ADVANCES IN THE SYNTHESES OF FUSARIUM-DERIVED NATURAL PRODUCTS: PROGRESS TOWARD IMMUNOMODULIDE AND THE TOTAL SYNTHESIS OF FUSAHEXIN

Claudia Natola

Thesis Submitted to the University of Ottawa
in partial Fulfillment of the requirements for the

Doctorate in Philosophy degree in Chemistry

Department of Chemistry and Biomolecular Sciences
Faculty of Science
University of Ottawa

Supervisor:
Dr. Christopher N. Boddy

© Claudia Natola, Ottawa, Canada, 2026

ABSTRACT

Fungal natural products represent a chemically diverse and pharmacologically rich source of bioactive scaffolds, yet the majority remain incompletely characterized at the level of structure, biosynthesis, and biological function. Across the 12-membered cyclic tridepsipeptide family, to which *Fusarium*-derived immunomodulide belongs, biochemically characterized biosynthetic gene clusters remain the exception rather than the rule, leaving stereochemical assignment dependent on total synthesis in the absence of reliable biosynthetic prediction. These structural and biosynthetic uncertainties place practical limits on real-world applications for these compounds. The development of immunomodulide as a sustainable plant immune potentiator has been limited by the absence of a validated pharmacophore model and unresolved polyketide stereochemistry, and investigation into fusahexin's proposed role in *Fusarium* virulence and cell surface hydrophobicity has been limited by the absence of synthetic access to both the natural product and its biosynthetic precursor.

This thesis describes the use of total synthesis, comparative spectroscopic analysis, and biosynthetic investigation to resolve these structural and functional gaps for two macrocyclic fungal natural products. We have established the first pharmacophore model for the 12-membered cyclic tridepsipeptide class, identifying the native D-Trp/L-Pip macrolactam configuration as essential for immunomodulide's plant immunopotentiating activity and confirming that this activity translates into reduced bacterial colonization *in planta*. We have narrowed the stereochemical assignment of immunomodulide's polyketide-derived fragment from sixteen possible permutations to a single synthetic lead using comparative ^{13}C NMR analysis, and have advanced its total synthesis to the macrolactamization precursor, providing a foundation for the future development of a lead scaffold for sustainable crop protection. Using a synthesis-supported workflow, CRISPR/Cas9 gene editing and comparative metabolomics, we have identified prefusahexin as the direct biosynthetic precursor to fusahexin and achieved the total syntheses of both natural products, with a reduction-triggered cyclization cascade delivering fusahexin's fused *N,O*-acetal in high yield. We have further shown that the fusahexin biosynthetic gene cluster is split across the genome and, through biomimetic oxidation of prefusahexin, implicated copper amine oxidases as the enzyme class responsible for the key oxidative transformation linking the two natural products. The synthetic and biosynthetic platforms presented in this thesis will be

fundamental to pursuing further biological and translational investigations of these fungal natural products.

DEDICATION

To Flavio, Mamma and Papà, who have always believed in me
more than I could ever believe in myself, I love you.

A Flavio, Mamma e Papà, che hanno sempre creduto in me
più di quanto io abbia mai creduto in me stessa. Vi voglio bene.

ACKNOWLEDGEMENTS

First and foremost, I must thank my PhD supervisor Dr. Christopher Boddy. I once heard that to have a great graduate school experience, you need three of three things. You need a project you're passionate about, a supportive supervisor and a great lab environment. You have given me three of three, and I will forever think back on this time in my life fondly because of that. No matter how many times I walked into your office with "bad news," you've always found a way to reframe my results as a "win," and out I walked with newfound energy to try yet again. You've taught me more than organic chemistry and biosynthesis, and I hope to one day lead a team just as you have been leading yours. I can't thank you enough.

To my committee members, thank you for taking the time to read my thesis work and for always being available for a scientific discussion, a career conversation or even a listening ear. Your guidance and support have been instrumental.

To my colleagues, this journey would certainly not have been the same without you. Thank you for the friendships and support throughout the years, and for making light of quite literally every failed experiment, embarrassing moment or difficult time. It has been a joy to work with and alongside you all. I am especially thankful to my colleagues-turned-lifelong-friends, Eryn, Jason, Sherif and Chad. Your talent, passion and hard work have inspired me day in and day out, and our friendship has gotten me through this degree.

To my family, Flavio, Stefania and Angelo, I could never have done this without your love and support. No matter how many kilometers have been between us in these past years, you three have been my rock. I will forever be grateful for you.

To David, thank you for always reminding me of what I was capable of, knowing exactly what to say and when to say it, and being my escape in times when I've needed it most.

TABLE OF CONTENTS

PART I. Total Synthesis of Immunomodulide

CHAPTER I. Emergence of a Structurally Coherent Family of Fungal PKS–NRPS-Derived Tridepsipeptides

1.1 Fungal PKS-NRPS Hybrid Natural Products 3
1.1.1 Fungal Secondary Metabolites....3
1.1.2 Fungal Polyketide Synthase–Nonribosomal Peptide Synthetase Hybrid Biosynthesis...3
1.1.3 Cyclic Depsipeptide Macrocycles in Fungal PKS–NRPS Systems....9
1.2 Emergence of a Structurally Conserved Subfamily of 12-Membered Cyclic Tridepsipeptides 10
1.2.1 Inclusion Criteria and Structural Definition 10
1.2.2 Structural Diversity....13
1.2.3 Biosynthetic Origins 16
1.2.4 Biological Activity....19
1.2.5 Total Synthesis Attempts....21
1.2.5.1 Colletopeptides and Colletotrichamides 22
1.2.5.2 Acremolides 25
1.2.5.3 HA23....33
1.2.5.4 Stereocalpins....36
1.2.6 Synthetic Challenges and Opportunities....45
1.3 An Introduction to Immunomodulide 52
1.3.1 Discovery, Isolation, and Biosynthetic Context 52
1.3.2 Immunomodulide Within the Fungal Tridepsipeptide Framework 53
1.3.3 Biological Activity and Significance....54
1.3.4 Configurational Ambiguity and Structural Assignment 54
1.4 Summary of Thesis Objectives (Part I)....55
1.5 References....57

CHAPTER II. Evaluating Macrolactamization Approaches Towards the Synthesis of the Immunomodulide Core

2.1 An Introduction to the Synthesis of Macrocycles....62
2.1.1 Macrocyclization: General Challenges and Strategies 62
2.1.2 Common Macrocyclization Methods....62
2.1.3 Macrolactamization in the Synthesis of Cyclic Tridepsipeptides....64
2.1.4 Retrosynthetic Analysis and Model System Design....65
2.2 Results and Discussion 67
2.2.1 Macrolactamization via Route B 67
2.2.2 Macrolactamization via Route C 73
2.3 Conclusions and Application to the Total Synthesis of Immunomodulide 77

2.4 Experimental Section 79
2.5 References 104
2.6 Appendix to Chapter III 107

CHAPTER III. Synthesis of Immunomodulide Analogues
3.1 Introduction 141
3.1.1 An Introduction to PAMP-Triggered Immunity and Immunomodulatory Natural Products in Plant Defense 141
3.1.2 Biological Activity of Immunomodulide and the Model System 142
3.1.3 Structure-Activity Relationships in Cyclic Depsipeptides: Precedent and Design Principles 144
3.1.4 Analogue Design Strategy and Pharmacophore Hypothesis 145
3.2 Results and Discussion 148
3.2.1 First-Generation Synthesis of the Analogue Library 144
3.2.2 Second-Generation Synthesis of the Analogue Library 153
3.2.3 Biological Evaluation of the Analogue Library 154
3.3 Conclusions and Future Directions 156
3.4 Experimental Section 159
3.5 References 191
3.6 Appendix to Chapter III 193

CHAPTER IV. Toward the Total Synthesis of Immunomodulide
4.1 Introduction 231
4.2 Defining the PKS Target (^{13}C NMR Stereochemical Assignment) 232
4.3 A Retrosynthetic Analysis of Immunomodulide 239
4.4 Results and Discussion 240
4.4.1 Enantioselective Synthesis of the PKS Fragment 240
4.4.1.1 First-Generation Synthesis 240
4.4.1.2 Second-Generation Synthesis 245
4.4.1.3 Diastereoselectivity of the Vinylogous Mukaiyama Aldol 247
4.4.2 Evaluation of Acyl Ketene Ring-Closure in a Model System 255
4.4.3 Sequence Optimizations to Construct Immunomodulide 258
4.5 Conclusions and Future Directions 264
4.6 Experimental Section 267
4.7 References 293
4.8 Appendix to Chapter IV 297

PART II. Total Synthesis and Biosynthetic Investigation of Fusahexin

CHAPTER V. Synthesis-Supported Discovery of Prefusahexin, a Direct Fusahexin Biosynthetic Precursor

5.1 Introduction to the Research Article Presented in this Chapter 335
5.2 Summary of Thesis Objectives (Part II) 337
5.3 Author Contributions 338
5.4 Copyright 338
5.5 Synthesis-Supported Discovery of Prefusahexin, a Direct Fusahexin Biosynthetic Precursor 339
5.5.1 Abstract 339
5.5.2 Main Text 339
5.5.3 Supplementary Information 346
5.6 Future Directions and Preliminary Results 370
5.6.1 Identifying the Oxidative Enzyme Responsible for Converting Prefusahexin to Fusahexin 370
5.6.2 Biomimetic Oxidation of Prefusahexin Using a Synthetic TPQ Mimic 371
5.7 Conclusions 372
5.8 References 374
5.9 Appendix to Chapter V 377

CHAPTER VI. Conclusions and Future Directions

6.1 Overview 392
6.2 The 12-Membered Cyclic Tridepsipeptide Family 393
6.3 Toward the Total Synthesis of Immunomodulide 393
6.4 Immunomodulide as a Plant Immune Potentiator 395
6.5 Biosynthesis and Synthesis of Fusahexin 396
6.6 Conclusion 398
6.7 References 399

LIST OF FIGURES

Chapter I

Figure 1.1. Generalized architecture and iterative biosynthetic logic of a fungal highly reducing polyketide synthase (hrPKS).....5
Figure 1.2. Generalized modular architecture and peptide elongation logic of a fungal non-ribosomal peptide synthetase (NRPS) 7
Figure 1.3. Generalized PKS-NRPS hybrid biosynthetic logic illustrated using the proposed biosynthesis of xylacremolides A and B.....9
Figure 1.4. Three-component core architecture of the 12-membered cyclic tridepsipeptide family 10
Figure 1.5. Members of the 12-membered cyclic tridepsipeptide family.....12
Figure 1.6. Structurally related fungal cyclic tridepsipeptides excluded from the defined compound class.....13
Figure 1.7. Three recurring macrocyclization disconnections (routes A-C) explored across reported synthetic campaigns.....22
Figure 1.8. Summary of synthetic strategy towards colletopeptide A and colletotrichamide A by Chen et al. 23
Figure 1.9. Summary of key synthetic steps in the total synthesis of colletopeptide A and colletotrichamide A.....24
Figure 1.10. Summary of ElMarrouni's strategy towards the synthesis of 2,5-diepi-acremolide B 25
Figure 1.11. Key strategic steps in the total synthesis of 2,5-diepi-acremolide B.....27
Figure 1.12. Summary of synthetic strategy of Yadav et al. towards the total synthesis of acremolides A–D 28
Figure 1.13. Summary of key steps in Yadav's forward synthesis towards the acremolides 29
Figure 1.14. Summary of synthetic strategy of Xiao et al. towards the total synthesis of acremolide A and B 30
Figure 1.15. Summary of key steps in linear synthesis of acremolide A and B by Xiao and coworkers.....32
Figure 1.16. Summary of synthetic strategy of Feng et al. towards the total synthesis of HA2333
Figure 1.17. Feng's forward synthesis of HA23 35
Figure 1.18. Summary of synthetic strategy of Ghosh et al. towards the total synthesis of 5-epi-stereocalpin A 36
Figure 1.19. Synthesis of 5-epi-stereocalpin A by Ghosh et al.....37
Figure 1.20. Summary of Reddy and coworkers' synthetic strategy to stereocalpin A 38
Figure 1.21. Reddy et al.'s synthetic attempts towards stereocalpin A.....39
Figure 1.22. Summary of retrosynthetic strategy towards stereocalpin A by Zhao et al.and first synthetic attempt by Zhao et al. demonstrating formation of undesired lactone.....41
Figure 1.24. Second and third synthetic attempts by Zhao et al. towards stereocalpin A 42
Figure 1.25. Summary of Kaneda and coworkers' synthetic strategy to stereocalpin A 43
Figure 1.26. Kaneda's synthesis of PKS fragments in pursuit of structural characterization and total synthesis of stereocalpin A 44

Figure 1.27. Completion of total synthesis of stereocalpin A by Kaneda 45
Figure 1.28. Macrolactonization (route A) attempts made towards acremolide and stereocalpin tridepsipeptide cores 46
Figure 1.29. Macrolactamization (route B) attempts made towards HA23 and stereocalpin tridepsipeptide cores 47
Figure 1.30. Macrolactamization (route C) successful implementation in synthesis of acremolides, colletopeptides A, colletotrichamide A, and stereocalpin A 48
Figure 1.31. Proposed biosynthetic gene cluster responsible for production of immunomodulide 52
Figure 1.32. Biosynthesis-supported predicted structure of immunomodulide 52

Chapter II

Figure 2.1. Summary of macrocyclization outcomes across routes A–C in reported synthetic campaigns targeting the 12-membered cyclic tridepsipeptide scaffold 64
Figure 2.2. Model system (**2.1**) employed for macrolactamization evaluation 65
Figure 2.3. Summary of retrosynthetic analysis of model system (**2.1**) via route B and route C 66
Figure 2.4. Synthesis of linear precursors **2.6a/b** and their macrolactamization via route B 67
Figure 2.5. Coupling reagent screen for macrolactamization via route B (L-Trp series, **2.6b**)...69
Figure 2.6. Coupling reagent screen for macrolactamization via route B (D-Trp series, **2.6a**)...71
Figure 2.7. Synthesis of linear precursors **2.7a/b** and their macrolactamization via route C 74
Figure 2.8. Mitsunobu-based route C macrolactamization employing reverse-prenylated D-Trp–L-Pip dipeptide **2.24** 76
Figure 2.9. Marfey's analysis of the pipecolic acid residue in macrolactam diastereomers obtained from routes B and C 102
Figure 2.10. Repeat Marfey's analysis of **2.1-anti'** from the L-Trp series (route C, **2.7b**), confirming the presence of D-Pip 102
Figure 2.11. Marfey's analysis of the tryptophan residue in macrolactam diastereomers obtained from routes B and C 103
Figure 2.12. Repeat Marfey's analysis of the tryptophan residue in **2.1-anti'** from the L-Trp series (route C, **2.7b**) 103

Chapter III

Figure 3.1. ROS burst potentiation assay results for immunomodulide in Arabidopsis thaliana leaf discs 143
Figure 3.2. DC3000 bacterial colonization assay results for immunomodulide and model system 2.1-anti 144
Figure 3.3. Stereochemical probe set: all four diastereomers of the model system macrolactam 146
Figure 3.4. Building block exchange analogue set with structural modifications at the PKS surrogate, L-Pip, and D-Trp positions 146
Figure 3.5. Tridepsipeptide family-inspired analogue set 147
Figure 3.6. General first-generation solution-phase route to the analogue library 149

Figure 3.7. Synthesis of reverse-prenylated Trp analogue 3.4 via alternative route C strategy 152
Figure 3.8. Second-generation SPPS-based route to the analogue library.....153
Figure 3.9. ROS burst potentiation assay results for **2.1-anti 3.6** and **3.3** analogue library subset 155
Figure 3.10. Synthetic scheme for SPPS-enabled workflow (general procedure A) 175

Chapter IV

Figure 4.1. Structures of immunomodulide and configurationally defined congeners used for ^{13}C NMR comparison.....232
Figure 4.2. Comparative ^{13}C NMR Δppm analysis of immunomodulide against configurationally defined tridepsipeptide congeners.....235
Figure 4.3. Comparative ^{13}C NMR Δppm analysis of immunomodulide against 3,5-diepi-acremolide B and acremolide B 236
Figure 4.4. Retrosynthetic analysis of immunomodulide 237
Figure 4.5. PKS portion retrosynthetic analysis highlighting stereocenter installation strategy 239
Figure 4.6. First-generation retrosynthetic analysis of PKS fragment **4.3** via disconnections A and B 241
Figure 4.7. Synthesis of Chan's diene (**4.6**) and attempted preparation of racemic aldehyde 4.11 242
Figure 4.8. Synthesis of cross-metathesis coupling partners **4.9** and **4.5** 243
Figure 4.9. Second-generation retrosynthetic analysis of aldehyde **4.8** via retro-Claisen fragmentation of 2-acetylcyclohexanone.....245
Figure 4.10. Second-generation forward synthesis of PKS aldehyde **4.8**.....246
Figure 4.11. Transition state models for diastereoselective nucleophilic addition to β-heteroatom-substituted and α-substituted aliphatic aldehydes.....248
Figure 4.12. Generation of COBI catalyst and proposed transition state for vinylogous Mukaiyama aldol reaction.....249
Figure 4.13. Assembly of model system **4.29** for evaluation of acyl ketene ring-closure 255
Figure 4.14. Thermal acyl ketene ring-closure of model system **4.29**, affording ring-closed product **4.31** and diketopiperazine **4.32**.....257
Figure 4.15. First attempted route B macrolactamization 258
Figure 4.16. TBS protection strategy and attempted C5 silyl ether deprotection of **4.38**.....259
Figure 4.17. Yamaguchi esterification between PKS-dioxinone fragment **4.26** and NRPS fragment **2.24** 261
Figure 4.18. Synthesis of macrolactamizsation (route C) precursor **4.40** and acyl ketene ring-closure.....262
Figure 4.19. LC-MS evidence for macrolactam product **4.43** in crude reaction mixture.....263

Chapter V

Figure 5.1. Structure of fusahexin (**5.1**) and prefusahexin (**5.3**).....335
Figure 5.2. Revised biosynthetic origine of fusahexin (**5.1**).....336

Figure 5.3. Revised biosynthesis of fusahexin (**5.1/1**), and prefusahexin (**5.3/3**) showing biosynthetic gene cluster and annotate NRPS4 340
Figure 5.4. Metabolomics data showing identification of prefusahexin (**5.3/3**) and supporting hypothesis 342
Figure 5.5. Total synthesis of fusahexin (**5.1**) and prefusahexin (**5.3**) via SPPS and DIBAL-H/acid-promoted cascade 343
Figure 5.S1. pRF-HU2 vector map 350
Figure 5.S2. Validation of knockout of NRPS4 gene (FGSG_02315) 350
Figure 5.S3. EIC and mass spectrum of prefusahexin (**5.3**) 354
Figure 5.S4. EIC and mass spectrum of synthetic intermediate **13** 357
Figure 5.S5. EIC and mass spectrum of synthetic intermediate **8** 363
Figure 5.S6. EIC and mass spectrum of synthetic intermediate **9** 365
Figure 5.S7. EIC and mass spectrum of synthetic intermediate **10** 366
Figure 5.S8. rp-HPLC chromatogram of fusahexin (**5.1**) 369

LIST OF TABLES

Chapter III

Table 3.1. Reaction optimization for saponification of dipeptide **3.1a'**. 147

Chapter IV

Table 4.1. Optimization of the cross-metathesis reaction between **4.9** and **4.5** 244
Table 4.2. Optimization of the vinylogous Mukaiyama aldol reaction between aldehyde **4.8** and Chan's diene **4.6** or TMS-dioxinone **4.24** 253
Table 4.3. Optimizations for esterification between dioxinone model **4.28** and simplified NRPS substrate **3.1b** 256
Table 4.4. Conditions evaluated for deprotection of the C5 silyl ether of **4.38** 260

Chapter V

Table 5.S1. Primers used in the amplification of the hygromycin repair template.....348
Table 5.S2. crRNA primer sequences used in the assembly of Cas-9 ribonucleoprotein complexes 349
Table 5.S3. Internal primers used for the confirmation of the absence of target gene 349
Table 5.S4. Complete spectroscopic characterization of prefusahexin.....359
Table 5.S5. Comparison of selected diagnostic ^{1}H NMR data for fusahexin and prefusahexin368

LIST OF SCHEMES

Chapter V

Scheme 5.S1. Synthesis of dihydrofusahexin (**5.2**) and prefusahexin (**5.3**).....352

LIST OF SPECTRA

Chapter II (Appendix, Section 2.6)

Spectra 2.1. ^{1}H and ^{13}C NMR spectra of compound **2.8** 107
Spectra 2.2. ^{1}H and ^{13}C NMR spectra of compound **2.9** 108
Spectra 2.3. ^{1}H and ^{13}C NMR spectra of compound **2.10** 109
Spectra 2.4. ^{1}H and ^{13}C NMR spectra of compound **2.11** 110
Spectra 2.5. ^{1}H and ^{13}C NMR spectra of compound **2.12** 111
Spectra 2.6. ^{1}H and ^{13}C NMR spectra of compound **2.13** 112
Spectra 2.7. ^{1}H and ^{13}C NMR spectra of compound **2.14a** 113
Spectra 2.8. ^{1}H and ^{13}C NMR spectra of compound **2.14b** 114
Spectra 2.9. ^{1}H and ^{13}C NMR spectra of compound **2.16a** 115
Spectra 2.10. COSY and HSQC NMR spectra of compound **2.16a** 116
Spectra 2.11. ^{1}H and ^{13}C NMR spectra of compound **2.16b** 117
Spectra 2.12. COSY and HSQC NMR spectra of compound **2.16b** 118
Spectra 2.13. ^{1}H and ^{13}C NMR spectra of compound **2.18** 119
Spectra 2.14. ^{1}H and ^{13}C NMR spectra of compound **2.19a** 120
Spectra 2.15. COSY and HSQC spectra of compound **2.19a** 121
Spectra 2.16. ^{1}H and VT NMR spectra of compound **2.19b** 122
Spectra 2.17. ^{13}C and COSY NMR spectra of compound **2.19b** 123
Spectra 2.18. HSQC NMR spectra of compound **2.19b** 124
Spectra 2.19. ^{1}H and ^{13}C NMR spectra of compound **2.20a** 125
Spectra 2.20. COSY and HSQC spectra of compound **2.20a** 126
Spectra 2.21. ^{1}H and ^{13}C NMR spectra of compound **2.20b** 127
Spectra 2.22. ^{1}H and ^{13}C NMR spectra of compound **2.21** 128
Spectra 2.23. ^{1}H and ^{13}C NMR spectra of compound **2.22** 129
Spectra 2.24. ^{1}H and ^{13}C NMR spectra of compound **2.1-anti** 130
Spectra 2.25. HSQC NMR spectra of compound **2.1-anti** 131
Spectra 2.26. ^{1}H and ^{13}C NMR spectra of compound **2.1-anti'** 132
Spectra 2.27. ^{1}H and ^{13}C NMR spectra of compound **2.1-syn** 133
Spectra 2.28. ^{1}H and ^{13}C NMR spectra of compound **2.1-syn'** 134
Spectra 2.29. ^{1}H NMR spectra of compounds **2.1-anti**, **2.1-anti', 2.1-syn** and **2.1-syn'** 135
Spectra 2.30. ^{1}H and ^{13}C NMR spectra of compound **2.23** 136
Spectra 2.31. ^{1}H and ^{13}C NMR spectra of compound **2.24** 137
Spectra 2.32. ^{1}H and ^{13}C NMR spectra of compound **2.25** 138
Spectra 2.33. HSQC NMR spectra of compound **2.25** 139

Chapter III (Appendix, Section 3.6)

Spectra 3.1. ^{1}H and ^{13}C NMR spectra of compound **3.1a'** 193
Spectra 3.2. ^{1}H and ^{13}C NMR spectra of compound **3.1b** 194
Spectra 3.3. ^{1}H and ^{13}C NMR spectra of compound **3.4c** 195

Spectra 3.4. ^{1}H and ^{13}C NMR spectra of compound **3.4d**.....196
Spectra 3.5. ^{1}H and ^{13}C NMR spectra of compound **3.14**.....197
Spectra 3.6. ^{1}H and ^{13}C NMR spectra of compound **3.2e**.....198
Spectra 3.7. ^{1}H and ^{13}C NMR spectra of compound **3.15**.....199
Spectra 3.8. ^{1}H and ^{13}C NMR spectra of compound **3.1c**.....200
Spectra 3.9. ^{1}H and ^{13}C NMR spectra of compound **3.1d**.....201
Spectra 3.10. ^{1}H and ^{13}C NMR spectra of compound **3.1e**.....202
Spectra 3.11. HSQC NMR spectrum of compound **3.1e**.....203
Spectra 3.12. ^{1}H and ^{13}C NMR spectra of compound **3.1**.....204
Spectra 3.13. HSQC NMR spectrum of compound **3.1**.....205
Spectra 3.14. ^{1}H and ^{13}C NMR spectra of compound **3.12**.....206
Spectra 3.15. ^{1}H and ^{13}C NMR spectra of compound **3.3a'**.....207
Spectra 3.16. ^{1}H and ^{13}C NMR spectra of compound **3.3b**.....208
Spectra 3.17. ^{1}H and ^{13}C NMR spectra of compound **3.3c**.....209
Spectra 3.18. ^{1}H and ^{13}C NMR spectra of compound **3.3d**.....210
Spectra 3.19. ^{1}H and ^{13}C NMR spectra of compound **3.3e**.....211
Spectra 3.20. ^{1}H and ^{13}C NMR spectra of compound **3.5d**.....212
Spectra 3.21. ^{1}H and ^{13}C NMR spectra of compound **3.5e**.....213
Spectra 3.22. ^{1}H and ^{13}C NMR spectra of compound **3.5f**.....214
Spectra 3.23. ^{1}H and ^{13}C NMR spectra of compound **3.6d**.....215
Spectra 3.24. ^{1}H and ^{13}C NMR spectra of compound **3.6e**.....216
Spectra 3.25. ^{1}H and ^{13}C NMR spectra of compound **3.6**.....217
Spectra 3.26. ^{1}H and ^{13}C NMR spectra of compound **3.7d**.....218
Spectra 3.27 ^{1}H and ^{13}C NMR spectra of compound **3.7e**.....219
Spectra 3.28. ^{1}H and ^{13}C NMR spectra of compound **3.7**.....220
Spectra 3.29. ^{1}H and ^{13}C NMR spectra of compound **3.9d**.....221
Spectra 3.30. ^{1}H and ^{13}C NMR spectra of compound **3.9**.....222
Spectra 3.31. ^{1}H and ^{13}C NMR spectra of compound **3.10d**.....223
Spectra 3.32. ^{1}H and ^{13}C NMR spectra of compound **3.10e**.....224
Spectra 3.33. ^{1}H and ^{13}C NMR spectra of compound **3.10**.....225
Spectra 3.34. HSQC NMR spectra of compound **3.10**.....226
Spectra 3.35. ^{1}H and ^{13}C NMR spectra of compound **3.11d**.....227
Spectra 3.36. ^{1}H and ^{13}C NMR spectra of compound **3.11e**.....228
Spectra 3.27. ^{1}H and ^{13}C NMR spectra of compound **3.11**.....229
Spectra 3.28. HSQC NMR spectra of compound **3.11**.....230

Chapter IV (Appendix, Section 4.8)
Spectra 4.1. ^{1}H and ^{13}C NMR spectra of compound **4.10**.....297
Spectra 4.2. ^{1}H and ^{13}C NMR spectra of compound **4.6**.....298
Spectra 4.3. ^{1}H and ^{13}C NMR spectra of compound **4.12**.....299
Spectra 4.4. ^{1}H and ^{13}C NMR spectra of compound **4.9**.....300

Spectra 4.5. ^{1}H and ^{13}C NMR spectra of compound **4.13** 301
Spectra 4.6. ^{1}H and ^{13}C NMR spectra of compound **4.14** 302
Spectra 4.7. ^{1}H and ^{13}C NMR spectra of compound **4.15** 303
Spectra 4.8. ^{1}H and ^{13}C NMR spectra of compound **4.5** 304
Spectra 4.9. ^{1}H spectra of compound **4.16** 305
Spectra 4.10. ^{1}H and ^{13}C NMR spectra of compound **4.19** 306
Spectra 4.11. ^{1}H and ^{13}C NMR spectra of compound **4.11** 307
Spectra 4.12. ^{1}H and ^{13}C NMR spectra of compound **4.21** 308
Spectra 4.13. ^{1}H and ^{13}C NMR spectra of compound **4.21-(R)-MTPA ester** 309
Spectra 4.14. ^{1}H and ^{13}C NMR spectra of compound **4.21-rac** 310
Spectra 4.15. ^{1}H and ^{13}C NMR spectra of compound **4.21-rac-MTPA ester** 311
Spectra 4.16. Expanded ^{1}H NMR spectrum of compound **4.21-(R)-MTPA** 312
Spectra 4.17. Expanded ^{1}H NMR spectrum of compound **4.21-rac-MTPA** 312
Spectra 4.18. ^{1}H and ^{13}C NMR spectra of compound **4.22** 313
Spectra 4.19. ^{1}H and ^{13}C NMR spectra of compound **4.17** 314
Spectra 4.20. ^{1}H and ^{13}C NMR spectra of compound **4.23** 315
Spectra 4.21. ^{1}H and ^{13}C NMR spectra of compound **4.8** 316
Spectra 4.22. ^{1}H and ^{13}C NMR spectra of compound **4.27** 317
Spectra 4.23. ^{1}H spectra of compound **4.25** (mixture of diastereomers) 318
Spectra 4.24. ^{13}C and HSQC NMR spectra of compound **4.25** (mixture of diastereomers) 319
Spectra 4.25. ^{1}H and ^{13}C NMR spectra of compound **4.26** 320
Spectra 4.26. ^{1}H and ^{13}C NMR spectra of compound **4.27** 321
Spectra 4.27. ^{1}H and ^{13}C NMR spectra of compound **4.32** 322
Spectra 4.28. ^{1}H and ^{13}C NMR spectra of compound **4.37** 323
Spectra 4.29. HSQC and VT ^{13}C NMR of compound **4.37** 324
Spectra 4.30. Expanded VT ^{13}C NMR spectra of compound **4.37** 325
Spectra 4.31. ^{1}H and ^{13}C NMR spectra of compound **4.38** 326
Spectra 4.32. HSQC spectrum of compound **4.38** 327
Spectra 4.33. ^{1}H and ^{13}C NMR spectra of compound **4.34** 328
Spectra 4.34. ^{1}H and ^{13}C NMR spectra of compound **4.36** 329
Spectra 4.35. ^{1}H and ^{13}C NMR spectra of compound **4.41** 330
Spectra 4.36. ^{1}H and ^{13}C NMR spectra of compound **4.35** 332
Spectra 4.37. HSQC spectrum of compound **4.35** 331
Spectra 4.38. ^{1}H NMR spectra of compound **4.40** 332

Chapter V (Appendix, Section 5.9)

Spectra 5.1. ^{1}H NMR spectra of compound **11** 377
Spectra 5.2. ^{13}C NMR spectra of compound **11** 377
Spectra 5.3. ^{1}H NMR spectra of compound **4** 378
Spectra 5.4. ^{13}C NMR spectra of compound **4** 378
Spectra 5.5. ^{1}H NMR spectra of compound **5** 379

Spectra 5.6. ^{13}C NMR spectra of compound **5** 379
Spectra 5.7. ^{1}H NMR spectra of compound **6** 380
Spectra 5.8. ^{13}C NMR spectra of compound **6** 380
Spectra 5.9. ^{1}H NMR spectra of compound **2 (5.2)** 381
Spectra 5.10. ^{13}C NMR spectra of compound **2 (5.2)** 381
Spectra 5.11. ^{1}H NMR spectra of compound **3 (5.3)** 382
Spectra 5.12. ^{13}C NMR spectra of compound **3 (5.3)** 382
Spectra 5.13. COSY NMR spectra of compound **3 (5.3)** 383
Spectra 5.14. HSQC NMR spectra of compound **3 (5.3)** 383
Spectra 5.15. TOCSY NMR spectra of compound **3 (5.3)** 384
Spectra 5.16. HMBC NMR spectra of compound **3 (5.3)** 384
Spectra 5.17. ^{1}H NMR spectra of compound **1 (5.1)** 385
Spectra 5.18. COSY NMR spectra of compound **1 (5.1)** 385
Spectra 5.19. HSQC NMR spectra of compound **1 (5.1)** 386
Spectra 5.20. TOCSY NMR spectra of compound **1 (5.1)** 386
Spectra 5.21. Overy ^{1}H NMR spectra of synthetic **1 (5.1)** and isolate **1 (5.1)** 387
Spectra 5.21. Overy ^{1}H NMR spectra of 1D selective ROSEY of **1 (5.1)** 388

LIST OF ABBREVIATIONS

A	adenylation domain
AAFC	Agriculture and Agri-Food Canada
ACP	acyl carrier protein
aq	aqueous
AT	acyltransferase domain
BGC	biosynthetic gene cluster
Bn	benzyl
Boc	tert-butoxycarbonyl
Boc_2O	di-tert-butyl dicarbonate
BINAP	2,2'-bis(diphenylphosphino)-1,1'-binaphthyl
BINOL	1,1'-bi-2-naphthol
C	condensation domain
CAO	copper amine oxidase
CBS	Corey–Bakshi–Shibata
CDI	1,1'-carbonyldiimidazole
CFU	colony-forming units
CM	cross-metathesis
CoA	coenzyme A
COBI	chiral oxazaborolidinium ion
COSY	correlation spectroscopy
CT	terminal condensation domain
D	D-configured (amino acid)
DCE	1,2-dichloroethane
DCM	dichloromethane
DEAD	diethyl azodicarboxylate
DH	dehydratase domain
DIAD	diisopropyl azodicarboxylate
DIBAL-H	diisobutylaluminium hydride
DIPEA	N,N-diisopropylethylamine
DKP	diketopiperazine
DMAP	4-dimethylaminopyridine
DMF	N,N-dimethylformamide
DMP	Dess–Martin periodinane
DMSO	dimethyl sulfoxide
dr	diastereomeric ratio
E	epimerization domain
EDC	1-ethyl-3-(3-dimethylaminopropyl)carbodiimide
EIC	extracted ion chromatogram
er	enantiomeric ratio
ER	enoyl reductase domain
ESI	electrospray ionization

Fmoc	fluorenylmethyloxycarbonyl
flg22	flagellin-derived 22-amino acid peptide
FLS2	FLAGELLIN-SENSING 2
G-I	Grubbs first-generation catalyst
G-II	Grubbs second-generation catalyst
HATU	1-[bis(dimethylamino)methylene]-1H-1,2,3-triazolo[4,5-b]pyridinium 3-oxide hexafluorophosphate
HBTU	2-(1H-benzotriazol-1-yl)-1,1,3,3-tetramethyluronium hexafluorophosphate
HDAC	histone deacetylase
HG-II	Hoveyda–Grubbs second-generation catalyst
HMBC	heteronuclear multiple bond correlation
HOAt	1-hydroxy-7-azabenzotriazole
HOBt	1-hydroxybenzotriazole
HRP	horseradish peroxidase
HRMS	high-resolution mass spectrometry
hrPKS	highly reducing polyketide synthase
HSQC	heteronuclear single quantum coherence
iPKS	iterative polyketide synthase
KF	kahalalide F
KR	ketoreductase domain
KS	ketosynthase domain
L	L-configured (amino acid)
LA	Lewis acid
LC-MS	liquid chromatography–mass spectrometry
LDA	lithium diisopropylamide
MAMP	microbe-associated molecular pattern
Me-CBS	methyl-Corey–Bakshi–Shibata
MS	molecular sieves; Murashige and Skoog (in biological context)
MT	methyltransferase domain
MTPA	α-methoxy-α-(trifluoromethyl)phenylacetic acid (Mosher's acid)
MW	molecular weight
N-Me	N-methyl
NMR	nuclear magnetic resonance
NRPS	nonribosomal peptide synthetase
OxymaPure	ethyl 2-cyano-2-(hydroxyimino)acetate
PAMP	pathogen-associated molecular pattern
PCP	peptidyl carrier protein
PDC	pyridinium dichromate
Pip	pipecolic acid
PKS	polyketide synthase
PRR	pattern recognition receptor
PTI	PAMP-triggered immunity

PyBOP	benzotriazol-1-yl-oxytripyrrolidinophosphonium hexafluorophosphate
R	reductase domain
RBOH	respiratory burst oxidase homolog
RCM	ring-closing metathesis
ROS	reactive oxygen species
rt	room temperature
SAM	S-adenosyl methionine
SAR	structure–activity relationship
SGI	seedling growth inhibition
SM	secondary metabolite
SPPS	solid-phase peptide synthesis
T	thiolation domain (see PCP)
T3P	propylphosphonic anhydride
TBAF	tetrabutylammonium fluoride
TBDPS	tert-butyldiphenylsilyl
TBS	tert-butyldimethylsilyl
TE	thioesterase domain
TFA	trifluoroacetic acid
THF	tetrahydrofuran
TLC	thin-layer chromatography
TMS	trimethylsilyl
TMSCl	trimethylsilyl chloride
TMSOTf	trimethylsilyl trifluoromethanesulfonate
TOF	time-of-flight
TPQ	topaquinone
UPLC	ultra-performance liquid chromatography
VMAR	vinylogous Mukaiyama aldol reaction
XIC	extracted ion chromatogram

PART I.

Total Synthesis of Immunomodulide

CHAPTER I.

Emergence of a Structurally Coherent Family of Fungal PKS–NRPS-Derived Tridepsipeptides

1.1 Fungal PKS-NRPS Hybrid Natural Products

1.1.1 Fungal Secondary Metabolites.

Fungal species occupy diverse ecological niches as endophytes, soil saprophytes, and host-associated pathogens, where they encounter intense competitive and environmental pressures over evolutionary timescales[1,2]. In response to these pressures, fungi have evolved a remarkable capacity for secondary metabolite (SM) biosynthesis, producing structurally diverse small molecules that enable them to mediate both biotic and abiotic interactions within their environment. Unlike the primary metabolites they produce, which are essential for survival, these specialized compounds serve adaptive functions including host interactions (pathogenic, symbiotic and endophytic), chemical signaling and abiotic stress responses. Collectively, fungal secondary metabolites enhance organismal fitness within a given environment, and encompass a chemically diverse repertoire of remarkable structural and functional breadth[3].

It is precisely this chemical diversity, shaped by millions of years of ecological pressure, that has made fungal secondary metabolites such a productive source of pharmaceutical and agrochemical leads. Penicillin, the cephalosporins, the statins, and the echinocandins represent landmark examples of clinically deployed fungal natural products spanning antibiotic, antifungal, and lipid-lowering activities[4,5]. Beyond these, fungal SMs encompass potent anticancer agents, mycotoxins with significant agricultural and clinical consequences, and virulence factors such as gliotoxin from *Aspergillus fumigatus*, which directly modulate host immune defense mechanisms[6].

The structural diversity and pharmacological range represented by these compounds is a reflection of the complex biosynthetic machinery encoded within fungal genomes, the nature and programming of which are the subject of the sections that follow. The work described in Part I of this thesis investigates immunomodulide, a fungal PKS–NRPS-derived 12-membered cyclic tridepsipeptide, through an integrated approach combining total synthesis, structure-activity relationship studies, and biosynthetic analysis. The sections below establish the biosynthetic and synthetic background required to understand this campaign.

1.1.2 Fungal Polyketide Synthase-Nonribosomal Peptides Synthetase Hybrid Biosynthesis

The biosynthetic instructions for fungal SMs are encoded within fungal genomes in the form of biosynthetic gene clusters (BGCs): co-localized sets of genes that together encode the enzymatic machinery, tailoring enzymes, and regulatory elements required for SM production. A

defining and historically frustrating feature of fungal BGCs is their pronounced tendency toward transcriptional silence under standard laboratory conditions[8], meaning that the majority of biosynthetic potential encoded within fungal genomes remains cryptic and unexplored[8]. This challenge is compounded by the complexity of eukaryotic fungal genomes themselves, which are intron-rich and subject to layers of epigenetic regulation, significantly complicating heterologous expression efforts and slowing the functional characterization of many clusters relative to their bacterial counterparts[9,10].

Structurally, fungal secondary metabolites are broadly classified by their biosynthetic origin: polyketides assembled by polyketide synthases (PKSs), non-ribosomal peptides assembled by non-ribosomal peptide synthetases (NRPSs), terpenoids derived from the mevalonate pathway, and indole alkaloids rooted in the shikimate pathway[11,12].

Polyketide Synthases.

Among the biosynthetic enzymes present within fungal systems, polyketide synthases represent one of the largest and most prolific families[13]. PKS enzymes elaborate acetyl units from the iterative condensation of short acyl-CoA thioesters, most commonly acetyl-CoA and malonyl-CoA, assembling them in sequence into highly functionalized carbon skeletons[14]. Fungal PKSs are further subcategorized by type: type I, II and III, depending on their structural arrangements and catalytic mechanisms[15]. Within the subset of type I PKSs, which are often larger and either functionally modular or iterative, multiple catalytic domains are found, covalently fused and each serving a specific purpose within the elongation and processing of CoA units. Type II PKSs are dissociated, multienzyme complexes primarily found in bacteria, and type III PKSs are homodimeric enzymes responsible for simpler condensation reactions such as chalcone biosynthesis in plants. The focus of this thesis is the type I PKS architecture, which dominates fungal SM biosynthesis.

The core catalytic domains found in type I PKSs are the following: the acyltransferase (AT) domain functioning by selecting and loading the appropriate acyl-CoA thioesters onto the module, the ketosynthase domain (KS) functioning as the main catalytic domain responsible for the decarboxylative Claisen condensation reaction that fuses each successive building block units. The growing chain is “shuttled” between the KS and other modifying domains by the acyl carrier

protein (ACP) which holds the polyketide chain via its flexible phosphopantetheine arm (**Figure 1.1A**).

Collectively, AT, ACP, and KS domains are the fundamental catalytic units, and are grouped into larger repetitive structures known as modules. Each module thus contains the full set of domains required to add one residue to the growing chain. Optional tailoring domains can also

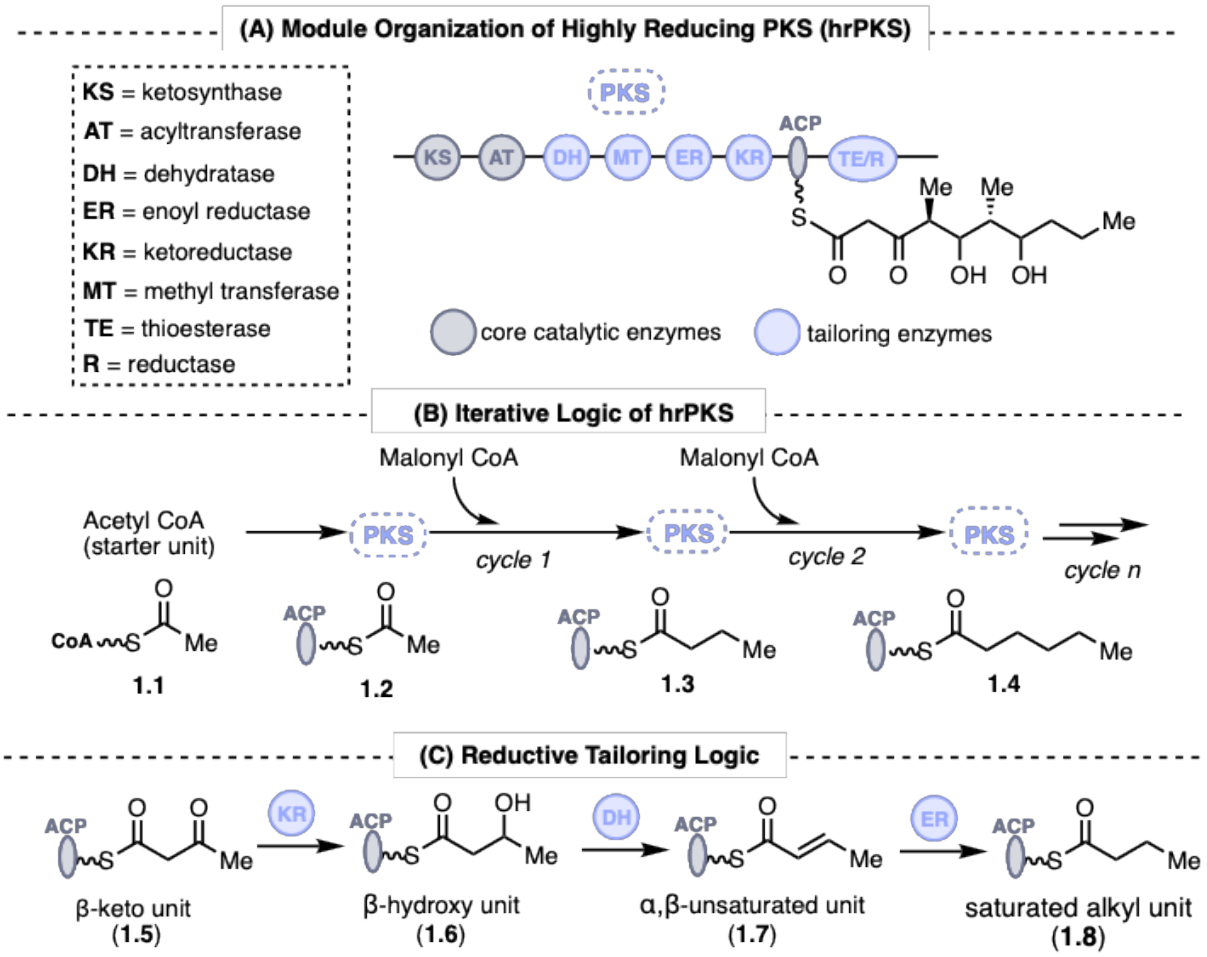


Figure 1.1. Generalized architecture and iterative biosynthetic logic of a fungal highly reducing polyketide synthase (hrPKS).

be found within any given module, examples of which are ketoreductase (KR), dehydratase (DH) and enoyl reductase (ER) process the β-carbon of each acyl CoA unit, uniquely controlling its final oxidation state. Additionally, all α-branching introduced along the polyketide chain arises through methyltransferase (MT) domain-mediated methylation of β-ketoacyl intermediates using the electrophilic methyl donor *S*-Adenosyl methionine (SAM), as no fungal PKS characterized to date

has been shown to incorporate branched extender CoA units (methyl/ethyl-malonyl) in the manner commonly observed in bacterial PKSs[16]. Off-loading of the polyketide chain is controlled by either a thioesterase (TE) or a C-terminal reductase (R) domain, releasing the functionalized carbon skeleton off the enzyme complex, either via hydrolysis forming the free acid, through cyclization via an intramolecular nucleophile or via the reduction to an aldehyde. In the PKS–NRPS hybrid systems relevant to this thesis and elaborated in **Section 1.3.1**, the PKS transfers its polyketide chain directly to the NRPS, where the terminal condensation (CT) domain is responsible for offloading the fully assembled hybrid product[17].

While bacteria often elaborate polyketide chains through modular type I PKSs, operating as well-defined assembly lines wherein each module is engaged precisely once per chain extension event in a predictable and co-linear fashion, fungal PKSs are iterative (iPKS)[18]. iPKSs are further subclassified by their reductive capacity; however, this thesis will focus on SM generated by the highly reducing PKSs (hrPKSs) subset, which fully engage their KR, DH, and ER domains to produce highly reduced, aliphatic polyketide chains. A simplified representation of this process is depicted in **Figure 1.1B,** where acetyl-CoA (**1.1**) is loaded on an iterative hrPKS (**1.2**), and extended in numerous cycles of iteration with the addition of malonyl-CoA units, leading to **1.3** and **1.4**. **Figure 1.1C** expands on the reductive tailoring logic for the reducing domains in these iterative hrPKSs. KR domains reduce β-keto units (**1.5**) into β-hydroxy units (**1.6**). The DH domain then reduces **1.6** to its corresponding α,β-hydroxy counterpart (**1.7**), after which the ER domain reduces the chain into a saturated alkyl unit (**1.8**).

Unlike modular bacterial PKSs, where each extension and tailoring event is encoded co-linearly by a discrete module, fungal iPKSs operate by reusing a single module, or set of domains, across multiple chain extension cycles. Consequently, identical catalytic domains may participate differently at distinct stages of chain assembly, such that the domain architecture alone is often insufficient to predict the final structural outcome. Due to the iterative nature of fungal PKSs, the programming logic governing starter unit selection, extension count, and reductive tailoring within each cycle is difficult to predict and remains poorly understood[19]. While this complexity produces an enormous diversity of fungal scaffolds, structural prediction and BGC reconstitution become considerably more demanding than in bacterial systems[20].

Non-Ribosomal Peptide Synthetases.

The second largest biosynthetic enzyme class found in fungal system is the non-ribosomal peptide synthetase (NRPS) subset. These catalytic enzymes are responsible for linking and functionalizing amino acid subunits into longer peptide structures. Similarly to PKSs, NRPS are multidomain proteins, composed of adenylation (A), peptidyl carrier protein (PCP) also known as thiolation (T) domains, and condensation (C) domains that play analogous roles in substrate selection, chain tethering, and elongation to the AT, ACP, and KS domains of PKS systems respectively (**Figure 1.2**), though through distinct mechanisms. Similarly to the PKS architecture, A, PCP and C domains in NRPS are also grouped into modules. Beyond these core domains, NRPS modules can also include accessory domains that provide further chemical diversity. Modifications during peptide elongation occur in the form of *N*-methylation via methyltransferases (MT), amino acid epimerization events occur by engaging epimerization (E) domains (**Figure 1.2**). Following selection and activation of an L-amino acid by the A domain and its loading onto the PCP domain, the E domain catalyzes epimerization of the PCP-bound residue to its D-configuration. The

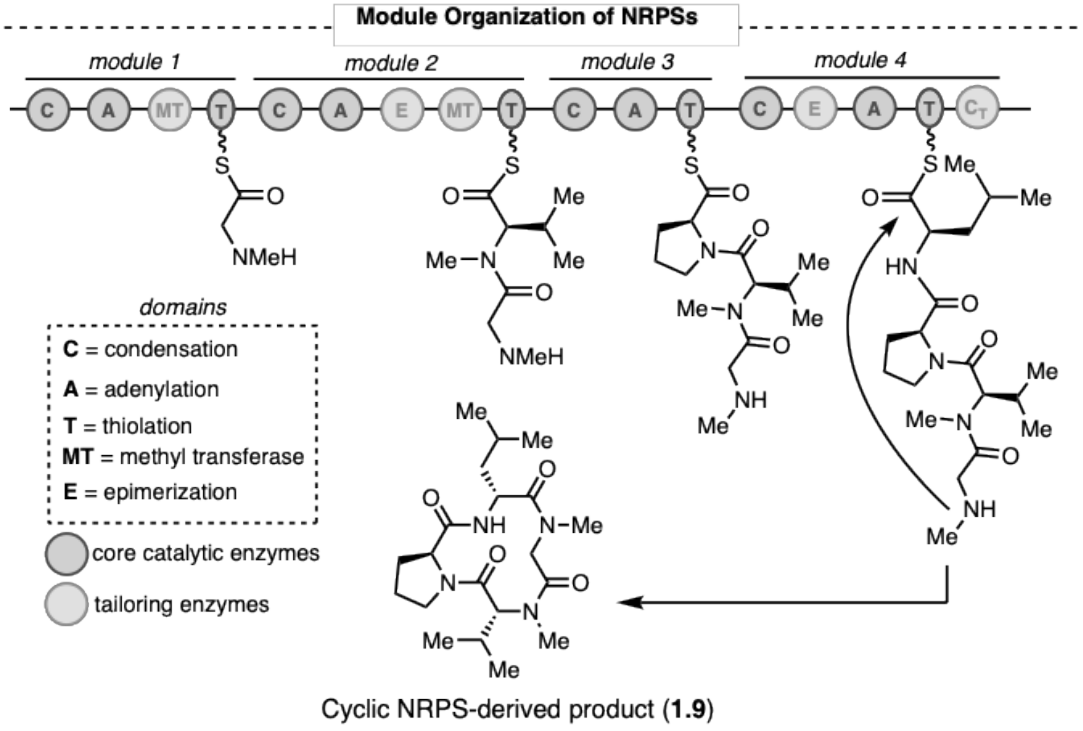


Figure 1.2 Generalized modular architecture and peptide elongation logic of a fungal non-ribosomal peptide synthetase (NRPS).

downstream condensation (C) domain displays stereochemical selectivity, preferentially accepting the appropriately configured substrate for condensation and thereby ensuring incorporation of the correct stereoisomer into the growing peptide chain.Oxidation fluctuations are facilitated by oxidation (Ox) and reduction (R) domains. Furthermore, intra-chain heterocyclization events are catalyzed by specialized Cy domains, which are functional variants of the standard condensation (C) domain. Chain termination in fungal NRPS systems is primarily catalyzed by terminal condensation (C_T) domains, which account for the majority of offloading domain types across fungal NRPS enzymes, with reductase (R) comprising the rest. For fungal cyclic peptide natural products, CT-mediated macrocyclization is the offloading mechanism, releasing cyclic products such as cyclosporin A and the echinocandins[21].

Fungal PKS-NRPS Hybrids.

Structural complexity of fungal-derived SM can be compounded by the hybrid arrangements or co-involvement of multiple distinct enzyme complexes, one example of which is the PKS-NRPS hybrid SM category discussed herein. Fungal metabolites assembled by PKS-NRPS hybrids incorporate both polyketide-derived and amino acid-derived building blocks into a single scaffold, generating a vast structural and stereochemical breadth that renders this compound class particularly compelling targets for total synthesis. The PKS and NRPS components can either be found fused, classifying them as megasynthases[20,22–25], co-localized within a BGC[26], or located on entirely separate gene clusters[27]. The architecture of fungal PKS-NRPS hybrids within the second category (co-localized enzymes within a BGC) often incorporates a hrPKS and a multi-modular NRPS enzyme where off-loading is mediated by the C_T domain of the NRPS, liberating the metabolite in the form of a macrocyclic lactone. A generalized representation of this biosynthetic logic, illustrated using the proposed biosynthesis of **1.10** (xylacremolide A) and **1.11** (xylacremolide B)[28], is shown in **Figure 1.3**. It is within this biosynthetic framework of co-localized PKS/NRPS enzymes, that the compounds central to this thesis (Part I) are situated. In

these systems, macrocycle formation proceeds through intramolecular nucleophilic attack of a polyketide-derived hydroxyl group onto the NRPS-tethered thioester, generating a macrocyclic ester upon product release[21,28,29]. The resulting scaffolds are, by definition, cyclic depsipeptides (CDPs), or hybrid macrocycles where at least one ester bond is found within a peptide backbone[30]. It is this structural motif that defines the compound class discussed in the sections that follow.

1.1.3 Cyclic Depsipeptide Macrocycles in Fungal PKS-NRPS Systems

Cyclic depsipeptides have gained research interest over the past three decades due to their unique structures and biological properties that include antitumor, antifungal, and antiviral activities[31–33]. Interestingly, among bacterial and fungal cyclic depsipeptides producers, fungi represent the most prolific class, accounting for up to 71% of all cyclic depsipeptides across endophytic fungi of plants (30.7%) , insect pathogenic fungi (14.04 %), and fungi of other origins

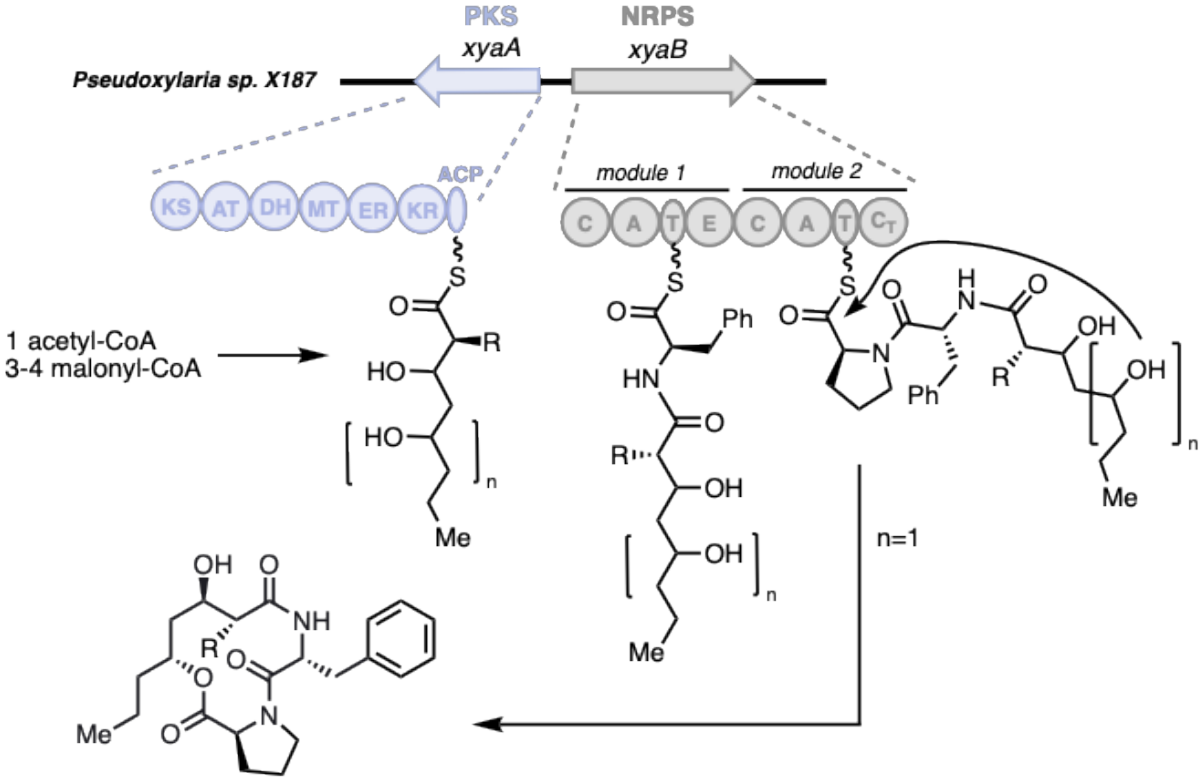


Figure 1.3 Representative BGC of xylacremolide A (**1.10**) and B (**1.11**), showing architecture of PKS-NRPS biosynthetic assembly line and resulting cyclic scaffold. An iterative hrPKS (*xyaA*) generates a polyketide fragment, which is transferred to a NRPS (*xyaB*) for the incorporation of two amino acids and formation of a CDP through C_T cyclization.

(27.19%)[34]. Structurally, fungal CDPs range from compact tridepsipeptides to substantially larger octa- and nonadepsipeptide macrocycles, reflecting the biosynthetic flexibility of fungal PKS-NRPS assembly systems[35]. Within the broader family of fungal PKS-NRPS-derived cyclic depsipeptides, a structurally conserved subset of 12-membered cyclic tridepsipeptides has emerged. In this subset, two NRPS-derived amino acid residues are converged with a hrPKS-derived hydroxy acid unit, generating the three-component core, cyclized through intramolecular macrolactonization (**Figure 1.4**).

Despite variation in amino acid composition, oxidation state, methylation pattern, and peripheral functionalization, these metabolites exhibit striking structural similarities suggestive of related biosynthetic origins. The constrained nature of the 12-membered ring, combined with the presence of *N*-methylated or conformationally restricted amino acid residues, imparts a conformational complexity that has repeatedly challenged stereochemical assignment and total synthesis efforts across this family.

The sections that follow examine the emergence of this structurally conserved family of fungal tridepsipeptides, with emphasis placed on their defining structural features and the recurring synthetic challenges associated with their construction.

1.2 Emergence of a Structurally Conserved Subfamily of 12-Membered Cyclic Tridepsipeptides

1.2.1 Inclusion Criteria and Structural Definition

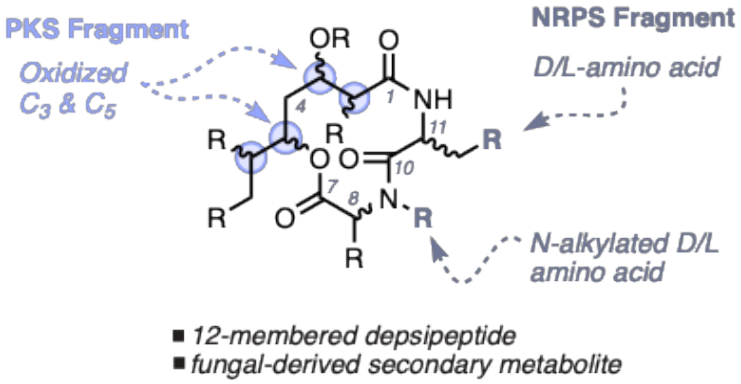


Figure 1.4 Structural inclusion criteria for fungal cyclic tridepsipeptides.

12-membered fungal-derived CDPs, previously described more broadly as cyclic tridepsipeptides[35], are characterized herein by three structural elements which are found highly

conserved across the family (**Figure 1.4**). Members of this class are displayed in **Figure 1.5** and include the acremolides[36], xylacremolides[28], colletopeptides[37,38], HA23[39,40], and stereocalpins[41,42], as well as immunomodulide, the compound central to Part I of this thesis. The first structural element is a predominantly aromatic amino acid residue incorporated by the NRPS module. The D-form for this structural feature dominates across most metabolites of this class (acremolides[36], xylacremolides[28], colletopeptides[37,38] and HA23[39,40]), although uniquely has been found in its L-form in the stereocalpin A and B subfamilies[41,42] (**Figure 1.5**). The second structural component defining this class is the is the presence of one *N*-alkylated or conformationally constrained amino acid residue incorporated by the NRPS module. This encompasses *N*-methyl amino acids, most prominently *N*-Me-Leu and *N*-Me-Ile, as well as cyclic secondary amines such as proline (Pro) and pipecolic acid (Pip), all of which share the common functional consequence of restricting backbone amide bond rotation and enforcing a compact, preorganized ring conformation that challenges synthetic attempts. The final element is a PKS-derived hydroxy acid handle that arises from an iterative hrPKS enzyme complex within the biosynthetic gene clusters of this family of natural products. Although the hydroxy acid fragment can be unique in length (stereocalpins A(**1.16**)[41] and B(**1.17**)[42]), oxidation (acremolide A(**1.12**) and B(**1.13**)[36]) or functionalization (colletopoeptides (**1.19 -1.25**)[38] and their glycosylated counterpart (**1.26 -1.30**)[37,43]), this recurring PKS-derived C5-hydroxyl group undergoes intramolecular esterification with the thioester-NRPS linked *N*-alkylated amino acid, closing the 12-membered ring as a depsipeptide. This macrolactonization event is the obligatory ring-closure step and furnishes the ester bond that formally defines these compounds as cyclic depsipeptides rather than cyclic peptides. Several fungal metabolites tangentially related to this subclass have also been reported, including xylacremolide C(**1.33**) and D(**1.34**)[28], saroclide A(**1.31**) and B(**1.32**)[44], calcaripeptide A-B(**1.35-1.36**)[45], FE399(**1.39**) and PM18110(**1.40**)[46] and valactamide A (**1.38**)[29] (**Figure 1.6**). Although

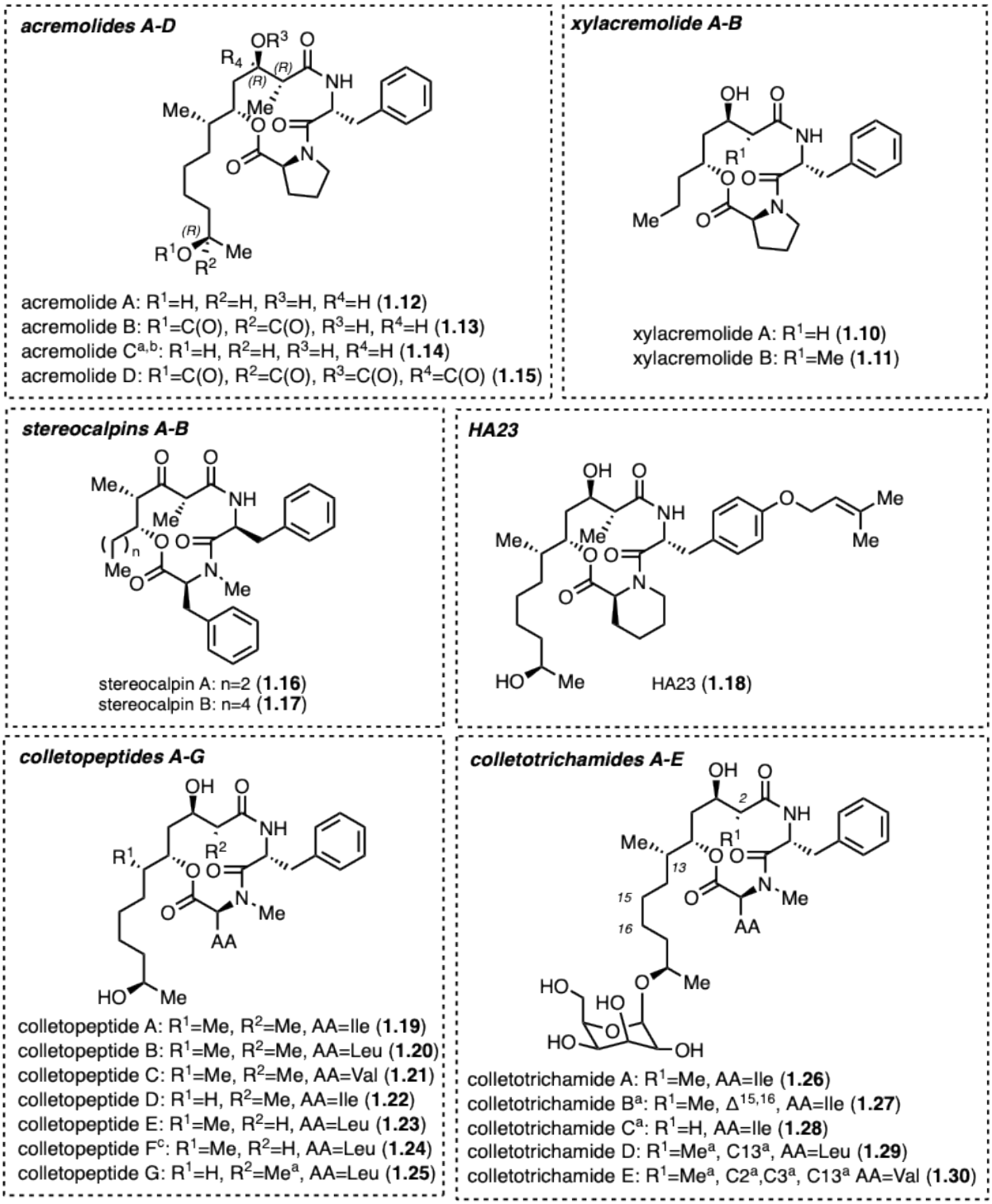


Figure 1.5 Members of the fungal-derived cyclic tridepsipeptides, grouped according to their reported natural product series. [a] unknown configuration. [b] D-Ile in place of D-Phe. AA=amino acid. [c] D-Leu in place of D-Phe

these compounds share the core three-component PKS–NRPS-derived macrolactam framework

seen across tridepsipeptides, they instead form larger 14- to 20-membered macrocycles due to either the absence of the conserved C5-hydroxyl or to its non-participation in the macrocyclization event.

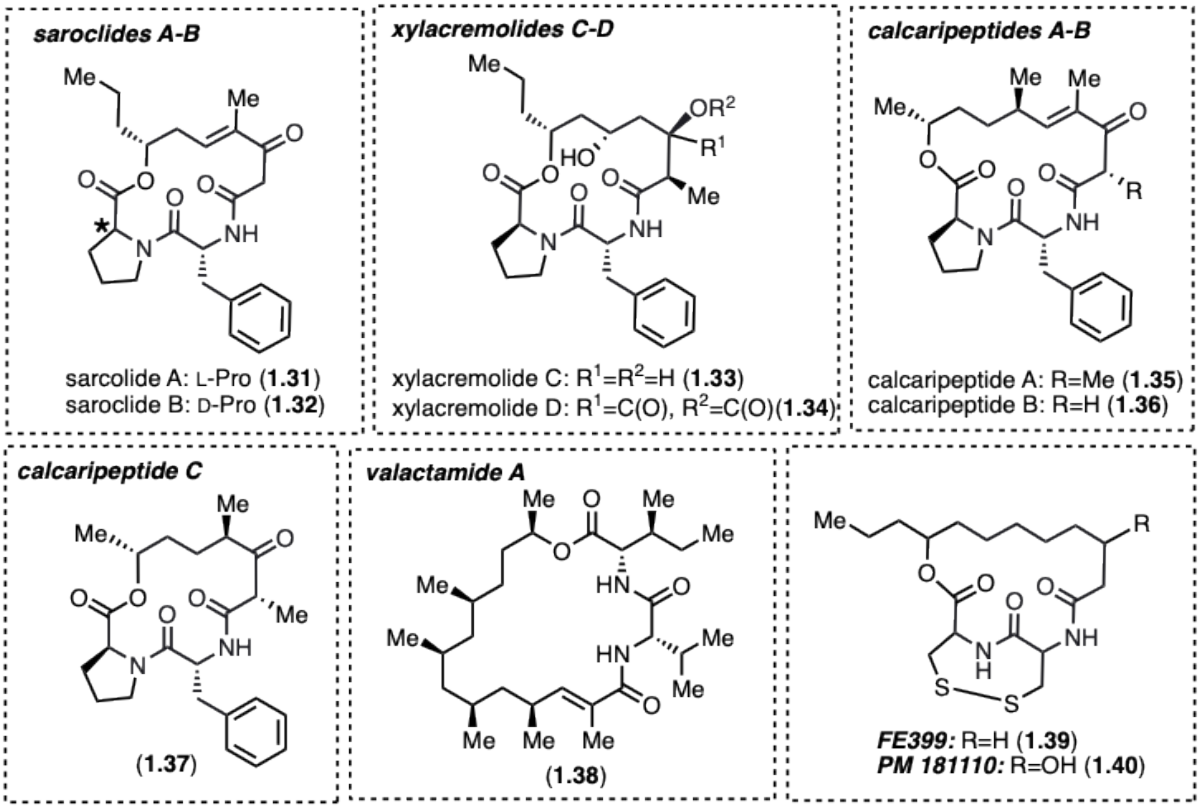


Figure 1.6. Structurally related fungal cyclic tridepsipeptides excluded from the defined compound class.

The remainder of this chapter will examine the structural diversity, biosynthesis, biological activity, and total synthesis attempts associated with this emerging family of fungal- derived 12-membered tridepsipeptides macrocycles, among which immunomodulide, the compound central to Part I, has been classified.

1.2.2 Structural Diversity

Structural diversity across this family of 12-membered cyclic tridepsipeptides arises through variation across the three defining components: *N*-alkylated amino acid, aromatic amino acid and the PKS-derived hydroxy acid. Additional structural diversity arises through secondary modifications including C-methylation, oxidation state changes along the polyketide chain, and glycosylation.

Polyketide Subunit Variation.

The hydroxy acid unit is the most variable structural element across the family and the primary determinant of ring size. In the acremolides[36], colletopeptides[37], colletotrichamides[43], and HA23[39] (**Figure 1.5**), a 12-carbon long hydroxy acid unit participates in ester bond formation via its C5-hydroxyl, consistently generating the 12-membered ring core. The xylacremolides A and B[28], and stereocalpins A[43] and B[44], share this same ring size through the cyclization of a shorter eight- or ten-carbon long hydroxy acid unit, where cyclization occurs at the C5-hydroxyl group. Xylacremolides C and D[28] incorporate a longer 3,5,7-trihydroxy-2-methyldecanoic acid unit that cyclizes at C7, generating a 14-membered ring and placing them formally outside the scope of this subfamily. The calcaripeptides A-C[45] and saroclides A-B[44] represent further structural outliers in this regard. Both series incorporate β-keto-bearing polyketide units with Δ4,5 olefins that cyclize at C7/C9 and C7, respectively, generating 14- and 16-membered rings, also placing them outside the scope of this family.

Oxidation state along the polyketide chain also varies in a structurally informative way. Acremolide A bears hydroxyl groups at both C3 and C11, while the C11 position in acremolide B is oxidized to a ketone. The colletopeptides carry a fully elaborated 3,5,11-trihydroxy-2-methyldodecanoic acid unit invariant in oxidation state across the series, with structural diversity arising exclusively from the amino acid components and methylation pattern. The stereocalpins are unique in bearing a β-keto group at C3 rather than the β-hydroxyl found across all other members, a feature that introduces significant synthetic and stereochemical complications. The β-keto motif at C3 is also found in the calcaripeptides and saroclides, suggesting it may arise from a shared deviation in KR domain engagement within otherwise potentially related hr-PKS enzymes, though this has not been confirmed biosynthetically for any of these series.

C2-methylation of the polyketide unit is also a recurrent but variable feature. C2-methylation is present in acremolide B, xylacremolide B, HA23, and all colletopeptides A-G with the exception of colletopeptide E[38] and colletotrichamide C. Presence of this C2 methylation is speculated to have conformational consequences, as reported in the publication of the xylacremolide series, where an upfield shift was noted in the C2-methyl NMR signal and attributed to shielding by the D-Phe aromatic ring within the constrained ring geometry[28]. Notably, as will be discussed further in Chapter IV, incorporation of the C2-methyl group is also associated with

substantial perturbations across the entire ^{13}C NMR spectrum, particularly among resonances corresponding to the macrocyclic core, further supporting its influence on overall ring conformation.

An additional distinguishing feature of the stereocalpins in particular is the methylation at C4 of the polyketide unit, suggesting incorporation of an additional methylation event within the hrPKS programming, which is otherwise not observed across the rest of the tridepsipeptide family.

Amino acid variation.

The *N*-alkylated or conformationally constrained residue is occupied by *N*-Me-Phe, *N*-Me-Leu, *N*-Me-Ile, *N*-Me-Val, Pro or Pip across the family. The colletopeptide series[37,38] illustrates this variation most clearly: colletopeptides A-D vary at this position between *N*-Me-Ile, *N*-Me-Leu, and *N*-Me-Val while retaining D-Phe at the aromatic position, generating a series of four analogues from a single invariant polyketide scaffold. Uniquely, in colletopeptide F, the aromatic D-Phe is replaced with a D-Leu, representing the only metabolite within this series that lacks an aromatic amino acid, while still retaining the mixed (D/L) amino acid configuration. The acremolides A and B[36] incorporate an invariant L-Pro–D-Phe dipeptide, as do the xylacremolides[28] across their series. However, acremolides C and D[36], exceptionally incorporate a D-Ile and D-Val in the place of the aromatic amino acid D-Phe. HA23[39] diverges even further from the canonical amino acid composition through incorporation of pipecolic acid alongside an *O*-prenyl-substituted tyrosine, representing the most heavily decorated amino acid composition within the family. The stereocalpins[41,42] stand apart from all other members in incorporating two L-configured amino acids (L-Phe and L-*N*-MePhe), in contrast to the D/L amino acid pairings that characterize the remainder of the family[41,42]. This unusual stereochemical arrangement has significantly complicated total synthesis efforts, with multiple studies instead resulting in the synthesis of stereochemical epimers of the natural products[47–49]. These synthetic challenges and the associated stereochemical reassignment studies will be discussed further in **Section 1.2.5.4**. Notably, saroclides A and B, which are only considered outside the scope due to their ring size, represent a rare case in which both the L-Pro and D-Pro epimers of an otherwise identical metabolite were isolated simultaneously from a single producing strain, suggesting the presence of an E domain within the NRPS module responsible for incorporation of the *N*-alkylated amino acid residue[44]. The concurrent formation of both epimers suggests improper C-domain discrimination between configurations during biosynthesis . This feature has not been proposed for any other member of

this structural family or its related analogues. Furthermore, D-Pro-containing saroclide B represents the first reported example within this subclass to possess a D/D-configured amino acid pairing, whereas all other known members display either mixed D/L configuration or, uniquely in the stereocalpins, an L/L-configured amino acid pairing.

Glycosylation.

The colletotrichamides A-E represent the only glycosylated members of this scaffold, bearing a β-D-mannose unit appended as an *O*-glycosidic linkage to the terminal polyketide hydroxyl[43]. This modification, reported for the first time in this series, does not alter the 12-membered core architecture but introduces significant polarity and steric bulk at the periphery of the molecule, with resulting consequences on biological activity[37,43]. The structural variations across the colletotrichamide series parallel those seen in the colletopeptides at the amino acid level, though the two series do not constitute a strictly paired glycosylated/aglycone set.

1.2.3 Biosynthetic Origins

To date, the only biosynthetic gene cluster that has been biochemically characterized and reported within this strict 12-membered tridepsipeptide definition is that of the xylacremolides, identified in *Pseudoxylaria* sp. X187 through genome mining guided by GNPS-based molecular networking[28]. This report demonstrated an arrangement of both hrPKS (*xyaA*) and NRPS (*xyaB*) -encoding genes co-localized within the same BGC and co-operating in their production of the xylacremolide A-C (**Figure 1.3**). The involvement of short-chain dehydrogenase/reductase encoded within the same BGC, engage an oxidation event at the C3-hydroxyl of xylacremolide C, resulting in the production of xylacremolide D. Interestingly, this report also notes sequence similarity to the biochemically characterized valactamides A-H-encoding enzymes, ValA and ValB from *Aspergillus terreus* ATCC 20542[29], with a 65% and 70% sequence similarity to XyaA and XyaB, respectively. Importantly, the biochemical characterization of the xylacremolide-producing BGC, by Schalk et al, enabled the identification of homologous BGCs in *Colletotrichum gloeosporioides* and *Acremonium chrysogenum*, producers of colletotrichamides and acremolides, respectively. The high degree of sequence similarity across those homologues (in the range of 53-75%) and close structural features support the idea of similar biosynthetic origins.

The discussion that follows, on the proposed PKS and NRPS programming predicted within our defined family of 12-membered cyclic tridepsipeptides, is founded in Schalk et al.'s encouraging results[28].

PKS programming.

The polyketide subunits across this family are predicted to be assembled by hrPKS, with the loading of one acetyl-CoA, followed by a minimum of three malonyl CoA, resulting in a PKS fragment chain length of 8 or more carbons. The highly conserved C2-methylation observed in most members of this family is predicted to be installed by the MT domain of the hrPKS via SAM-mediated methylation of a β-ketoacyl intermediate, consistent with the established mechanism of fungal hrPKS methyltransferases[50]. This is further supported by the presence of MT domain in the hrPKS of XyaA (KS-AT-DH-MT-ER-KR-ACP)[28] and ValA (KS-AT-DH-MT-ER-KR-ACP)[51]. The most direct experimental confirmation of this proposed PKS programming within the broader structural family was provided by ^{13}C-feeding studies on calcaripeptide A, which demonstrated acetate incorporation throughout the polyketide chain and SAM-derived methylation at C2, C4, and C6, thereby validating the iterative acetate extension and MT-domain-mediated methylation pattern, consistent with that proposed for the 12-membered members of this subclass[45]. PKS programming also affects the oxidation state at each β-carbon position incorporated into the growing chain. Whether retained as a ketone, reduced to a hydroxyl, or fully reduced, reflects the selective engagement of the KR, DH, and ER domains at each extension cycle and gives rise to the variation in hydroxylation pattern described in the structural diversity section above (**Section 1.2.2**).

A conceptual advancement in understanding the stereochemical output of this PKS programming was provided by the biochemistry-based stereochemical prediction model developed by Takino et al.[52] and subsequently applied by Xiao et al. to the acremolides[53] and by Feng et al. to HA23[41]. This model is grounded in the processing logic of experimentally characterized fungal reduced polyketides and related hrPKS and functions as a useful "rule of thumb" although not without its limitations[52]. This rule was applied successfully to acremolides A and B and to the polyketide fragment of HA23, discussed in **Section 1.2.5**, and has also been extended to related hrPKS products in the same broader biosynthetic logic, including valactamides[51]. Although still heuristic and not exception-free, the model supports that these compounds could be products of

evolutionarily related hrPKS enzymes with conserved domain stereochemistry, though this has not been confirmed through BGC analysis, and with the significant variations in oxidation and methylation patterns seen within related subsets of tridepsipeptides, the reality of the hrPKS programming likely much more complex.

Amino acid incorporation and *N*-methylation.

The two amino acid residues are incorporated by NRPS modules, following PKS processing. *A* domain selectivity and E domain engagement within the first module of the NRPS is predicted to be broadly consistent across the family, as D-configured aromatic residue (Phe or Tyr) prevail as one of the most common features of this cyclic tridepsipeptides class. This proposed biosynthesis is consistent with the architecture of the xylacremolides, D-Phe is invariably incorporated across all family members as a consequence of processing through the first module of XyaB containing the epimerization (E) domain[28].

The second NRPS module appears to exhibit reduced conservation, both across fungal producers of this family and within individual strains themselves, as evidenced by the variable amino acids incorporated at this position across closely related (i.e. L-configured *N*-Me-Ile, *N*-Me-Leu, *N*-Me-Val, in colletopeptides A, B and C, respectively) or distantly related metabolites (i.e. L-Pro in xylacremolides vs. L-Pip in HA23). Notably, however, the incorporated residues consistently retain either *N*-alkylated amino acids, proline, or pipecolic acid, reinforcing the same functional consequence of restricting amide bond rotation. It is predicted that an MT domain is present within this second module of BGC producing *N*-alkylated residues, although this has not yet been confirmed by biochemical characterization within strains producing cyclic tridepsipeptides with this functionality.

Despite this broader variability in residue identity, several studies suggest that substrate selection within individual biosynthetic systems remains highly stringent and mechanistically programmed. Feeding studies on the ring-expanded calcaripeptides further demonstrated the strict A-domain substrate selectivity of this NRPS machinery, where supplementation with L-Trp, L-Tyr, and L-His failed to substitute for L-Pro or L-Phe, suggesting that amino acid incorporation within these biosynthetic systems *can* still remain highly specific despite the close structural relatedness of the substrates[45].

Although these conserved NRPS-based biosynthetic trends predominate across the family, several notable outliers suggest that divergence in NRPS domain architecture may also occur. The unique occurrence of two L-configured amino acids in the stereocalpins implies that the corresponding NRPS enzyme within the producing BGC either lacks an E domain or possesses a silent E domain[41,42]. This represents putative biosynthetic divergence within this otherwise conserved family that has yet to be validated through phylogenetic analysis. A similarly unusual deviation is observed in the larger 14-membered macrocyclic saroclides, where both the L-Pro and D-Pro epimers were isolated from a single producing strain[44], representing the first report within the broader class of tridepsipeptides where both stereoisomers of the conformationally restricted amino acid are found.

Macrocyclization.

The xylacremolide BGC (**Figure 1.2**) confirms the presence of the C_T domain on the NRPS, able to generate the macrocyclic ester linkage that formally defines these compounds as cyclic depsipeptides. Although the BGCs of the rest of this class remain uncharacterized, it is speculated that macrocyclization is catalyzed by a similar NPRS domain. The shift to C7 or C9 hydroxyl engagement in xylacremolides C and D, the calcaripeptides, and the saroclides, producing 14- and 16-membered rings from longer polyketide units, illustrates that hydroxyl-site selection during macrocyclization, likely due to conformational accessibility and geometric preorganization of the hydroxyl nucleophiles for intramolecular attack, acts as the principal determinant of ring size within this broader biosynthetic framework.

1.2.4 Biological Activity

The biological activities reported across the 12-membered cyclic tridepsipeptide family are diverse and, in several cases, pharmacologically compelling, though the overall coverage remains uneven: many members were isolated without any reported activity, and for others only narrow bioassay panels have been applied.

Anti-inflammatory and immunomodulatory activity.

The most consistent and pharmacologically relevant activity profile across the family is anti-inflammatory and immunomodulatory. All four colletopeptides A-D inhibited LPS-induced

nitric oxide production in RAW264.7 macrophages, with colletopeptide A showing the greatest potency (IC_{50} 8.3 μM). Colletopeptide A additionally suppressed IL-6 and TNF-α production and attenuated NF-κB signalling through decreased phosphorylation of IκBα and p65[37]. Colletopeptides B and F were further identified as strong promoters of adiponectin secretion, a finding with potential implications for metabolic inflammation[37,38]. Stereocalpin B displayed anti-inflammatory activity in LPS-induced RAW264.7 macrophages (IC_{50} 5-7 μM)[42], consistent with the activity profile of the colletopeptide aglycones. The recurring emergence of anti-inflammatory activity across these structurally related members isolated from phylogenetically distant organisms suggests the compact *N*-alkylated macrolactone scaffold represents a privileged motif for modulating innate immune signalling.

Cytotoxicity.

Cytotoxic activity has been reported for several members, though potency and selectivity vary. Stereocalpin A (**1.16**) exhibited moderate cytotoxic activity against three human solid tumor cell lines including HT-29, B16/F10, and HepG2 in the original report[41]. Stereocalpin B (**1.17**) inhibited HCT116 colon cancer cell proliferation with an IC_{50} of 20 ± 1.20 μM[42]. Although outside the structural scope, PM181110 (**1.40**), exhibited potent anticancer activity against 40 human cancer cell lines with a mean IC_{50} of 0.089 μM, the most potent cytotoxic activity reported for any member tangentially related to the tridepsipeptide class of compounds[54].

Neuroprotective activity.

Colletotrichamide C (**1.21**), the glycosylated congener of the colletopeptide scaffold, exhibited strong neuroprotective activity against glutamate-induced toxicity in hippocampal HT22 cells, a biological profile entirely distinct from the anti-inflammatory activity of the aglycone series[37]. This observation suggests that glycosylation at the polyketide terminus not only alters the physicochemical properties of the scaffold but may redirect its biological target engagement.

Antifungal and protease inhibitory activity.

Xylacremolides A (**1.10**) and B (**1.11**) showed moderate antifungal activity against *Aspergillus nidulans* spore germination at early time points, with activity declining at longer incubation suggesting tolerance or detoxification by the growing fungus[28]. Additionally, low

protease inhibitory activity was observed at 200 μM across a panel of proteases (rhodesain, cruzain, cathepsin L, sortase A, and the viral proteases SARS-CoV-2 M^{pro}, PL^{pro}, DENV-2, and ZIKV NS2B-NS3. , with the strongest effects observed for xylacremolide B against rhodesain (15% inhibition) and ZIKV NS2B-NS3 (17% inhibition). Weak HDAC inhibitory activity was also observed for xylacremolides A and B at relatively high concentrations (0.25–1.0 mM), with substantially lower activity than the reference inhibitors valproic acid and trichostatin A[28].

Unknown or absent biological roles.

The original acremolides A-D (**1.12**-**1.15**) displayed no cytotoxic activity in the initial biological evaluation[36], and HA23 (**1.18**) itself showed no activity in antimicrobial or cytotoxicity bioassays despite being co-isolated with the antifungal W493-B[39]. The calcaripeptides A-C (**1.35-1.37**) similarly showed no detectable activity across a broad panel of 43 assays[45], and saroclides A and B (**1.31-1.32**) were inactive against all cancer cell lines and pathogenic microorganisms tested, with saroclide A notably exhibiting lipid-lowering activity in oleic acid-stimulated HepG2 cells as its sole reported bioactivity[44]. The biological roles of these metabolites in their ecological context including their function in abiotic and biotic interactions, remain entirely unexplored, as is the case for the majority of members within this emerging subfamily, a point which will become particularly relevant in Chapter (IV).

1.2.5 Total Synthesis Attempts

The 12-membered cyclic tridepsipeptides have attracted sustained synthetic interest driven both by the configurational ambiguity of their polyacetate-derived PKS fragments and the conformational complexity of their densely substituted macrocyclic cores. The discussion that follows aims to summarize this synthetic investigation by encompassing unsuccessful synthetic attempts, stereochemical reassignment campaigns, and completed total syntheses, and revealing recurring challenges associated with macrocyclization strategy, amino acid epimerization, diketopiperazine formation, and stereochemical characterization of the polyacetate-derived PKS

fragments. Broader synthetic trends and lessons emerging across this family will be comparatively analyzed in **Section 1.2.6.**

To streamline the discussion that follows, the campaigns described are grouped according to natural product family and further subcategorized chronologically by their first reported synthetic investigations. The reported syntheses across this family repeatedly explore one of three

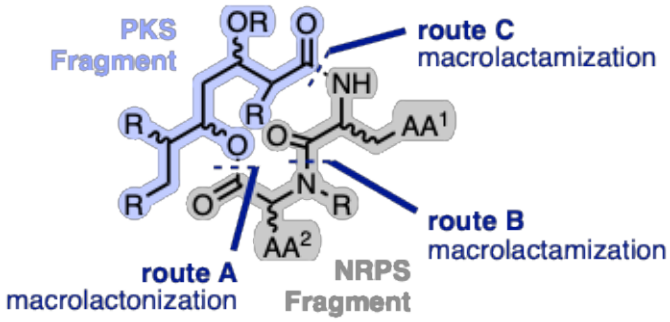


Figure 1.7 Generalized structure of the 12-membered cyclic tridepsipeptide scaffold illustrating the three recurring macrocyclization disconnections (routes A–C) employed across reported synthetic campaigns. The PKS-derived polyacetate fragment (light blue) and the NRPS dipeptide fragment (grey), comprising amino acids residues AA^1 and AA^2, are labeled according to the naming convention adapted throughout this chapter.

recurring macrocyclization disconnections, herein designated routes A-C (**Figure 1.7**) to facilitate discussions and comparisons across the approaches. Moreover, the tridepsipeptide scaffolds will be discussed according to their constituent fragments, using "PKS fragment" and "NRPS fragment" as a naming convention, where applicable. Finally, throughout this chapter, unsuccessful synthetic strategies, undesired products, and key synthetic limitations are highlighted in yellow.

1.2.5.1 Colletopeptides and Colletotrichamides

Chen, 2019 (Colletopeptide A and Colletotrichamide A).

In what still stands as the only synthetic attempt targeting this series of fungal tridepsipeptides, the relative and absolute configurations of colletopeptide A[39] and colletotrichamide A[43] were confirmed in 2019, with a strategic divergent total synthesis by Chen et al[55]. This synthesis featured an early-stage cross metathesis strategy to incorporate three of the five stereocenters along the PKS fragment, the last two of which were introduced through an asymmetric Brown's crotylation, and a ring-closure via route C macrolactamization (**Figure 1.8**).

These efforts strategically furnished a common late-stage intermediate **1.51** (**Figure 1.9**), from which both colletopeptide A and colletotrichamide A could be accessed divergently.

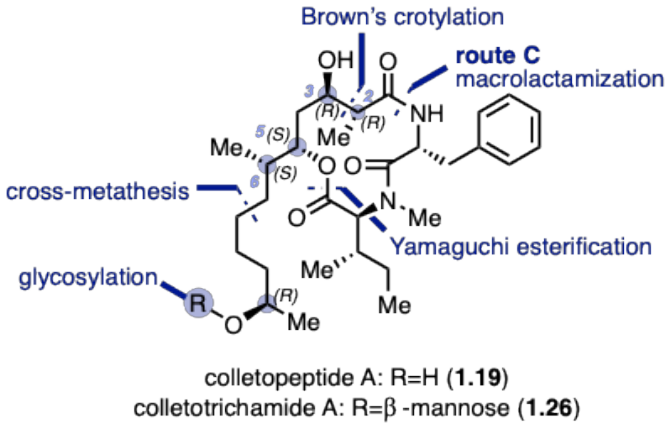


Figure 1.8. Summary of synthetic strategy towards colletopeptide A and colletotrichamide A by Chen et al.

Assembly of the linear precursor was initiated through the convergence of two known enantiopure alkenes **1.41**[56] and **1.42**[57] via cross-metathesis (**Figure 1.9**), furnishing the first three successive stereogenic centres of the PKS fragment (**1.43**). A Yamaguchi esterification was employed next, to install the *N*-Me-Leu (**1.44**) residue, followed by standard peptide coupling, and several reductions and protecting group manipulations, ultimately resulting in advanced linear precursor **1.47**. Oxidation to the aldehyde and Brown's crotylation followed, installing the C2-methyl in **1.48.** Ozonolysis and oxidation of the terminal alkene in **1.48** then delivered the fully elaborated linear substrate for macrocyclization (**1.49**). The decision to pursue macrolactamization via route C rather than route B or macrolactonization (route A), was not explicitly discussed in the report, although inspiration might have been drawn from reported attempts of similar cyclic tridepsipeptides that predicated, in which the routes A and B were reported to complicate ring-closure and/or stereogenic integrity. These reports will be discussed in detail in the sections that follow. Despite the significant conformational constraint imposed by the densely substituted tridepsipeptide scaffold, Chen's cyclization proceeded without detectable epimerization at C2, although only moderate yields of colletopeptide A (**1.19**) (51%) were obtained. Interestingly, no diketopiperazine (DKP) formation was reported, although this side reaction was observed in the stereocalpin A synthesis by Zhao[48] and Kaneda[58], in which a similar ring-closure approaches was pursued.

Chen's route diverged following macrocyclization, with a common intermediate **1.51,** enabling access to both colletopeptide A (**1.19**) and colletotrichamide A (**1.26**). Particularly

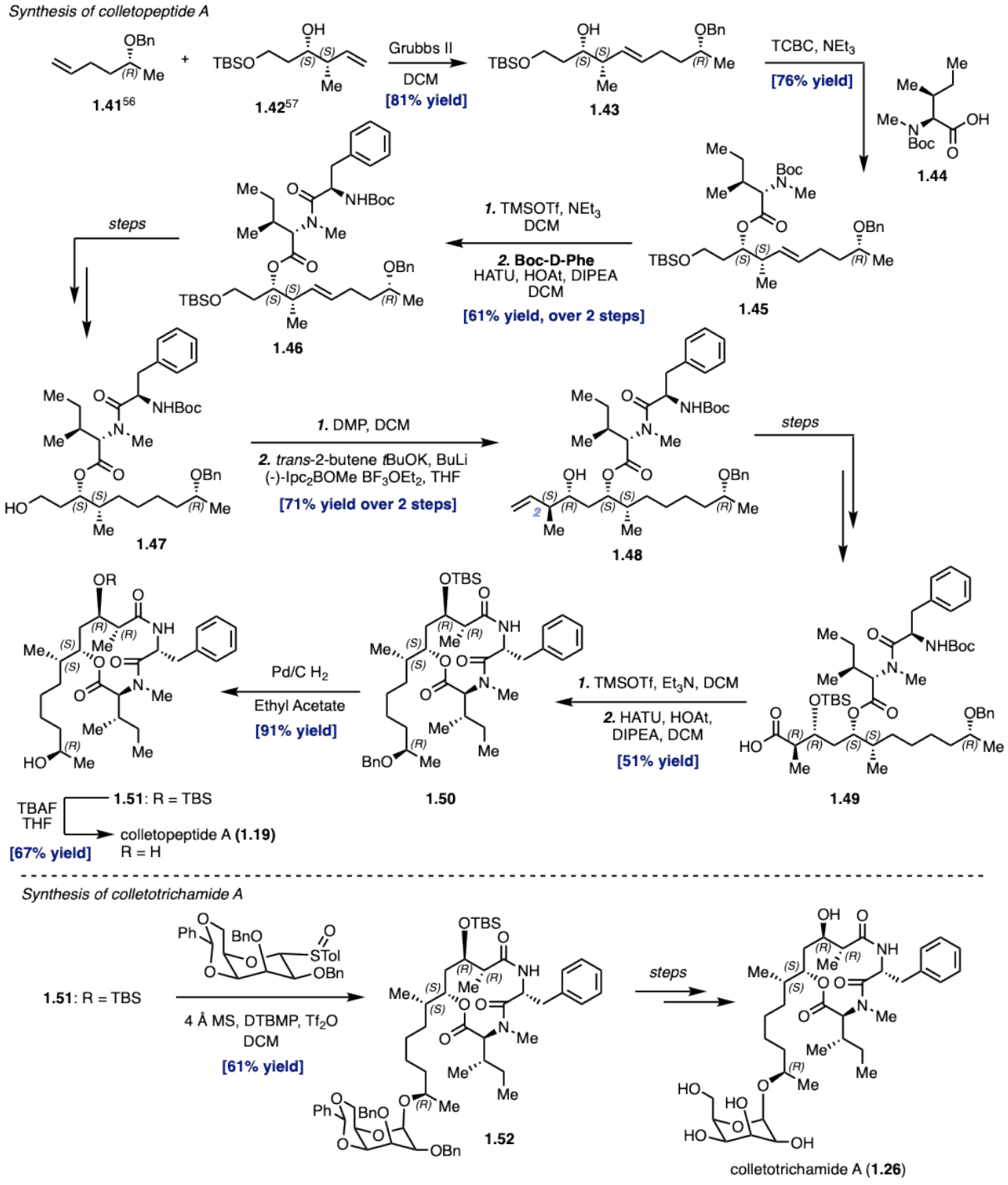


Figure 1.9. Summary of key synthetic steps in the total synthesis of colletopeptide A and colletotrichamide A, adapted from ref. 55

notable was the installation of the β-mannosidic linkage in colletotrichamide A through sulfoxide-

mediated glycosylation, which proceeded with complete stereocontrol despite the sterically congested macrocyclic acceptor. A significant advantage of this campaign relative to later studies within this family was the absence of stereochemical ambiguity surrounding the configuration of the PKS fragment, owing to the prior X-ray crystallographic assignments accomplished in the isolation report[37]. Overall, Chen et al., reported an efficient divergent route to colletopeptide A (3.2% overall yield) and colletotrichamide A (1.5% overall yield).

1.2.5.2 Acremolides

ElMarrouni, 2010

The first synthetic campaign targeting this scaffold was reported by ElMarrouni et al. in 2010[59], ultimately delivering 2,5-diepi-acremolide B (**1.62**) rather than the natural product, in 16 steps and 7.6% overall yield[59]. The route was designed around four key disconnections: a cross-metathesis to construct the PKS fragment side chain, a Yamaguchi esterification to append the dipeptide unit, two sequential stereoselective allylation/crotylation reactions to establish the PKS

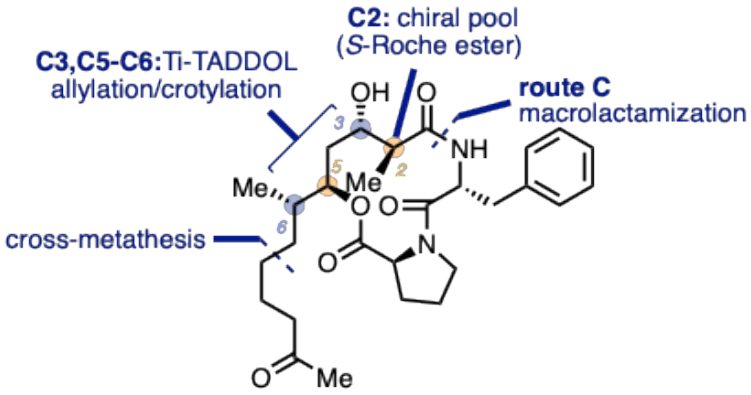


Figure 1.10. Summary of ElMarrouni's strategy towards the synthesis of 2,5-diepiacremolide B

fragment stereocenters, and a macrolactamization via route C to close the 12-membered ring. The (*S*)-Roche ester provided a chiral-pool entry point into the PKS fragment, while the three remaining stereocenters at C3, C5, and C6 were installed by two independent Ti(TADDOLate)-mediated reactions (**Figure 1.11**). Importantly, because the absolute stereochemistry of the PKS fragment remained unresolved at the time of this study, the route was strategically designed to

permit stereochemical flexibility, allowing access to alternative diastereomeric outcomes through modification of the chiral auxiliary, crotylation geometry, or Roche ester enantiomer employed.

With their strategy, ElMarrouni and coworkers successfully constructed the C1-C8 PKS fragment as a single stereoisomer. The Fmoc-D-Phe-L-Pro (**1.58**) dipeptide unit was prepared independently in three steps and appended to the polyketide fragment via Yamaguchi esterification, installing both amino acids simultaneously**.** This convergent peptide-installation strategy distinguishes the route from later syntheses within this family, where the amino acid residues were instead introduced sequentially onto the polyketide framework. Notably, no DKP formation was reported in this esterification step, even in the presence of a turn-inducing L-proline, an observation which becomes pertinent in later discussions (Chapter IV).

A major strategic limitation of the original route emerged late-stage. Following EDCI/HOBt-mediated macrolactamization to furnish the 12-membered macrolactam, all attempts to complete the PKS fragment by cross-metathesis between **1.61** and 5-hexen-2-one using the Hoveyda–Grubbs catalyst failed to produce the desired product. This outcome was attributed to either ruthenium coordination to the lactone carbonyl of the macrocycle generating a catalytically inactive species, or sequestration of the metal within the ring[59]. To circumvent this, the authors redesigned the sequence in a second strategy, performing the cross-metathesis with 5-hexen-2-one on the open-chain fragment **1.63,** prior to dipeptide installation and macrolactamization. This sequence successfully delivered the disubstituted olefin, which was subsequently hydrogenated selectively while maintaining the integrity of the TBS ether protecting group. Following dipeptide installation and oxidation to the corresponding carboxylic acid, **1.65**, route C macrolactamization proceeded smoothly, furnishing the strained 12-membered macrocycle in 60% yield over two steps and without detectable epimerization. Final TBAF-mediated desilylation completed the synthesis of epi-acremolide B.

Comparison of the spectroscopic and physical data of 2,5-diepi-acremolide B with those reported for the natural product ultimately confirmed that a stereoisomer had been synthetized. Importantly, the authors noted that the cyclic nature of the product makes it particularly difficult to speculate on which of the C2, C3, C5, and C6 centres bears the incorrect configuration, as a single stereochemical inversion in a macrocycle can have a cascading effect on all chemical shifts. Although not pursued, the stereochemically flexible nature of ElMarrouni's synthesis permitted,

in theory, access to all stereochemical variants of acremolide B, highlighting the strategic value of this approach.

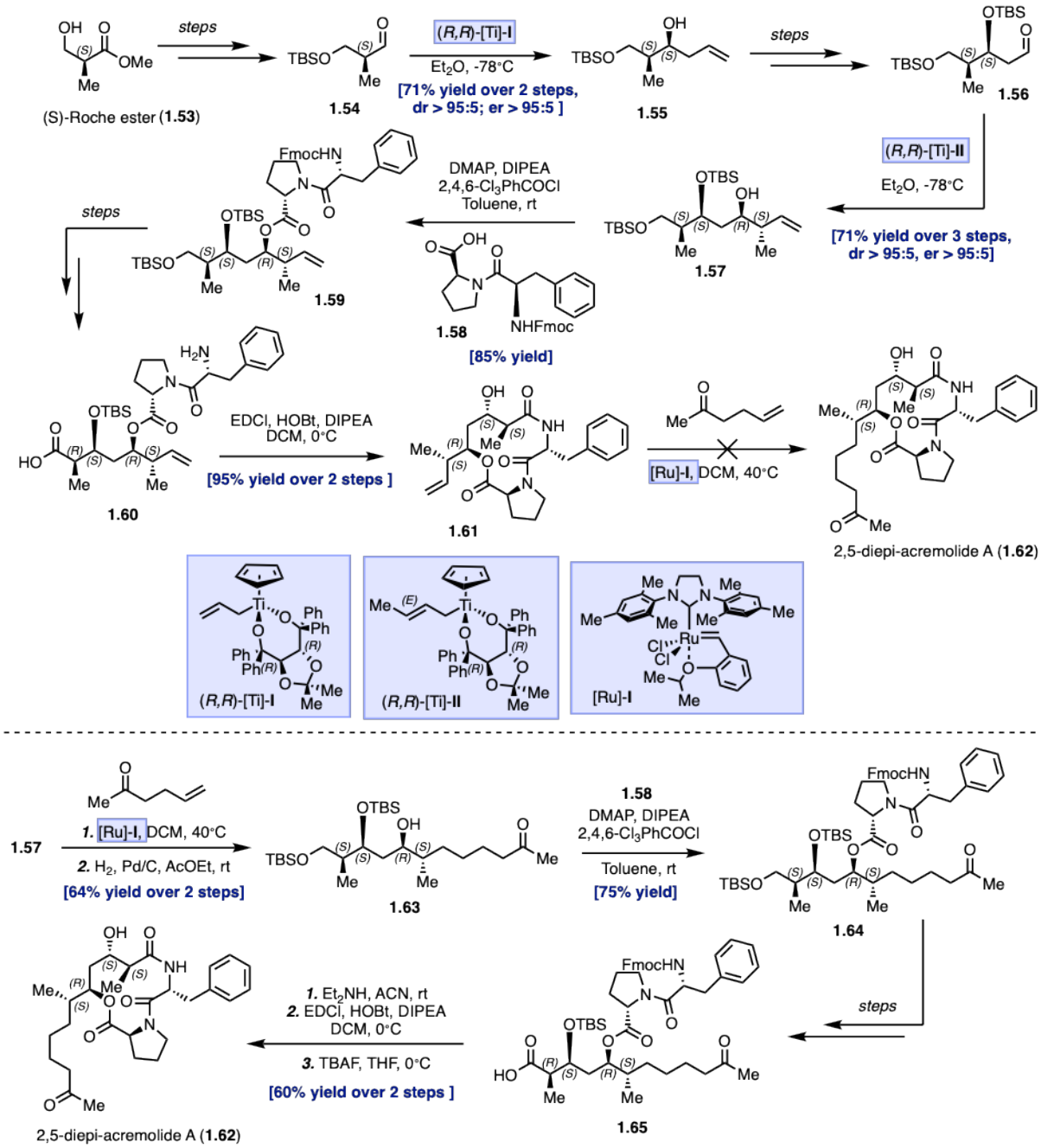


Figure 1.11. Key strategic steps in the total synthesis of epi-acremolide B. Adapted from ref. 59.

Yadav, 2017.

The next synthetic attempt towards acremolide B was reported by Yadav and coworkers[60], who sought to develop a unified and modular strategy capable of accessing multiple members of the acremolide family through late-stage diversification. In contrast to the macrolactamization

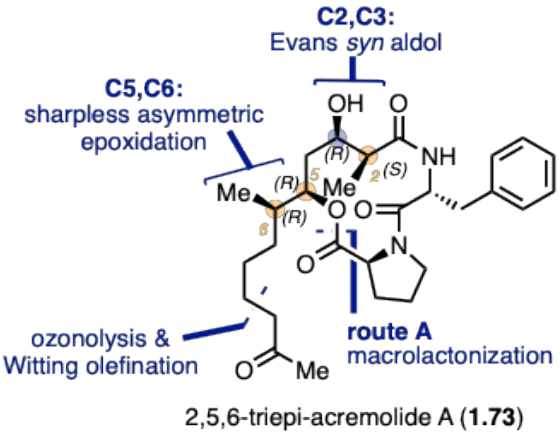


Figure 1.12. Summary of synthetic strategy of Yadav et al towards the total synthesis of acremolide A-D.

strategy employed by ElMarrouni, their retrosynthetic analysis was predicated on a late-stage *macrolactonization* (route A) instead, ring-closing a seco-acid intermediate, assembled via convergent coupling of a fully elaborated polyacetate fragment and a variable dipeptide unit. This design was intended to enable rapid interchange of the amino acid component, thereby providing a flexible entry point to acremolides A-D (**Figure 1.12**); however, efforts towards intramolecular macrolactonization were ultimately unsuccessful. The challenge encountered at this stage can be rationalized by several factors: (1) esterification-based macrocyclization may be inherently disfavoured over amidation-based. (2) the (2*S*,3*R*,5*R*,6*R*)-polyacetate fragment (**1.67**) targeted in this study differs at three stereogenic centres from the (then unknown) natural configuration of acremolide B (2*R*,3*R*,5*S*,6*S*), such that formation of a non-native stereoisomer may further exacerbate the energetic barrier to cyclization. (3) the linear seco-acid (**1.70, Figure 1.13**) may lack the requisite conformational preorganization to adopt a productive cyclization geometry, with competing intramolecular hydrogen bonding or steric interactions biasing the molecule toward conformations that disfavor effective orbital alignment for ester bond formation. Notably, this study represents the only synthetic effort within this class to pursue macrocyclization via macrolactonization; all subsequent retrosynthetic strategies instead converge on

macrolactamization as the ring-closing disconnection, underlining the inherent limitations of esterification-based approaches for this scaffold.

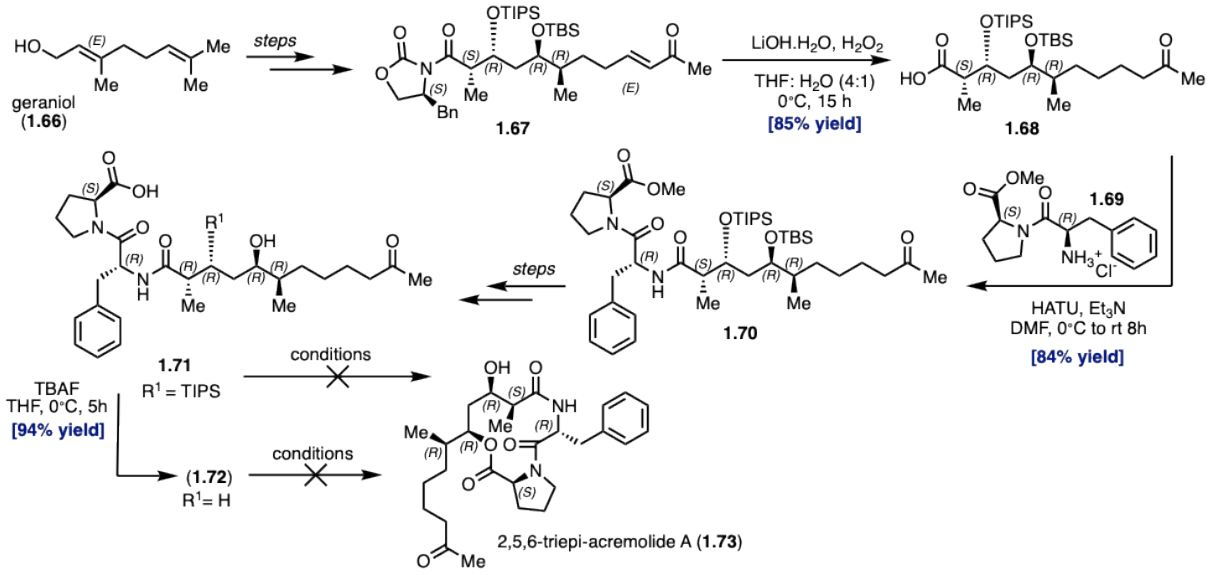


Figure 1.13. Summary of key steps in Yadav's forward synthesis towards the acremolides. Adapted from ref. 60

Nevertheless, the Yadav synthesis serves as an impressive demonstration of fragment design, strategically elaborating the polyacetate fragment from geraniol (**1.66**), utilizing Sharpless asymmetric epoxidation and Evans *syn* aldol chemistry to install all four stereogenic centres in a controlled and modular fashion. Subsequent functional group manipulations including ozonolysis/Wittig olefination and hydrogenation furnished fully elaborated acid fragment **1.67**, suitable for coupling. In parallel, the D-Phe–L-Pro (**1.69**) dipeptide was prepared in three steps from commercially available amino acids and coupled to the polyacetate fragment under HATU-mediated conditions to furnish the linear precursor in high yield. Selective deprotection and ester hydrolysis then provided access to the key seco-acid intermediate (**1.70**) poised for macrocyclization. Despite the apparent convergence and efficiency of this assembly, all attempts to effect macrolactonization under a range of established conditions, including Yamaguchi, MNBA, and PyBOP-mediated protocols resulted either in decomposition or complete recovery of starting material. A final attempt of the TIPS group removal to alleviate conformational constraints still resulted in no productive cyclization, suggesting that the failure was not solely steric in origin and may instead reflect unfavorable conformational preferences of the linear precursor that limit

access to a cyclization-competent geometry, although this proposal was not supported by computational analysis.

Collectively, these findings underscore the sensitivity of ring-closing strategy to both conformational and electronic factors in this unique class of strained fungal PKS-NRPS macrocyclic systems, and reinforce macrolactamization as the more viable disconnection for accessing the macrocyclic core within this class.

Xiao, 2024.

The definitive stereochemical resolution of acremolides A and B was achieved by Xiao et al. in 2024 through the first confirmed total syntheses of both natural products, accomplished in 12 and 10 linear steps and 8.3% and 19% overall yield, respectively[53]. This synthesis campaign benefitted from the use of the authors' biochemistry-based stereochemical prediction model rooted in the known stereochemical logic of fungal hr-PKSs[61]. Notably, in its first application, this model was successful in unravelling the stereochemical puzzle of the Valactamides, reducing the 32 possible stereoisomers to one target lead, and resulting in the stereochemical characterization and total synthesis of valactamide A[51]. Similarly, application of their "Biochemistry-based rule" reduced the synthetic efforts of the acremolides, from a sixteen-isomer search to a single targeted

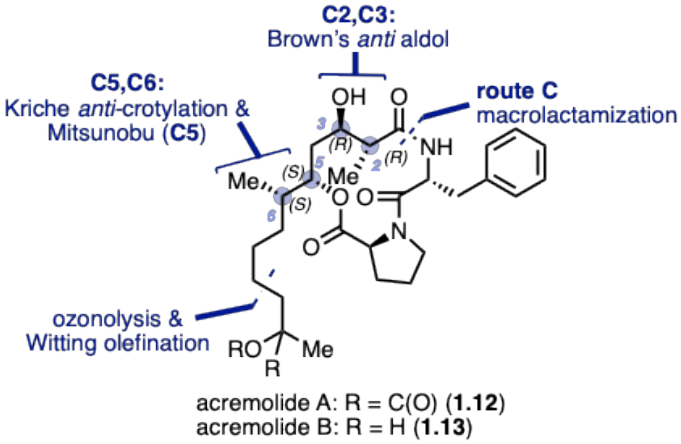


Figure 1.14. Summary of synthetic strategy of Xiao et al towards the total synthesis of acremolide A and B.

synthesis, predicting that the KR domain would furnish *R*-configured C11, *S*-configured C5, and *R*-configured C3, the enoyl reductase domain would deliver *S*-configured C6, and the MT domain

would install the *R*-configured C2 methyl branch. This conceptual advancement alone distinguishes this work from all prior campaigns in this series, and a summary of the synthetic strategy that followed is provided in **Figure 1.14**.

The synthesis of acremolide B commenced with a Krische *anti*-crotylation employing chiral iridium catalyst Ir(*S*)-SEGPHOS to furnish the *R5*-hydroyxl and S6 methyl stereogenic centres with great diastereoselectivty (*dr* > 20:1) (**1.74, Figure 1.15**). A Mitsunobu-mediated stereochemical inversion at C5 was used to converge the *R5*-hydroyxl in **1.74** with the preassembled dipeptide (Boc-D-Phe-L-Pro, **1.75**) affording the ester **1.76**. Next, a cross-metathesis (CM) between olefin **1.76** and 5-hexen-2-one proved unsuccessful, underscoring the inherent severe steric hindrance at the α and β positions of trisubstituted olefin **1.76** experienced also by ElMarrouni et al. in their first-strategy failure where a similar motif was employed in an attempted CM. A strategic reordering of synthetic events, where the CM was prioritized followed by the Mitsunobu, furnished **1.78** successfully. Next, a hydrogenation of the olefin, followed by DMP oxidation revealed the intermediate aldehyde **1.80,** that was employed in a subsequent Brown *anti*-crotylation enabling successful diastereoselective installation the last two stereogenic centres (*dr* > 20:1) of polyketide chain. In their discussion, the authors noted a tendency of C3-hydroxyl elimination both in forcing oxidative conditions (Pinnick) and acidic conditions required for N-Boc removal. Therefore, in a sequence similar to Chen's synthesis of colletopeptide and colletotrichamide A[55], terminal alkene **1.81** was subject to ozonolysis and mild-TEMPO-mediate oxidation, to furnish acid handle necessary for ring-closure. Following this, a deprotection of Boc revealed the amine handle and mitigated C3-hydroxyl elimination. Macrolactamization under HATU/HOAt/DIPEA conditions then furnished acremolide B in 67% yield over two steps. The ^{1}H and ^{13}C NMR spectra and optical rotation of synthetic acremolide B were fully consistent with those of the natural product, confirming the predicted absolute configuration of 2*R*, 3*R*, 5*S*, 6*S*, and resulting in the first unambiguous stereochemical assignment for any member of the acremolide series.

The authors then proceeded with the synthesis of acremolide A, which diverged from the acremolide B route at the early CM stage. Here, alkene **1.74** was instead coupled with TBS-protected allylic alcohol **1.83** as the CM partner. A similar synthetic route was followed to elaborate acremolide A, with the addition of a TBS-protection of the C3-hydroxyl following Brown crotylation, a departure from the harsher TFA-mediated deprotection conditions to remove

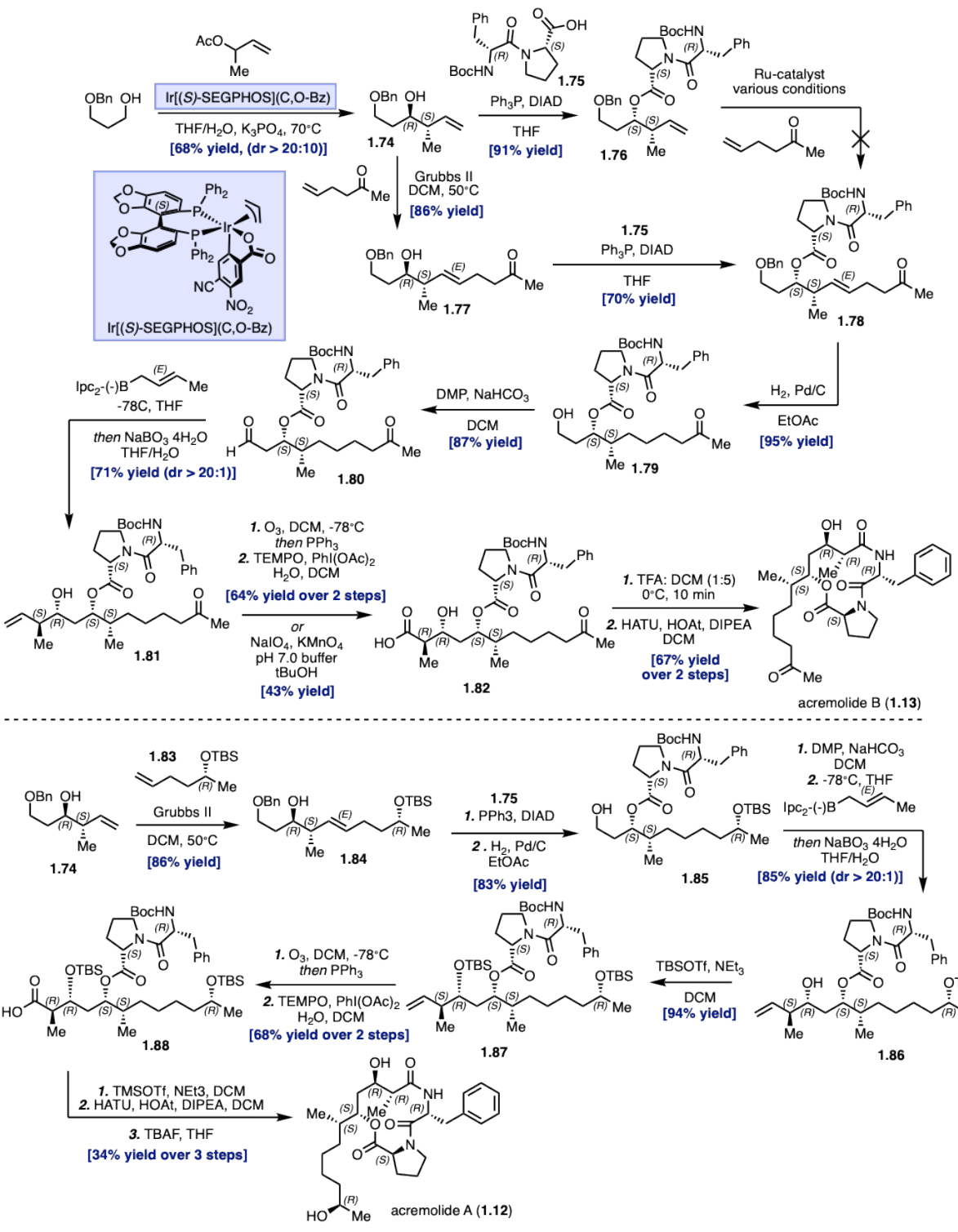


Figure 1.15. Summary of key steps in linear synthesis of acremolide A and B by Xiao and coworkers. Adapted from ref. 53.

the Boc, and a final TBAF-mediate global desilyation. Spectroscopic comparison with natural

acremolide A confirmed complete agreement, establishing the absolute configuration as 2*R*, 3*R*, 5*S*, 6*S*, 11*R,* and underpinning the reliability of the authors "biochemistry-based rule" in predicting the configuration of the polyketide unit.

1.2.5.3 HA23

Feng, 2025.

The total synthesis of HA23 was reported 23 years after its isolation, by Feng et al. and accomplished in 18 linear steps with a 6.9% overall yield[40]. As with the acremolide campaign of Xiao et al., the synthetic strategy was predicated on a biochemistry-based stereochemical prediction: applying the fungal hrPKS stereochemical rules established by Takino et al. 2021[61]. Unsurprisingly, this approach predicted a polyketide configuration identical to that seen in acremolide A, colletopeptide A, colletotrichamide A.

A unique feature of this strategy was the bond chosen for ring-closure. Unlike most other reported synthetic attempts within this broader class of tridepsipeptides, Feng et al. opted for macrolactamization at the amide between L-Tyr and L-Pip (route B) on the grounds that pipecolic acid's inherent tendency to adopt a cis-amide geometry was expected to pre-organize the linear precursor for efficient ring closure. Additionally, the acid-labile *O*-prenyl substituent on tyrosine was strategically deferred to a late-stage cross-metathesis with 2-methyl-2-butene under second-generation Grubbs conditions to avoid compatibility issues during the earlier protecting group manipulations.

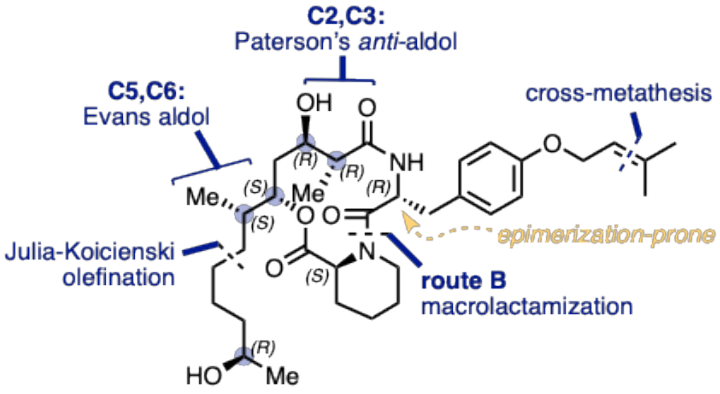


Figure 1.16. Summary of synthetic strategy of Feng et al towards the total synthesis of HA23.

Construction of the polyketide commenced with known alkene **1.89,** which was elaborated int two steps to sulfone **1.92**. Coupling of **1.92** was achieved via a Julia–Kocienski olefination with fragment **1.93**, preconstructed via Evans aldol to contain key stereocenters C5 and C6. Following a hydrogenation of the olefin **1.94** and oxidation to the aldehyde, a Patterson *anti*-aldol reaction enabled the installation of the remaining C2 and C3 stereocenters, of which the C3 hydroxyl was silylated with TBSOTf. The terminal acid handle of polyketide unit **1.99** was accessed subsequently by a ketone reduction, revealing a periodate-cleavable terminal diol handle which was later oxidized to the acid via the Pinnick oxidation. Notably, no mention of C3-hydroxyl elimination (reported in Xiao et al.'s synthesis of acremolide A) was made, presumably due to the fact that it was carried forward protected, as a silyl-enol ether. Amino acid tethering to the polyketide unit proceeded in succession, starting with a HATU-mediated amide coupling between the polyketide acid **1.99** and L-Tyr(O-allyl)-Fm. A selective TES deprotection of **1.100** followed, revealing the alcohol handle primed for a Yamaguchi esterification between the resulting hydroxyl handle and N-Fmoc-L-pipecolic acid. Gratifyingly, a global deprotection mediated by diethylamine smoothly removed Fmoc and Fm-ester, enabling a telescoped HATU/HOAt/DIPEA-mediated macrolactamization. Upon ring-closure, desired macrolactam **1.102** was isolated along with its epimer **1.103**, arising from partial epimerization at the activated tyrosine ester during cyclization which was confirmed by Marfey's analysis.

Comparative ^{13}C NMR analysis against the natural product then revealed, rather serendipitously, a complete structural agreement of the D-Tyr macrocycle with natural HA23, including matching ^{1}H NMR, HRMS, and optical rotation[40]. This constituted a structural revision of HA23 which, was made possible by the epimerization-prone macrolactamization strategy (unbeknownst to the authors) employed for ring-closure. The authors attribute the original misassignment to epimerization occurring during the harsh acid hydrolysis conditions employed for Marfey's analysis[62]. A second, epimerization-free synthesis confirming the D-Tyr assignment was then executed starting directly from D-Tyr(O-allyl)-Fm, delivering **1.106** in 59% yield over the final three steps with no detected epimerization, completing the total synthesis and unambiguously establishing the revised absolute configuration.

Collectively, the synthesis revealed that macrolactamization of 12-membered rings containing an L/L amino acid pair at the cyclization site is prone to epimerization, whereas D/L

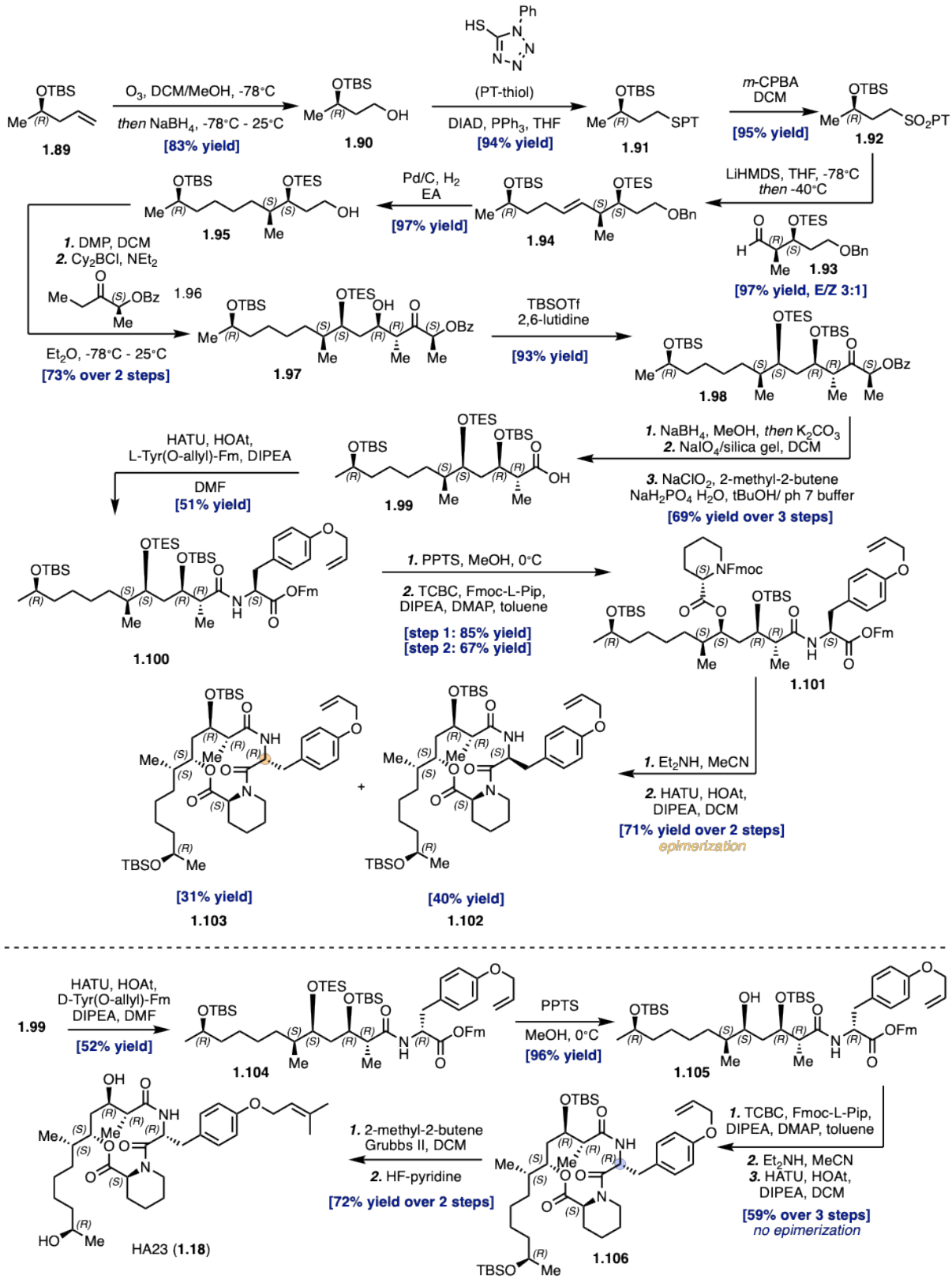


Figure 1.17. Feng's forward synthesis of HA23. Adapted from ref. 40

combinations effectively suppress this process, a practically important observation for future

synthetic work in this family.

1.2.5.4 Stereocalpins

Ghosh, 2009.

The first synthetic investigation targeting stereocalpin A, and first synthetic attempt overall amongst this broader family of tridepsipeptides, was reported by Ghosh et al. in 2009[49]. Their synthetic strategies and ultimate outcomes were contingent on a ring-closure strategy involving macrolactamization between the two amino acids (route B, **Figure 1.18**) constituting the 12-membered core. The route also employed Ghosh's TiCl-promoted *anti*-aldol and Evans' *syn*-aldol reaction as the key steps to control the C2, C4 and C5 stereocenters to be *R*, *S* and *S*-

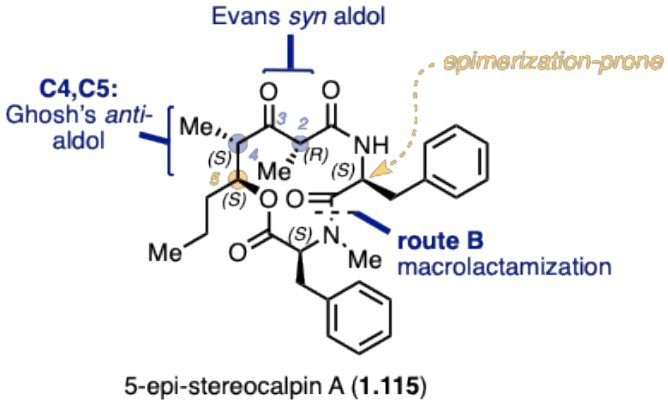
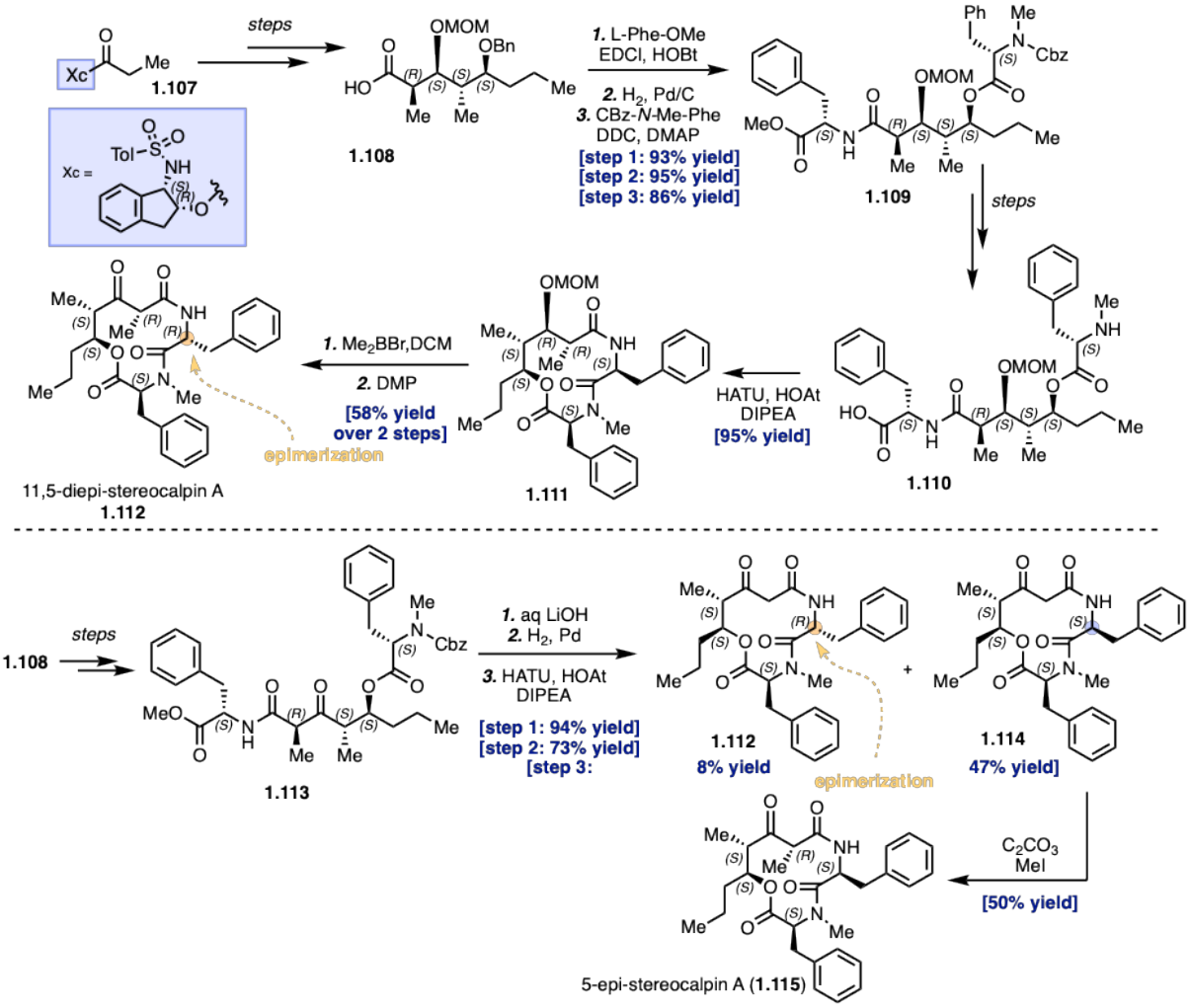


Figure 1.18. Summary of synthetic strategy of Feng et al towards the total synthesis of 5-epi-stereocalpin A.

configured, respectively, with high diastereoselectivity, producing PKS fragment **1.108** (**Figure 1.19**). Notably, the authors targeted this stereochemical assignment (later determined to be 5-epistereocalpin A) as proposed in the isolation paper by Seo et al. in 2008[41]. The amino acids were then installed onto the polyketide unit in succession, via high-yielding HATU and DCC-mediated amidation and esterification conditions. Following a chemoselective LiOH methyl ester hydrolysis and CBz hydrogenation revealing the free acid and amine handles of intermediate **1.110**, ring-closure was attempted employing HATU/HOAt/DIPEA. The synthesis was completed with the removal of the MOM protecting group under dimethylboron bromide conditions, and oxidation to the desired β-keto group was successfully achieved via mild DMP oxidation.

The synthesis delivered a single product (**1.112**), although it was not a match to the spectroscopic data of the natural product reported. X-ray data and Marfey's analysis of macrocycle

revealed complete epimerization of L-Phe α-proton, which was consistent across all other coupling conditions tested (TBTU and BOP) and represented, at the time, the first report of complete



stereochemical inversion during ring-closure (route B). The observed facile epimerization of the substrate was attributed to the steric compression between the C2 methyl, C3 MOM group, and the C11 benzyl group present in the linear substrate.

Figure 1.19. Synthesis of 5-epi-stereocalpin by Ghosh et al. Adapted from ref. 49

Interestingly, in their second synthetic iteration (**Figure 1.19**), where a late-stage methylation of the β-keto macrocycle was employed to de-risk epimerization upon macrolactamization and C2-racemization, 47% of the stereochemically intact macrocycle (**1.114**) was isolated and only 8% of the epimerized product (**1.112**) after the same ring-closing conditions were employed. However, pronounced discrepancies in the NMR data between the synthetic and

natural samples of stereocalpin A suggested an incorrect stereochemical assignment in the original report[41], thereby necessitating further synthetic studies to definitively establish its structure. Ultimately, Kaneda et al.'s synthesis in 2018 unambiguously characterized stereocalpin A (vide infra), and revealed Ghosh's synthesis had targeted the 5-epi-stereocalpin A instead.

Reddy, 2011. — Synthetic Studies toward Stereocalpin A

The second synthetic investigations targeting stereocalpin A were reported by Reddy et al. in 2011[47]. Given Ghosh's results suggesting an incorrect stereochemical assignment in the original isolation report[49], Reddy and coworkers directed their efforts at establishing the absolute configuration of the natural product by synthesis of candidate stereoisomers.

The route employed a Paterson aldol reaction as the key step for construction of the β-hydroxy ketone polyacetate fragment, utilizing chiral boron enolate chemistry to install both C4–

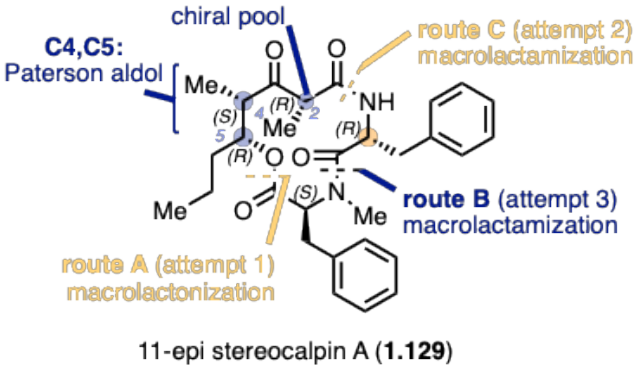


Figure 1.20. Summary of Reddy and coworkers synthetic strategy to stereocalp
in A, resulting in the synthesis of 11-epi-stereocalpin A.

C5 *syn* and *anti* isomers in the polyketide subunit. Following construction of **1.117a** and **1.117b**, the *N*-MePhe–Phe dipeptide was appended through standard amidation conditions to set the stand for ring-closure via macrolactonization (route A). Unfortunately, Yamaguchi conditions did not provide the desired macrocycle (**1.122**), representing another example in which macrolactonization was not productive, and efforts were shifted to macrolactamization via route C instead. After the construction of the required linear precursor (**1.125**), no condition tested resulted in the desired cyclized product via this second attempt, presumably due to formation of the DKP, although this was not directly commented on by the authors in their report.

In a last resort (attempt 3, **Figure 1.21**), the authors adapted their PKS isomer fragments for route B ring-closure, installing the *N*-MePhe via Yamaguchi esterification first generating **1.126**, followed by the installation of the L-Phe on the acid handle of the PKS fragment. Following

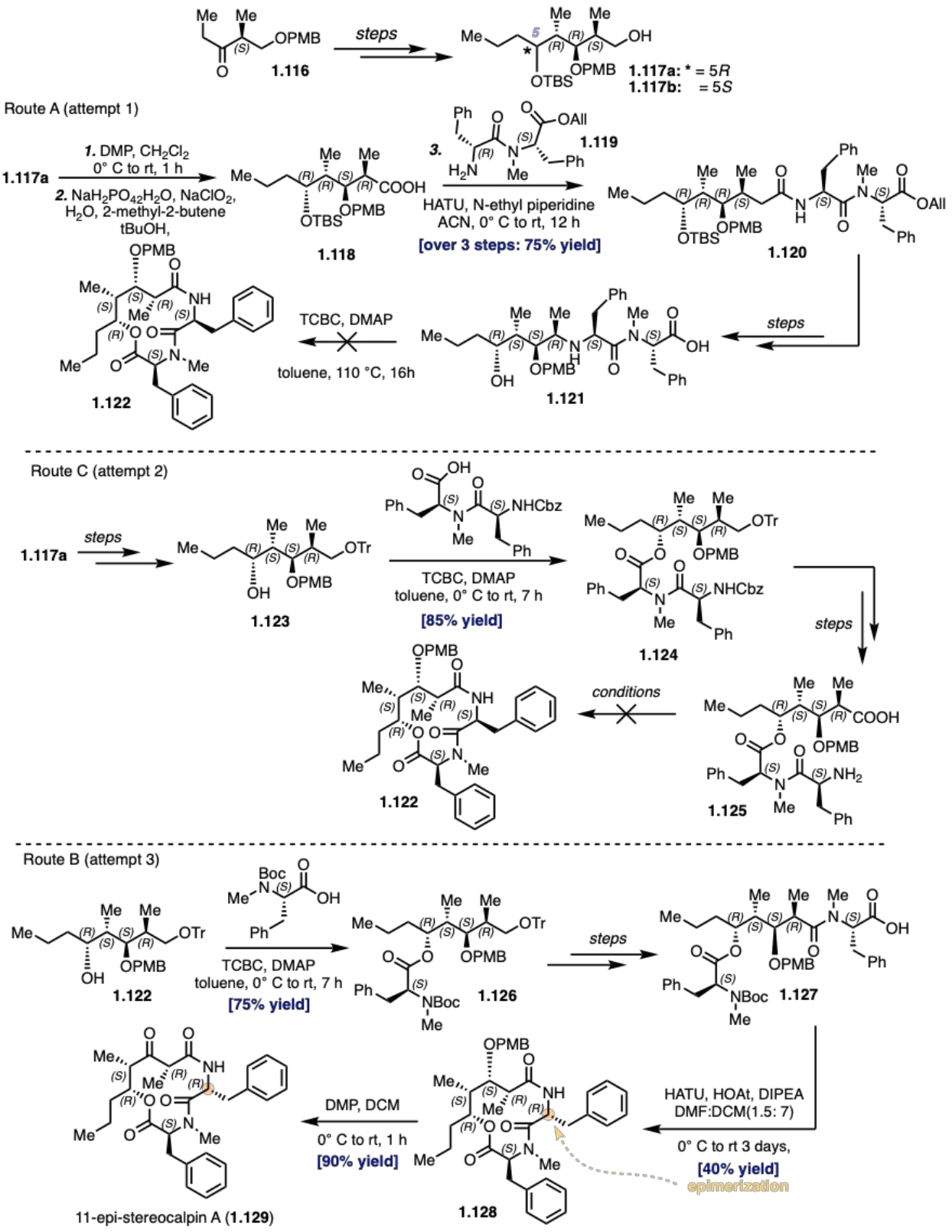


Figure 1.21. Reddy et al.'s synthetic attempts towards stereocalpin A. Adapted from ref. 47

deprotection conditions, HATU/HOAt conditions were successful in delivering the macrocyclic

products derived by both C4–C5 *syn* and *anti* PKS isomers. A late-stage DMP-mediated oxidation to afford the C3 ketone from the C3 hydroxyl, was employed as a mitigation strategy to prevent unwanted stereochemical scrambling of C2-methyl stereocenter. The synthesis delivered two diastereomers: 11-*epi*-stereocalpin A (**1.129, Figure 1.21)** and 5,11-di*epi*-stereocalpin A (not depicted here) from the C4-C5 *syn* (**1.117a**) and *anti* (**1.117b**) PKS isomers, respectively. Similarly to Ghosh's approach, a complete stereo-inversion of C11 from the L-Phe to D-Phe upon macrolactamization conditions was noted. This phenomenon that was also later reported by Feng et al. in their 2025 synthesis of HA23[40] whereby ring-closure about the same bond (route B) was initially attempted on a similarly L/L-configured linear precursor. This problem was attributed to the activated ester conditions in the presence of the adjacent β-keto group (C1), which acidified the α-proton and facilitated racemization under the coupling conditions.

The NMR discrepancies between the synthetic epimers and natural stereocalpin A were informative, as the campaign established the synthetic accessibility of the 12-membered ring system under macrolactamization conditions and identified epimerization at C11 as the central practical challenge. However, the configurational question remained unresolved.

Zhao, 2017

In a partial retraction and correction of an earlier synthesis from the same laboratory[63], Zhao, Wu, and Li re-examined the route and, in doing so, provided the most mechanistically explicit account to date of the inherent synthetic challenges of the stereocalpin A scaffold.

The Cbz-L-Phe–L-MePhe dipeptide subunit **1.132 (Figure 1.23)** was assembled via EDCI/HOAt-mediated amidation conditions, followed by methyl ester saponification, reproducing the earlier work reliably at this stage. Control of the stereogenic centres along the PKS subunit was achieved as before through Evans' asymmetric aldol reaction of the α-methyl ketone with

butyraldehyde under dicyclohexylboron chloride conditions, delivering the C2, C4 and C5

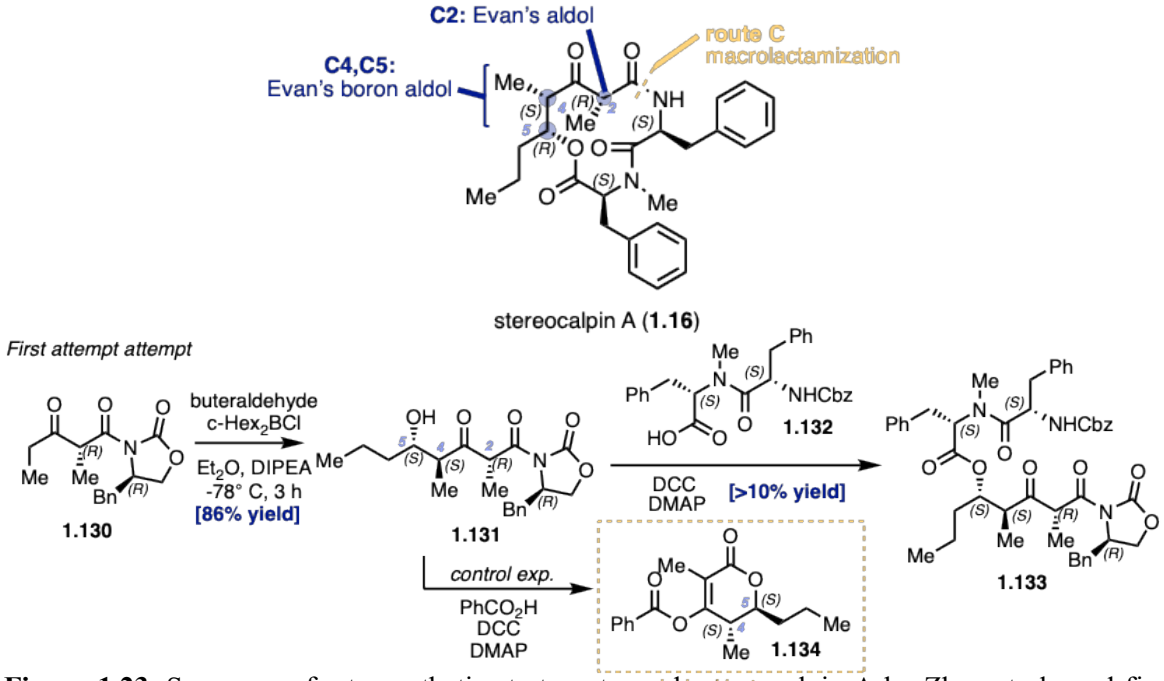


Figure 1.23. Summary of retrosynthetic strategy towards stereocalpin A by Zhao et al., and first synthetic attempt demonstrating formation of undesired lactone. Adapted from ref. 63

stereocenters to be *R*, *S* and *S*-configured (**1.131**). However, attempted DCC/DMAP-mediated esterification to unite the two fragments did not proceed in high yields as previously reported. Instead, control experiments revealed that the dominant pathway was intramolecular lactonization of the β-hydroxy group onto the adjacent enolizable ketone, delivering an undesired six-membered lactone byproduct **1.134**, with the loss of Evans auxiliary. This incompatibility between the free secondary alcohol and the β-keto carbonyl at the point of fragment union represents a genuine constraint on route design that is not immediately apparent from inspection of the linear substrate but becomes decisive under activation conditions. To circumvent this, the C3 ketone **1.131,** was reduced prior to fragment coupling (**Figure 1.24**), resulting in a smooth successive EDCI/HOAt-mediated esterification Cbz-*N*-Me-Phe (**1.136**), followed by Cbz hydrogenation and installation of the second amino acid residue via HATU-mediated amidation, delivering **1.138**. Interestingly, removal of Evans auxiliary under LiOH/H_2O_2 conditions resulted in poor yields of the desired linear acid **1.139** due the labile ester that resulted in a series of lactone side products **1.140** and

1.141. This observation becomes relevant in Chapter IV where our total synthesis efforts towards

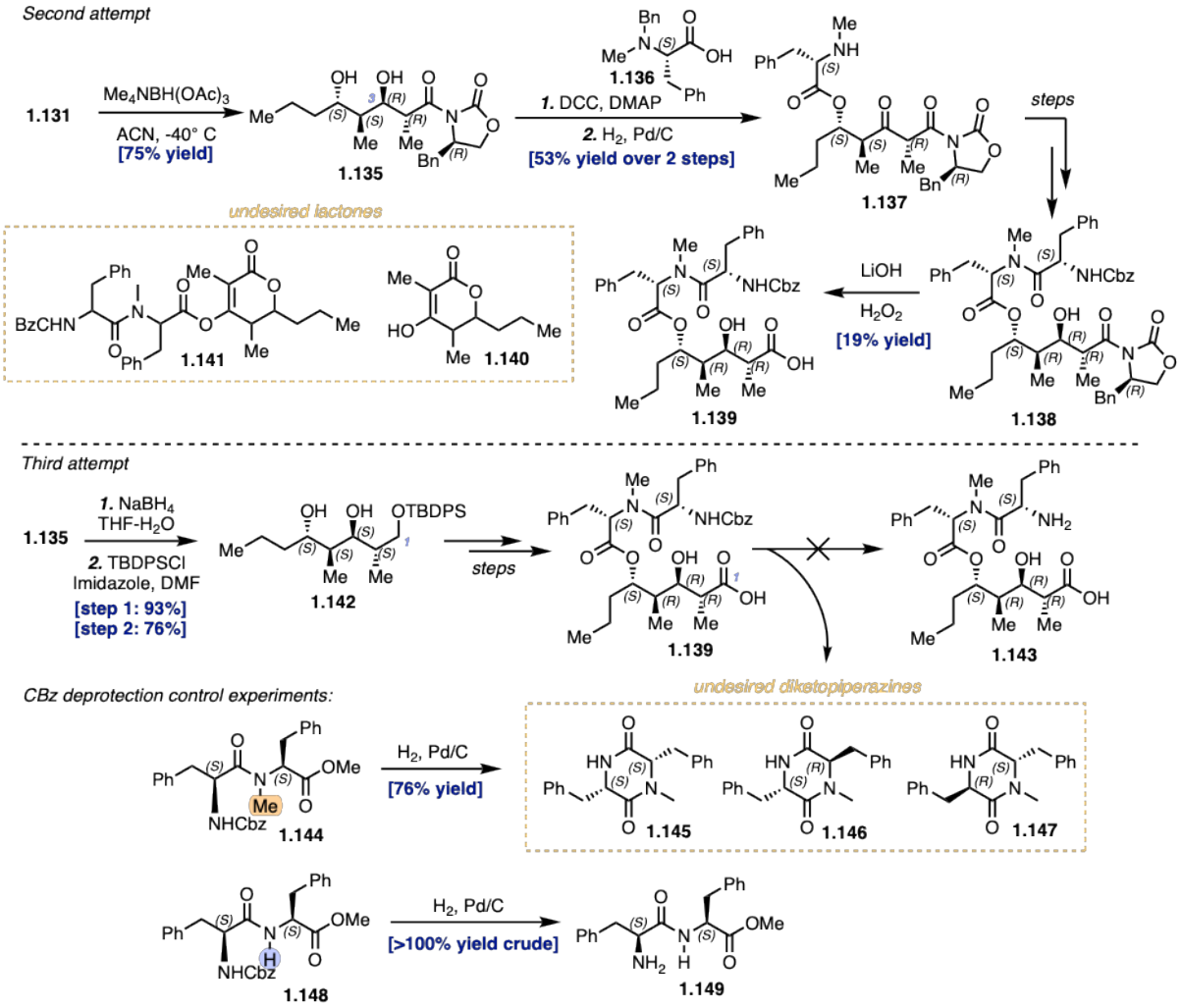


Figure 1.24. Second and third synthetic attempts by Zhao et al. towards the synthesis of stereocalpin A, and CBz deprotection control experiments. Adapted from ref 63.

immunomodulide become challenged by a similar labile ester intermediate.

Zhao and coworkers proceeded in a third attempt (**Figure 1.24**) by unmasking the auxiliary via a two-step reduction-then-protection sequence early in the synthesis, delivering intermediate **1.142**. Installation of each amino acids followed, via standard carbodiimide conditions (DCC, DMAP), and C1 deprotection followed by oxidation delivered the linear precursor primed for ring-closure **1.139**. More consequentially, were Zhao et al.'s challenges in unmasking CBz protected *N*-terminus of this advanced linear intermediate prior to macrolactamization. Hydrogenation at this stage led uniformly to diketopiperazine formation (**1.145-1.147**) rather than the desired free amine

required for ring-closure **1.143**, regardless of catalyst or additive. The authors attributed this outcome to the conformational bias imposed by the *N*-methyl group on the adjacent amide, which enforces a folded chain geometry that positions the primary amine in proximity to the labile ester linkage, making intramolecular aminolysis kinetically competitive with the intended macrolactamization. This argument was reinforced by their control studies in which the same hydrogenation conditions were carried out on both Cbz-L-Phe–L-*N*-MePhe (**1.144)** and Cbz-L-Phe–L-Phe (**1.148)**. DKP byproducts (**1.145-1.147)** were exclusively obtained in the L-*N*-MePhe case, whereas deprotection of the CBz proceeded smoothly otherwise, delivering (**1.149)**. This structural argument simultaneously explains why Ghosh's ring-closure at the *N*-MeNH bond (route B) succeeded whereas their attempts in implementing route C ring-closure did not[49].

Ultimately, the partial retraction report of Zhao and coworkers highlighted the complications attributed to the synthetic strategy of route C, which are broadly applicable even outside the unique C3 oxidized and L/L-configured stereocalpin A scaffold. Their conclusions stressed that subsequent synthetic attempts targeting this strained ring core via macrolactamization at route C should consider mitigation techniques in the construction of the lactonization-prone PKS fragment as well as deprotection conditions/sequences that reduce the lifetime of the vulnerable free amine advanced intermediate prone to DKP formation.

Kaneda, 2018

The definitive resolution of stereocalpin A's structure was achieved by Kaneda and colleagues in 2018[58] through the most comprehensive stereochemical campaign reported for any member of this compound family. Recognizing that the amino acid configurations had been

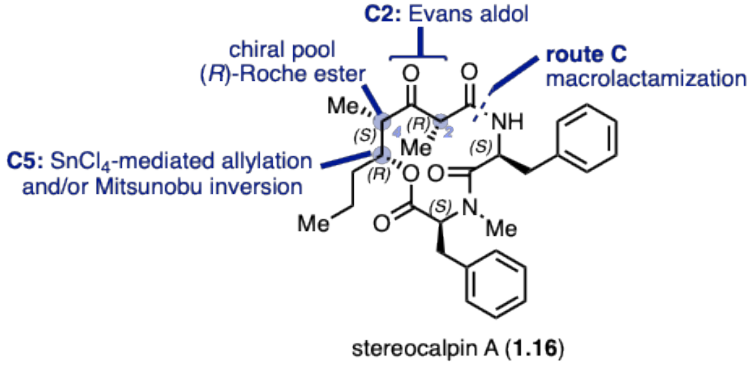


Figure 1.25. Summary of Kaneda and coworkers' synthetic strategy to stereocalp in A.

reliably established by Marfey's analysis in the original isolation report, the authors confined the configurational ambiguity to the three polyketide stereocenters at C2, C4, and C5, reducing the relevant isomer space from 32 to eight. The authors strategically implemented a "mirror image strategy" enabling an expedient preparation of only four of the eight possible PKS fragments by utilizing D/D-dipeptides as surrogates for the four remaining L/L-amino acid enantiomers, halving the synthetic burden. Kaneda and coworkers also noted the importance of route selection for the construction of the macrocycle, given the precedence for epimerization[40,47,49], PKS fragment lactonization[48] and DKP formation[48]. Ultimately, the authors opted for route C, utilizing a one-pot deprotection-cyclization approach to mitigate DKP formation.

The synthesis was initiated from the (*R*)-Roche ester alcohol (**1.150**) as a chiral pool source fixing the configuration of C4 across the PKS isomers. C5 was installed via $SnCl_4$-mediated addition of allyltributylstannane to give an *anti*-homoallyl alcohol **1.151** which could be inverted via the Mitsunobu reaction. Across the series, C2 was controlled through the use of Evans' asymmetric aldol with either matched or mismatched chiral oxazolidinones (**1.153** or **1.154**).

For each of the four PKS configurations synthesized through this sequence (**1.156-1.159, Figure 1.26**), the D/D-configured (not depicted) and L/L-configured amino acids combinations were installed one amino acid at a time, via esterification first between *N*-Me-Phe and the C5

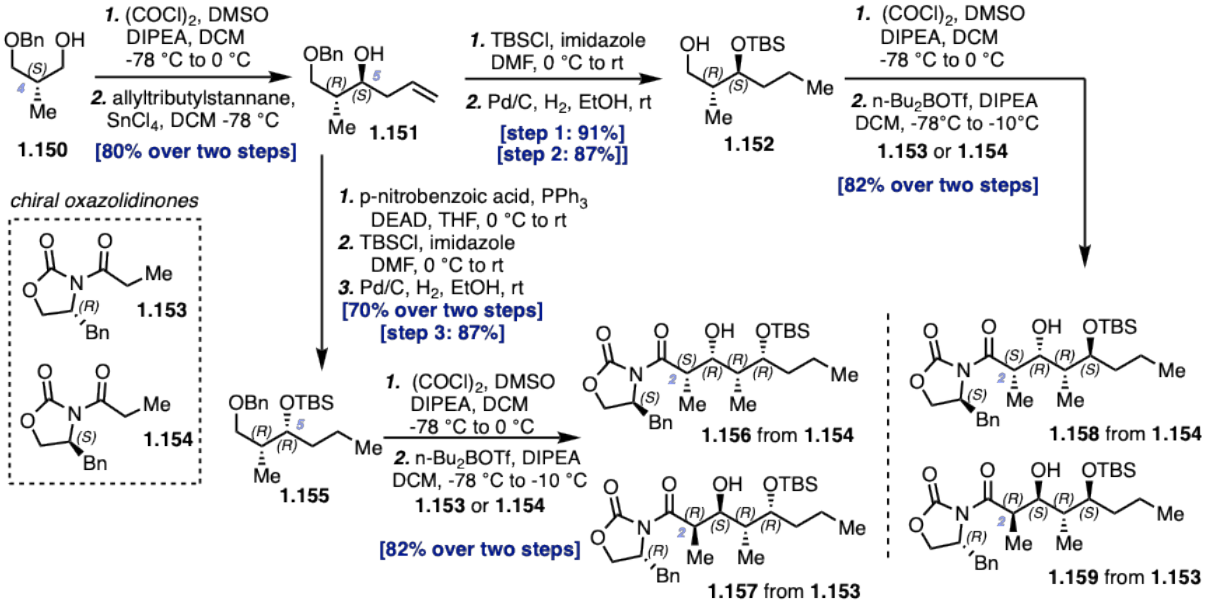


Figure 1.26. Kaneda's synthesis of PKS fragments in pursuit of structural characterization and total synthesis of stereocalpin A. Adapted from ref. 58.

hydroxyl, followed by deprotection and HATU-mediated amidation for the installation of the subsequent CBz-protected-Phe amino acid (**Figure. 1.27**) With the eight stereoisomers in hand, one-pot CBz deprotection-HATU/HOAt-cyclization provided the desired corresponding macrocycles and suppressing competitive diketopiperazine formation (advancement of isomer **1.159** leading to the formation stereocalpin A is displayed in Figure **1.27**). Finally, a late-stage C3-hydroyxl oxidation approach, similar to that of Ghosh synthesis was implemented to retain the stereochemical integrity of C2-methyl, affording all eight synthetic isomers in high enantiopurities.

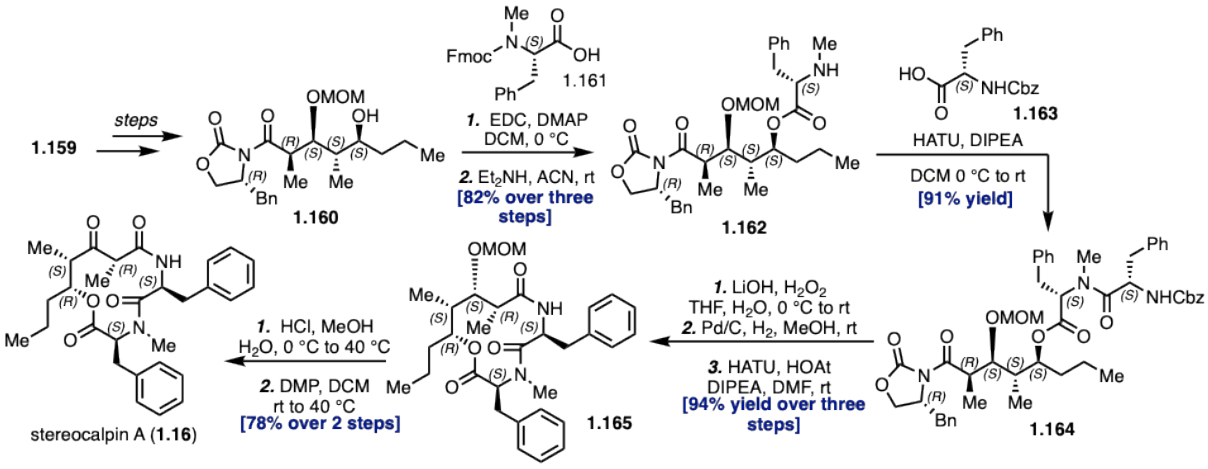


Figure 1.27. Completion of total synthesis of stereocalpin A by Kaneda. Adapted from ref 58.

Comparison of the ^{1}H and ^{13}C NMR spectra and optical rotations of all eight synthetic isomers with those of natural stereocalpin A unambiguously identified the natural product as the 2*R*,4*S*,5*R*-configured isomer incorporating the L-Phe and L-N-Me-Phe amino acids, a structural revision of the originally proposed configuration. A retrospective NOESY analysis confirmed that the NOE correlations relied upon in the initial isolation report were shared amongst 4*S*,5*S* and 4*S*,5*R* diastereomers, and signal overlap at C5 complicated determination of its configuration. This work constitutes the most complete stereochemical campaign in the entire family reviewed here and establishes the mirror-image approach as a general strategy for configurational assignment of polyketide natural products with multiple unresolved stereocenters when the isomer space is manageable.

1.2.6 Synthetic Challenges and Opportunities

Macrocyclization Strategy and Disconnection Site Selection

Across the synthetic campaigns reviewed in **Section 1.2.5**, the choice of macrocyclization disconnection emerges as the single most consequential strategic decision, with route selection directly determining whether ring-closure is achievable at all, and whether the configurations of important stereocenters are retained. The three recurring disconnections (route A, route B and route C; **Figure1.7**) explored throughout the synthetic attempts of tridepsipeptides discussed, carry distinct advantages and failures that have been revealed progressively across this series and are summarized in the discussion that follows.

Macrolactonization via route A. Across all attempts that explored macrolactonization, the approach proved uniformly unsuccessful. Yamaguchi conditions failed entirely in the Yadav

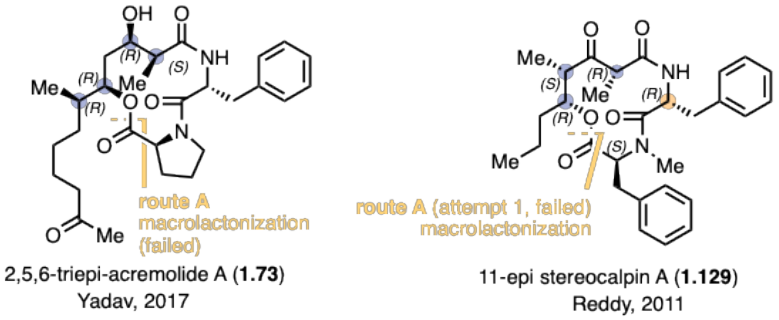


Figure 1.28. Macrolactonization (route A) attempts made towards acremolide and stereocalpin tridepsipeptide cores.

acremolide campaign, with no macrocyclic product recovered under any condition tested[60], and Reddy's initial attempt at stereocalpin A via the same route was similarly unsuccessful[47]. The inherent difficulty of esterification-based macrocyclization relative to amide-bond formation appear to be compounded in the context of this this densely substituted 12-membered ring, where conformational demands, and epimerization liabilities dominate. The observation that route A has not been successfully implemented by any group across the entire family reviewed here strongly suggests that esterification-based ring closure should be deprioritized in future synthetic planning for these targets.

Macrolactamization via route B. Route B macrolactamization, closing the N-methylamide bond between the two amino acids, was successfully exploited by Ghosh in accessing stereocalpin A[49] and by Feng in the synthesis of HA23[40]. The main advantage of

macrolactamization via this route is that it generates no free primary amine intermediate capable

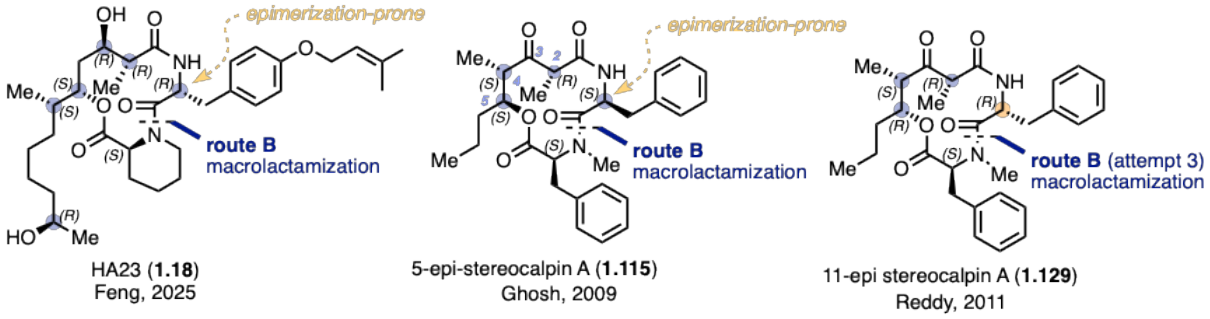


Figure 1.29. Macrolactamization (route B) attempts made towards HA23, and stereocalpin tridepsipeptide cores. Epimerization-prone stereocenter indicated in yellow.

of competing with the macrolactamization pathway, thereby avoiding diketopiperazine formation entirely. However, route B is complicated by the tendency for epimerization at the C-terminus of the aromatic amino acid which could be attributed to the prolonged lifetime of its activated ester due to the increase in steric demand about the nucleophilic partner (*N*-Me amine). This prolonged lifetime could result in the competing epimerization side reaction becoming dominant over ring-closure, which become obvious specifically in the context of L/L-configured advanced linear precursors such as in the stereocalpin A case, as reported by Ghosh[49] and Reddy[47], but also in Feng's structural revisions of HA23[40] (**Figure 1.29**).

Macrolactamization via route C. Macrolactamization via route C presents as the strategy most frequently attempted across all synthetic campaigns within the cyclic tridepsipeptide family. This approach was successfully implemented in Chen's synthesis of colletopeptide A/colletotrichamide A[55], Xiao's synthesis of acremolide A and B[53], and Kaneda's synthesis of stereocalpin A[58]. Ring-closure here is enabled by an amidation between the acid of the PKS fragment and the terminal primary amine of the aromatic amino acid. Its primary appeal is that the nucleophilic partner, unlike in route B, is the less sterically encumbered primary amine of the aromatic amino acid residue. However, route C suffers from the competing DKP pathway

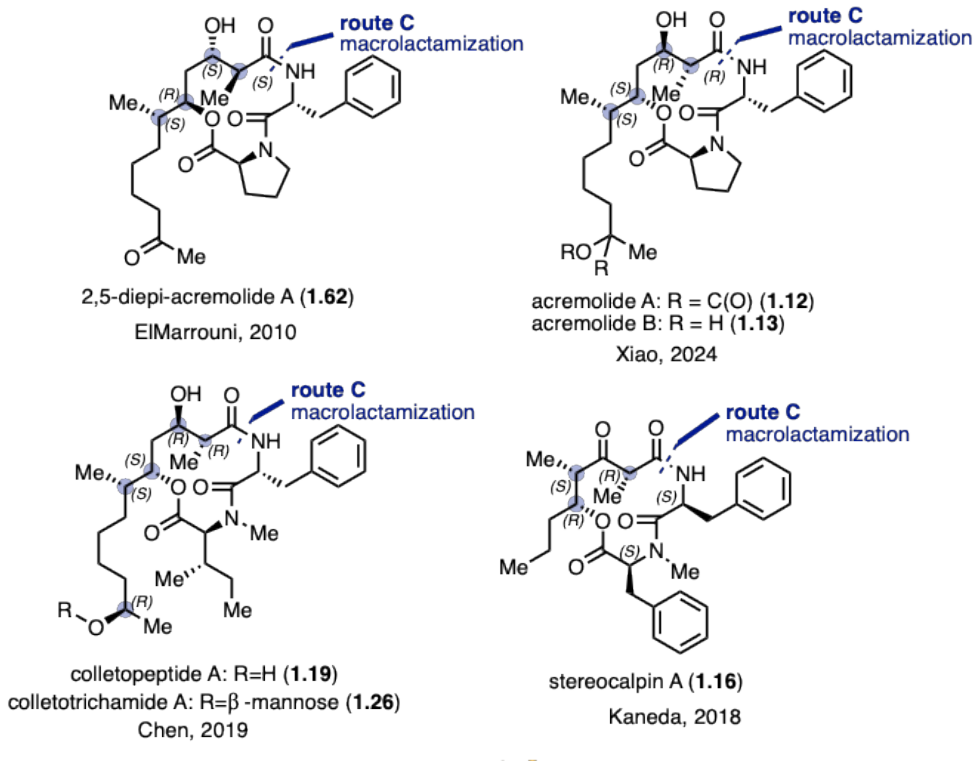


Figure 1.30. Macrolactamization (route C) successful implementation in synthesis of acremolides, colletopeptides A, colletotrichamide A and stereocalpin.

(discussed below) and demands careful monitoring of deprotection and cyclization to minimize the lifetime of the reactive free amine intermediate.

Diketopiperazine Formation

Diketopiperazine formation is inherent to this class by definition of the conserved *N*-alkyl amino acid moiety, that defines the tridepsipeptides. In cyclic secondary amines such as proline and pipecolic acid, the ring architecture enforces the *cis* amide geometry, while in *N*-Me amino acids, *N*-alkylation reduces the energetic difference between *cis* and *trans* conformers, increasing the *cis* population relative to unalkylated systems. In either case, the elevated *cis* geometry biases the dipeptide portion of synthetic intermediate towards a folded arrangement that positions the terminal amine in proximity to the adjacent ester carbonyl, making six-membered lactam formation kinetically competitive. As established by Zhao et al.'s control studies[48] discussed in **Section 1.2.5.4** the decomposition pathway was prevalent in route C, but also in a simplified dipeptide intermediate, when it was subject to the same hydrogenation conditions for N-Me

deprotection. DKP formation was eradicated their control dipeptide lacking *N*-methylation, which highlights the extent of conformational biasing that takes place in *N*-methylated derivatives. Conversely, in ElMarrouni[59] or Yadav's[60] syntheses of the acremolide series, no DKP complicated were reported, even in the presence of the turn-inducing L-proline amino acid which is well-reported to exhibit similar conformational biasing that facilitates diketopiperazine formation[64].

The successful implementation of a one-pot deprotection-cyclization protocol by Kaneda in the synthesis of stereocalpin A[58], and a similar telescoped approach by Xiao in his synthesis of the acremolides[53], demonstrates that DKP formation is manageable with optimizations. However, best-practice approaches for suppressing diketopiperazine formation generally rely on low temperatures and minimizing base exposure[65–67].

Epimerization

Epimerization at the α-centres of amino acid moieties represents the most pervasive stereochemical liability across this compound family. Two major manifestations of this problem have been repeated documented across the synthetic campaigns discussed.

The first epimerization concern appears at the C-terminal aromatic amino acid in route B closures (vide supra, **Figure 1.29**), where the ring closing conditions that activated the C-terminus render the α-proton of the amino acid acidic and susceptible to stereochemical scrambling. As mentioned before, this problem is exacerbated by the sterically encumbered *N*-Me amine nucleophile which increases the lifetime of the activated ester intermediate and enables epimerization pathways to dominate.

The second manifestation is distinct in that it persists throughout the synthesis, specifically in the stereocalpin series, due to the α-methyl β-keto ester motif. This functionality increases acidity of the proton at the C2 position, rendering that stereocenter inherently susceptible to scrambling under basic and oxidative conditions. Two strategic responses have been developed. Ghosh's approach performed macrolactamization on a C2-unmethylated substrate and installed the α-methyl group post-cyclization under basic conditions, removing the acidifying influence of the β-keto carbonyl during the ring-closing step and recovering the stereochemically intact macrocycle in the second-generation route. Kaneda's approach instead deferred installation of the ketone entirely, carrying a protected C3 hydroxyl throughout the synthesis and performing an oxidation to the β-keto group at the penultimate step. This strategy enabled complete C2 stereochemical

integrity across all eight synthetic isomers made, validating this as the preferred solution. The lessons that emerge here is that a strategy should be put in place to retain the integrity of the C2 stereocenter across the compound series, particularly in the case where a C3 carbonyl is present (stereocalpin).

Stereochemical Assignment

The configurational assignment of polyacetate-derived PKS fragments in particular, have proven systematically unreliable by NMR-based methods alone, evident by the structural elucidations and reassignments of the acremolides and stereocalpins. Moreover, because the producing organisms employ iterative rather than modular PKSs, the biosynthetic gene clusters provide limited predictive insight into the stereochemical configuration of the resulting metabolites, making configurational assignment from genomic analysis alone particularly difficult

Kaneda's stereochemical revision demonstrates that NOE/NOESY-derived assignments alone may be insufficient for reliable conformational analysis in macrocyclic systems[58]. Furthermore, the conformational averaging and restricted bond rotation of the L/L- and D/D-configured tridepsipeptides synthesized in Kaneda's report exhibited pronounced signal doubling in their NMR spectra, obscuring important diagnostic NOE cross-peaks. The implication from this work is that NOESY-based configurational assignment of polyacetate macrolides of this ring size and substitution density should not be considered definitive without synthetic corroboration.

Two complementary strategies have emerged for addressing this problem. The exhaustive synthetic approach, refined by Kaneda through the mirror-image strategy[58], provides unambiguous assignment, although still synthetically labour intensive. Alternatively, the biochemistry-guided approach of Xiao et al. derives stereochemical information from biosynthetic studies of the producing organism rather than from the conformationally compromised macrocycle itself[53]. While conceptually powerful, the success of this strategy remains limited, having thus far been demonstrated in only two members of this class, both of which conveniently feature configurationally identical polyacetate-derived PKS fragments (acremolide A[36] and HA23[39,40]).

The challenges associated with configurational assignment are not restricted to the PKS-derived fragment. In the case of HA23, stereochemical assignments of the peptide-derived residues obtained through Marfey's analysis in the isolation report[39], were later revised with the completion of Feng's total synthesis[40]. This further highlights the difficulty of securing definitive

stereochemical assignments, even when exploiting Marfey's techniques, presumably due to the tendency of conformational scrambling in the acid-mediated hydrolysis stage.

Collectively, these studies highlight the substantial challenges associated with configurational assignment in fungal tridepsipeptides, while simultaneously underscoring the important role of total synthesis in structural validation, stereochemical reassignment, and biosynthetic investigation within this class of natural products.

Opportunities and Outlook

Several opportunities for future advancement within this class remain largely unexplored. The most immediate of which is expanding the currently structural and stereochemical diversity accessed synthetically across fungal tridepsipeptides. To date, only a small subset of family membered have been subject to total synthesis, despite the growing number of structurally related metabolites emerging from fungal genome mining and metabolomics studies, the majority of which have demonstrated bioactivity[28,37,38,41–43,54].

From a methodological perspective, macrocyclization itself remains an unresolved opportunity rather than a solved problem. The inherent difficulty associated with macrocyclization across the competing disconnection strategies remains poorly defined, as comparisons between approaches are often confounded by differences in substrate structure and stereochemical configuration. Systematic evaluation of ring-closing methodologies in simplified model systems could prove valuable in characterizing the inherent feasibility of individual macrocyclization events and detangling conformational effects from substrate-specific complications. On this same methodological perspective, the recurring problems of diketopiperazine formation and epimerization highlight opportunities for the development of new protecting-group strategies, milder activation methods, and telescoped transformations specifically tailored to these conformationally biased cyclic tridepsipeptides.

An especially promising direction concerns the development of generalized, stereochemically programmable synthetic approaches capable of rapidly accessing multiple PKS stereoisomers from common intermediates. While Kaneda's mirror-image strategy elegantly reduced the stereochemical burden associated with stereocalpin A, analogous stereodivergent approaches have yet to be broadly implemented across the family. Such strategies could become

increasingly important as new isomers continue to emerge with unresolved or partially assigned configurations.

More broadly, the synthetic accessibility of these compounds opens opportunities extending beyond structural validation alone, enabling systematic structure-activity relationship studies, biosynthetic investigations, and chemical biology efforts aimed at understanding the functional significance of their privileged macrocyclic scaffolds.

1.3. An Introduction to Immunomodulide

1.3.1 Discovery, Isolation, and Biosynthetic Context

Immunomodulide (**1.165**) is a fungal-derived cyclic depsipeptide natural product originally isolated from *Fusarium avenaceum* by our collaborators in the Overy Lab at Agriculture Agri-Foods Canada (AAFC). Following its identification via metabolomic
profiling, a detailed analysis utilizing HRMS, and 2D NMR experiments was carried out, revealing a predicted structure and candidate gene cluster identified by AntiSmash (**Figure 1.31**). Genetic

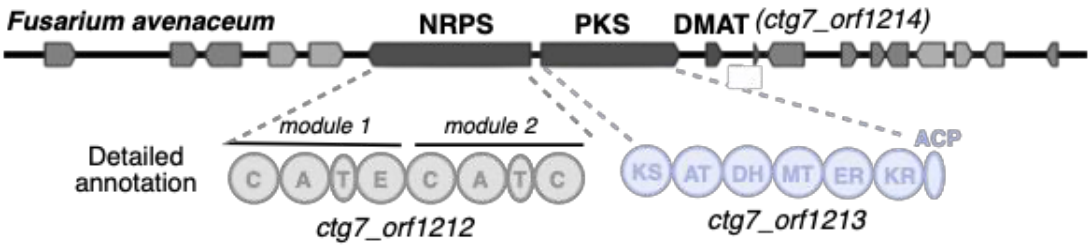


Figure 1.21. Proposed biosynthetic gene cluseter responsible for production of immunomodulide. AntiSMASH analysis identified a candidate hybrid PKS-NRPS biosynthetic gene cluster comprising an NRPS (ctg_orf1212), a highly reducing PKS (ctg_orf1213) and a putative dimethylallyltransferase (DMAT).

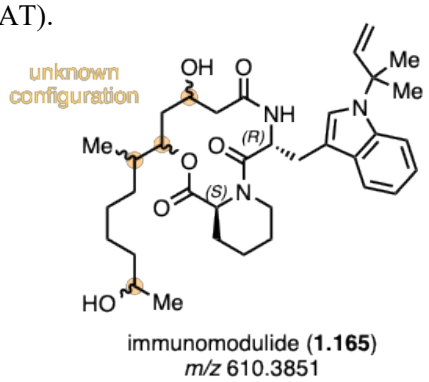


Figure 1.32. Biosynthesis-supported predicted structure of immunomodulide

disruption and complementation studies confirmed that biosynthesis of the novel metabolite hit (*m/z* 610.3851) was dependent upon the associated NRPS-containing biosynthetic gene cluster. The core biosynthetic enzymes within the proposed candidate cluster consisted of an single module PKS (KS-AT-DH-MT-ER-KR-ACP), flanked by a bimodular NRPS (C-A-PCP-E-C-A-PCP-CT) and a tryptophan dimethylallyltransferase (DMAT), which was consistent with an *N*-indole reverse prenylation event that was evident by NMR investigations.

Taken together, the domain arrangement and sequence of the PKS-NRPS assembly line strongly supported the proposed structural assignment in **Figure 1.32**. The iterative PKS was predicted to generate a methylated and highly reduced PKS fragment derived from six acetate units, consistent with the observed polyacetate architecture of Immunomodulide. The peptide-derived fragment was instead composed of an *N*-reverse prenylated D-tryptophan consistent with the presence of the epimerization domain in the NRPS and DMAT in the BGC. Structural analysis predicted L-pipecolic as the second amino acid motif incorporated by the NRPS enzyme. Moreover, the C terminal domain identified at in the NRPS was consistent with the presence of a 12-membered macrocycle, which was evident by the distinct NMR signals of the isolated compound as well as HRMS-provided accurate mass and degrees of unsaturation.

Collectively, the combined metabolomic, spectroscopic, and biosynthetic analyses positioned immunomodulide within the emerging family of fungal PKS-NRPS-derived cyclic tridepsipeptides discussed throughout this thesis.

1.3.2 Immunomodulide Within the Fungal Tridepsipeptide Framework

Immunomodulide aligns perfectly with the fungal tridepsipeptide classification framework developed throughout this thesis. Like the acremolides, stereocalpins, HA23, colletopeptides, and related congeners discussed previously, immunomodulide contains a densely substituted polyacetate-derived PKS fragment embedded within a compact 12-membered cyclic tridepsipeptide scaffold. The macrocycle is constructed through linkage of the PKS-derived fragment to two amino acid residues through alternating ester and amide bonds, generating the conserved depsipeptide architecture characteristic of the family. Additionally, the presence of an N-alkylated amino acid residue (Pip) further reinforces its alignment with the broader fungal tridepsipeptide family and contributes to the conformationally restricted characteristic of these macrocycles. While immunomodulide preserves the broader structural characteristic of the

tridepsipeptide class, notable and unique features are its reverse-prenylated indole motif, a modification otherwise only loosely reflected in the prenylated architecture of HA23, as well as the absence of the otherwise relatively conserved C2 methyl substituent within the PKS fragment, a feature similarly observed in colletopeptide E.

Overall, immunomodulide represents both a logical continuation of synthetic investigations within this emerging class of fungal natural products and an opportunity to further interrogate the structural and stereochemical complexity associated with fungal tridepsipeptides.

1.3.3 Biological Activity and Significance

Immunomodulide attracted considerable interest following its initial isolation due to its reported immunomodulating activity. Preliminary biological evaluation demonstrated enhancement of the innate immune response, observed through increased reactive oxygen species (ROS) burst production upon co-administration with the bacterial flagellin-derived peptide flg22, a well-established pathogen-associated molecular pattern (PAMP) recognized by plant immune systems. These studies suggested that immunomodulide may function as a potentiator of plant innate immunity, highlighting its potential biological relevance in host-pathogen signalling and fungal chemical ecology.

More broadly, fungal tridepsipeptides collectively exhibit diverse biological activities including cytotoxic, antifungal, antiviral, anti-inflammatory, and enzyme inhibitory properties[28,37,38,41–43,54]. The recurring bioactivity observed throughout the family suggests that the conformationally restricted macrocyclic scaffold may function as a privileged pharmacophore whose biological properties are highly sensitive to stereochemistry, oxidation state, and substitution pattern. In the case of immunomodulide, the densely functionalized macrocycle likely contributes directly to molecular recognition through its constrained three-dimensional architecture.

Consequently, reliable synthetic access to immunomodulide is important not only for structural validation, but also for enabling deeper biological interrogation and future structure–activity relationship studies. At present, however, investigation of the natural product remains constrained by limited material availability from isolation sources. Total synthesis therefore represents a critical enabling platform for accessing stereochemically defined material and structurally modified analogues inaccessible through fermentation alone.

1.3.4 Configurational Ambiguity and Structural Assignment

Despite extensive spectroscopic and biosynthetic analysis, the stereochemical configuration of immunomodulide could not be unambiguously established from the isolation data alone. While the overall connectivity and macrocyclic architecture of the natural product were strongly supported by HRMS and 2D NMR experiments, the relative and absolute configurations of the PKS-derived stereocenters remained unresolved (unknown configurations in yellow, **Figure 1.32**). The densely substituted polyacetate fragment contained four elusive stereogenic centres, corresponding to sixteen possible stereochemical permutations of the PKS fragment alone. Consequently, definitive configurational assignment by NMR analysis alone proved particularly challenging. Although biosynthetic analysis provided tentative support for the D-tryptophan and L-pipecolic acid assignments, the stereochemical outcome of the iterative hrPKS remained significantly more difficult to predict. Furthermore, the extremely limited quantity of isolated material available (~2 mg) rendered X-ray crystallographic analysis impractical. Consequently, the stereochemical assignment of the PKS-derived fragment remained entirely tentative at the outset of this work.

Within this context, total synthesis became necessary not only for material access, but also for structural validation itself. A stereochemically programmable synthetic strategy capable of accessing candidate stereoisomers of the PKS fragment would permit direct comparison of spectroscopic and physical data against the isolated natural product, thereby enabling rigorous configurational assignment. Accordingly, one of the principal objectives motivating the work presented in this thesis was the development of a synthetic platform capable of interrogating and resolving the unresolved stereochemical configuration of immunomodulide.

1.4 Summary of Thesis Objectives (Part I)

Given the unresolved stereochemical configuration of the Immunomodulide, and its intriguing biological activity, the work presented in Part I of this thesis was directed toward the development of a total synthesis strategy that would enable full stereochemical and structural elucidation of this novel natural product. This objective was pursued in the form of three integrated objectives (summarized below) which will constitute Chapters II-IV of Part I of this thesis.

1. Evaluating Macrolactamization Approaches Towards the Synthesis of the Immunomodulide Core (Chapter II). This objective involved the investigation of macrocycle construction within this structurally constrained class of natural products. As highlighted throughout Chapter I, the intrinsic feasibility of competing macrocyclization disconnections remains poorly understood due to substantial confounding effects arising from substrate structure and stereochemical configuration. Accordingly, a simplified model system was pursued to characterize the inherent difficulty of ring-closure across route B and C ring-closing strategies to better understand the limitations of each approach within the Immunomodulide scaffold.

2. Synthesis of Immunomodulide Analogs (Chapter III). Building on the results of Chapter II model analogs that, rather serendipitously, were found to also pose immunomodulatory activity, the platform for model substrates was expanded to encompass synthetic analogs capable of probing structure-activity relationships. Within this objective, the route to construction of these analogs was optimized to prioritize efficiency both in the form of scaffold diversification and operational simplicity, resulting in the integration of solid-phase peptide synthesis (SPPS) as a solution to this end.

3. Towards the Total Synthesis of Immunomodulide (Chapter IV). From a synthetic perspective, the primary objective of this work was the development of a convergent and stereochemically programmable route toward the immunomodulide scaffold. Emphasis was placed on the design of a stereochemically tailorable route towards PKS fragment construction, strategic incorporation of the peptide-derived residues, and the application of lessons learned in Chapter II to guide macrocyclization disconnection rationale with the conformationally restricted 12-membered depsipeptide core. Given the recurring synthetic complications observed throughout related fungal tridepsipeptide syntheses, including diketopiperazine formation, epimerization, and macrocyclization failure, the work additionally sought to identify synthetic sequences and protecting-group strategies capable of minimizing these liabilities.

1.5 References:

(1) Bhunjun, C. S.; Phukhamsakda, C.; Hyde, K. D.; McKenzie, E. H. C.; Saxena, R. K.; Li, Q. *Fungal Divers. 2023 1251* **2023**, *125* (1), 73–98.

(2) Kusari, S.; Hertweck, C.; Spiteller, M. *Chem. Biol.* **2012**, *19* (7), 792–798.

(3) Mousa, W. K.; Raizada, M. N. *Front. Microbiol.* **2013**, *4*, 65.

(4) Saxena, S.; Chhibber, M.; Singh, I. P. *Curr. Bioact. Compd.* **2018**, *15* (2), 211–231.

(5) Aly, A. H.; Debbab, A.; Proksch, P. *Fungal Divers. 2011 501* **2011**, *50* (1), 3–19.

(6) Arias, M.; Santiago, L.; Vidal-García, M.; Redrado, S.; Lanuza, P.; Comas, L.; Domingo, M. P.; Rezusta, A.; Gálvez, E. M. *Front. Immunol.* **2018**, *9*, 2549.

(7) Brakhage, A. A.; Schroeckh, V. *Fungal Genet. Biol.* **2011**, *48* (1), 15–22.

(8) Scherlach, K.; Hertweck, C. *Nat. Commun. 2021 121* **2021**, *12* (1), 3864-.

(9) Liu, Z.; Lin, Z.; Nielsen, J. *Synth. Syst. Biotechnol.* **2021**, *6* (1), 20–22.

(10) Mózsik, L.; Iacovelli, R.; Bovenberg, R. A. L.; Driessen, A. J. M. *Front. Bioeng. Biotechnol.* **2022**, *10*, 901037.

(11) Wadhwa, K.; Kapoor, N.; Kaur, H.; Abu-Seer, E. A.; Tariq, M.; Siddiqui, S.; Yadav, V. K.; Niazi, P.; Kumar, P.; Alghamdi, S. *Mycobiology* **2024**, *52* (6), 335–387.

(12) Jinna, Z.; Khan, T.; Kanwal, N.; Zhenji, W. *Cell. Mol. Biol.* **2025**, *71* (5), 43–48.

(13) Stroe, M. C.; Gao, J.; Pitz, M.; Fischer, R. *Mol. Microbiol.* **2024**, *121* (1), 18–25.

(14) Lin, P.; Fu, Z.; Li, Y.; Yoon, Y. J.; Lee, S. Y. *Nat. Prod. Rep.* **2026**.

(15) Chooi, Y.-H.; Tang, Y. *J. Org. Chem.* **2012**, *77* (22), 9933–9953.

(16) Hertweck, C. *Angew. Chem. Int. Ed.* **2009**, *48* (26), 4688–4716.

(17) Chooi, Y.-H.; Tang, Y. *J. Org. Chem.* **2012**, *77* (22), 9933–9953.

(18) Fujii, I. *J. Antibiot. 2010 635* **2010**, *63* (5), 207–218.

(19) Wang, J.; Deng, Z.; Liang, J.; Wang, Z. *Nat. Prod. Rep.* **2023**, *40* (9), 1498–1520.

(20) Minami, A.; Ugai, T.; Ozaki, T.; Oikawa, H. *Sci. Rep.* **2020**, *10* (1), 13556.

(21) Gao, X.; Haynes, S. W.; Ames, B. D.; Wang, P.; Vien, L. P.; Walsh, C. T.; Tang, Y. *Nat. Chem. Biol. 2012 810* **2012**, *8* (10), 823–830.

(22) Brown, A. S.; Calcott, M. J.; Owen, J. G.; Ackerley, D. F. **2018**.

(23) Cox, R. J. *Org. Biomol. Chem.* **2007**, *5* (13), 2010–2026.

(24) Zhang, J. M.; Wang, H. H.; Liu, X.; Hu, C. H.; Zou, Y. *J. Am. Chem. Soc.* **2020**, *142* (4), 1957–1965.

(25) D, B.; C, H. *Chembiochem Eur. J. Chem. Biol.* **2013**, *14* (1), 28–42.

(26) Wolff, P. B.; Nielsen, M. L.; Slot, J. C.; Andersen, L. N.; Petersen, L. M.; Isbrandt, T.; Holm, D. K.; Mortensen, U. H.; Nødvig, C. S.; Larsen, T. O.; Hoof, J. B. *Fungal Genet. Biol.* **2020**, *139*, 103378.

(27) Huang, X.; Zhang, W.; Tang, S.; Wei, S.; Lu, X. *Angew. Chem. - Int. Ed.* **2020**, *59* (11), 4349–4353.

(28) Schalk, F.; Fricke, J.; Um, S.; Conlon, B. H.; Maus, H.; Jäger, N.; Heinzel, T.; Schirmeister, T.; Poulsen, M.; Beemelmanns, C. *RSC Adv.* **2021**, *11* (31), 18748–18756.

(29) Clevenger, K. D.; Bok, J. W.; Ye, R.; Miley, G. P.; Verdan, M. H.; Velk, T.; Chen, C.; Yang, K. H.; Robey, M. T.; Gao, P.; Lamprecht, M.; Thomas, P. M.; Islam, M. N.; Palmer, J. M.; Wu, C. C.; Keller, N. P.; Kelleher, N. L. *Nat. Chem. Biol. 2017 138* **2017**, *13* (8), 895–901.

(30) Sivanathan, S.; Scherkenbeck, J. *Molecules* **2014**, *19* (8), 12368.

(31) Moore, R. E. *J. Ind. Microbiol. Biotechnol.* **1996**, *16* (2), 134–143.

(32) Negi, B.; Kumar, D.; Rawat, D. S. *Curr. Protein Pept. Sci.* **2016**, *18* (9), 885–904.

(33) Nihei, K.; Itoh, H.; Hashimoto, K.; Miyairi, K.; Okuno, T. *Biosci. Biotechnol. Biochem.* **1998**, *62* (5), 858–863.

(34) Liu, S. X.; Ou-Yang, S. Y.; Lu, Y. F.; Guo, C. L.; Dai, S. Y.; Li, C.; Yu, T. Y.; Pei, Y. H. *Front. Microbiol.* **2023**, *14*, 1276928.

(35) Wang, X.; Gong, X.; Li, P.; Lai, D.; Zhou, L. *Mol.* **2018**, *23* (1), 169.

(36) Ratnayake, R.; Fremlin, L. J.; Lacey, E.; Gill, J. H.; Capon, R. J. *J. Nat. Prod.* **2008**, *71* (3), 403–408.

(37) Feng, L.; Wang, J.; Liu, S.; Zhang, X.-J.; Bi, Q.-R.; Hu, Y.-Y.; Wang, Z.; Tan, N.-H. *J Nat. Prod.* **2019**, *82*, 12.

(38) Lee, C.; Gong, J.; Kim, J.; Ko, H.; An, S.; Bang, S.; Deyrup, S. T.; Noh, M.; Shim, S. H. *J. Nat. Prod.* **2022**, *85* (3), 501–510.

(39) Feng, Y.; Blunt, J. W.; Cole, A. L. J.; Munro, M. H. G. *Org. Lett.* **2002**, *4* (12), 2095–2096.

(40) Feng, J.; Liu, J.; Ye, T. *Org. Lett.* **2025**, *27* (33), 9299–9303.

(41) Seo, C.; Yim, J. H.; Lee, H. K.; Park, S. M.; Sohn, J. H.; Oh, H. *Tetrahedron Lett.* **2008**, *49* (1), 29–31.

(42) Lee, S.; Jeong, S. Y.; Nguyen, D. L.; So, J. E.; Kim, K. H.; Kim, J. H.; Han, S. J.; Suh, S. S.; Lee, J. H.; Youn, U. J. *Metabolites* **2022**, *12* (2), 141.

(43) Bang, S.; Lee, C.; Kim, S.; Song, J. H.; Kang, K. S.; Deyrup, S. T.; Nam, S. J.; Xia, X.; Shim, S. H. *J. Org. Chem.* **2019**, *84* (17), 10999–11006.

(44) Guo, W.; Wang, S.; Li, N.; Li, F.; Zhu, T.; Gu, Q.; Guo, P.; Li, D. *J. Nat. Prod.* **2018**, *81* (4), 1050–1054.

(45) Silber, J.; Ohlendorf, B.; Labes, A.; Näther, C.; Imhoff, J. F. *J. Nat. Prod.* **2013**, *76* (8), 1461–1467.

(46) Tonoi, T.; Ikeda, M.; Sato, T.; Inohana, T.; Kawahara, R.; Murata, T.; Shiina, I. *Eur. J. Org. Chem.* **2020**, *2020* (32), 5119–5125.

(47) Reddy, K. M.; Shashidhar, J.; Pottireddygari, G. R.; Ghosh, S. *Tetrahedron Lett.* **2011**, *52* (45), 5987–5991.

(48) Zhao, Z.; Wu, Y.; Li, Y. *Chin. J. Chem.* **2017**, *35* (7), 1185–1194.

(49) Ghosh, A. K.; Xu, C. X. *Org. Lett.* **2009**, *11* (9), 1963–1966.

(50) Storm, P. A.; Herbst, D. A.; Maier, T.; Townsend, C. A. *Cell Chem. Biol.* **2017**, *24* (3), 316–325.

(51) Zhang, T.; Feng, J.; Oikawa, H.; Guo, Y.; Ye, T. *Precis. Chem.* **2024**, *2* (3), 120–126.

(52) Takino, J.; Kotani, A.; Ozaki, T.; Peng, W.; Yu, J.; Guo, Y.; Mochizuki, S.; Akimitsu, K.; Hashimoto, M.; Ye, T.; Minami, A.; Oikawa, H. *Angew. Chem. - Int. Ed.* **2021**, *60* (43), 23403–23411.

(53) Xiao, Y.; Liu, J.; Jiang, Y.; Guo, Y.; Ye, T. *Molecules* **2024**, *29* (15), 3599.

(54) Verekar, S. A.; Mishra, P. D.; Sreekumar, E. S.; Deshmukh, S. K.; Fiebig, H. H.; Kelter, G.; Maier, A. *J. Antibiot. 2014 6710* **2014**, *67* (10), 697–701.

(55) Chen, J.; Jiang, Y.; Yan, J.; Xu, C.; Ye, T. *Molecules* **2023**, *28* (20), 7194.

(56) García-Fortanet, J.; Carda, M.; Alberto Marco, J. *Tetrahedron* **2007**, *63* (49), 12131–12137.

(57) Wang, P.; Kim, Y.-J.; Navarro-Villalobos, M.; Rohde, B. D.; Gin, D. Y. *J. Am. Chem. Soc.* **2005**, *127* (10), 3256–3257.

(58) Kaneda, M.; Inuki, S.; Ohno, H.; Oishi, S. *J. Org. Chem.* **2018**, *83* (6), 3047–3060.

(59) Elmarrouni, A.; Fukuda, A.; Heras, M.; Arseniyadis, S.; Cossy, J. *J. Org. Chem.* **2010**, *75* (24), 8478–8486.

(60) Yadav, J. S.; Amrutapu, S. K.; Pabbaraja, S. *ChemistrySelect* **2017**, *2* (5), 1850–1853.

(61) Takino, J.; Kotani, A.; Ozaki, T.; Peng, W.; Yu, J.; Guo, Y.; Mochizuki, S.; Akimitsu, K.; Hashimoto, M.; Ye, T.; Minami, A.; Oikawa, H. *Angew. Chem. Int. Ed.* **2021**, *60* (43), 23403–23411.

(62) Szókán, G.; Mezö, G.; Hudecz, F. *J. Chromatogr. A* **1988**, *444*, 115–122.

(63) Huang, Y.; Wu, Y. *Chin. J. Chem.* **2011**, *29* (6), 1185–1191.

(64) Kaushal, M.; Kumar, A.; Gamal, H.; Mthembu, S. N.; Sheyi, R.; Kou, X.; de la Torre, B. G.; Albericio, F. *Chemistry–Methods* **2025**, *5* (11), e202500035.

(65) Wang, J.; Berglund, M. R.; Braden, T.; Embry, M. C.; Johnson, M. D.; Groskreutz, S. R.; Sayyed, F. B.; Tsukanov, S. V.; White, T. D.; Jalan, A.; Seibert, K. D.; Kopach, M. E. *ACS Omega* **2022**, *7* (50), 46809–46824.

(66) Goolcharran, C.; Borchardt, R. T. *J. Pharm. Sci.* **1998**, *87* (3), 283–288.

(67) Zhang, Z.; Raab, S. A.; Hales, D. A.; Clemmer, D. E. *J. Phys. Chem. B* **2021**, *125* (11), 2952–2959.

CHAPTER II.

Evaluating Macrolactamization Approaches Towards the Synthesis of the Immunomodulide Core

2.1 An introduction to The Synthesis of Macrocycles

2.1.1 Macrocyclization: General Challenges and Strategies

Macrocycles are broadly defined as ring systems containing 12 or more atoms and are among the most frequently encountered structural motifs in biologically active natural products and pharmaceutical agents[1–4]. The cyclic architecture benefits from inherent conformational restriction that pre-organizes the molecule for target binding, often translating to enhanced potency and selectivity relative to acyclic analogues[5–7]. In the context of macrocyclic peptides and depsipeptides specifically, cyclization has been shown to improve metabolic stability and membrane permeability relative to their linear counterparts[3,4,8–10]. These beneficial properties have driven considerable interest in this compound class within medicinal chemistry, and innovative solutions to constructing macrocyclic structures is ever-growing[11–15].

The construction of these macrocyclic ring systems, however, presents several challenges that vary considerably with ring size. The most pervasive difficulty is the competition between intramolecular cyclization and intermolecular oligomerization or polymerization[16], which is most often addressed with high dilution technique or syringe-pump (slow addition) protocols. Both techniques bias towards intramolecular cyclization by reducing the probability of bimolecular mechanisms[17,18].

Outside of this challenge, 12 membered ring systems, which constitute the macrocyclic core central to this thesis, occupy a particularly difficult niche of ring-size space[17,19,20]. Sitting at the boundary between medium rings (8–11 atoms) and true macrocycles (12 or more atoms), these systems combine the transannular strain and conformational rigidity characteristic of medium rings with the entropic cost of organizing a longer chain for cyclization[21,22]. Transannular interactions, arising from steric and electronic repulsions across the ring interior, impose significant strain energy in rings of this size, and the rigid linear precursor chain increase the difficulty of the reactive termini being brought into proximity[22]. Taken together, these factors mean that 12-membered ring-forming reactions can prove more challenging than their larger macrocyclic counterparts and underscore the synthetic difficulty central to this chapter.

2.1.2 Common Macrocyclization Methods

Several strategic approaches to macrocyclization have been developed to address these challenges, with the optimal choice depending on the functional groups available for ring closure

and the sensitivity of the substrate. The most widely employed methods in the context of polyketide and depsipeptide natural product synthesis are macrolactonization, macrolactamization, and ring-closing metathesis[23,24]. Macrolactamization and lactonization will be discussed below as they pertain to the functional groups present in the scaffold of interest.

Macrolactonization, which proceeds through formation of a macrocyclic ester bond characteristic to depsipeptides, has been extensively developed for the synthesis of polyketide-derived natural products and represents one of the most reliable macrocyclization strategies available. Amongst the most common and robust macrolactonization strategies are the Yamaguchi protocol, employing 2,4,6-trichlorobenzoyl chloride (TCBC) and DMAP under high-dilution conditions, and the Corey-Nicolaou method, utilizing 2,2'-dipyridyl disulfide and triphenylphosphine, with both serve to activate the acid by increasing its electrophilicity[25]. The Mitsunobu reaction offers a mechanistically distinct alternative, activating the alcohol rather than the acid through formation of an alkoxyphosphonium intermediate. Given that the carboxylate serves as the nucleophile in a S_N2 displacement, its α centre is left undisturbed, making this strategy particularly beneficial in acid coupling partners that are sensitive to stereochemical scrambling at their α centre[26].

Macrolactamization instead proceeds through ring closure via an amide bond and primarily operates on the basis of acid activation as the mechanism for bond formation. Relative to macrolactonization, amide bond-forming reactions benefit from the inherently greater nucleophilicity of amines compared to alcohols, generally affording more robust and higher yielding cyclizations[27]. Given the pervasiveness of amide bonds across pharmaceutically relevant compounds, extensive methodology has been developed for their construction, and several peptide coupling reagents have emerged as being particularly well-suited for macrolactamization. These include uronium-based reagents such as HATU and HBTU, phosphonium-based reagents such as PyBOP and PyAOP, and reagents developed specifically for macrocyclic applications such as T3P (propylphosphonic anhydride). Among these, HATU in combination with a hindered base such as DIPEA or collidine is among the most commonly employed for macrolactamization in complex molecule synthesis, offering a balance of reactivity and selectivity[28].

Ring-closing metathesis has also been employed as a macrocyclization strategy in natural product synthesis through the use of ruthenium-based Grubbs catalysts[29–31]. Its application, however, is contingent on the presence of suitable olefin handles in the substrate or the synthetic

viability of reducing the resulting alkene late-stage. As this strategy falls outside the scope of the present work, it will not be elaborated further.

2.1.3 Macrolactamization in the Synthesis of Cyclic Tridepsipeptides

As discussed across **Sections 1.2.5** and **1.2.6**, macrolactamization routes (route B and C) emerged as the ring-closing strategies of choice across synthetic campaigns directed toward the 12-membered cyclic tridepsipeptide family, as all macrolactonization (route A) attempts resulted in unsuccessful cyclization. Yamaguchi-mediated macrolactonization failed to deliver the desired macrocycle in Yadavs acremolide campaign under all conditions tested[17,32], and Reddy's initial route A attempt in the stereocalpin A series was similarly unproductive[33]. In both cases, the conformational demands of the linear substrates and were identified as the contributing factors leading to these failures.

Conversely, macrolactamization either via route B and C yielded successful macrocyclic products across the synthetic attempts within this class[33–39], albeit with two well-documented challenges of epimerization at the activated amino acid α-centre and competitive diketopiperazine formation (**Figure 2.1**).

These challenges, elaborated in **Section 1.2.6**, are directly relevant to the immunomodulide scaffold: route B ring-closure has been repeatedly associated with epimerization at the α-centre of the *C*-terminal aromatic amino acid, particularly in L/L-configured substrates where the steric demand of the *N*-methyl amine nucleophile prolongs the lifetime of the activated ester intermediate[33,37,38]. Route C, though more broadly successful, remained susceptible to competitive

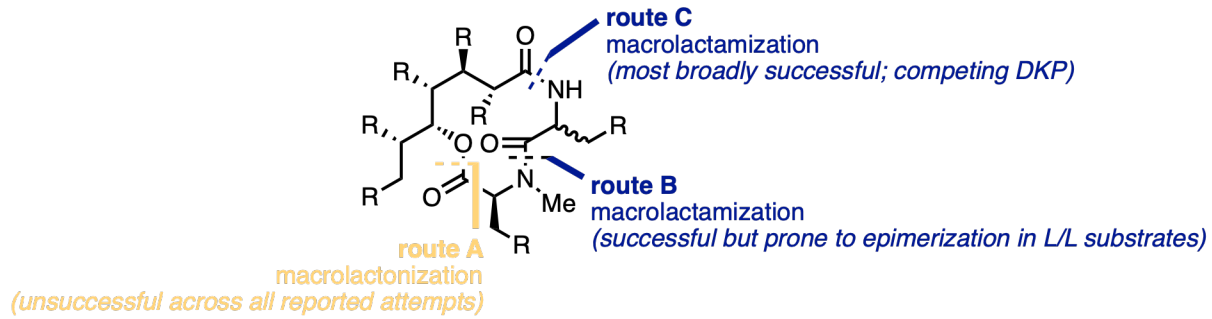


Figure 2.1. Summary of macrocyclization outcomes across routes A-C in reported synthetic campaigns targeting the 12-membered cyclic tridepsipeptide scaffold. Yellow denotes unsuccessful or complication-prone disconnections.

DKP formation upon *N*-terminal deprotection, arising from the conformational biasing imposed by the conserved *N*-alkyl amino acid residue (**Figure 2.1**)[35,39,40].

These precedents directly inform the macrolactamization strategy investigated in this chapter, and the design of the model system described in **Section 2.2** reflects the lessons drawn from the synthetic campaigns reviewed.

2.1.4 Retrosynthetic Analysis and Model System Design

Given the synthetic risk associated with macrocyclization at a late stage in a fully elaborated substrate and the well-documented complications associated with both route B and route C ring-closure within the tridepsipeptides[33,37–40], a model system approach was adopted to evaluate the feasibility of each synthetic approach.

The model system (**2.1**) employed in this work centred on the replacement of the PKS fragment of immunomodulide with commercially available 1,5-pentanediol (**2.2**), which preserves the chain length and the hydroxyl handle required for ester bond formation while eliminating the four unresolved stereocenters of the polypropionate unit (see immunomodulide (**1.165**), **Figure 2.2**). This simplification carries two practical benefits. First, it allows the macrocyclization routes B and C to be evaluated independently of the stereochemical ambiguities in the PKS fragment of immunomodulide, where any complications arising at the ring-closing step can be attributed to the disconnection site itself rather than to substrate-specific conformational effects. Second, and perhaps more consequentially, the simplified PKS fragment can later be exchanged for the fully

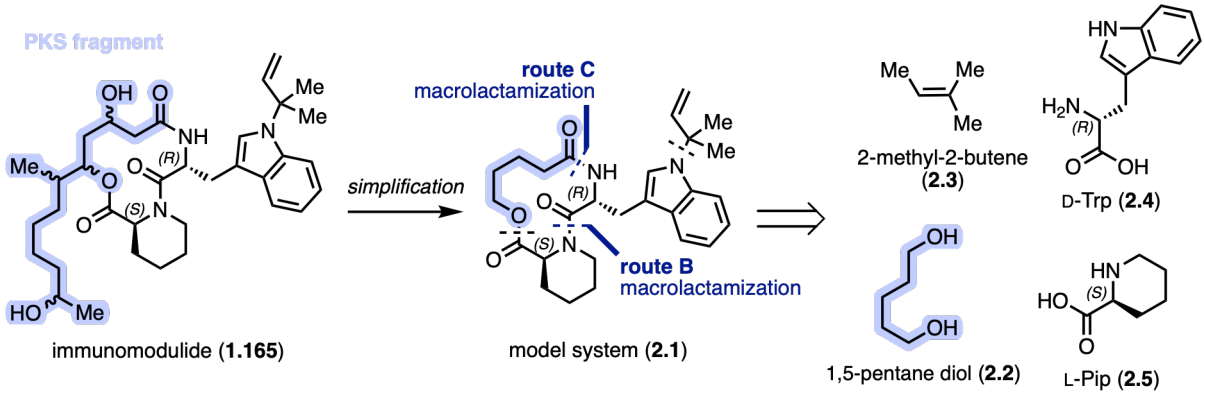


Figure 2.2 Simplification strategy of Immunomodulide (**1.165**) to the model system (**2.1**) and summary of retrosynthesis with key macrolactamization strategies (route B and C) annotated in dark blue.

elaborated polypropionate unit (PKS fragment) once the correct stereochemical configuration has been established. In isolating the challenges of selecting a ring-closure strategy and elucidating the configuration of the elusive stereochemical centres, the synthesis of immunomodulide could be de-risked significantly. The NRPS fragment, comprising D-tryptophan (D-Trp) and L-pipecolic acid (L-Pip), was retained in its native form. These residues define the amide bond geometry and steric environment at the ring-closing site, making them structurally critical elements for evaluating both ring-closure feasibility and more importantly, its susceptibility to epimerization and DKP formation. The reverse prenylation of the Trp indole nitrogen, a structurally distinctive feature of immunomodulide, was initially excluded from the macrolactamization analysis, and later investigated in the context of route C, as described in **Section 2.3.2**.

The retrosynthetic analysis developed for the model system is summarized in **Figure 2.2** and **Figure 2.3.** Disconnection of the 12-membered macrolactam at route B reveals a linear intermediate precursor (**2.6**) in which the activated D-Trp carboxylic acid is positioned for amide bond formation with the secondary amine of L-Pip. Disconnection at route C instead reveals a linear precursor (**2.7**) in which the activated acid handle of the simplified PKS fragment is positioned for amide bond formation with the primary amine of D-Trp. In both cases, the linear precursor is assembled from three components: 1,5-pentanediol (**2.2**) as the PKS surrogate, D-Trp (**2.4**), and L-Pip (**2.5**), connected through a combination of ester and amide bond-forming reactions prior to macrolactamization.

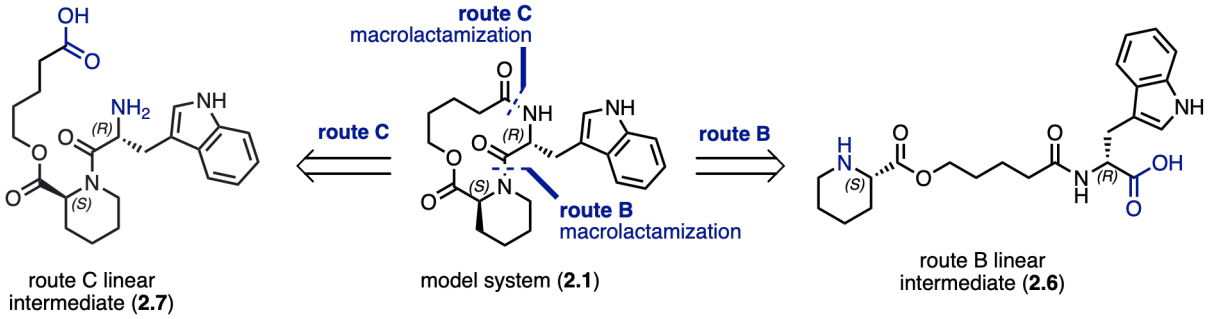


Figure 2.3. Summary of retrosynthetic analysis of model system (**2.1**) via route B and route C

2.2 Results and Discussion

2.2.1 Macrolactamization via Route B

Exploration of macrolactamization via route B began with a gram-scale Boc protection of commercially available L-pipecolic acid, affording L-Boc-pipecolic acid (**2.8**) in near-quantitative yield. Mono-tertbutyldimethylsilyl (TBS)-protected diol (**2.9**) was then prepared according to protocol by Wilke B. et al.[8], after which it was condensed onto **2.8** in an esterification reaction (EDC, DMAP) to form ester **2.10** in 62.7% yield. Deprotection of TBS was achieved by (1M) TBAF in THF after which primary alcohol **2.11** was subject to two rounds of successive oxidation, via the Parikh Doering reaction followed by the Pinnick reaction, to obtain acid **2.13**. D-Trp-OBn (**2.15a**) was elaborated in two steps carrying out an esterification (EDC, DMAP) with Boc-D-Trp followed by an acid-mediated deprotection.

2.15a was subsequently used in an amide bond forming step (HATU, DIPEA) to join the three subunits that constituted our model system, producing **2.16a** in moderate yields (62%). Finally, deprotection of the benzyl ester via hydrogenation (H_2, Pd/C) followed by an acid-mediated Boc-deprotection afforded our linear substrate **2.6a,** ready for ring-closure. With this compound in hand, we sought to explore the feasibility of a diastereoselective macrolactamization.

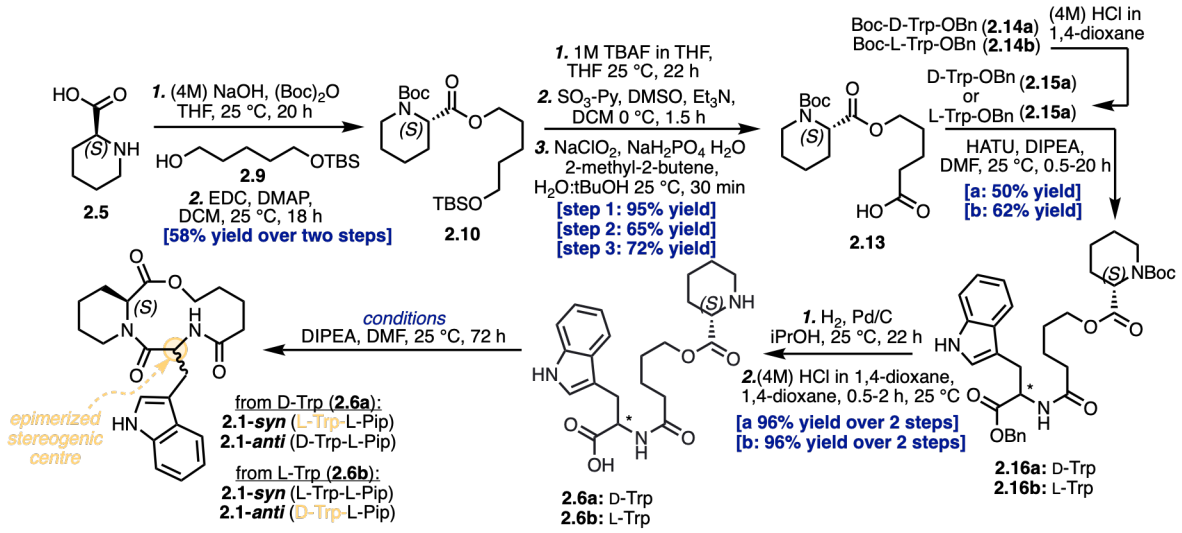


Figure 2.4. Synthesis of linear precursors **2.6a/b** and their macrolactamization via route B to afford diastereomeric macrolactams **2.1-*syn*** and **2.1-*anti***. Series diverge at the amide coupling step through coupling with either D-Trp-OBn (**2.15a**) or L-Trp-OBn (**2.15b**); epimerization at the Trp α-centre during macrolactamization affords two macrolactam diastereomers across both series. Epimerized stereocenters indicated in orange.

A parallel sequence employing L-Trp in place of D-Trp was subsequently carried out to access the L/L-configured linear precursor **2.6b (Figure 2.4)**, given the elevated susceptibility to epimerization documented for L/L substrates amongst HA23 and the stereocalpin class[33,38,41].

The prospect of epimerization at the activated L or D-Trp α-centre under ring-closing conditions was recognized as the principal stereochemical risk of this route. This concern is well-precedented in the reports on the synthesis of HA23 by Feng[37] and those of stereocalpin A by Ghosh[38] and subsequently that of Reddy and coworkers[33] (see **Section 1.2.6**). The sterically encumbered secondary amine of L-Pip relative to a primary amine nucleophile in route C compounds this issue, as reduced rates of bond formation extends intermediate lifetime and amplifies epimerization risk. Within this context, HATU has emerged as a particularly effective coupling reagent for macrolactamization reactions involving sterically encumbered *N*-alkyl amino acid nucleophiles, with its superiority attributed to the HOAt-derived active ester. The 7-aza-hydroxybenzotriazole moiety of HOAt operates through two complementary mechanisms: suppression of *N*-acylurea formation, which diverts productive activation toward ester formation, and hydrogen-bond-mediated assistance of the incoming nucleophile through coordination with the adjacent pyridine nitrogen[28,42]. However, the effectiveness of any given coupling reagent in preserving stereochemical integrity during macrolactamization is well established to be highly substrate-dependent, with ring size, side-chain steric demand, and the relative configuration of the amino acid residues all contributing to the diastereomeric outcome of ring closure[43].

To evaluate the influence of activation mode on the diastereoselectivity of macrolactamization, a systematic screen of amide bond-forming reagents was conducted on linear substrates **2.6a** and **2.6b.** The screen encompassed carbodiimide- (EDCl), uronium- (HATU, HBTU), and phosphonium-based (PyBOP, T3P) coupling reagents, as well as HOBt and OxymaPure as additives, to probe the effect of differential activation on the diastereomeric ratio of the macrolactam product. All reactions were performed in dilute solution (0.025 M, DMF) with DIPEA as base to favor intramolecular cyclization and suppress oligomerization, a known pitfall of macrocyclization attempts (see **Section 2.1.1**).The diastereomeric ratio (d.r.) of macrolactam products arising from each series (a: D-Trp and b: L-Trp, **Figure 2.4**) are identified as either **2.1-*syn*** and **2.1-*anti***, where *syn* and *anti* denote macrocycles bearing amino acid residues of uniform (L/L) or mixed configurations (D/L), respectively. Product distribution was evaluated by LC-MS by monitoring the distinct retention times of each diastereomer detected in the extracted ion

chromatograms corresponding to the $[M+H]^+$ mass (XIC of *m/z* 398.20). In the initial macrolactamization attempt employing the L/L-configured (b series) linear precursor **2.6b**, the major product was isolated and subjected to Marfey's analysis (see **Figure 2.9-2.12**) and NMR characterization, which together confirmed that epimerization had occurred at the Trp α-centre, establishing the major product as the D/L-configured **2.1-*anti***. The retention time and NMR data of **2.1-*anti*** were subsequently used as reference points to assign the diastereomeric identity of all macrolactam products obtained across the remainder of the screen.

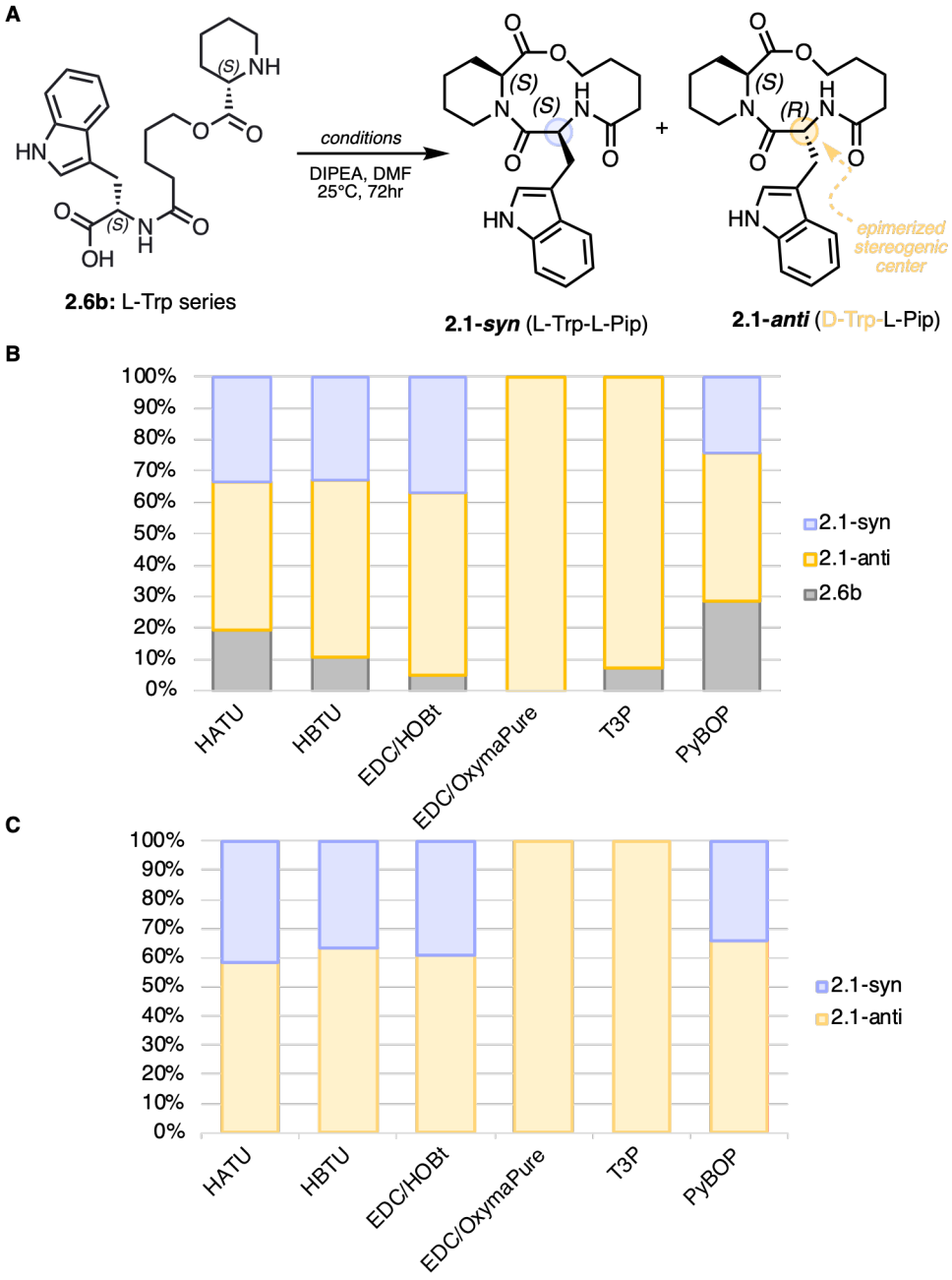


Figure 2.5. Coupling reagent screen for macrolactamization via route B. (A) General reaction scheme showing macrolactamization of linear precursors **2.6b** (L-Trp series) under dilute conditions (0.025 M, DMF, DIPEA, 25 °C, 72 h). (B) Diastereomeric ratio (*anti*:*syn*) of macrolactam products **2.1-*anti*** (epimerized product, in yellow) and **2.1-*syn*** across all coupling reagents screened, determined by area under the curve (AUC) of extracted ion chromatography peaks (XIC, *m/z* 398.20, $[M+H]^+$; retention times 10.36 and 10.48 min). (C) Reaction profile and product distribution expressed as relative AUC from extracted ion chromatograms of macrolactam products (as in B) and recovered starting material (*m/z* 416.2, $[M+H]^+$; retention time 7.28 min).

Initial screening of the L/L-configured linear precursor **2.6b** revealed that all coupling reagents tested resulted in epimerization at the *C*-terminal α-centre to some degree, with **2.1-*anti*** favoured as the major product in every case (**Figure 2.5**). This outcome was not surprising given the well-established thermodynamic preference for conformationally mixed macrocycles bearing alternating D/L stereocenters over their all-L counterparts[44–46]. The extent of epimerization was found to be strongly dependent on the coupling reagent employed (**Figure 2.5B and C**). EDC/OxymaPure and T3P afforded **2.1-*anti*** as the sole detectable product with full consumption of **2.6b**, indicating complete epimerization at the Trp α-centre prior to ring closure under these conditions. HATU, HBTU and PyBOP consistently delivered **2.1-*anti*** as the major product, albeit with low diastereoselectivity (dr ~ 6:4 **2.1-*anti***: **2.1-*syn***; **Figure 2.5C**) and with moderate-to-good consumption of starting material (**Figure 2.5B**), indicating that uronium and phosphonium-based OBt or OAt esters are insufficient at outpacing epimerization. EDC/HOBt provided higher consumption of **2.6b** compared to the uronium-based entries consumption (**Figure 2.5B**) with a dr broadly consistent with the uronium-based entries, suggesting that despite proceeding via a mechanistically distinct *O*-acylisourea pathway, the OBt active ester generated in situ presents a similar profile to that of the uronium-derived OBt esters once formed. Notably, no reagent in the **2.6b** series was capable of suppressing epimerization sufficiently to deliver **2.1-*syn*** as the major product, a result that is consistent with the degree of epimerization being governed by the competition between ring closure and α-centre scrambling at the activated intermediate stage. It should be noted that, as starting material and product ionize with different efficiencies under ESI conditions, the relative AUC values reported do not reflect absolute molar conversion. Rather, the total AUC at 72 h was normalized to 100% and subdivided into starting material and product

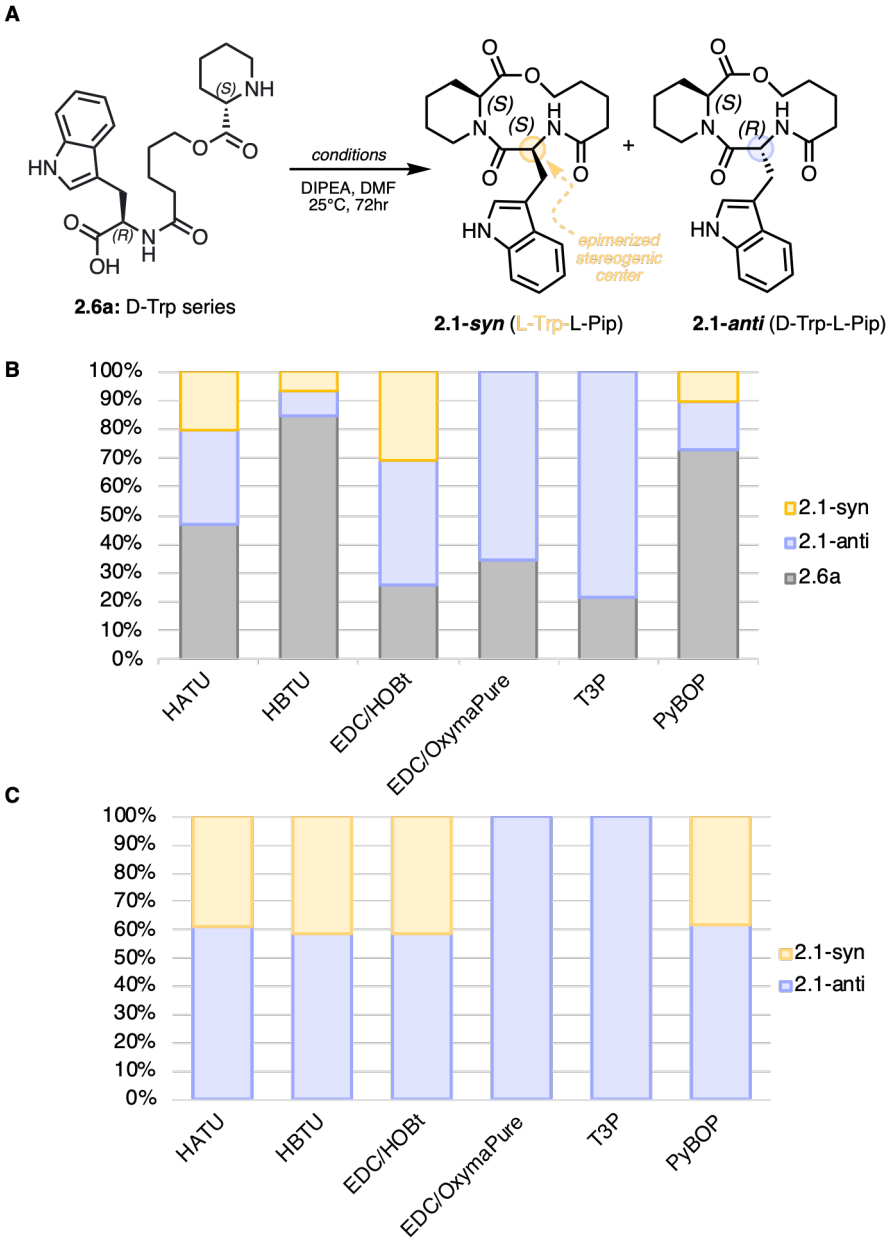


Figure 2.6. Coupling reagent screen for macrolactamization via route B. (A) General reaction scheme showing macrolactamization of linear precursors **2.6a** (D-Trp series) under dilute conditions (0.025 M, DMF, DIPEA, 25 °C, 72 h). (B) Diastereomeric ratio (*anti*:*syn*) of macrolactam products **2.1-*anti*** and **2.1-*syn*** (epimerized product, in yellow) across all coupling reagents screened, determined by area under the curve (AUC) of extracted ion chromatography peaks (XIC, *m/z* 398.20, $[M+H]^+$; retention times 10.36 and 10.48 min). (C) Reaction profile and product distribution expressed as relative AUC from extracted ion chromatograms of macrolactam products (as in B) and recovered starting material (*m/z* 416.2, $[M+H]^+$; retention time 7.28 min).

contributions to provide a semi-quantitative assessment of relative consumption and product

distribution across entries.

Macrolactamization of the D/L-configured linear precursor **2.6a** interestingly, delivered similar reaction profiles when evaluated under identical conditions. Consistent with the behavior observed for **2.6b**, EDC/OxymaPure and T3P afforded **2.1-*anti*** as the exclusive product with good starting material consumption, while EDC/HOBt, was similarly comparable in starting material consumption, while not successful at controlling dr significantly (dr ratio of 6:4). HATU again showed poor consumption with a moderate dr of approximately 6:4 (*anti*:*syn*), while HBTU and PyBOP both displayed minimal starting material consumption (remaining starting material AUC: 84% and 72% of total, respectively, for the **2.16a** series; **Figure 2.6B**), with dr's across the products similar to those of HATU. The similarity in product distribution obtained from both **2.6a** and **2.6b** across all coupling reagents tested is notable and will be discussed further below.

The most consequential finding of the screen was the consistent *anti*-selectivity observed across all coupling reagents and both linear precursors. In no entry across either series was the *syn* diastereoisomer obtained as the major product, demonstrating that macrolactamization via route B is inherently *anti*-selective under all activation conditions evaluated, and that epimerization precedes ring-closure. While EDC/OxymaPure and T3P afforded **2.1-*anti*** as the sole detectable product in both series, all other reagents delivered the *anti* diastereoisomer as the major product with a consistent dr of approximately 6:4 (*anti*:*syn*) and variable consumption of starting material. OxymaPure generates a more electrophilic active ester than HOBt owing to its superior leaving group ability[47,48], and T3P operates through a mechanistically distinct phosphate-carboxylate mixed anhydride intermediate of comparable electrophilicity[49]. In **2.7b**, the exclusive formation of **2.1-*anti*** under EDC/OxymaPure and T3P conditions is consistent with complete epimerization at the Trp α-centre prior to ring closure, driven by the high reactivity of their respective activated intermediates. In the case of **2.7a**, where the D/L configuration is already present in the linear precursor, the same *anti*-selective outcome is observed, consistent with ring closure occurring predominantly from the D/L epimeric activated intermediate regardless of starting configuration. This suggests that the product ratio is governed primarily by the properties of the activated intermediate rather than by the starting configuration of the linear precursor.

From the results obtained, three conclusions can be made: Firstly, the dr outcome is consistent with epimerization at the Trp α-centre occurring at the stage of activation, prior to ring closure. Given that the diastereomeric outcome remains consistent across both conformationally

distinct starting materials, it is suggested that the activated intermediate is the primary determinant of stereochemical outcome rather than the configuration of the linear precursor. Secondly, it is proposed that the degree of epimerization is governed by the reactivity of the activated intermediate: EDC/OxymaPure and T3P drive epimerization to completion, affording **2.1-*anti*** as the sole detectable product, while less reactive intermediates afford a consistent dr of approximately 6:4 (*anti*:*syn*) across both precursors. Thirdly, preferential *anti*-lactam formation across the screen suggests that conformational differences upon activation contribute to a different capacity to adopt the geometry required for ring closure within the 12-membered macrolactam.

These observations are consistent with the epimerization tendencies of L/L-precursors reported under route B conditions across the synthetic campaigns of HA23[37] and stereocalpin A[33,38] where the anti-lactam product is reported to form preferentially over the syn-product. However, they contrast the results reported by HA23, in which testing of macrolactamization of the D/L-configured linear precursor proceeded without epimerization, though the moderate yields reported may not fully account for epimerized product lost during isolation. Finally, these results extend reported findings by demonstrating that the epimerization outcome is governed by the reactivity of the activated intermediate rather than the configuration of the linear precursor.

The incomplete consumption of starting material and moderate dr achieved even under the best conditions identified indicate that route B does not offer a practical diastereoselective entry to the target macrolactam. These findings motivated the exploration of the alternative ring-closing disconnection described in **Section 2.3**.

2.2.2 Macrolactamization via Route C

Exploration of macrolactamization via route C began with the preparation of methyl ester **2.18,** in near-quantitative yield (99%) via TMSCl-mediated esterification of L-pipecolic acid in MeOH. Amide bond formation (HATU, DIPEA) with either Boc-D-Trp (**2.17a**) or Boc-L-Trp (**2.17b**), followed by LiOH-mediated saponification of the methyl ester, afforded Trp-Pip dipeptides **2.20a** and **2.20b** respectively, each bearing a free acid handle for subsequent elaboration. Esterification of **2.20a** and **2.20b** with fragment **2.22** (via EDC, DMAP) then furnished the fully assembled linear precursors **2.7a** and **2.7b**, though this step was later identified as the source of epimerization, as confirmed by ^{1}H NMR and Marfey's analysis (**Figure 2.9 - 2.12**) of the resulting macrocyclic products. Global Boc deprotection was achieved with TFA in DCM

and monitored by LC-MS; a counter-ion exchange with HCl was found necessary prior to ring closure, as TFA adduct formation was observed as a competitive side reaction in an initial screen. Macrolactamization of **2.7a** and **2.7b** under standard conditions (HATU, DIPEA) afforded separatable diastereomeric product pairs in each case, with *anti*:*syn* ratios of 3:1 and 2:1 arising from the **2.7a** and **2.7b** racemates respectively.

In contrast to route B, macrolactamization via route C was initially appealing in that ring closure does not proceed through activation of an epimerizable centre. Nevertheless, diastereomer formation was observed upon ring closure of both linear precursors, prompting investigation into its origin. Marfey's analysis (**Figure 2.9 - 2.12**) of each diastereomeric product pair unambiguously attributed epimerization to the early-stage esterification step rather than to the macrolactamization itself. In the case of linear precursor **2.7a**, the major product **2.1-*anti*** was assigned the D-Trp-L-Pip configuration, while the minor product **2.1-*syn'*** bore the D-Trp-D-Pip configuration, confirming that **2.1-*syn'*** arose from epimerization at the stereocenter of Pip during esterification. Product distribution, determined at the stage of the macrocycle purification, favoured the

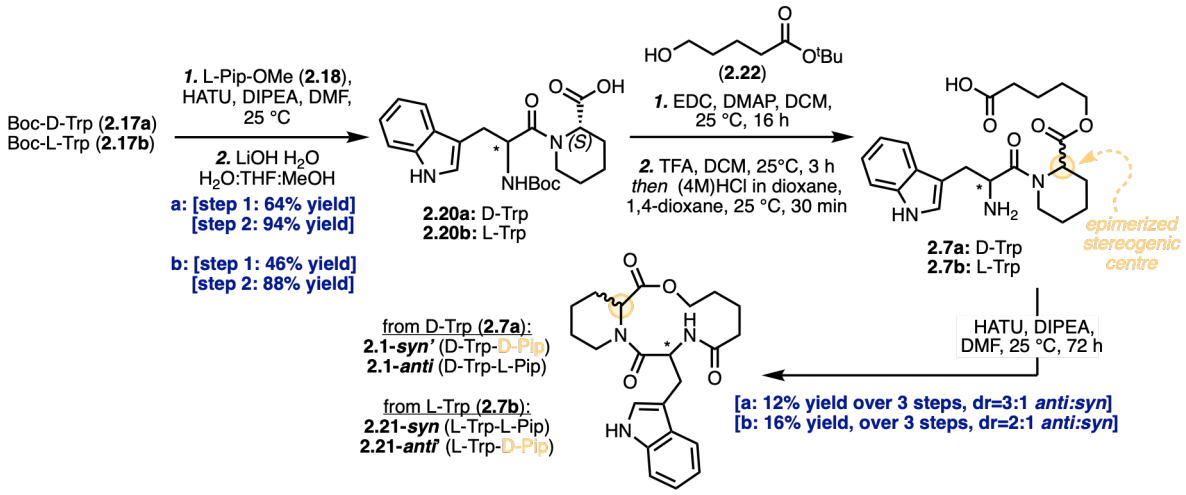


Figure 2.7. Synthesis of linear precursors **2.7a** and **2.7b** and their macrolactamization via route C to afford diastereomeric macrocycles **2.1-*syn'***, **2.1-*anti*** and **2.1-*syn*** and **2.1-*anti'***, respectively. Epimerization at the pipecolic α-centre during EDC-mediated esterification affords two macrolactam diastereomers across both series. Epimerized stereocenters indicated in yellow.

conformationally mixed *anti* macrocycle in a 3:1 ratio. An analogous outcome was observed for linear precursor **2.7b**: **2.1-*anti'*** was assigned the L-Trp-D-Pip configuration and **2.1-*syn*** the L-Trp-L-Pip configuration, with the *anti* product, again arising from α-Pip epimerization during the early-

stage esterification. Product distribution once again favored the *anti* macrocycle, in a 2:1 ratio. The stereochemical relatedness of all four macrocyclic isomers was confirmed by NMR, where the enantiomer relationship between **2.1-*anti*** and **2.1-*anti'*,** as well as that of **2.1-*syn*** and **2.1-*syn'*** was expectedly indistinguishable upon spectral analysis (see **Spectra 2.29** for comparison).

Although route B was initially promising in circumventing epimerization at the ring-closing step, Marfey's analysis (**Figure 2.9 - 2.12**) did revealed that the esterification about the Pipecolic acid-terminus of the dipeptide constitutes the critical stereochemical liability of this approach. Notably, the analogous esterification of Boc-L-Pip (**2.8**) with the mono-protected alcohol fragment (**2.9**) in route B proceeds without detectable epimerization in generating ester **2.10** under otherwise comparable EDC/DMAP conditions (**Figure 2.4**), highlighting the role of the carbamate *N*-protecting group in suppressing epimerization. This difference is attributed to the greater susceptibility of *N*-acyl-protected amino acids to oxazolone-mediated epimerization relative to their *N*-carbamate-protected counterparts, a well-precedented phenomenon in peptide chemistry[50].

It is worth noting that esterification reactions across this bond within synthetic campaigns directed toward the cyclic tridepsipeptide class have generally employed either Yamaguchi-mediated esterification conditions or stepwise installation of individual amino acid residues as their N-carbamate protected forms[32–39]. Interestingly, no campaign reported epimerization as a liability of their strategy for esterification when the Yamaguchi was employed on the dipeptide directly[33,34]. However, in their report towards the synthesis of stereocalpin A, Zhao et al. utilized DCC-mediated esterification conditions to install their dipeptide fragment onto the PKS unit and reported only low yields and competitive lactone formation as liabilities of this approach (see Chapter I)[40].

In a final attempt to circumvent epimerization at the esterification step, the Mitsunobu reaction was investigated as a stereochemically retentive alternative to EDC-mediated coupling at this stage. Initial attempts employing an unprotected indole were unsuccessful, necessitating "*N*-indole protection" achieved in the form of reverse prenylation before proceeding. With the protected substrate (**2.24**) in hand, Mitsunobu esterification proceeded smoothly, affording **2.25** in 81% yield and global deprotection followed by macrolactamization afforded the desired

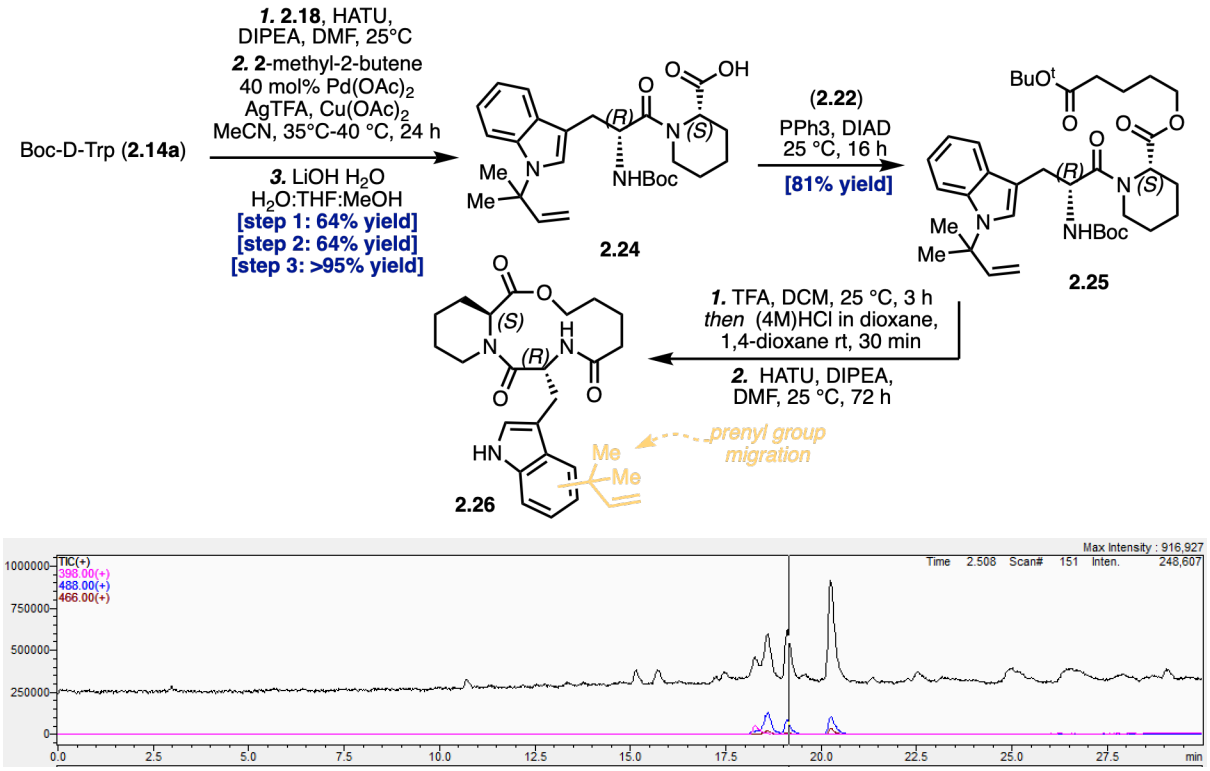


Figure 2.8. Mitsunobu-based route C macrolactamization employing reverse prenylated D-Trp-L-Pip dipeptide **2.24**. Migration of the reverse prenyl group under acidic conditions, affords **2.26** (XIC *m/z* 466 for $[M+H]^+$ and 488 $[M+Na]^+$) bearing a rearranged prenyl substituent. Prenyl migration indicated in yellow on scheme and blue/brown in MS chromatogram. **m/z* 398 corresponds to a pervasive column impurity.

macrolactam (**Figure 2.8**). However, by LC-MS it was apparent that migration of the reverse prenyl group had occurred about the indole ring under the strongly acidic deprotection conditions employed, as the resulting chromatogram resulted in multiple peaks on the XIC corresponding in mass to the expected product **2.26** (*m/z* 466 for [M+H]+ and 488 [M+Na]+) **(Figure 2.8).** An attempted HPLC purification of each **2.26** regioisomer product from this ring-closing reaction was

unsuccessful. This rearrangement, which is presumed to occur via an acid-accelerated aza-Cope rearrangement has been documented for both reverse- and regular-prenylated indole nitrogens and phenols under both Lewis and Brønsted acid conditions[51–54], and ultimately rendered the desired reverse prenylated product inaccessible via this sequence. Nevertheless, these results served as a useful proof of concept: the Mitsunobu esterification was demonstrated to be a reliable and stereochemically robust alternative to carbodiimide-mediated esterification at this stage, fully preserving the integrity of the pipecolic α-centre. The observed prenyl migration under strongly acidic conditions (TFA/HCl) further established an important constraint on protecting group strategy that is addressed in the context of the total synthesis in Chapter IV.

2.3 Conclusions and Application to the Total Synthesis of Immunomodulide

The macrolactamization studies described in this chapter were undertaken to evaluate the feasibility of routes B and C as ring-closing strategies for the synthesis of immunomodulide and to identify the stereochemical liabilities associated with each disconnection prior to their application to a fully elaborated substrate.

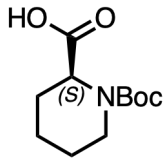
Route B macrolactamization was found to be inherently *anti*-selective under all activation conditions evaluated, with epimerization at the Trp α-centre occurring at the stage of activation and preceding ring closure regardless of the starting linear precursor configuration. The product distribution was found to be governed primarily by the reactivity of the activated intermediate rather than the configuration of the linear precursor, with more electrophilic intermediates driving epimerization to completion and less reactive intermediates affording a consistent anti:syn ratio of approximately 6:4. These results establish that diastereoselective access to the native syn macrolactam via route B is not achievable under standard coupling conditions, and that this disconnection is therefore not suitable as a ring-closing strategy for the total synthesis of immunomodulide.

In Route C, although macrolactamization was found to proceed smoothly, epimerization at the stage of esterification mediated by carbodiimide reagents (EDC) and implemented on the dipeptide fragment, resulted in significant epimerization detected upon ring-closure. However, the Mitsunobu reaction was demonstrated to be a stereochemically robust alternative, preserving the integrity of the pipecolic α-centre. Furthermore, its application to a reverse prenylated model substrate revealed a second important consideration for the forward synthesis. Strongly acidic Boc

deprotection conditions were found to promote migration of the reverse prenyl group on the Trp indole nitrogen, establishing that milder deprotection conditions will be required in any synthetic sequence bearing this functionality. It should also be noted that competitive diketopiperazine formation was not monitored for in the present model study and cannot be excluded as a liability of route C ring closure under the conditions evaluated. Given the precedent established in the stereocalpin campaign by Zhao et al.[40] (Chapter I), where DKP formation was attributed to the conformational bias imposed by the *N*-alkyl Phe residue upon *N*-terminal deprotection, its assessment in the context of the fully elaborated immunomodulide substrate remains an important consideration for the forward synthesis.

Taken together, these findings establish route C as the more promising disconnection for the total synthesis of immunomodulide, with two key constraints identified for the forward synthesis: esterification-stage epimerization must be suppressed through the adoption of Yamaguchi or Mitsunobu conditions in place of carbodiimide-mediated coupling, and mild Boc deprotection conditions must be employed to preserve the reverse prenyl group. These considerations inform the synthetic strategy described in Chapter VI.

2.4 Experimental Section



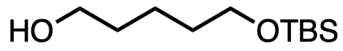
Preparation of (S)-1-(tert-butoxycarbonyl)piperidine-2-carboxylic acid (2.8): Prepared as per reference[55]. To a vigorously stirred solution of commercially available *L*-pipecolic acid (2.0 g, 15.5 mmol, 1.0 eq.) and triethylamine (2.4 mL, 17.2 mmol, 1.1 eq.) in methanol (22 mL) at 50°C was added di-tert-butyl dicarbonate (6.8 g, 31.0 mmol, 2.0 eq.). The mixture was stirred at room temperature for 1h after which the solvent was removed under reduced pressure. The crude was suspended in EtOAc washed with saturated $NaHCO_3$ (2 x15mL) and brine (1x15 mL). Aqueous layers were combined, brought to pH 2.0 with (2M) HCl and immediately extracted in EtOAc (3 x 5 mL). The combined organic layers were washed with dilute (1M) HCl , dried over Na_2SO_4, filtered and evaporated to give compound **2.8** as a white solid (3.3 g, 14.5 mmol, 93%). Spectral data are consistent with reported values[55].

TLC (10%MeOH/DCM, Ninhydrin): R_f=0.55

^{1}H NMR (400 MHz, $CDCl_3$) δ 10.61 (s, 1H), 4.82 (d, 1H), 3.95 (dd, 1H), 2.92 (dd, 1H), 2.21 (t, *J* = 14.2 Hz, 1H), 1.72 – 1.55 (m, 3H), 1.45 – 1.39 (m, 9H), 1.41 – 1.37 (m, 1H), 1.33 – 1.19 (m, 1H).

^{13}C NMR (101 MHz, $CDCl_3$) δ 177.64, 156.16, 80.31, 54.71, 53.58, 42.10, 41.04, 28.34, 26.62, 24.76, 20.80.

HRMS (ESI-TOF) *m/z* calcd for $C_{11}H_{19}NO_4Na$ [M+Na]+ 252.1184, found 252.1212.



Preparation of5-((tert-butyldimethylsilyl)oxy)pentan-1-ol (2.9): Prepared as per reference[2]. A flame-dried flask equipped with a Teflon-coated magnetic stir bar was charged with a 160 mL of a 3:1 ratio of Hexanes to acetonitrile and commercially available 1,5-pentane diol (2.0 mL, 19.2 mmol, 1.0 eq.). The flask was flushed with $N_{2(g)}$ after which TBSCl (2.9 g, 19.2 mmol, 1.0 eq.) was added and the reaction was left to stir vigorously overnight at room temperature. The mixture was quenched with a saturated solution of NH_4Cl, and extracted with EtOAc (15 mL x 2) and

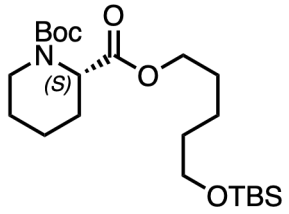
washed with brine (2 x 15 mL). The organic phases were combined, dried over Na_2SO_4, filtered and concentrated. The product was purified via gel flash chromatography (10 -15% EtOAc/Hexane) yielding pure compound **2.9** (2.7 g, 12.5 mmol, 65%) as a clear colourless oil. Spectral data are consistent with reported values[3]

TLC (30% EtOAc/Hexane, CAM stained): R_f=0.29

^{1}H NMR (400 MHz, $CDCl_3$) δ 3.63 (dq, *J* = 17.8, 6.5 Hz, 4H), 1.63 – 1.54 (m, 3H), 1.41 (dtd, *J* = 8.9, 6.3, 2.5 Hz, 2H), 0.89 (s, 9H), 0.04 (s, 6H).

^{13}C NMR (101 MHz, $CDCl_3$) δ 63.14, 62.96, 62.80, 32.50, 32.36, 25.99(3C), 22.03, (2C) -5.27.

HRMS (ESI-TOF) *m/z* calcd for $C_{11}H_{26}O_2SiNa$ [M+Na]+ 241.1602, found 241.1600.



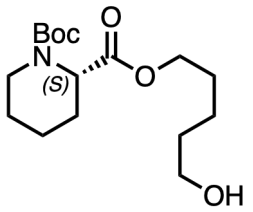
Preparation of 1-(tert-butyl) 2-(5-((tert-butyldimethylsilyl)oxy)pentyl) (S)-piperidine-1,2-dicarboxylatecompound (2.10): A flame-dried flask equipped with a Teflon-coated magnetic stir bar was charged with acid **2.8** (3.3 g, 14.5 mmol, 1.0 eq), EDC (5.5 g, 29 mmol, 2.0 eq), DMAP (175 mg, 1.4 mmol, 0.1 eq), and 40 mL of DCM. After 15 minutes of stirring, alcohol **2.9** (3.5 g, 15.8 mmol, 1.1 eq) was added portion-wise. Stirring was continued at room temperature for 16 h after which saturated $NaHCO_3$ was added. The mixture was transferred to a separatory funnel, extracted with DCM (3 x 15 mL) and washed with brine (2 x 15 mL). The organic layers were combined, dried over Na_2SO_4, filtered, and concentrated under reduced pressure. Purification by silica gel flash chromatography (10% EtOAc/Hexane) yielded pure compound **2.10** (3.6 g, 9.02 mmol, 63%) as a clear colourless oil.

TLC (10%EtOAc/Hexane): R_f=0.25

^{1}H NMR (600 MHz, $CDCl_3$) δ 4.90 – 4.65 (m, 1H), 4.14 (t, *J* = 6.6 Hz, 2H), 4.05 – 3.87 (m, 1H), 3.60 (t, *J* = 6.4 Hz, 2H), 2.99 – 2.84 (m, 1H), 2.22 (d, *J* = 15.0 Hz, 1H), 1.68 – 1.64 (m, 4H), 1.53 (dd, *J* = 8.5, 6.5 Hz, 2H), 1.46 (s, 9H), 1.42 – 1.35 (m, 4H), 1.22 (ddd, *J* = 17.0, 9.5, 3.9 Hz, 1H), 0.88 (s, 9H), 0.04 (s, 6H).

^{13}C NMR (151 MHz, $CDCl_3$) δ (1C) 172.33 & 172.12, (1C) 156.12 & 155.65, 105.65, 80.01, 65.18, 63.07, (1C) 55.08 & 53.98, (1C) 42.26 & 41.23, 32.50, 28.64, (3C) 28.50, (3C) 26.09, (1C) 25.00 & 24.76, 22.46, (1C) 21.01 & 20.82, 18.49, (2C) -5.16.

HRMS (ESI-TOF) *m/z* calcd for $C_{22}H_{43}NO_5SiNa$ + [M+Na]+ 452.2799, found 452.2808.



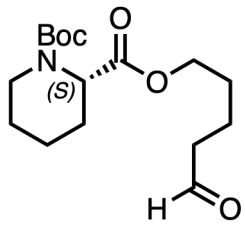
Preparation of 1-(tert-butyl) 2-(5-hydroxypentyl) (S)-piperidine-1,2-dicarboxylate (2.11): In a round bottom flask equipped with a Teflon-coated magnetic stir bar, TBS-protected alcohol, **2.10** (3.26 g, 9.0 mmol, 1.0 eq.) was dissolve in 10.5 mL of THF. The suspension was cooled to 0°C, after which (1M) TBAF in THF (13.5 mL, 15.5 mmol, 1.5 eq.) was added dropwise. Mixture was left to stir and warm to room temperature for 3hr, after which it was diluted with Et_2O (10 mL), washed with H_2O (10 mL) and brine (10 mL). Organic fractions were combined, dried over Na_2SO_4, filtered, and concentrated under reduced pressure. Purification by silica gel flash chromatography (50% EtOAc/Hexane) yielded pure compound **2.11** (1.9 g, 6.0 mmol, 67.2%) as a clear colourless oil. TBS-protected starting material **2.10** (0.98 g, 2.7 mmol) was also recovered from purification.

TLC (50%EtOAc/Hexane, Ninhydrin stained): R_f=0.35

^{1}H NMR (400 MHz, $CDCl_3$) δ 4.92 – 4.62 (m, 1H), 4.14 (td, *J* = 6.5, 2.9 Hz, 2H), 3.96 (dd, 1H), 3.64 (t, *J* = 6.4 Hz, 2H), 2.89 (dt, 1H), 2.20 (t, 1H), 1.70 – 1.55 (m, 7H), 1.44 (d, *J* = 7.4 Hz, 9H), 1.23 (tt, *J* = 13.5, 4.1 Hz, 1H).

^{13}C NMR (151 MHz, $CDCl_3$) δ (1C)172.32 & 172.15, 156.14, 105.67, 80.10, 65.07, 62.66, (1C) 55.11 & 53.95, (1C) 42.27 & 41.29, 32.32, (3C) 28.49, 26.86, (1C) 24.96, 24.72, 22.29, (1C) 20.95 & 20.80.

HRMS (ESI-TOF) *m/z* calcd for $C_{16}H_{29}NO_5Na$ [M+Na]+ 338.1950, found 338.1943.



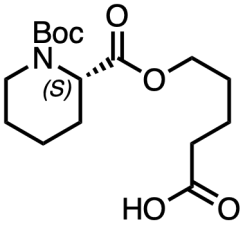
Preparation of 1-(tert-butyl) 2-(5-oxopentyl) (S)-piperidine-1,2-dicarboxylate (2.12): In a flame-dried round bottom flask equipped with a Teflon-coated magnetic stir bar, DMSO (12.0 mL, 0.5 M) was added to a spinning mixture of 6 mL DCM and sulfur trioxide pyridine complex (2.9 g, 18.2 mmol, 3.0 eq). This mixture was left to activate for 15 min at room temperature. In a separate flame-dried round bottom flask, alcohol **2.11** (1.9 g, 6.1 mmol, 1.0 eq.) was dissolved in 6mL DCM and DIPEA (3.2 g, 18.2 mmol, 3.0 eq.) at 0°C, after which the activated DMSO complex was added to this mixture drop-wise via syringe. Reaction progress was monitored via TLC and quenched at 1.5 h with the addition of saturated NH_4Cl. The reaction mixture was diluted with DCM (10 mL) and washed with H_2O (10 mL) and brine (10 mL). Organic fractions were combined, dried over Na_2SO_4, filtered, and concentrated under reduced pressure. Crude product **2.12** was obtained as a clear colourless oil (1.2 g, 3.92 mmol) and telescoped to the next step.

TLC (50%EtOAc/Hexane, Ninhydrin stained): R_f=0.68

^{1}H NMR (400 MHz, $CDCl_3$) δ 9.76 (t, *J* = 1.5 Hz, 1H), 4.78 (d, 1H), 4.14 (t, *J* = 5.7 Hz, 2H), 3.96 (dd, 1H), 2.89 (dt, 1H), 2.48 (q, 2H), 2.24 – 2.13 (m, 1H), 1.73 – 1.57 (m, 7H), 1.43 (d, 9H), 1.40 – 1.37 (m, 1H), 1.27 – 1.14 (m, 1H).

^{13}C NMR (101 MHz, $CDCl_3$) δ 201.98, 172.08, 156.08, 80.06, 64.52, (1C) 55.05 & 53.92, 43.37, (1C) 42.25 & 41.22, (3C) 28.47, 28.21, 26.89, 24.93, 20.95, 18.63.

HRMS (ESI-TOF) m/z calcd for $C_{16}H_{27}NO_5Na$ [M+Na]+ 336.1805, found 336.1787.



Preparation of (S)-5-((1-(tert-butoxycarbonyl)piperidine-2-carbonyl)oxy)pentanoic acid (2.13): Crude aldehyde **2.12** (1.2 g, 3.92 mmol, 1.0 eq.) was dissolved in 20.1 mL of ^{t}BuOH. Suspension was cooled to 0°C, after which 2-methyl-2-butene (2.6 mL, 24.2 mmol, 6.0 eq.) was

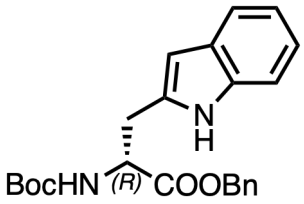
added. In a separate flask, a solution of $NaClO_2$ (730.8 mg, 8.1 mmol, 2.0 eq.) and NaH_2PO_4 monohydrate (1.9 g, 16.3 mmol, 4.0 eq.) was prepared in 20.2 mL of H_2O and was added drop-wise to the first mixture. The final mixture was left to stir and warm to room temperature over 30 min after which H_2O was added and the pH was adjusted to 5.0 with acetic acid. The mixture was washed with Et_2O (3x), the organic fractions were combined, dried over $MgSO_4$, filtered, and concentrated under reduced pressure. Crude product **(2.13)**, isolated as a clear oil (954 mg, 2.9 mmol, 72%), was sufficiently pure to use in the next step without purification.

TLC (50%EtOAc/Hexane, Ninhydrin stained): R_f=0.35

^{1}H NMR (400 MHz, $CDCl_3$) δ 8.07 (s, 1H), 4.77 (d, 1H), 4.13 (t, 2H), 3.96 (dd, 1H), 2.88 (dt, 1H), 2.36 (t, 2H), 2.17 (t, *J* = 9.1 Hz, 1H), 1.73 – 1.56 (m, 7H), 1.45 – 1.38 (m, 9H), 1.21 (tt, *J* = 13.2, 3.7 Hz, 1H).

^{13}C NMR (101 MHz, $CDCl_3$) δ 178.67, (1C) 172.18 & 172.04, (1C) 156.16 &155.68, 80.23, 64.55, (1C) 55.02 & 53.92, (1C) 42.23 & 41.22, 33.50, (3C) 28.42, 26.83, (1C) 24.87 & 24.66, 21.26, (1C) 20.89 & 20.74.

HRMS (ESI-TOF) *m/z* calcd for $C_{16}H_{27}NO_6Na$ [M+Na]+ 353.1716, found 352.1736.



Preparation of benzyl (tert-butoxycarbonyl)-D-tryptophanate (2.14a): A flame-dried flask equipped with a Teflon-coated magnetic stir bar was charged with commercially available Boc-D-Trp-OH (4.0 g, 10.1 mmol, 1.0 eq.), EDC (3.9 g, 20.3 mmol, 2.0 eq.), DMAP (124 mg, 1.0 mmol, 0.1 eq.), and 51 mL of DCM. After 15 min of stirring, commercially available benzyl alcohol (1.2 mL, 11.2 mmol, 1.1 eq) was added portion-wise. Stirring was continued at room temperature for 16 hr after which saturated $NaHCO_3$ was added. The mixture was transferred to a separatory funnel, extracted with DCM (3 x15 mL) and washed with brine (2 x 15 mL). The organic layers were combined, dried over Na_2SO_4, filtered, and concentrated under reduced pressure. Purification by silica gel flash chromatography (30% Acetone/Hexane) yielded a mixture of **2.14a** and excess benzyl alcohol. Excess benzyl alcohol was removed via recrystallization in cold hexanes. Pure

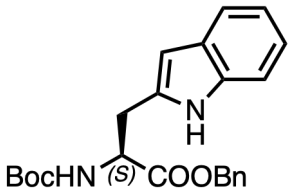
2.14a was obtained as a white powder (3.1 g, 6.1 mmol, 60%). Spectral data are consistent with reported values[56].

TLC (30%Acetone/Hexane): R_f=0.31

^{1}H NMR (400 MHz, $CDCl_3$) δ 8.08 (s, 1H), 7.55 (d, *J* = 7.9 Hz, 1H), 7.36 – 7.31 (m, 4H), 7.25 – 7.22 (m, 2H), 7.19 (dt, *J* = 7.0, 1.2 Hz, 1H), 7.11 (tdd, *J* = 8.0, 7.1, 1.1 Hz, 1H), 6.80 (s, 1H), 5.09 (d, *J* = 10.1 Hz, 2H), 4.70 (q, 1H), 3.30 (d, *J* = 5.5 Hz, 2H), 1.43 (s, 9H).

^{13}C NMR (101 MHz, $CDCl_3$) δ 172.31, 155.39, 136.21, 135.43, 128.63, 128.52, 128.44, 123.00, 122.22, 119.67, 118.85, 111.30, 110.00, 79.98, 67.16, 54.44, 28.43, 28.06.

HRMS (ESI-TOF) *m/z* calcd for $C_{23}H_{26}N_2O_4Na$ [M+Na]+ 417.1790, found 417.1799.



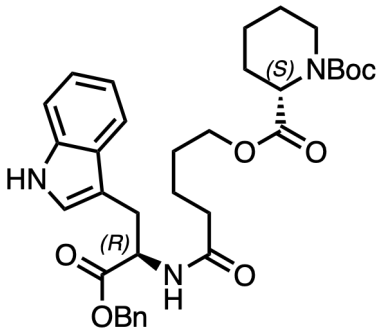
Preparation of benzyl (tert-butoxycarbonyl)-L-tryptophanate (2.14b): follows same procedure as **preparation of compound 2.14a.** Pure **2.14b** was obtained as a white powder (507 mg, 1.7 mmol, 65%). Spectral data are consistent with reported values[57].

TLC (30%Acetone/Hexane): R_f=0.38

^{1}H NMR (400 MHz, $CDCl_3$) δ 8.10 (s, 1H), 7.56 (d, 1H), 7.37 – 7.31 (m, 4H), 7.26 – 7.22 (m, 2H), 7.19 (dt, *J* = 7.0, 1.2 Hz, 1H), 7.11 (dt, *J* = 7.0, 1.1 Hz, 1H), 6.80 (s, 1H), 5.09 (d, *J* = 10.3 Hz, 2H), 4.71 (q, *J* = 5.5 Hz, 1H), 3.30 (d, *J* = 5.6 Hz, 2H), 1.43 (s, 9H).

^{13}C NMR (101 MHz, $CDCl_3$) δ 172.29, 155.38, 136.21, 135.47, 128.65, 128.56, 128.46, 122.97, 122.28, 119.73, 118.92, 111.27, 110.14, 79.98, 67.17, 54.44, 28.45, 28.10.

HRMS (ESI-TOF) *m/z* calcd for $C_{23}H_{26}N_2O_4Na$ [M+Na]+ 417.1790, found 417.1821.



Preparation of 2-(5-(((R)-1-(benzyloxy)-3-(1H-indol-3-yl)-1-oxopropan-2-yl)amino)-5-oxopentyl) 1-(tert-butyl) (S)-piperidine-1,2-dicarboxylate (2.16a): A round-bottom flask equipped with a Teflon-coated magnetic stir bar was charged with **2.14a** (237 mg, 0.47 mmol) in 1mL of 1,4-dioxane. To this suspension, 1 mL of (4M) HCl in dioxane was added dropwise and the mixture was left to stir for 2 h. Solvents were removed under vacuum to afford crude amine product **2.15a,** which was used in next step without further purification.

A flame-dried flask equipped with a Teflon-coated magnetic stir bar and flushed with $N_{2(g)}$ was charged with acid **2.13** (595 mg, 1.8 mmol, 1.0 eq), and dissolved in 4.5 mL DMF. HATU (1.0 g, 2.7 mmol, 1.5 eq.) was added portion-wise at 0 °C and left to stir for 30 min. In a second round-bottom flask flushed with $N_{2(g)}$, amine **2.15a** (0.9 g, 2.7 mmol, 1.5 eq.) was suspended in 1.5 mL of DMF, and DIPEA (0.63 mL, 3.6 mmol, 2.0 eq.) was added dropwise. After activation of **2.13** was complete (solution turns cloudy white from transparent clear), the mixture of amine **2.15a** and DIPEA in DMF was transferred via syringe through dropwise addition to the activated ester at 0 °C. The final mixture was left to stir overnight and warm to room temperature. Once reaction was complete, quenching was achieved with (1M) HCl (dropwise addition) followed by immediate extraction with EtOAc. The organic layer was washed saturated $NaHCO_3$ (5 mL x 3), brine (5 mL x 2), dried over $MgSO_4$, filtered and concentrated under reduced pressure. Purification by silica gel flash chromatography (30% Acetone/Hexane) yielded pure compound **2.16a** (545.2 mg, 0.9 mmol, 50%) as an orange oil.

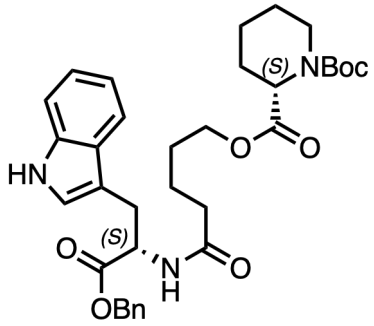
TLC (30%Acetone/Hexane): 0.24

^{1}H NMR (600 MHz, $CDCl_3$) δ 8.88 – 8.46 (m, 1H), 7.50 (d, *J* = 7.8 Hz, 1H), 7.34 (s, 4H), 7.28 – 7.26 (m, 2H), 7.17 (t, *J* = 7.6 Hz, 1H), 7.08 (t, *J* = 7.5 Hz, 1H), 6.84 – 6.78 (m, 1H), 6.14 – 6.03 (m, 1H), 5.14 – 5.08 (m, 2H), 4.98 (dt, *J* = 7.8, 5.7 Hz, 1H), 4.90 – 4.66 (m, 1H), 4.13 – 3.88 (m,

3H), 3.34 (dd, *J* = 14.8, 5.5 Hz, 1H), 3.29 (dd, *J* = 14.9, 5.9 Hz, 1H), 2.91 (dt, 1H), 2.19 – 2.11 (m, 3H), 1.69 – 1.53 (m, 7H), 1.49 – 1.42 (m, 9H), 1.41 – 1.36 (m, 1H), 1.20 (dt, *J* = 13.5, 3.6 Hz, 1H).

^{13}C NMR (151 MHz, $CDCl_3$) δ 172.21, 172.01, (1C)156.30 & 155.81, 136.30, 135.38, 128.70, 128.55, 127.73, 123.19, 123.07, 122.16, 119.59, 118.53, 111.50, 109.78, 109.58, 80.27, 67.30, (1C) 64.79 & 64.66, (1C) 55.10 & 53.91, 53.00, 52.91, (1C) 42.25 & 41.32, 35.87, (3C) 28.50, (1C) 28.21 & 27.94, 27.67, 26.86, (1C) 24.89 & 24.68, 21.97, 20.83.

HRMS (ESI-TOF) *m/z* calcd for $C_{34}H_{43}N_3O_7Na$ [M+Na]+ 628.2972, found 628.2999.



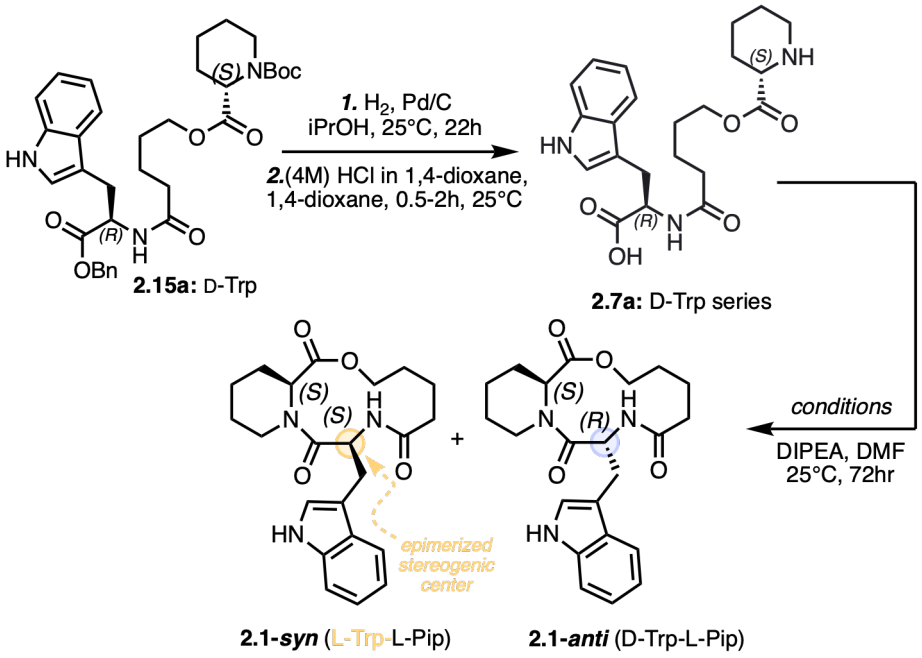
Preparation of compound (2.16b): follows same procedure as **preparation of compound (2.16a)** using **2.14b** to generate the **2.15a** amine. Purification by silica gel flash chromatography (30% Acetone/Hexane) yielded pure compound **(2.16b)** (682 mg, 1.2 mmol, 62%) as an orange oil.

TLC (30%Acetone/Hexane): R_f=0.22

^{1}H NMR (400 MHz, $CDCl_3$) δ 8.86 – 8.55 (m, 1H), 7.49 (d, *J* = 7.9 Hz, 1H), 7.37 – 7.33 (m, 4H), 7.30 – 7.26 (m, 2H), 7.17 (t, *J* = 7.5 Hz, 1H), 7.08 (t, *J* = 7.5 Hz, 1H), 6.81 (d, *J* = 2.4 Hz, 1H), 6.06 (d, *J* = 9.0 Hz, 1H), 5.11 (s, 2H), 4.98 (dt, *J* = 8.0, 5.6 Hz, 1H), 4.91 – 4.66 (m, 1H), 4.10 – 3.90 (m, 3H), 3.32 (qd, *J* = 14.9, 5.6 Hz, 2H), 2.90 (dt, 1H), 2.21 – 2.12 (m, 3H), 1.69 – 1.54 (m, 7H), 1.46 (d, *J* = 14.9 Hz, 9H), 1.37 (dt, *J* = 13.0, 4.1 Hz, 1H), 1.27 – 1.17 (m, 1H).

13C NMR (151 MHz, CDCl3) δ 172.19, 172.04, 156.30, 136.31, 135.39, (2C) 128.73, 128.59, (2C) 128.58, 127.75, 123.17, 122.19, 119.62, 118.56, 111.51, 109.61, 80.30, 67.35, 64.80, (1C) 55.14 & 53.91, 52.99, 52.82, (1C) 42.27 & 41.35, (1C) 36.00 & 35.91, (3C) 28.51, (1C) 28.27 & 28.00, 27.66, 26.88, (1C) 24.92 & 24.68, (1C) 22.15 & 21.99, 20.85

HRMS (ESI-TOF) *m/z* calcd for $C_{34}H_{43}N_3O_7Na$ [M+Na]+ 628.2976, found 628.2999.

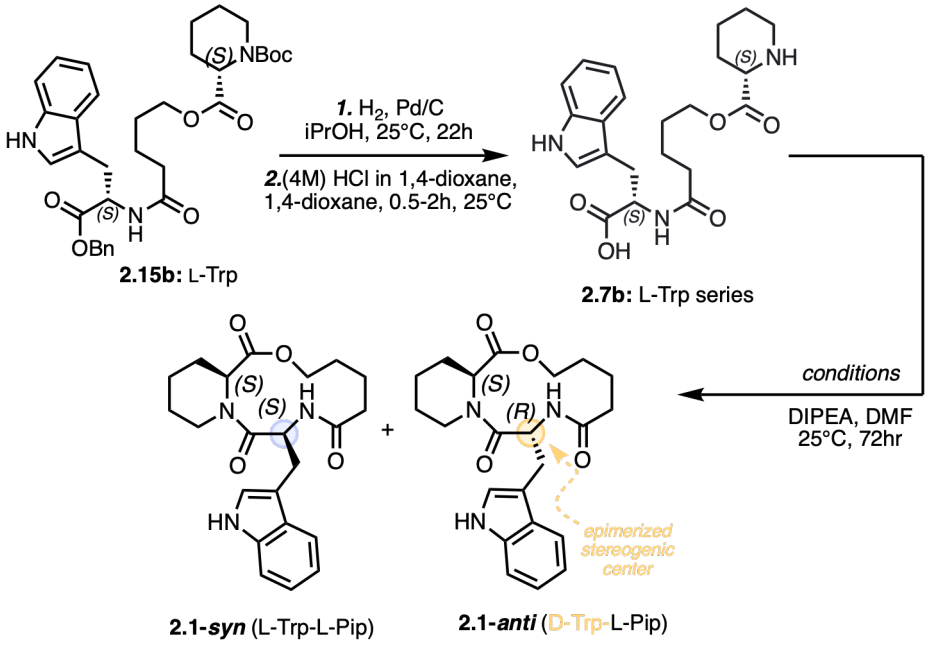


General Procedure (GP2.1) for macrolactamization screen.

Preparation of (9S,15aS)-9-((1H-indol-3-yl)methyl)decahydropyrido[2,1-c][1]oxa[4,7]diazacyclododecine-1,7,10(12H)-trione (2.1-*syn*) and **(9R,15aS)-9-((1H-indol-3-yl)methyl)decahydropyrido[2,1-c][1]oxa[4,7]diazacyclododecine-1,7,10(12H)-trione (2.1-*anti*). 2.16a** (61 mg, 0.1 mmol, 1.0 eq.) was suspended in 0.5 mL of iPrOH in a round-bottom flask equipped with a teflon-coated magnetic stir bar. To this suspension, Pd/C (10%) (1 mg, 0.01 mmol, 0.1 eq.) was added after which the flask was flushed with $H_{2(g)}$, sealed, and left to stir overnight at room temperature until reaction is complete. The mixture was filtered through celite and washed with iPrOH, after which the combined filtrate was concentrated under reduced pressure. The crude product acid was isolated as a transparent yellow oil and used in the next step without purification.

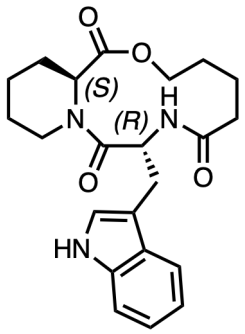
A round-bottom flask equipped with a Teflon-coated magnetic stir bar was charged with crude acid in 0.2 mL of 1,4-dioxane. To this suspension, 0.2 mL of (4M) HCl in dioxane was added dropwise and the mixture was left to stir for 30 min. Solvents were removed under vacuum to afford crude product **2.6a** as a dark purple powder (39.8 mg, 0.96 mmol, 96%) which was used in next step without further purification.

Six separate 1-dram vials equipped with a Teflon-coated magnetic stir bars and flushed with $N_{2(g)}$ were each charged with **2.6a** (5 mg, 0.01 mmol, 1.0 eq.), and dissolved in 0.44 mL DMF. One coupling reagent (HATU, HBTU, EDC/HOBt, EDC/OxymaPure, T3P, PyBOP) (0.033 mmol, 3.0 eq.) was added to each vial, followed by dropwise addition of DIPEA (0.02 mL, 0.1 mmol, 9.0 eq.). The mixtures were monitored over the course of 72 hr via LCMS. Preparation of the LCMS samples was achieved by taking aliquots from each vial and suspending them in a 1:1 mixture of LCMS Optima grade acetonitrile and LCMS Optima grade H_2O. Reaction profile was monitored by LCMS using a Shimadzu LC20A HPLC coupled with a Shimadzu LCMS2020 single quad mass spectrometer with an ESI source, using a 5%-to-95% H2O in Acetonitrile with 0.05% formic acid gradient over 15 min. The starting material consumption and diastereomeric ratio (d.r.) was quantified on the basis of peak area from the extracted ion chromatogram of the product [M+H]+ peak (*m/z* 398.20; retention times 10.36 min and 10.48 min) and starting material [M+H]+ peak (*m/z* 416.2; retention time: 7.28 min). See **Figure 2.6** for results.



Preparation of (9S,15aS)-9-((1H-indol-3-yl)methyl)decahydropyrido[2,1-c][1]oxa[4,7]diazacyclododecine-1,7,10(12H)-trione (2.1-*syn*) and **(9R,15aS)-9-((1H-indol-3-yl)methyl)decahydropyrido[2,1-c][1]oxa[4,7]diazacyclododecine-1,7,10(12H)-trione (2.1-*anti*).** Preparation of this screen followed the same procedure as in GP2.1 starting from **2.16b** and

yielding **2.6b** as a dark purple powder (51 mg, 0.12 mmol, 96%) which was used in without further purification. **2.6b** was then used to screen coupling conditions as per GP2.1. See **Figure 2.5** for results.



2.1-*anti* (D-Trp-L-Pip)

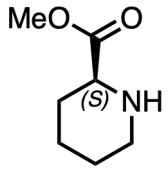
Preparation of 9R,15aS)-9-((1H-indol-3-yl)methyl)decahydropyrido[2,1-c][1]oxa[4,7]diazacyclododecine-1,7,10(12H)-trione (2.1a-*anti*). Preparation was achieved as per the EDC/OxymaPure entry in **GP 2.1. 2.6a** (123 mg, 0.27 mmol, 1.0 eq.), 10.8 mL DMF, EDC (155.9 mg, 0.8 mmol, 3.0 eq), OxymaPure (116.5 mg, 0.8 mmol, 3.0 eq.) and DIPEA (0.44 mL, 2.4 mmol, 9.0 eq.). At 72 h , the mixture was quenched with (1M) HCl then extracted with EtOAc. Organic fractions were washed with saturated $NaHCO_3$ (x3), brine (x2), dried over $MgSO_4$, filtered and concentrated under reduced pressure. Purification was achieved by silica gel flash chromatography (50% Acetone/Hexane) to yielded single diastereomer (L-Trp) **(2.1a-*anti*)** (10.7 mg, 0.03 mmol, 10%) as an orange sticky powder.

TLC (10%MeOH/DCM): R_f=0.42

^{1}H NMR (600 MHz, CDCl3) δ 8.03 (s, 1H), 7.65 (d, J = 7.9 Hz, 1H), 7.36 (d, J = 8.2 Hz, 1H), 7.22 – 7.18 (m, 1H), 7.14 (ddd, J = 8.0, 7.1, 1.0 Hz, 1H), 7.07 (d, J = 2.2 Hz, 1H), 6.59 (d, J = 10.0 Hz, 1H), 5.60 (td, J = 9.8, 6.0 Hz, 1H), 5.31 (dd, J = 6.5, 4.3 Hz, 1H), 3.84 (td, J = 10.9, 2.5 Hz, 1H), 3.74 – 3.64 (m, 1H), 3.36 – 3.22 (m, 1H), 3.17 (dd, J = 14.3, 6.0 Hz, 1H), 2.86 (dd, J = 13.2, 3.1 Hz, 1H), 2.33 (ddd, J = 12.9, 6.3, 2.7 Hz, 1H), 2.31 – 2.25 (m, 1H), 2.15 (dd, J = 12.9, 3.0 Hz, 1H), 2.02 – 1.92 (m, 1H), 1.86 – 1.72 (m, 2H), 1.56 – 1.45 (m, 2H), 1.42 (d, J = 14.0 Hz, 1H), 1.33 (tdd, J = 13.6, 5.8, 3.9 Hz, 1H), 1.16 (qt, J = 13.2, 3.7 Hz, 1H), 0.65 (qt, J = 13.2, 4.2 Hz, 1H).

^{13}C NMR (151 MHz, CDCl3) δ 174.9, 174.4, 170.5, 136.4, 127.2, 122.7, 122.4, 119.9, 118.8, 111.3, 105.0, 66.0, 53.2, 48.8, 45.2, 37.1, 27.4, 25.5, 25.1, 24.7, 23.3, 20.5.

HRMS (ESI-TOF) m/z calcd for $C_{22}H_{27}N_3O_4Na$ [M+Na]+ 420.1899, found 420.1903.



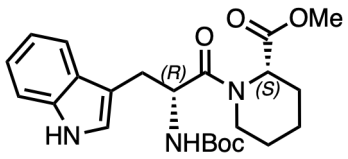
Preparation of methyl (S)-piperidine-2-carboxylate (2.18): To a flame-dried flask flushed with N_2(g) and equipped with a Teflon-coated magnetic stir bar, commercially available *L*-pipecolic acid (1.5g, 11.6mmol, 1.0eq.) was suspended in 25mL MeOH and cooled to 0 °C, after which TMSCl (3.8mL, 34.8mmol, 3.0eq.) was added dropwise via syringe and the reaction was left to warm to room temperature and stir overnight. Solvent and excess reagents were removed under reduced pressure to afford crude compound **(2.18)** (2.1g, 11.5mmol, 98.6%) as a pale green powder which was used in the next reaction without further purification.

TLC (10% MeOH in DCM, Ninhydrin): R_f=0.28

^{1}H NMR (400 MHz, D_2O) δ 4.03 (dd, *J* = 11.8, 3.6 Hz, 1H), 3.80 (s, 3H), 3.48 – 3.41 (m, 1H), 3.07 – 2.99 (m, 1H), 2.27 (ddd, *J* = 14.2, 3.6, 1.5 Hz, 1H), 1.90 – 1.83 (m, 2H), 1.76 – 1.56 (m, 3H).

^{13}C NMR (101 MHz, D_2O) δ 170.12, (1C) 56.98 & 56.70, 53.52, (1C) 44.03 & 43.85, (1C) 25.77 & 25.53, 21.29, 21.15.

HRMS (ESI-TOF) *m/z* calcd for $C_7H_{14}NO_2$ [M+H]+ 144.1037, found 144.1025.



Preparation of methyl (S)-1-((tert-butoxycarbonyl)-D-tryptophyl)piperidine-2-carboxylate (2.19a): A flame-dried flask equipped with a Teflon-coated magnetic stir bar and flushed with $N_{2(g)}$ was charged with acid **2.18** (1.2 g, 4.0 mmol, 1.2 eq.), and dissolved in 5.25mL DMF. HATU (1.5 g, 4.0 mmol, 1.2 eq.) was added portion-wise at 0 °C and left to stir for 30 mins. In a second round-bottom flask flushed with $N_{2(g)}$, commercially available Boc-*D*-Trp-OH (0.6 g, 3.34 mmol, 1.0 eq.) was suspended in 1.75mL of DMF, and DIPEA (1.2mL,6.7mmol,2.0eq.) was added

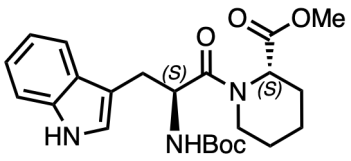
dropwise. After activation of **2.18** was complete (solution turns cloudy white from transparent clear), the mixture of tryptophan amino acid and DIPEA in DMF was transferred via syringe through dropwise addition to the activated ester at 0 °C. The final mixture was left to stir overnight and warm to room temperature. Once reaction was complete, quenching was achieved with (1M) HCl (dropwise addition) followed by immediate extraction with EtOAc. The organic layer was washed saturated $NaHCO_3$ (5 mL x 3), brine (5 mL x 2), dried over $MgSO_4$, filtered and concentrated under reduced pressure. Purification by silica gel flash chromatography (30% EtOAc/Hexane) yielded pure compound **2.19a** as viscous orange oil (917 mg, 2.14 mmol, 64% yield)

TLC (30%EtOAc in Hexane): R_f=0.19

^{1}H NMR (600 MHz, $CDCl_3$) δ 8.15 (s, 1H), 7.66 (d, *J* = 7.9 Hz, 1H), 7.32 (d, *J* = 8.1 Hz, 1H), 7.17 (ddd, *J* = 8.3, 7.0, 1.2 Hz, 1H), 7.10 (ddd, *J* = 7.4, 7.0, 1.0 Hz, 1H), 7.05 (d, *J* = 2.3 Hz, 1H), 5.56 (d, *J* = 8.5 Hz, 1H), 5.18 – 5.12 (m, 1H), 5.02 (td, *J* = 8.8, 5.2 Hz, 1H), 3.67 (s, 3H), 3.51 – 3.47 (m, 1H), 3.22 (dd, *J* = 14.0, 5.2 Hz, 1H), 3.15 (dd, *J* = 14.1, 9.1 Hz, 1H), 3.01 (td, *J* = 13.1, 3.0 Hz, 1H), 2.06 – 2.00 (m, 1H), 1.45 (s, 9H), 1.37 – 1.34 (m, 1H), 1.18 – 1.13 (m, 1H), 1.11 – 0.97 (m, 2H), 0.22 – 0.08 (m, 1H).

^{13}C NMR (151 MHz, $CDCl_3$) δ 172.43, 171.55, 155.29, 136.19, 128.02, 122.94, 122.30, 119.83, 119.02, 111.18, 111.01, 79.64, 52.40, 52.35, 50.77, 43.92, 30.60, (3C) 28.53, 26.30, 24.07, 20.60.

HRMS (ESI-TOF) m/z calcd for $C_{23}H_{31}N_3O_5Na$ [M+Na]+ 452.2162, found 452.2161.



Preparation of methyl (S)-1-((tert-butoxycarbonyl)-L-tryptophyl)piperidine-2-carboxylate (2.19b): follows same procedure as **preparation of compound (2.19a).** ^{1}H and ^{13}C NMR reveals 7:3 mixture of rotamers. Only the mwajor rotomer as characterized. (659mg , 1.56 mmol, 46% yield)

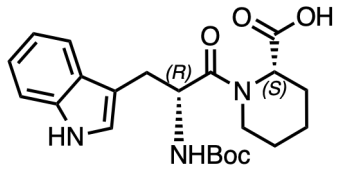
TLC (50%EtOAc in Hexane): R_f=0.42

1H NMR (600 MHz, CDCl3) δ 8.28 – 8.18 (m, 1H), 7.68 – 7.60 (m, 1H), 7.33 (d, J = 8.1 Hz, 1H), 7.18 – 7.15 (m, 1H), 7.12 – 7.00 (m, 2H), 5.45 – 5.40 (m, 2H), 5.04 (dt, J = 8.8, 6.1 Hz, 1H),

3.80 – 3.74 (m, 1H), 3.72 (s, 3H), 3.28 (dd, J = 14.8, 6.2 Hz, 1H), 3.08 – 3.01 (m, 1H), 2.30 – 2.21 (m, 1H), 1.73 – 1.56 (m, 3H), 1.45 – 1.39 (m, 11H), 1.30 (dt, J = 13.2, 3.8 Hz, 1H).

13C NMR (151 MHz, CDCl3) δ 171.8, 171.7, 155.3, 136.1, 128.2, 123.6, 121.9, 119.5, 118.9, 111.2, 110.3, 79.6, 52.4, 52.3, 50.9, 43.6, 28.5, 28.5, 26.8, 25.4, 21.1.

HRMS (ESI-TOF) m/z calcd for $C_{23}H_{31}N_3O_5$ [M+Na]+ 452.2167, found 452.2161.



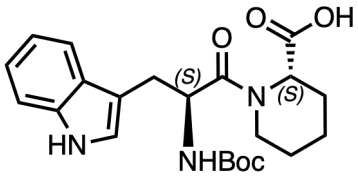
Preparation of (S)-1-((tert-butoxycarbonyl)-D-tryptophyl)piperidine-2-carboxylic acid (2.20a): To a stirring mixture of **(2.19a)** (161.1mg, 0.37mmol, 1.0eq.) in 1.8mL of THF:MeOH:H_2O, LiOH monohydrate (78.8mg, 1.9mmol, 5.0eq.) was added. Stirring was continued at room temperature until reaction was deemed complete (monitored via TLC). Upon reaction completion, acidification of the mixture was achieved via dropwise addition of (1M) HCl to a pH of 5.0, followed by immediate extraction in EtOAc. Organic fractions were washed with brine (x3), dried over $MgSO_4$, filtered, and concentrated under reduced pressure. Compound **(2.20a)** was isolated as a pale-yellow powder (144mg, 0.35mmol, 94%) and used in subsequent chemical step without need for further purification.

TLC (40%EtOAc in Hexane with 1% acetic acid): Rf=0.05

^{1}H NMR (600 MHz, $CDCl_3$) δ 8.58 – 8.24 (m, 1H), 7.64 – 7.58 (m, 1H), 7.33 (d, *J* = 8.1 Hz, 1H), 7.20 – 7.14 (m, 1H), 7.14 – 7.08 (m, 1H), 7.05 (s, 1H), 5.68 (d, *J* = 8.3 Hz, 1H), 5.15 (dd, *J* = 6.2, 2.1 Hz, 1H), 5.00 (td, *J* = 8.6, 5.5 Hz, 1H), 3.55 – 3.45 (m, 1H), 3.25 – 3.09 (m, 2H), 3.01 (td, *J* = 13.2, 2.7 Hz, 1H), 2.06 (d, *J* = 13.8 Hz, 1H), 1.44 – 1.39 (m, 9H), 1.37 – 1.31 (m, 2H), 1.16 (d, *J* = 12.6 Hz, 1H), 0.98 (ddt, *J* = 11.8, 8.1, 4.8 Hz, 1H), 0.16 (dt, *J* = 13.1, 4.1 Hz, 1H).

^{13}C NMR (151 MHz, $CDCl_3$) δ 174.07, 173.00, 155.57, 136.10, 127.75, 123.06, 122.19, 119.72, 118.71, 111.18, 110.42, 80.02, 52.43, 50.85, 43.99, (3C) 28.37, 23.93, 20.33.

HRMS (ESI-TOF) m/z calcd for $C_{22}H_{29}N_3O_5Na$ [M+Na]+ 438.2005, found 438.2005.



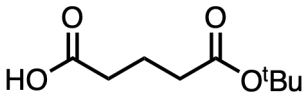
Preparation of (S)-1-((tert-butoxycarbonyl)-L-tryptophyl)piperidine-2-carboxylic acid (2.20b): follows same procedure as **preparation of compound (2.20a)**. **2.19b** was isolated as a pale-yellow powder (135mg, 0.33mmol, 88% yield). Major rotomer characterized only.

TLC (50%EtOAc in Hexane with 1% acetic acid): Rf=0.15

1H NMR (600 MHz, CDCl3) δ 8.96 (s, 1H), 7.62 – 7.60 (m, 1H), 7.23 (d, J = 7.7 Hz, 1H), 7.09 – 7.05 (m, 3H), 5.53 (d, J = 8.6 Hz, 1H), 5.35 – 5.32 (m, 1H), 5.06 (td, J = 7.7, 4.2 Hz, 1H), 3.75 – 3.67 (m, 1H), 3.29 (dd, J = 14.5, 7.3 Hz, 1H), 3.13 – 3.10 (m, 1H), 3.07 – 3.00 (m, 1H), 2.30 – 2.24 (m, 1H), 1.67 – 1.58 (m, 3H), 1.44 – 1.42 (m, 10H), 1.23 – 1.15 (m, 1H).

13C NMR (151 MHz, CDCl3) δ 174.53, 172.58, 171.97, 155.35, 136.19, 128.29, 124.94, 121.45, 119.14, 118.65, 111.34, 108.81, 79.64, 53.36, 51.14, 43.65, 28.55, 25.47, 20.99.

HRMS (ESI-TOF) m/z calcd for $C_{22}H_{29}N_3O_5Na$ [M+Na]+ 438.1988, found 438.2005.



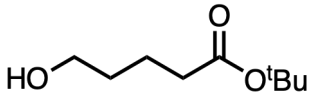
Preparation of 5-(tert-butoxy)-5-oxopentanoic acid (2.21): A flame-dried flask equipped with a Teflon-coated magnetic stir bar and flushed with $N_{2(g)}$ was charged with commercially available $ZnCl_2$ (11.9mg, 0.1mmol, 0.01eq.) in 1.7mL of dry tBuOH until a white emulsion appeared. To this suspension, commercially available glutaric anhydride (1.0g, 8.7mmol, 1.0eq) was added and the mixture was heated to reflux (80°C) and left to stir overnight. The mixture was transferred to a separatory funnel, diluted with EtOAc and washed thoroughly with 5% $NaHSO_4$ (x3). Organic fractions were combined, washed with brine (x1), dried over Na_2SO_4, filtered and concentrated under reduced pressure. Crude product **(2.21)** (540.5mg, 2.9mmol, 33%) was isolated as a clear transparent oil and used in subsequent chemical step without need for further purification. Characterization data is consistent with reported values

TLC (50%EtOAc in Hexanes, 1% acetic acid, cerium III sulfate stain): R_f=0.1

1H NMR (400 MHz, CDCl3) δ 2.41 (t, J = 7.4 Hz, 2H), 2.29 (t, J = 7.3 Hz, 2H), 1.90 (p, J = 7.3 Hz, 2H), 1.43 (s, 9H).

^{13}C NMR (101 MHz, $CDCl_3$) δ 179.07, 172.33, 80.60, 34.49, 33.05, (3C) 28.16, 20.04.

HRMS (ESI-TOF) m/z calcd for $C_9H_{16}O_4Na$ [M+Na]+ 211.0951, found 211.0946.



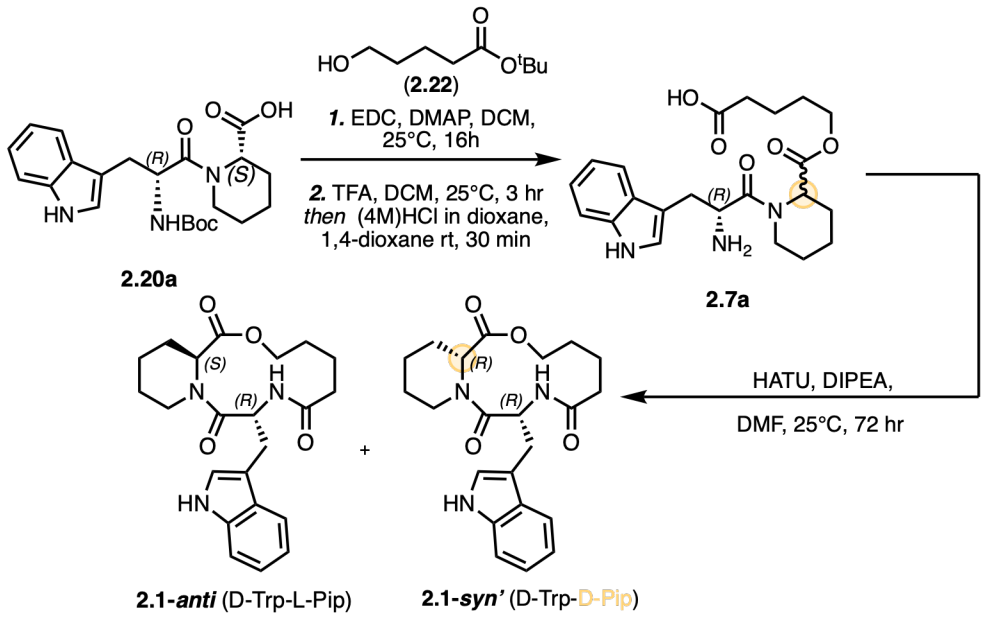
Preparation of tert-butyl 5-hydroxypentanoate (2.22): A flame-dried flask equipped with a Teflon-coated magnetic stir bar and flushed with $N_{2(g)}$ was charged with **(2.21)** (540.5mg, 2.9 mmol, 1.0 eq.) in 12 mL of THF. The stirring suspension was cooled to -78 °C and BH_3Me_2S (0.55 mL, 5.7 mmol, 2.0 eq.) was added dropwise via syringe. The mixture was then allowed to slowly warm to room temperature and stirring was continued for 1.5 - 3 h. The mixture was quenched carefully with slow addition of MeOH and evaporated to dryness under reduced pressure. The crude mixture was diluted with EtOAc, transferred to a separatory funnel, and washed with brine (x3). Organic fractions were combined, dried over $MgSO_4$, filtered and concentrated under reduced pressure to afford **2.22** as a clear colourless viscous oil (348.4 mg, 2.0 mmol, 70%). **2.21** was used in subsequent chemical step without need for further purification.

TLC (50%EtOAc in Hexanes, 1% acetic acid, cerium III sulfate stain): R_f=0.46

^{1}H NMR (400 MHz, $CDCl_3$) δ 3.63 (t, *J* = 6.2 Hz, 2H), 2.25 (t, *J* = 7.1 Hz, 2H), 1.72 – 1.62 (m, 2H), 1.62 – 1.53 (m, 2H), 1.43 (s, 9H).

^{13}C NMR (101 MHz, $CDCl_3$) δ 173.25, 80.26, 62.24, 35.10, 32.08, 28.10, 21.08.

HRMS (ESI-TOF) *m/z* calcd for $C_9H_{17}O_3Na$ [M+Na]+ 196.1030, found 196.1075.



Preparation of (9R,15aS)-9-((1H-indol-3-yl)methyl)decahydropyrido[2,1-c][1]oxa[4,7]diazacyclododecine-1,7,10(12H)-trione (2.1-*anti*) and **(9R,15aR)-9-((1H-indol-3-yl)methyl)decahydropyrido[2,1-c][1]oxa[4,7]diazacyclododecine-1,7,10(12H)-trione (2.1-*syn'*):** A flame-dried flask equipped with a Teflon-coated magnetic stir bar was charged with acid **2.20a** (70 mg, 0.17 mmol, 1.0 eq.), EDC (64.7 mg, 0.34 mmol, 2.0 eq.), DMAP (1.0 mg, 0.01 mmol, 0.05 eq.), and 0.9mL of DCM. After 15 minutes of stirring, alcohol **(2.22)** (87 mg, 0.5 mmol, 3.0 eq.) was added. Stirring was continued at room temperature for 16 h after which saturated $NaHCO_3$ was added. The mixture was transferred to a separatory funnel, extracted with DCM (3 x 2 mL) and washed with brine (2 x 2mL). The organic layers were combined, dried over Na_2SO_4, filtered, and concentrated under reduced pressure. Purification by silica gel flash chromatography (20-30% EtOAc/Hexane) yielded the ester intermediate (33-48%), as a pale yellow powder, that was immediately used in the next reaction. Next, in flame-dried flask equipped with a Teflon-coated magnetic stir bar, ester intermediate (6.3 mg, 0.01 mmol, 1.0 eq.) was suspended in in 0.12mL DCM and cooled to 0 °C, after which TFA (0.01 mL, 0.07 mmol, 6.0 eq.) was added dropwise. TLC was used to monitor reaction progress. Once complete, solvents and excess reagents were removed under reduced pressure. Compound was resuspended in 0.12 mL 1,4-dioxane and 0.12 mL (4M) HCl was added. Mixture was allowed to stir at room temperature for 30mins to complete the counter-ion exchange, after which solvents were removed under reduced pressure and an ^{19}F-NMR in d-chloroform was taken to ensure all TFA was removed. **2.7a**

was obtained in quantitative yields as deep purple powders and used without further purification in subsequent chemical step.

HRMS (ESI-TOF) *m/z* calcd for $C_9H_{18}O_3Na$ [M+Na]+ 197.1154, found 197.1150.

In a round-bottom flask equipped with Teflon-coated magnetic stir bar **2.7a** (164.8mg, 0.36 mmol, 1.0 eq.) was suspended in 14.4 mL of DMF, to this suspension, HATU (416.0mg, 1.1 mmol, 3.0 eq.) was added, followed by DIPEA (0.54 mL, 3.9 mmol, 9.0 eq.). The reaction was left stir at room temperature overnight, and monitored via LCMS for the formation of macrocycle. Upon completion, the mixture was quenched with (1M) HCl then extracted with EtOAc. Organic fractions were washed with saturated $NaHCO_3$ (x3), brine (x2), dried over $MgSO_4$, filtered and concentrated under reduced pressure. Separation and purification of the two diastereomer products **2.1-*anti*** and **2.1-*syn'*** was achieved by silica gel flash chromatography (20-30% Acetone/Hexane). **2.1-*anti*** and **2.1-*syn'*** diastereomers (17 mg, 0.043 mmol, 12%, d.r.=3:1) were isolated as orange sticky powders.

2.1-*anti*: spectral data matched with **2.1-*anti*** characterized for route B (See **Spectra 2.29**)

TLC (50%EtOAc in Hexanes, 1% acetic acid, cerium III sulfate stain): R_f=0.48

HRMS (ESI-TOF) *m/z* calcd for $C_{22}H_{27}N_3O_4Na$ [M+Na]+ 420.1899, found 420.1871.

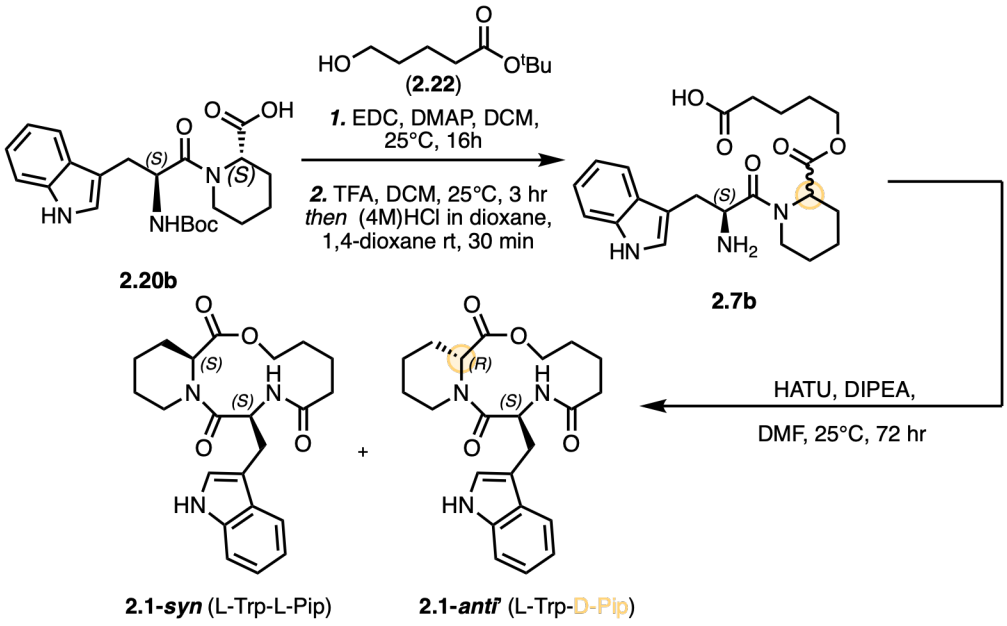
2.1-*syn'*:

TLC (50%EtOAc in Hexanes, 1% acetic acid, cerium III sulfate stain): R_f=0.36

1H NMR (600 MHz, CDCl3) δ 8.09 (s, 1H), 7.66 (d, J = 7.9 Hz, 1H), 7.34 (dt, J = 8.1, 0.9 Hz, 1H), 7.17 (ddd, J = 8.1, 7.0, 1.2 Hz, 1H), 7.11 (ddd, J = 8.0, 7.0, 1.0 Hz, 1H), 7.09 (d, J = 2.2 Hz, 1H), 6.00 (d, J = 10.2 Hz, 1H), 5.47 (dt, J = 10.3, 7.3 Hz, 1H), 4.87 (d, J = 5.4 Hz, 1H), 4.46 (d, J = 13.6 Hz, 1H), 4.27 (ddd, J = 11.7, 9.7, 2.3 Hz, 1H), 3.98 (ddd, J = 11.2, 5.8, 2.8 Hz, 1H), 3.34 (dd, J = 14.7, 7.8 Hz, 1H), 3.21 – 3.15 (m, 1H), 2.56 (td, J = 13.2, 2.9 Hz, 1H), 2.29 – 2.25 (m, 1H), 2.18 – 2.12 (m, 1H), 1.93 – 1.87 (m, 3H), 1.69 – 1.61 (m, 3H), 1.47 – 1.37 (m, 2H), 1.30 – 1.27 (m, 1H), 1.19 (ddt, J = 13.0, 8.0, 4.1 Hz, 1H).

13C NMR (151 MHz, CDCl3) δ 172.7, 171.5, 170.9, 136.2, 127.7, 122.8, 122.1, 119.7, 118.8, 111.4, 111.2, 66.7, 56.5, 48.2, 40.6, 38.6, 28.4, 27.7, 26.6, 24.7, 23.9, 20.6.

HRMS (ESI-TOF) *m/z* calcd for $C_{22}H_{27}N_3O_4Na$ [M+Na]+ 420.1899, found 420.1895.



Preparation of (9S,15aR)-9-((1H-indol-3-yl)methyl)decahydropyrido[2,1-c][1]oxa[4,7]diazacyclododecine-1,7,10(12H)-trione (2.1-*anti'*) and **(9S,15aS)-9-((1H-indol-3-yl)methyl)decahydropyrido[2,1-c][1]oxa[4,7]diazacyclododecine-1,7,10(12H)-trione (2.1-*syn*):** follows same procedure as **preparation of compounds (2.1-*anti*) & (2.1-*syn'*).** From **2.20b** and **2.22** to access intermediate **2.7b** confirmed via HRMS.

2.7b: HRMS (ESI-TOF) *m/z* calcd C9H18O3Na [M+Na]+ 197.1154, found 197.1152.

Separation and purification of the two diastereomer products **2.1-*anti'*** and **2.1-*syn*** was achieved by silica gel flash chromatography (20-30% Acetone/Hexane). **2.1-*anti'*** and **2.1-*syn*** diastereomers (24mg, 0.06mmol, 16%, d.r.=2:1) were isolated as a orange sticky powders.

2.1-*anti'*:

TLC (50%EtOAc in Hexanes, 1% acetic acid, cerium III sulfate stain): R_f=0.48

1H NMR (400 MHz, CDCl3) δ 8.16 (s, 1H), 7.66 (d, J = 7.8 Hz, 1H), 7.34 (d, J = 0.9 Hz, 1H), 7.18 (ddd, J = 8.2, 7.0, 1.2 Hz, 1H), 7.11 (ddd, J = 8.0, 7.0, 1.1 Hz, 2H), 7.06 (d, J = 2.4 Hz, 1H), 6.10 (d, J = 10.1 Hz, 1H), 5.54 (td, J = 9.7, 6.2 Hz, 1H), 5.33 (d, J = 5.6 Hz, 1H), 4.11 (dt, J = 10.9, 3.6 Hz, 1H), 3.82 (td, J = 10.6, 3.3 Hz, 1H), 3.67 (d, J = 13.3 Hz, 1H), 3.32 (dd, J = 14.3, 9.4 Hz, 1H), 3.15 (dd, J = 14.2, 6.1 Hz, 1H), 2.87 – 2.80 (m, 1H), 2.32 – 2.28 (m, 1H), 2.27 – 2.23 (m,

1H), 2.10 – 2.05 (m, 1H), 1.95 – 1.89 (m, 1H), 1.81 – 1.77 (m, 2H), 1.53 – 1.47 (m, 2H), 1.42 – 1.38 (m, 1H), 1.34 – 1.29 (m, 1H), 1.18 – 1.11 (m, 1H), 0.67 (tdd, J = 13.2, 9.0, 4.1 Hz, 1H).

13C NMR (151 MHz, CDCl3) δ 174.3, 174.0, 170.9, 136.3, 127.3, 122.6, 122.3, 119.8, 118.9, 111.3, 105.7, 65.8, 52.9, 48.7, 44.9, 37.4, 27.7, 25.6, 25.2, 24.8, 23.2, 20.7.

HRMS (ESI-TOF) *m/z* calcd for $C_{22}H_{27}N_3O_4Na$ [M+Na]+ 420.1899, found 420.1912.

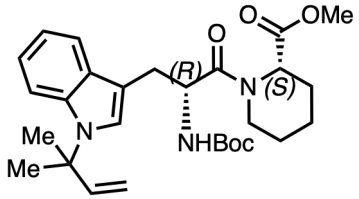
2.1-*syn*:

TLC (50%EtOAc in Hexanes, 1% acetic acid, cerium III sulfate stain): R_f=0.36

1H NMR (400 MHz, CDCl3) δ 8.06 (s, 1H), 7.67 (d, J = 7.8 Hz, 1H), 7.34 (dt, J = 8.1, 0.9 Hz, 1H), 7.18 (ddd, J = 8.1, 7.0, 1.3 Hz, 1H), 7.14 – 7.10 (m, 1H), 7.09 (d, J = 2.0 Hz, 1H), 5.94 (d, J = 10.3 Hz, 1H), 5.47 (dt, J = 10.4, 7.3 Hz, 1H), 4.87 (d, J = 5.4 Hz, 1H), 4.46 (d, J = 13.7 Hz, 1H), 4.27 (td, J = 10.3, 2.3 Hz, 1H), 3.99 (ddd, J = 11.1, 5.7, 2.8 Hz, 1H), 3.37 – 3.32 (m, 1H), 3.20 – 3.16 (m, 1H), 2.56 (td, J = 13.4, 3.0 Hz, 1H), 2.27 (dd, J = 11.6, 7.9 Hz, 1H), 1.92 – 1.84 (m, 3H), 1.69 – 1.59 (m, 3H), 1.45 – 1.35 (m, 2H), 1.30 – 1.25 (m, 1H), 1.18 (dt, J = 13.6, 4.4 Hz, 1H).

13C NMR (101 MHz, CDCl3) δ 172.61, 170.94, 122.75, 122.14, 119.68, 118.84, 111.47, 111.19, 66.72, 56.44, 48.17, 40.59, 38.57, 31.08, 28.37, 27.67, 26.60, 24.75, 23.90, 20.63.

HRMS (ESI-TOF) *m/z* calcd for $C_{22}H_{27}N_3O_4Na$ [M+Na]+ 420.1899, found 420.1868.



Preparation of methyl (S)-1-((tert-butoxycarbonyl)-D-tryptophyl)piperidine-2-carboxylate (2.23): A flame-dried flask equipped with a Teflon-coated magnetic stir bar and flushed with N2(g) was charged with acid **2.19a** (3.4g, 7.9mmol, 1.0eq.), and dissolved in 79 mL of dry ACN. To the stirring suspension, $Cu(OAc)_2$ (3.5 g, 15.8 mmol, 2.0 eq) AgTFA (3.1 g, 15.8 mmol, 2.0 eq.) were added, and N2(g) was bubbled into the reaction vessel as stirring was continued for 15 min. To the stirring mixture, Pd(OAc)2 (176 mg, 0.79 mmol, 0.1 eq) was added, immediately followed by 2-methyl-2-butene (6.5 mL, 237 mmol, 30.0 eq.). Again, the reaction vessel was flushed with $N_{2(g)}$ and allowed to stir at 35°C for 1h. Three more additions of $Pd(OAc)_2$ (176 mg, 0.79 mmol, 0.1 eq)

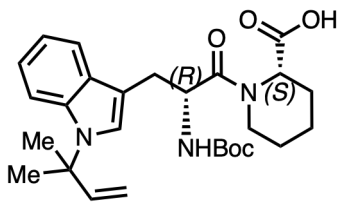
were carried out every hour, after which the reaction was left to stir overnight at 35 °C. Once complete, the solvent and volatile reagents were removed by rotary evaporation, and the crude product was placed directly on a silica column for purification. Purification by silica gel flash chromatography (30% EtOAc/Hexane) yielded pure compound **2.23** as viscous orange oil (2.5 g, 5.1 mmol, 64% yield).

TLC (50% EtOAc in Hexanes): R_f=0.8

1H NMR (400 MHz, CDCl3) δ 7.65 – 7.62 (m, 1H), 7.48 – 7.43 (m, 1H), 7.19 (s, 1H), 7.11 – 7.02 (m, 2H), 6.09 (dd, J = 17.5, 10.7 Hz, 1H), 5.56 (d, J = 8.6 Hz, 1H), 5.23 – 5.16 (m, 3H), 5.03 (td, J = 9.1, 5.2 Hz, 1H), 3.67 (s, 3H), 3.45 (d, J = 11.6 Hz, 1H), 3.23 (dd, J = 14.1, 5.2 Hz, 1H), 3.10 (dd, J = 14.0, 9.5 Hz, 1H), 3.00 – 2.93 (m, 1H), 2.07 – 1.96 (m, 1H), 1.71 (s, 6H), 1.46 (d, J = 1.3 Hz, 9H), 1.29 (td, J = 12.2, 5.7 Hz, 1H), 1.11 – 0.92 (m, 3H), 0.03 – -0.13 (m, 1H).

13C NMR (101 MHz, CDCl3) δ 172.6, 171.5, 155.3, 144.2, 135.6, 129.8, 124.0, 121.1, 119.2, 119.1, 113.7, 113.6, 108.9, 79.6, 59.0, 52.4, 52.3, 50.7, 43.9, 31.0, 28.6, 28.4, 28.0, 26.3, 24.0, 20.5, 18.8, 17.6.

HRMS (ESI-TOF) *m/z* calcd for $C_{28}H_{40}N_3O_5$ [M+H]+ 498.2968, found: 498.2973



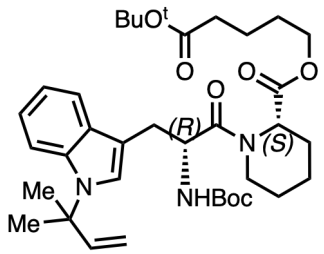
Preparation of (S)-1-((tert-butoxycarbonyl)-D-tryptophyl)piperidine-2-carboxylic acid (2.24): To a stirring mixture of **2.23** (103.3mg, 0.21mmol, 1.0eq.) in 1.0mL of THF:MeOH:H2O, LiOH monohydrate (43.5mg, 1.04mmol, 5.0eq.) was added. Stirring was continued at room temperature until reaction was deemed complete (monitored via TLC). Upon reaction completion, acidification of the mixture was achieved via dropwise addition of (1M) HCl to a pH of 5.0, followed by immediate extraction in EtOAc. Organic fractions were washed with brine (x3), dried over MgSO4, filtered, and concentrated under reduced pressure. Compound **2.24** was isolated as a pale-yellow powder (96.5mg, 0.2mmol, >95%) and used in subsequent chemical step without need for further purification.

TLC (50% Acetone in Hexane): R_f=0.25

1H NMR (400 MHz, CDCl3) δ 7.64 – 7.58 (m, 1H), 7.49 – 7.43 (m, 1H), 7.18 (s, 1H), 7.08 (ddt, J = 9.8, 7.1, 3.6 Hz, 2H), 6.09 (dd, J = 17.5, 10.7 Hz, 1H), 5.60 (d, J = 7.9 Hz, 1H), 5.24 – 5.15 (m, 3H), 4.98 (td, J = 9.0, 5.4 Hz, 1H), 3.46 (d, J = 13.3 Hz, 1H), 3.22 (dd, J = 13.9, 5.2 Hz, 1H), 3.12 (dd, J = 13.8, 9.8 Hz, 1H), 2.94 (td, J = 13.1, 3.0 Hz, 1H), 2.09 – 2.04 (m, 1H), 1.71 (s, 6H), 1.44 (d, J = 4.0 Hz, 9H), 1.23 – 1.01 (m, 3H), 0.97 – 0.88 (m, 1H), -0.07 (d, J = 12.1 Hz, 1H).

13C NMR (101 MHz, CDCl3) δ 174.4, 173.3, 155.7, 144.1, 135.6, 129.6, 124.1, 121.2, 119.3, 119.0, 113.8, 113.7, 108.6, 80.1, 59.0, 52.4, 50.9, 44.1, 30.3, 28.5, 28.4, 28.0, 25.9, 24.0, 20.7, 20.4.

HRMS (ESI-TOF) *m/z* calcd for $C_{27}H_{38}N_3O_5$ [M+H]+ 484.2811, found: 484.2828



Preparation of 5-(tert-butoxy)-5-oxopentyl (S)-1-(Nα-(tert-butoxycarbonyl)-1-(2-methylbut-3-en-2-yl)-D-tryptophyl)piperidine-2-carboxylate (2.25): A flame-dried flask equipped with a Teflon-coated magnetic stir bar and flushed with $N_{2(g)}$ was charged with **2.22** (56.4mg, 0.32 mmol, 1.2 eq.) and PPh3 (115.4mg, 0.44mmol, 1.2 eq.) in dry THF (2 mL). The stirring mixture was cooled to 0°C and DIAD (0.08mL, 0.44 mmol, 1.2 eq.) was added drop-wise over 2 min. The mixture was left to stir for 15 min, after which a suspension of **2.24** (131.4 mg, 0.27 mmol, 1.0 eq) in THF 0.7 mL was added drop-wise. The mixture was then allowed to slowly warm to room temperature and stirring was continued overnight. Volatiles were removed via rotary evaporation and the crude was subject directly to purification via silica gel flash chromatography (20% EtOAc/Hexane) to yield pure compound **2.25** as an orange oil (139 mg, 0.21 mmol, 81 % yield).

TLC (30% Acetone in Hexane): R_f=0.40

1H NMR (600 MHz, CDCl3) δ 7.63 – 7.59 (m, 1H), 7.47 (d, J = 7.9 Hz, 1H), 7.18 (s, 1H), 7.12 – 7.04 (m, 2H), 6.08 (dd, J = 17.4, 10.7 Hz, 1H), 5.56 (d, J = 7.8 Hz, 1H), 5.24 – 5.15 (m, 3H), 4.99 – 4.93 (m, 1H), 3.65 (t, J = 6.3 Hz, 2H), 3.45 (d, J = 13.2 Hz, 1H), 3.22 (dd, J = 13.9, 5.1 Hz, 1H), 3.12 (dd, J = 13.9, 9.9 Hz, 1H), 2.97 – 2.89 (m, 1H), 2.25 (d, J = 7.2 Hz, 2H), 2.07 (d, J =

14.2 Hz, 1H), 1.71 (s, 6H), 1.68 – 1.64 (m, 2H), 1.61 – 1.57 (m, 3H), 1.44 (s, 9H), 1.44 (s, 9H), 1.05 (d, J = 13.0 Hz, 1H), 0.98 – 0.82 (m, 2H), -0.08 (dq, J = 13.1, 6.6 Hz, 1H).
13C NMR (151 MHz, CDCl3) δ 173.4, 173.3, 173.2, 155.6, 144.0, 135.5, 129.5, 124.0, 121.0, 119.2, 118.8, 113.7, 113.6, 108.4, 80.3, 80.0, 62.3, 58.9, 52.2, 50.8, 44.0, 35.1, 32.1, 30.1, 29.7, 28.4, 28.3, 28.1, 27.9, 27.9, 27.6, 25.7, 23.8, 22.5, 21.1, 20.2.

Marfey's Analysis: *(Results and experimental description provided and performed by Carmen Hicks at Agriculture and Agri-Foods Canada)*

Marfey's analysis was performed as follows. Approximately 0.25 mg of each synthetic compound was transferred to an HPLC vial in MeOH and dried under a stream of N_2. Acid hydrolysis was effected by addition of 6 N HCl (100 µL), after which vials were sealed and heated at 100 °C for 5 hours at 500 rpm on a thermomixer. The hydrolysate was dried under N_2, resuspended in 1 M $NaHCO_3$ (20 µL), and treated with a solution of L-FDAA (1-fluoro-2,4-dinitrophenyl-5-L-leucinamide; 0.4 mg in 380 µL acetone). Derivatization was carried out at 40 °C for 1 hour at 600 rpm, after which reactions were quenched by addition of 1 M HCl (20 µL). All samples, including amino acid standards processed in parallel under identical conditions, were filtered through 0.2 µm PTFE syringe filters prior to injection.

UPLC-HRMS analysis was performed on a 50 × 2.1 mm C18 column using a binary gradient of H_2O + 0.1% formic acid (solvent A) and CH_3CN + 0.1% formic acid (solvent B) at a flow rate of 0.4 mL/min. The gradient was as follows: 5% to 40% B over 0–55 min, 40% to 100% B over 55–57 min, held at 100% B from 57–60 min, followed by return to initial conditions.

Results from analysis displayed across **Figures 2.9-2.12** (see below)

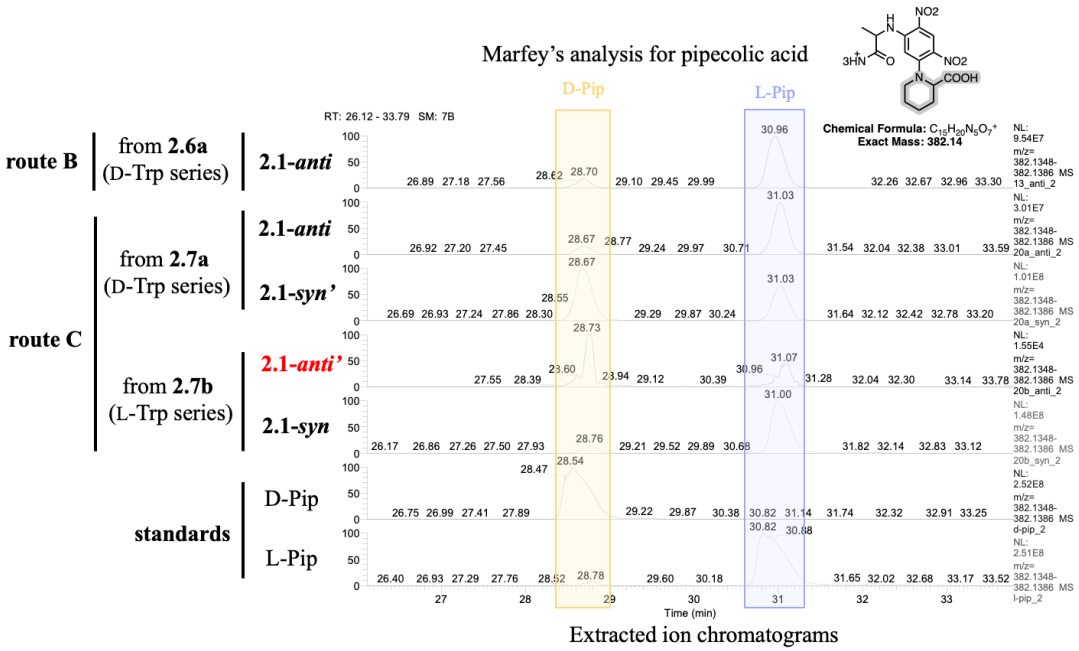


Figure 2.9. Marfey's analysis of the pipecolic acid residue in macrolactam diastereomers obtained from routes B and C. Extracted ion chromatograms (*m/z* 382.1348–382.1386, $[M+H]^+$) of L-FDAA-derivatized hydrolysates are shown alongside D-Pip and L-Pip standards. Retention times within the D-Pip (yellow) and L-Pip (blue) windows confirm the pipecolic acid configuration in each diastereomer. Results from **2.1-*anti'*** are inconclusive (highlighted in red) and subject to redo (**Figure 2.10**)

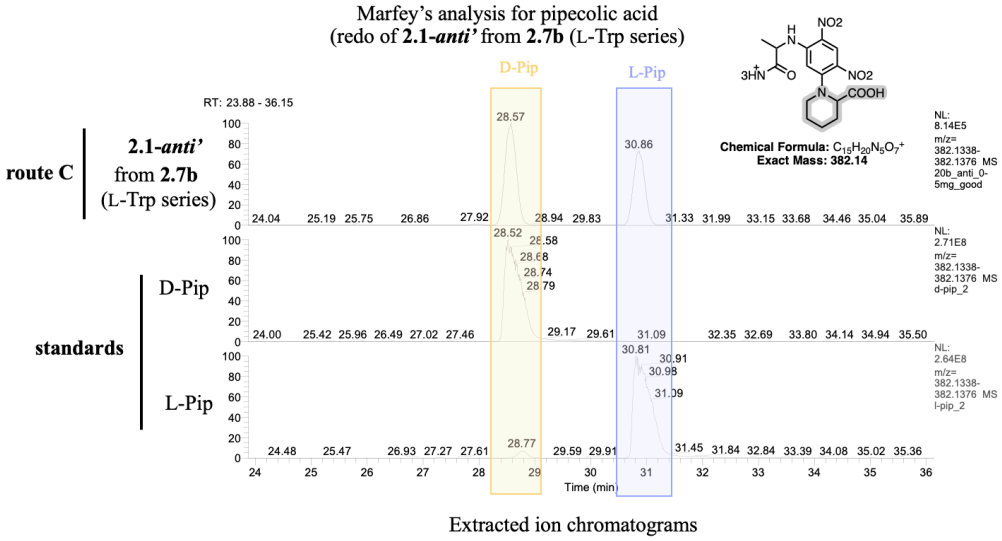


Figure 2.10. Repeat Marfey's analysis of **2.1-anti'** from the L-Trp series (route C, **2.7b**), confirming the presence of D-Pip. The initial assay was repeated due to inconclusive results across Pip and Trp Marfey's analyses.

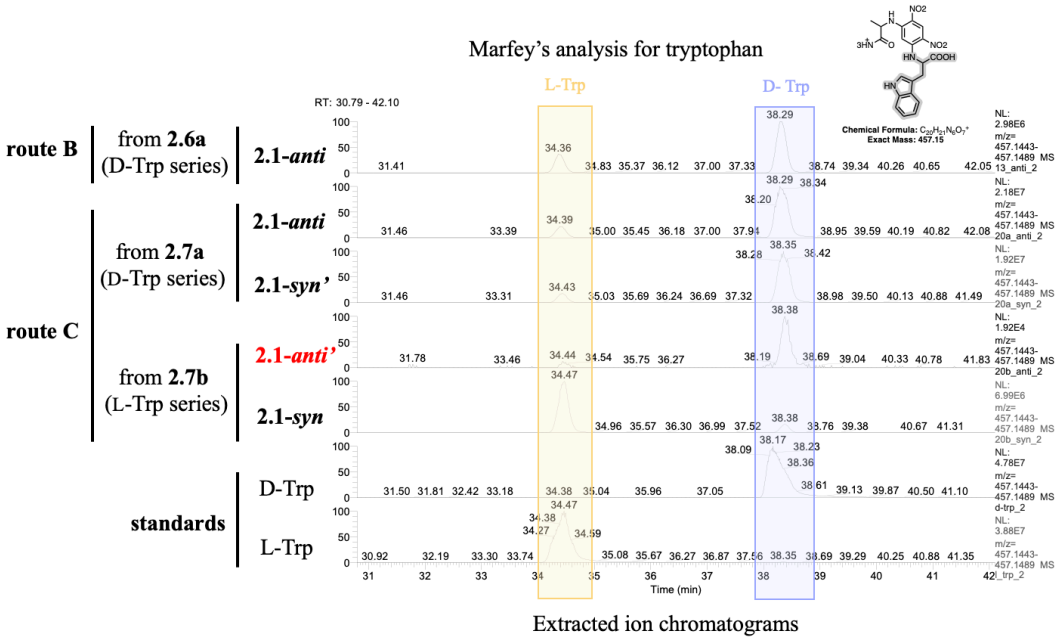


Figure 2.11. Marfey's analysis of the tryptophan residue in macrolactam diastereomers obtained from routes B and C. Extracted ion chromatograms (*m/z* 457.1443–457.1489, $[M+H]^+$) of L-FDAA-derivatized hydrolysates are shown alongside D-Trp and L-Trp standards. Retention times within the L-Trp (yellow) and D-Trp (blue) windows confirm the tryptophan configuration in each diastereomer. Results from **2.1-*anti'*** are inconclusive (highlighted in red) and subject to redo (**Figure 2.12**).

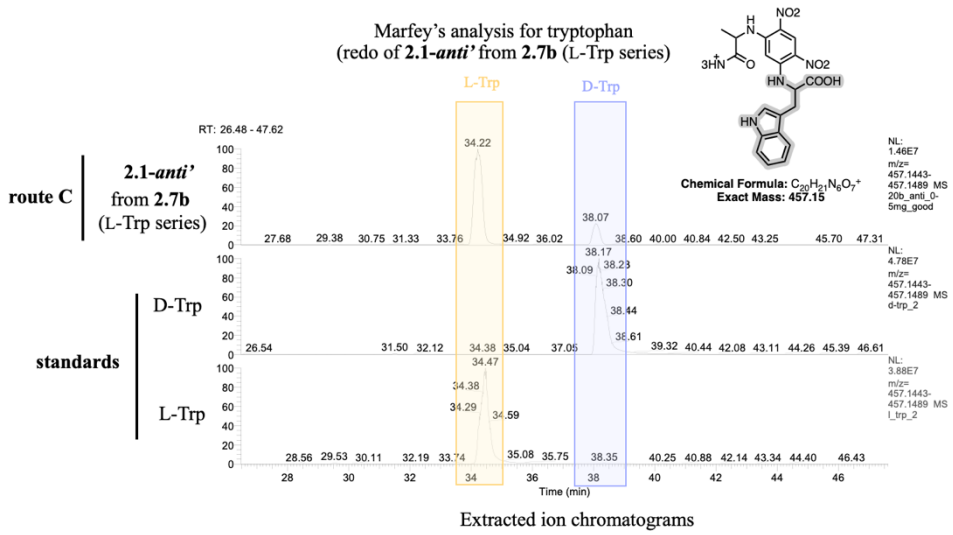


Figure 2.12. Repeat Marfey's analysis of the tryptophan residue in **2.1-*anti'*** from the L-Trp series (route C, **2.7b**), confirming the presence of L-Trp The initial assay was repeated due to inconclusive results across Pip and Trp Marfey's analyses.

2.5 References

(1) Yudin, A. K. *Chem. Sci.* **2015**, *6* (1), 30–49.

(2) Wessjohann, L. A.; Ruijter, E.; Garcia-Rivera, D.; Brandt, W. *Mol. Divers.* **2005**, *9* (1), 171–186.

(3) Mallinson, J.; Collins, I. *Future Med. Chem.* **2012**, *4* (11), 1409–1438.

(4) Driggers, E. M.; Hale, S. P.; Lee, J.; Terrett, N. K. *Nat. Rev. Drug Discov.* **2008**, *7* (7), 608–624.

(5) Kim, T.; Baek, E.; Kim, J. *Pharmaceuticals* **2025**, *18* (5), 617.

(6) Zhang, C.; Liu, F.; Zhang, Y.; Song, C. *Eur. J. Med. Chem.* **2024**, *268*, 116234.

(7) Fang, Z.; Song, Y.; Zhan, P.; Zhang, Q.; Liu, X. *Future Med. Chem.* **2014**, *6* (8), 885–901.

(8) He, J.; Ghosh, P.; Nitsche, C. *Chem. Sci.* **2024**, *15* (7), 2300–2322.

(9) Fouché, M.; Schäfer, M.; Berghausen, J.; Desrayaud, S.; Blatter, M.; Piéchon, P.; Dix, I.; Martin Garcia, A.; Roth, H.-J. *ChemMedChem* **2016**, *11* (10), 1048–1059.

(10) Faris, J. H.; Adaligil, E.; Popovych, N.; Ono, S.; Takahashi, M.; Nguyen, H.; Plise, E.; Taechalertpaisarn, J.; Lee, H.-W.; Koehler, M. F. T.; Cunningham, C. N.; Lokey, R. S. *J. Am. Chem. Soc.* **2024**, *146* (7), 4582–4591.

(11) Fang, P.; Pang, W.-K.; Xuan, S.; Chan, W.-L.; Leung, K. C.-F. *Chem. Soc. Rev.* **2024**, *53* (24), 11725–11771.

(12) Wang, H.; Bi, T.; Yang, W. *Acc. Chem. Res.* **2025**, *58* (19), 3096–3110.

(13) Amrhein, J. A.; Knapp, S.; Hanke, T. *J. Med. Chem.* **2021**, *64* (12), 7991–8009.

(14) Saridakis, I.; Kaiser, D.; Maulide, N. *ACS Cent. Sci.* **2020**, *6* (11), 1869–1889.

(15) Donald, J. R.; Unsworth, W. P. *Chem. – Eur. J.* **2017**, *23* (37), 8780–8799.

(16) Zalessky, I.; Wootton, J. M.; Tam, J. K. F.; Spurling, D. E.; Glover-Humphreys, W. C.; Donald, J. R.; Orukotan, W. E.; Duff, L. C.; Knapper, B. J.; Whitwood, A. C.; Tanner, T. F. N.; Miah, A. H.; Lynam, J. M.; Unsworth, W. P. *J. Am. Chem. Soc.* **2024**, *146* (8), 5702–5711.

(17) Fürstner, A. *Acc. Chem. Res.* **2021**, *54* (4), 861–874.

(18) Garnes-Portolés, F.; Leyva-Pérez, A. *ACS Catal.* **2023**, *13* (14), 9415–9426.

(19) Nubbemeyer, U. Synthesis of Medium-Sized Ring Lactams. In *Stereoselective Heterocyclic Synthesis III*; Metz, P., Ed.; Springer: Berlin, Heidelberg, 2001; pp 125–196.

(20) Zhang, X.; Lin, L.; Li, J.; Duan, S.; Long, Y.; Li, J. *Chin. J. Org. Chem.* **2021**, *41* (5), 1878.

(21) Clarke, A. K.; Unsworth, W. P. *Chem. Sci.* **2020**, *11* (11), 2876–2881.

(22) Bogdan, A. R.; Jerome, S. V.; Houk, K. N.; James, K. *J. Am. Chem. Soc.* **2012**, *134* (4), 2127–2138.

(23) Paquette, A. R.; Boddy, C. N. *Org. Biomol. Chem.* **2023**, *21* (40), 8043–8053.

(24) Bechtler, C.; Lamers, C. *RSC Med. Chem.* **2021**, *12* (8), 1325.

(25) Cochrane, J. R.; Yoon, D. H.; McErlean, C. S. P.; Jolliffe, K. A. *Beilstein J. Org. Chem.* **2012**, *8*, 1344–1351.

(26) Swamy, K. C. K.; Kumar, N. N. B.; Balaraman, E.; Kumar, K. V. P. P. *Chem. Rev.* **2009**, *109* (6), 2551–2651.

(27) Lobo-Ruiz, A.; Tulla-Puche, J. 2 - Synthetic Approaches of Naturally and Rationally Designed Peptides and Peptidomimetics. In *Peptide Applications in Biomedicine, Biotechnology and Bioengineering*; Koutsopoulos, S., Ed.; Woodhead Publishing, 2018; pp 23–49.

(28) El-Faham, A.; Albericio, F. *Chem. Rev.* **2011**, *111* (11), 6557–6602.

(29) Požgan, F.; Štefane, B.; Kiđemet, D.; Smodiš, J.; Zupet, R. *Tetrahedron* **2012**, *68* (25), 5081–5086.

(30) Brillon, D.; Deslongchamps, P. *Can. J. Chem.* **1987**, *65* (1), 43–55.

(31) Cordes, M.; Kalesse, M. Synthesis of 12- to 16-Membered-Ring Lactones. In *Synthesis of Saturated Oxygenated Heterocycles II: 7- to 16-Membered Rings*; Cossy, J., Ed.; Springer: Berlin, Heidelberg, 2014; pp 369–427.

(32) Yadav, J. S.; Amrutapu, S. K.; Pabbaraja, S. *ChemistrySelect* **2017**, *2* (5), 1850–1853.

(33) Reddy, K. M.; Shashidhar, J.; Pottireddygari, G. R.; Ghosh, S. *Tetrahedron Lett.* **2011**, *52* (45), 5987–5991.

(34) Elmarrouni, A.; Fukuda, A.; Heras, M.; Arseniyadis, S.; Cossy, J. *J. Org. Chem.* **2010**, *75* (24), 8478–8486.

(35) Xiao, Y.; Liu, J.; Jiang, Y.; Guo, Y.; Ye, T. *Molecules* **2024**, *29* (15), 3599.

(36) Chen, J.; Jiang, Y.; Yan, J.; Xu, C.; Ye, T. *Molecules* **2023**, *28* (20), 7194.

(37) Feng, J.; Liu, J.; Ye, T. *Org. Lett.* **2025**, *27* (33), 9299–9303.

(38) Ghosh, A. K.; Xu, C. X. *Org. Lett.* **2009**, *11* (9), 1963–1966.

(39) Kaneda, M.; Inuki, S.; Ohno, H.; Oishi, S. *J. Org. Chem.* **2018**, *83* (6), 3047–3060.

(40) Zhao, Z.; Wu, Y.; Li, Y. *Chin. J. Chem.* **2017**, *35* (7), 1185–1194.

(41) Feng, Y.; Blunt, J. W.; Cole, A. L. J.; Munro, M. H. G. *Org. Lett.* **2002**, *4* (12), 2095–2096.

(42) Carpino, L. A.; Imazumi, H.; Foxman, B. M.; Vela, M. J.; Henklein, P.; El-Faham, A.; Klose, J.; Bienert, M. *Org. Lett.* **2000**, *2* (15), 2253–2256.

(43) Yudin, A. K. *Chem. Sci.* **2014**, *6* (1), 30–49.

(44) Martí-Centelles, V.; Pandey, M. D.; Burguete, M. I.; Luis, S. V. *Chem. Rev.* **2015**, *115* (16), 8736–8834.

(45) Perlman, Z. E.; Bock, J. E.; Peterson, J. R.; Lokey, R. S. *Bioorg. Med. Chem. Lett.* **2005**, *15* (23), 5329–5334.

(46) Huang, Z.-S.; Wang, W.-R.; Yang, F.-H.; Gou, F.; Jiang, L.; Qiu, C.-C.; Tai, Y.-Y.; Yan, X.-S.; Wu, X.; Jiang, T.; Jiang, Y.-B. *JACS Au 6* (2), 1319–1326.

(47) Manne, S. R.; Sharma, A.; Sazonovas, A.; El-Faham, A.; de la Torre, B. G.; Albericio, F. *ACS Omega* **2022**, *7* (7), 6007–6023.

(48) Subirós-Funosas, R.; Prohens, R.; Barbas, R.; El-Faham, A.; Albericio, F. *Chemistry* **2009**, *15* (37), 9394–9403.

(49) Wang, Z.; Barrows, R. D.; Emge, T. J.; Knapp, S. *Org. Process Res. Dev.* **2017**, *21* (3), 399–407.

(50) Peptide Synthesis. In *Peptides: Chemistry and Biology*; John Wiley & Sons, Ltd, 2009; pp 175–315.

(51) Mahmoodi, N.; Qian, Q.; Luk, L. Y. P.; Tanner, M. E. *Pure Appl. Chem.* **2013**, *85* (10), 1935–1948.

(52) Roe, J. M.; Webster, R. A. B.; Ganesan, A. *Org. Lett.* **2003**, *5* (16), 2825–2827.

(53) Beholz, L. G.; Stille, J. R. *J. Org. Chem.* **1993**, *58* (19), 5095–5100.

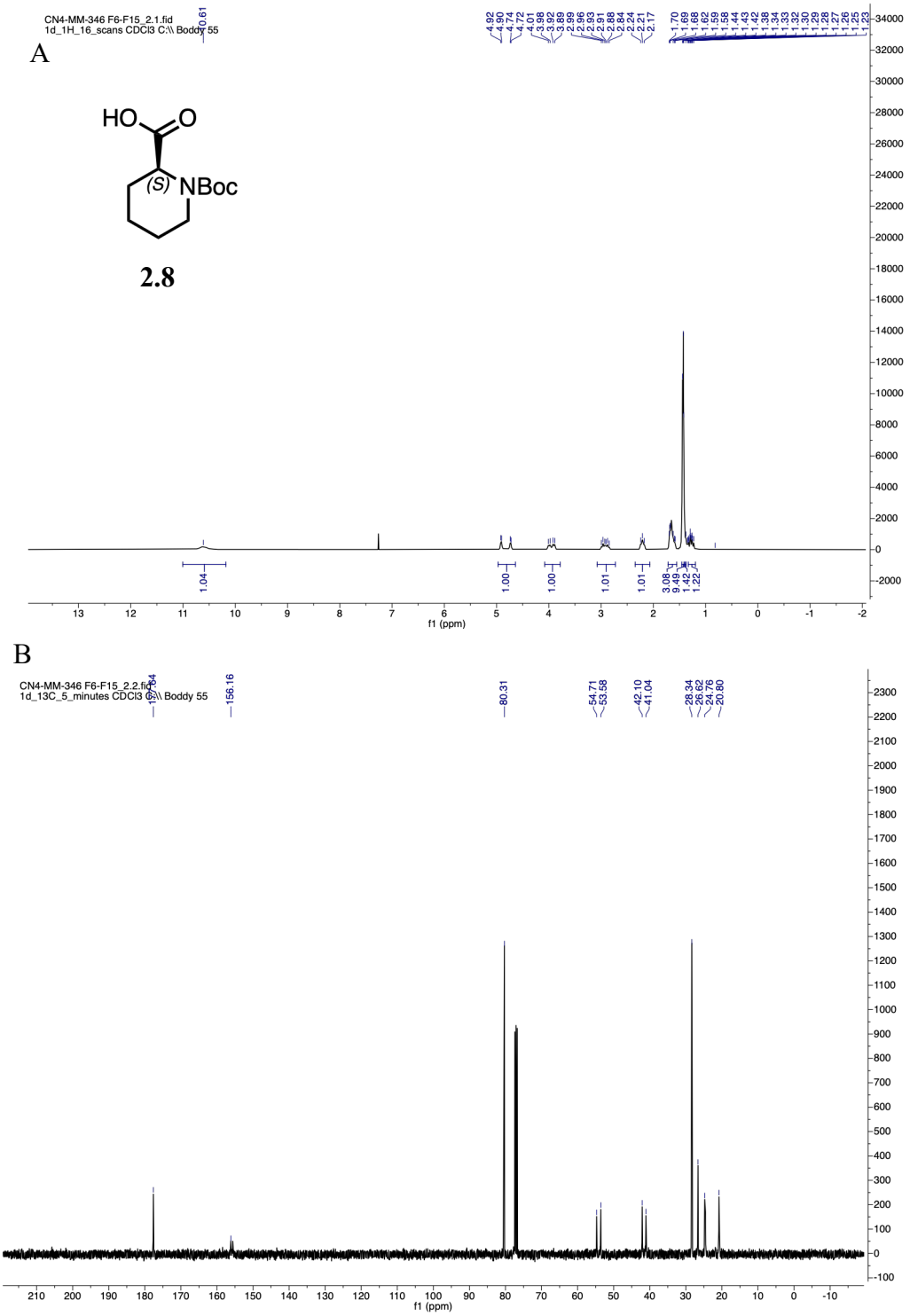
(54) Mahmoodi, N.; Tanner, M. E. *ChemBioChem* **2013**, *14* (15), 2029–2037.

(55) Thai, D. L.; Sapko, M. T.; Reiter, C. T.; Bierer, D. E.; Perel, J. M. *J. Med. Chem.* **1998**, *41* (4), 591–601.

(56) Kavanagh, M. E.; Gray, J. L.; Gilbert, S. H.; Coyne, A. G.; McLean, K. J.; Davis, H. J.; Munro, A. W.; Abell, C. *ChemMedChem* **2016**, *11* (17), 1924–1935.

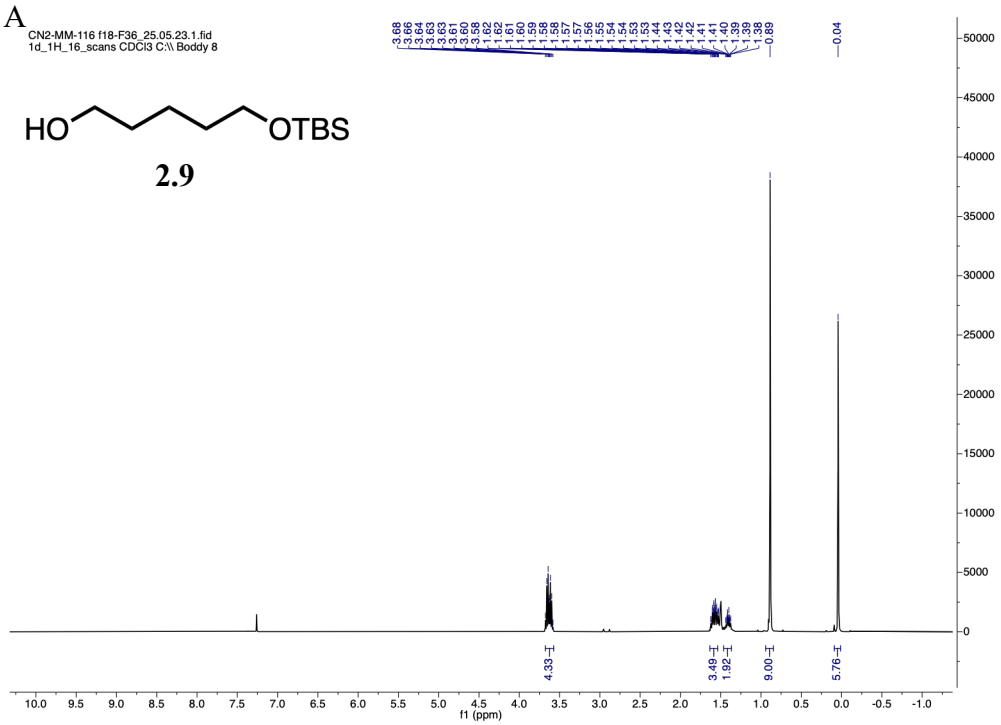
(57) Naganna, N.; Madhavan, N. *J. Org. Chem.* **2014**, *79* (23), 11549–11557.

2.6 Appendix to Chapter II

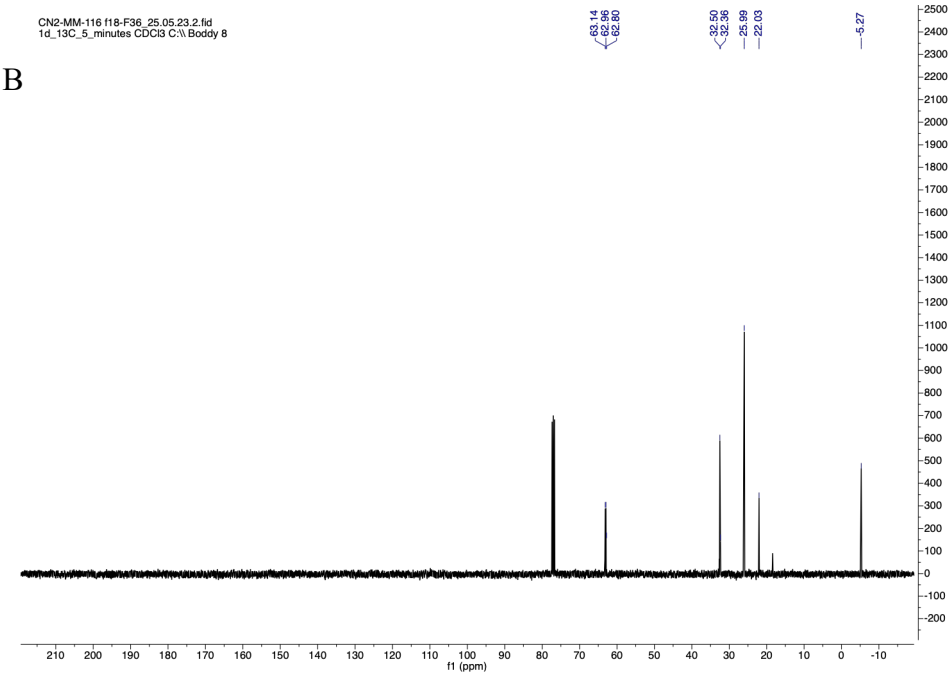


Spectra 2.1 Spectra of compound **2.8** (A) 1H NMR (400 MHz, CDCl3) and (B) 13C NMR (101MHz, CDCl3)

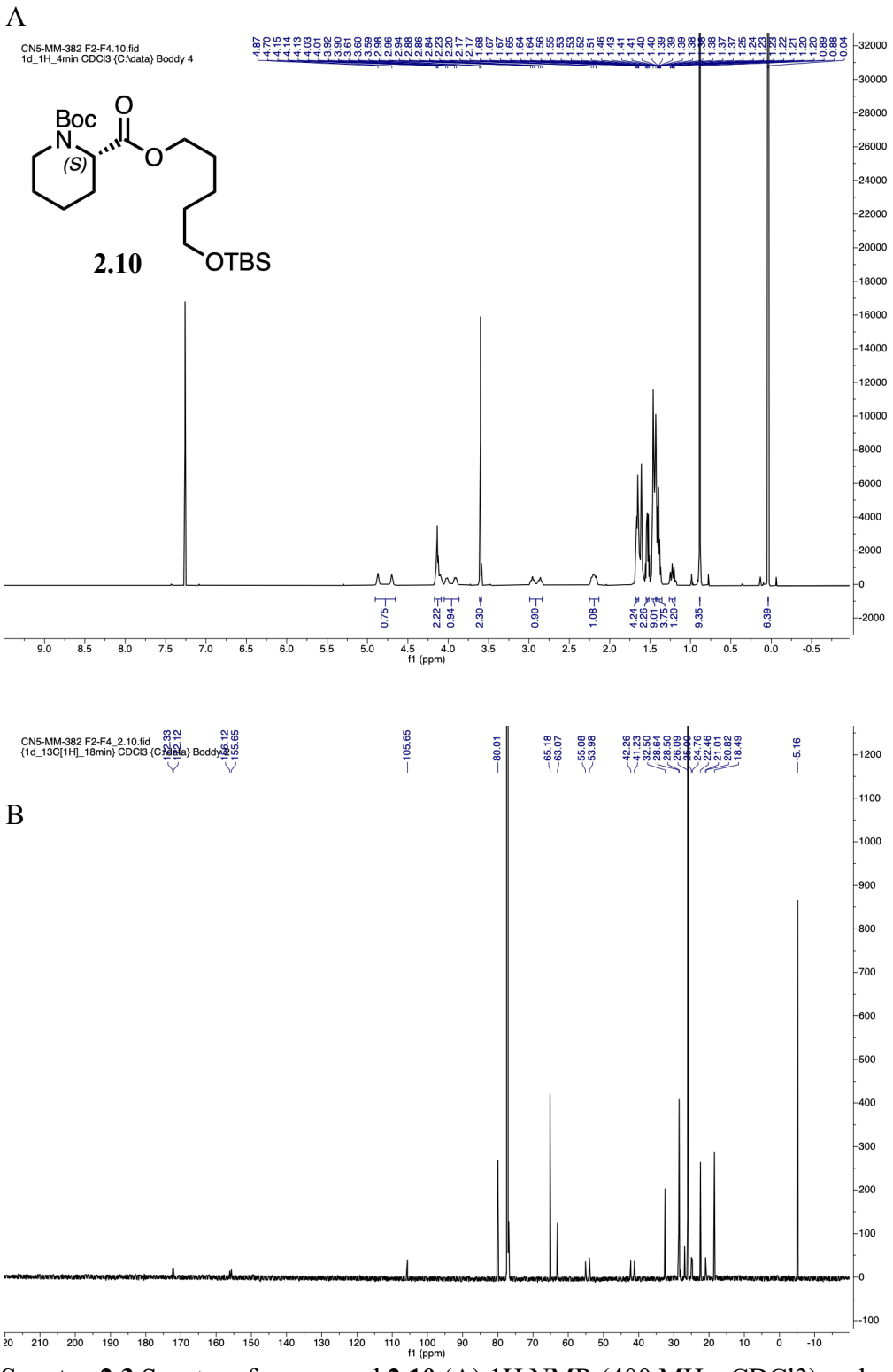
A



B

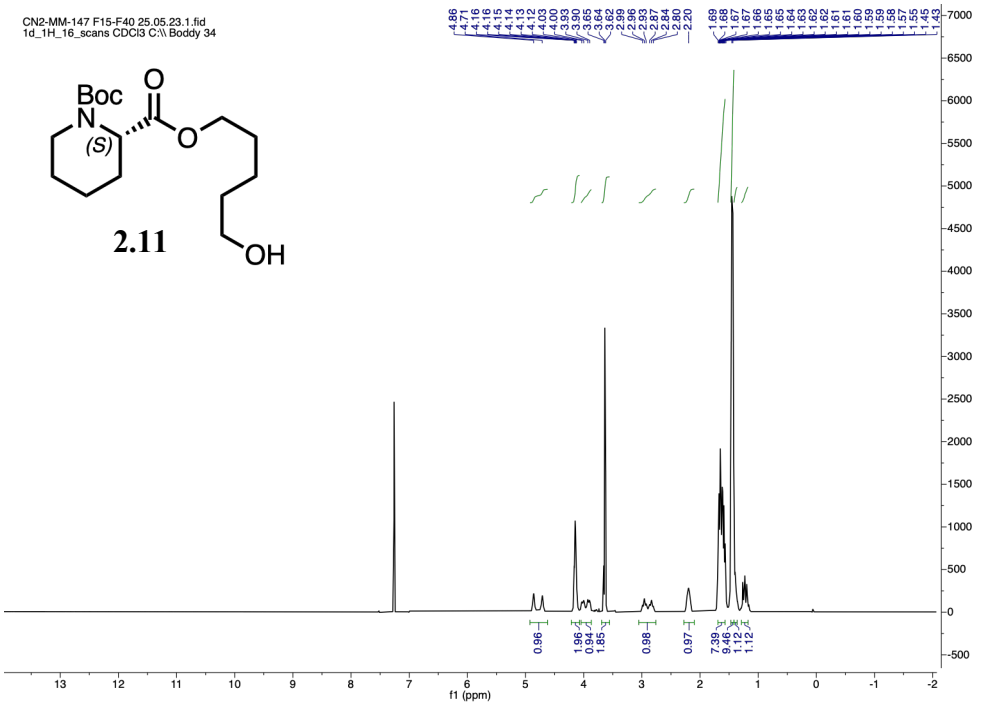


Spectra 2.2 Spectra of compound **2.9** (A) 1H NMR (400 MHz, CDCl3) and (B) 13C NMR (101MHz, CDCl3)

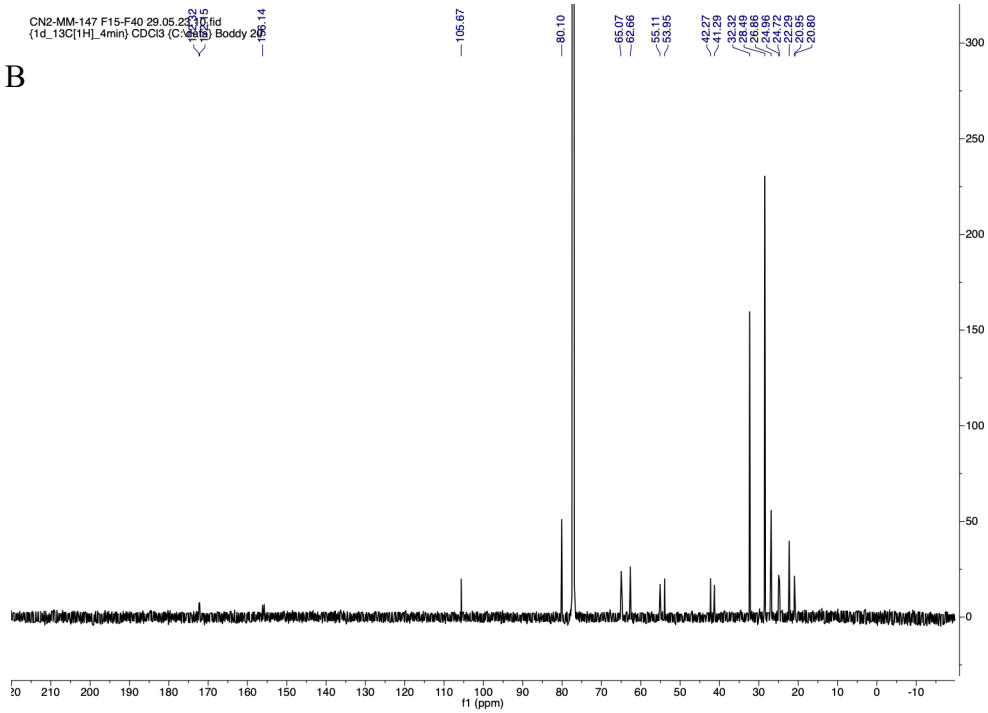


Spectra 2.3 Spectra of compound **2.10** (A) 1H NMR (400 MHz, CDCl3) and (B) 13C NMR (101MHz, CDCl3)

A

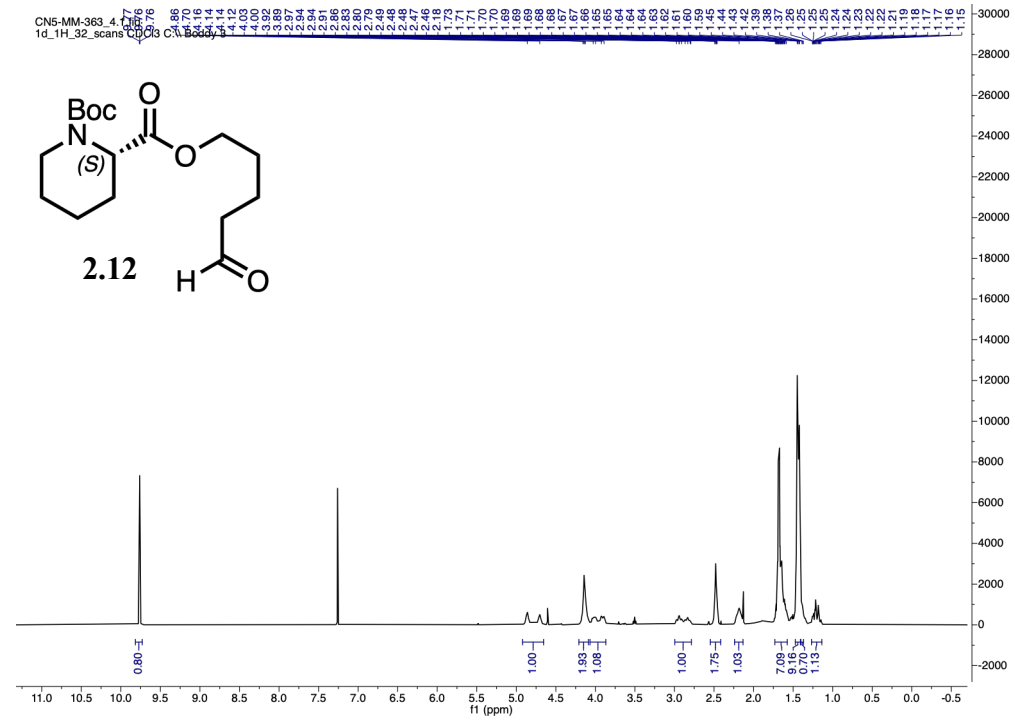


B

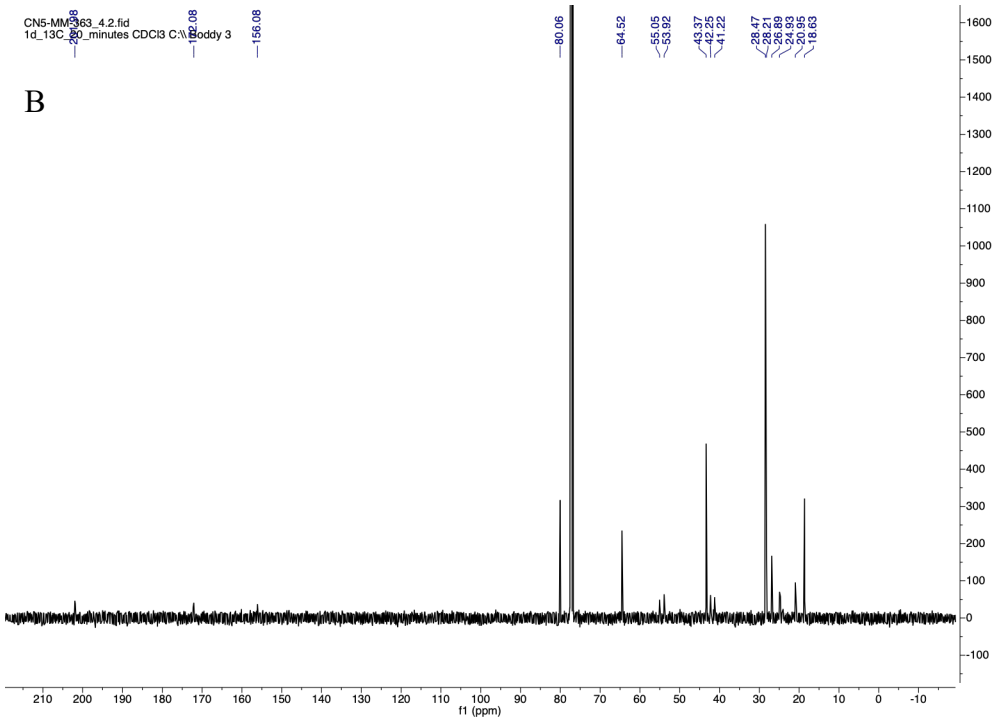


Spectra 2.4 Spectra of compound **2.11** (A) 1H NMR (400 MHz, CDCl3) and (B) 13C NMR (101MHz, CDCl3)

A

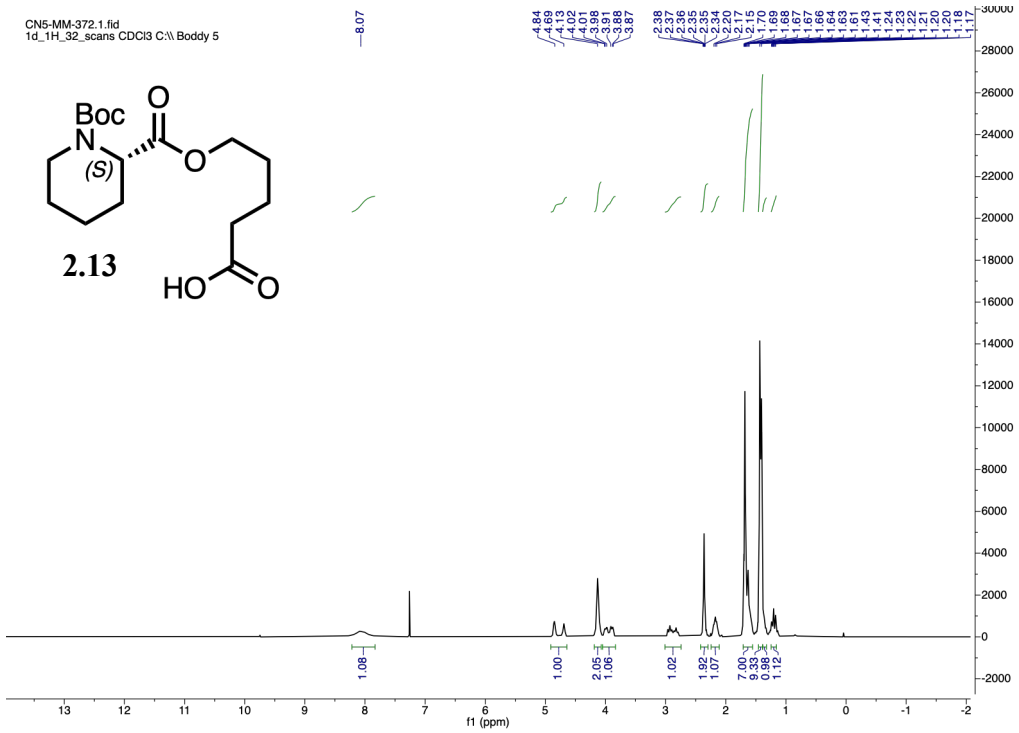


B

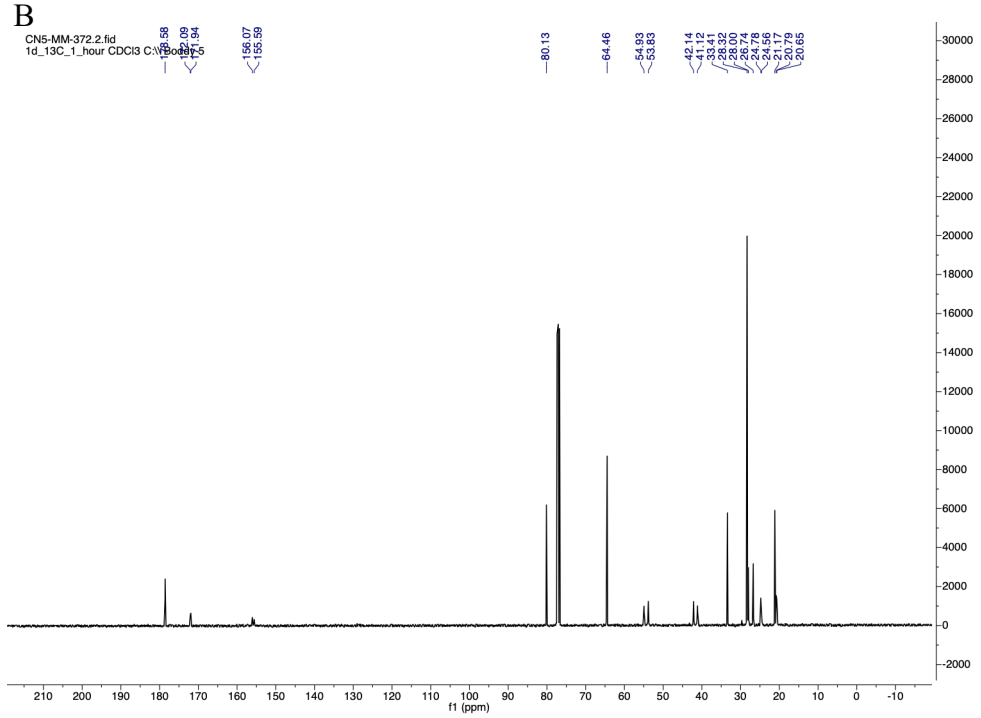


Spectra 2.5 Spectra of compound **2.12** (A) 1H NMR (400 MHz, CDCl3) and (B) 13C NMR (101MHz, CDCl3)

A

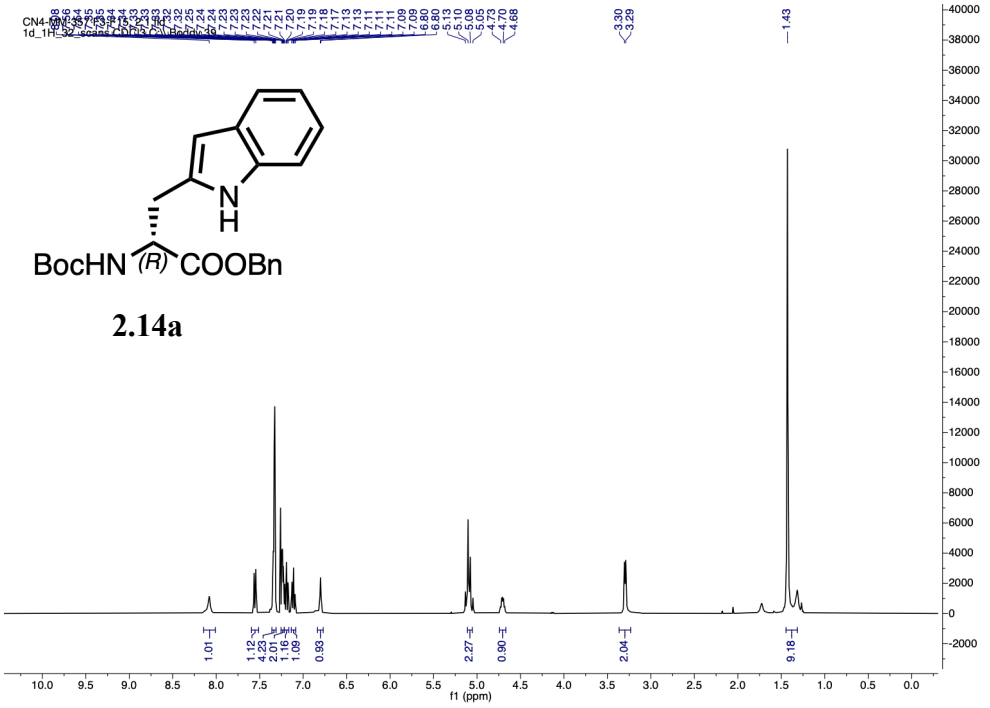


B

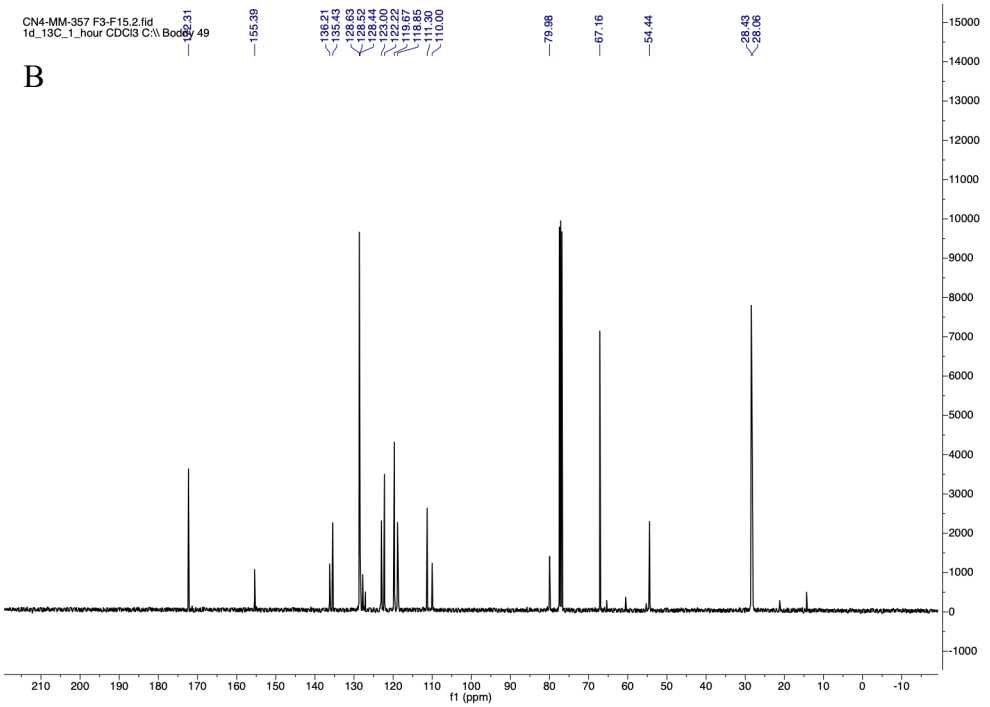


Spectra 2.6 Spectra of compound **2.13** (A) 1H NMR (400 MHz, CDCl3) and (B) 13C NMR (101MHz, CDCl3)

A

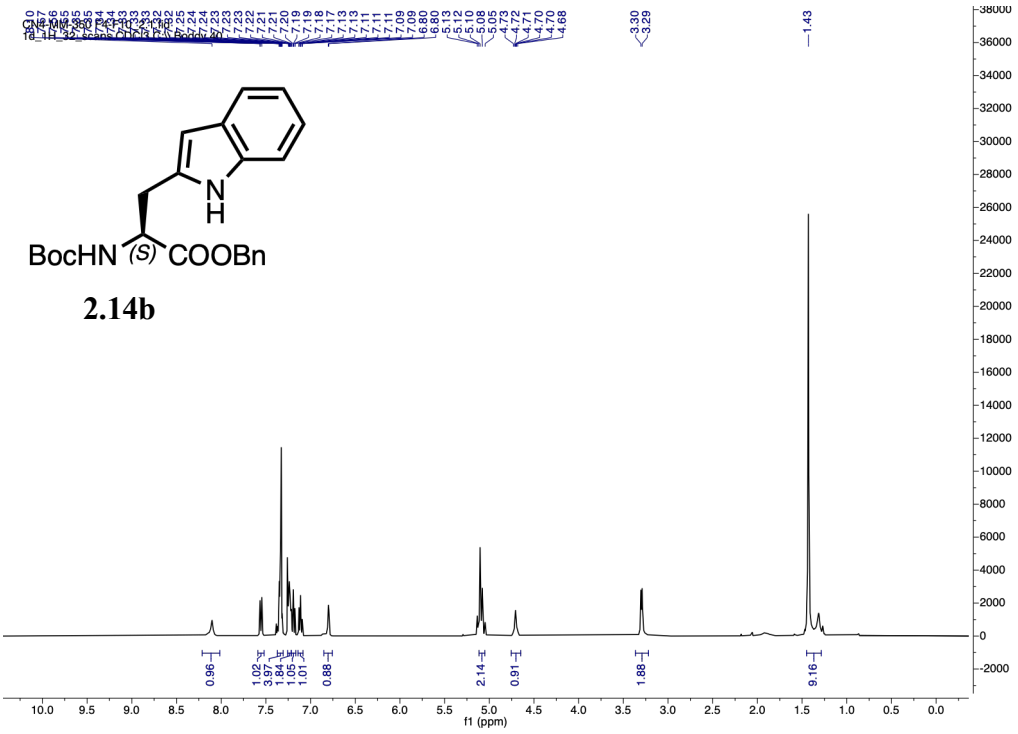


B

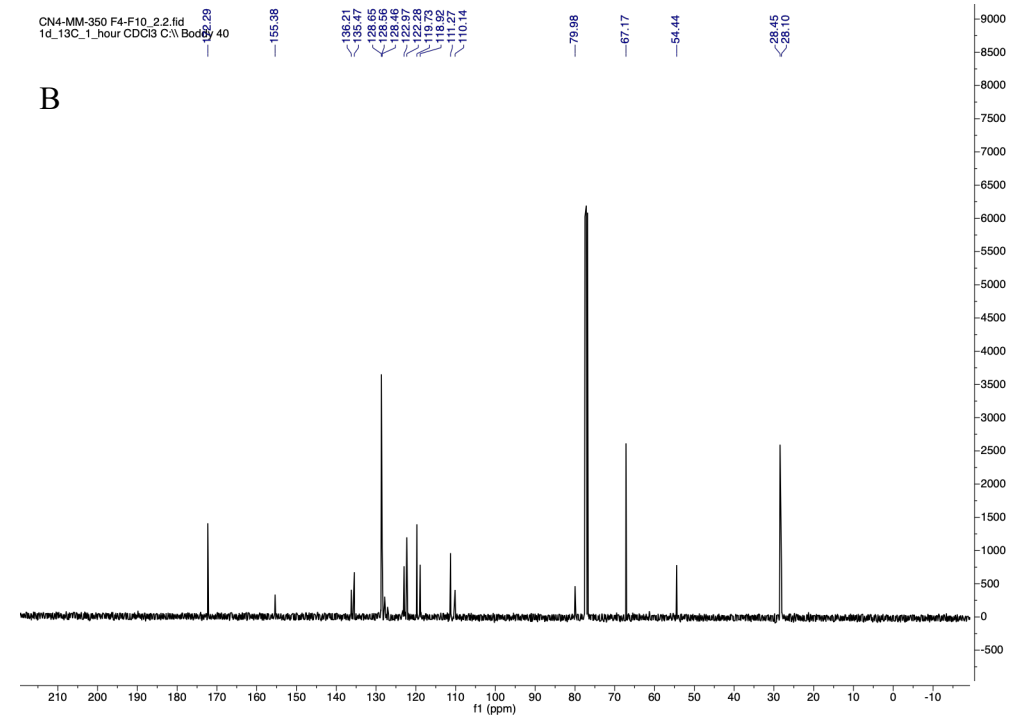


Spectra 2.7 Spectra of compound **2.14a** (A) 1H NMR (400 MHz, CDCl3) and (B) 13C NMR (101MHz, CDCl3)

A

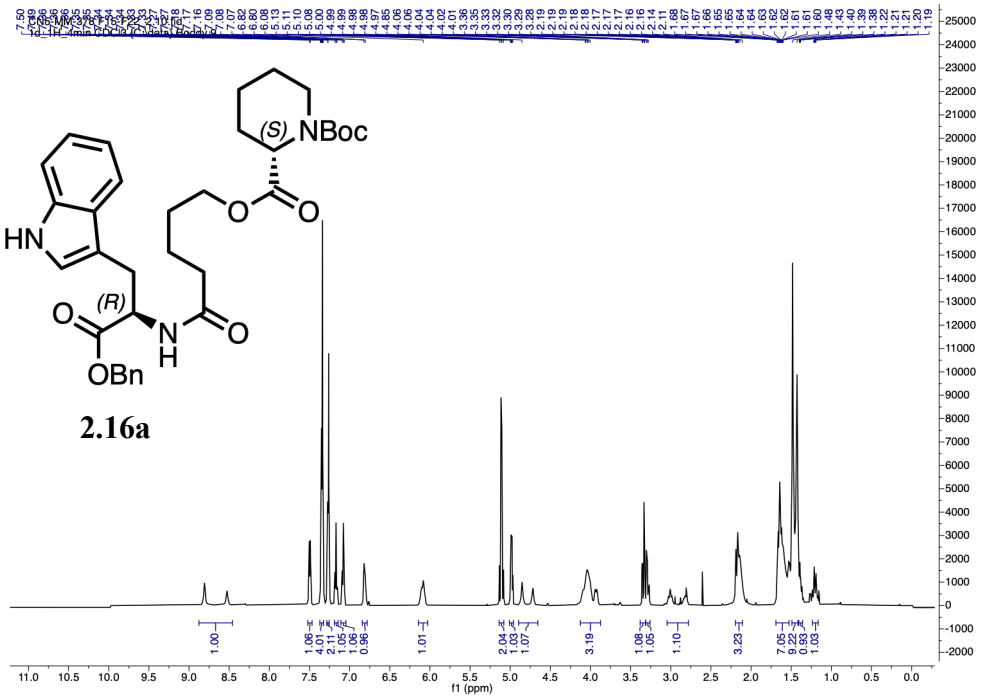


B

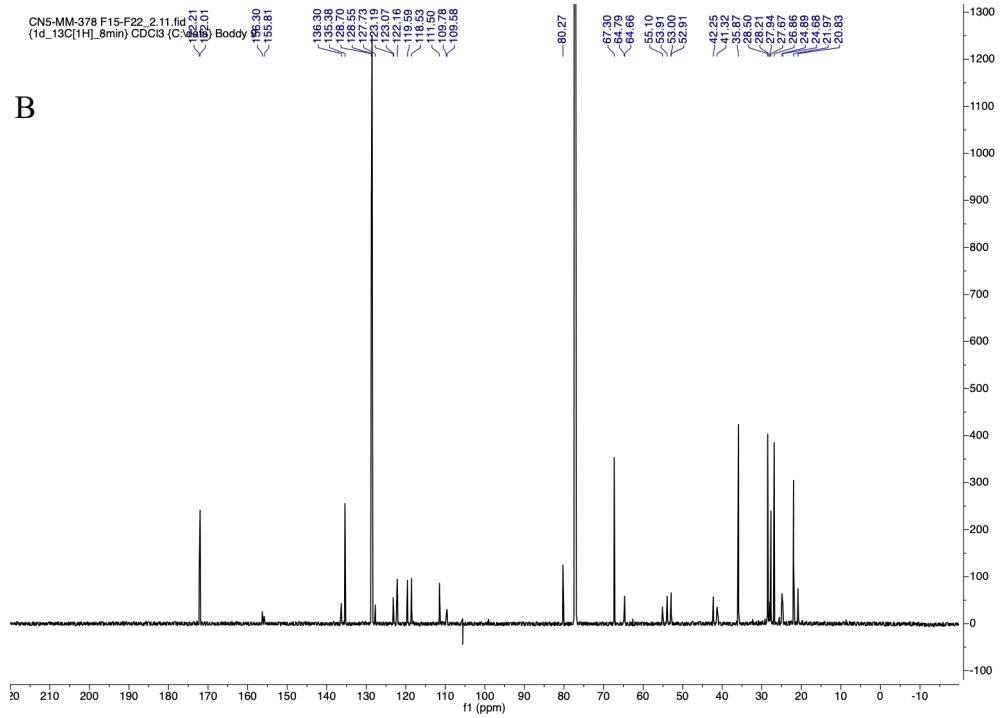


Spectra 2.8 Spectra of compound **2.14b** (A) 1H NMR (400 MHz, CDCl3) and (B) 13C NMR (101MHz, CDCl3)

A

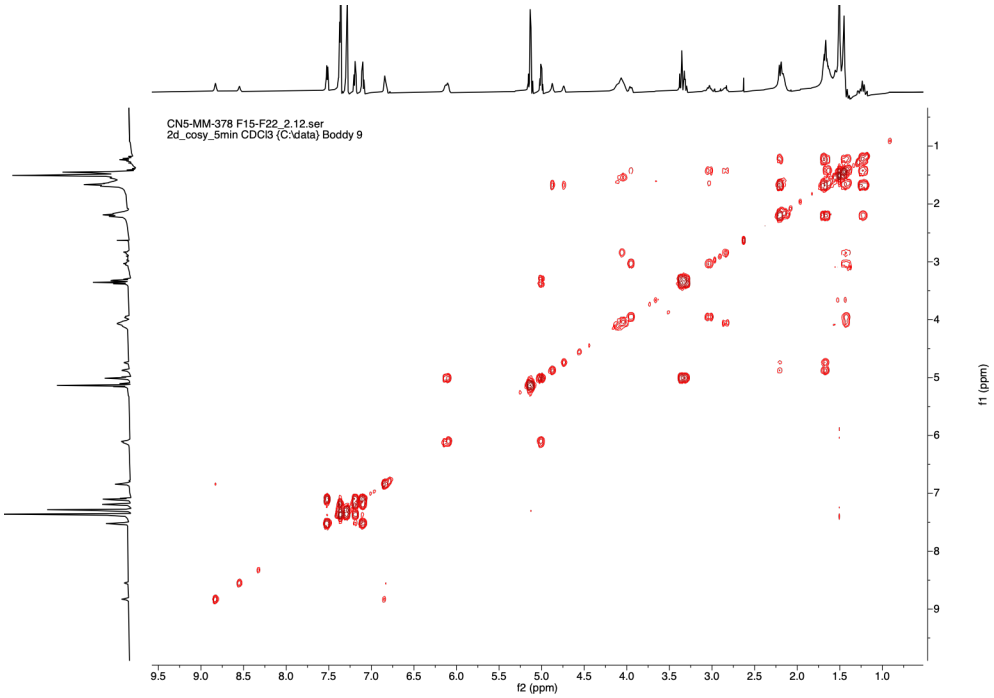


B

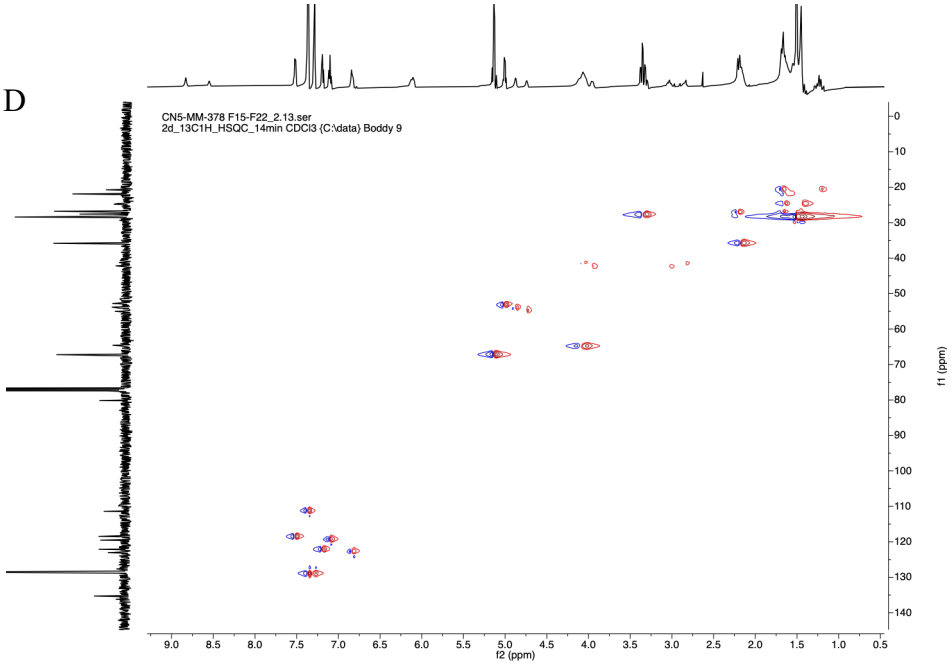


Spectra 2.9 Spectra of compound **2.16a** (A) 1H NMR (400 MHz, CDCl3) and (B) 13C NMR (101MHz, CDCl3)

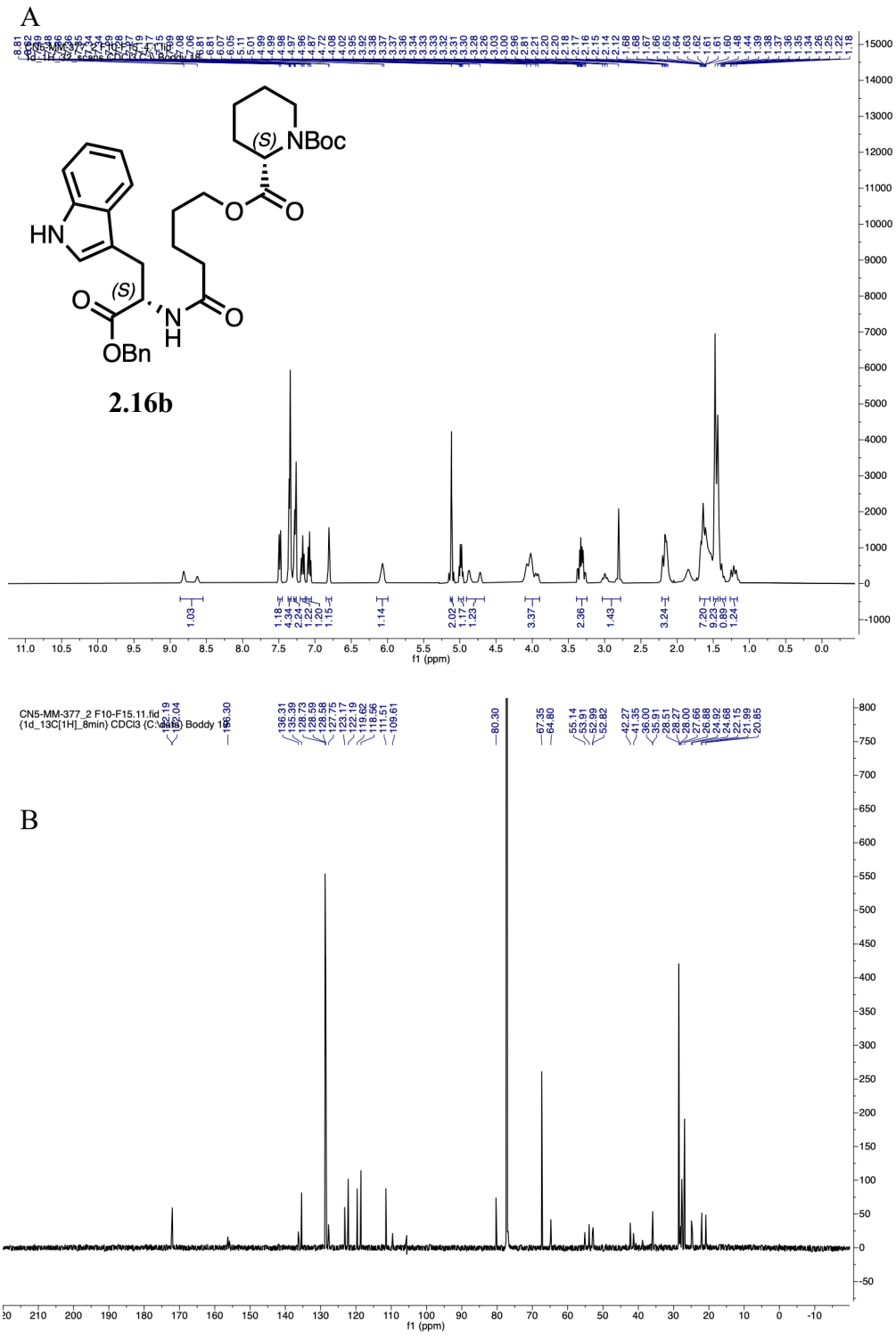
C



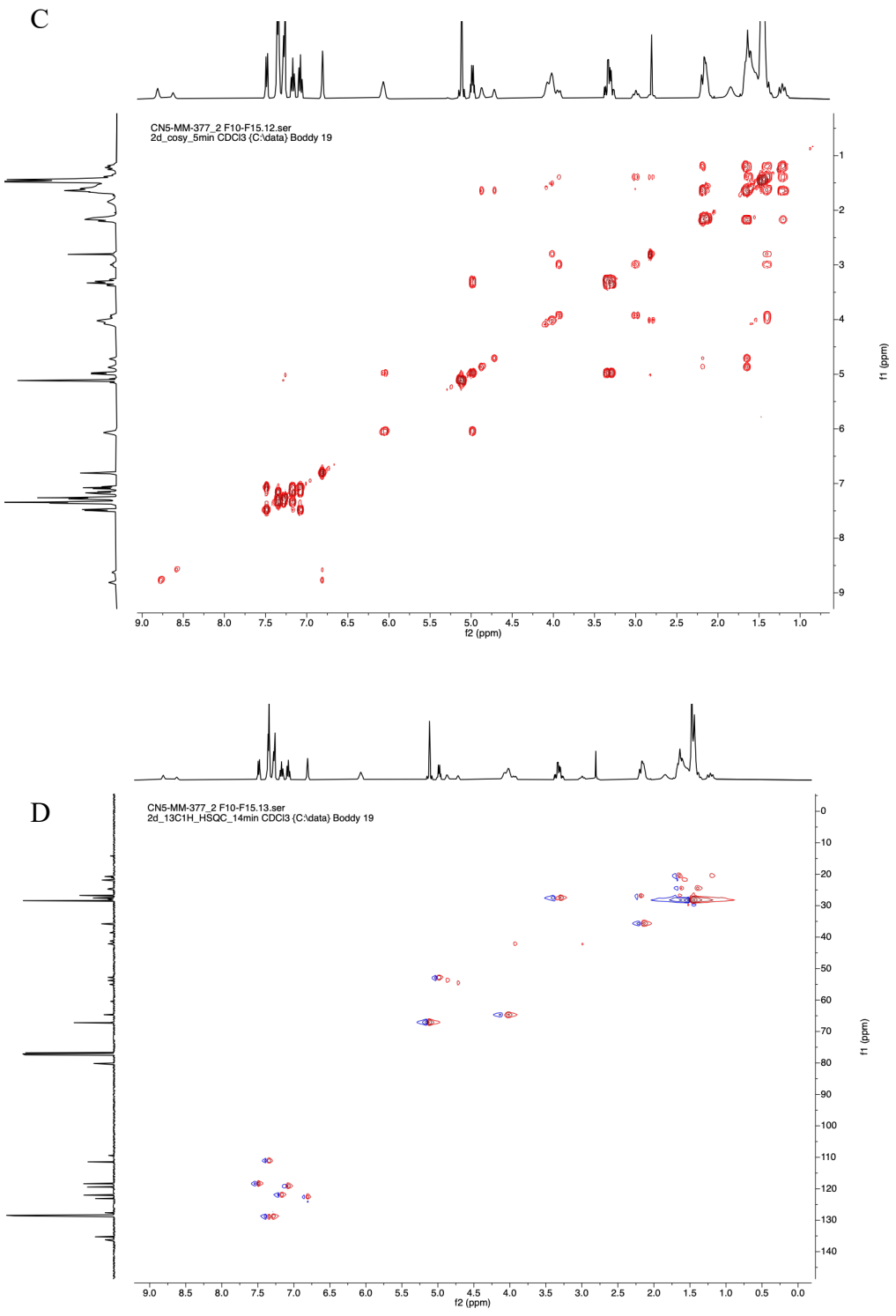
D



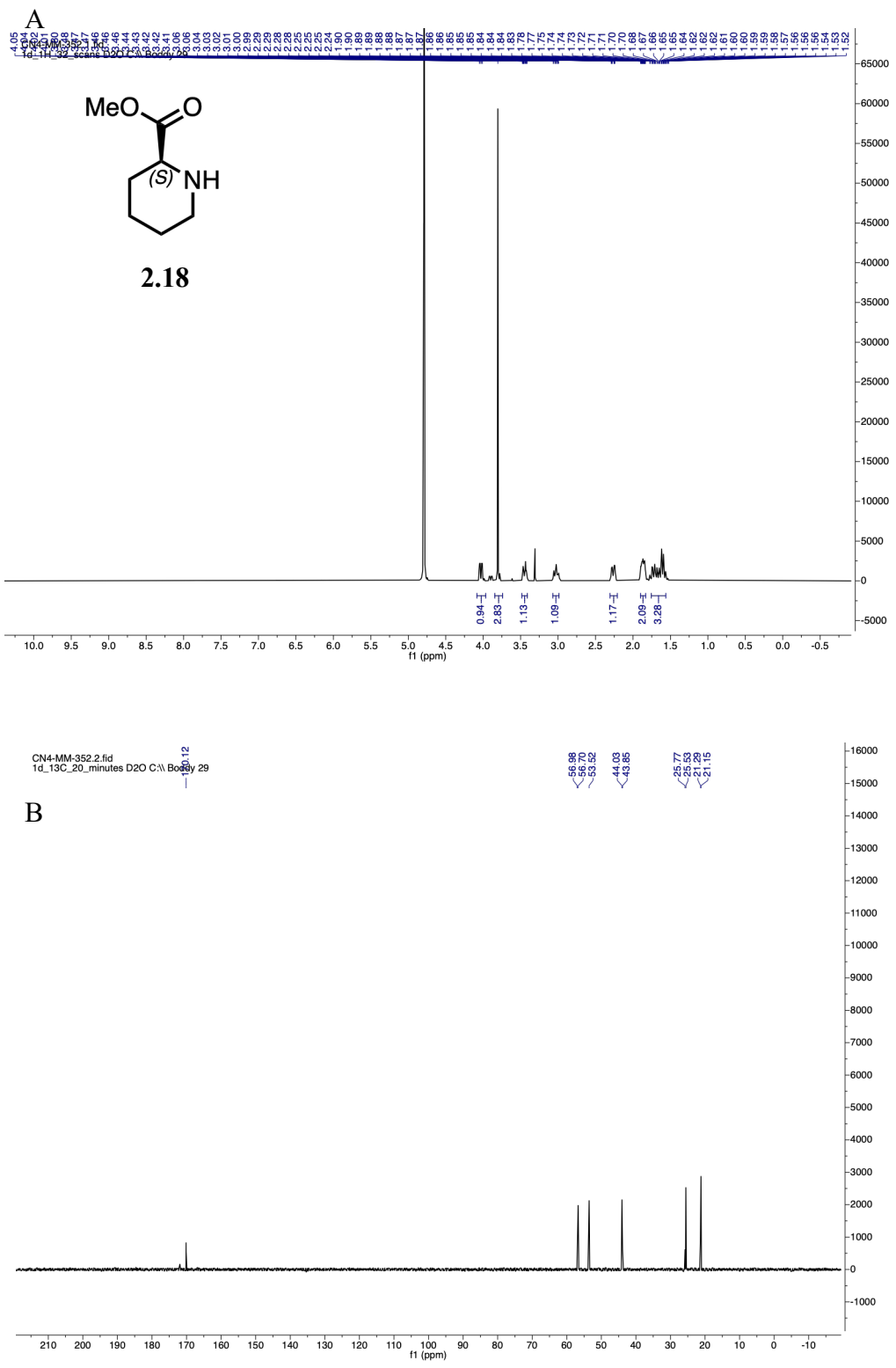
Spectra 2.10 Spectra of compound **2.16a** (C) COSY (CDCl3) and (D) HSQC (CDCl3)



Spectra 2.11 Spectra of compound **2.16b** (A) 1H NMR (400 MHz, CDCl3) and (B) 13C NMR (101MHz, CDCl3)

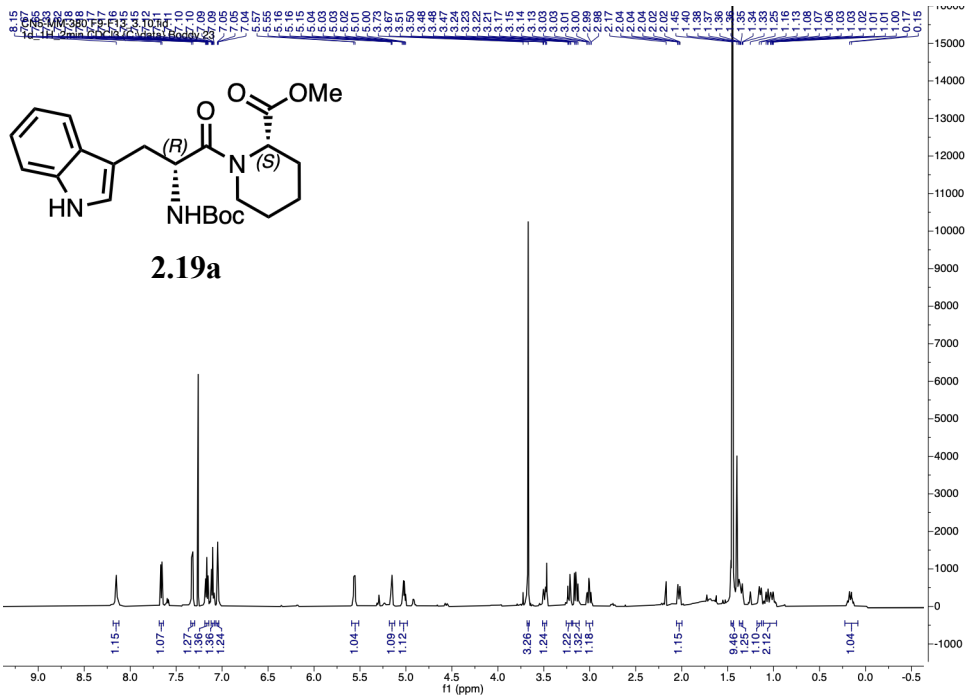


Spectra 2.12 Spectra of compound **2.16b** (C) COSY (CDCl3) and (D) HSQC (CDCl3)



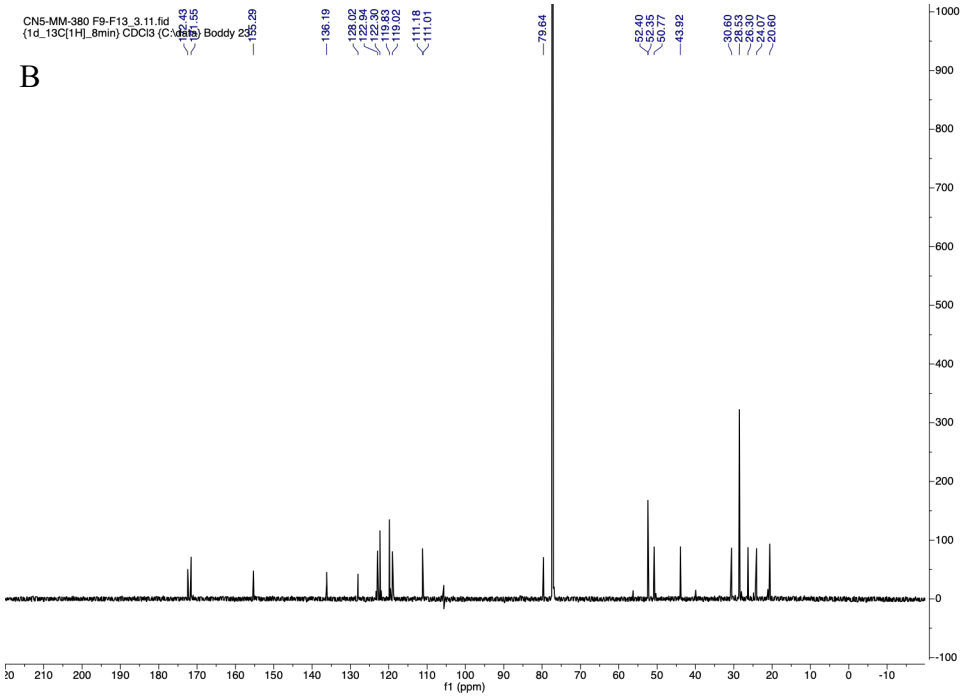
Spectra 2.13 Spectra of compound **2.18** (A) 1H NMR (400 MHz, CDCl3) and (B) 13C NMR (101MHz, CDCl3)

A



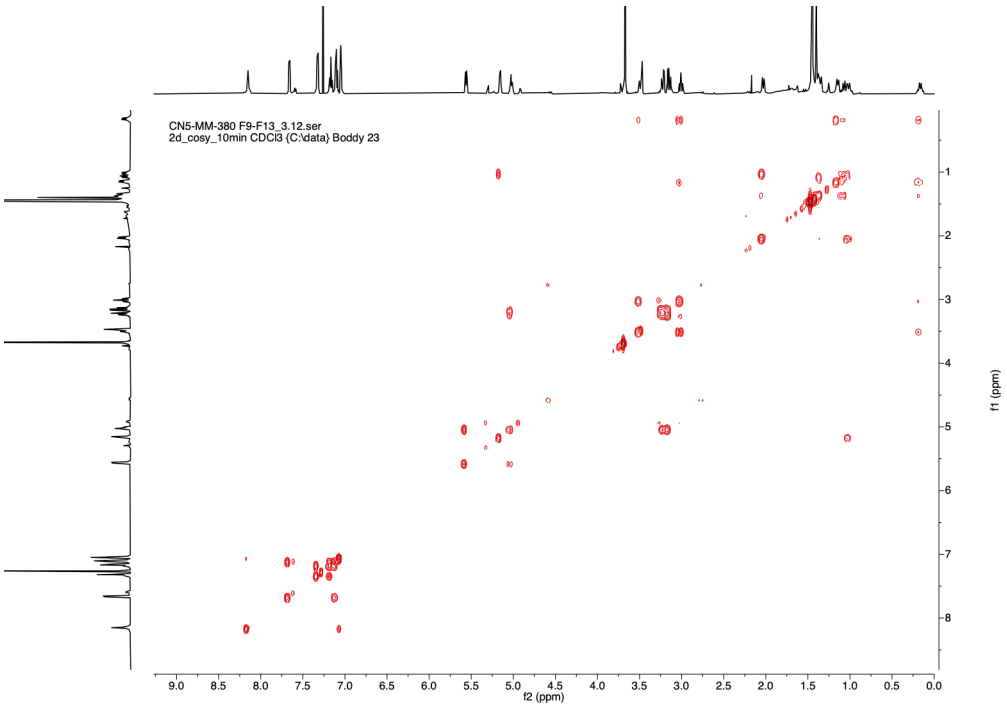
2.19a

B

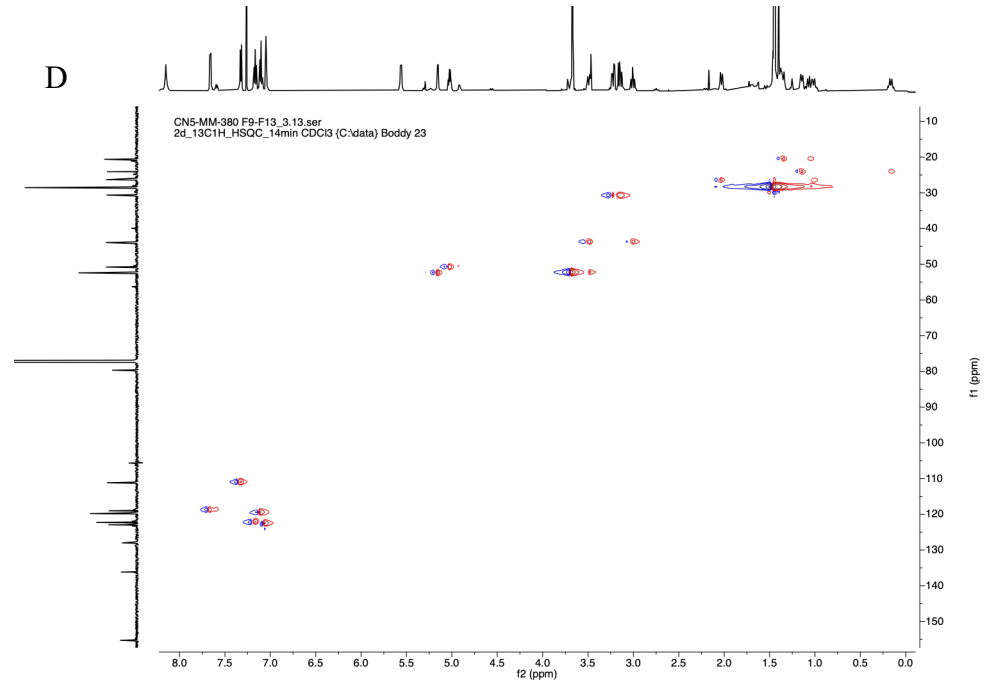


Spectra 2.14 Spectra of compound **2.19a** (A) 1H NMR (400 MHz, CDCl3) and (B) 13C NMR (101MHz, CDCl3)

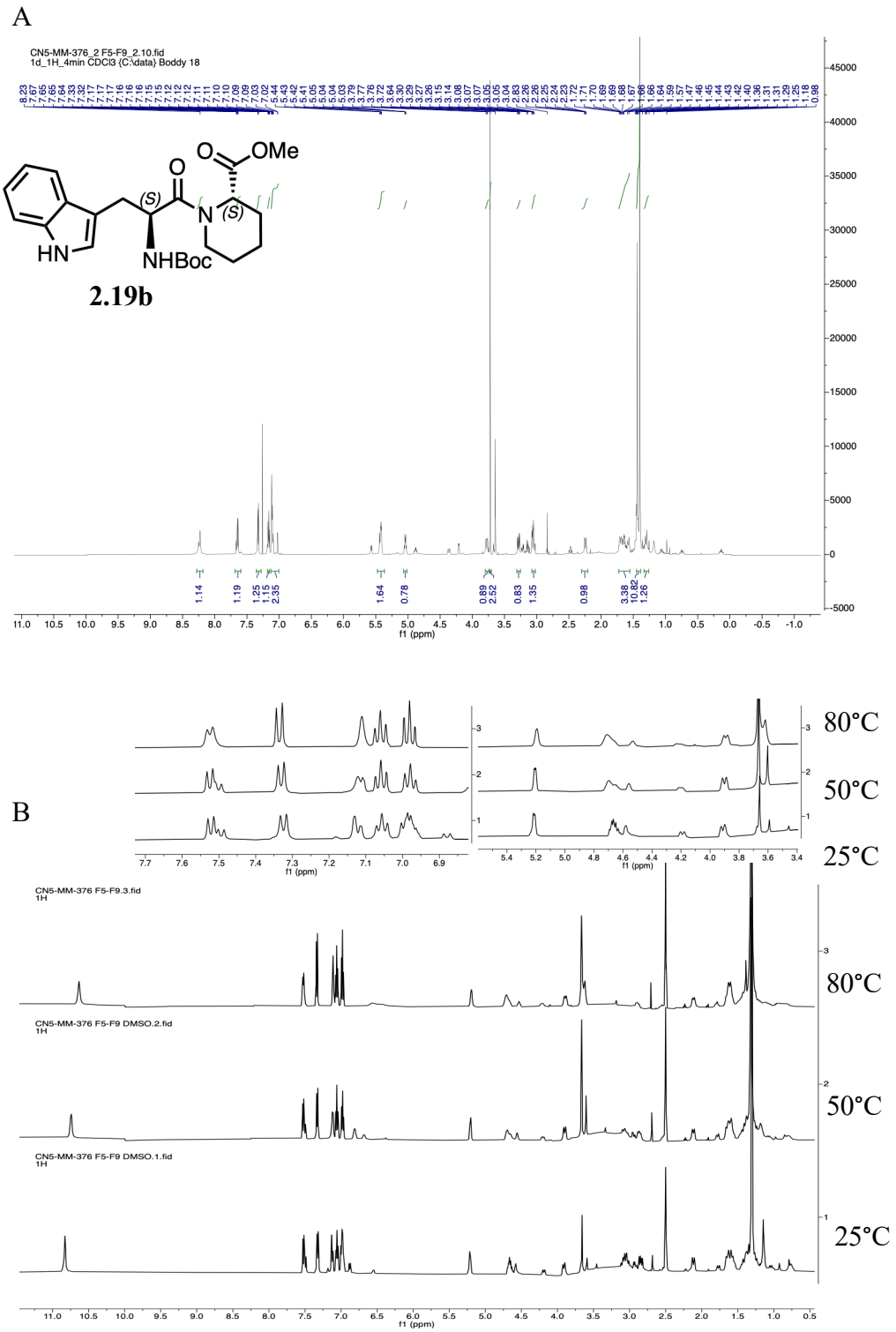
C



D

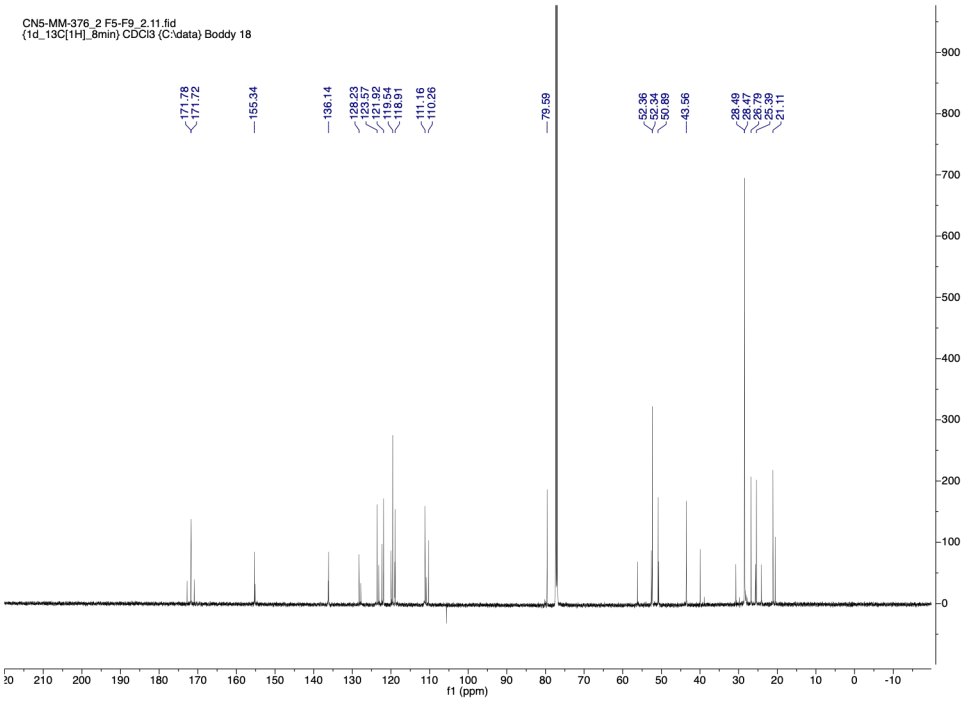


Spectra 2.15 Spectra of compound **2.19a** (C) COSY (CDCl3) and (D) HSQC (CDCl3)

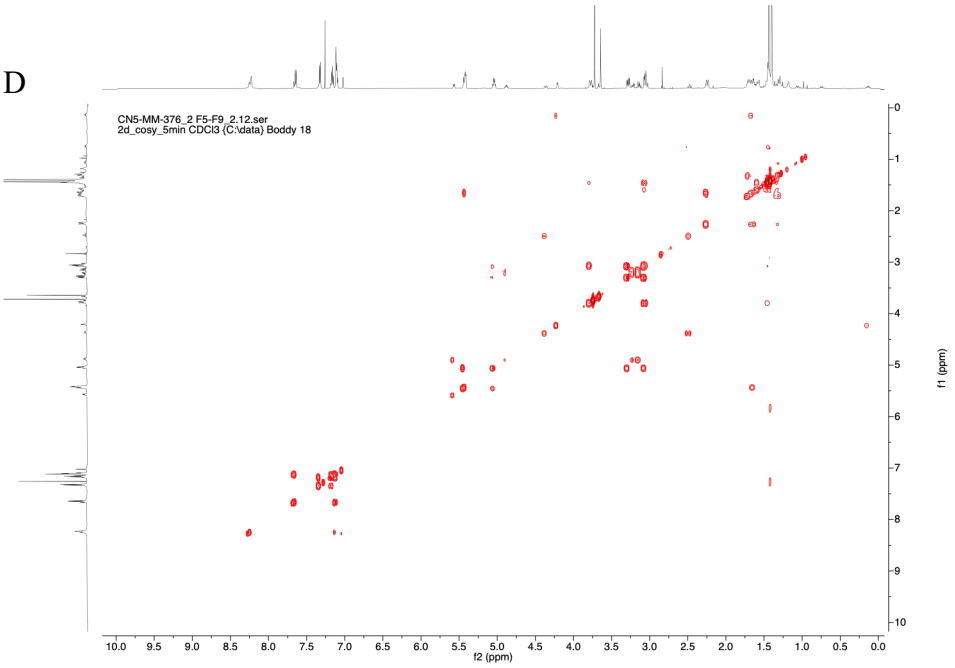


Spectra 2.16 Spectra of compound **2.19b** (A) 1H NMR (400 MHz, CDCl3) and (B) Variable temperature (VT) 1H NMR (500 MHz, d-DMSO) collected at 25°C, 50°C and 80°C

C

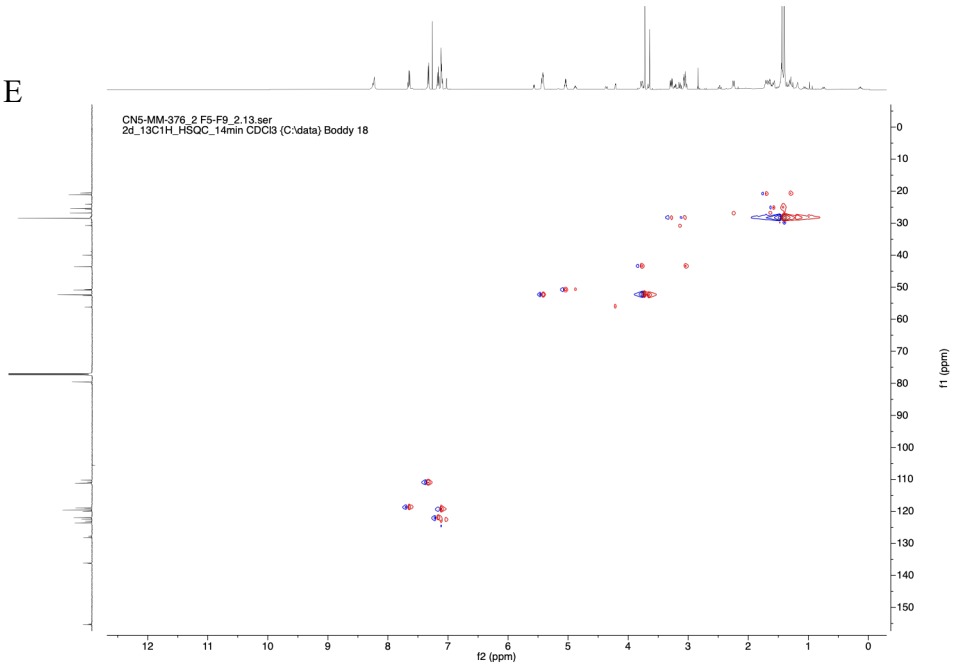


D



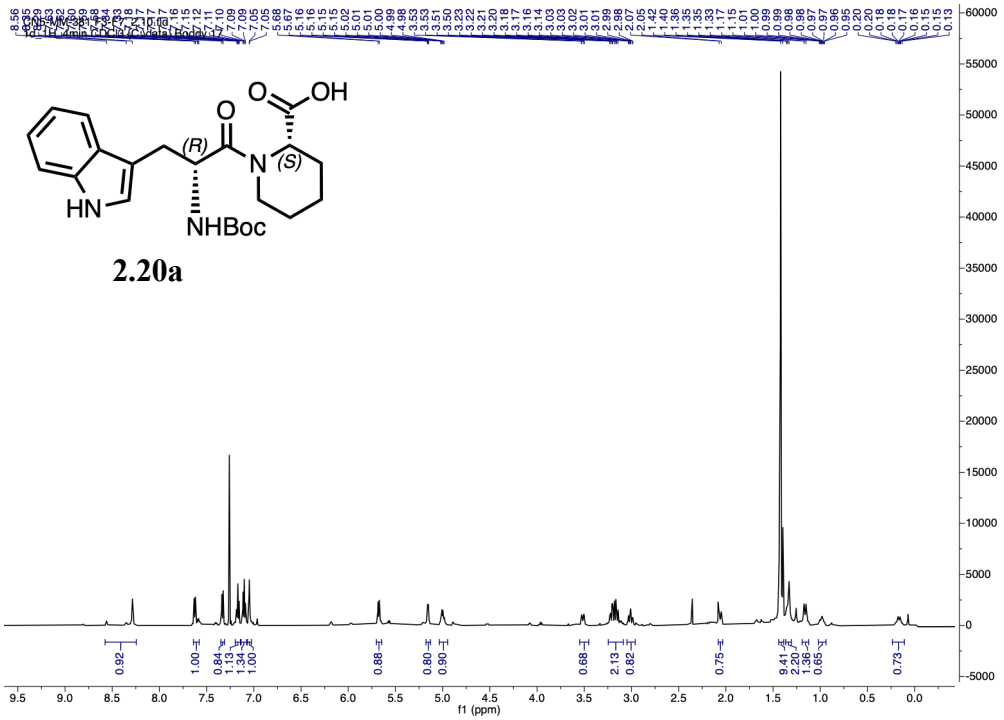
Spectra 2.17 Spectra of compound **2.19b** (C) 1H NMR (400 MHz, CDCl3) and (D) 13C NMR (101MHz, CDCl3)

E



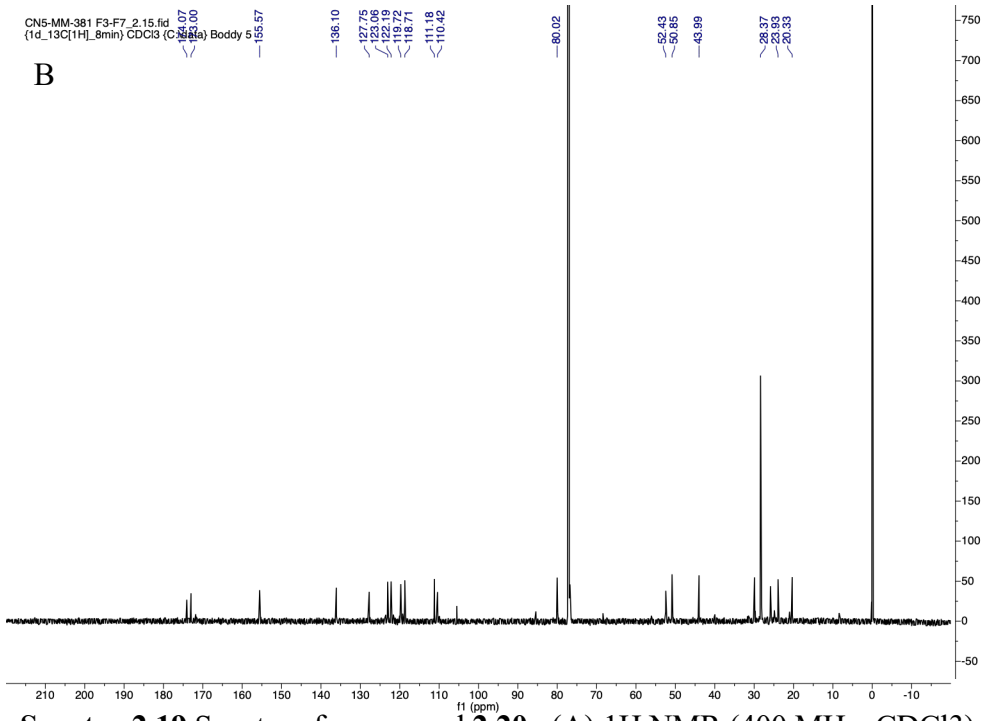
Spectra 2.18 Spectra of compound **2.19b** (E) HSQC (CDCl3)

A



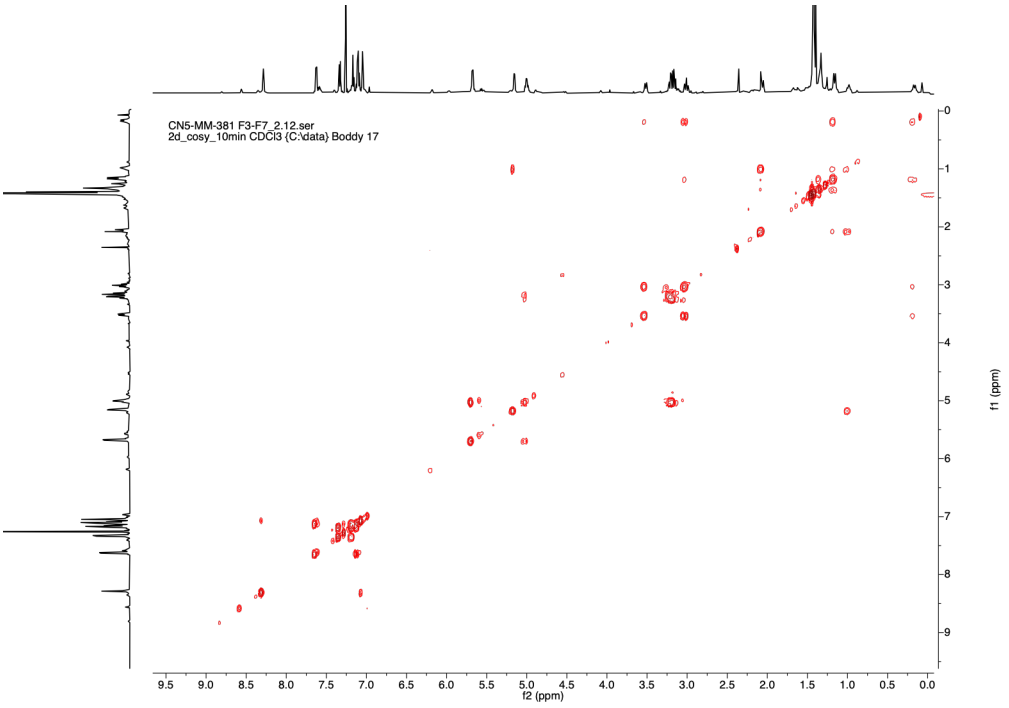
2.20a

B

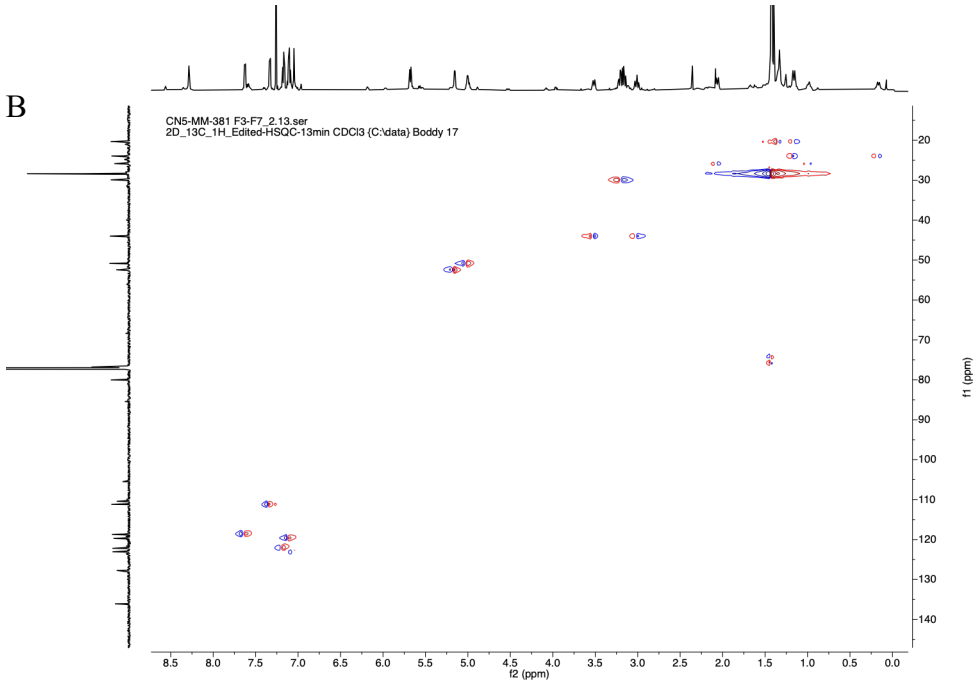


Spectra 2.19 Spectra of compound **2.20a** (A) 1H NMR (400 MHz, CDCl3) and (B) 13C NMR (101MHz, CDCl3)

A

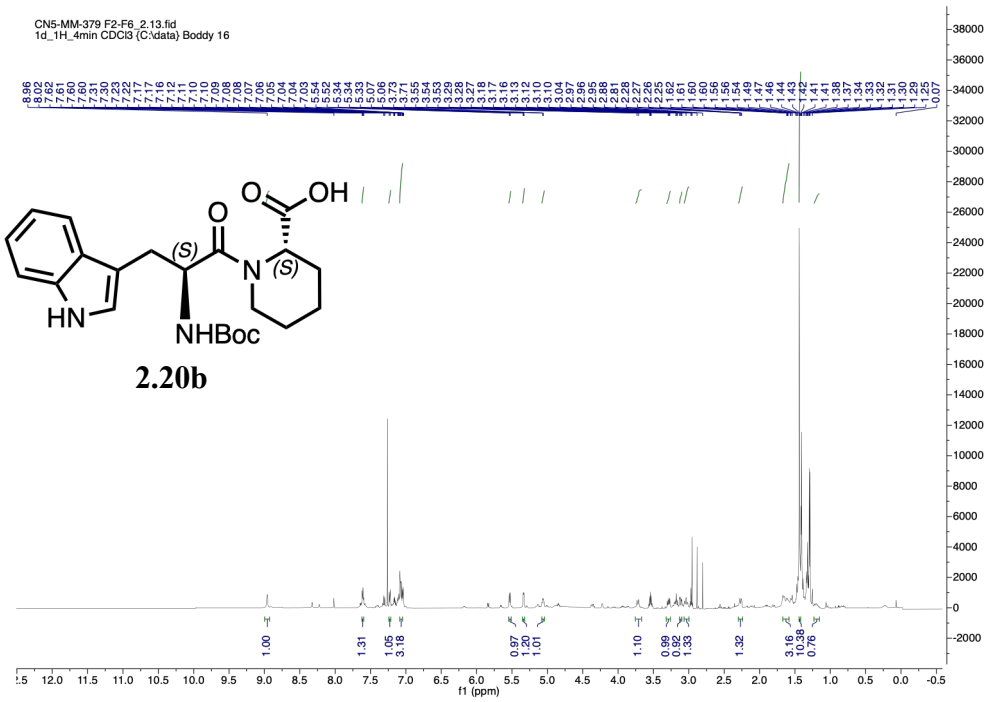


B



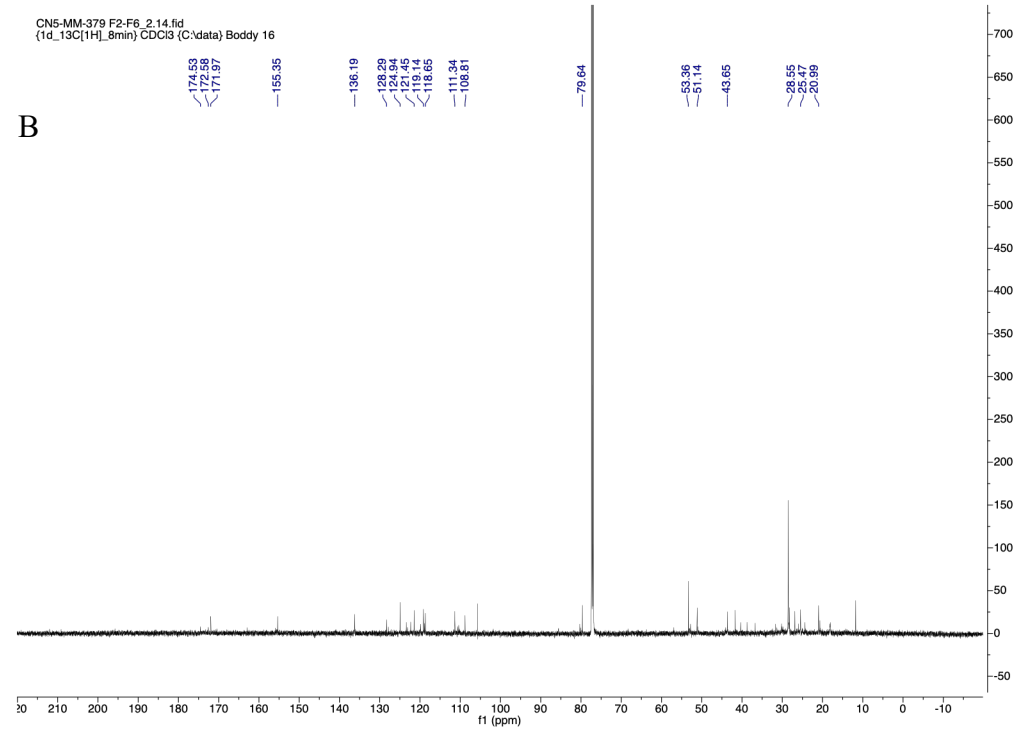
Spectra 2.20 Spectra of compound **2.20a** (C) COSY (CDCl3) and (D) HSQC (CDCl3)

A



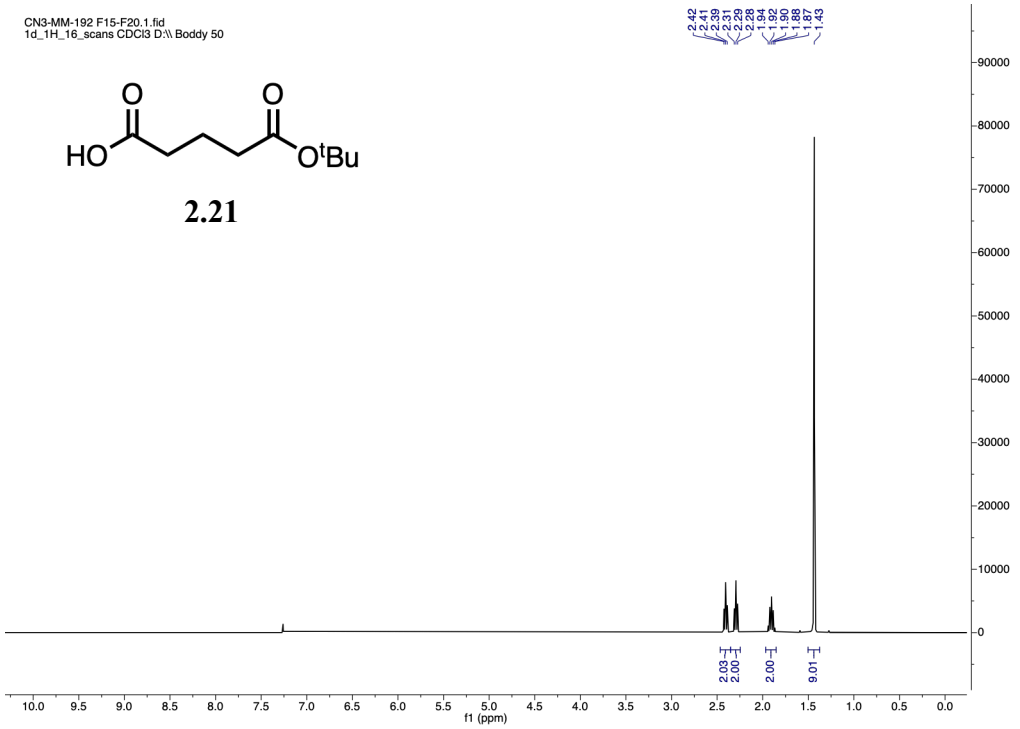
2.20b

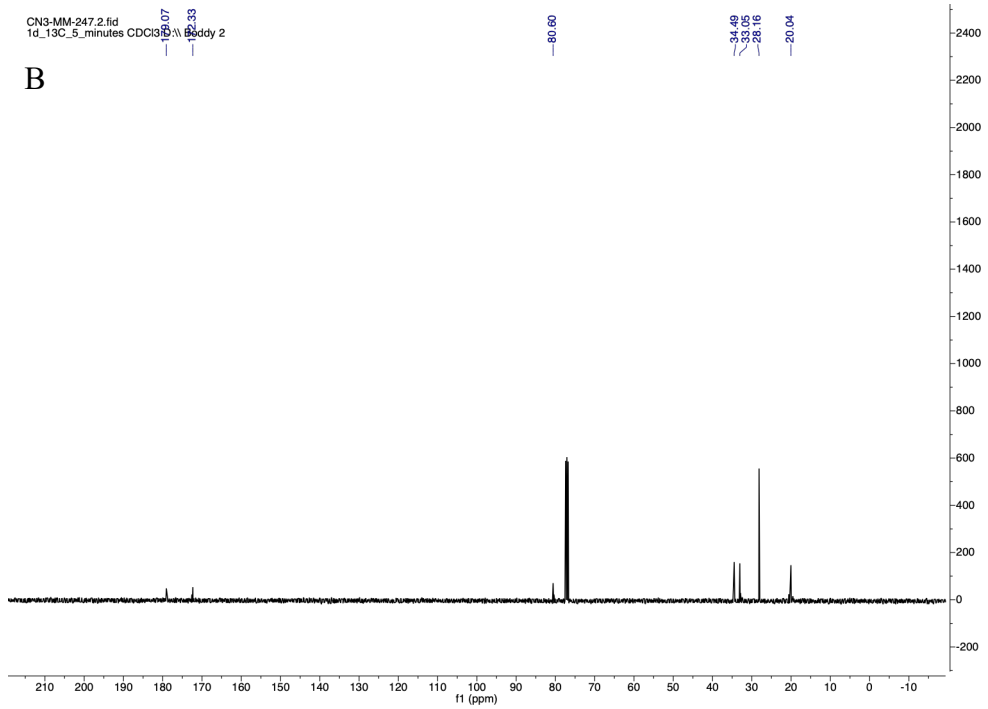
B



Spectra 2.21 Spectra of compound **2.20b** (A) 1H NMR (400 MHz, CDCl3) and (B) 13C NMR (101MHz, CDCl3)

A

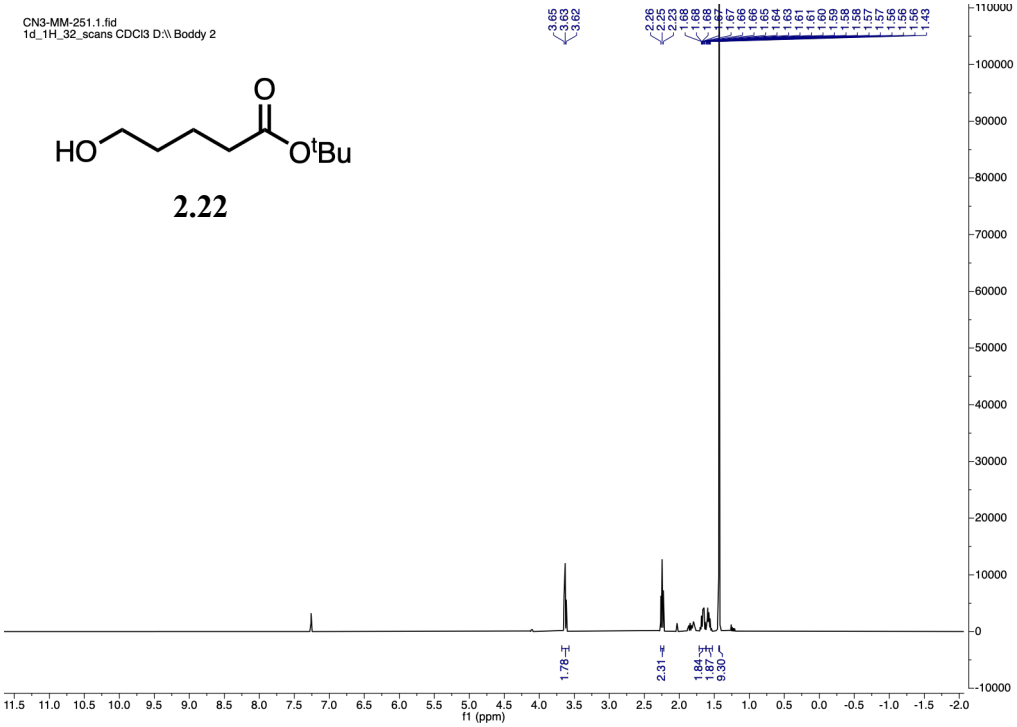




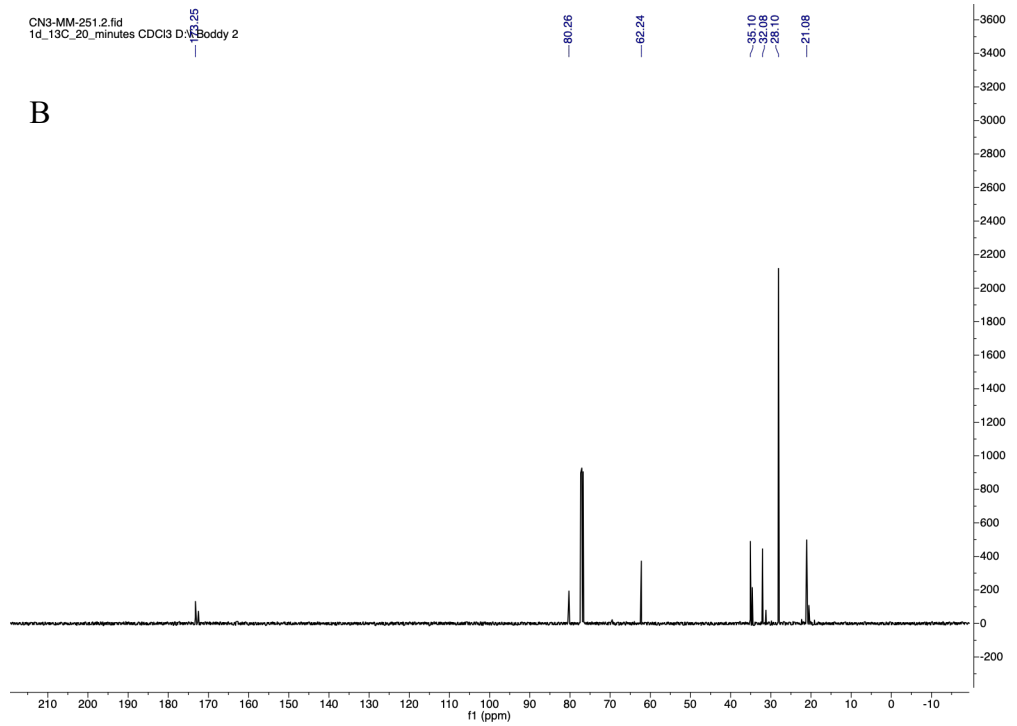
B

Spectra 2.22 Spectra of compound **2.21** (A) 1H NMR (400 MHz, CDCl3) and (B) 13C NMR (101MHz, CDCl3)

A

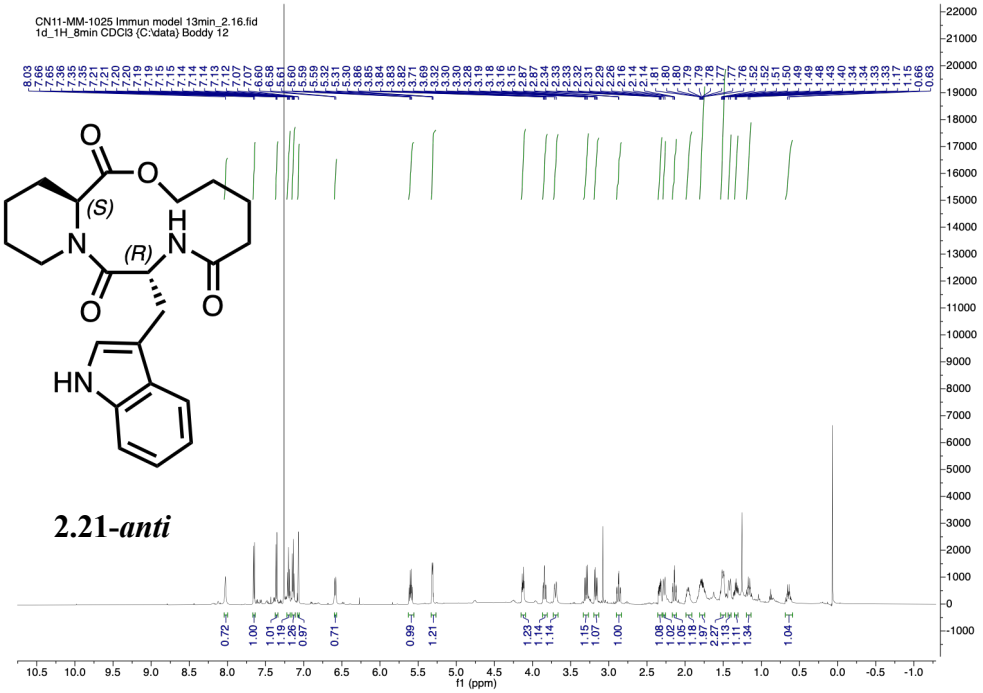


B

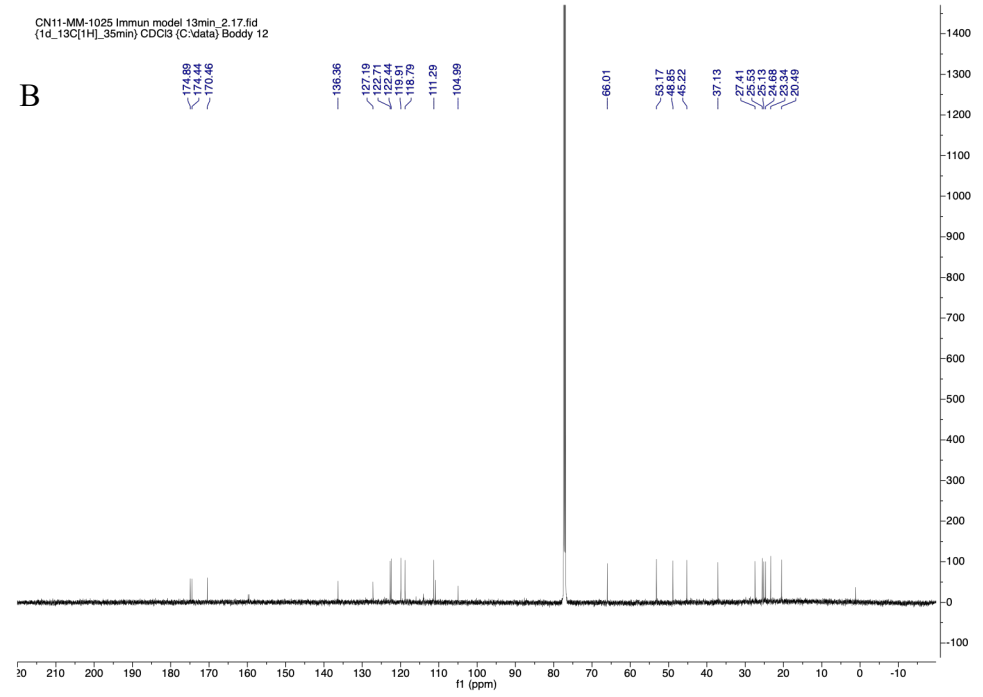


Spectra 2.23 Spectra of compound **2.22** (A) 1H NMR (400 MHz, CDCl3) and (B) 13C NMR (101MHz, CDCl3)

A

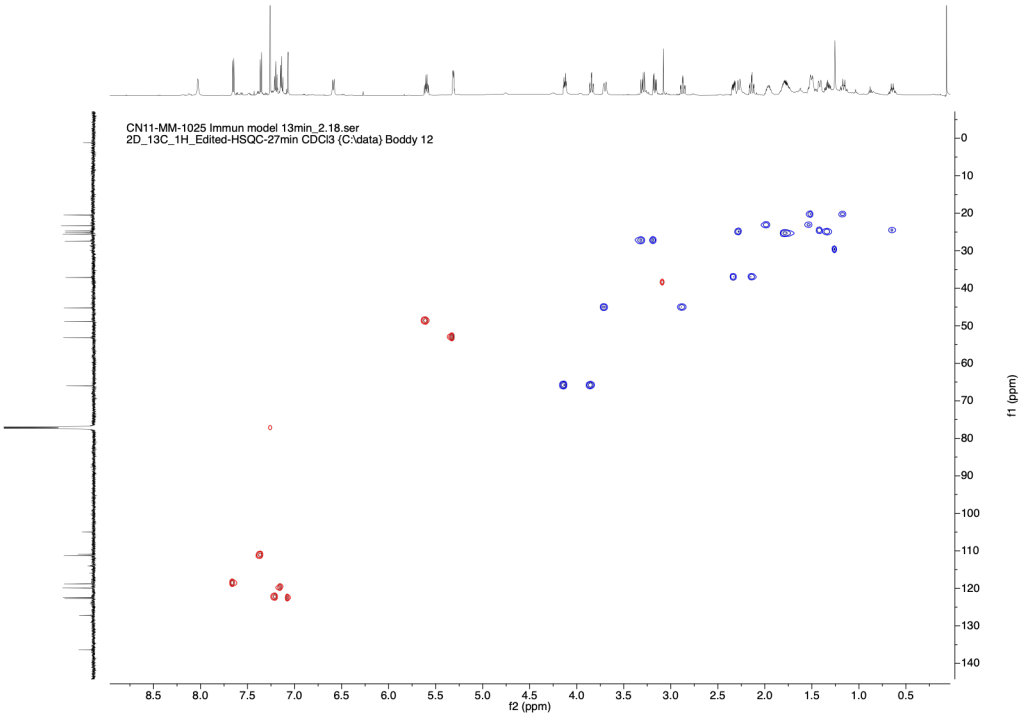


B



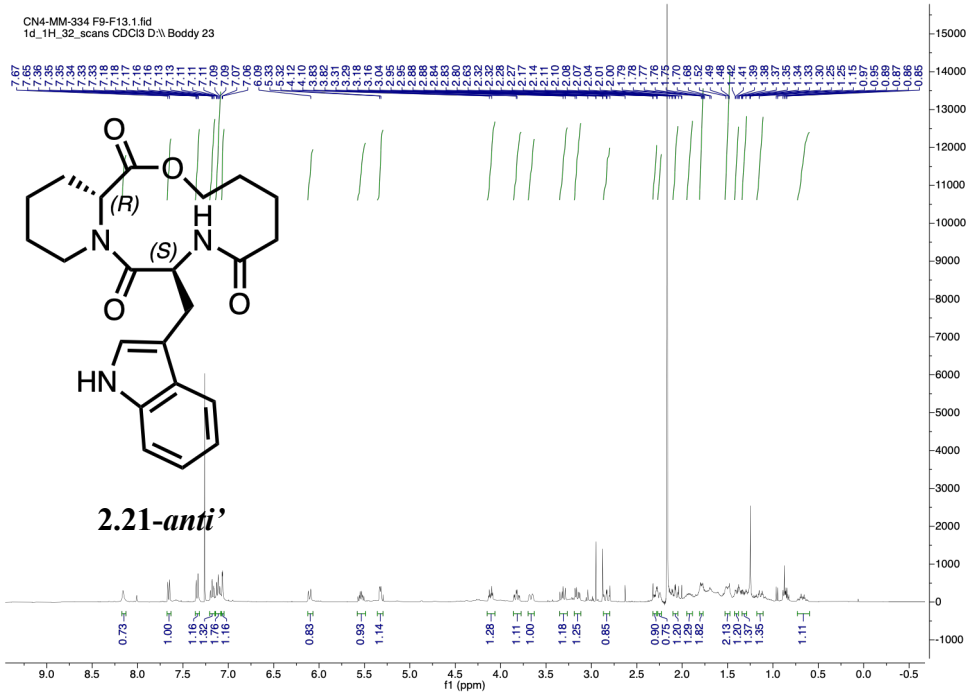
Spectra 2.24 Spectra of compound **2.21-*anti*** (A) 1H NMR (600 MHz, CDCl3) and (B) 13 NMR (101 MHz, CDCl3)

C

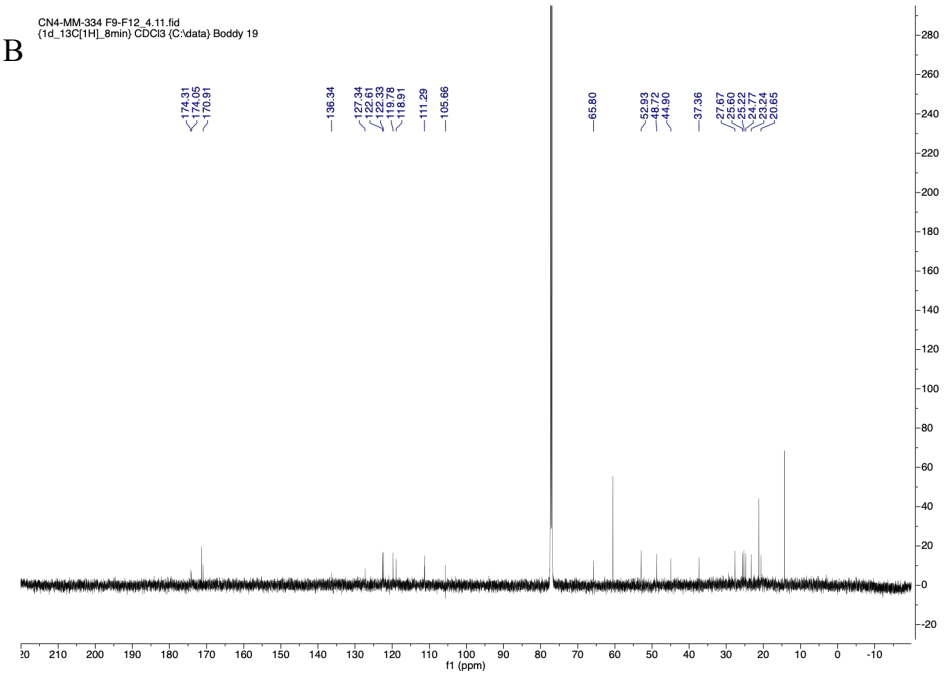


Spectra 2.25 HSQC Spectra of compound **2.21-*anti***

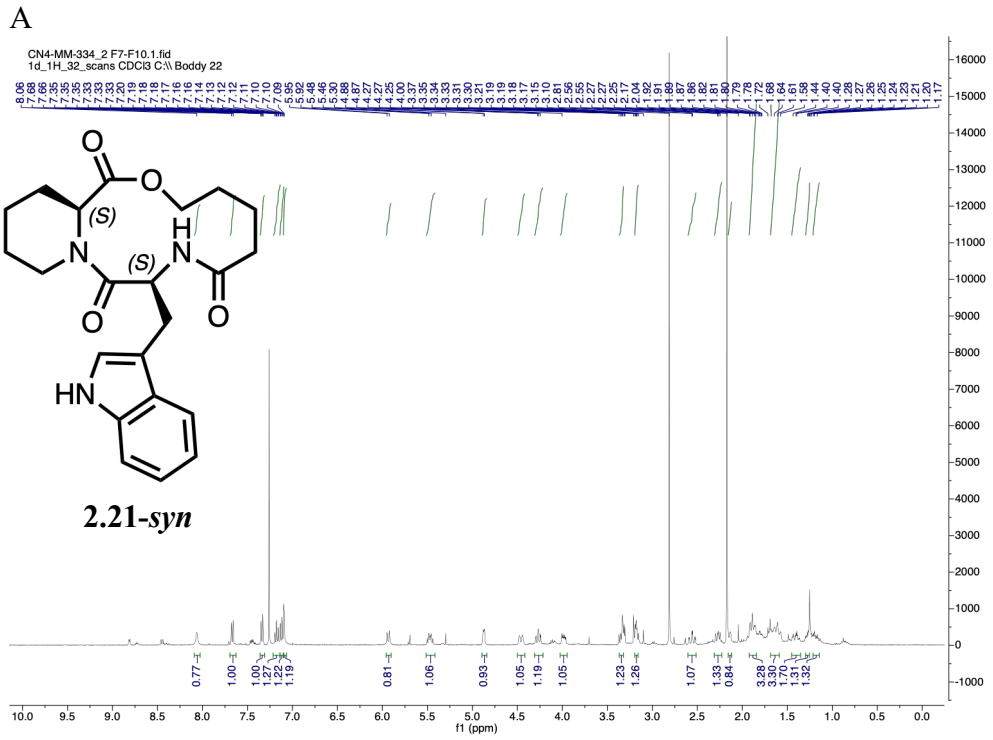
A

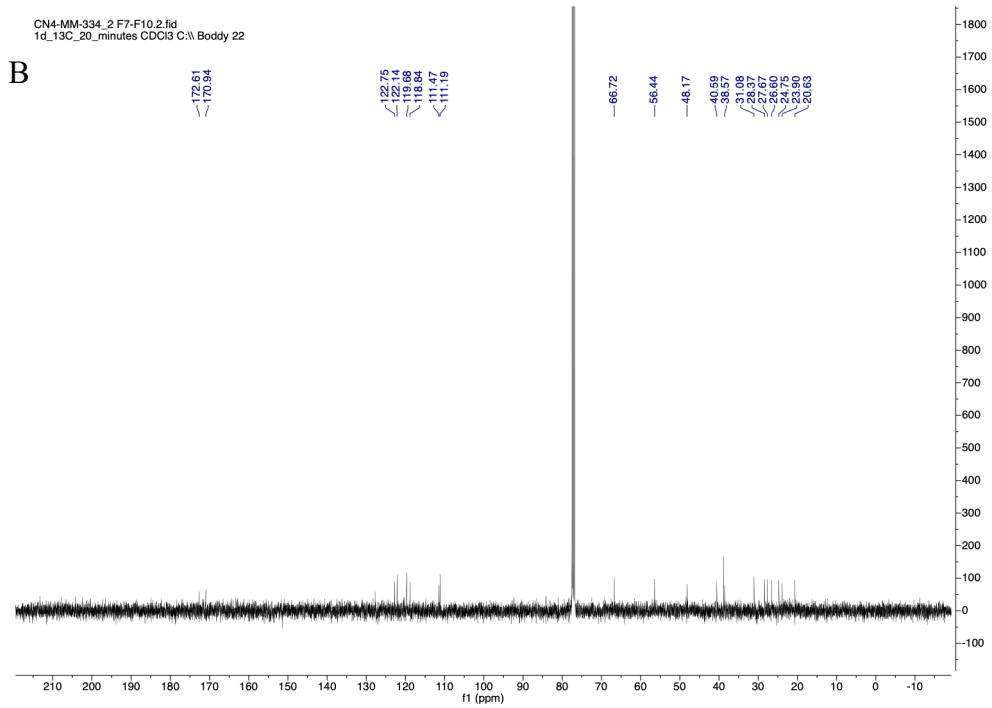


B



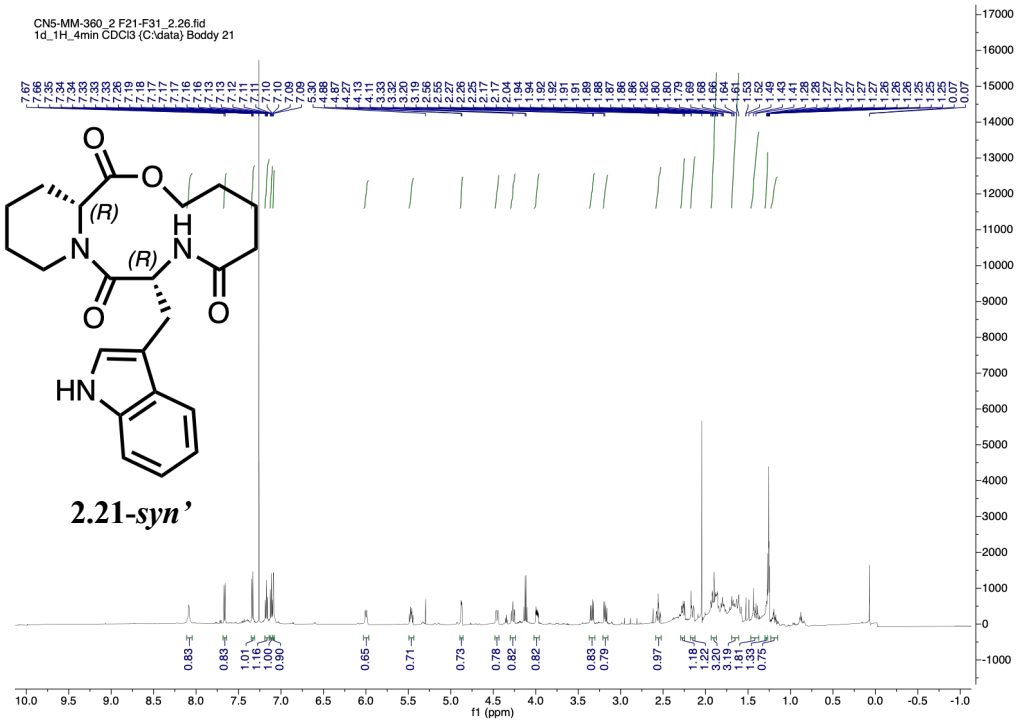
Spectra 2.26 Spectra of compound **2.21-*anti'*** (A) 1H NMR (400 MHz, CDCl3) and (B) 13C NMR (101MHz, CDCl3)



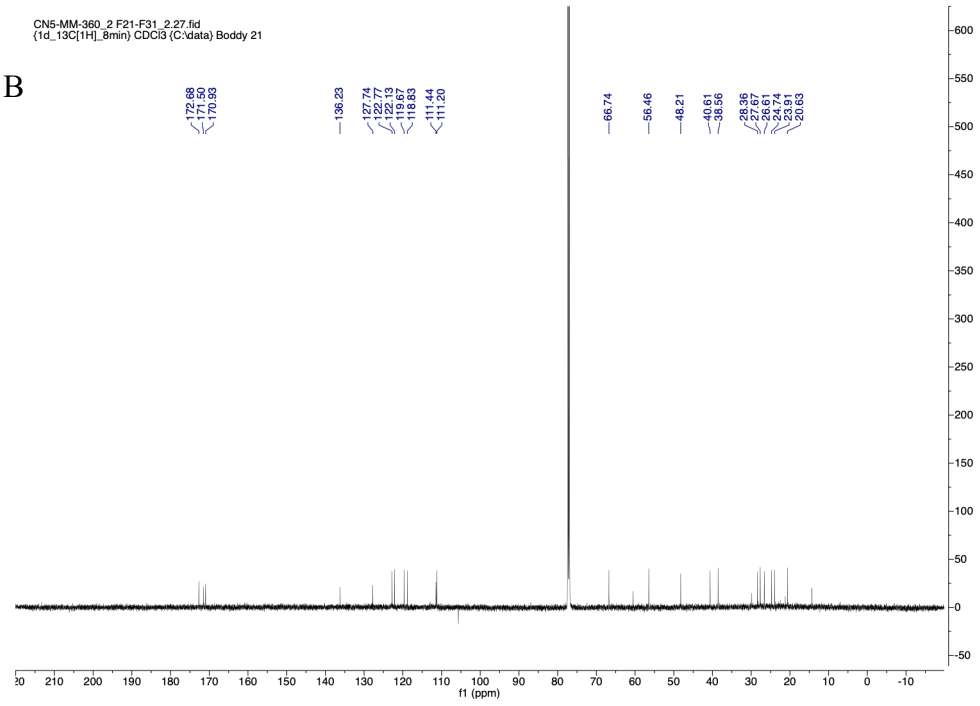


Spectra 2.27 Spectra of compound **2.21-*syn*** (A) 1H NMR (400 MHz, CDCl3) and (B) 13C NMR (101MHz, CDCl3)

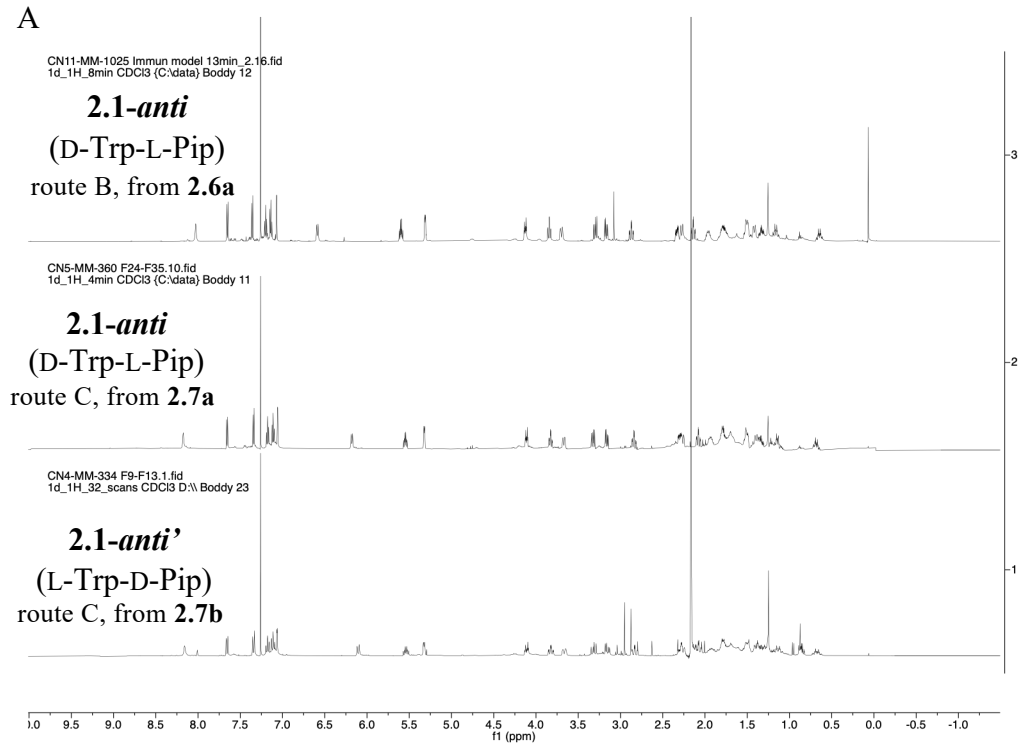
A

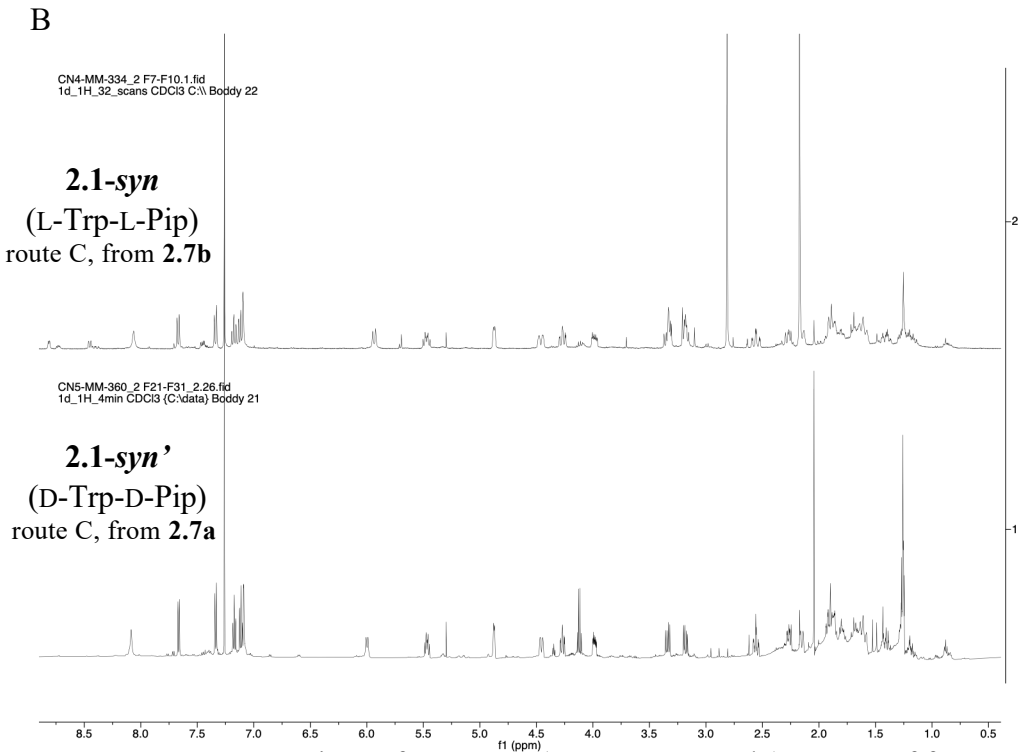


B

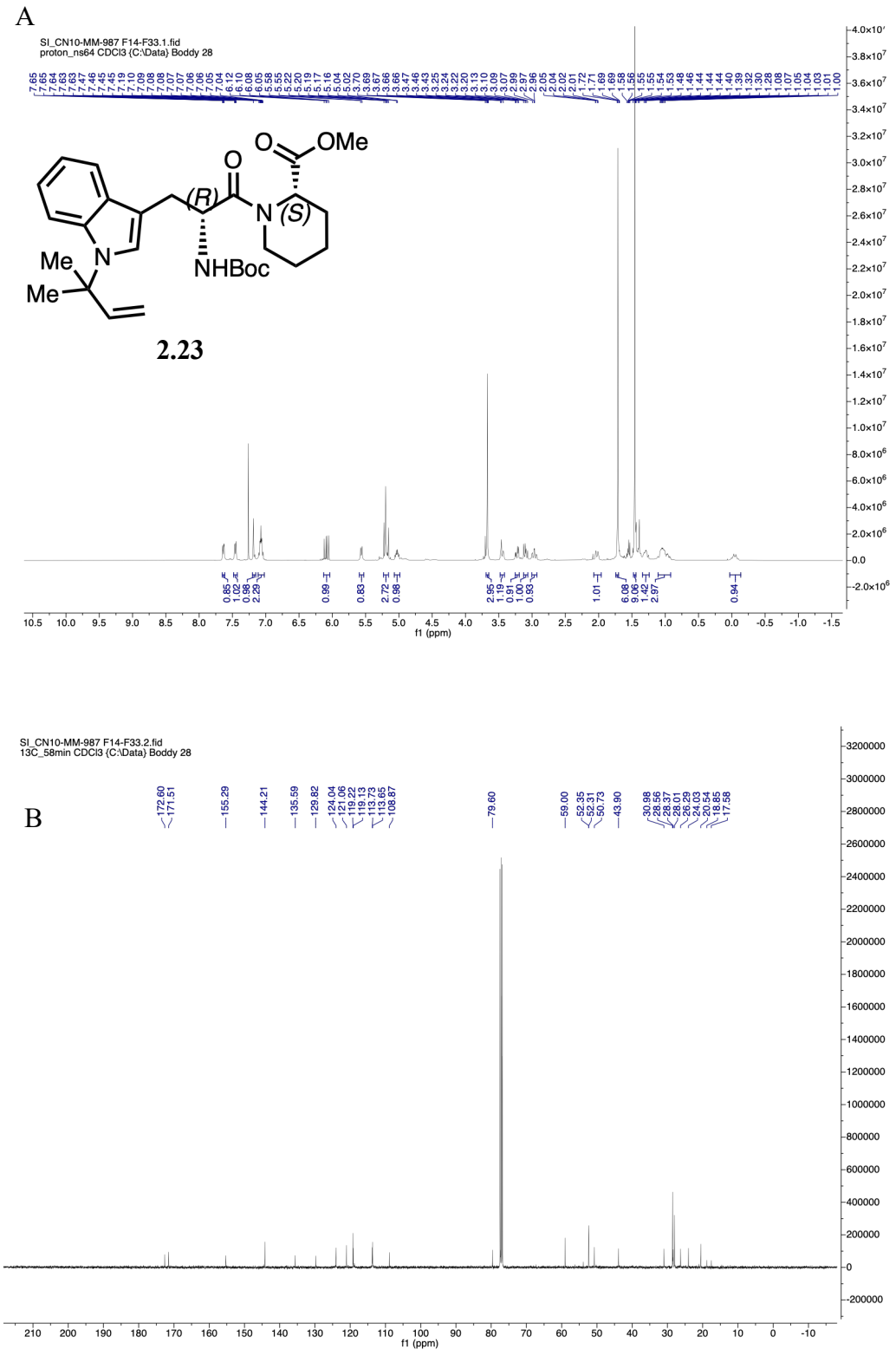


Spectra 2.28 Spectra of compound **2.21-*syn'*** (A) 1H NMR (400 MHz, CDCl3) and (B) 13C NMR (101MHz, CDCl3)



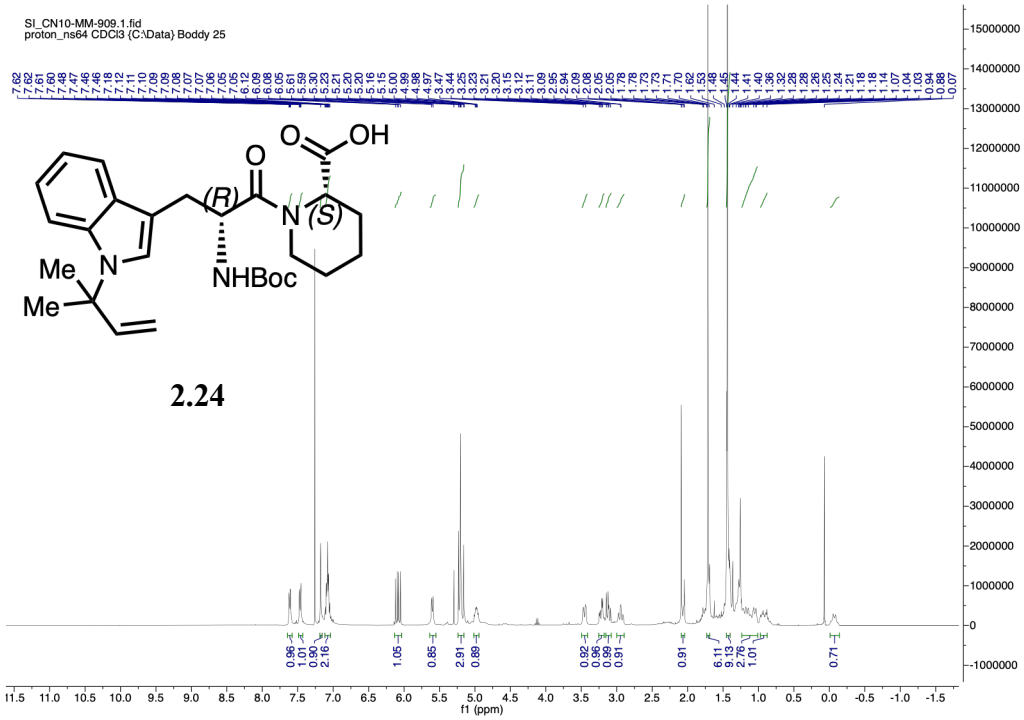


Spectra 2.29 Comparison of 1H NMR (400 MHz, CDCl3) spectra of four macrocyclic compounds (A) **2.1-*anti,* 2.1-*anti'*** (B) **2.21-*syn*** ,**2.21-*syn'***



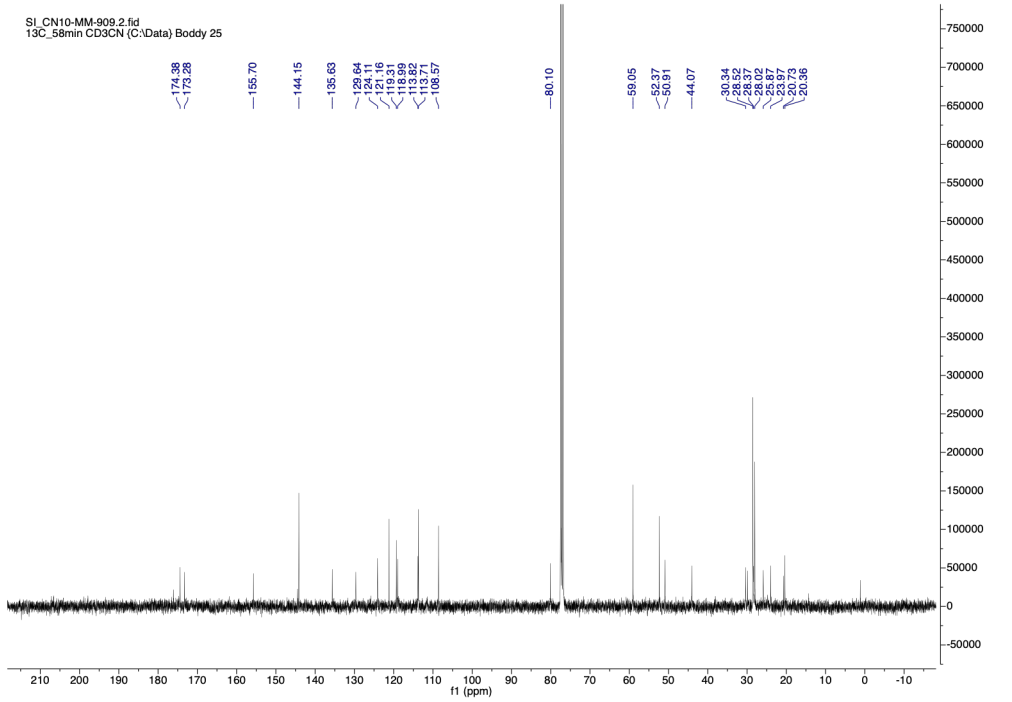
Spectra 2.30 Spectra of compound **2.23** (A) 1H NMR (400 MHz, CDCl3) and (B) 13C NMR (101MHz, CDCl3)

A



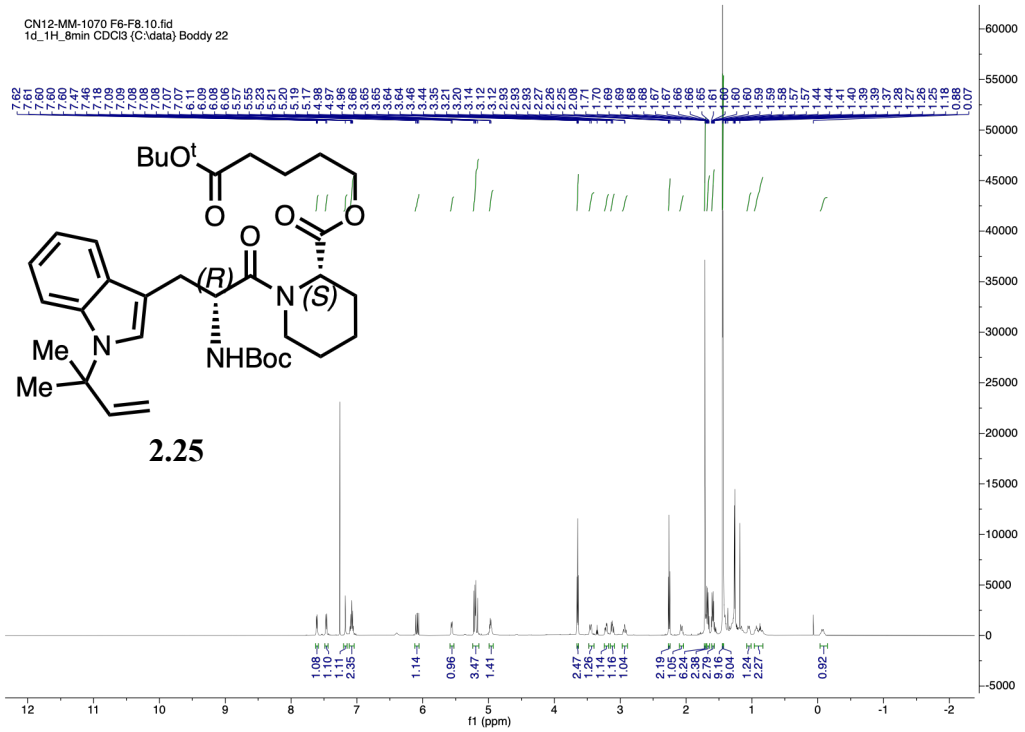
2.24

B



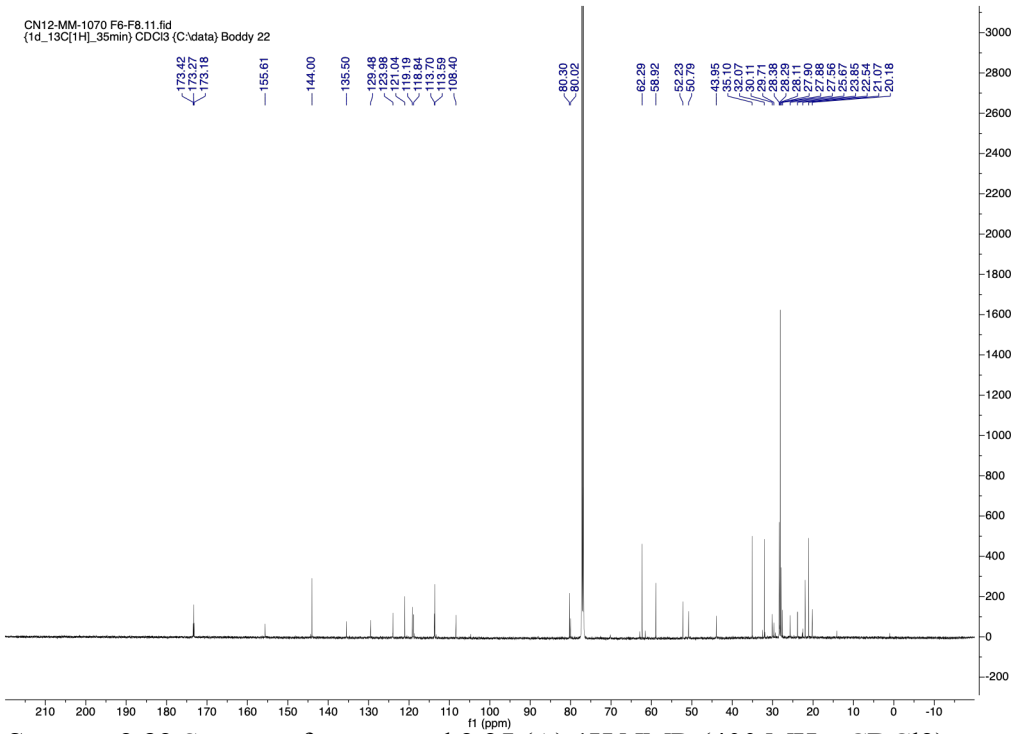
Spectra 2.31 Spectra of compound **2.24** (A) 1H NMR (400 MHz, CDCl3) and (B) 13C NMR (101MHz, CDCl3)

A

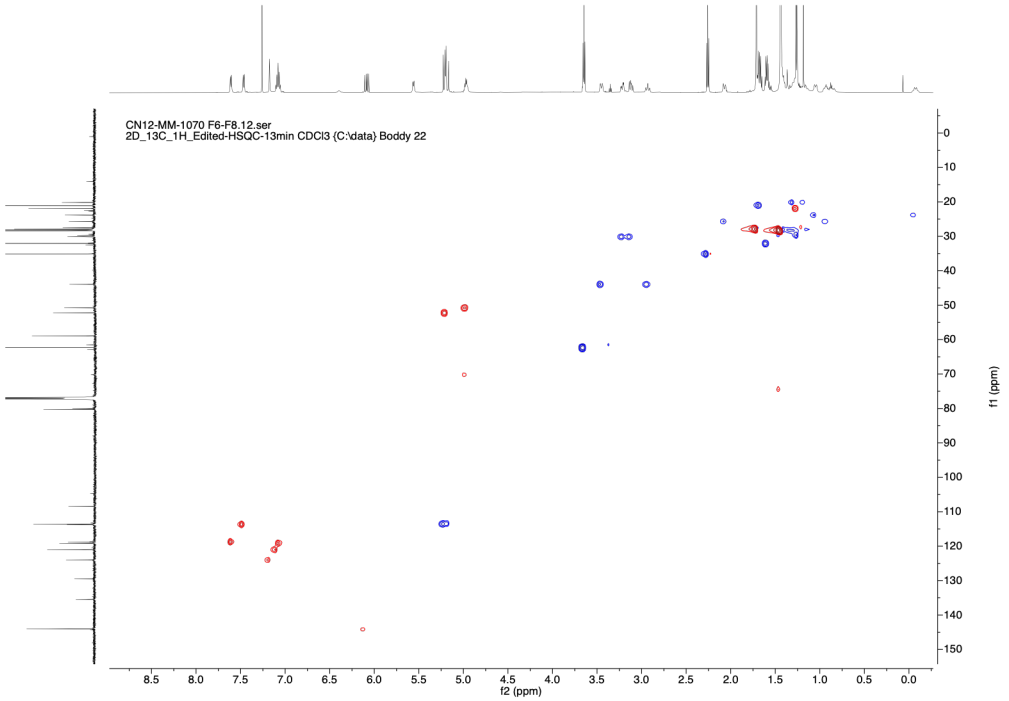


2.25

B



Spectra 2.32 Spectra of compound **2.25** (A) 1H NMR (400 MHz, CDCl3) and (B) 13C NMR (101MHz, CDCl3)



Spectra 2.33 HSQC of compound **2.25**

CHAPTER III.

Synthesis of Immunomodulide Analogues

3.1 Introduction

The model system developed in Chapter 2 was designed primarily as a synthetic surrogate for immunomodulide, intended to evaluate macrolactamization feasibility independently of the unresolved stereocenters of the PKS fragment. Its evaluation in plant immunity assays by collaborators at Agriculture and Agri-Food Canada, however, revealed that the model system was biologically active in both in detach ROS leaf assays (see **Figure 3.9**) and in suppressing bacterial colonization in *Arabidopsis thaliana* (see **Figure 3.2**). This unexpected finding shifted the focus of the immunomodulide project toward an investigation of the structural requirements for biological activity, resulting in the analogue synthesis campaign described in this chapter.

3.1.1 An Introduction to PAMP-Triggered Immunity and Immunomodulatory Natural Products in Plant Defense

Unlike animals, which rely on both an innate and adaptive immune systems, plants only possess an innate immune system to detect and respond to pathogens within their environment. This immune response relies on the recognition of conserved structures known as pathogen-associate molecular patterns (PAMPs), by pattern recognition receptors (PRRs) located on the plant's cell surface[1]. Upon binding of PAMPs to PRRs, a coordinated immune response is triggered known as the PAMP-triggered immunity (PTI) which results in the production of reactive oxygen species (ROS) within the extracellular matrix of plant cells, leading to a cascade of kinase activation and transcriptional reprograming of defence related genes in the plant[2]. The ROS burst in particular, serves as a hallmark of PTI activation and is widely used as a readout of immune responsiveness in plant biology research[3–6]. Flg22 is among the PAMPs used to study and quantify the PTI response. This 22-amino acid peptide derived from bacterial flagellin is recognized by specialized PRRs in *Arabidopsis thaliana* known as FLS2 and represents one of the most widely used PAMPs for PTI quantification[7–9].

Plant pathogens such as *Pseudomonas syringae*, *Ustilago maydis* and *Verticillium dahlia* have evolved effector proteins to suppress, disrupt or neutralize the PTI response, enabling colonization of their plant hosts[10]. Therefore, compounds able to potentiate or restore the PTI response represent an attractive lead for the development of novel crop protection agents. Within this context, several natural products sourced from plants, fungi and microbes, such as chitosan, salicylic acid, laminarin and harpin proteins have been identified as potentiators of plant immunity

and represent a sustainable alternative to conventional chemical pesticides that face increasing pathogen resistance and cause environmental pollution[11–13].

From a chemical perspective, however, the growing interest in sourcing natural immune inducers and potentiators has been complicated by the structural complexity that often characterizes these scaffolds, limiting their development as crop protection agents. Beyond their synthetic challenge alone, the sheer scale at which active compounds would be need to be produced to afford meaningful protection imposes significant economic and logistical constraints[14,15]. In this context, the identification of simplified analogues that retain the biological activity of a complex natural product lead while offering a more tractable synthetic route is of considerable practical value[16]. This strategy is central in translating natural product discoveries toward agrochemical applications and forms the basis of the work described in this chapter.

3.1.2 Biological Activity of Immunomodulide and the Model System

The compound central to Part I of this thesis, immunomodulide, was isolated by collaborators in the laboratory of Dr. David Overy at Agriculture and Agri-Food Canada (AAFC) and identified as a potentiator of the plant immune response. Its intriguing biological activity, combined with an incomplete structural characterization at the time of its discovery, prompted the total synthesis campaign described in this thesis.

The immunomodulatory activity of immunomodulide was evaluated in a detached leaf ROS burst assay using *Arabidopsis thaliana* leaf disks (**Figure 3.1**). Leaf disks were treated with the flagellin-derived PAMP flg22 (1 nM) in the presence or absence of immunomodulide at varying concentrations (10 nM, 100 nM, and 1 μM), and ROS production was quantified by luminescence. From these assays it was found that immunomodulide alone, across all concentrations tested, did not elicit a significant ROS response relative to the DMSO vehicle control, confirming that it does not act as a PAMP mimic. However, co-administration of immunomodulide with flg22 produced a statistically significant enhancement of the ROS burst at 1 μM ($p \leq 0.005$), while the 10 nM and 100 nM co-treatment conditions were not significantly different from flg22 alone. These results establish immunomodulide as a dose-dependent potentiator of PTI rather than a direct elicitor of the immune response.

To assess whether the biological activity of immunomodulide was dependent on the structural complexity of its PKS fragment, the model system (**2.1-*anti***) developed in Chapter II

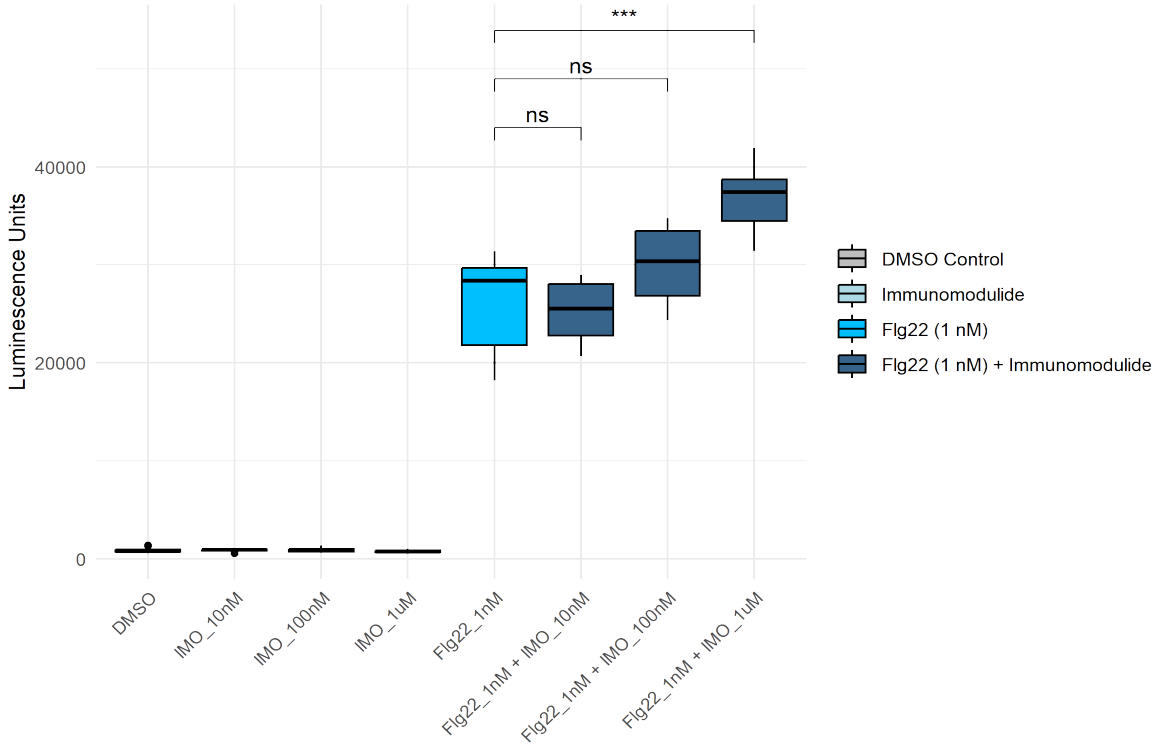


Figure 3.1. Immunomodulide potentiates flg22-triggered ROS production in *Arabidopsis* detached leaf assays. ROS production was measured by luminescence in response to flg22 (1 nM) alone or in combination with immunomodulide (IMO) at the indicated concentrations. Statistical comparisons are relative to flg22 alone. Figure provided by Dr. David Overy (Agriculture and Agri-Food Canada). ns: not significant; *:p ≤0.05; *: p ≤ 0.005.

was subsequently evaluated by AAFC collaborators in a complementary in planta bacterial colonization assay. *Arabidopsis thaliana* leaves were syringe-infiltrated with *Pseudomonas syringae* pv. tomato DC3000 in the presence of either immunomodulide or the model system at 1 µM, and bacterial colonization was quantified as colony-forming units per gram of leaf tissue (CFU/g) (**Figure 3.2**). Treatment with immunomodulide at 1 µM resulted in a statistically significant reduction in DC3000 colonization relative to the DMSO vehicle control ($p \leq 0.005$). Interestingly, the model system afforded an enhanced suppression of bacterial growth under identical conditions, reducing CFU/g to levels approaching zero. This suppression was superior to immunomodulide itself ($p \leq 0.005$) and provided the motivation to explore the model system further.

Structurally, the model system retained only the macrocyclic core of immunomodulide composed of the dipeptide backbone D-Trp-L-Pip dipeptide and a short 5-carbon mimic of the PKS

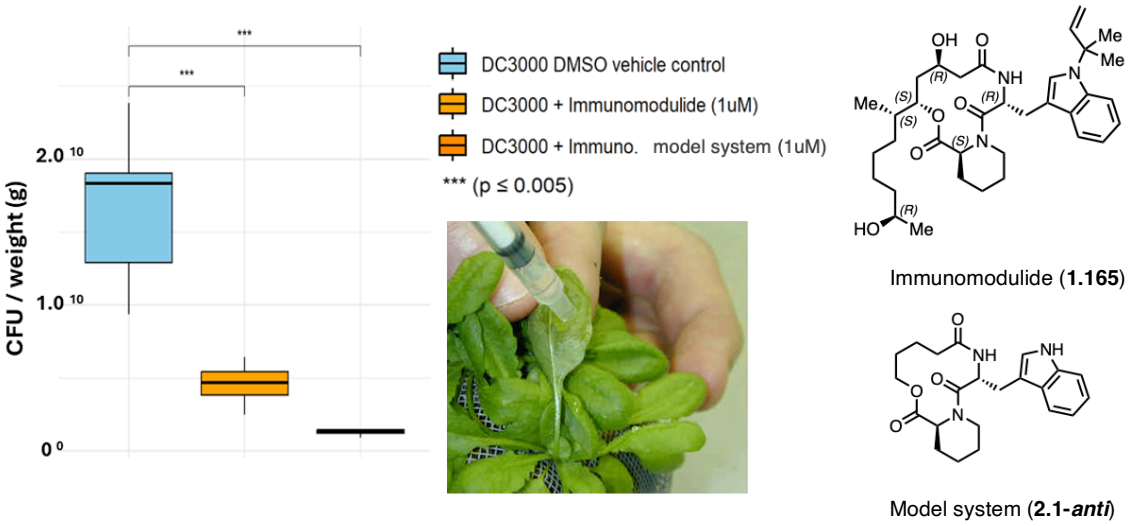


Figure 3.2. Immunomodulide (**1.165**) and the model system (**2.1-anti)** reduce *P. syringae* DC3000 colonization in *Arabidopsis*. Colony-forming units (CFU) per gram of leaf tissue were quantified following infiltration with DC3000 in the presence of immunomodulide or the immunomodulide model system (1 μM each). Structures of immunomodulide and the model system are shown. ***: $p \leq 0.005$. Figure provided by Dr. David Overy (Agriculture and Agri-Food Canada).

fragment (**Figure 3.2**). The assay results suggested then that all four stereocenters of the PKS fragment and the reverse prenyl group present on the indole nitrogen were not structural determinants of activity, suggesting that instead the pharmacopohore is retained within the simplified model system. This finding motivated the structure-activity relationship (SAR) study described in this chapter, in which systematic structural modifications to the model system (**2.1-*anti***) were undertaken to identify the pharmacophoric elements required for activity and to evaluate the effect of stereochemical, building block, and scaffold-level changes on biological potency, as determined by ROS burst and infection model assays discussed above.

3.1.3 Structure-Activity Relationships in Cyclic Depsipeptides: Precedent and Design Principles

SAR studies on bioactive cyclic depsipeptides have established that stereochemistry, amino acid identity, and *N*-methylation pattern are among the most consequential variables governing biological activity in this compound class, and that systematic analogue synthesis can reveal structural features essential for activity that are not apparent from the native scaffold alone.

Jiménez et al. demonstrated through a systematic analogue campaign on kahalalide F (KF), a marine cyclic depsipeptide, that KF is highly sensitive to stereochemical perturbation at the α-carbon of backbone residues but broadly tolerant of side chain substitution, implicating macrocyclic backbone conformation as the primary determinant of target engagement[17]. Romidepsin (FK228) provides a complementary example in which analogue synthesis clarified the mechanistic basis of activity, demonstrating that the thiol-containing side chain rather than the macrolactam backbone was the pharmacophoric element responsible for zinc coordination at the HDAC active site[18]. More recently, Sato et al. demonstrated using *N*-desmethyl and *N*-methyl analogues of destruxin E, a 19-membered cyclodepsipeptide, that *N*-methylation at individual backbone positions serves distinct roles, contributing either to the conformational constraint required for activity or to the cell permeability necessary for potency[19]. Together, these studies illustrate that the pharmacophore of a cyclic depsipeptide is not self-evident from its structure, and that systematic evaluation of backbone conformation, building block substitution, and macrocyclic core perturbation through analogue synthesis is the most reliable tool for its delineation.

Notably, no systematic SAR study has been reported for the 12-membered cyclic tridepsipeptide class to which immunomodulide belongs. While several members of this family have been the subject of total synthesis campaigns (see Chapter I, **Section 1.2.5**), these efforts have been directed primarily toward structural confirmation and macrolactamization methodology rather than biological evaluation through analogue synthesis. The SAR study described in this chapter therefore represents the first systematic investigation of the structural requirements for biological activity within this compound class.

3.1.4 Analogue Design Strategy and Pharmacophore Hypothesis

The retention of biological activity in the model system advanced the hypothesis that the macrolactam backbone constitutes the primary pharmacophoric element. However, the structural requirements about the core, remained unknown. To elucidate these requirements, the analogue library was designed around two major categories of structural modifications.

The first category comprised a stereochemical probe set, in which the configurations at the Trp α-centre and the Pip α-centre were systematically inverted to generate all four possible diastereomers of the model system (configurational inversions highlighted in yellow, **Figure 3.3**). All four diastereomers, namely **2.1-*syn***, **2.1-*anti***, **2.1-*syn'***, and **2.1-*anti'***, were obtained directly

from the cyclization studies described in Chapter II, where epimerization at the Trp and Pip α-centres under the ring-closing and esterification conditions evaluated yielded the complete

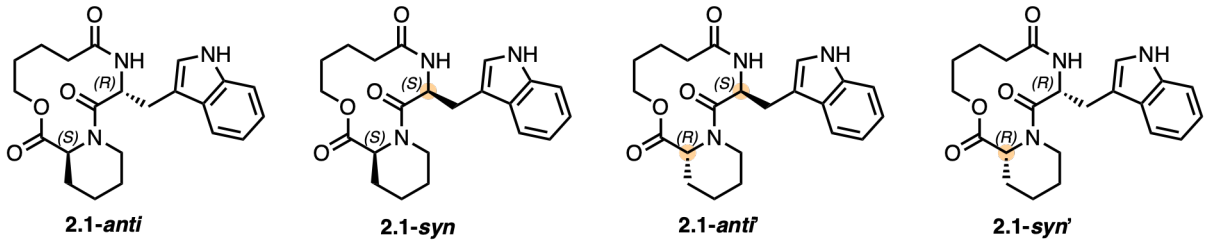


Figure 3.3. The four diastereomers of the model system constituting the stereochemical probe set, generated through inversion at the Trp and Pip α-centres in Chapter II: **2.1-*anti*** (D-Trp/L-Pip, native configuration), **2.1-*syn*** (L-Trp/L-Pip), **2.1-*anti'*** (L-Trp/D-Pip), and **2.1-*syn'*** (D-Trp/D-Pip).

diastereomeric series (see **Sections 2.2.1** and **2.2.2**). Given the sensitivity of cyclic depsipeptide activity to the backbone amino acid configuration established in the kahalalide F[17] and destruxin E[19] series, this probe set was designed to determine whether the native D-Trp/L-Pip configuration is an absolute requirement for activity or whether alternative stereochemical arrangements are tolerated.

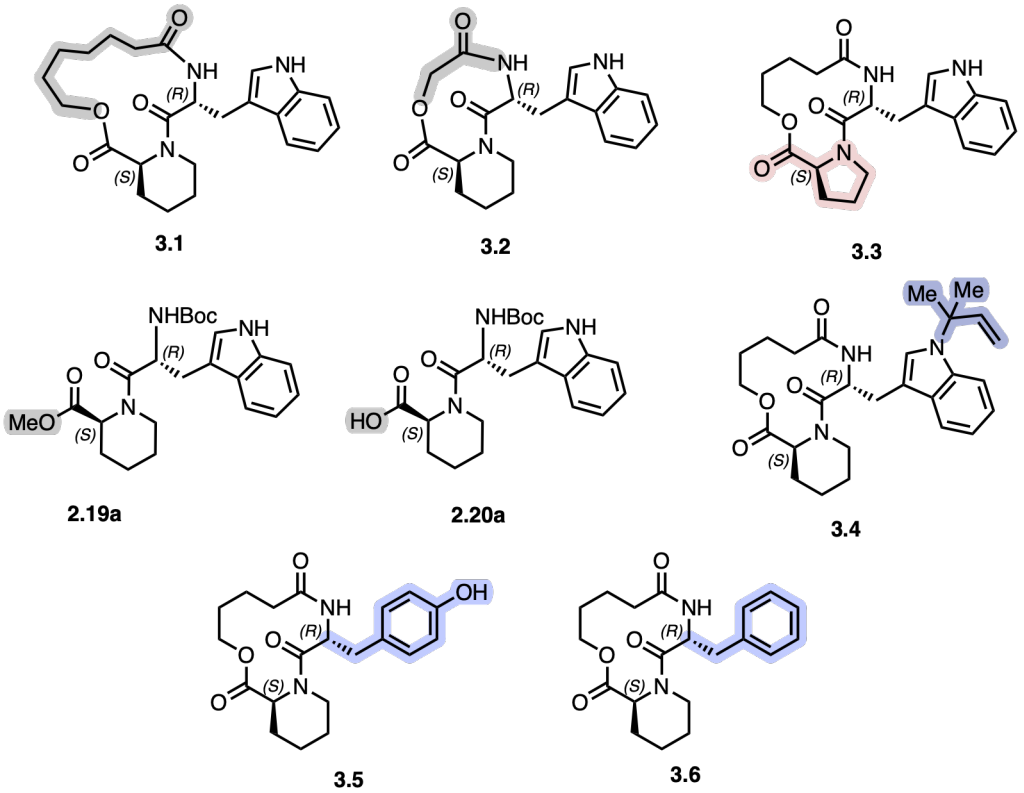


Figure 3.4. The building block exchange set. Ring-size and ester variants: 7C (**3.1**) and 3C (**3.2**) PKS tether analogues (grey). Pip substitution: L-Pro analogue (**3.3**, pink). Acyclic dipeptide controls: methyl ester (**2.19a**) and free acid (**2.19b**) variants. Trp substitutions: reverse-prenylated D-Trp (**3.4**, blue), D-Tyr (**3.5**, blue), and D-Phe (**3.6**, blue) analogues.

The second category comprised a building block exchange set (**Figure 3.4**), in which individual residues and ring-forming components of the model system were systematically replaced. Three subcategories of substitution were explored. First, the ring size was varied by modifying the PKS fragment (in grey, **Figure 3.4**), with 3-carbon (**3.2**) and 7-carbon diols (**3.1**) evaluated alongside the acyclic variants (methyl ester (**2.19a)** and carboxylic acid (**2.20a**)) to probe the effect of the macrocyclic and its ring size on activity. The acyclic variants were prepared as per protocols in Chapter II. Second, modifications to L-Pip (in pink, **Figure 3.4**) was made by replacing it with isostere L-Pro, a cyclic *N*-alkylated amino acid that differs from L-Pip only in ring size. L-Pro also recurs as the *N*-alkylated residue in the acremolide[20] and xylacremolide

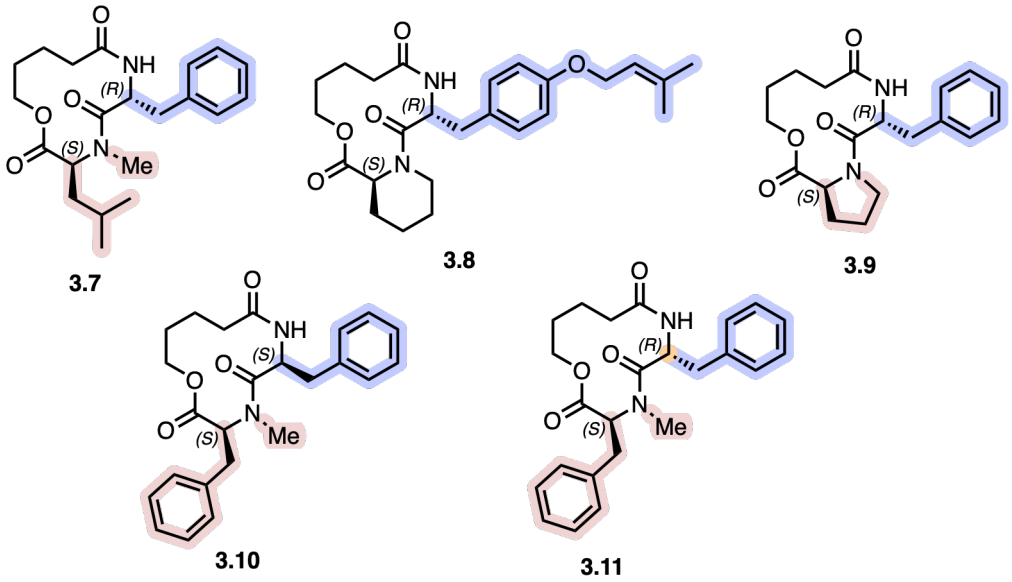


Figure 3.5. The tridepsipeptide family analogueues (supplementary set). Colletopeptide/colletotrichamide analogue, bearing D-Phe and *N*-Me-L-Ile (**3.7**). HA23 analogue bearing *O*-prenylated D-Tyr (**3.8**). Acremolide analogue, bearing D-Phe and L-Pro (**3.9**). Stereocalpin analogue, bearing D-Phe and *N*-Me-D-Phe (**3.10**). Epi-stereocalpin analogue (**3.11**), diastereomeric to **3.10** at the *N*-Me-Phe stereocenter.

series[21], further supporting this modification on the basis of the natural precedent within the tridepsipeptide family. Third, D-Trp was modified (in blue, **Figure 3.4**) with isosteric amino acids

bearing aromatic side chains, including D-Phe (**3.6**) and D-Tyr (**3.5**), and with a reverse-prenylated Trp derivative (**3.4**), to determine whether the indole side chain and its prenylation state contribute to the pharmacophore or whether a simpler aromatic moiety is sufficient. These residues were again selected on the basis of their recurrence across the 12-membered tridepsipeptide family, namely across the acremolides[20], xylacremolides[21], colletopeptides[22,23], HA23[24] and stereocalpins[25,26].

Beyond the two principal analogue categories, the simplified scaffold was further elaborated to prepare analogues corresponding to the best-characterized members of select 12-membered cyclic tridepsipeptide families, namely acremolide A[20,27](**3.9**), colletopeptide/colletotrichamide A[22,28,29] (**3.7**), HA23[24,30] (**3.8**), and stereocalpin A/B[25,26,31] (**3.10**), each bearing the native amino acid combination of the respective natural product within the pentanediol-based macrolactam scaffold (**Figure 3.5**). Notably, an epi-stereocalpin analogue (**3.11**) was also prepared, motivated by the observation that the L/L configuration at the Trp and Pip α-centres is unique to the stereocalpin series within the tridepsipeptide family. This set was designed to determine whether the pharmacophore identified in the immunomodulide model system is conserved across structurally related members of the class, and to assess whether the atypical L/L backbone geometry of stereocalpin is a prerequisite for or detrimental to biological activity.

Taken together, the stereochemical probe set, building block exchange set, and tridepsipeptide family analogues constitute a library of 18 compounds in total, designed to systematically map the structural requirements for immunomodulide-type modulation of the plant immune response to be evaluated by ROS burst potentiation and *Pseudomonas syringae* DC3000 colonization assays.

3.2 Results and Discussion

3.2.1 First-Generation Synthesis of the Analogue Library

The first-generation synthesis of the analogue library was predicated on successes in synthesis of the model system series (**2.1-*anti*, 2.1-*anti'*, 2.1-*syn*, and 2.1-*syn'***) which employed route C as a ring-closure strategy. This disconnection closes the macrolactam at the amide bond between the PKS fragment and the primary amine of the amino acid with the aromatic residue (see **Section 2.2**). The additional observation of epimerization-prone esterification in implementing this route

in Chapter II, led to the adoption of a Mitsunobu-based esterification approach, rather than a carbodiimide-based esterification, in the attachment of the PKS surrogate to the dipeptide backbone. Given the robustness and reliability of this disconnection established, route C macrolactamization was extended to the synthesis of the remaining members of the analogue library using a consistent protecting group strategy. Thus, this route was applied to the synthesis of the ring size (**3.1** and **3.2**) and acyclic (**3.4** and **3.5**) variants, the L-Pro analogue (**3.3**), and the reverse-prenylated analogue (**3.4**). The entry-point for the synthesis of **3.4** was the Mitsunobu step, as the required acid intermediate (Boc-D-Trp(*N*-reverse-prenyl)-L-Pip-OH) was sourced from model system route explorations in Chapter II (see **Figure 2.8**).

The general route to the first-generation analogue library is summarized in **Figure 3.6,** where "X" defines the specific compound number assigned to each analogue, with lettered suffixes identifying the corresponding synthetic intermediate along its route. Each analogue series begins with a methyl esters L-Pip-OMe (**2.18**) or L-Pro-OMe (**3.12**) made with TMSCl in MeOH, according to conditions reported in Chapter II. Then, HATU-mediated amide coupling between methyl esters **2.18**/**3.12** and the corresponding Boc-D-protected amino acid, installing the second

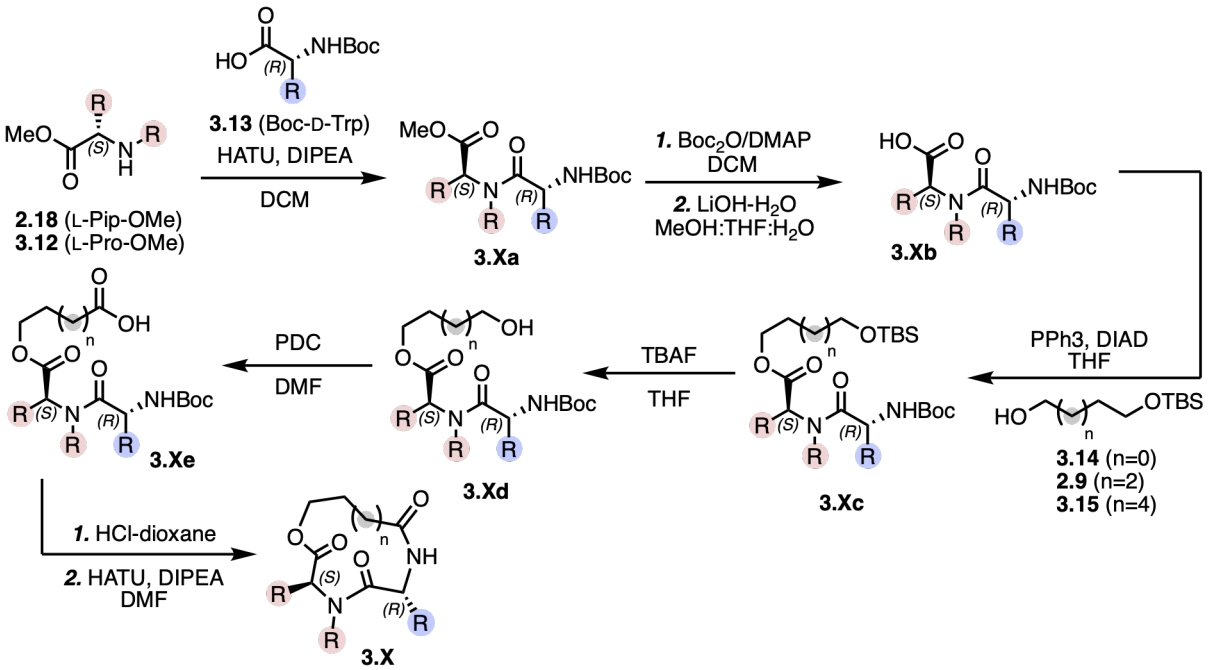


Figure 3.6. General route to the first-generation analogue library. "X" denotes the compound number assigned to each analogue; lettered suffixes (a–e) denote the corresponding synthetic intermediate. Modifications at L-Pip (in pink), D-Trp (in blue) and PKS fragment (in grey).

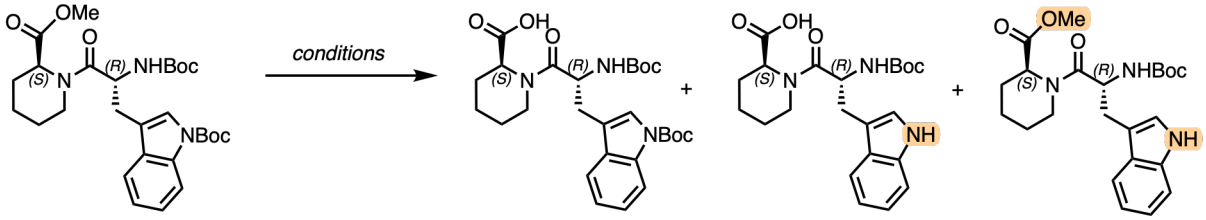
residue of the dipeptide backbone. For Trp-containing analogues, an additional di-Boc protection of the indole nitrogen (Boc2O, DMAP) was carried out at this stage to afford **3.Xa'**, introduced to circumvent oxidative side reactions at the unprotected indole observed later in the sequence. Saponification of the resulting methyl ester (**3.Xa**, or **3.Xa',** for Trp-containing analogues) under LiOH-mediated hydrolysis then affords free acid **3.Xb**, providing the handle required for installation of the PKS surrogate fragment. Attachment of the PKS surrogate (**3.14, 2.9** or **3.15;** synthesized according to procedures in Chapter II) proceeds via Mitsunobu esterification between **3.Xb** and the mono-TBS-protected diol fragment, also consistent with the stereochemically robust esterification strategy established in Chapter II, affording ester **3.Xc**. TBAF-mediated removal of the TBS group then reveals the free primary alcohol **3.Xd**, which is oxidized directly to the corresponding carboxylic acid **3.Xe** under PDC conditions. With the linear precursor fully elaborated, a two-step sequence of Boc deprotection (HCl-dioxane) and HATU-mediated macrolactamization furnishes the desired macrolactam **3.X**, completing the synthesis of each analogue.

Application of this general route to Trp-containing analogues revealed that the indole-Boc group introduced at **3.1a′** was not orthogonal to the LiOH-mediated hydrolysis conditions used to access **3.1b,** without optimization. Under the originally employed conditions (5.0 eq $LiOH \cdot H_2O$, THF:MeOH:H_2O), competitive removal of the indole carbamate complicated was observed alongside methyl ester hydrolysis, affording **3.1a** and **2.20a** as a byproduct in a 1:1 ratio, determined by LCMS (**Table 3.1**). Given this lack of selectivity, an optimization of hydrolysis conditions was carried out by varying LiOH equivalents, solvent composition, and reaction time (**Table 3.1**).

Reducing the LiOH loading to 1.5 equivalents and limiting the reaction time to 2 h substantially improved selectivity for the desired bis-protected product, affording a 93:7 ratio of desired acid to indole-deprotected byproduct under otherwise identical solvent conditions (THF:MeOH:H_2O, 1:1:1, rt). Chemoselectivity decreased with extended reaction times even at reduced LiOH equivalencies (entry 2), with the ratio declining to 72:28 after 16 h, confirming that indole-Boc loss is a time-dependent process competing kinetically with the intended methyl ester hydrolysis. Substitution of LiOH with the milder base K_2CO_3 in MeOH instead resulted in incomplete consumption of starting material (entry 3), and removing methanol from the solvent

cocktail (entry 4) similarly failed to outperform the optimized tri-component mixture, presumably, due to incomplete dissolution of the reagents.

The optimized conditions (entry 2; 1.5 eq LiOH·H_2O, THF:MeOH:H_2O 1:1:1, rt, 2 h) were thus adopted for the synthesis of all Trp-containing analogues. The penultimate step in the analogue synthesis sequence involving HCl-mediate Boc deprotection was successful in achieving *global* deprotection in the case of all "di-Boc" Trp-containing analogues.



Entry	Reagent	Solvent	Temp.	Time (h)	Reaction profile ratio			
					3.1a'	**3.1b**	**2.20a**	**2.19a**
1	LiOH·H_2O (5.0 eq)	THF:MeOH:H2O (1:1:1)	25 °C	16	-*	50*	50*	-*
2	**LiOH·H_2O (1.5 eq)**	**THF:MeOH:H2O (1:1:1)**	25 °C	**2**	**-**	**93**	**7**	**-**
				4	-	92	8	-
				16	-	72	28	-
3	K_2CO_3 (1.5 eq)	MeOH	25 °C	2	93	6	-	-
				4	90	2	8	-
4	LiOH·H_2O (1.1 eq)	THF:H2O (1:1)	25 °C	2	90	10	-	-
				4	58	42	-	-
				16	10	87	3	-
5	LiOH·H_2O (1.1 eq)	THF:MeOH:H2O (1:1:1)	25 °C	2	56	44	-	-
				4	52	47	1	-
				16	50	47	1	2

Table 3.1 Reaction optimization for saponification of dipeptide **3.1a'.** Ratios determined by AUC of LCMS trace at 214nm. *isolated yields.

Across the first-generation analogues, the general route afforded acyclic variants **2.19a** and **2.20a**, in 63% and 59% overall yields (as per Chapter II results), respectively. Furthermore the 7C ring-size variant **3.1** in 15% overall yield and the L-Pro (**3.3**, 9% overall yield) variant were accessed without complications.

In contrast, application of this route to the 3C ring-size variant (**3.2**) was unsuccessful. Upon activation of acid **3.2e** under standard macrolactamization conditions (HATU, DIPEA), LCMS analysis revealed complete decomposition of the linear precursor, with the dipeptide acid recovered as the major identifiable product instead of the desired macrocycle. This outcome is consistent with an E1cb-type elimination pathway, in which deprotonation at the C2 position alpha to the activated PKS carboxylic acid promotes elimination to furnish the dipeptide acid and the corresponding α,β-unsaturated acrylic acid byproduct. This pathway is in direct competition with the intended macrolactamization, The shortened 3C PKS tether reduces the targeted ring size from the native 12-membered macrolactam to a 10-membered system, a ring-closing event expected to be considerably more difficult given the increased transannular strain characteristic of medium-sized rings (see **Section 2.1.1**). Thus, rather unsurprisingly, under these more demanding cyclization conditions, the competing elimination pathway appears to outcompete macrolactamization entirely. Due to the inaccessibility of this analogue, this analogue was excluded from the targeted analogue scope.

Synthesis of the reverse-prenylated Trp analogue (**3.4**) presented another distinct complication as treatment of the free alcohol intermediate under PDC conditions resulted in complete decomposition of the substrate by LCMS, with no identifiable oxidized product (**3.6e**) detected. This was due to the sensitivity of the indole to oxidation, which was still persistent even



Figure 3.7. Synthesis of the reverse-prenylated Trp analogue from advanced intermediate **2.25** (Chapter II). Global deprotection (TMSOTf, 2,6-lutidine) and HATU-mediated macrolactamization afford macrolactam **3.4**.

with the early-stage installation of the reverse-prenylation at the indole nitrogen. An alternative two-step oxidation sequence, employing Parikh-Doering oxidation to the aldehyde followed by Pinnick oxidation to the corresponding acid, was attempted to circumvent this outcome, however, decomposition was again observed at the Pinnick step. Consequently, the reverse-prenylated Trp analogue could not be accessed via the first-generation route. Instead, this analogue was accessed using traditional route C strategy described in Chapter II, in which the reverse-prenylated dipeptide was esterified directly with pre-functionalized PKS surrogate **2.22**, affording intermediate **2.25** (see Chapter II, **Figure 2.8**). The final steps involved the use of TMS-OTf and 2,6-lutidine as a mild alternative enabling global Boc and tert-butyl deprotection, affording then linear precursor to cyclization (**Figure 3.7**). Strong acidic conditions were specifically avoided due to the tendency for migration of the reverse-prenyl group, as had been previously seen and described in Chapter II, **Section 2.2.2**. Finally, employing standard ring-closing conditions (HATU, DIPEA) afforded the desired product in 35% yields (full spectroscopic characterization is pending). A related strategy is being pursued by Jason Ma in the synthesis of the corresponding HA23 analogue, where its *O*-prenylated Tyr residue presents a comparable susceptibility to acid-mediated prenyl migration under the strongly acidic Boc-deprotection conditions required for cyclization.

3.2.2 Second-Generation Synthesis of the Analogue Library

While the first-generation route successfully delivered the majority of the targeted analogues, its solution-phase design proved labour-intensive with each analogue requiring between nine and ten linear steps and up to seven individual purifications per analogue. Given the size of the analogue library and the need to access multiple structurally distinct compounds in

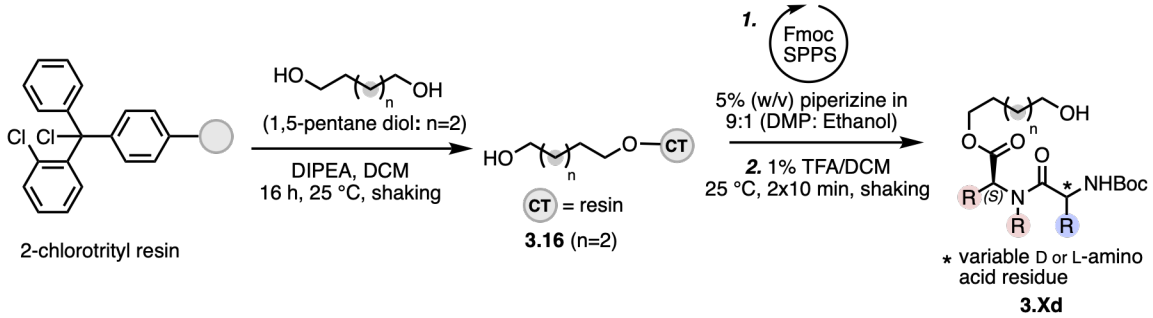


Figure 3.8. Second-generation (SPPS) route. Loading of the diol fragment onto 2-chlorotrityl resin (DIPEA, DCM) affords **3.16**; Fmoc-SPPS and TFA-mediated cleavage afford same three-component intermediate **3.Xd**, corresponding to the first-generation intermediate.

parallel, a second-generation strategy employing solid-phase peptide synthesis (SPPS) was proposed by Jason Ma and implemented jointly to streamline analogue production (**Figure 3.8**).

The second-generation route begins with loading of the diol fragment onto 2-chlorotrityl (CT) resin under DIPEA-mediated conditions (**Figure 3.8**), installing the PKS fragment to the solid support through its free hydroxyl terminus. Resin loading was determined by a standard Fmoc loading test following installation of the first Fmoc-protected amino acid residue onto the resin-bound diol, providing a quantitative measure of the functionalization efficiency at this stage. Fmoc-SPPS, employing standard piperazine-mediated Fmoc deprotection and a HATU-mediated coupling, was then used to install the remaining amino acid residue. Following a TFA-mediated resin-cleavage step, the three-component intermediate (**3.Xd**) was accessed. This single SPPS-enabled process, requiring just two hours from **3.X** and a single purification, consolidated what previously took six to seven synthetic steps and 4 to 5 individual purifications and thus provided a substantial reduction in synthetic effort and time. From **3.Xd**, the remaining three steps to access each macrolactam (PDC-mediated oxidation to the carboxylic acid, Boc-deprotection, and HATU-mediated macrolactamization) were identical to those employed in the first-generation route.

This route was applied to the synthesis of the remaining members of the analogue library. The D-Phe (**3.6**, 8% overall yield) and acremolide (**3.9**, 28% overall yield) and colletopeptide (**3.7, 13**% overall yield) analogues were prepared by Jason Ma using this general route, while the synthesis of the D-Tyr (**3.5**) and HA23 (**3.8**) remains ongoing (with full characterization data pending). The stereocalpin (**3.10, 20**% overall yield) and epi-stereocalpin (**3.11, 45**% overall yield) analogues were prepared as part of this work

Collectively, the second-generation SPPS strategy enabled rapid access to the remaining members of the analogue library, substantially reducing the synthetic burden relative to the first-generation route. With the majority of the targeted analogue library now in hand, preliminary biological evaluation of a subset of these compounds is presented in the following section.

3.2.3 Biological Evaluation of the Analogue Library

Preliminary biological evaluation of a subset of the analogue library was carried out using the ROS burst potentiation assay described in Section 3.1.2, in which compound-mediated enhancement of the Flg22-triggered immune response is measured by luminescence.

The stereochemical probe set (**2.1-*syn***, **2.1-*anti***, **2.1-*syn'***, **2.1-*anti'***) was evaluated first, given its direct relevance to the pharmacophore hypothesis outlined in Section 3.1.4 (Results not shown). Of the four diastereomers, only **2.1-*anti***, bearing the native D-Trp/L-Pip configuration of immunomodulide, potentiated the Flg22-triggered ROS burst relative to Flg22 alone (1 nM). None of the remaining three diastereomers, each bearing an inverted configuration at the Trp or Pip α-centre relative to the native arrangement, retained this activity. This result indicates that the configuration of the macrolactam backbone is critical for activity, with only the native D-Trp/L-Pip configuration retaining the immunopotentiating effect.

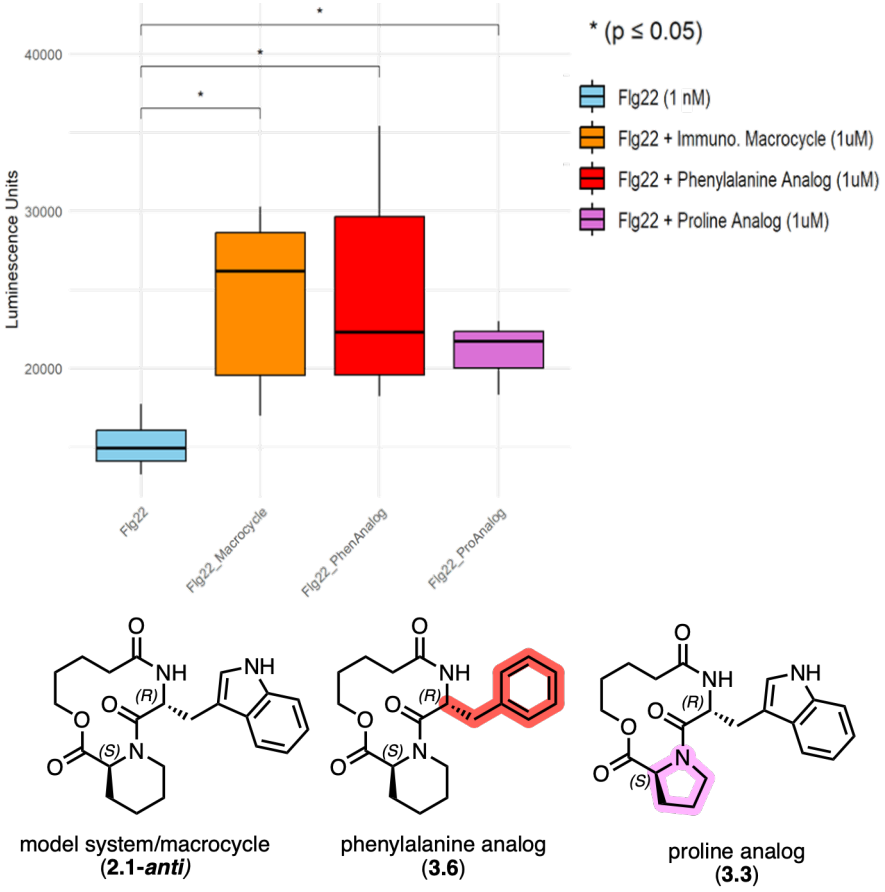


Figure 3.9. ROS burst potentiation assay evaluating the model macrolactam (**2.1-*anti***) and building block exchange set analogues. Luminescence was measured following treatment with Flg22 (1 nM) alone or in combination with the model macrolactam, D-Phe analogue (**3.6**), or L-Pro analogue (**3.3**) (each at 1 μM). All three compound-treated conditions show a statistically significant increase in ROS burst relative to Flg22 alone (* $p \leq 0.05$).

The building block exchange set was evaluated next, focusing on the D-Phe and L-Pro analogues, which were available at the time of analysis (**Figure 3.X**). Both analogues significantly potentiated the Flg22-triggered ROS burst relative to Flg22 alone (1 nM, $p \leq 0.05$), comparable to the parent immunomodulide model macrolactam (**2.1-*anti***). Notably, both modifications retain structural features and configurations of the native residue they replaced. The D-Phe analogue preserves an aromatic side chain in place of the D-Trp indole, suggesting that the hydrogen bonding of the nitrogen in the indole of D-Trp is not required for activity. Similarly, as the L-Pro analogue retains the cyclic, *N*-alkylated character of L-Pip while reducing the ring size from a six to five-membered system, the comparable activity in this analogue suggests that is ring size is not a determinant of activity, or rather, that a one-carbon reduction in ring size does not erode it. Although these results begin to define the tolerance window at each position, the boundaries of that window cannot be fully established from active analogues alone. Systematic modifications that specifically remove aromaticity at the Trp position or *N*-alkylation at the Pip position are needed to determine where activity is gained and lost, given that inactive analogues are equally as informative as active ones in defining the structural limits of the pharmacophore.

Taken together, these preliminary results support the model in which the macrolactam backbone serves as the primary pharmacophoric determinant of activity. They demonstrate that conservative substitutions at the aromatic side chain and *N*-alkyl positions are tolerated and retain activity. However, they inform that strict D- and L- configurational requirements must be met at the *N*-alkylated amino acid as well as the amino acid with the aromatic side chain, respectively, for activity to be maintained.

Biological evaluation of the remaining members of the analogue library, including the supplementary tridepsipeptide family analogues and the colonization assay readout described in **Section 3.1.2**, remains ongoing at the time of writing.

3.3 Conclusions and Future Directions

The analogue synthesis campaign described in this chapter was undertaken to investigate the structural requirements for the immunomodulatory activity first identified in the model system (**2.1-*anti***), and to establish a preliminary structure-activity relationship for the 12-membered cyclic tridepsipeptide class.

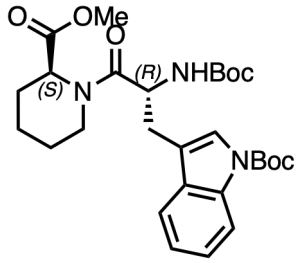
Synthetic access to the analogue library was achieved through two complementary strategies. The first-generation solution-phase route, building directly on the route C macrolactamization established in Chapter II, successfully delivered the analogues **3.1**, and **3.3**, while two notable complications arose. Firstly, in the 3C ring-size variant (**3.2**), which underwent E1cb-type elimination upon in macrolactamization conditions, delivering a decomposition product rather than the conformationally demanding 10-membered product. Additionally, the reverse-prenylated Trp analogue (**3.4**), whose indole proved incompatible with the oxidation conditions required to access the corresponding PKS fragment acid and was instead accessed through the alternative, pre-oxidized fragment strategy established in Chapter II. The subsequent transition to a solid-phase synthetic strategy, consolidating up to seven solution-phase steps into a single automated process, substantially improved the throughput of analogue production and enabled access to the remaining analogues of the building block exchange set **3.5** and **3.6** as well as the tridepsipeptide family-inspired analogues **3.7**-**3.11.**

Preliminary biological evaluation of the stereochemical probe set established that the native D-Trp/L-Pip configuration of the macrolactam backbone is essential for activity, and that α-centre inversion at either stereocenter was sufficient to abolish ROS burst potentiation. This finding identifies the configurational integrity of the macrolactam backbone as a strict pharmacophoric requirement. Moreover, D-Phe (**3.6**) and L-Pro (**3.3**) analogues tested alongside the native model system (**2.1**-***anti***) revealed that these substitutions were tolerated and resulted in no decrease in ROS burst potentiation. However, the degree of structural tolerance at these positions needs to be fully defined by furthering the scope to include failure models (negative controls) and testing the full breadth of the library synthesized here.

Three priorities follow directly from this work. First, the boundaries of this tolerance window must be established through the synthesis and evaluation of analogues that directly interrogate the "aromatic" side chain and *N*-alkylation requirement of the D-Trp and L-Pip substitutions, respectively. Second, biological evaluation of the remaining analogue library, including the tridepsipeptide family analogues and the *Pseudomonas syringae* DC3000 colonization assay, must be completed to determine whether the trends observed in the ROS burst assay extend to a second, independent measure of immunopotentiating activity. Third, given that the mechanism by which this scaffold potentiates the plant immune response remains unknown, future directions of this project could explore synthesis of a clickable analogue, installed at a

position confirmed tolerant of modification. This would enable activity-based protein profiling or fluorescent labeling to identify the molecular target and localize the compound's site of action within the plant.

3.5 Experimental Section

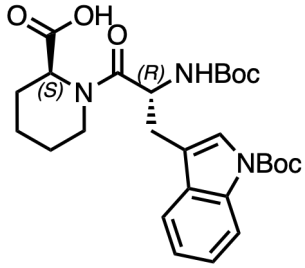


***tert*-butyl 3-((*R*)-2-((*tert*-butoxycarbonyl)amino)-3-((*S*)-2-(methoxycarbonyl)piperidin-1-yl)-3-oxopropyl)-1*H*-indole-1-carboxylate (3.1a').** A flame-dried flask equipped with a Teflon-coated magnetic stir bar and flushed with $N_{2(g)}$ was charged with the free-indole dipeptide (1.26g, 2.94mmol, 1.0eq.) and 7.4mL of DCM. To this stirring solution, NEt_3 (0.82mL, 5.88mmol, 2.0eq) was added dropwise, followed by DMAP (17.9mg, 0.15mmol, 0.05eq), and Boc_2O (750mg, 3.43mmol, 1.17eq). The mixture was left to stir overnight. Upon completion, the organic layer was washed with (1M) HCl, brine (2x5mL), dried over Na_2SO_4, filtered, and concentrated in vacuo. Purification by silica gel flash chromatography (20% EtOAc/Hexane) yielded pure final compound as an orange oil (1.14g, 2.16mmol, 73% yield).

TLC (30%EtOAc in Hexane): Rf= 0.36

NMR (400 MHz, $CDCl_3$) δ 8.12 (d, *J* = 8.2 Hz, 1H), 7.62 (d, *J* = 7.8 Hz, 1H), 7.43 (s, 1H), 7.30 (t, *J* = 7.9 Hz, 1H), 7.25 – 7.21 (m, 1H), 5.55 (d, *J* = 8.3 Hz, 1H), 5.18 (s, 1H), 5.00 (q, *J* = 7.7 Hz, 1H), 3.69 (d, *J* = 2.3 Hz, 3H), 3.55 – 3.45 (m, 1H), 3.10 (dd, *J* = 17.2, 8.6 Hz, 2H), 2.15 – 2.09 (m, 1H), 1.65 (s, 11H), 1.47 (s, 9H), 1.29 – 1.25 (m, 1H), 1.21 – 1.07 (m, 2H), 0.39 (d, *J* = 11.5 Hz, 1H).

13C NMR (101 MHz, $CDCl_3$) δ 171.9, 171.4, 155.2, 149.7, 130.8, 124.7, 124.3, 122.9, 119.1, 115.7, 115.4, 83.7, 79.8, 52.5, 52.4, 50.2, 43.9, 30.2, 28.5, 28.3, 27.7, 26.5, 24.3, 20.7.



(*S*)-1-(*Nα*,1-bis(*tert*-butoxycarbonyl)-*D*-tryptophyl)piperidine-2-carboxylic acid (3.1b). To a solution of methyl ester **3.1a'** (1.1g, 2.4mmol, 1.0eq), dissolved in 12mL of a 1:1:1 mixture of

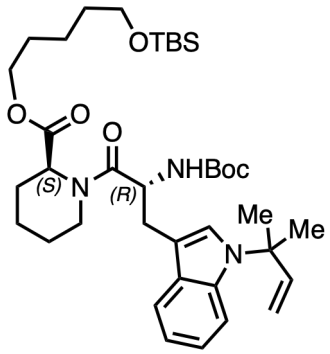
H_2O:THF:MeOH, LiOH monohydrate (203.1mg, 4.84mmol, 1.5eq) was added. The reaction was vigorously stirred for 2h. The pH was adjusted to 2.0 with (1M) HCl and mixture was extract immediately with EtOAc. The organic layers were washed with brine (2x10mL), dried and concentrated in vacuo to yield 70% of the acid product (0.861g, 1.67mmol), of which 50% was boc-deprotected at the indole nitrogen. Optimization attempts are summarized in Table 1.0 below. Desired product of Entry 2 (2h) was product was purified via silica column chromatography (50% EtOAc/Hexane + 1% acetic acid) affording 0.86 g (1.7 mmol, 70% yield) of pale-yellow oil.

TLC (50%EtOAc in Hexane, 1% acetic acid): Rf= 0.27

^{1}H NMR (600 MHz, $CDCl_3$) δ 10.84 (s, 1H), 8.14 – 8.05 (m, 1H), 7.60 (d, *J* = 7.8 Hz, 1H), 7.43 (s, 1H), 7.30 (ddd, *J* = 8.3, 7.1, 1.2 Hz, 1H), 7.24 (td, *J* = 7.5, 1.1 Hz, 1H), 5.67 (d, *J* = 8.2 Hz, 1H), 5.22 – 5.15 (m, 1H), 4.99 (td, *J* = 8.5, 5.5 Hz, 1H), 3.56 – 3.49 (m, 1H), 3.18 – 3.02 (m, 3H), 2.17 – 2.10 (m, 1H), 1.64 (d, *J* = 11.9 Hz, 12H), 1.43 (s, 9H), 1.25 – 1.18 (m, 1H), 1.15 – 1.08 (m, 1H), 0.44 – 0.32 (m, 1H).

13C NMR (151 MHz, $CDCl_3$) δ 175.1, 172.5, 155.4, 149.7, 130.7, 124.7, 124.3, 122.9, 119.1, 115.5, 115.4, 83.8, 80.0, 52.5, 50.3, 44.0, 29.8, 28.5, 28.3, 27.8, 26.2, 24.2, 20.5.

HRMS (ESI-TOF) m/z: [M+H]+ Calcd for $C_{27}H_{38}N_3O_7$ 516.2710; Found 516.2715.



5-((*tert*-butyldimethylsilyl)oxy)pentyl (*S*)-1-(*Nα*-(*tert*-butoxycarbonyl)-1-(2-methylbut-3-en-2-yl)-*D*-tryptophyl)piperidine-2-carboxylate (3.4c). A flame-dried flask equipped with a Teflon-coated magnetic stir bar and flushed with $N_{2(g)}$ was charged with mono-protected alcohol (83.7 mg, 0.38 mmol, 1.0eq), PPh_3 (155.2 mg, 0.59 mmol, 1.3eq) and DIAD (0.11 mL, 0.59 mmol, 1.3eq) added dropwise to 4 mL of dry THF. The mixture was left to stir at 0°C for 15-30 min, after which a solution of dipeptide acid (223.0 mg, 0.46 mmol, 1.2eq) dissolved in 1mL dry THF, was

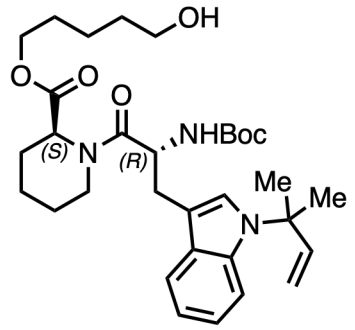
added. The resulting mixture was allowed to warm to room temperature and stir overnight. Once complete, solvent was removed via rotary evaporation and the crude mixture was directly purified by flash silica chromatography (5-10% EtOAc in Hexanes) to afford 160.3 mg (0.23 mmol, 51% yield) of pure compound as a colourless oil.

TLC (30%EtOAc in Hexane): Rf=0.41

^{1}H NMR (400 MHz, $CDCl_3$) δ 7.67 – 7.61 (m, 1H), 7.45 (dt, *J* = 6.7, 3.0 Hz, 1H), 7.19 (s, 1H), 7.07 (tt, *J* = 7.1, 5.4 Hz, 2H), 6.16 – 6.03 (m, 1H), 5.55 (d, *J* = 8.5 Hz, 1H), 5.25 – 5.11 (m, 3H), 5.02 (td, *J* = 9.1, 5.1 Hz, 1H), 4.07 (t, *J* = 6.7 Hz, 2H), 3.58 (t, *J* = 6.4 Hz, 2H), 3.48 – 3.39 (m, 1H), 3.23 (dd, *J* = 14.1, 5.2 Hz, 1H), 3.10 (dd, *J* = 14.0, 9.5 Hz, 1H), 3.04 – 2.92 (m, 1H), 2.12 – 1.99 (m, 1H), 1.71 (s, 6H), 1.61 (p, *J* = 7.0 Hz, 2H), 1.50 (dd, *J* = 8.5, 6.3 Hz, 2H), 1.46 (s, 9H), 1.37 – 1.28 (m, 3H), 1.08 – 0.94 (m, 3H), 0.88 (s, 9H), 0.03 (s, 6H), -0.01 – -0.08 (m, 1H).

^{13}C NMR (101 MHz, $CDCl_3$) δ 172.4, 170.9, 155.1, 144.1, 135.5, 129.7, 123.9, 120.9, 119.1, 119.0, 113.6, 113.5, 108.8, 79.4, 77.2, 65.2, 62.9, 58.9, 52.2, 50.6, 43.7, 32.3, 30.9, 28.4, 28.3, 27.9, 26.2, 26.0, 23.9, 22.2, 20.4, 18.3, 1.0, -5.3.

HRMS (ESI-TOF) m/z: [M+H]+ Calcd for $C_{38}H_{62}N_3O_6Si$ 684.4408; Found 684.4402



5-hydroxypentyl (*S*)-1-(*Nα*-(*tert*-butoxycarbonyl)-1-(2-methylbut-3-en-2-yl)-*D*-tryptophyl)piperidine-2-carboxylate (3.4d). An RBF equipped with a Teflon-coated magnetic stir bar was charged with the TBS-protected intermediate **3.4c** (160.3 mg, 0.25 mmol, 1.0 eq) and dissolved in dry 0.5mL of dry THF. The flask was sparged with $N_{2(g)}$ and cooled in an ice bath. To the stirring suspension, TBAF (1M in THF, 0.35 mL 0.35 mmol, 1.5 eq) was added dropwise and the mixture was left to warm to room temperature and stir overnight. Once complete, the solvent was removed via rotary evaporation and the mixture was re-dissolved in roughly 10mL of diethyl ether. The organic layer was washed with water (2x 5mL), brine (1x5mL), dried over $MgSO_4$ and

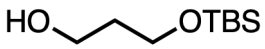
concentrated to give the crude of the alcohol product as a colourless oil in 57% yield (75 mg, 0. 131 mmol). The product was sufficiently pure to proceed without further purification.

TLC (50%EtOAc in Hexane): Rf=0.13

^{1}H NMR (600 MHz, $CDCl_3$) δ 7.62 (d, *J* = 7.6 Hz, 1H), 7.45 (d, *J* = 7.9 Hz, 1H), 7.18 (s, 1H), 7.10 – 7.00 (m, 2H), 6.08 (ddd, *J* = 17.4, 10.7, 1.4 Hz, 1H), 5.66 (d, *J* = 8.7 Hz, 1H), 5.24 – 5.11 (m, 3H), 5.03 (td, *J* = 8.8, 5.5 Hz, 1H), 4.10 – 4.07 (m, 2H), 3.66 – 3.56 (m, 2H), 3.47 (ddd, *J* = 12.5, 5.6, 2.9 Hz, 1H), 3.20 (dd, *J* = 14.1, 5.3 Hz, 1H), 3.09 (dd, *J* = 14.0, 9.4 Hz, 1H), 2.94 (t, 1H), 2.03 (d, 1H), 1.70 (d, *J* = 1.5 Hz, 6H), 1.66 – 1.57 (m, 2H), 1.56 – 1.50 (m, 2H), 1.45 (d, *J* = 1.4 Hz, 9H), 1.39 (dd, *J* = 13.0, 6.3 Hz, 3H), 1.33 – 1.28 (m, 1H), 1.06 (d, *J* = 12.7 Hz, 1H), 0.98 (td, *J* = 11.1, 6.6 Hz, 1H), -0.01 (td, *J* = 13.2 Hz, 1H).

^{13}C NMR (151 MHz, $CDCl_3$) δ 172.6, 171.0, 155.3, 144.2, 135.5, 129.7, 124.0, 121.0, 119.2, 119.1, 113.7, 113.6, 108.8, 79.6, 65.1, 62.4, 59.0, 52.4, 50.7, 44.0, 32.2, 30.9, 28.5, 28.5, 28.4, 28.3, 28.0, 26.1, 24.0, 22.3, 21.1, 20.5.

HRMS (ESI-TOF) m/z: [M+H]+ Calcd for $C_{32}H_{48}N_3O_6$570.3543; Found: 570.3551



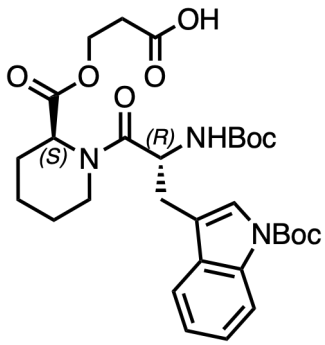
3-((*tert*-butyldimethylsilyl)oxy)propan-1-ol. (3.14) To a stirring solution of 1,3-propane diol (0.5mL, 6.9mmol, 1.0eq) in 7mL of DCM, NEt_3 (1.92mL, 13.8mmol, 2.0eq) was added dropwise, along with DMAP (42mg, 0.31mmol, 0.05eq) and TBSCl (1.25g, 8.35mmol, 1.2eq). The solution was stirred vigorously overnight after which all volatiles were removed in vacuo and the resulting mixture was immediately purified via flash silica column chromatography (gradient of 100% hexanes to 80% hexanes in EtOAc), and tracked via $KMnO_4$ staining of TLCs to yield 0.59 g (3.12 mmol, 45% yield).

TLC (20%EtOAc in Hexane): Rf=0.3

^{1}H NMR (400 MHz, $CDCl_3$) δ 3.87 – 3.76 (m, 4H), 2.55 (s, 1H), 1.80 – 1.72 (m, 2H), 0.91 – 0.88 (m, 9H), 0.11 – 0.03 (m, 6H).

^{13}C NMR (101 MHz, $CDCl_3$) δ 63.1, 62.6, 34.3, 26.0, 18.3, -5.4.

HRMS (ESI-TOF) m/z: [M+H]+ Calcd for $C_9H_{23}O_2Si$ 191.1467; Found 191.1479.



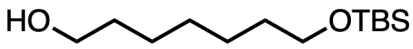
3-(((*S*)-1-(*Nα*,1-bis(*tert*-butoxycarbonyl)-*D*-tryptophyl)piperidine-2-carbonyl)oxy)propanoic acid (3.2e). A flame-dried flask equipped with a Teflon-coated magnetic stir bar and flushed with $N_{2(g)}$ was charged with mono-protected alcohol **3.14** (88.4mg, 0.46mmol, 1.0eq), PPh_3 (146.1mg, 0.56mmol, 1.2eq) and DIAD (0.11mL, 0.56mmol, 1.2eq) added dropwise to 5mL of dry THF. The mixture was left to stir at 0C for 15-30minutes, after which a solution of dipeptide acid **3.1b** (287.9mg, 0.56mmol, 1.2eq) dissolved in 1mL dry THF, was added. The resulting mixture was allowed to warm to room temperature and stir overnight. Upon disappearance of the starting material on TLC, 0.724mL (0.72mmol, 1.5eq) of a TBAF solution (1M in THF) was added dropwise and the resulting mixture was left to stir overnight at room temperature. Once complete, solvent was removed via rotary evaporation and the mixture was re-dissolved in roughly 10mL of diethyl ether. The organic layer was washed with water (2x 5mL), brine (1x5mL), dried over $MgSO_4$ and concentrated to give the crude mixture of the alcohol product. This crude mixture was taken up in 2mL of DMF, 940mg (2.5mmol, 5,0eq) PDC was added in one portion, and the resulting solution was left to stir under inert conditions overnight. After the reaction was confirmed to be complete via TLC, roughly 2g of celite, 2mL of saturated NH_4Cl solution and 2mL of EtOAc was added directly to the reaction flask. The resulting mixture was filtered through a pad of celite, the aqueous layer was extracted with EtOAc (2x 5mL). The organic layers were combined and washed with brine (3x 5mL) to remove residual DMF and before concentrating under vacuo. Purification by silica gel flash chromatography (50% EtOAc/Hexane *then* 50% EtOAc/Hexane with 1% acetic acid) yielded pure compound **3.2e** as a clear colourless oil (136.8mg, 0.23mmol, 41% overall yield).

TLC (20%EtOAc in Hexane): Rf=0.3

1H NMR (600 MHz, $CDCl_3$) δ 8.12 (s, 1H), 7.57 (d, J = 7.7 Hz, 1H), 7.45 (d, J = 8.3 Hz, 1H), 7.32 – 7.29 (m, 1H), 7.25 – 7.22 (m, 1H), 5.66 – 5.58 (m, 1H), 5.21 (d, J = 4.1 Hz, 1H), 4.99 – 4.95 (m, 1H), 4.42 (dt, J = 11.3, 5.8 Hz, 1H), 4.31 (dt, J = 11.1, 6.3 Hz, 1H), 3.54 (d, J = 13.8 Hz, 1H), 3.13 – 3.06 (m, 3H), 2.63 (t, J = 6.0 Hz, 2H), 2.18 – 2.12 (m, 1H), 1.65 (s, 11H), 1.44 (s, 9H), 1.23 – 1.19 (m, 1H), 1.15 (s, 1H), 1.15 – 1.11 (m, 1H), 0.60 – 0.36 (m, 1H).

^{13}C NMR (151 MHz, $CDCl_3$) δ 173.1, 171.9, 155.9, 149.7, 135.5, 130.7, 124.7, 124.2, 122.9, 119.0, 115.5, 115.4, 83.8, 80.5, 52.6, 52.5, 50.3, 43.9, 33.7, 30.0, 28.5, 28.3, 26.2, 24.4, 20.5.

HRMS (ESI-TOF) m/z: [M+H]+ Calcd for $C_{30}H_{42}N_3O_9$ 588.2921; Found 588.2925.



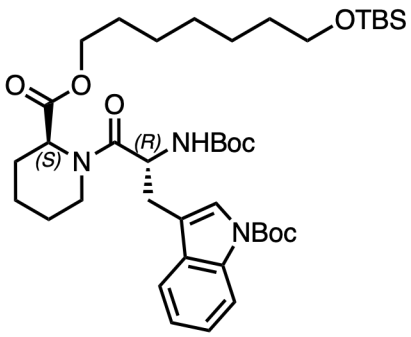
7-((*tert*-butyldimethylsilyl)oxy)heptan-1-ol (3.15): To a stirring solution of 1,7-propane diol (0.5mL, 3.6mmol, 1.0eq) in 3.6 mL of DCM, NEt_3 (1.0 mL, 7.2 mmol, 2.0eq) was added dropwise, along with DMAP (21 mg, 0.18 mmol, 0.05 eq) and TBSCl (650 mg, 4.3 mmol, 1.2eq). The solution was stirred vigorously overnight after which all volatiles were removed in vacuo and the resulting mixture was immediately purified via flash silica column chromatography (gradient of 100% hexanes to 80% hexanes in EtOAc), and tracked via $KMnO_4$ staining of TLCs to yield 49 % of pure product (437 mg, 1.77 mmol).

TLC (20%EtOAc in Hexane): Rf=0.32

1H NMR (400 MHz, $CDCl_3$) δ 3.64 (t, J = 6.6 Hz, 2H), 3.60 (t, J = 6.6 Hz, 2H), 1.63 – 1.43 (m, 4H), 1.43 – 1.29 (m, 6H), 0.89 (s, 9H), 0.04 (s, 6H).

13C NMR (101 MHz, $CDCl_3$) δ 63.4, 63.2, 33.0, 32.9, 29.4, 26.1, 25.9, 25.9, 18.5, -5.1.

HRMS (ESI-TOF) m/z: [M+H]+ Calcd for $C_{13}H_{31}O_2Si$ 247.2093; Found 247.2103



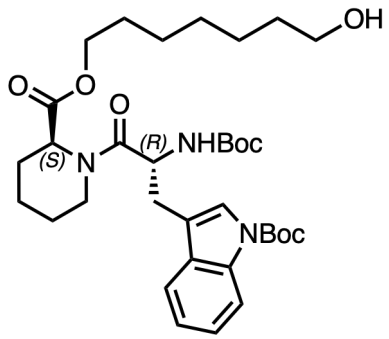
***tert*-butyl 3-((*R*)-2-((*tert*-butoxycarbonyl)amino)-3-((*S*)-2-(((7-((*tert*-butyldimethylsilyl)oxy)heptyl)oxy)carbonyl)piperidin-1-yl)-3-oxopropyl)-1*H*-indole-1-carboxylate (3.1c):** A flame-dried flask equipped with a Teflon-coated magnetic stir bar and flushed with $N_{2(g)}$ was charged with mono-protected alcohol **3.15** (81.4 mg, 0.33 mmol, 1.0eq), PPh_3 (134.1 mg, 0.51 mmol, 1.3eq) and DIAD (0.1 mL, 0.51 mmol, 1.3eq) added dropwise to 4mL of dry THF. The mixture was left to stir at 0°C for 15-30 min, after which a solution of dipeptide acid **3.1b** (204.6 mg, 0.4 mmol, 1.2eq) dissolved in 1mL dry THF, was added. The resulting mixture was allowed to warm to room temperature and stir overnight. Once complete, solvent was removed via rotary evaporation and the crude mixture was directly purified by flash silica chromatography (5-10% EtOAc in Hexanes) to afford 190.2 mg (0.25 mmol, 64% yield) of pure **3.1c** as a colourless oil.

TLC (30%EtOAc in Hexane): Rf=0.34

1H NMR (600 MHz, $CDCl_3$) δ 8.12 (s, 1H), 7.63 (d, J = 7.8 Hz, 1H), 7.43 (s, 1H), 7.30 (t, J = 7.8 Hz, 1H), 7.25 – 7.21 (m, 1H), 5.53 (d, J = 8.2 Hz, 1H), 5.15 (d, J = 4.8 Hz, 1H), 5.00 (q, J = 8.1 Hz, 1H), 4.08 (q, J = 6.2 Hz, 2H), 3.61 – 3.55 (m, 3H), 3.52 – 3.48 (m, 1H), 3.16 – 3.05 (m, 3H), 2.11 (d, J = 11.2 Hz, 1H), 1.67 – 1.64 (m, 11H), 1.61 – 1.56 (m, 4H), 1.52 – 1.47 (m, 3H), 1.45 (s, 9H), 1.39 – 1.36 (m, 3H), 1.14 – 1.10 (m, 2H), 0.89 (s, 9H), 0.40 (q, J = 12.8 Hz, 1H), 0.04 (s, 8H).

13C NMR (151 MHz, $CDCl_3$) δ 171.9, 170.9, 155.2, 149.7, 135.6, 130.8, 124.7, 124.3, 122.9, 119.2, 115.7, 115.4, 83.7, 79.7, 65.4, 63.3, 52.6, 50.3, 43.9, 32.9, 30.2, 29.1, 28.6, 28.5, 28.4, 26.5, 26.1, 25.9, 25.8, 24.3, 20.7, 18.5, 1.2, -5.1.

HRMS (ESI-TOF) m/z: [M+H]+ Calcd for $C_{40}H_{66}N_3O_8Si$ 744.4619; Found 744.4622



***tert*-butyl 3-((*R*)-2-((*tert*-butoxycarbonyl)amino)-3-((*S*)-2-(((7-hydroxyheptyl)oxy)carbonyl)piperidin-1-yl)-3-oxopropyl)-1*H*-indole-1-carboxylate (3.1d):**

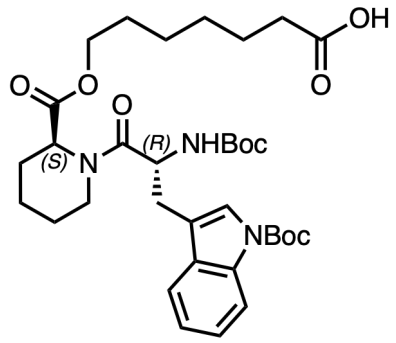
An RBF equipped with a Teflon-coated magnetic stir bar was charged with the TBS-protected intermediate **3.1c** (190.2 mg, 0.25 mmol, 1.0 eq) and dissolved in dry 0.5mL of dry THF. The flask was sparged with $N_{2(g)}$ and cooled in an ice bath. To the stirring suspension, TBAF (1M in THF, 0.38 mL 0.38 mmol, 1.5 eq) was added dropwise and the mixture was left to warm to room temperature and stir overnight. Once complete, the solvent was removed via rotary evaporation and the mixture was re-dissolved in roughly 10mL of diethyl ether. The organic layer was washed with water (2x 5mL), brine (1x5mL), dried over $MgSO_4$ and concentrated to give the crude of the alcohol product **3.1d** as a colourless oil in 80% yield (128.1 mg, 0.2 mmol). The product was sufficiently pure to proceed without further purification.

TLC (40%EtOAc in Hexane): Rf=0.20

1H NMR (600 MHz, $CDCl_3$) δ 8.14 – 8.09 (m, 1H), 7.62 (d, J = 7.7 Hz, 1H), 7.43 (s, 1H), 7.32 – 7.28 (m, 1H), 7.25 – 7.22 (m, 1H), 5.58 (d, J = 8.3 Hz, 1H), 5.16 – 5.13 (m, 1H), 5.00 (td, J = 8.5, 5.3 Hz, 1H), 4.08 (td, J = 6.6, 1.2 Hz, 2H), 3.62 (t, J = 6.6 Hz, 2H), 3.50 (dd, J = 10.0, 6.8 Hz, 1H), 3.16 – 3.05 (m, 3H), 2.13 – 2.08 (m, 1H), 1.65 (s, 9H), 1.60 (t, J = 6.7 Hz, 2H), 1.56 – 1.53 (m, 2H), 1.45 (s, 9H), 1.39 – 1.37 (m, 2H), 1.35 – 1.32 (m, 3H), 1.27 – 1.25 (m, 2H), 1.14 – 1.10 (m, 2H), 0.44 – 0.35 (m, 1H).

13C NMR (151 MHz, $CDCl_3$) δ 171.9, 170.9, 155.2, 149.7, 135.5, 130.8, 124.7, 124.3, 122.9, 119.1, 115.7, 115.3, 83.7, 79.8, 65.3, 63.0, 52.6, 50.2, 43.9, 32.7, 30.2, 28.8, 28.5, 28.3, 26.5, 25.8, 25.6, 24.3, 20.6.

HRMS (ESI-TOF) m/z: [M+H]+ Calcd for $C_{34}H_{52}N_3O_8$ 630.3754; Found 630.3754



7-(((*S*)-1-(*Nα*,1-bis(*tert*-butoxycarbonyl)-*D*-tryptophyl)piperidine-2-carbonyl)oxy)heptanoic acid (3.1e): A RBF equipped with a Teflon-coated magnetic stir bar was charged with 128.7 mg of alcohol intermediate (0.2 mmol, 1.0 eq) and 0.8 mL of wet DMF. 383 mg of PDC (1.02 mmol,

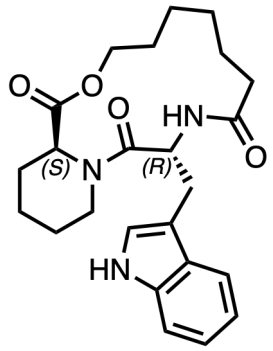
5.0 eq) was added to stirring suspension, and the reaction was left to stir overnight at 25°C. Upon completion, ~1g of celite, 10mL of NH_4Cl saturated solution and 10mL EtOAc were added, and stirring was continued for 30 min, after which the mixture was directly applied to a separatory funnel and the organic layers was extracted. The aqueous layers were washed (15mL x 5) with EtOAc, and organic layers were combined. The organic layer was washed (15mL x 5) with brine, dried over MgSO4, filtered, and concentrated under reduced pressure to afford the crude acid product. Purification was achieved by flash silica column chromatography (50% EtOAc in Hexanes, 1% acetic acid) yielding 65 mg (0.1 mmol, 50% yield) of pure acid **3.1e**.

TLC (70%EtOAc in Hexane, 1% acetic acid): Rf=0.30

1H NMR (400 MHz, $CDCl_3$) δ 8.73 (s, 1H), 8.12 (d, J = 8.2 Hz, 1H), 7.61 (d, J = 7.7 Hz, 1H), 7.43 (s, 1H), 7.33 – 7.28 (m, 1H), 7.26 – 7.18 (m, 1H), 5.68 – 5.57 (m, 1H), 5.19 – 5.13 (m, 1H), 5.02 (q, J = 7.7 Hz, 1H), 4.10 (ddt, J = 8.9, 6.5, 3.3 Hz, 2H), 3.54 (d, J = 13.4 Hz, 1H), 3.14 – 3.04 (m, 3H), 2.33 (t, J = 7.3 Hz, 2H), 2.15 – 2.06 (m, 1H), 1.65 (s, 11H), 1.44 (s, 10H), 1.40 – 1.32 (m, 7H), 1.13 (s, 1H), 0.85 (dd, J = 7.0, 3.2 Hz, 1H), 0.45 – 0.39 (m, 1H).

^{13}C NMR (101 MHz, $CDCl_3$) δ 178.1, 172.0, 170.7, 155.2, 149.6, 135.4, 124.6, 124.2, 122.8, 119.0, 115.5, 115.2, 83.6, 79.7, 65.1, 52.5, 50.1, 43.8, 33.7, 30.0, 29.7, 28.4, 28.4, 28.3, 28.2, 26.4, 25.4, 24.4, 24.4, 20.5.

HRMS (ESI-TOF) m/z: [M+H]+ Calcd for $C_{34}H_{50}N_3O_9$ 644.3547; Found 644.3548



(11*R*,17a*S*)-11-((1*H*-indol-3-yl)methyl)dodecahydropyrido[2,1-*c*][1]oxa[4,7]diazacyclotetradecine-1,9,12(14*H*)-trione (3.1): In a RBF equipped with a Teflon-coated magnetic stir bar, 63.9 mg (0.1 mmol, 1.0 eq) pure acid **3.1e** was dissolved in 0.2 mL of DCM. 0.2 mL of TFA was added dropwise to this stirring suspension and the reaction was left to stir at 25°C for 1h or until deprotection was determined complete by TLC. Once complete, the

volatiles were removed under reduced pressure and the resulting crude unprotected intermediate was used directly in the subsequent step without further purification.

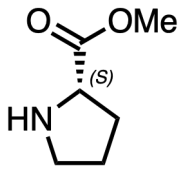
The crude product was dissolved in 1 mL DCM and sparged with nitrogen. A solution of HATU (114 mg, 0.3 mmol, 3.0 eq) in 2 mL of DMF was added to this stirring suspension, after which DIPEA (0.15 mL, 0.9 mmol, 9.0 eq) was added dropwise and the reaction was left to stir at 25°C overnight. Upon completion, the reaction was quenched with sat. $NaHCO_3$ and transferred to a separatory funnel. The organic layers were extracted, washed with brine (5x), dried over Na2SO4, filtered, and concentrated under reduced pressure to afford the crude macrocycle. Purification was achieved by semipreparative reverse-phase HPLC (flowrate of 10mL/min from 5%-95% (ACN in H_2O) over 20 min) to afford 25mg (0.06 mmol, 59% yield) of pure **3.1** macrocycle.

TLC (10%MeOH in DCM, 1% acetic acid): Rf=0.38

^{1}H NMR (600 MHz, $CDCl_3$) δ 8.05 (s, 1H), 7.66 (dt, *J* = 7.9, 1.0 Hz, 1H), 7.35 (dt, *J* = 8.2, 0.9 Hz, 1H), 7.19 (ddd, *J* = 8.1, 7.0, 1.2 Hz, 1H), 7.12 (ddd, *J* = 8.2, 7.1, 1.0 Hz, 1H), 7.11 (s, 1H), 6.77 (d, *J* = 9.3 Hz, 1H), 5.53 (td, *J* = 9.9, 5.4 Hz, 1H), 5.20 (d, *J* = 5.6 Hz, 1H), 4.32 (ddd, *J* = 10.9, 6.5, 3.2 Hz, 1H), 3.80 (ddd, *J* = 11.2, 8.7, 2.8 Hz, 1H), 3.59 (d, *J* = 13.5 Hz, 1H), 3.26 (dd, *J* = 13.9, 10.4 Hz, 1H), 3.17 (dd, *J* = 13.9, 5.3 Hz, 1H), 2.69 (td, *J* = 13.1, 2.8 Hz, 1H), 2.47 (ddd, *J* = 14.0, 6.7, 3.1 Hz, 1H), 2.09 (d, *J* = 9.8 Hz, 1H), 2.02 (ddd, *J* = 14.1, 11.3, 3.0 Hz, 1H), 1.90 (dddd, *J* = 14.1, 11.5, 8.8, 3.4 Hz, 1H), 1.60 (dtd, *J* = 12.1, 6.1, 3.0 Hz, 3H), 1.50 – 1.40 (m, 2H), 1.32 – 1.26 (m, 3H), 1.17 – 1.11 (m, 1H), 1.11 – 1.06 (m, 2H), 0.97 – 0.91 (m, 1H), -0.06 (tt, *J* = 13.1, 4.1 Hz, 1H).

^{13}C NMR (101 MHz, $CDCl_3$) δ 172.9, 170.6, 136.3, 127.4, 122.9, 122.5, 120.0, 118.9, 111.2, 95.8, 90.5, 77.4, 67.2, 65.7, 60.5, 52.5, 44.7, 36.9, 29.3, 28.5, 26.0, 25.3, 24.4, 24.2.

HRMS (ESI-TOF) m/z: [M+H]+ Calcd for $C_{24}H_{32}N_3O_4$ 426.2393; Found 426.2383



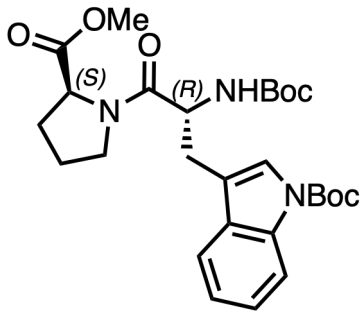
Methyl *L*-prolinate (3.12): In a RBF equipped with a Teflon-coated magnetic stir bar, 2g (17.4 mmol, 1.0 eq) L-proline was dissolved in 35 mL of methanol. To this stirring suspension, TMSCl (6.5 mL, 52 mmol, 3.0 eq) was added dropwise and the reaction was vigorously stirred at 25°C

overnight. Upon completion, the volatiles were removed through rotary evaporation. The crude product collected (2.1 g, 16.5 mmol, 95% yield) was sufficiently pure to be used in the following step without the need for further purification.

1H NMR (400 MHz, MeOD) δ 4.53 – 4.32 (m, 1H), 3.86 (dt, J = 2.2, 1.1 Hz, 3H), 3.49 – 3.34 (m, 2H), 2.44 (dq, J = 14.3, 7.3 Hz, 1H), 2.25 – 1.93 (m, 3H).

^{13}C NMR (101 MHz, MeOD) δ 170.51, 60.66, 53.93, 47.15, 29.28, 24.52.

HRMS (ESI-TOF) m/z: [M+H]+ Calcd for $C_6H_{12}NO_2$ 130.0868; Found 130.0880



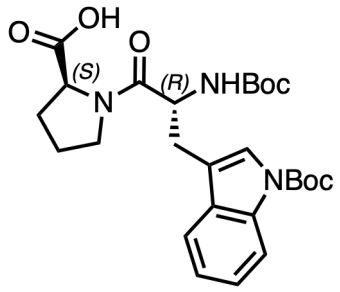
tert-butyl 3-((R)-2-((tert-butoxycarbonyl)amino)-3-((S)-2-(methoxycarbonyl)pyrrolidin-1-yl)-3-oxopropyl)-1H-indole-1-carboxylate (3.3a'). A flame-dried flask equipped with a Teflon-coated magnetic stir bar and flushed with $N_{2(g)}$ was charged with Boc-*D*-Trp-OH (**3.16**) (0.56g, 1.85mmol, 1.0eq.), **3.12** (0.25 mg, 2.03 mmol, 1.1 eq) and 18.5 mL of DCM. HATU (0.844 mg, 2.22 mmol, 1.2 eq.) was added at 0 °C and, followed by DIPEA (0.6 mL, 3.7 mmol, 2.0 eq) dropwise. The reaction was left to warm to 25 °C and stir overnight. Upon completion, quenching was achieved with (1M) HCl (dropwise addition) followed by immediate extraction with EtOAc. The organic layer was washed with saturated $NaHCO_3$ (5mLx3), brine (5mLx2), dried over $MgSO_4$, filtered, and concentrated under reduced pressure. Purification by silica gel flash chromatography (40% EtOAc/Hexane) yielded pure product as viscous orange oil (0.73 g, 1.78 mmol, 94% yield). The product was then taken up 4.0 mL DCM, to which NEt3 (0.49 mL, 3.54 mmol, 2.0 eq) and DMAP (21 mg, 0.17 mmol, 0.1 eq) were added, followed by (Boc)2O (0.43 g, 1.9 mmol, 1.1 eq). The reaction was left to stir overnight at 25 °C. Upon completion, the mixture was directly concentrated by rotary evaporation and purified via silica column chromatography (20-30% EtOAc in Hexanes) to afford 0.794 g (1.54 mmmol, 87% yield) of **3.3a'** isolated as a pale-yellow oil.

TLC (30%EtOAc in Hexane): Rf=0.23

^{1}H NMR (400 MHz, $CDCl_3$) δ 8.12 (d, *J* = 8.2 Hz, 1H), 7.55 (d, *J* = 7.7 Hz, 1H), 7.46 (s, 1H), 7.30 (t, *J* = 7.6 Hz, 1H), 7.23 (t, *J* = 7.4 Hz, 1H), 5.47 (d, *J* = 8.4 Hz, 1H), 4.69 (td, *J* = 8.9, 5.2 Hz, 1H), 4.19 (dd, *J* = 8.7, 3.5 Hz, 1H), 3.71 (s, 3H), 3.51 (q, *J* = 7.4 Hz, 1H), 3.16 (dd, *J* = 13.8, 5.2 Hz, 1H), 3.07 (dd, *J* = 13.9, 9.1 Hz, 1H), 2.69 (q, *J* = 8.1 Hz, 1H), 1.76 (tt, *J* = 10.8, 6.6 Hz, 2H), 1.65 (s, 9H), 1.45 (s, 9H), 1.33 – 1.26 (m, 2H).

^{13}C NMR (101 MHz, $CDCl_3$) δ 172.4, 170.6, 155.2, 149.7, 130.5, 124.7, 124.4, 122.7, 119.1, 115.7, 115.3, 83.8, 79.8, 77.4, 59.0, 52.8, 52.4, 47.0, 29.8, 28.9, 28.5, 28.4, 24.4.

HRMS (ESI-TOF) m/z calcd for $C_{27}H_{38}N_3O_7$ [M+H]+ 516.2710, found 516.2708.



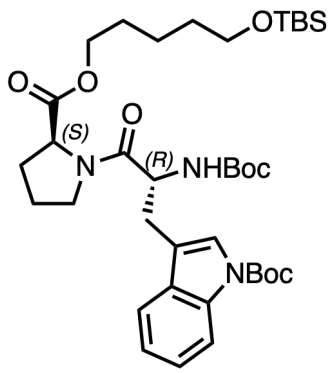
***Nα*,1-bis(*tert*-butoxycarbonyl)-*D*-tryptophyl-*L*-proline (3.3b).** To a solution of methyl ester **3.3a'** (0.51 g, 1.0 mmol, 1.0eq), dissolved in 5 mL of a 1:1:1 mixture of H_2O:THF:MeOH, LiOH monohydrate (62.9 mg, 1.5 mmol, 1.5eq) was added. The reaction was vigorously stirred for 2h. The pH was adjusted to 2.0 with (1M) HCl and mixture was extract immediately with EtOAc. The organic layers were washed with brine (2x10mL), dried and concentrated in vacuo to the acid product in quantitative yields (0.5 g, 1.0 mmol , >95% yields) without the need for further purification.

TLC (50%EtOAc in Hexane, 1% acetic acid): Rf=0.06

^{1}H NMR (400 MHz, $CDCl_3$) δ 8.12 (d, *J* = 8.2 Hz, 1H), 7.55 (d, *J* = 7.7 Hz, 1H), 7.46 (s, 1H), 7.30 (t, *J* = 7.6 Hz, 1H), 7.23 (t, *J* = 7.4 Hz, 1H), 5.47 (d, *J* = 8.4 Hz, 1H), 4.69 (td, *J* = 8.9, 5.2 Hz, 1H), 4.19 (dd, *J* = 8.7, 3.5 Hz, 1H), 3.71 (s, 3H), 3.51 (q, *J* = 7.4 Hz, 1H), 3.16 (dd, *J* = 13.8, 5.2 Hz, 1H), 3.07 (dd, *J* = 13.9, 9.1 Hz, 1H), 2.69 (q, *J* = 8.1 Hz, 1H), 1.76 (tt, *J* = 10.8, 6.6 Hz, 2H), 1.65 (s, 9H), 1.45 (s, 9H), 1.33 – 1.26 (m, 2H).

^{13}C NMR (101 MHz, $CDCl_3$) δ 172.4, 170.6, 155.2, 149.7, 130.5, 124.7, 124.4, 122.7, 119.1, 115.7, 115.3, 83.8, 79.8, 77.4, 59.0, 52.8, 52.4, 47.0, 29.8, 28.9, 28.5, 28.4, 24.4.

HRMS (ESI-TOF) m/z Calcd for $C_{26}H_{36}N_3O_7$ [M+H]+ 502.2553, found 502.2551.



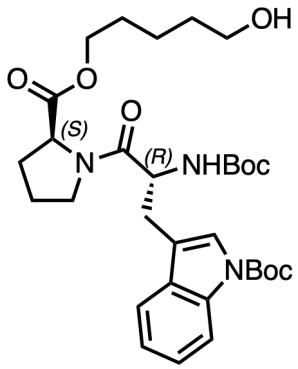
tert-butyl 3-((R)-2-((tert-butoxycarbonyl)amino)-3-((S)-2-(((5-((tert-butyldimethylsilyl)oxy)pentyl)oxy)carbonyl)pyrrolidin-1-yl)-3-oxopropyl)-1H-indole-1-carboxylate (3.3c) A flame-dried flask equipped with a Teflon-coated magnetic stir bar and flushed with $N_{2(g)}$ was charged with mono-protected alcohol **2.9** (53.0 mg, 0.24 mmol, 1.0eq), PPh_3 (100 mg, 0.38 mmol, 1.3eq) and DIAD (0.07 mL, 0.38 mmol, 1.3eq) added dropwise to 2mL of dry THF. The mixture was left to stir at 0°C for 15-30 min, after which a solution of dipeptide acid **3.3b** (146.1 mg, 0.30 mmol, 1.2eq) dissolved in 1mL dry THF, was added. The resulting mixture was allowed to warm to room temperature and stir overnight. Once complete, solvent was removed via rotary evaporation and the crude of **3.3c** was sufficiently pure to use in the subsequent step without further purification.

TLC (20%EtOAc in Hexane): Rf=0.23

1H NMR (600 MHz, $CDCl_3$) δ 8.12 (d, J = 8.5 Hz, 1H), 7.57 (d, J = 7.8 Hz, 1H), 7.46 (s, 1H), 7.30 (t, J = 7.8 Hz, 1H), 7.27 – 7.21 (m, 4H), 5.48 (d, J = 8.4 Hz, 1H), 4.70 (td, J = 8.8, 5.0 Hz, 1H), 4.22 – 4.18 (m, 1H), 4.14 – 4.05 (m, 2H), 3.60 (t, J = 1.3 Hz, 2H), 3.50 (dt, J = 10.2, 6.4 Hz, 1H), 3.16 (dd, J = 14.0, 5.0 Hz, 1H), 3.08 (dd, J = 14.0, 9.2 Hz, 1H), 2.70 (dt, J = 8.4 Hz, 1H), 1.75 (dq, J = 11.4, 6.9 Hz, 2H), 1.66 (d, J = 1.4 Hz, 9H), 1.64 – 1.61 (m, 2H), 1.59 – 1.56 (m, 1H), 1.52 (p, J = 7.0 Hz, 2H), 1.45 (s, 9H), 1.40 – 1.35 (m, 2H), 1.32 – 1.29 (m, 0H), 0.88 (s, 11H), 0.04 (s, 7H).

13C NMR (151 MHz, $CDCl_3$) δ 172.0, 170.5, 155.2, 149.7, 124.7, 124.4, 122.8, 119.2, 115.8, 115.3, 105.0, 83.8, 79.8, 65.3, 63.0, 59.1, 52.8, 47.0, 32.5, 32.4, 29.8, 29.0, 28.5, 28.5, 28.4, 26.1, 24.4, 22.3, 18.5, -5.1, -5.2.

HRMS (ESI-TOF) *m/z* Calcd for $C_{37}H_{60}N_3O_8Si$ [M+H]+ 702.4150; Found 702.4161



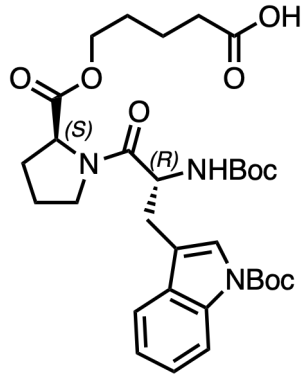
***tert*-butyl 3-((*R*)-2-((*tert*-butoxycarbonyl)amino)-3-((*S*)-2-(((5-hydroxypentyl)oxy)carbonyl)pyrrolidin-1-yl)-3-oxopropyl)-1*H*-indole-1-carboxylate (3.3d).** A RBF equipped with a Teflon-coated magnetic stir bar was charged with the TBS-protected intermediate **3.3c** and dissolved in dry 0.5mL of dry THF. The flask was sparged with $N_{2(g)}$ and cooled in an ice bath. To the stirring suspension, TBAF (1M in THF, 0.37 mL 0.37 mmol, 1.5 eq) was added dropwise and the mixture was left to warm to room temperature and stir overnight. Once complete, the solvent was removed via rotary evaporation, and the mixture was re-dissolved in roughly 10mL of diethyl ether. The organic layer was washed with water (2x 5mL), brine (1x5mL), dried over $MgSO_4$ and concentrated to give the crude alcohol product that was purified by flash silica gel chromatography in (60% EtOAc in Hexanes). **3.3d** alcohol compound was isolated as a pale-yellow oil (126.1 mg , 0.21 mmol, 74% yield over two steps).

TLC (40%EtOAc in Hexane): Rf=0.23

1H NMR (600 MHz, $CDCl_3$) δ 8.15 – 8.09 (m, 1H), 7.56 (d, J = 7.7 Hz, 1H), 7.45 (s, 1H), 7.31 – 7.27 (m, 1H), 7.25 – 7.20 (m, 1H), 5.74 (d, J = 8.7 Hz, 1H), 4.73 (td, J = 8.8, 5.4 Hz, 1H), 4.22 – 4.17 (m, 2H), 4.07 (dd, J = 10.8, 6.2 Hz, 1H), 3.64 (td, J = 6.0, 4.0 Hz, 2H), 3.57 – 3.51 (m, 1H), 3.09 (qd, J = 14.0, 7.4 Hz, 2H), 2.77 – 2.70 (m, 1H), 1.80 – 1.72 (m, 2H), 1.68 (d, J = 7.7 Hz, 2H), 1.65 (s, 9H), 1.63 (d, J = 1.8 Hz, 1H), 1.60 – 1.54 (m, 3H), 1.47 (d, J = 6.5 Hz, 1H), 1.44 (s, 9H), 0.88 – 0.83 (m, 1H).

13C NMR (151 MHz, $CDCl_3$) δ 172.0, 170.8, 155.3, 149.7, 135.5, 130.5, 124.7, 124.4, 122.7, 119.1, 115.7, 115.3, 83.8, 79.8, 65.0, 62.3, 59.4, 52.7, 47.1, 32.1, 29.7, 29.0, 28.5, 28.3, 28.2, 24.4, 22.0.

HRMS (ESI-TOF) *m/z* Calcd for $C_{31}H_{46}N_3O_8$ [M+H]+ 588.3285; Found 588.3270



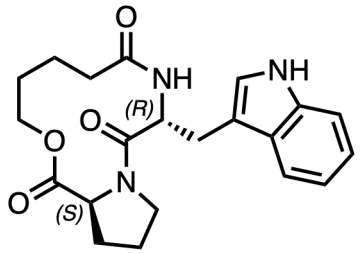
5-((*Nα*,1-bis(*tert*-butoxycarbonyl)-*D*-tryptophyl-*L*-prolyl)oxy)pentanoic acid (3.3e). A RBF equipped with a Teflon-coated magnetic stir bar was charged with 126.2 mg of alcohol intermediate **3.3d** (0.21 mmol, 1.0 eq) and 0.9 mL of wet DMF. 403 mg of PDC (1.1 mmol, 5.0 eq) was added to stirring suspension, and the reaction was left to stir overnight at 25°C. Upon completion, ~1g of celite, 10mL of NH_4Cl saturated solution and 10mL EtOAc were added, and stirring was continued for 30 min, after which the mixture was directly applied to a separatory funnel and the organic layers was extracted. The aqueous layers were washed (15mL x 5) with EtOAc, and organic layers were combined. The organic layer was washed (15mL x 5) with brine, dried over MgSO4, filtered, and concentrated under reduced pressure to afford the crude acid product. Purification was achieved by flash silica column chromatography (50% EtOAc in Hexanes, 1% acetic acid) yielding 36 mg (0.06 mmol, 28% yield) of pure **3.3e** acid product.

TLC (50%EtOAc in Hexane, 1% acetic acid): Rf=0.15

^{1}H NMR (600 MHz, $CDCl_3$) δ 8.12 (d, *J* = 8.3 Hz, 1H), 7.58 – 7.49 (m, 1H), 7.49 – 7.42 (m, 1H), 7.32 – 7.27 (m, 1H), 7.23 (dd, *J* = 7.3, 1.0 Hz, 1H), 5.63 (d, *J* = 8.5 Hz, 1H), 4.72 (td, *J* = 8.9, 5.4 Hz, 1H), 4.21 (dd, *J* = 8.6, 3.5 Hz, 1H), 4.12 (q, *J* = 4.5 Hz, 2H), 3.54 (ddd, *J* = 10.2, 7.5, 5.3 Hz, 1H), 3.14 (dd, *J* = 14.1, 5.3 Hz, 1H), 3.08 (dd, *J* = 13.9, 9.2 Hz, 1H), 2.73 (q, *J* = 8.1 Hz, 1H), 2.42 – 2.35 (m, 2H), 1.76 (ddd, *J* = 14.8, 10.9, 7.0 Hz, 2H), 1.70 (qd, *J* = 5.9, 3.0 Hz, 4H), 1.65 (d, *J* = 3.4 Hz, 9H), 1.44 (s, 9H), 1.34 (m, 2H).

^{13}C NMR (151 MHz, $CDCl_3$) δ 177.7, 171.8, 170.8, 155.3, 132.2, 128.7, 124.7, 124.4, 122.8, 119.1, 115.7, 115.3, 83.8, 79.9, 64.7, 59.2, 52.8, 46.8, 33.4, 29.7, 29.0, 28.5, 28.3, 28.0, 24.4, 21.4.

HRMS (ESI-TOF) m/z: [M+H]+ Calcd for $C_{31}H_{44}N_3O_9$ 602.3078; Found 602.3070



(9*R*,14a*S*)-9-((1*H*-indol-3-yl)methyl)decahydro-1*H*-pyrrolo[2,1-*c*][1]oxa[4,7]diazacyclododecine-1,7,10-trione (3.3).In a RBF equipped with a Teflon-coated magnetic stir bar, 32.9 mg (0.054 mmol, 1.0 eq) acid **3.3e** was dissolved in 0.1 mL of DCM. 0.1 mL of TFA was added dropwise to this stirring suspension and the reaction was left to stir at 25°C for 1h or until deprotection was determined complete by TLC. Once complete, the volatiles were removed under reduced pressure and the resulting crude unprotected intermediate was used directly in the subsequent step without further purification.

The crude product was dissolved in 1 mL DCM and sparged with nitrogen. A solution of HATU (57 mg, 0.15 mmol, 3.0 eq) in 2 mL of DMF was added to this stirring suspension, after which DIPEA (0.08 mL, 0.45 mmol, 9.0 eq) was added dropwise and the reaction was left to stir at 25°C overnight. Upon completion, the reaction was quenched with sat. $NaHCO_3$ and transferred to a separatory funnel. The organic layers were extracted, washed with brine (5x), dried over Na2SO4, filtered, and concentrated under reduced pressure to afford the crude macrocycle. Purification was achieved by semipreparative reverse-phase HPLC (flowrate of 10mL/min from 5%-95% (ACN in H_2O) over 20 min) to afford 7.6 mg (0.02 mmol, 40% yield) of pure macrocycle.

TLC (5%MeOH in DCM): Rf=0.10

HRMS (ESI-TOF) m/z: [M+H]+ Calcd for $C_{21}H_{26}N_3O_4$ 384.1923 ; Found: 384.1935

General Experimental Procedures:

General Procedure A (GPA): *Procedure for synthesis of analogues using manual solid-phase peptide (SPPS)*

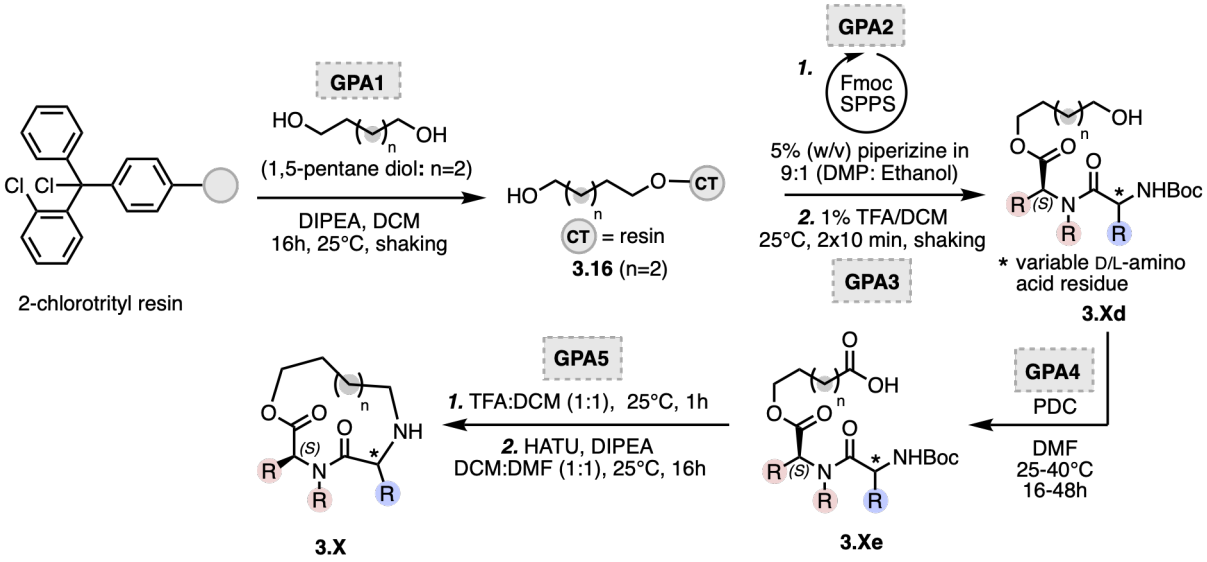


Figure 3.10 synthetic scheme for general procedure A (GPA) showing workflow for SPPS-enabled second-generation Synthesis of analogues.

GPA1 (resin loading): 2-chlorotritryl chloride (1.0 g, 200-400 mesh, 0.4 mmol/g) in a fritted peptide vessel was added DCM (10 mL), allowing the resin to swell at room temperature for 30 min. The solution as flushed and washed with DCM (10 mL × 3). Diol (3.2 mmol, 4.0 eq), DIPEA (0.7 mL, 4.0 mmol, 5.0 eq) and 8mL DCM were added. The fritted vessel was agitated uncapped for 20 s and later capped and agitated overnight. The solution as flushed and washed with DCM (10 mL × 4).

GPA2 (Fmoc SPPS): Separately in an RBF, N-alkylated amino acid (1.6 mmol, 4.0 eq), DIC (0.5 mL, 3.2 mmol, 8.0 eq) and DMAP (12 mg, 0.04 mmol, 0.1 eq) were suspended in 8mL DMF and left to pre-active at room temperature for 5 min. Following pre-activation, this mixture was added to the fritted vessel. The vessel was capped and left to shake for 3h-16h, after which the fritted vessel was flushed thoroughly with DMF (10 ml x 2) and DCM (10 mL × 3). The loading rate was determined with 2% DBU solution and spectrometric analysis (Sigma-Aldrich, Fmoc Loading Test) to afford Fmoc-L-(N-alkylated amino acid)-diol-TrtCl resin. The amino acid-bound resin in

the fritted vessel was charged with 5.0 mL of a deprotection cocktail (of 5% (w/v) piperazine in 9:1 (DMP:Ethanol)) and left to shake gently for 5 min. The resin was flushed thoroughly with DCM (10 mL × 3) and this process was repeated until a microcleavage shows complete Fmoc deprotection. For this microcleavage, ~1-2 mg of resin were placed into a vial containing a solution of TFA:DCM and stirred gently 5 min. The mixture was filtered through a cotton pad and concentrated for LCMS analysis. Separately in an RBF, Boc-amino acid (1.6 mmol, 4.0 eq), DIC (0.25 mL, 1.6 mmol, 4.0 eq) and OxymaPure (227 mg, 1.6 mmol, 4.0 eq) were suspended in 8mL DMF and left to pre-active at room temperature for 5 min. Following pre-activation, this mixture was added to the fritted vessel containing the free-N-terminus amino acid-bound resin. The vessel was capped and left to shake for 3h-16h, after which the fritted vessel was flushed thoroughly with DMF (10 ml x 2) and DCM (10 mL × 3). Once complete, the resin was washed thoroughly with DMF (10 ml x 2) and DCM (10 mL × 3).

GPA3 (Resin cleavage): A 20 mL of the resin cleavage cocktail was prepared (1% TFA in DCM) and 10mL were applied to the resin in the fritted vessel. The vessel was left to shake gently at room temperature for 10 min. The contents of the vessel were drained directly into a separatory funnel containing 20mL of saturated $NaHCO_3$ solution. The remaining 10mL of resin cleavage cocktail used in a second round of resin cleavage, after which the contents were flushed directly into the same separatory funnel. The organic layers were combined, dried over Na_2SO_4, filtered, and concentrated under reduced pressure to afford the crude tripartite product. Where necessary, purification was achieved by flash silica column chromatography (50%-60% EtOAc in Hexanes).

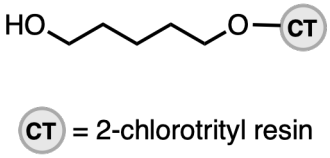
GPA4 (PDC oxidation): An RBF equipped with a Teflon-coated magnetic stir bar was charged with the tripartite pure product (1.0 eq) and wet DMF (0.1M). PDC (5.0 eq) was added to stirring suspension, and the reaction was left to stir between 25°C-40°C for 16-48h, and monitored by TLC. Upon completion, ~1g of celite, 10mL of NH_4Cl saturated solution and 10mL EtOAc were added, and stirring was continued for 30 min, after which the mixture was directly applied to a separatory funnel and the organic layers was extracted. The aqueous layers were washed (15mL x 5) with EtOAc, and organic layers were combined. The organic layer was washed (15mL x 5) with brine, dried over MgSO4, filtered, and concentrated under reduced pressure to afford the crude

acid product. Purification was achieved by flash silica column chromatography (3:7 EtOAc:Hexanes, 1% acetic acid) yielding the pure acid product as a pale yellow oil.

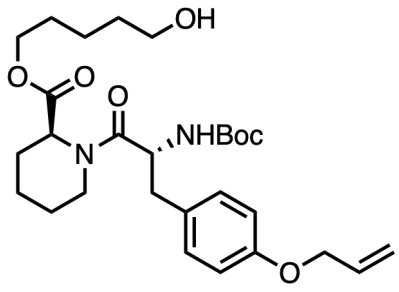
GPA5 (Macrolactamization):

In a RBF equipped with a Teflon-coated magnetic stir bar, the pure acid was dissolved in DCM (0.5M). TFA (0.5M) was added dropwise to this stirring suspension and the reaction was left to stir at 25°C for 1h or until deprotection was determined complete by TLC. Once complete, the volatiles were removed under reduced pressure and the resulting crude unprotected intermediate was used directly in the subsequent step without further purification.

The crude product was dissolved in DCM (0.05M) and sparged with nitrogen. A solution of HATU (3.0 eq) in DMF (0.05M) was added to this stirring suspension, after which DIPEA (9.0 eq) was added dropwise and the reaction was left to stir at 25°C overnight. Upon completion, the reaction was quenched with sat. $NaHCO_3$ and transferred to a separatory funnel. The organic layers were extracted, washed with brine (5x), dried over Na2SO4, filtered, and concentrated under reduced pressure to afford the crude macrocycle. Purification was achieved by semipreparative reverse-phase HPLC (flowrate of 10mL/min from 5%-95% (ACN in H_2O) over 20 min) to afford the pure macrocycle analogues.



5-hydroxypentyl-O-Trt resin (3.16). Prepared according to GPA1 using 1,5-pentane diol (335 mg , 3.2 mmol, 4.0 eq) to afford the resin-bound diol which was used in the subsequent step without the need for further purification.



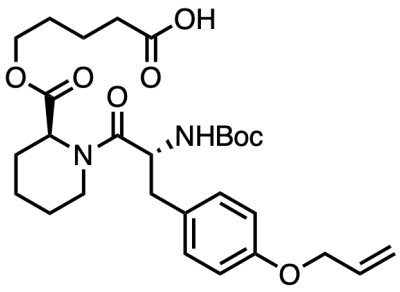
5-hydroxypentyl (S)-1-((R)-3-(4-(allyloxy)phenyl)-2-((tert-butoxycarbonyl)amino)propanoyl)piperidine-2-carboxylate (3.5d). Prepared according to GPA2 using 5-hydroxypentyl-O-Trt resin and Fmoc-Pip-OH (562 mg, 1.6 mmol, 4 eq) for the installation of the N-alkylated amino acid, with a loading rate of 0.40 mmol/g. Boc-D-Tyr(OAll)-OH (0.514 g, 1.6 mmol, 4.0eq) was installed subsequently. Following resin cleavage and purification (50% EtOAc/Hexanes), 125.7 mg (0.242 mmol, 61% yield) of pure product was obtained as a clear oil.

TLC (50%EtOAc in Hexanes): Rf=0.33

^{1}H NMR (600 MHz, $CDCl_3$) δ 7.08 (d, *J* = 8.6 Hz, 2H), 6.81 (d, 2H), 6.01 (ddt, *J* = 17.4, 10.5, 5.3 Hz, 1H), 5.53 (d, *J* = 8.7 Hz, 1H), 5.37 (dd, *J* = 17.3, 1.7 Hz, 1H), 5.29 – 5.19 (m, 2H), 4.86 (q, *J* = 7.5 Hz, 1H), 4.56 – 4.45 (m, 2H), 4.18 – 4.06 (m, 2H), 3.65 – 3.55 (m, 3H), 3.10 (td, *J* = 13.3, 3.0 Hz, 1H), 2.93 – 2.68 (m, 2H), 2.21 – 2.16 (m, 1H), 1.66 – 1.58 (m, 2H), 1.58 – 1.47 (m, 3H), 1.47 – 1.31 (m, 13H), 1.27 – 1.17 (m, 1H), 0.71 (qt, *J* = 13.1, 4.3 Hz, 1H).

^{13}C NMR (101 MHz, $CDCl_3$) δ 171.8, 170.9, 157.6, 155.2, 133.4, 130.6, 128.7, 117.6, 114.9, 79.7, 68.9, 65.2, 62.4, 52.6, 51.3, 43.9, 39.7, 32.2, 28.5, 28.3, 26.4, 24.6, 22.3, 20.7.

HRMS (ESI-TOF) m/z: [M+H]+ Calcd for $C_{28}H_{43}N_2O_7$ 519.3070; Found 519.3068



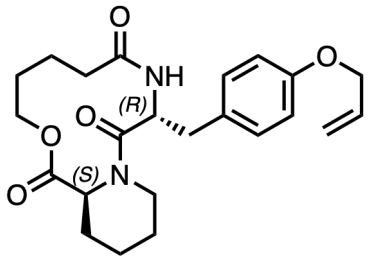
5-(((S)-1-((R)-3-(4-(allyloxy)phenyl)-2-((tert-butoxycarbonyl)amino)propanoyl)piperidine-2-carbonyl)oxy)pentanoic acid (3.5e). Prepared according to GPA4 using 86,6 mg (0.084 mmol, 1.0 eq) of primary alcohol. Following purification (50% EtOAc/Hexane + 1% AcOH) 23.6 mg (0.044 mmol, 53% yield) was obtained as clear colorless oil.

TLC (50%EtOAc in Hexanes + 1% AcOH): Rf=0.26

^{1}H NMR (600 MHz, $CDCl_3$) δ 7.10 (d, *J* = 8.4 Hz, 2H), 6.83 (d, *J* = 8.5 Hz, 2H), 6.02 (ddt, *J* = 17.2, 10.5, 5.2 Hz, 1H), 5.52 (d, *J* = 8.4 Hz, 1H), 5.38 (dd, *J* = 17.3, 1.5 Hz, 1H), 5.28 – 5.22 (m, 2H), 4.94 – 4.85 (m, 1H), 4.51 (d, *J* = 5.2 Hz, 2H), 4.14 – 4.09 (m, 2H), 3.64 (d, *J* = 13.1 Hz, 1H), 3.15 (td, *J* = 13.2, 2.6 Hz, 1H), 2.92 (d, *J* = 6.9 Hz, 2H), 2.38 – 2.35 (m, 2H), 2.20 (d, *J* = 13.6 Hz, 1H), 1.71 – 1.67 (m, 4H), 1.57 (d, *J* = 13.3 Hz, 1H), 1.41 (s, 11H), 1.33 – 1.28 (m, 1H), 1.25 (d, *J* = 4.8 Hz, 1H), 0.78 – 0.69 (m, 1H).

^{13}C NMR (101 MHz, $CDCl_3$) δ 177.0, 171.9, 170.9, 157.7, 155.3, 133.4, 130.7, 128.7, 117.7, 114.9, 79.9, 77.4, 77.2, 76.9, 69.0, 64.9, 52.6, 51.4, 44.0, 39.7, 33.4, 28.5, 27.9, 26.6, 24.6, 21.5, 20.8.

HRMS (ESI-TOF) m/z: [M+H]+ Calcd for $C_{28}H_{41}N_2O_8$ 533.2863; Found 533.2858



(9R,15aS)-9-(4-(allyloxy)benzyl)decahydropyrido[2,1-c][1]oxa[4,7]diazacyclododecine-1,7,10(12H)-trione (3.5f). Prepared according to GPA5 using 14.2 mg (0.027 mmol, 1.0 eq) of starting acid. Following purification (60% EtOAc/Hexanes) 5.6 mg (0.014 mmols, 50% yield) of pure macrocycle was obtained as clear colorless oil.

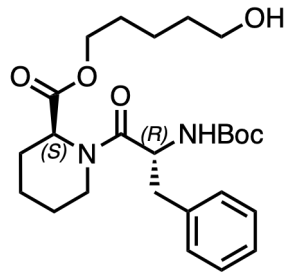
TLC (60% EtOAc in Hexanes): R_f=0.23

^{1}H NMR (600 MHz, $CDCl_3$) δ 7.14 (d, *J* = 7.9 Hz, 2H), 6.84 (d, *J* = 7.8 Hz, 2H), 6.04 (dt, *J* = 10.8, 5.3 Hz, 1H), 5.98 (s, 1H), 5.40 (d, *J* = 17.2 Hz, 1H), 5.34 (s, 2H), 5.27 (d, *J* = 10.5 Hz, 1H), 4.51 (d, *J* = 4.5 Hz, 2H), 4.12 (d, *J* = 7.8 Hz, 1H), 3.84 (s, 1H), 3.70 (d, *J* = 12.7 Hz, 1H), 3.14 – 3.07 (m, 1H), 2.93 – 2.87 (m, 2H), 2.32 – 2.26 (m, 2H), 2.11 – 2.08 (m, 1H), 1.96 – 1.92 (m, 1H),

1.79 – 1.77 (m, 2H), 1.58 – 1.54 (m, 3H), 1.42 – 1.40 (m, 1H), 1.30 – 1.29 (m, 1H), 0.95 – 0.92 (m, 1H).

^{13}C NMR (101 MHz, $CDCl_3$) δ 173.9, 173.8, 170.9, 157.6, 133.4, 130.2, 129.1, 117.8, 115.0, 77.4, 77.2, 76.9, 69.0, 65.8, 52.9, 49.6, 44.9, 37.3, 36.9, 25.6, 25.3, 25.0, 22.8, 20.7.

HRMS (ESI-TOF) m/z: [M+H]+ Calcd for $C_{23}H_{31}N_2O_5$ 415.2233; Found 415.2238



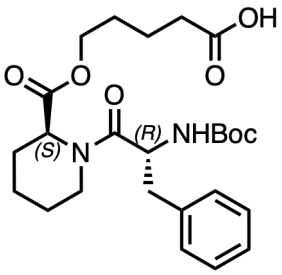
5-hydroxypentyl (S)-1-((tert-butoxycarbonyl)-D-phenylalanyl)piperidine-2-carboxylate (3.6d). Prepared according to GPA2 using 5-hydroxypentyl-O-Trt resin **3.16** and Fmoc-Pip-OH (281 mg, 0.8 mmol, 2 eq) for the installation of the N-alkylated amino acid, with a loading rate of 0.44 mmol/g. Boc-D-Phe-OH (0.424 g, 1.6 mmol, 4.0eq) was installed subsequently. Following resin cleavage and purification (40% EtOAc/Hexane), 103.3 mg (0.22 mmol, 50% yield) of pure product was obtained as a clear oil.

TLC (50%EtOAc in Hexanes): Rf=0.25

^{1}H NMR (400 MHz, $CDCl_3$) δ 7.28 – 7.15 (m, 5H), 5.56 (d, *J* = 8.7 Hz, 1H), 5.22 – 5.18 (m, 1H), 4.90 (q, *J* = 7.7 Hz, 1H), 4.10 (t, *J* = 6.3 Hz, 2H), 3.65 – 3.55 (m, 3H), 3.08 (td, *J* = 13.2, 3.0 Hz, 1H), 2.97 – 2.90 (m, 2H), 2.20 – 2.13 (m, 1H), 1.66 – 1.58 (m, 2H), 1.58 – 1.48 (m, 3H), 1.39 (s, 12H), 1.26 – 1.14 (m, 1H), 0.61 (qt, *J* = 13.1, 4.3 Hz, 1H).

^{13}C NMR (101 MHz, $CDCl_3$) δ 171.7, 170.9, 155.1, 136.5, 129.7, 128.5, 126.9, 79.7, 65.1, 62.3, 52.5, 51.2, 43.9, 40.6, 32.1, 28.4, 28.2, 26.3, 24.4, 22.2, 20.6.

HRMS (ESI-TOF) *m/z* Calcd for $C_{25}H_{38}N_2O_6Na$ [M+Na]+ 485.2628 ; Found: 485.2639



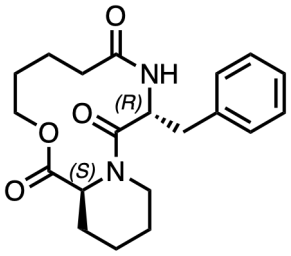
5-(((S)-1-((tert-butoxycarbonyl)-D-phenylalanyl)piperidine-2-carbonyl)oxy)pentanoic acid (3.6e). Prepared according to GPA4 using 87.5 mg (0.189 mmol, 1.0 eq) of primary alcohol **3.6d**. Following purification (40% EtOAc/Hexane + 1% AcOH) 35.5 mg (0.075, 42% yield) was obtained as clear colorless oil.

TLC (40%EtOAc in Hexanes + 1% AcOH): Rf=0.44

^{1}H NMR (400 MHz, $CDCl_3$) δ 7.29 – 7.14 (m, 5H), 5.55 (d, *J* = 8.6 Hz, 1H), 5.23 (d, *J* = 5.9 Hz, 1H), 4.93 (q, *J* = 7.9 Hz, 1H), 4.11 (q, *J* = 6.6 Hz, 2H), 3.62 (d, *J* = 13.7 Hz, 1H), 3.14 (td, *J* = 13.3, 3.0 Hz, 1H), 3.07 – 2.90 (m, 2H), 2.36 (d, *J* = 9.5 Hz, 2H), 2.18 (d, *J* = 13.7 Hz, 1H), 1.69 (q, *J* = 3.8 Hz, 3H), 1.57 – 1.51 (m, 1H), 1.41 (d, *J* = 5.8 Hz, 9H), 1.27 – 1.16 (m, 3H), 0.90 – 0.81 (m, 1H), 0.69 – 0.58 (m, 1H).

^{13}C NMR (101 MHz, $CDCl_3$) δ177.4, 171.8, 170.9, 155.3, 136.5, 129.7, 128.6, 127.0, 79.9, 77.4, 77.2, 76.9, 64.9, 52.6, 51.3, 44.0, 40.6, 33.5, 28.5, 27.9, 26.5, 24.5, 21.5, 20.7.

HRMS (ESI-TOF) *m/z* Calcd for $C_{25}H_{37}N_2O_7$ [M+H]+ 477.2601 ; Found: 477.2602

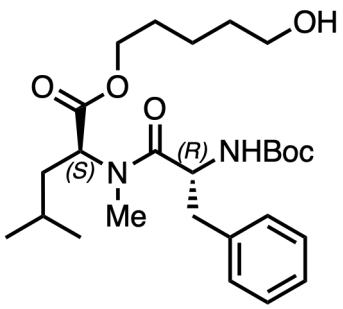


(9R,15aS)-9-benzyldecahydropyrido[2,1-c][1]oxa[4,7]diazacyclododecine-1,7,10(12H)-trione (3.6). Prepared according to GPA5 using 35.5 mg (0.075 mmol, 1.0 eq) of starting acid, **3.6e**. Following purification by HPLC, 10.5 mg, (0.029 mmol, 37% yield) of pure macrocycle was obtained as a pale yellow oil.

^{1}H NMR (400 MHz, $CDCl_3$) δ 7.29 (t, *J* = 7.1 Hz, 2H), 7.23 (d, *J* = 7.2 Hz, 3H), 6.52 (d, *J* = 9.9 Hz, 1H), 5.43 (q, *J* = 9.7 Hz, 1H), 5.33 (d, *J* = 5.0 Hz, 1H), 4.13 (d, *J* = 11.1 Hz, 1H), 3.84 (t, *J* = 10.8 Hz, 1H), 3.73 (d, *J* = 12.8 Hz, 1H), 3.18 – 3.07 (m, 1H), 2.99 (dd, *J* = 13.2, 5.5 Hz, 1H), 2.92 (t, *J* = 13.1 Hz, 1H), 2.31 (d, *J* = 13.8 Hz, 2H), 2.11 (t, *J* = 12.8 Hz, 1H), 1.96 (d, *J* = 6.4 Hz, 1H), 1.79 (s, 1H), 1.57 (t, *J* = 12.2 Hz, 2H), 1.49 (t, *J* = 12.4 Hz, 1H), 1.40 (t, *J* = 13.6 Hz, 1H), 1.24 – 1.16 (m, 1H), 0.89 (dd, *J* = 17.2, 10.3 Hz, 1H).

^{13}C NMR (101 MHz, $CDCl_3$) δ 174.7, 173.9, 170.5, 136.5, 129.4, 129.1, 128.8, 127.1, 77.4, 77.2, 76.9, 66.0, 53.2, 49.6, 45.2, 37.5, 37.1, 25.5, 25.2, 24.9, 23.3, 20.6.

HRMS (ESI-TOF) *m/z* Calcd for $C_{20}H_{26}N_2O_4$ [M+H]+ 359.1917 ; Found: 359.1955



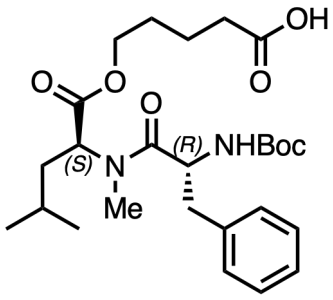
5-hydroxypentyl N-((tert-butoxycarbonyl)-D-phenylalanyl)-N-methyl-L-leucinate (3.7d). Prepared according to GPA2 using 5-hydroxypentyl-O-Trt resin and Fmoc-N-Me-Leu-OH (588 mg, 1.6 mmol, 4 eq) for the installation of the N-alkylated amino acid, with a loading rate of 0.39 mmol/g. Boc-D-Phe-OH (0.425 g, 1.6 mmol, 4.0eq) was installed subsequently. Following resin cleavage and purification (3% MeOH/DCM), 153.7 mg (0.343 mmol, 80% yield) of pure product was obtained as a clear oil.

TLC (3%MeOH in DCM): Rf=0.27

^{1}H NMR (400 MHz, $CDCl_3$) δ 7.25 – 7.17 (m, 5H), 5.53 (d, *J* = 9.1 Hz, 1H), 5.15 (dd, *J* = 10.8, 5.0 Hz, 1H), 4.91 (td, *J* = 8.4, 6.1 Hz, 1H), 4.06 (ddt, *J* = 17.2, 10.9, 5.4 Hz, 2H), 3.62 – 3.57 (m, 3H), 3.00 – 2.89 (m, 2H), 2.73 (s, 3H), 1.63 – 1.58 (m, 3H), 1.53 (dtd, *J* = 11.7, 6.2, 2.6 Hz, 2H), 1.50 – 1.43 (m, 1H), 1.39 (s, 11H), 1.10 – 1.03 (m, 1H), 0.82 (dd, *J* = 11.6, 6.6 Hz, 6H).

^{13}C NMR (101 MHz, $CDCl_3$) δ 172.9, 171.6, 155.2, 136.4, 129.5, 129.4, 128.5, 126.9, 79.8, 65.0, 62.3, 54.7, 51.8, 40.0, 37.1, 32.1, 31.2, 28.4, 28.3, 28.2, 24.6, 23.2, 22.2, 21.5.

HRMS (ESI-TOF) *m/z* Calcd for $C_{26}H_{43}N_2O_6$ [M+H]+ 479.3121; Found: 479.3117



(6R,9S)-6-benzyl-9-isobutyl-2,2,8-trimethyl-4,7,10-trioxo-3,11-dioxa-5,8-diazahexadecan-16-oic acid (3.7e). Prepared according to GPA4 using 153.7 mg (0.321 mmol, 1.0 eq) of primary

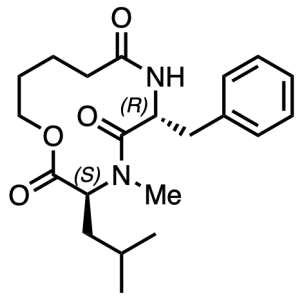
alcohol. Following purification (30% EtOAc/Hexane + 1% AcOH) 28.3 mg (0.057, 42% yield) was obtained as clear colorless oil.

TLC (30%EtOAc in Hexanes + 1% AcOH): Rf=0.29

^{1}H NMR (400 MHz, $CDCl_3$) δ 7.26 – 7.19 (m, 5H), 5.49 (d, *J* = 9.0 Hz, 1H), 5.16 (td, *J* = 10.8, 5.0 Hz, 1H), 4.93 (q, *J* = 7.4 Hz, 1H), 4.12 – 4.03 (m, 3H), 2.97 (tt, *J* = 14.0, 7.7 Hz, 2H), 2.75 (d, *J* = 13.6 Hz, 3H), 2.37 (d, *J* = 5.7 Hz, 2H), 1.71 – 1.46 (m, 6H), 1.40 (s, 9H), 1.09 (td, *J* = 11.4, 6.0 Hz, 1H), 0.89 – 0.81 (m, 6H).

^{13}C NMR (101 MHz, $CDCl_3$) δ 177.0, 173.1, 171.6, 155.4, 136.4, 129.6, 128.6, 127.0, 80.0, 64.9, 54.8, 51.9, 40.1, 37.3, 33.5, 31.3, 28.5, 27.9, 24.7, 23.3, 21.6, 21.5.

HRMS (ESI-TOF) m/z: [M+H]+ Calcd for $C_{26}H_{41}N_2O_7$ 493.2914; Found: 493.2924



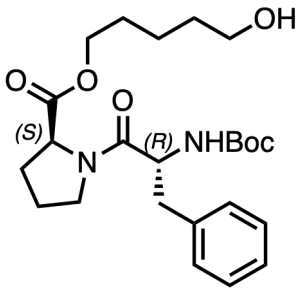
(3S,6R)-6-benzyl-3-isobutyl-4-methyl-1-oxa-4,7-diazacyclododecane-2,5,8-trione (3.7). Prepared according to GPA5 using 23.2 mg (0.047 mmol, 1.0 eq) of starting acid. Following purification (5% MeOH/DCM) 6.9 mg (0.018, 39% yield) of pure macrocycle was obtained as clear colorless oil.

TLC (8% Methanol in DCM): R_f=0.41

^{1}H NMR (400 MHz, $CDCl_3$) δ 7.26 – 7.20 (m, 5H), 6.39 (d, *J* = 10.1 Hz, 1H), 5.36 (qd, *J* = 11.5, 4.9 Hz, 2H), 4.24 (d, *J* = 10.9 Hz, 1H), 3.72 (t, *J* = 11.2 Hz, 1H), 3.18 (t, *J* = 11.9 Hz, 1H), 2.96 (dd, *J* = 12.8, 5.1 Hz, 1H), 2.70 (s, 3H), 2.35 (dd, *J* = 12.4, 4.9 Hz, 1H), 2.10 (t, *J* = 13.0 Hz, 1H), 1.99 – 1.91 (m, 1H), 1.78 (s, 1H), 1.74 – 1.62 (m, 2H), 1.60 – 1.47 (m, 2H), 1.05 – 1.00 (m, 1H), 0.81 (dd, *J* = 12.1, 6.6 Hz, 6H).

^{13}C NMR (101 MHz, $CDCl_3$) δ 174.7, 174.4, 170.6, 136.4, 129.1, 128.6, 127.0, 65.0, 55.0, 50.7, 37.4, 36.9, 35.1, 30.7, 25.7, 24.5, 23.2, 23.1, 21.0.

HRMS (ESI-TOF) *m/z* Calcd for $C_{21}H_{31}N_2O_4$ [M+H]+ 375.2284 ; Found: 375.2280



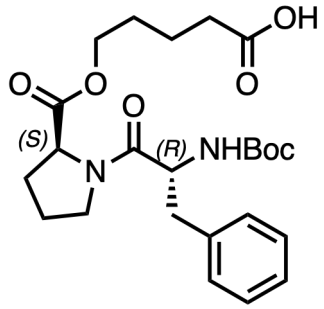
5-hydroxypentyl (tert-butoxycarbonyl)-D-phenylalanyl-L-prolinate (3.9d). Prepared according to GPA2 using 5-hydroxypentyl-O-Trt resin, **3.16** and Fmoc-Pro-OH (540 mg, 3.2 mmol, 8.0 eq) for the installation of the N-alkylated amino acid, with a loading rate of 0.40 mmol/g. Boc-D-Phe-OH (0.850 g, 3.2 mmol, 8.0 eq) was installed subsequently. Following resin cleavage and purification (5% MeOH/DCM), 117 mg (0.34 mmol, 85% yield) of pure product **3.9d** was obtained as a clear oil.

TLC (5%MeOH in DCM): Rf=0.38

^{1}H NMR (400 MHz, $CDCl_3$) δ 7.24 – 7.22 (m, 3H), 7.20 – 7.17 (m, 3H), 5.62 (d, *J* = 8.9 Hz, 1H), 4.62 (td, *J* = 9.2, 5.6 Hz, 1H), 4.23 (dd, *J* = 8.4, 4.0 Hz, 1H), 4.19 – 4.13 (m, 1H), 4.07 (dt, *J* = 10.9, 6.2 Hz, 1H), 3.61 (td, *J* = 6.1, 2.8 Hz, 2H), 3.54 (ddd, *J* = 10.0, 7.1, 5.1 Hz, 1H), 3.00 (dd, *J* = 12.9, 5.6 Hz, 1H), 2.89 (dd, *J* = 12.9, 9.5 Hz, 1H), 2.64 (dt, *J* = 9.8, 7.0 Hz, 1H), 1.92 – 1.79 (m, 3H), 1.64 – 1.60 (m, 2H), 1.55 (t, *J* = 6.9 Hz, 2H), 1.51 – 1.46 (m, 1H), 1.40 (s, 11H)

^{13}C NMR (101 MHz, $CDCl_3$) δ 171.9, 170.5, 157.3, 155.1, 136.5, 129.5, 128.5, 127.0, 79.7, 65.0, 62.1, 59.1, 53.6, 46.9, 42.1, 40.3, 32.1, 29.1, 28.4, 28.2, 24.5, 23.5, 22.0.

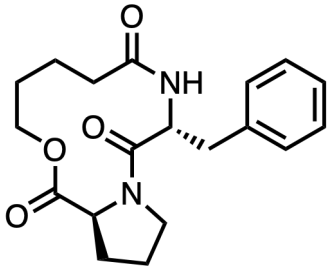
HRMS (ESI-TOF) *m/z* Calcd for $C_{24}H_{37}N_2O_6$ [M+H]+ 449.2660 ; Found: 449.2652



5-(((tert-butoxycarbonyl)-D-phenylalanyl-L-prolyl)oxy)pentanoic acid (3.9e). Prepared according to GPA4 using 52 mg (0.116 mmol, 1.0 eq) of primary alcohol. The product was

sufficiently pure to proceed without further purification, obtained 21.4 mg (0.046, 39% yield) as a clear colorless oil.

TLC (3%MeOH in DCM): Rf=0.21



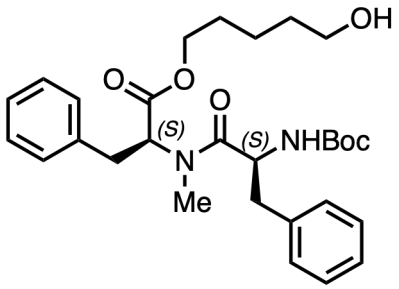
(9R,14aS)-9-benzyldecahydro-1H-pyrrolo[2,1-c][1]oxa[4,7]diazacyclododecine-1,7,10-trione (3.9). Prepared according to GPA5 using 21.3 mg (0.046 mmol, 1.0 eq) of starting acid. Following purification (5% MeOH/DCM) 13.1 mg (0.038, 83% yield) of pure macrocycle was obtained as clear colorless oil.

TLC (5%MeOH in DCM): Rf=0.36

^{1}H NMR (400 MHz, $CDCl_3$) δ 7.28 (t, *J* = 7.5 Hz, 2H), 7.23 (d, *J* = 7.3 Hz, 3H), 6.13 (d, *J* = 10.2 Hz, 1H), 5.04 (td, *J* = 10.2, 5.9 Hz, 1H), 4.47 (dd, *J* = 8.5, 4.3 Hz, 1H), 4.13 (t, *J* = 9.9 Hz, 1H), 4.07 – 4.00 (m, 1H), 3.80 (ddd, *J* = 11.0, 4.5, 2.8 Hz, 1H), 3.12 (dd, *J* = 13.1, 10.4 Hz, 1H), 2.94 (dt, *J* = 13.0, 7.2 Hz, 2H), 2.28 – 2.23 (m, 1H), 2.10 – 2.03 (m, 2H), 1.95 (tq, *J* = 12.2, 6.1 Hz, 2H), 1.90 – 1.76 (m, 3H), 1.70 (qt, *J* = 11.4, 5.1 Hz, 1H), 1.53 (t, *J* = 13.4 Hz, 1H).

^{13}C NMR (101 MHz, $CDCl_3$) δ 174.7, 171.9, 171.7, 136.7, 129.6, 129.2, 128.7, 127.1, 77.4, 77.2, 76.9, 66.2, 59.7, 52.6, 47.2, 37.6, 37.2, 29.3, 29.1, 26.0, 24.6, 23.8.

HRMS (ESI-TOF) *m/z* Calcd for $C_{19}H_{25}N_2O_4$ [M+H]+ 345.1814 ; Found: 345.1805



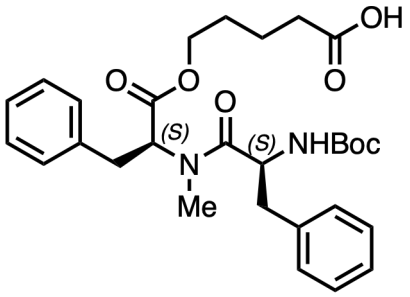
5-hydroxypentyl *N*-((*tert*-butoxycarbonyl)-*L*-phenylalanyl)-*N*-methyl-*L*-phenylalaninate (3.10d). Prepared according to GPA2 using 5-hydroxypentyl-O-Trt resin and Fmoc-N-Me-Phe-OH (0.641 g, 1.6 mmol, 4.0 eq) for the installation of the N-alkylated amino acid, with a loading rate of 0.39mmol/g. Boc-Phe-OH (0.424 g, 1.6 mmol, 4.0eq) was installed subsequently. Following resin cleavage and purification (100% Hexanes – 5% EtOAc/Hexanes), 95.6 mg (0.186 mmol 45%yield) of pure product was obtained as a clear oil.

TLC (10%EtOAc in Hexanes): Rf=0.20

^{1}H NMR (400 MHz, $CDCl_3$) δ 7.25 – 7.15 (m, 8H), 7.06 – 7.03 (m, 2H), 5.28 (dd, *J* = 9.7, 6.2 Hz, 1H), 4.89 (dd, *J* = 9.8, 5.6 Hz, 1H), 4.79 – 4.70 (m, 1H), 4.21 (dt, *J* = 10.8, 6.5 Hz, 1H), 4.10 – 4.04 (m, 1H), 3.64 – 3.58 (m, 2H), 3.32 (dt, *J* = 14.2, 5.7 Hz, 1H), 3.03 – 2.92 (m, 2H), 2.85 – 2.81 (m, 1H), 2.78 (s, 3H), 1.62 (ddd, *J* = 8.6, 6.3, 4.0 Hz, 2H), 1.58 – 1.52 (m, 2H), 1.44 – 1.39 (m, 2H), 1.37 (s, 9H).

^{13}C NMR (101 MHz, $CDCl_3$) δ 172.2, 170.4, 155.1, 137.2, 136.6, 129.7, 129.0, 128.6, 128.5, 126.9, 126.8, 79.7, 65.3, 62.3, 60.5, 51.6, 39.2, 34.8, 34.1, 32.1, 28.4, 28.2, 22.1.

HRMS (ESI-TOF) m/z: [M+H]+ Calcd for $C_{29}H_{41}N_2O_6$ 513.2965; Found: 513.2966



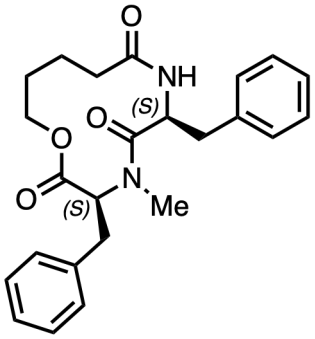
(6*S*,9*S*)-6,9-dibenzyl-2,2,8-trimethyl-4,7,10-trioxo-3,11-dioxa-5,8-diazahexadecan-16-oic acid (3.10e). Prepared according to GPA4 using 95.5mg (0.186 mmol, 1.0 eq) of primary alcohol **3.10d**. Following purification (30% EtOAc in Hexanes) 83.5 mg (0.158, 85% yield) of **3.10e** was obtained as clear colorless oil.

TLC (50%EtOAc in Hexanes): Rf=0.47

1H NMR (600 MHz, $CDCl_3$) δ 7.26 – 7.15 (m, 8H), 7.11 – 6.91 (m, 2H), 5.13 (d, J = 9.1 Hz, 1H), 5.05 (dd, J = 9.9, 6.0 Hz, 1H), 4.74 (q, J = 7.5 Hz, 1H), 4.22 – 4.13 (m, 1H), 4.09 (dd, J = 10.9, 5.4 Hz, 1H), 3.36 – 3.31 (m, 1H), 3.01 – 2.96 (m, 2H), 2.85 – 2.81 (m, 1H), 2.80 (s, 3H), 2.36 (q, J = 6.2 Hz, 2H), 1.71 (t, J = 5.9 Hz, 4H), 1.38 – 1.29 (m, 9H).

13C NMR (151 MHz, $CDCl_3$) δ 172.3, 137.0, 136.5, 129.7, 129.0, 128.7, 128.5, 126.9, 126.9, 79.8, 64.9, 59.8, 51.8, 39.3, 34.9, 33.6, 33.2, 28.4, 27.9, 21.4.

HRMS (ESI-TOF) m/z: [M+H]+ Calcd for $C_{29}H_{39}N_2O_7$ 527.2757 ; Found: 527.2763

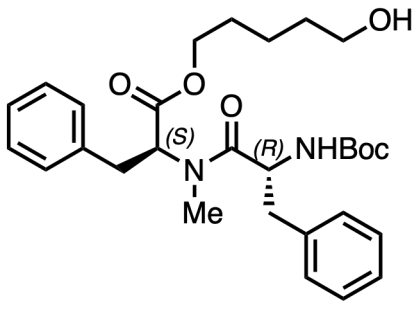


(3*S*,6*S*)-3,6-dibenzyl-4-methyl-1-oxa-4,7-diazacyclododecane-2,5,8-trione. (3.10) Prepared according to GPA5 using 61.6 mg (0.116 mmol, 1.0 eq) of starting acid. Following purification by HPLC, 24.4 mg, 0.059 mmol, 51% yield) of pure macrocycle was obtained as a pale yellow oil. Major rotamer was characterized only.

1H NMR (600 MHz, CDCl3) δ 7.38 – 7.35 (m, 1H), 7.24 – 7.22 (m, 1H), 7.21 – 7.12 (m, 6H), 6.96 – 6.92 (m, 2H), 6.23 (d, J = 10.4 Hz, 1H), 5.28 (dd, J = 11.2, 4.0 Hz, 1H), 4.97 (q, J = 8.1 Hz, 1H), 4.23 (tt, J = 10.8, 2.2 Hz, 1H), 3.97 (dd, J = 10.6, 4.9 Hz, 1H), 3.32 (dd, J = 14.8, 4.0 Hz, 1H), 2.93 (dd, J = 14.7, 11.2 Hz, 1H), 2.85 (s, 3H), 2.81 – 2.78 (m, 2H), 2.30 (dq, J = 15.4, 4.9 Hz, 1H), 1.92 (dq, J = 15.4, 7.5 Hz, 2H), 1.84 – 1.80 (m, 2H), 1.63 – 1.58 (m, 1H).

13C NMR (151 MHz, $CDCl_3$) δ 172.7, 172.3, 170.2, 136.7, 136.7, 129.5, 129.1, 129.1, 129.1, 129.0, 128.7, 128.7, 128.5, 127.2, 126.6, 66.8, 61.6, 49.0, 38.7, 37.9, 34.2, 29.8, 28.1, 23.6.

HRMS (ESI-TOF) *m/z* Calcd for $C_{24}H_{29}N_2O_4$ [M+H]+ 409.2127 ; Found: 409.2129



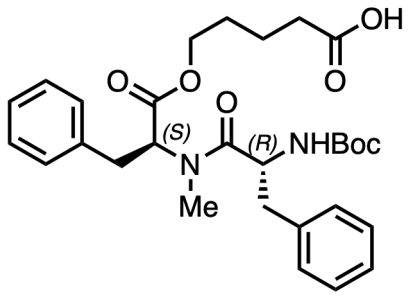
5-hydroxypentyl *N*-((*tert*-butoxycarbonyl)-*D*-phenylalanyl)-*N*-methyl-*L*-phenylalaninate (3.11d). Prepared according to GPA2 using 5-hydroxypentyl-O-Trt resin and Fmoc-N-Me-Phe-OH (0.641 g, 1.6 mmol, 4.0 eq) for the installation of the N-alkylated amino acid, with a loading rate of 0.45mmol/g. Boc-D-Phe-OH (0.424 g, 1.6 mmol, 4.0eq) was installed subsequently. Following resin cleavage and purification (100% Hexanes – 5% EtOAc/Hexanes), 213.3 mg (0.416, 92 %yield) of pure **3.11d** was obtained as a clear oil.

TLC (50%EtOAc in Hexanes): Rf=0.39

^{1}H NMR (400 MHz, $CDCl_3$) δ 7.29 (dd, *J* = 8.4, 6.2 Hz, 2H), 7.24 – 7.13 (m, 6H), 6.96 (dd, *J* = 7.0, 2.4 Hz, 2H), 5.34 (dd, *J* = 10.5, 5.8 Hz, 1H), 5.29 (d, *J* = 6.3 Hz, 1H), 4.75 (q, *J* = 7.4 Hz, 1H), 4.19 (dt, *J* = 10.7, 6.3 Hz, 1H), 4.11 (dt, *J* = 10.7, 6.2 Hz, 1H), 3.65 – 3.57 (m, 2H), 3.34 (dd, *J* = 14.5, 5.8 Hz, 1H), 2.95 – 2.88 (m, 1H), 2.80 (s, 3H), 2.59 (dd, *J* = 14.0, 6.2 Hz, 1H), 2.51 (dd, *J* = 13.9, 7.5 Hz, 1H), 1.68 – 1.60 (m, 2H), 1.59 – 1.50 (m, 2H), 1.46 – 1.39 (m, 2H), 1.37 (s, 9H).

^{13}C NMR (101 MHz, $CDCl_3$) δ 172.9, 170.6, 137.0, 136.4, 129.4, 129.0, 128.8, 128.5, 127.1, 126.9, 79.8, 65.4, 58.6, 51.7, 39.1, 34.8, 32.5, 32.2, 28.4, 28.2, 22.3.

HRMS (ESI-TOF) m/z: [M+H]+ Calcd for $C_{29}H_{41}N_2O_6$ 513.2965 ; Found: 513.2989



(6*R*,9*S*)-6,9-dibenzyl-2,2,8-trimethyl-4,7,10-trioxo-3,11-dioxa-5,8-diazahexadecan-16-oic acid (3.11e). Prepared according to GPA4 using 213.3mg (0.416 mmol, 1.0 eq) of primary alcohol **3.11d**. Following purification (30-50% EtOAc in Hexanes) 218.8 mg (0.416, >95% yield) of **3.11e** was obtained as clear colorless oil.

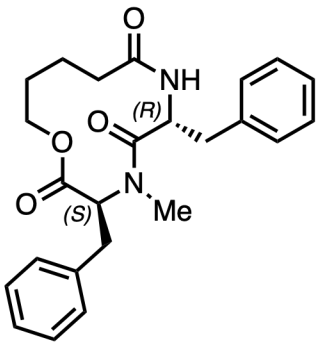
TLC (50%EtOAc in Hexanes): Rf=0.47

1H NMR (600 MHz, $CDCl_3$) δ 7.29 (dd, J = 8.7, 6.7 Hz, 2H), 7.22 – 7.18 (m, 6H), 6.98 – 6.93 (m, 2H), 5.40 (dd, J = 10.7, 5.7 Hz, 1H), 5.32 – 5.26 (m, 1H), 4.74 (td, J = 8.2, 5.7 Hz, 1H), 4.18 (p, J = 4.6 Hz, 1H), 4.14 – 4.09 (m, 1H), 3.36 (dd, J = 14.6, 5.8 Hz, 1H), 2.97 – 2.91 (m, 1H), 2.84

(s, 3H), 2.54 (dd, J = 14.1, 5.9 Hz, 1H), 2.44 (dd, J = 14.0, 7.8 Hz, 1H), 2.36 (ddd, J = 14.4, 6.3, 3.5 Hz, 2H), 1.70 (tt, J = 5.9, 3.6 Hz, 4H), 1.36 (s, 9H).

13C NMR (151 MHz, $CDCl_3$) δ 175.5, 172.9, 170.6, 155.6, 136.8, 136.4, 129.4, 129.0, 128.8, 128.5, 127.1, 126.9, 80.2, 65.2, 58.4, 51.8, 39.0, 34.9, 33.4, 32.4, 28.4, 27.8, 21.7.

HRMS (ESI-TOF) m/z: [M+H]+ Calcd for $C_{29}H_{39}N_2O_7$ 527.2757; Found: 527.2761



(3*S*,6*R*)-3,6-dibenzyl-4-methyl-1-oxa-4,7-diazacyclododecane-2,5,8-trione (3.11). Prepared according to GPA5 using 121.1 mg (0.23 mmol, 1.0 eq) of starting acid. Following purification by HPLC, 22.4 mg, 0.059 mmol, 51% yield) of pure **3.11** macrocycle was obtained as a pale yellow oil.

^{1}H NMR (600 MHz, $CDCl_3$) δ 7.30 – 7.28 (m, 1H), 7.27 – 7.27 (m, 1H), 7.26 – 7.25 (m, 1H), 7.17 – 7.12 (m, 3H), 7.11 – 7.07 (m, 2H), 7.02 (d, *J* = 7.2 Hz, 2H), 6.57 (d, *J* = 10.2 Hz, 1H), 5.80 – 5.75 (m, 1H), 5.34 (td, *J* = 10.2, 4.5 Hz, 1H), 4.38 – 4.30 (m, 1H), 3.82 (td, *J* = 11.1, 2.4 Hz, 1H), 3.44 (dd, *J* = 15.7, 5.2 Hz, 1H), 3.22 – 3.15 (m, 1H), 2.93 – 2.85 (m, 2H), 2.84 – 2.79 (m, 3H), 2.39 (ddt, *J* = 13.1, 5.9, 2.1 Hz, 1H), 2.16 (tt, *J* = 12.9, 2.4 Hz, 1H), 2.03 – 1.93 (m, 1H), 1.89 – 1.78 (m, 1H), 1.78 – 1.70 (m, 1H), 1.61 – 1.53 (m, 1H).

13C NMR (151 MHz, $CDCl_3$) δ 174.8, 174.1, 170.0, 136.2, 136.2, 128.6, 128.2, 126.7, 126.7, 65.4, 57.1, 50.4, 37.3, 36.8, 32.9, 31.0, 25.9, 23.2.

HRMS (ESI-TOF) *m/z* Calcd for $C_{24}H_{29}N_2O_4$ [M+H]+ 409.2127 ; Found: 409.2120

ROS Burst Potentiation Assay

The immunopotentiating activity of the analogue library was evaluated using a luminol-based reactive oxygen species (ROS) burst assay in Arabidopsis thaliana leaf discs, adapted from the protocol of Bredow et al[6]. *Arabidopsis thaliana* (Col-0) plants were grown on soil under standard

short-day conditions (22 °C, 10 h light, 65–70% relative humidity) for 4-5 weeks prior to assay. Leaf discs (4 mm diameter) were harvested using a biopsy punch from fully expanded rosette leaves, avoiding the mid-vein, and transferred to a 96-well luminometer plate containing 100 µL of double-distilled water per well. Leaf discs were recovered overnight at room temperature to allow metabolic stabilization following wounding. Prior to immune elicitation, the water was removed and replaced with 100 µL of reaction solution containing 100 µM luminol, 10 µg/mL horseradish peroxidase (HRP), and flg22 (1 nM) as the immune elicitor, prepared in sterile double-distilled water. Test compounds were dissolved in DMSO and added to the reaction solution at the indicated concentrations, with vehicle control wells receiving an equivalent volume of DMSO. ROS production was quantified as the maximal luminescence recorded at the peak apex of the ROS burst and is presented relative to the flg22-only control. All assays were performed in the laboratory of Dr. Gopal Subramaniam (Carleton University) in collaboration with the laboratory of Dr. David Overy (Agriculture and Agri-Food Canada).

3.5 References

(1) Schulze-Lefert, P. *Clin. Exp. Immunol.* **2010**, *160* (1), 62–69.

(2) Yu, X.; Feng, B.; He, P.; Shan, L. *Annu. Rev. Phytopathol.* **2017**, *55* (Volume 55, 2017), 109–137.

(3) Zielonka, J.; Lambeth, J. D.; Kalyanaraman, B. *Free Radic. Biol. Med.* **2013**, *65*, 1310–1314.

(4) Zhang, Y.; Dai, M.; Yuan, Z. *Anal. Methods* **2018**, *10* (38), 4625–4638.

(5) Sang, Y.; Macho, A. P. Analysis of PAMP-Triggered ROS Burst in Plant Immunity. In *Plant Pattern Recognition Receptors: Methods and Protocols*; Shan, L., He, P., Eds.; Springer: New York, NY, 2017; pp 143–153.

(6) Bredow, M.; Sementchoukova, I.; Siegel, K.; Monaghan, J. *J. Vis. Exp. JoVE* **2019**, No. 147, e59437.

(7) Li, R.; Schaller, A.; Stintzi, A. Quantitative Measurement of Pattern-Triggered ROS Burst as an Early Immune Response in Tomato. In *Plant Peptide Hormones and Growth Factors*; Schaller, A., Ed.; Springer US: New York, NY, 2024; pp 157–167.

(8) Keinath, N. F.; Kierszniowska, S.; Lorek, J.; Bourdais, G.; Kessler, S. A.; Shimosato-Asano, H.; Grossniklaus, U.; Schulze, W. X.; Robatzek, S.; Panstruga, R. *J. Biol. Chem.* **2010**, *285* (50), 39140–39149.

(9) Boller, T.; Felix, G. *Annu. Rev. Plant Biol.* **2009**, *60* (Volume 60, 2009), 379–406.

(10) Toruño, T. Y.; Stergiopoulos, I.; Coaker, G. *Annu. Rev. Phytopathol.* **2016**, *54*, 419–441.

(11) Jiang, Y.; Gao, Y.; Liu, J.; Zhang, H.; Latif, M. Z.; Fang, K.; Lu, C.; Yin, Z.; Li, Y.; Ding, X. *Plant Commun.* **2026**, *7* (3), 101631.

(12) Naz, M.; Zhang, D.; Liao, K.; Chen, X.; Ahmed, N.; Wang, D.; Zhou, J.; Chen, Z. *Genes* **2024**, *15* (9), 1237.

(13) Zhu, F.; Cao, M.-Y.; Zhang, Q.-P.; Mohan, R.; Schar, J.; Mitchell, M.; Chen, H.; Liu, F.; Wang, D.; Fu, Z. Q. *J. Adv. Res.* **2024**, *57*, 15–42.

(14) Jiang, Y.; Gao, Y.; Liu, J.; Zhang, H.; Latif, M. Z.; Fang, K.; Lu, C.; Yin, Z.; Li, Y.; Ding, X. *Plant Commun.* **2025**, *7* (3), 101631.

(15) Mubeen, B.; Murtaza, S.; Yaqoob, S.; Aregbe, A. Y.; Boasiako, T. A.; Xiong, Y.; Ma, Y. *South Afr. J. Bot.* **2025**, *179*, 280–292.

(16) Wang, S.; Dong, G.; Sheng, C. *Chem. Rev.* **2019**, *119* (6), 4180–4220.

(17) Jiménez, J. C.; López-Macià, A.; Gracia, C.; Varón, S.; Carrascal, M.; Caba, J. M.; Royo, M.; Francesch, A. M.; Cuevas, C.; Giralt, E.; Albericio, F. *J. Med. Chem.* **2008**, *51* (16), 4920–4931.

(18) Pojani, E.; Barlocco, D. *Curr. Med. Chem.* **2021**, *28* (7), 1290–1303.

(19) Sato, H.; Murase, H.; Ishida, Y.; Sugiyama, H.; Uekusa, H.; Nakagawa, H.; Yoshida, M.; Doi, T. *Bioorg. Med. Chem.* **2024**, *108*, 117777.

(20) Ratnayake, R.; Fremlin, L. J.; Lacey, E.; Gill, J. H.; Capon, R. J. *J. Nat. Prod.* **2008**, *71* (3), 403–408.

(21) Schalk, F.; Fricke, J.; Um, S.; Conlon, B. H.; Maus, H.; Jäger, N.; Heinzel, T.; Schirmeister, T.; Poulsen, M.; Beemelmanns, C. *RSC Adv.* **2021**, *11* (31), 18748–18756.

(22) Feng, L.; Wang, J.; Liu, S.; Zhang, X.-J.; Bi, Q.-R.; Hu, Y.-Y.; Wang, Z.; Tan, N.-H. *J Nat Prod* **2019**, *82*, 12.

(23) Lee, C.; Gong, J.; Kim, J.; Ko, H.; An, S.; Bang, S.; Deyrup, S. T.; Noh, M.; Shim, S. H. *J. Nat. Prod.* **2022**, *85* (3), 501–510.

(24) Feng, Y.; Blunt, J. W.; Cole, A. L. J.; Munro, M. H. G. *Org. Lett.* **2002**, *4* (12), 2095–2096.

(25) Seo, C.; Yim, J. H.; Lee, H. K.; Park, S. M.; Sohn, J. H.; Oh, H. *Tetrahedron Lett.* **2008**, *49* (1), 29–31.

(26) Lee, S.; Jeong, S. Y.; Nguyen, D. L.; So, J. E.; Kim, K. H.; Kim, J. H.; Han, S. J.; Suh, S. S.; Lee, J. H.; Youn, U. J. *Metabolites* **2022**, *12* (2), 141.

(27) Xiao, Y.; Liu, J.; Jiang, Y.; Guo, Y.; Ye, T. *Molecules* **2024**, *29* (15), 3599.

(28) Bang, S.; Lee, C.; Kim, S.; Song, J. H.; Kang, K. S.; Deyrup, S. T.; Nam, S. J.; Xia, X.; Shim, S. H. *J. Org. Chem.* **2019**, *84* (17), 10999–11006.

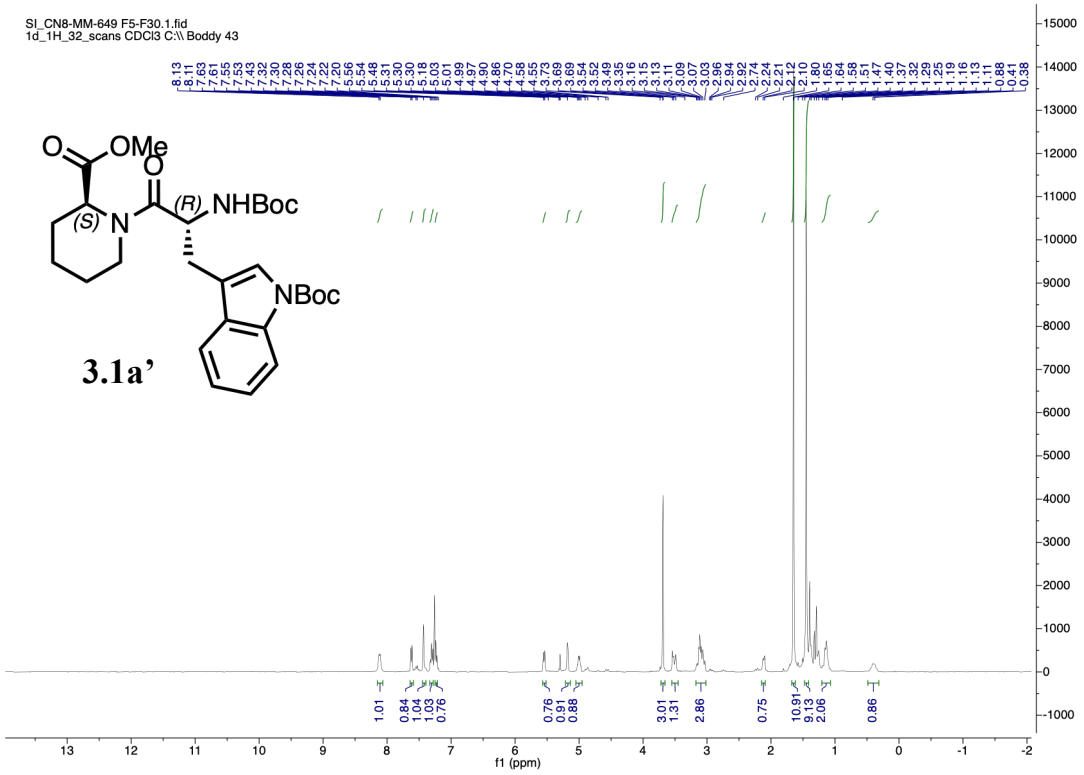
(29) Chen, J.; Jiang, Y.; Yan, J.; Xu, C.; Ye, T. *Molecules* **2023**, *28* (20), 7194.

(30) Feng, J.; Liu, J.; Ye, T. *Org. Lett.* **2025**, *27* (33), 9299–9303.

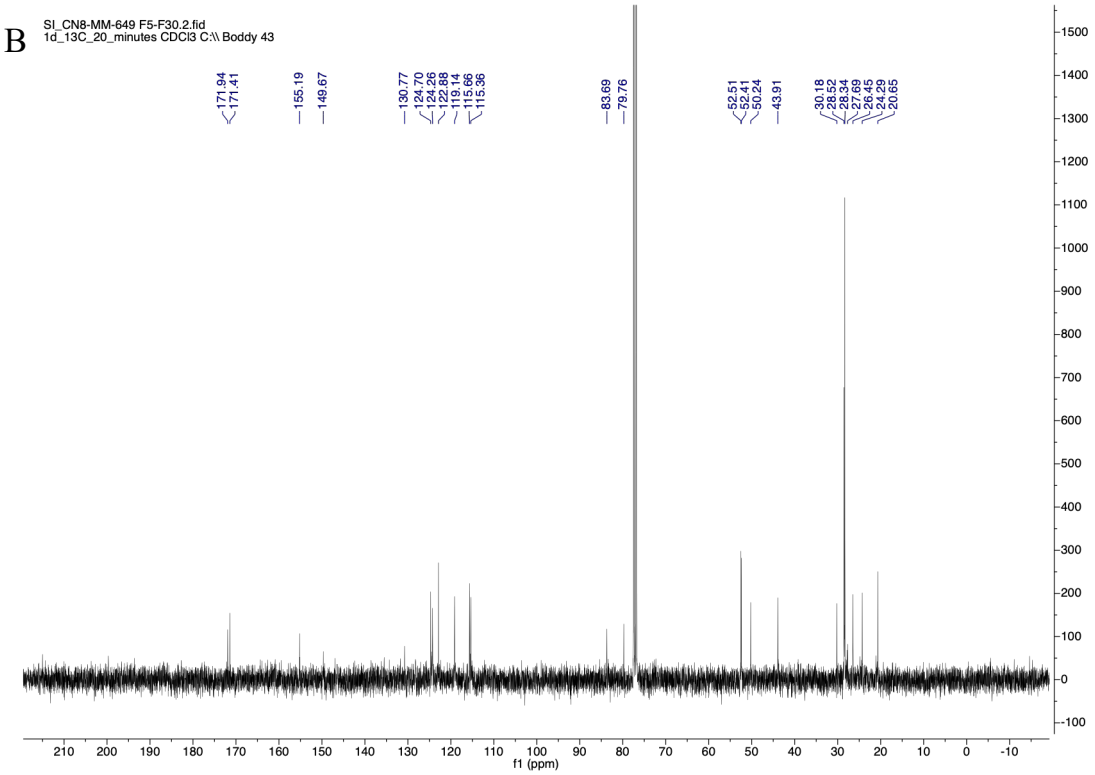
(31) Kaneda, M.; Inuki, S.; Ohno, H.; Oishi, S. *J. Org. Chem.* **2018**, *83* (6), 3047–3060.

3.6 Appendix for Chapter III
NMR Spectra:

A

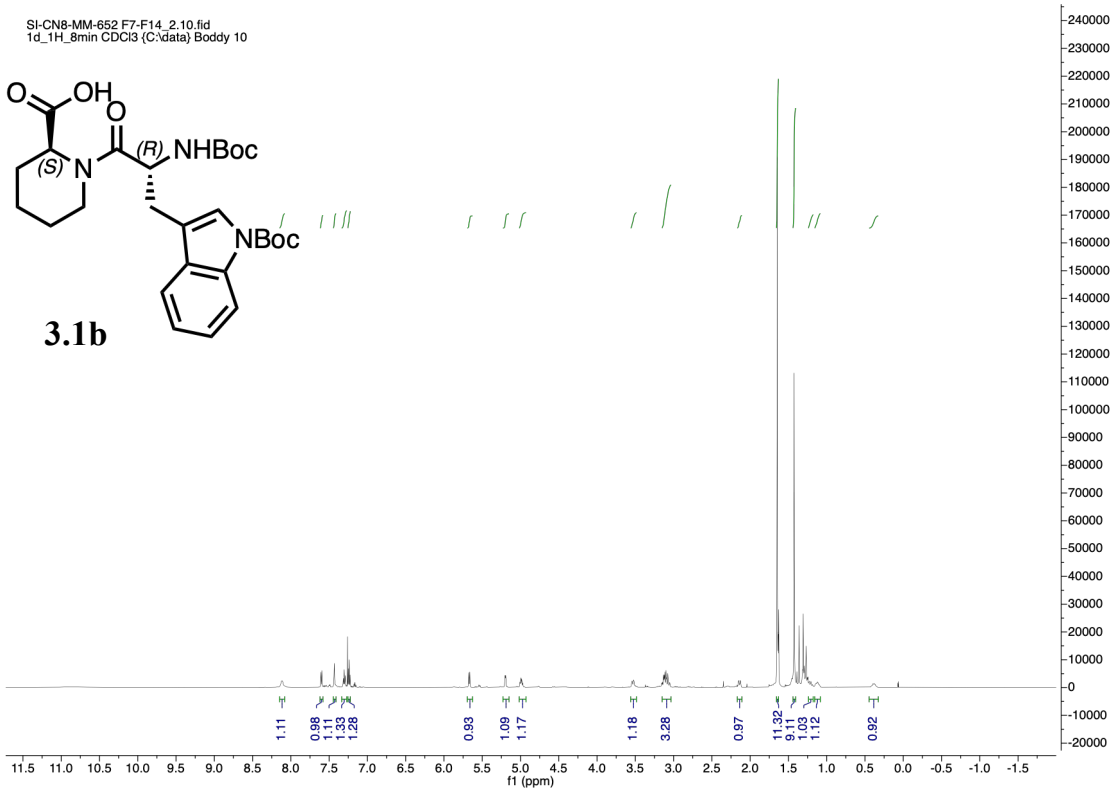


B

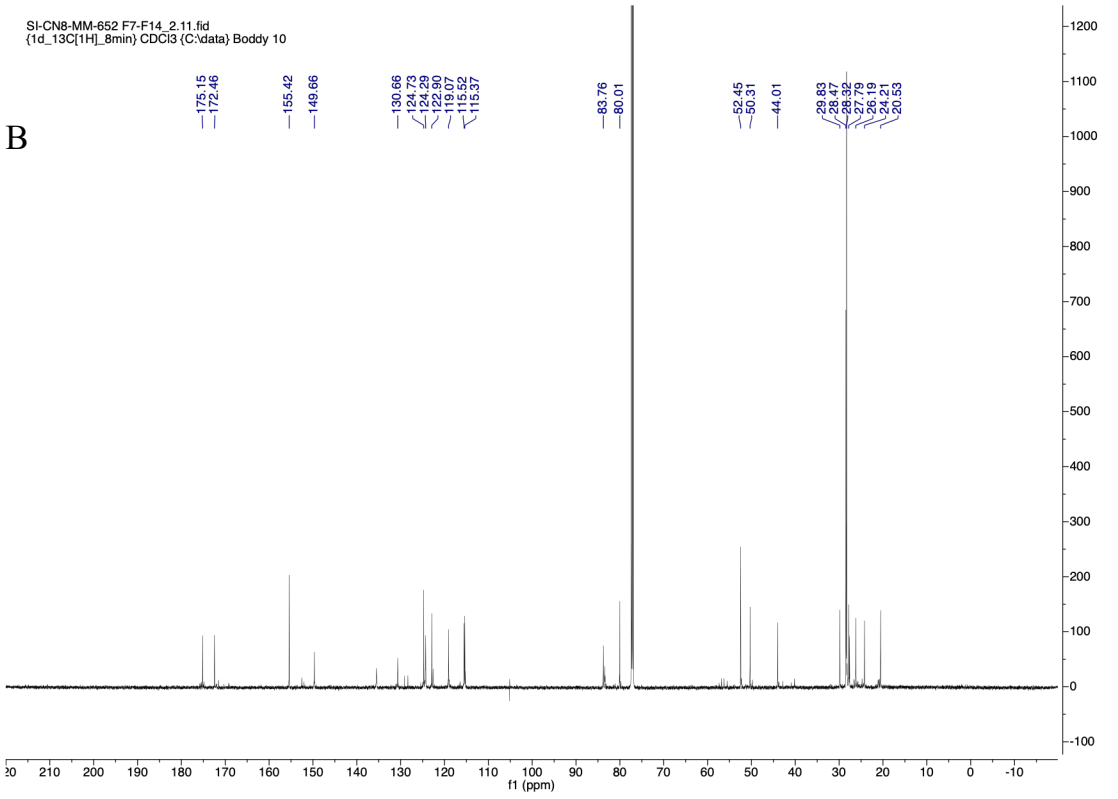


Spectra 3.1 of compound **3.1a'** (A) ^{1}H NMR (400 MHz, $CDCl_3$) and (B) ^{13}C NMR (101MHz, CDCl3)

A

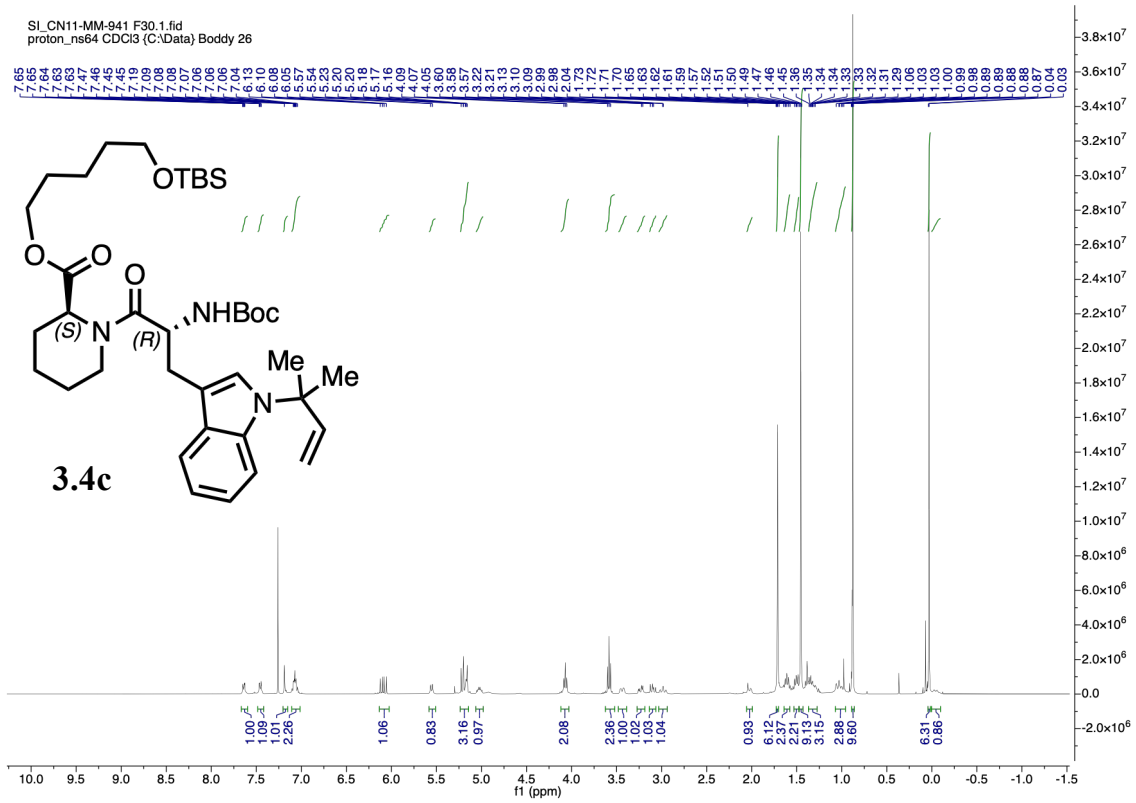


B

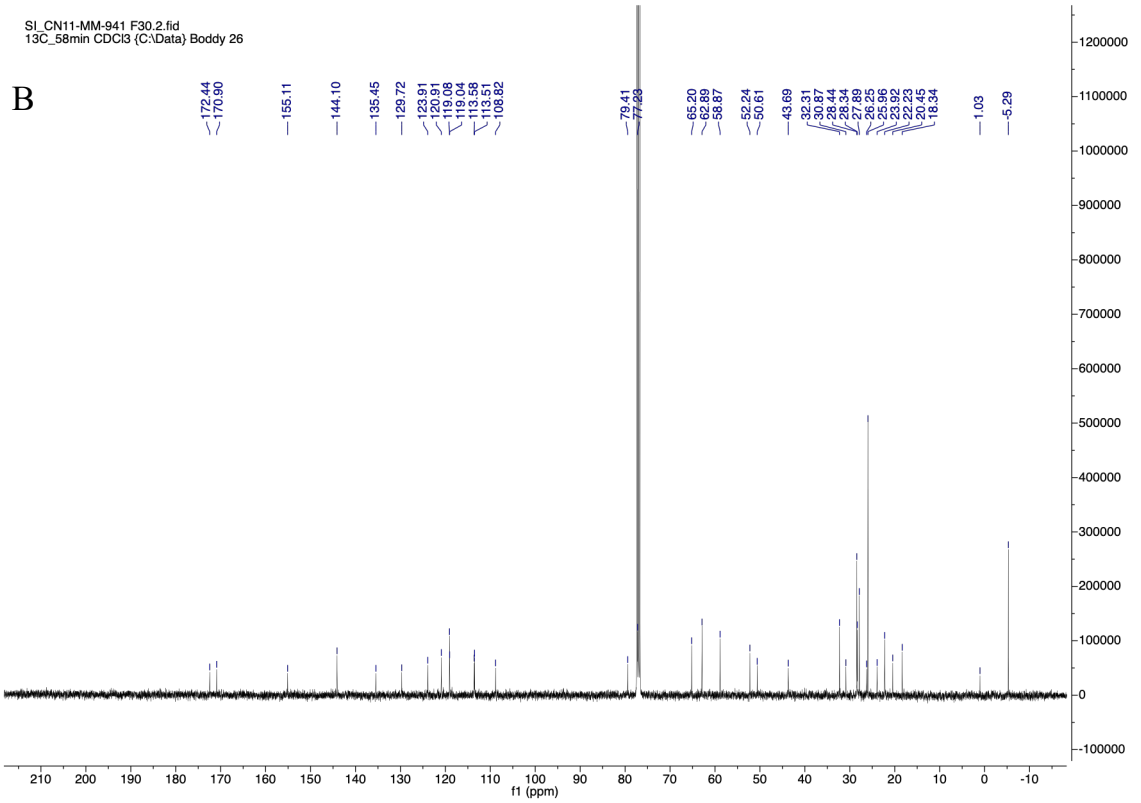


Spectra 3.2 of compound **3.1b** (A) ^{1}H NMR (400 MHz, $CDCl_3$) and (B) ^{13}C NMR (101MHz, CDCl3)

A

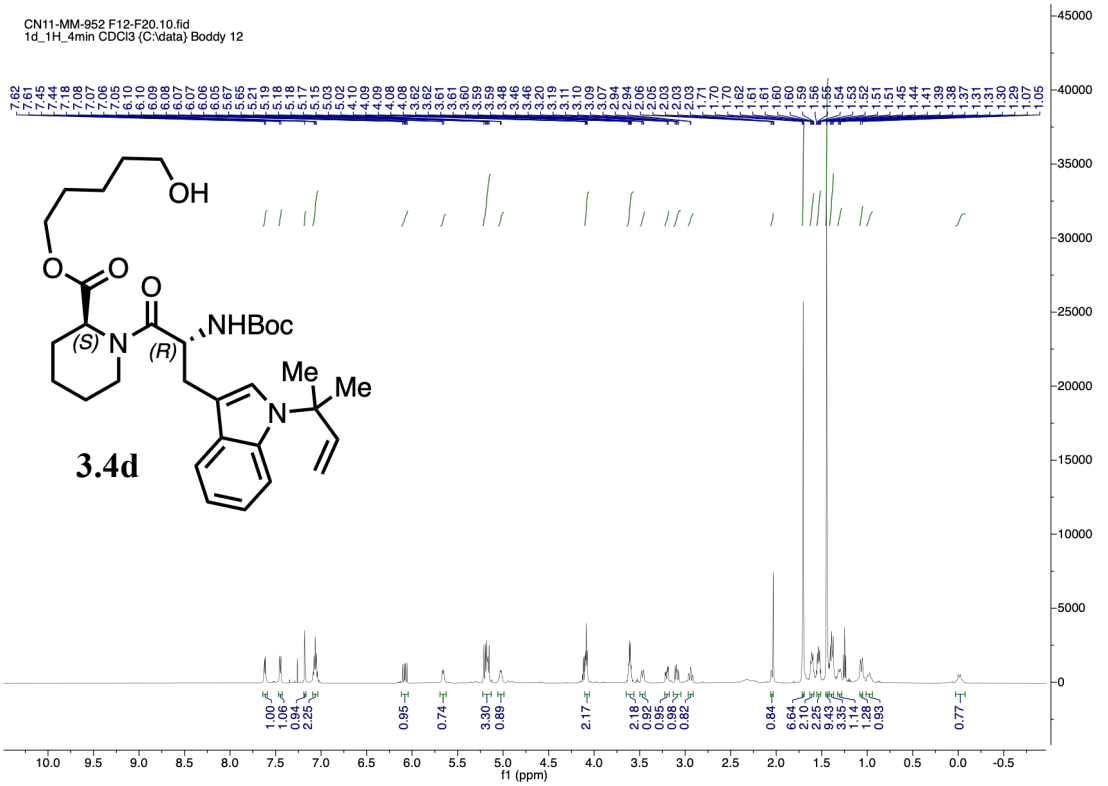


B

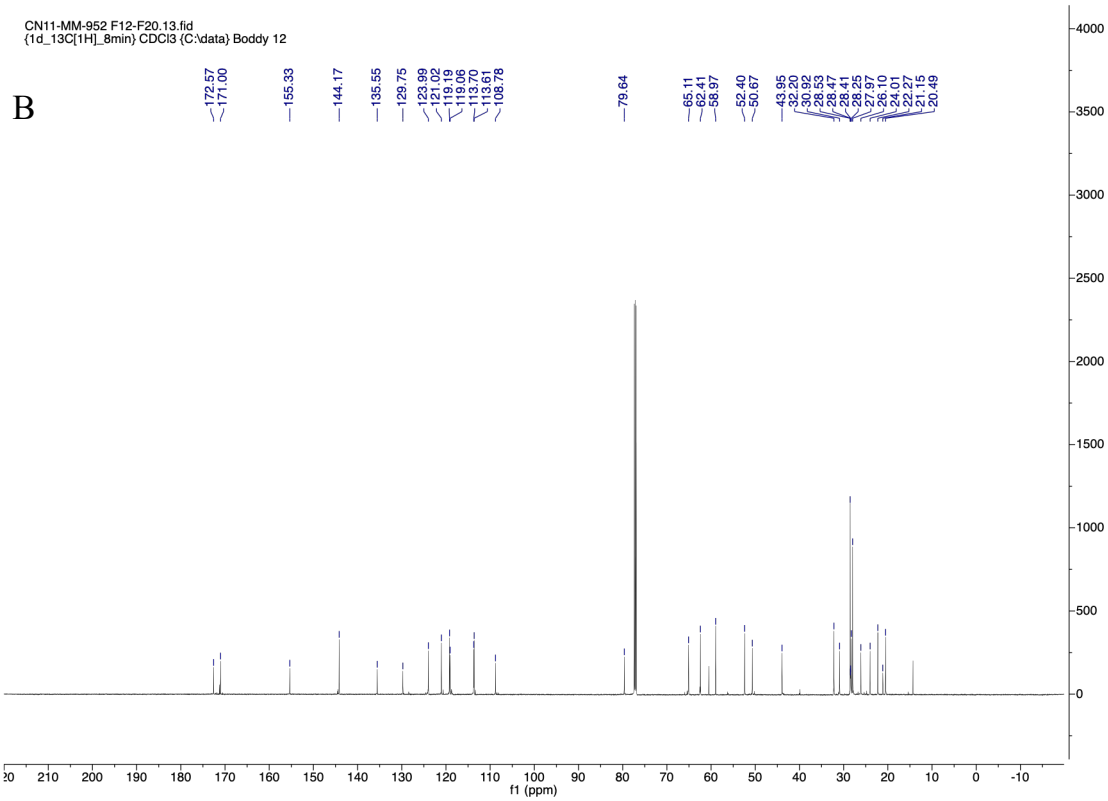


Spectra 3.3 of compound **3.4c** (A) ^{1}H NMR (400 MHz, $CDCl_3$) and (B) ^{13}C NMR (101MHz, CDCl3)

A

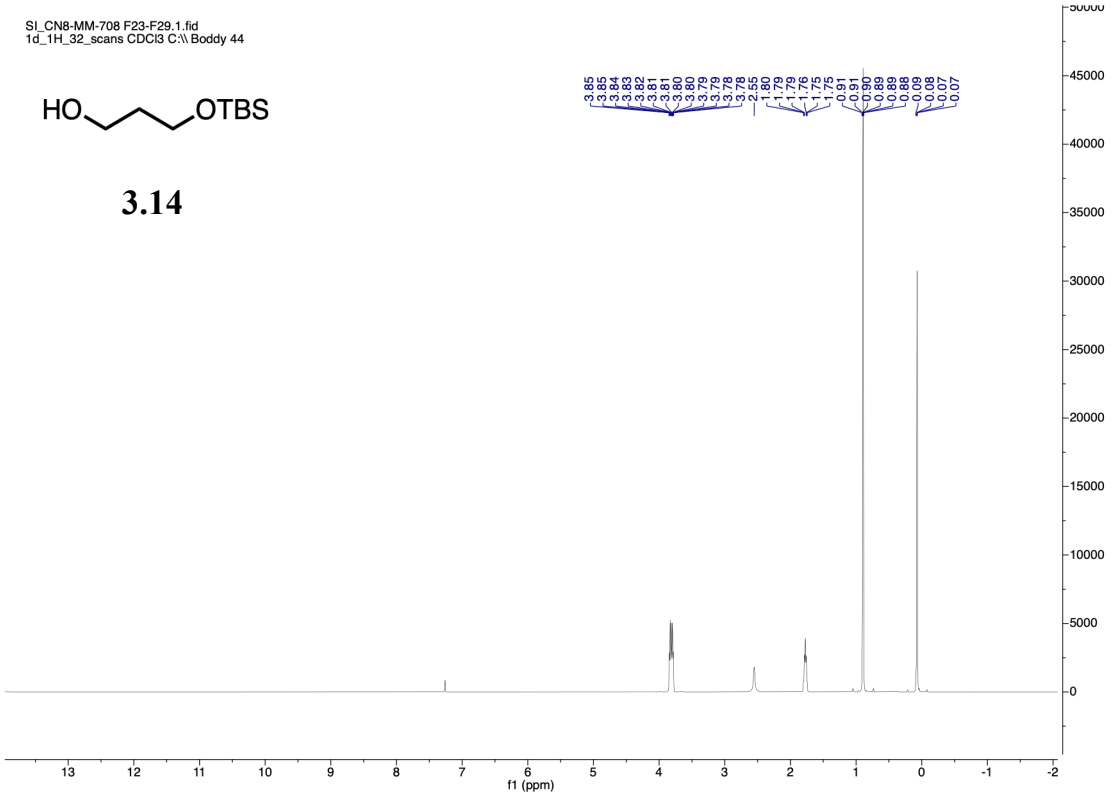


B

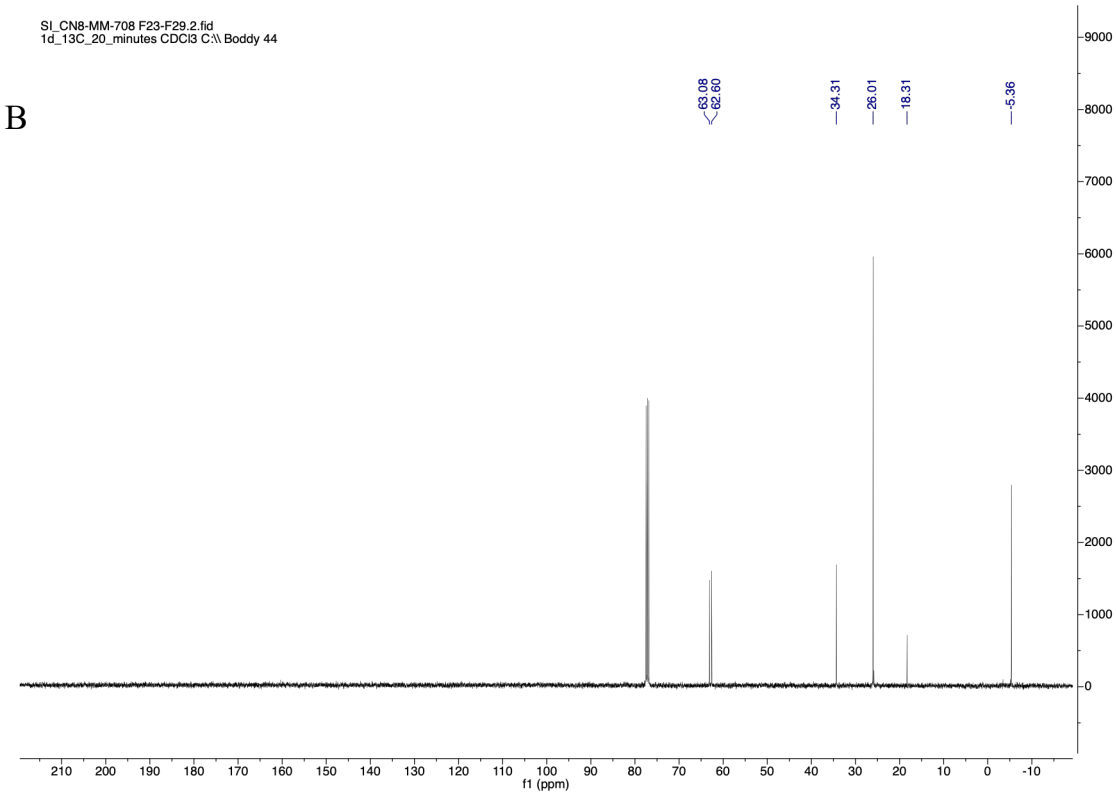


Spectra 3.4 of compound **3.4d** (A) ^{1}H NMR (400 MHz, $CDCl_3$) and (B) ^{13}C NMR (101MHz, CDCl3)

A

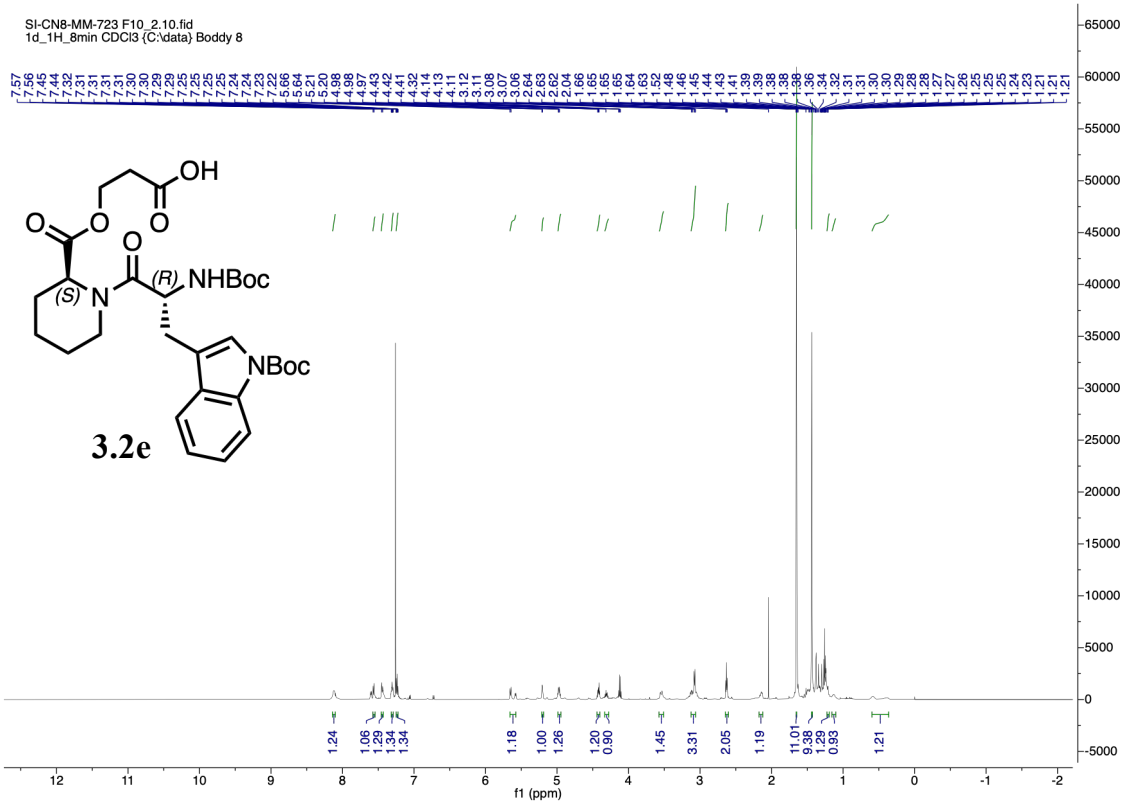


B

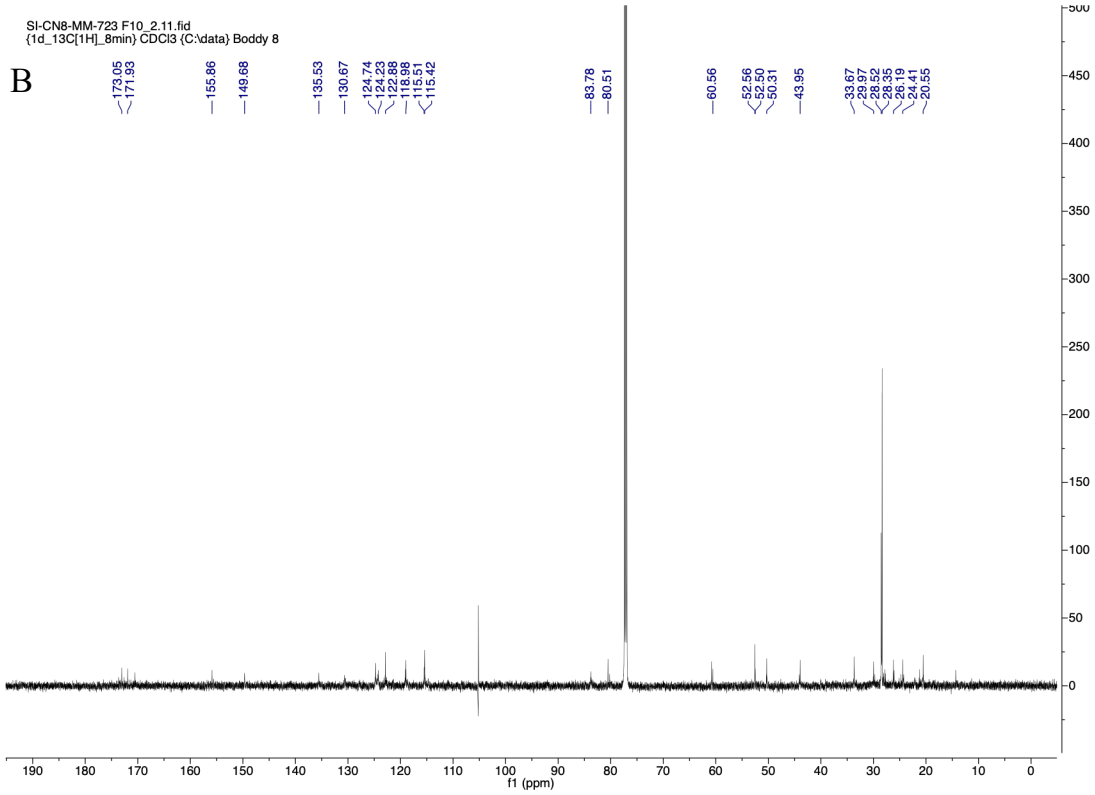


Spectra 3.5 of compound **3.14** (A) ^{1}H NMR (400 MHz, $CDCl_3$) and (B) ^{13}C NMR (101MHz, CDCl3)

A

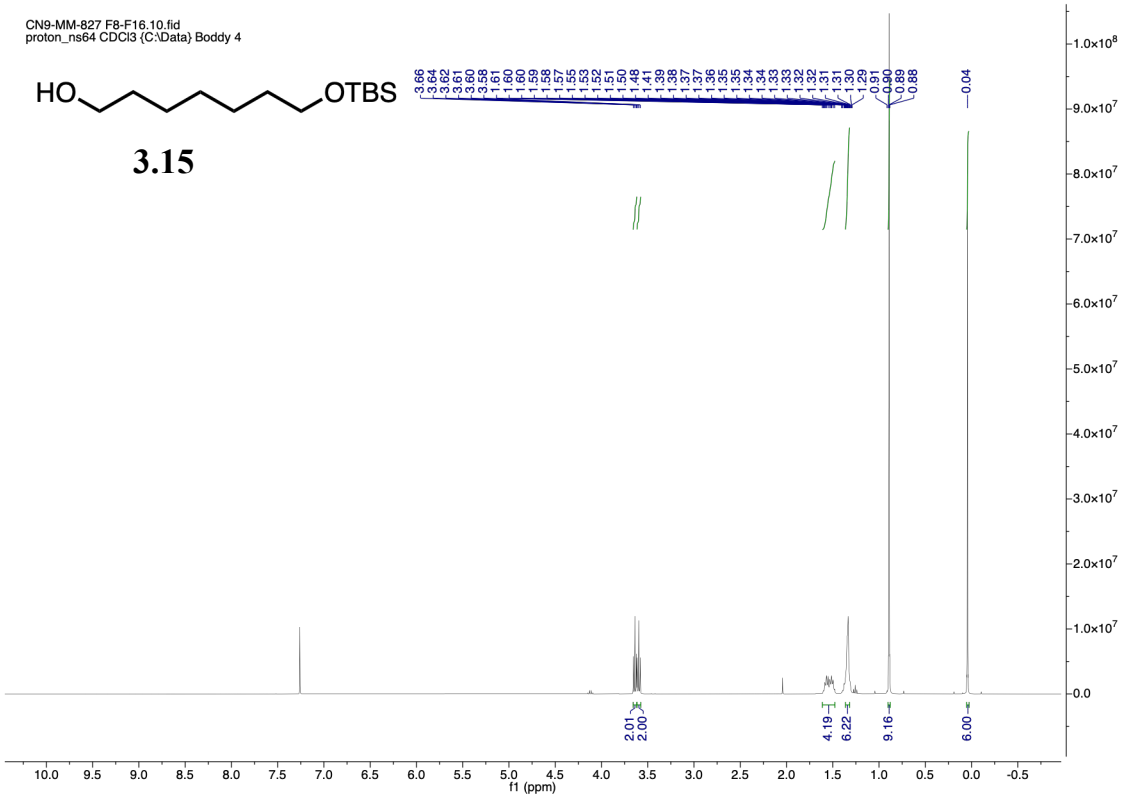


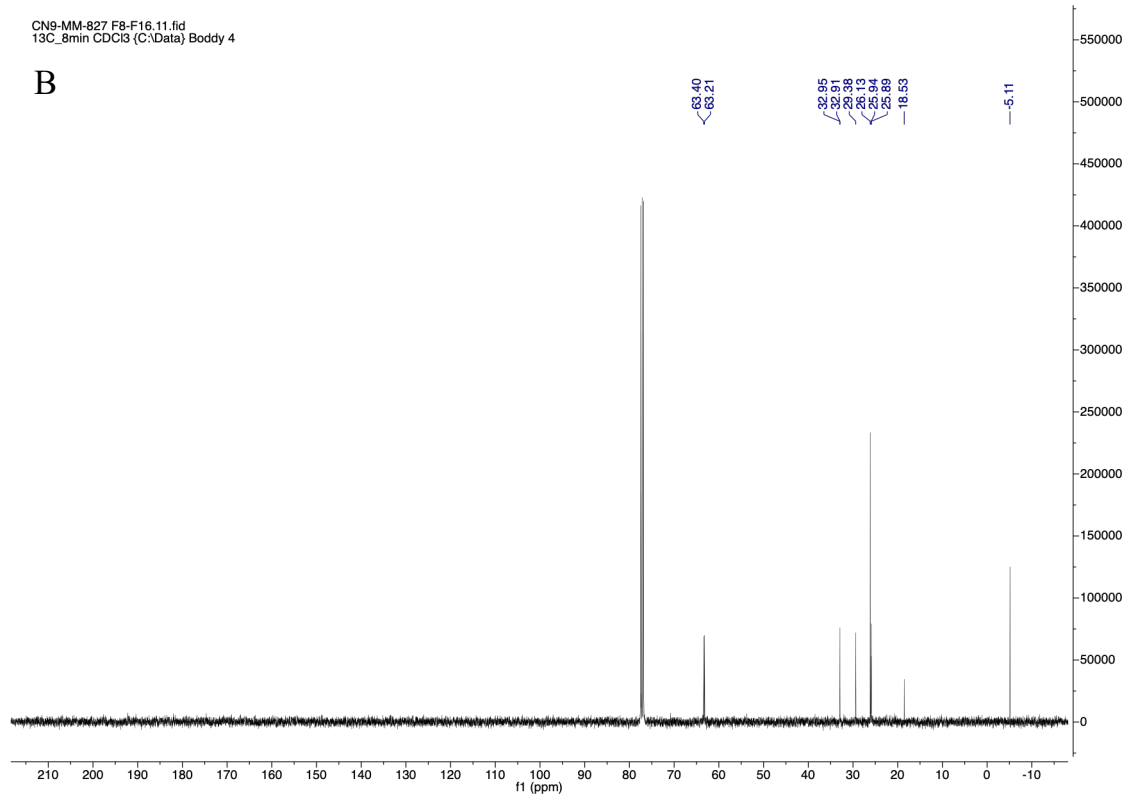
B



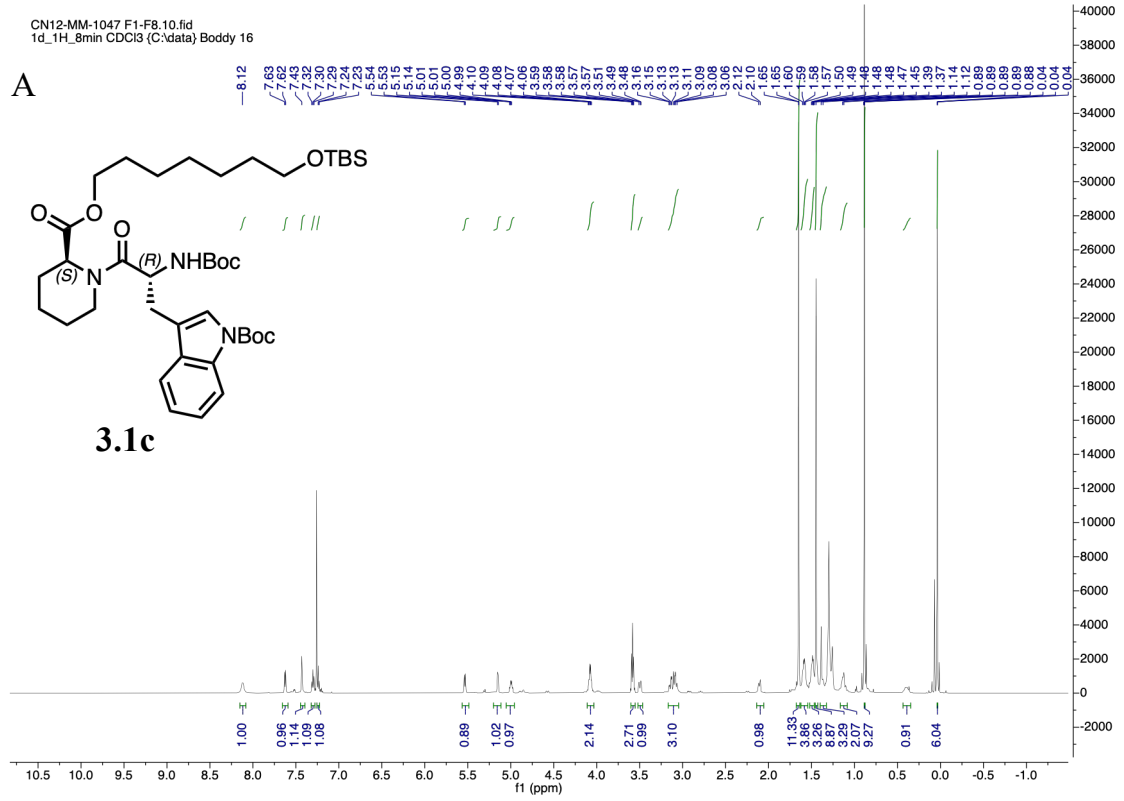
Spectra 3.6 of compound **3.2e** (A) ^{1}H NMR (400 MHz, $CDCl_3$) and (B) ^{13}C NMR (101MHz, CDCl3)

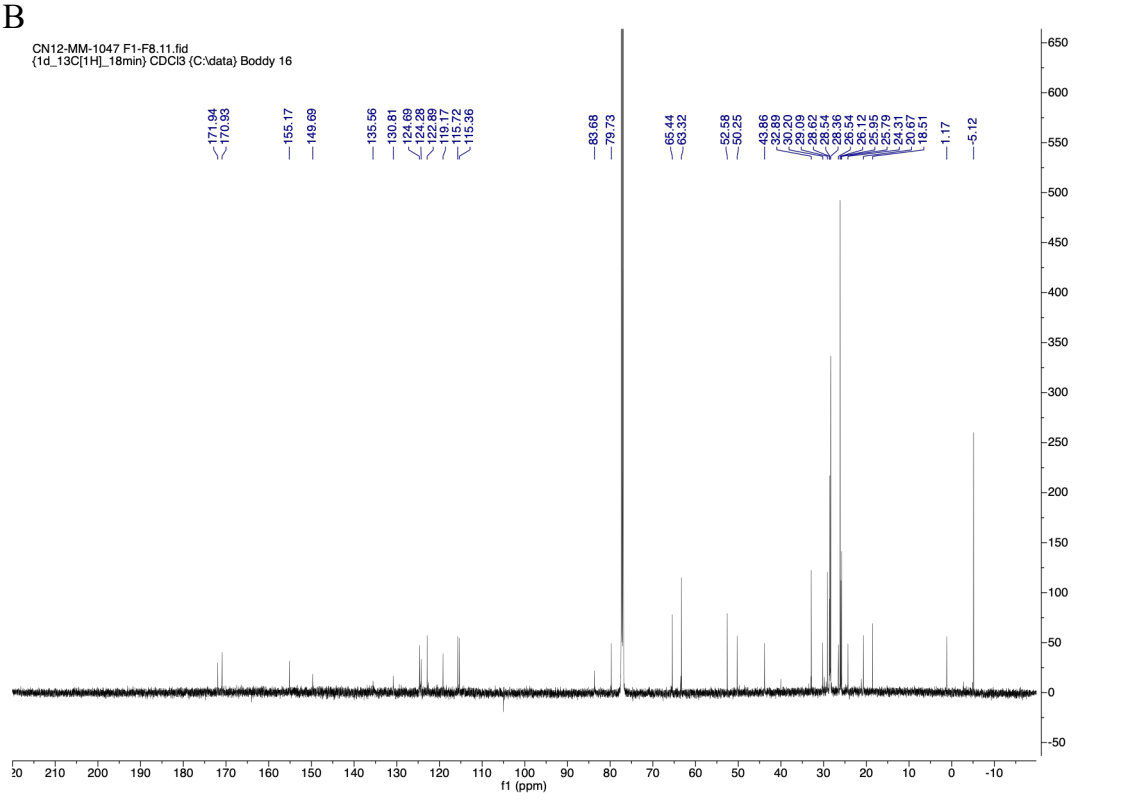
A



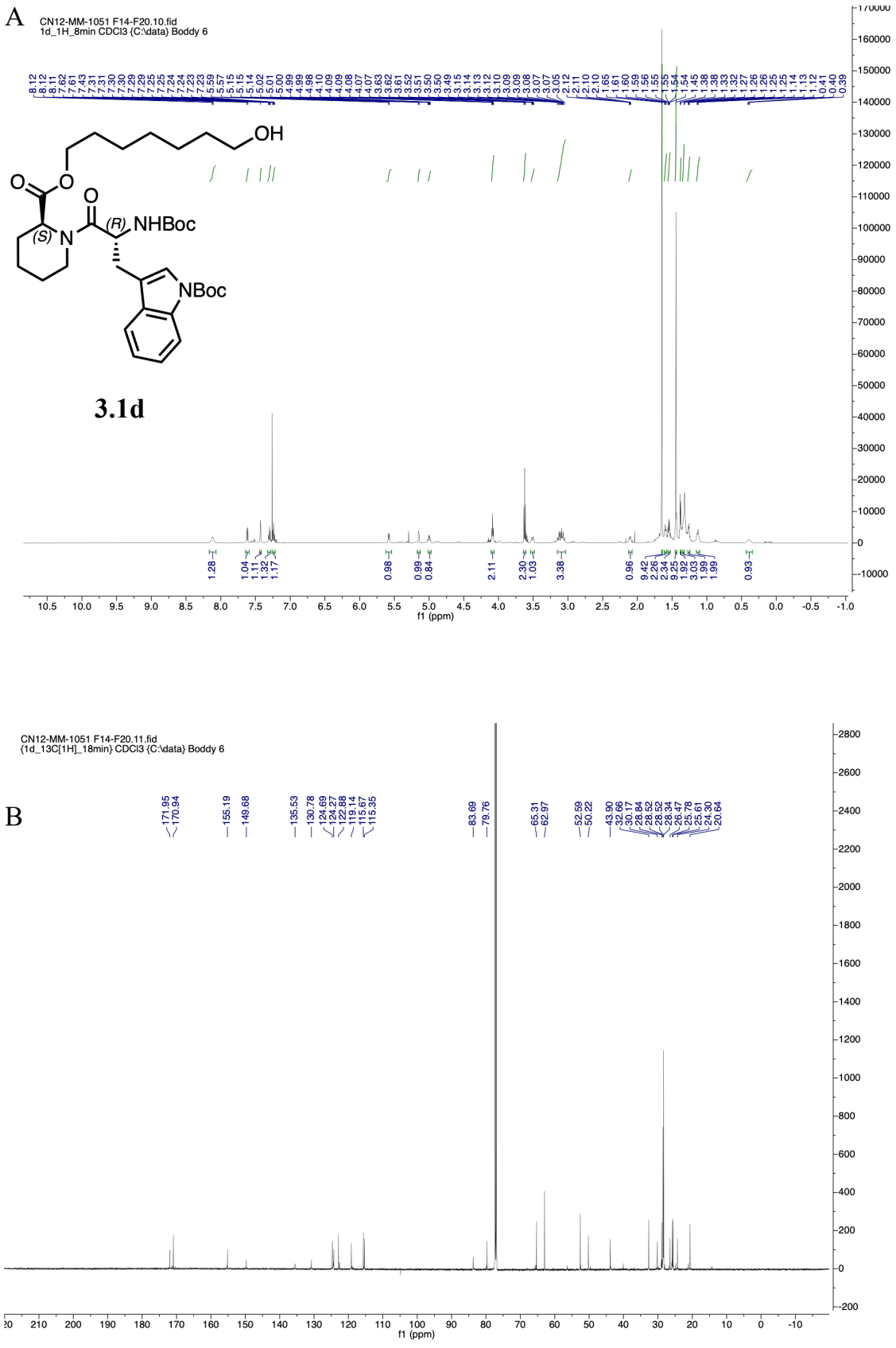


Spectra 3.7 of compound **3.15**(A) ^{1}H NMR (400 MHz, $CDCl_3$) and (B) ^{13}C NMR (101MHz, CDCl3)

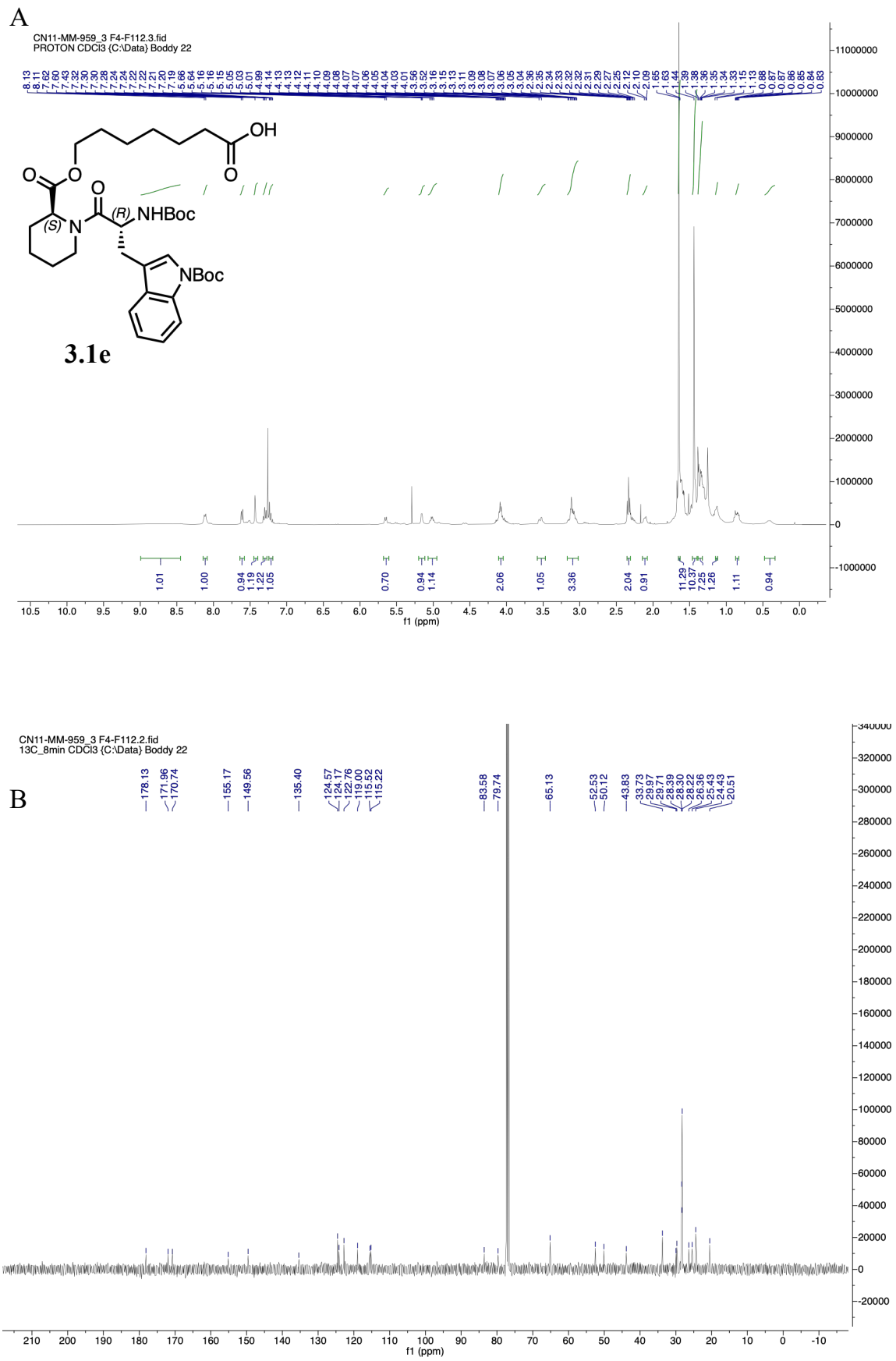




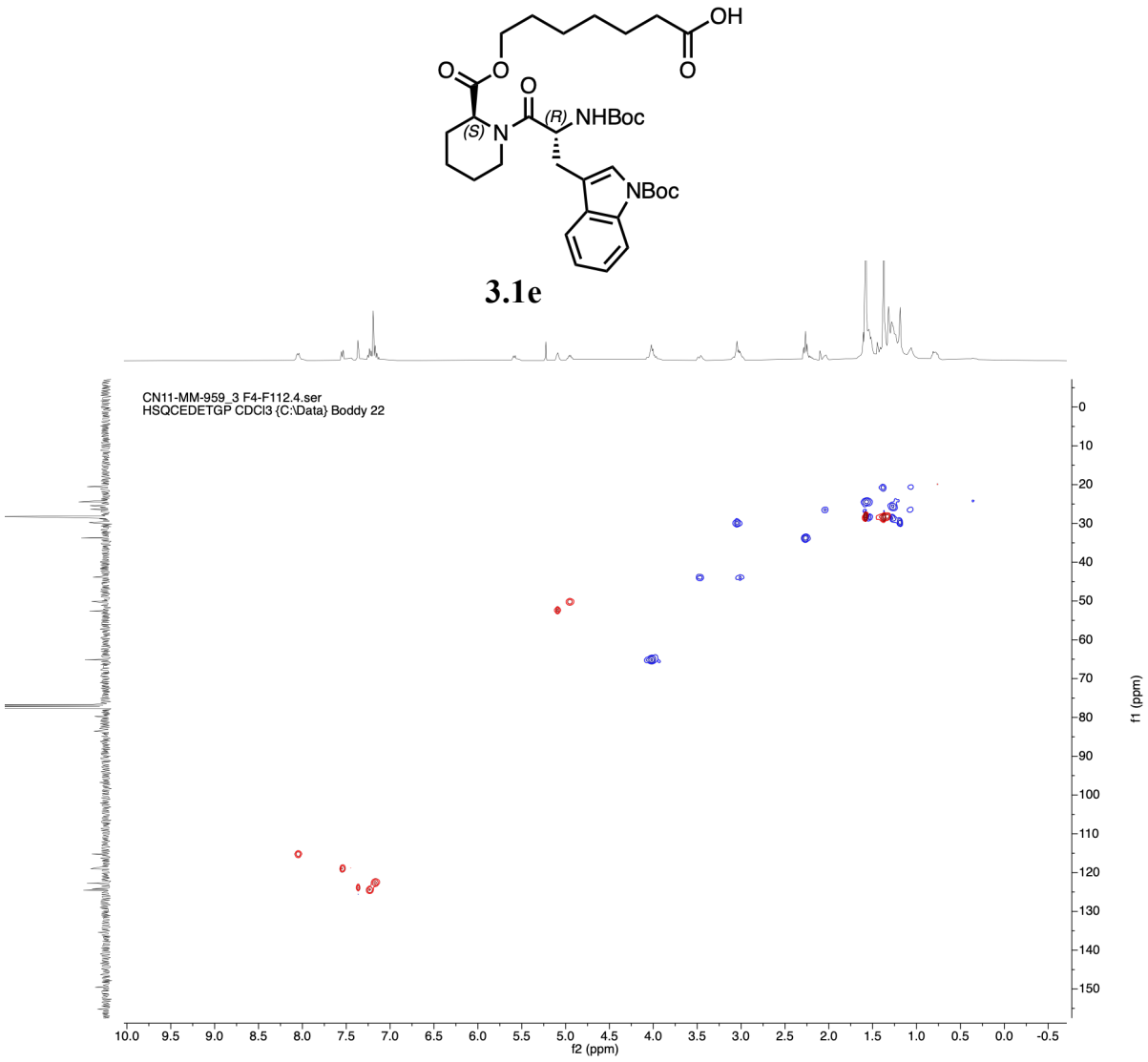
Spectra 3.8 of compound **3.1c** (A) ^{1}H NMR (400 MHz, $CDCl_3$) and (B) ^{13}C NMR (101MHz, CDCl3)



Spectra 3.9 of compound **3.1d** (A) ^{1}H NMR (400 MHz, $CDCl_3$) and (B) ^{13}C NMR (101MHz, CDCl3)

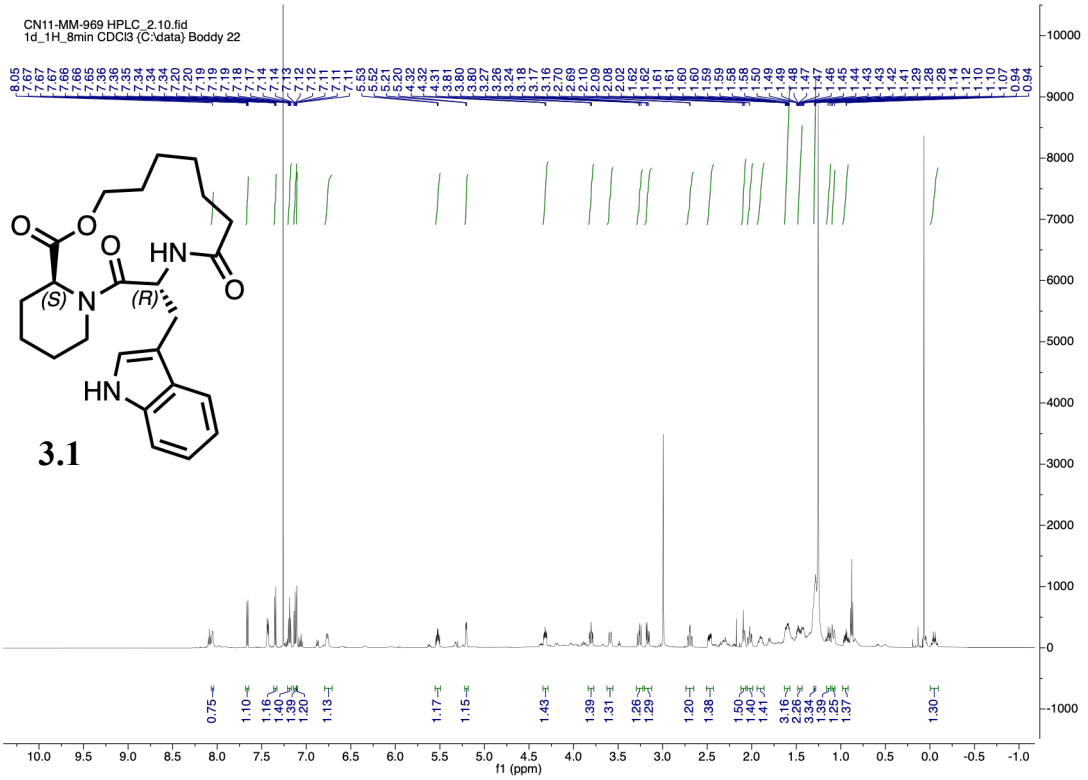


Spectra 3.10 of compound **3.1e** (A) ^{1}H NMR (400 MHz, $CDCl_3$) and (B) ^{13}C NMR (101MHz, CDCl3)

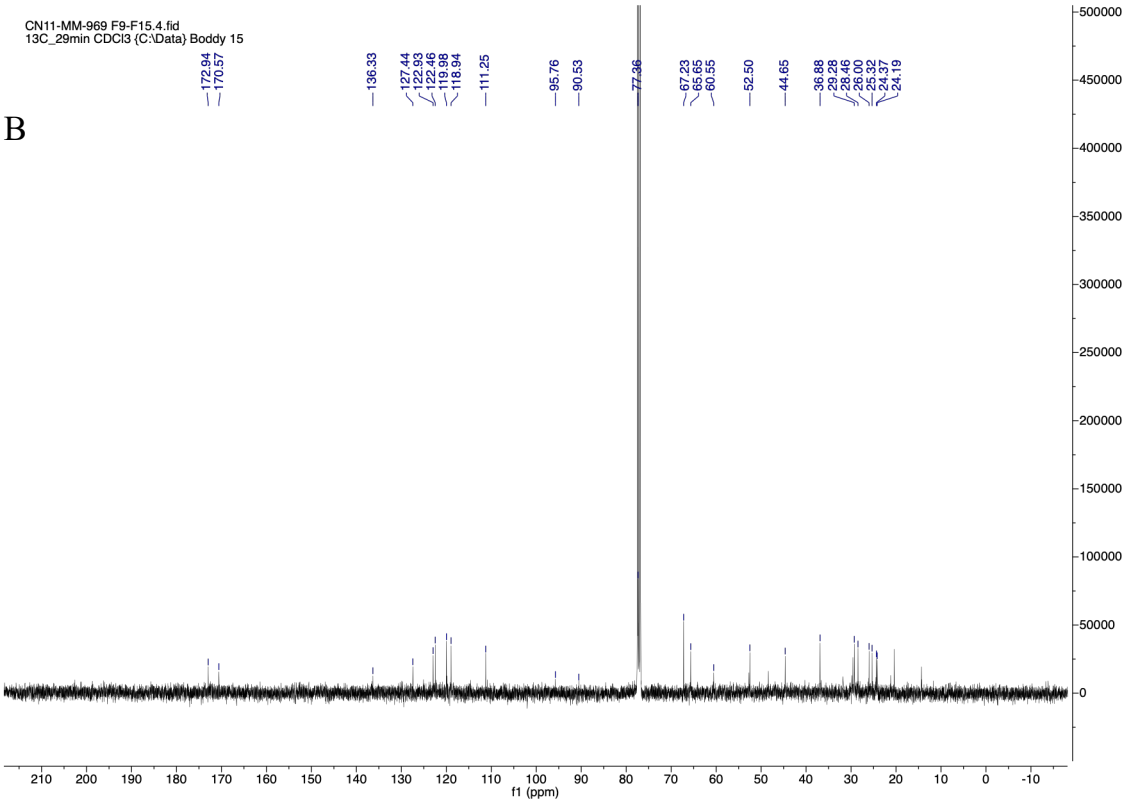


Spectra 3.11 of compound **3.1e** HSQC (CDCl3)

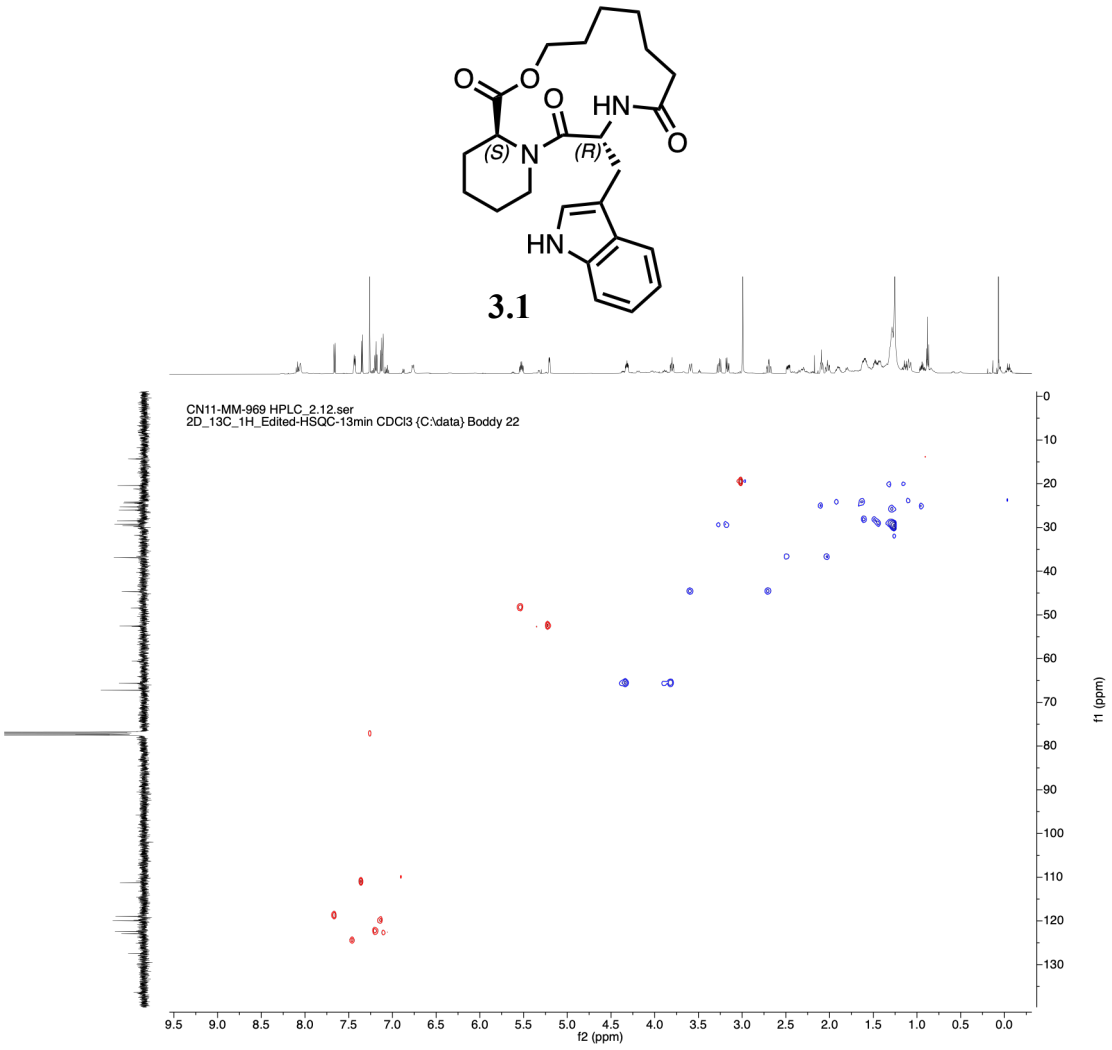
A



B

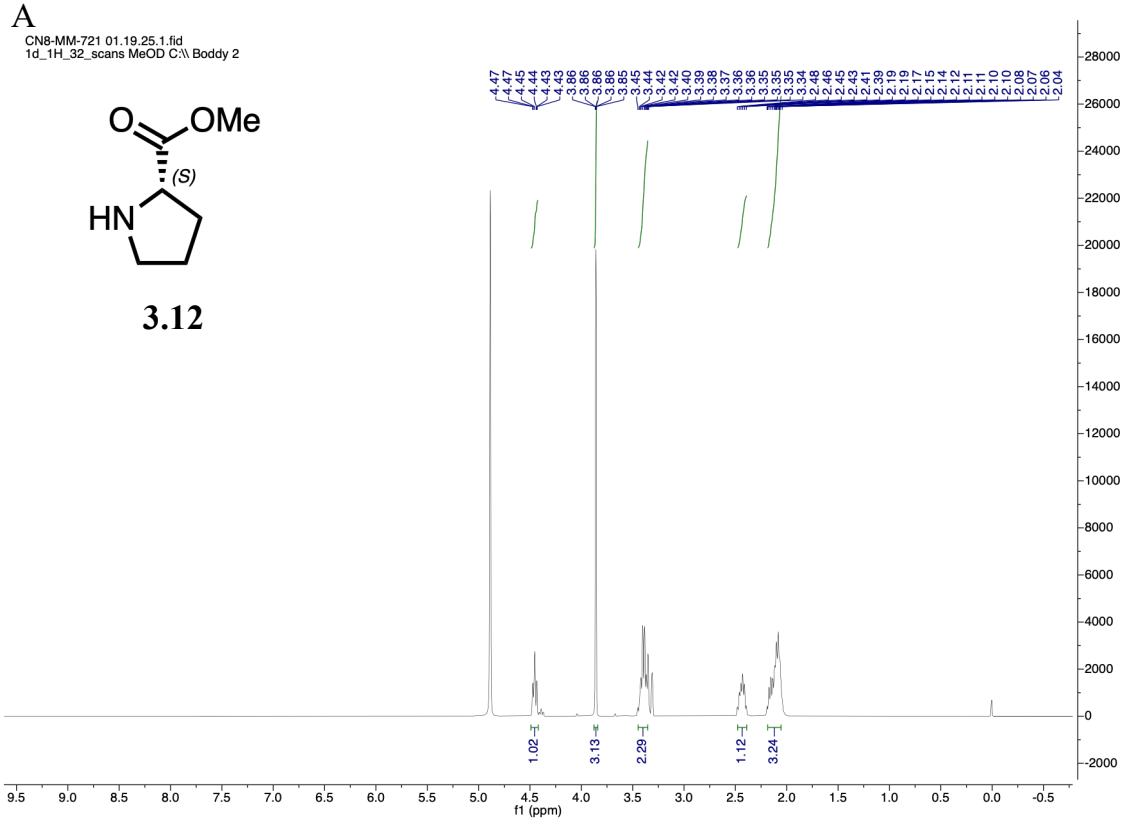


Spectra 3.12 of compound **3.1** (A) ^{1}H NMR (600 MHz, $CDCl_3$) and (B) ^{13}C NMR (101MHz, CDCl3)

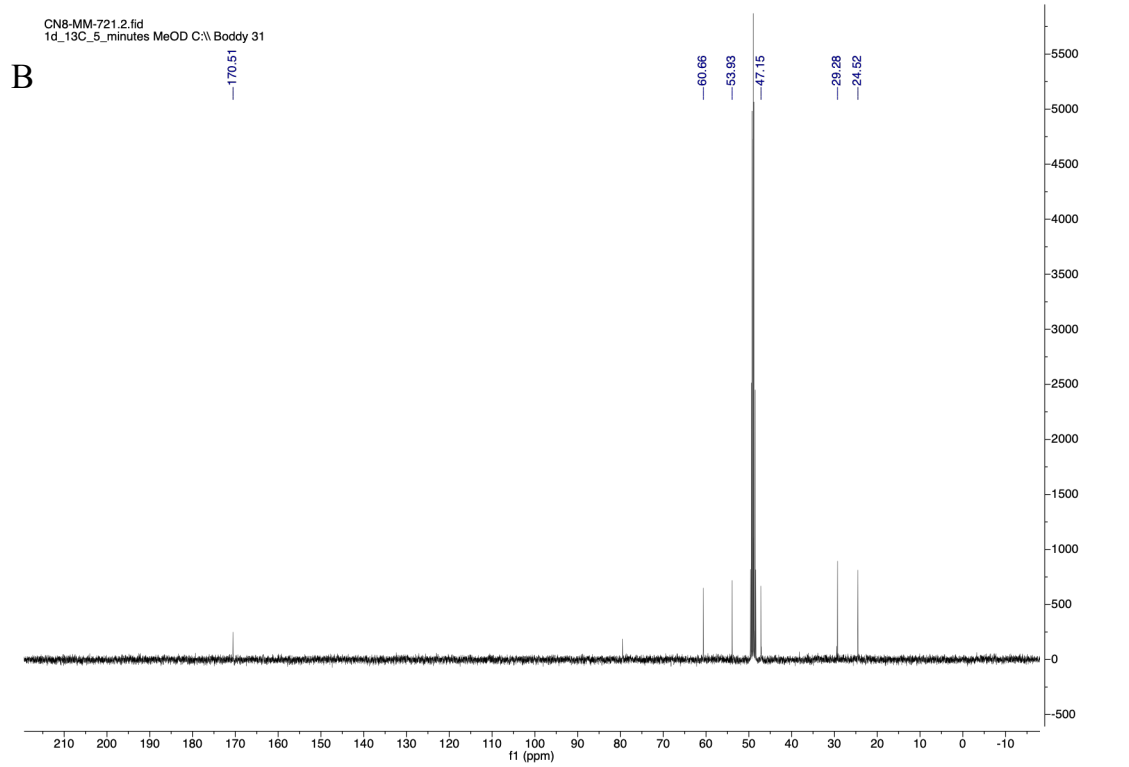


Spectra 3.13 of compound **3.1** HSQC (CDCl3)

A

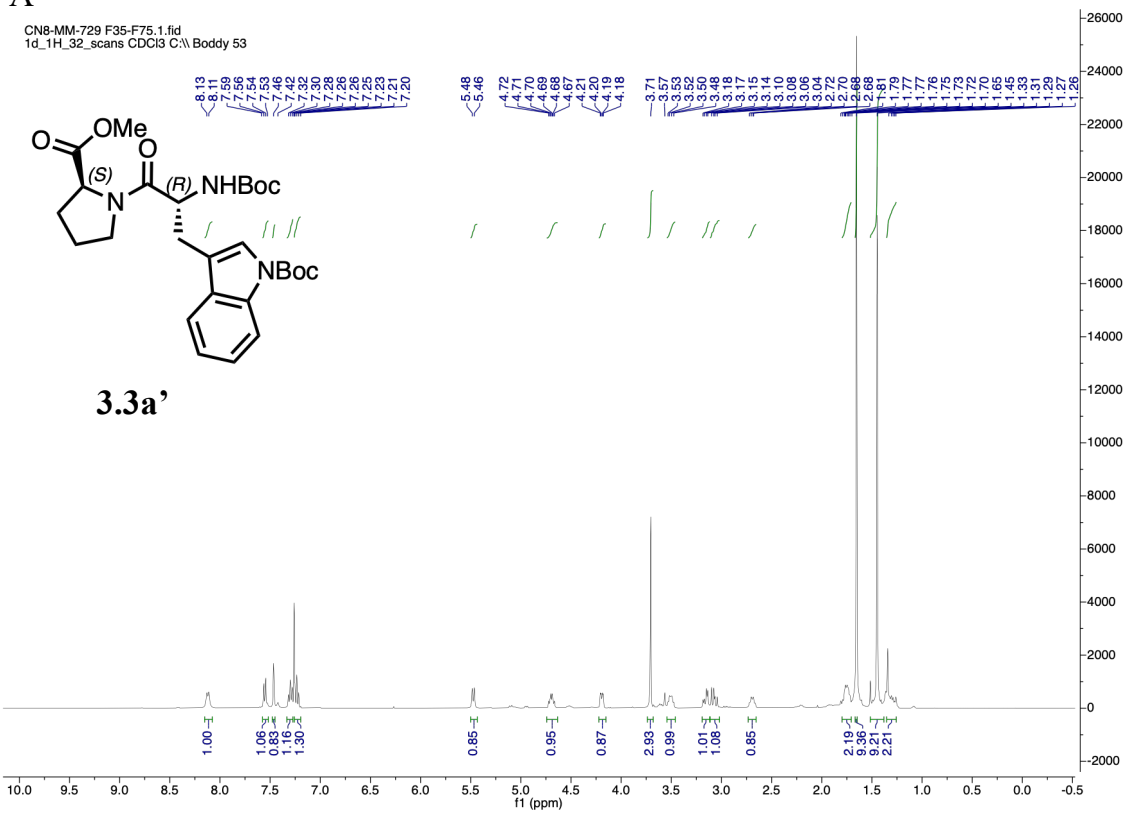


B



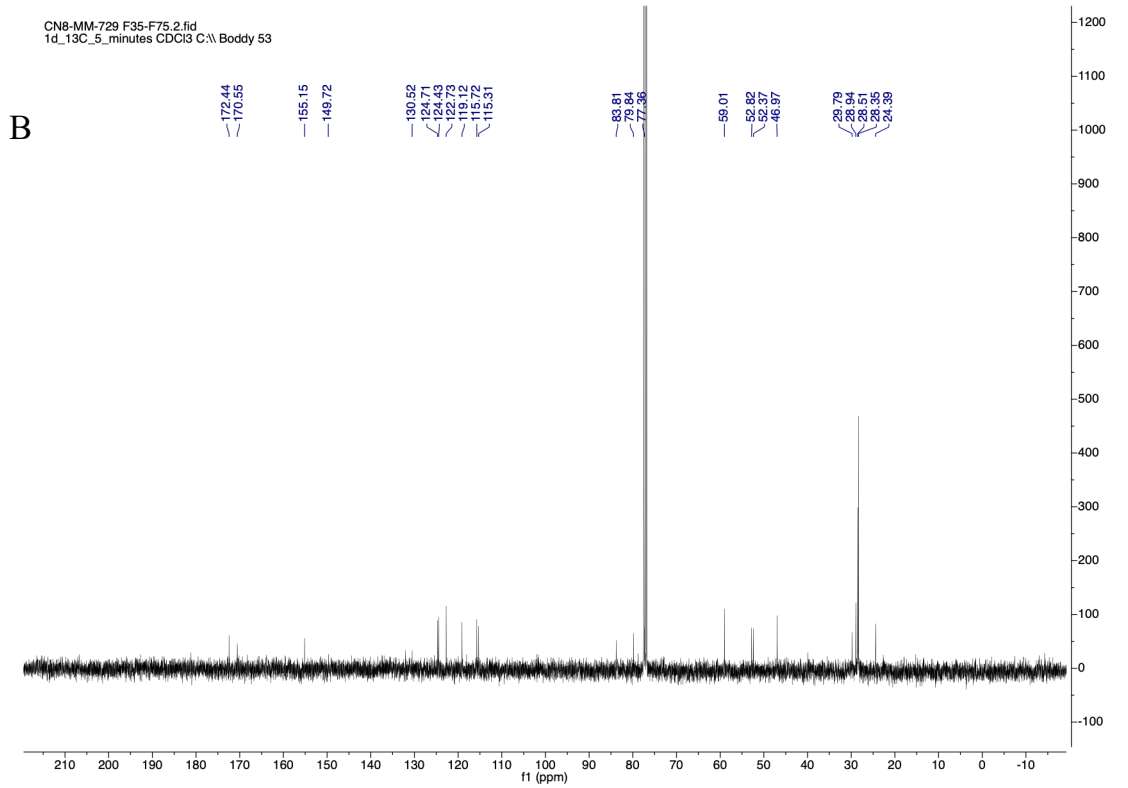
Spectra 3.14 of compound **3.12** (A) ^{1}H NMR (600 MHz, $CDCl_3$) and (B) ^{13}C NMR (101MHz, CDCl3)

A

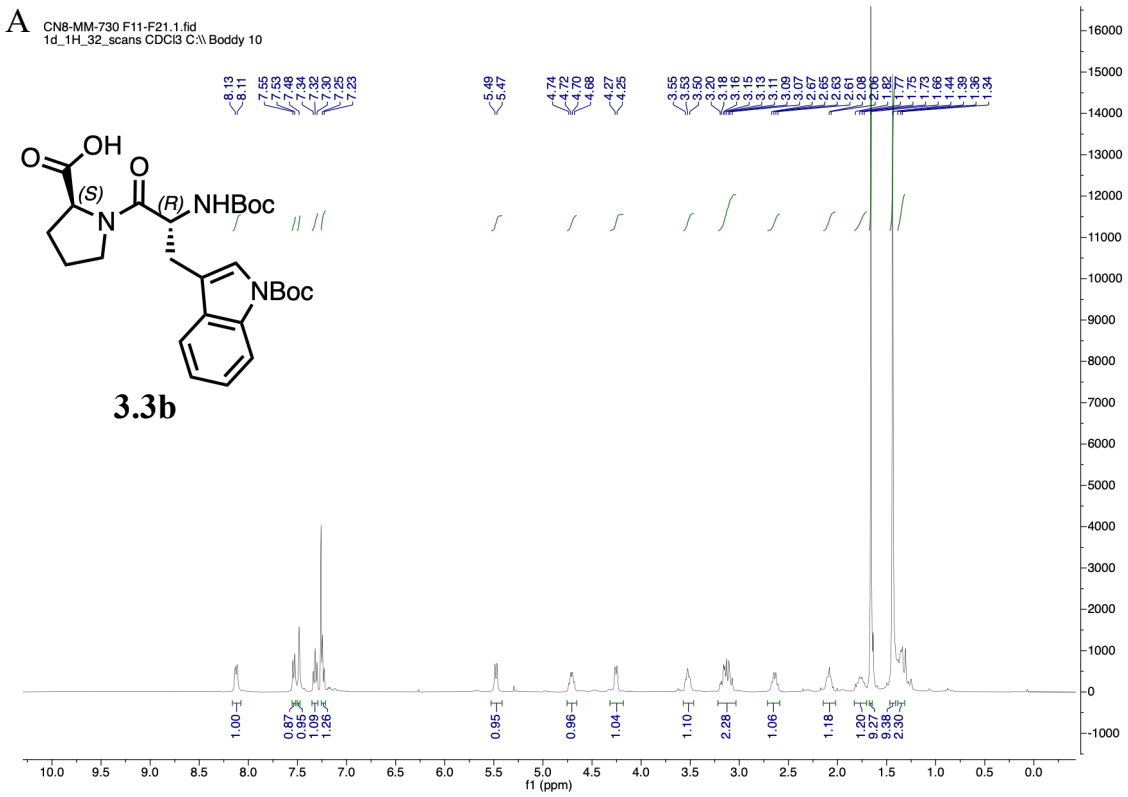


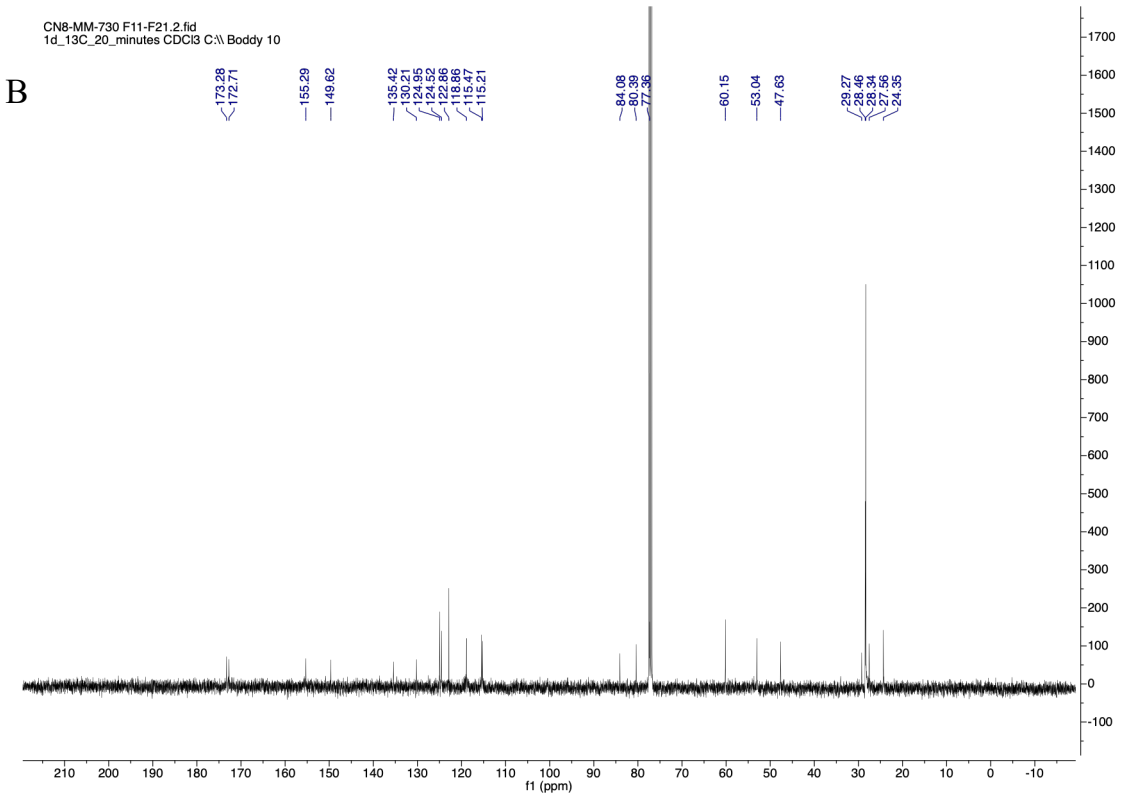
3.3a'

B



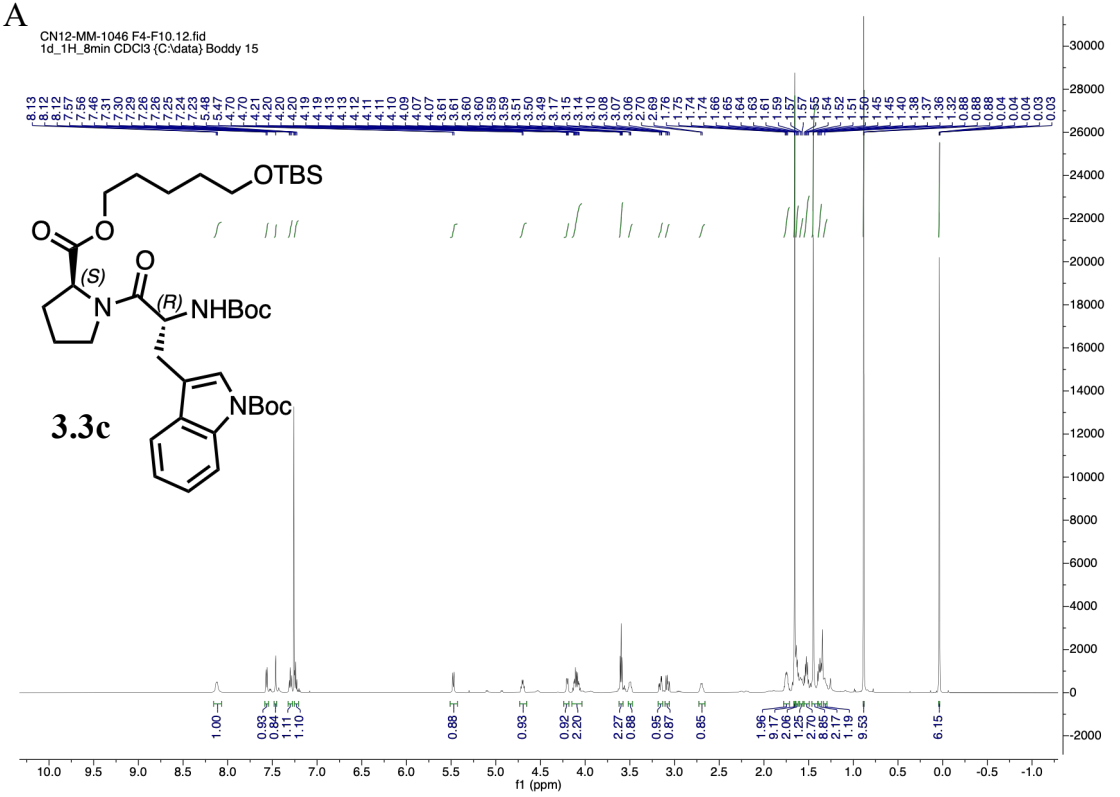
Spectra 3.15 of compound **3.3a'** (A) ^{1}H NMR (600 MHz, $CDCl_3$) and (B) ^{13}C NMR (101MHz, CDCl3)



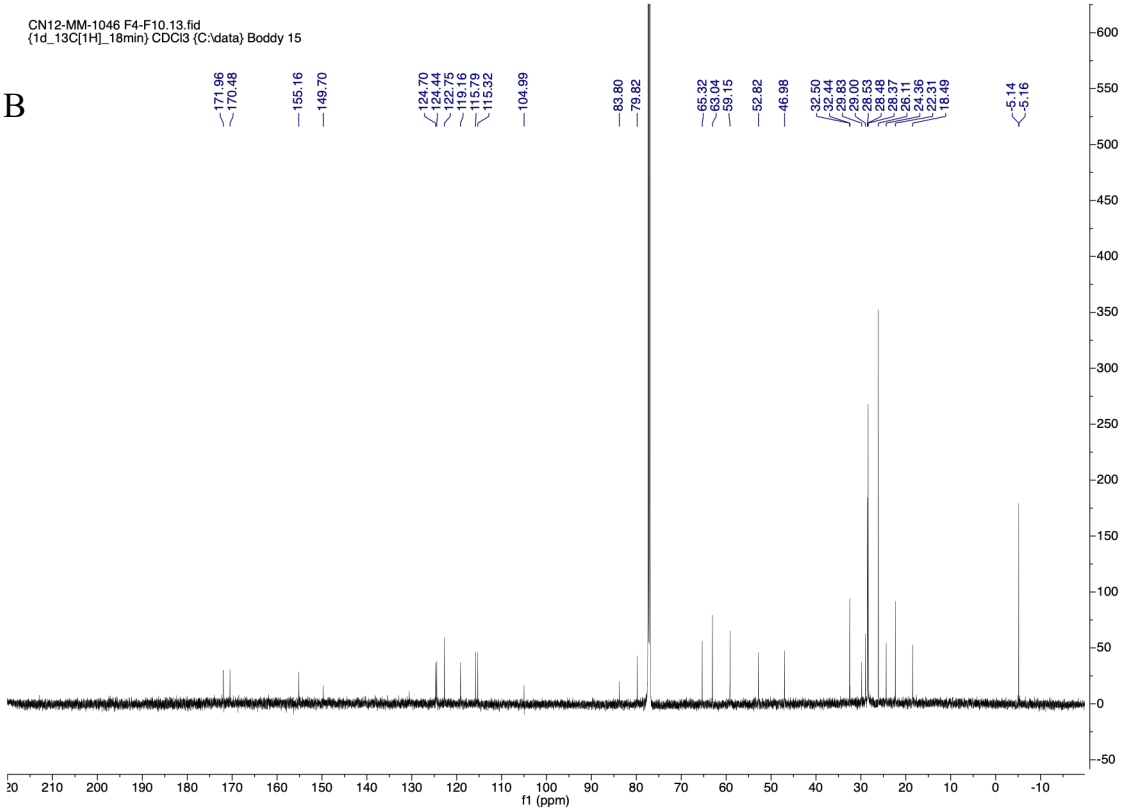


Spectra 3.16 of compound **3.3b** (A) ^{1}H NMR (600 MHz, $CDCl_3$) and (B) ^{13}C NMR (101MHz, CDCl3)

A

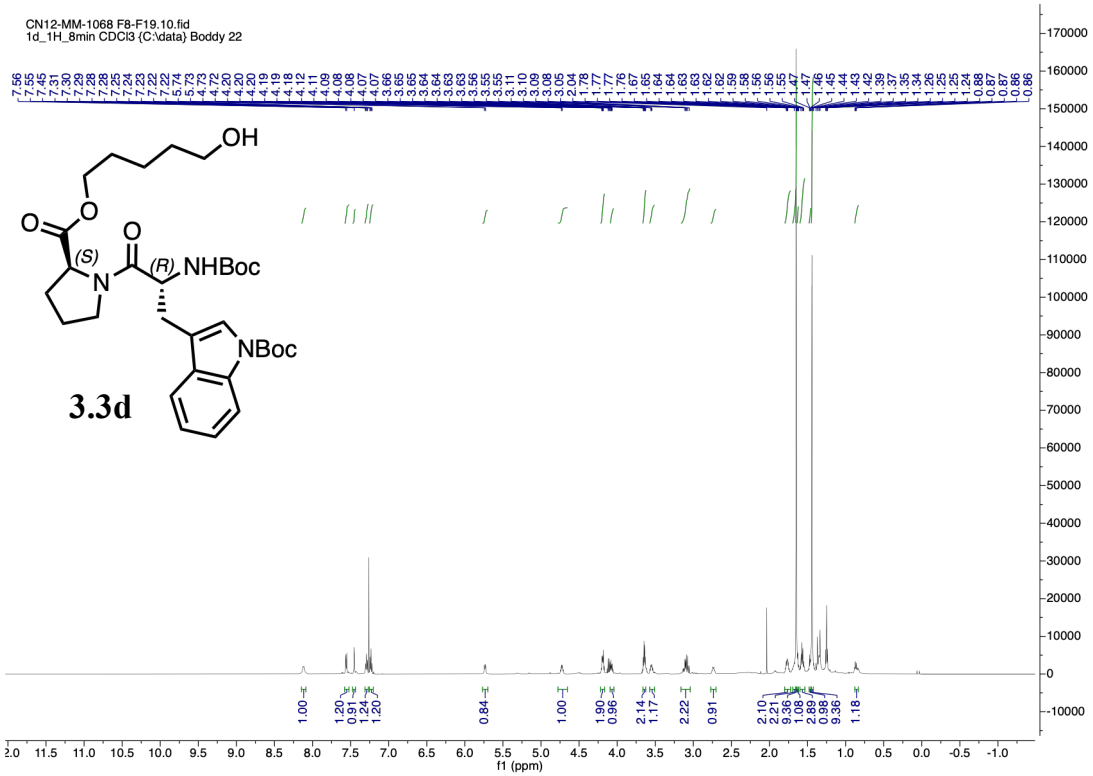


B

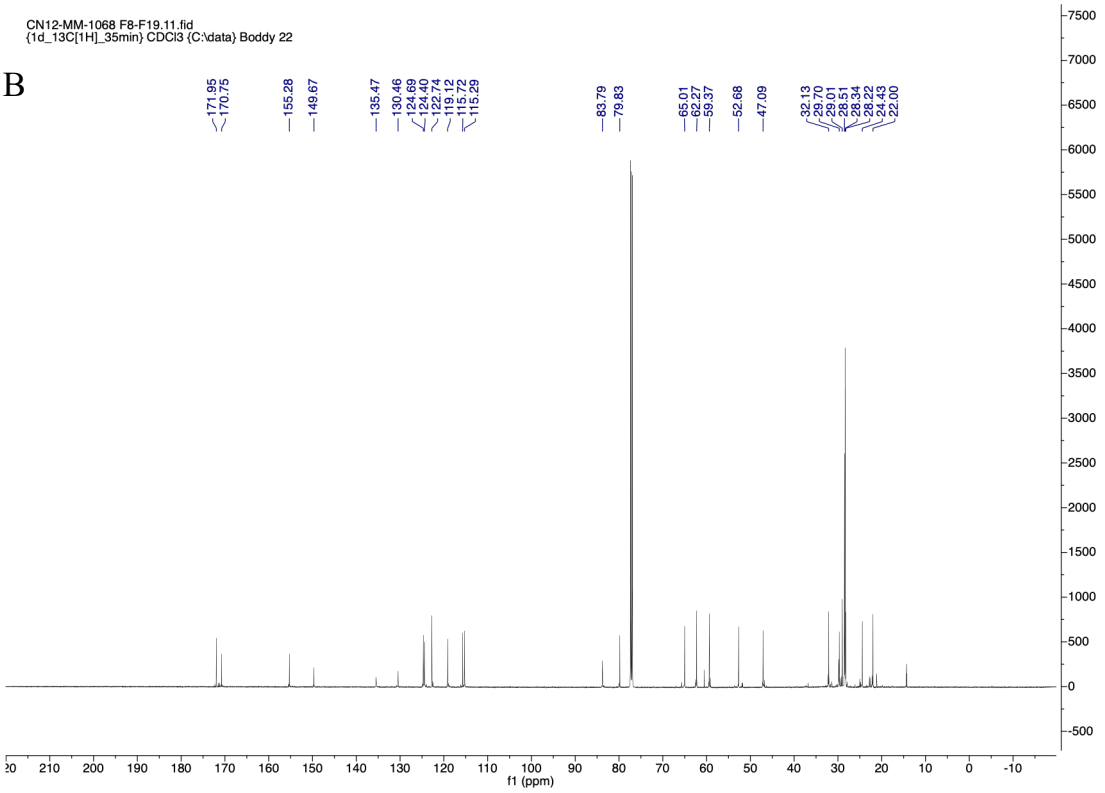


Spectra 3.17 of compound **3.3c** (A) ^{1}H NMR (600 MHz, $CDCl_3$) and (B) ^{13}C NMR (101MHz, CDCl3)

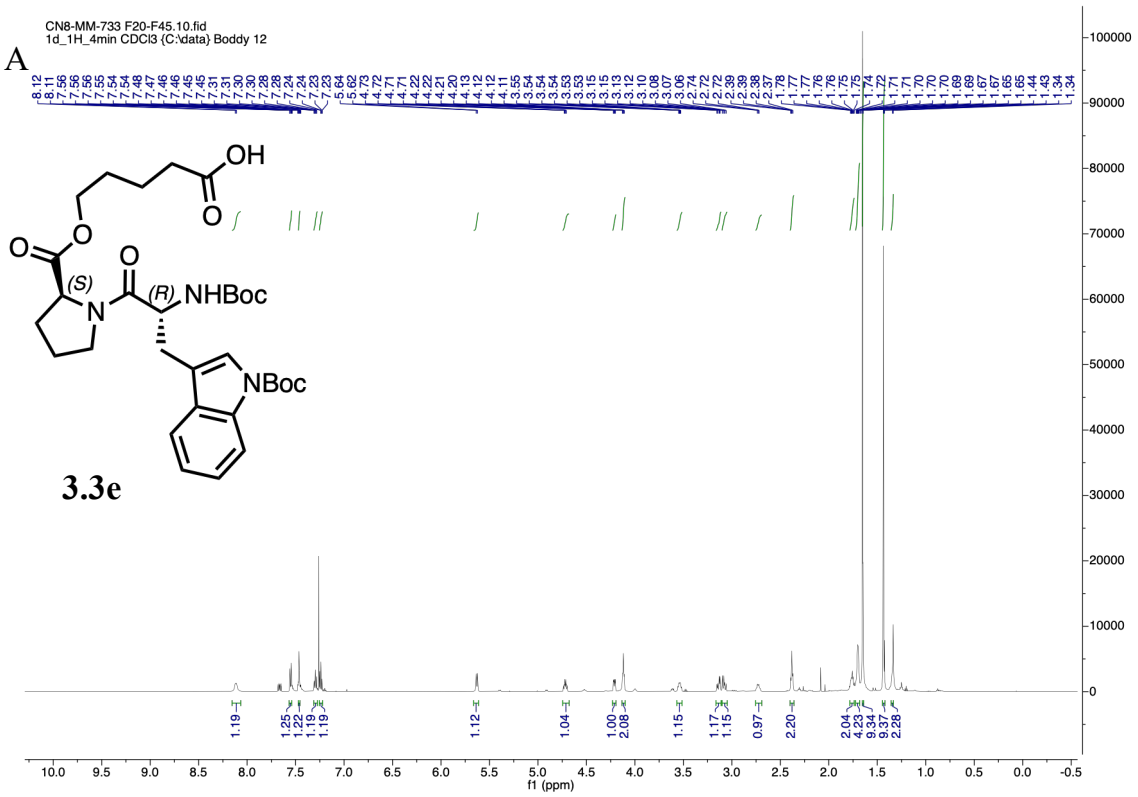
A

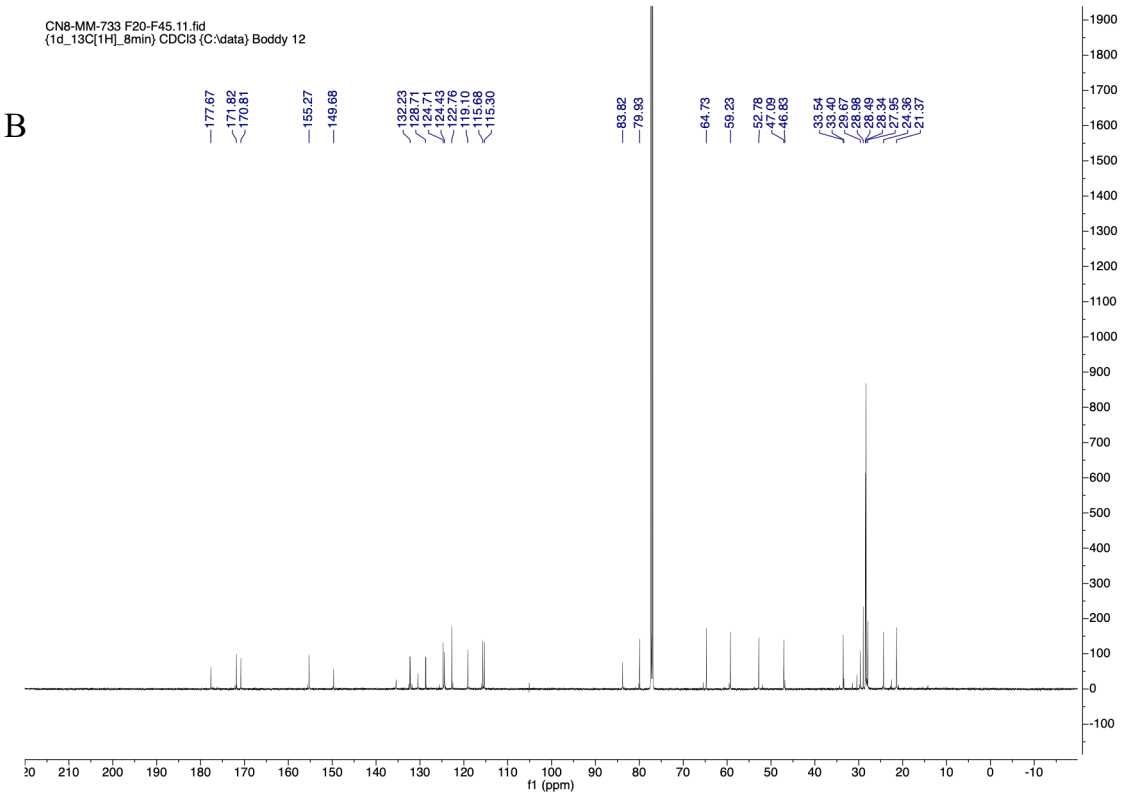


B



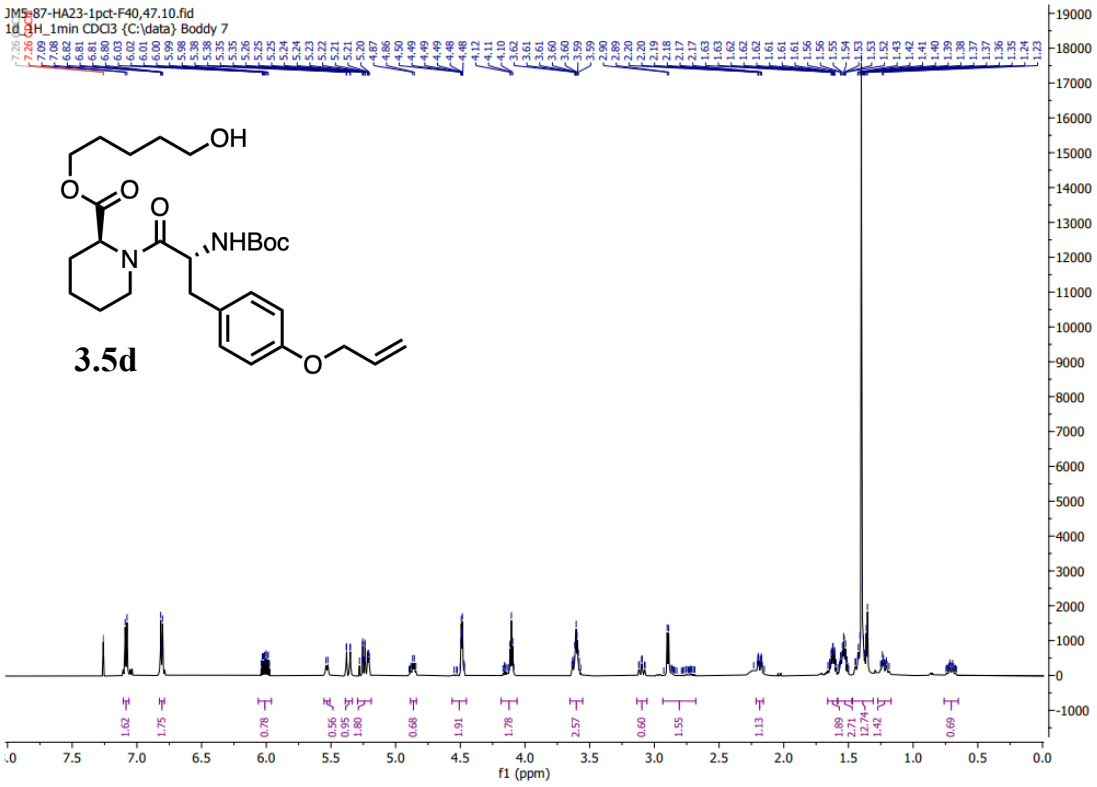
Spectra 3.18 of compound **3.3d** (A) ^{1}H NMR (600 MHz, $CDCl_3$) and (B) ^{13}C NMR (101MHz, CDCl3)



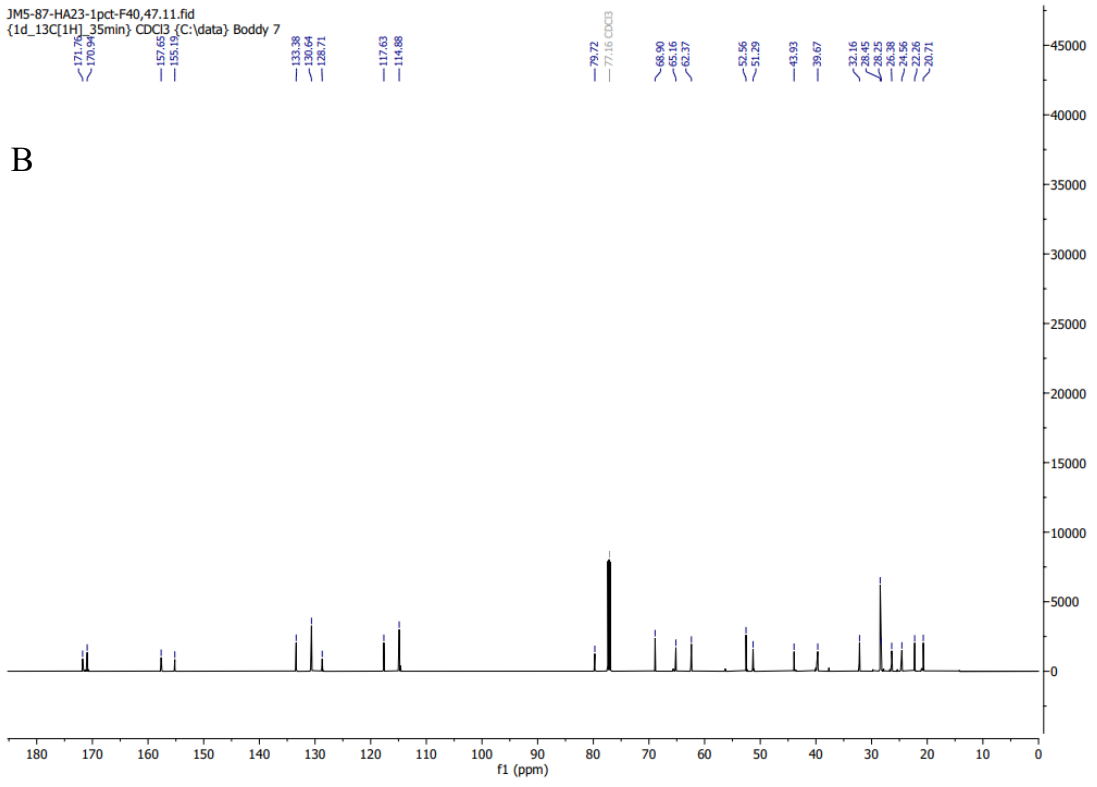


Spectra 3.19 of compound **3.3e** (A) ^{1}H NMR (600 MHz, $CDCl_3$) and (B) ^{13}C NMR (101MHz, CDCl3)

A

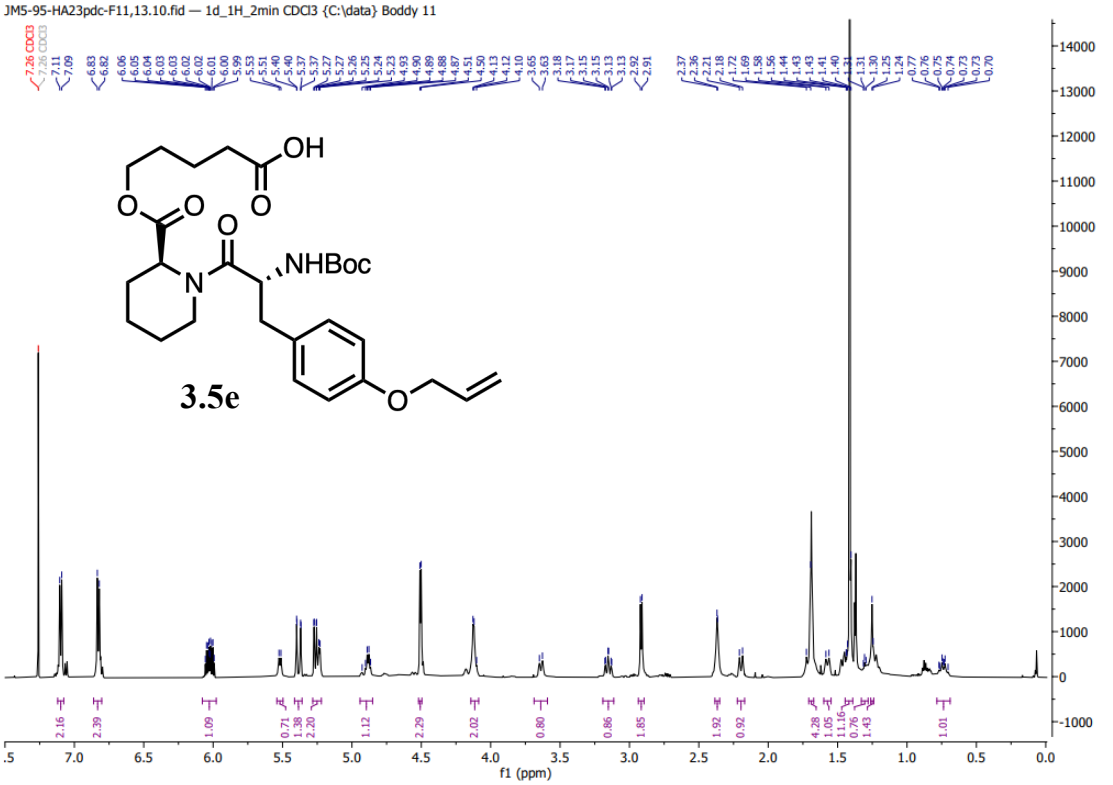


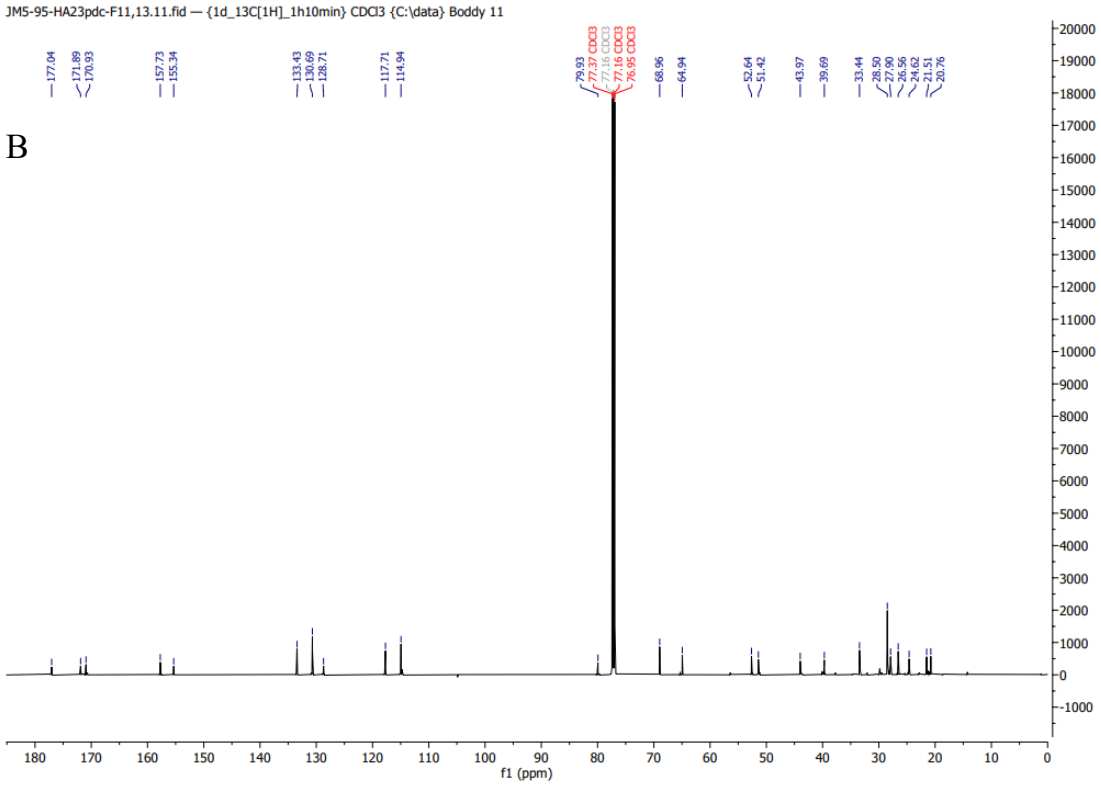
B



Spectra 3.20 of compound **3.5** (A) ^{1}H NMR (600 MHz, $CDCl_3$) and (B) ^{13}C NMR (101MHz, CDCl3)

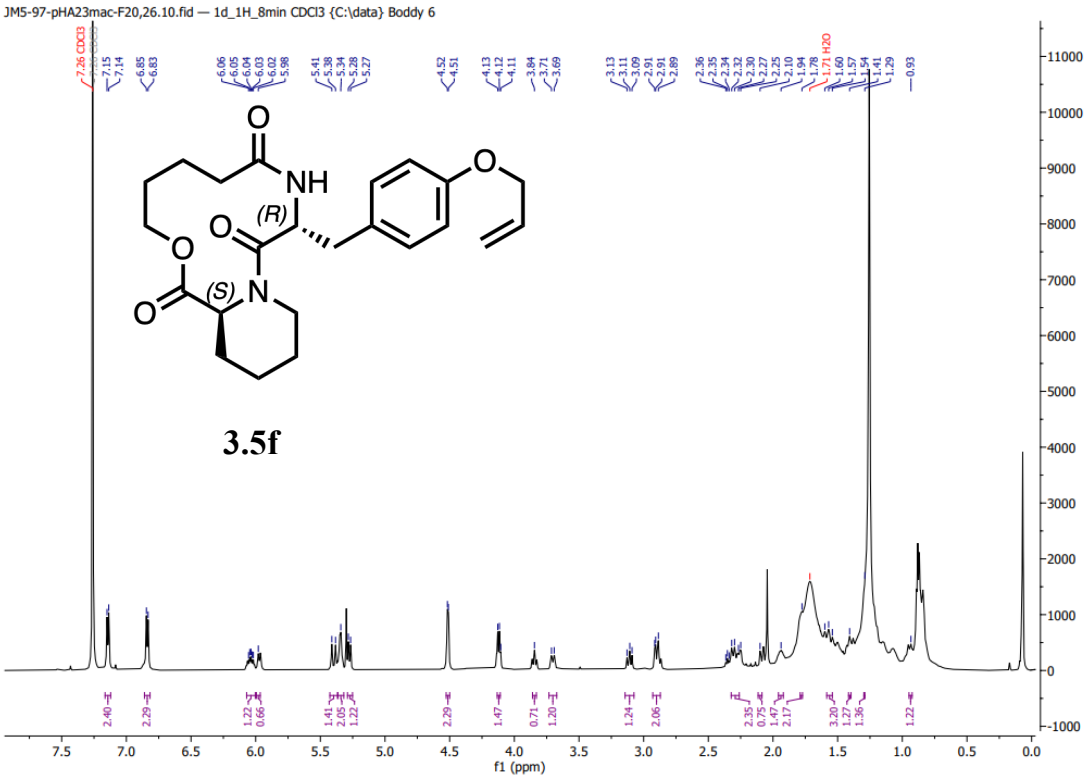
A



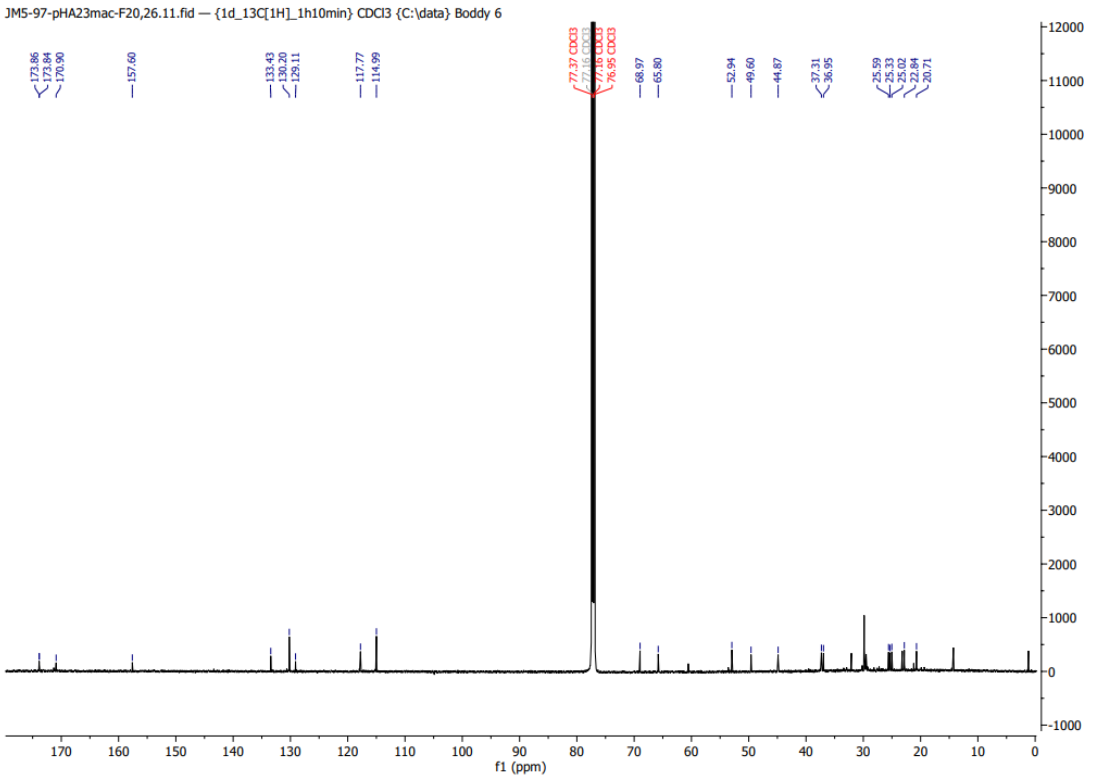


Spectra 3.21 of compound **3.5** (A) ^{1}H NMR (600 MHz, $CDCl_3$) and (B) ^{13}C NMR (101MHz, CDCl3)

A

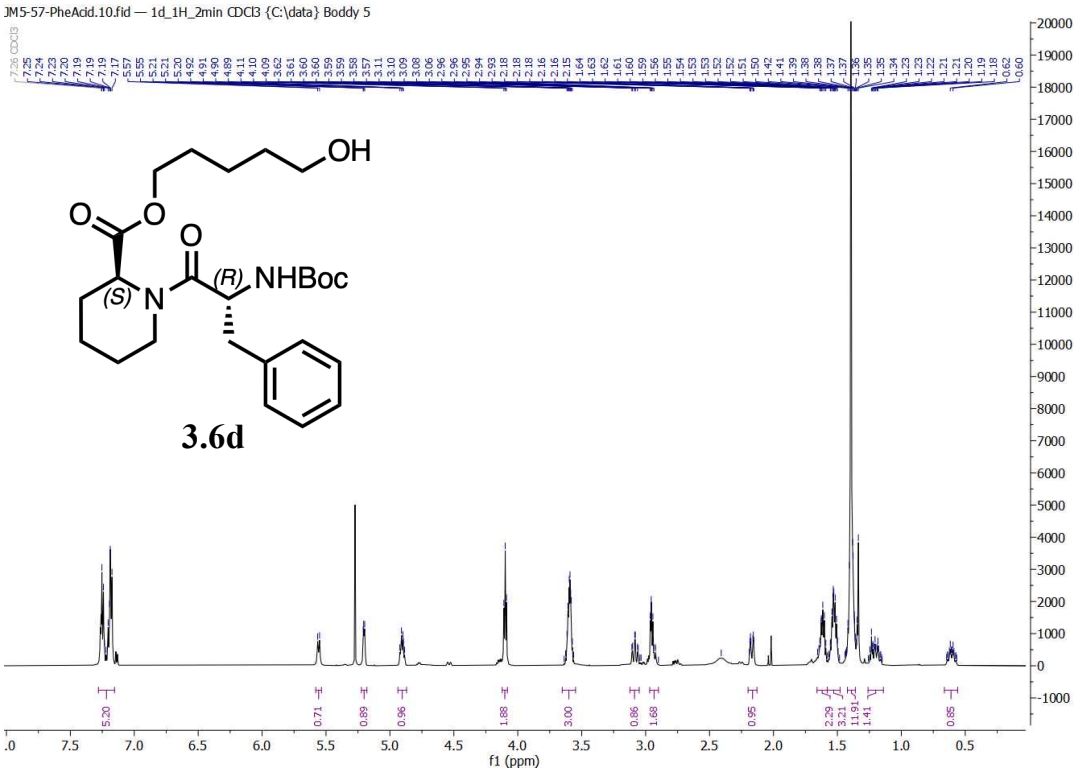


B

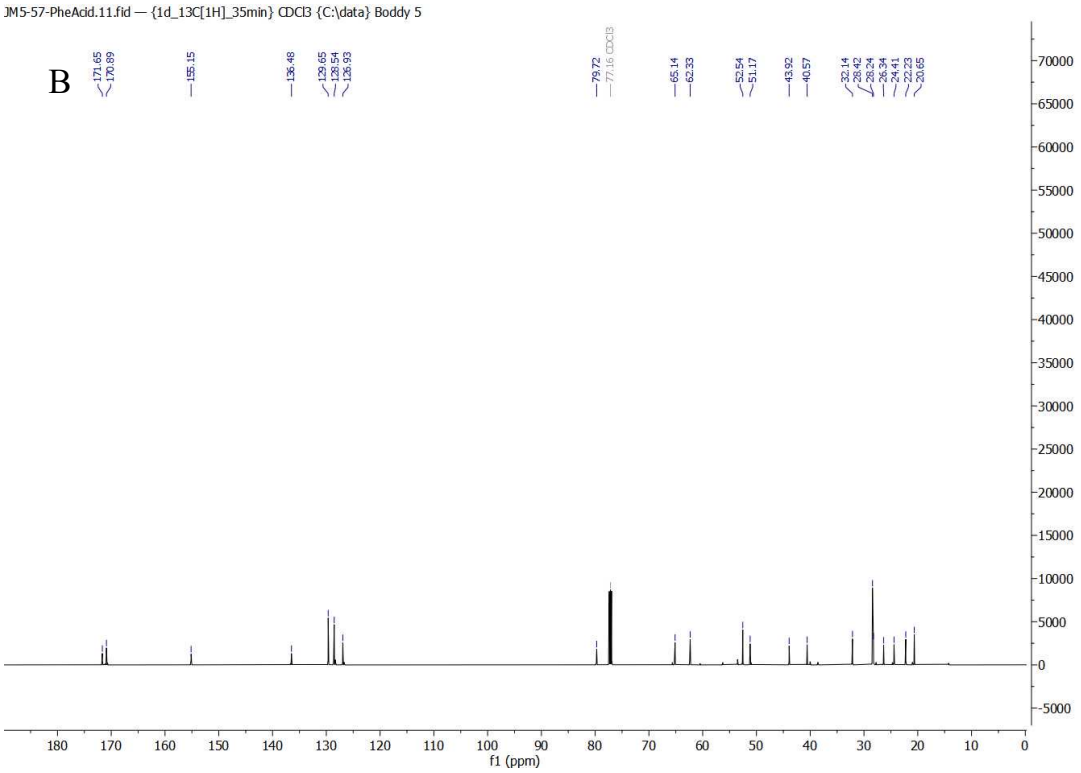


Spectra 3.22 of compound **3.5** (A) ^{1}H NMR (600 MHz, $CDCl_3$) and (B) ^{13}C NMR (101MHz, CDCl3)

A

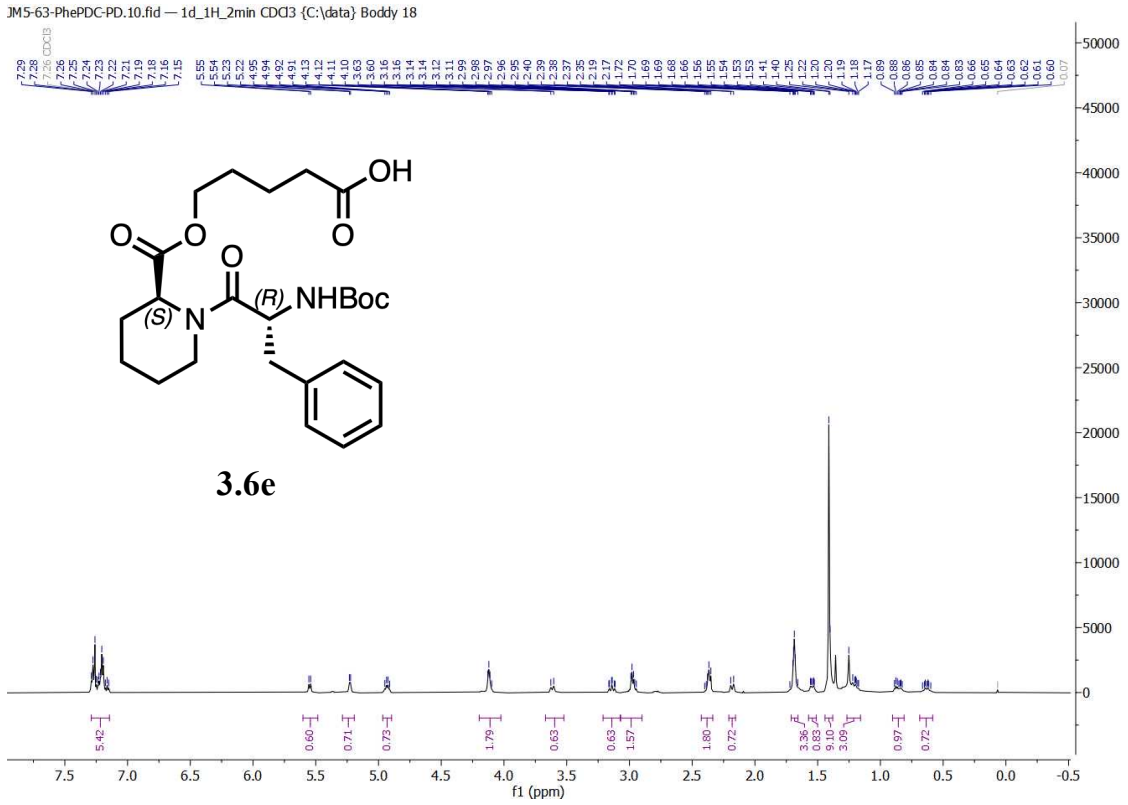


B



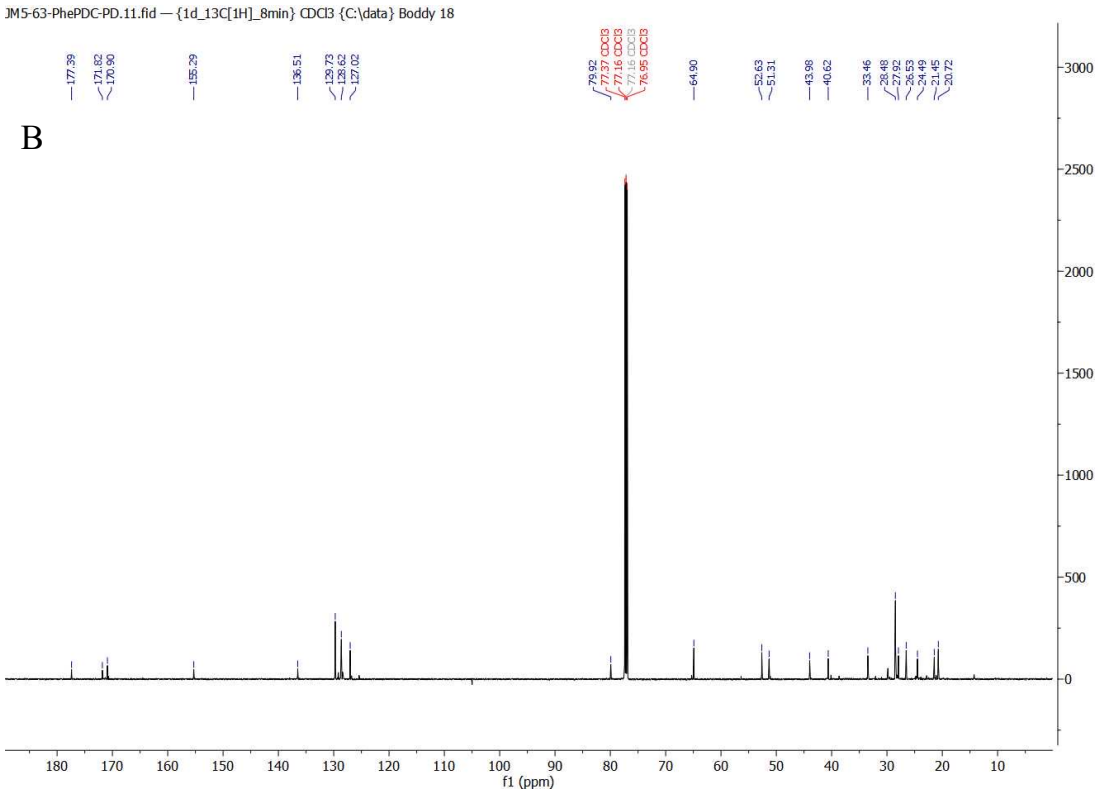
Spectra 3.23 of compound **3.6d** (A) ^{1}H NMR (600 MHz, $CDCl_3$) and (B) ^{13}C NMR (101MHz, CDCl3)

A

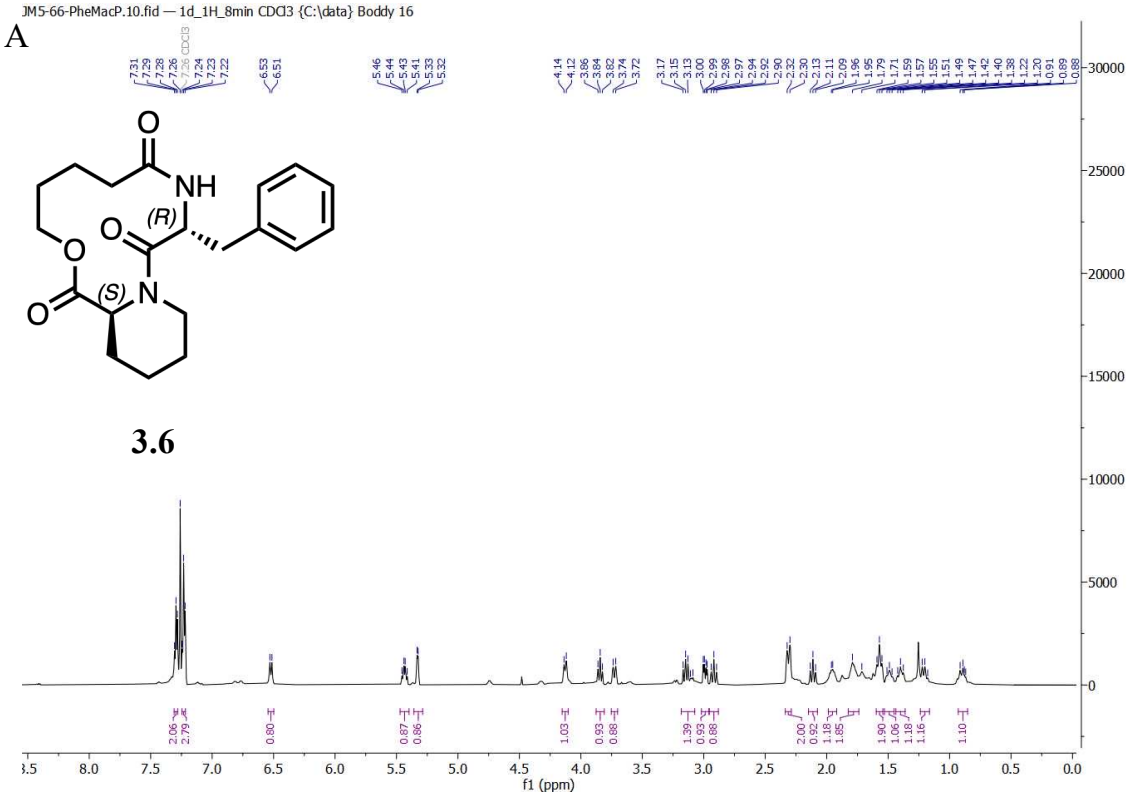


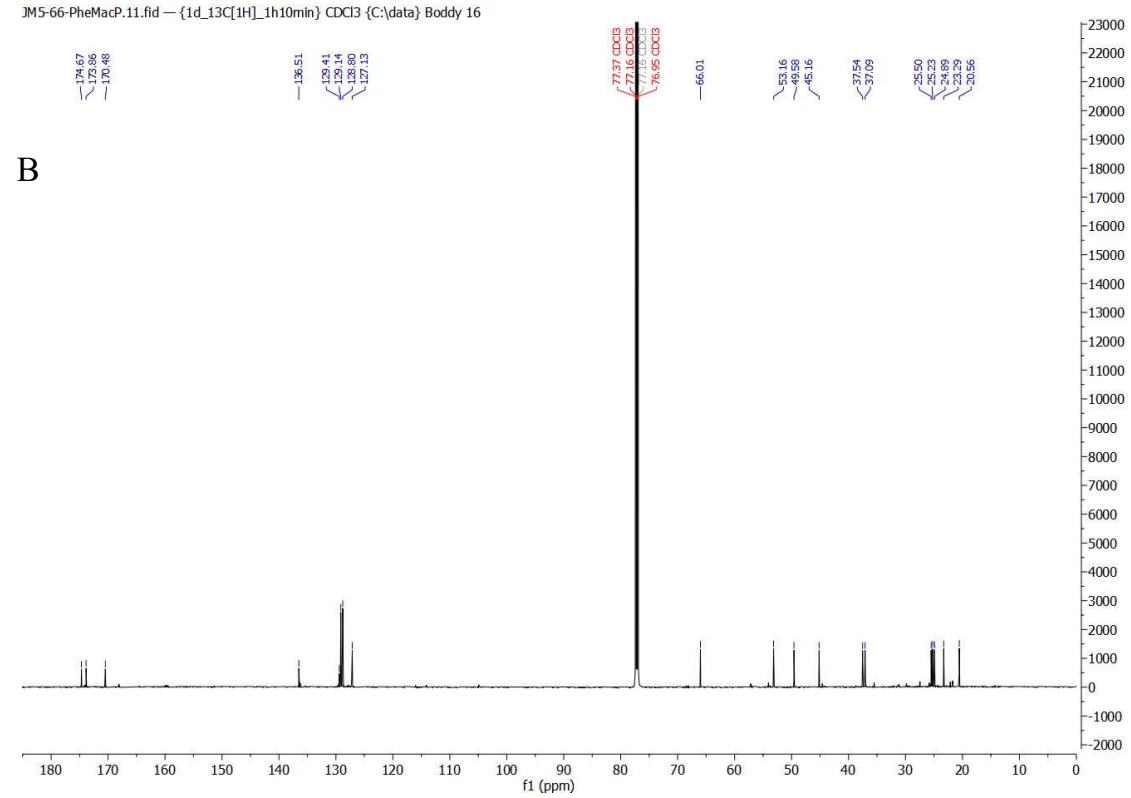
3.6e

B



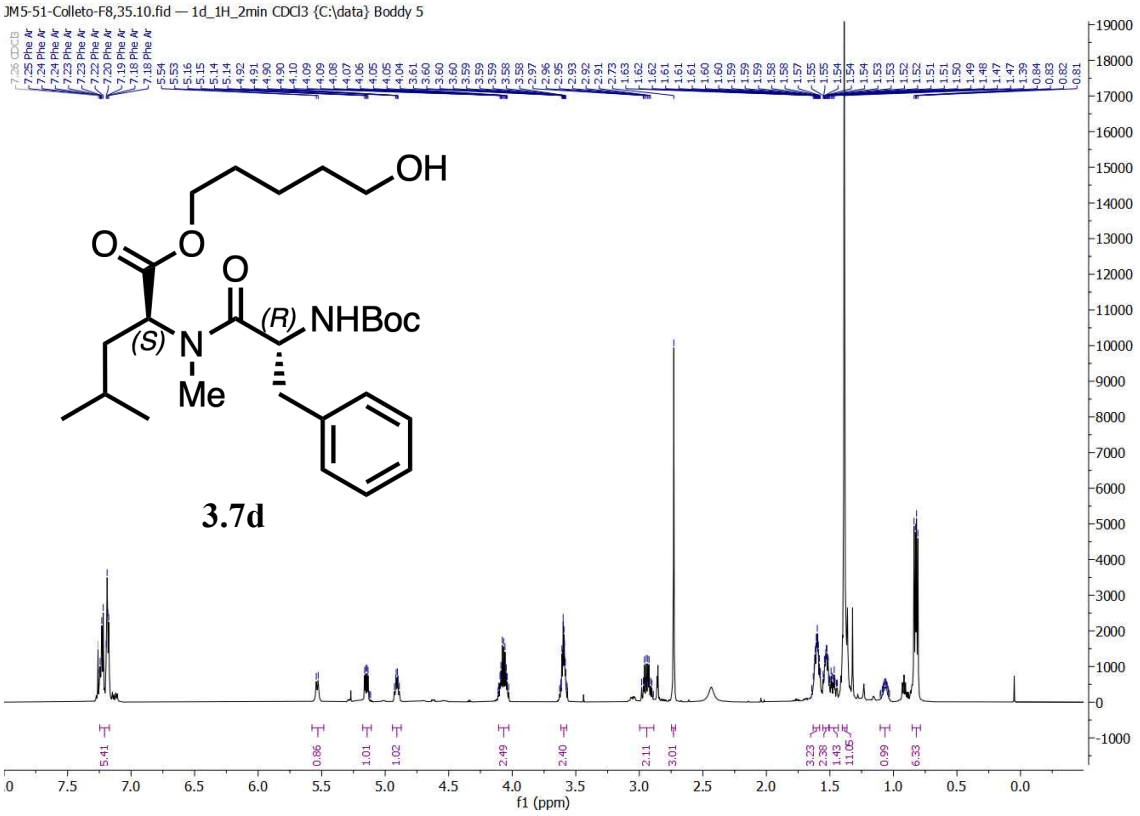
Spectra 3.24 of compound **3.6e** (A) ^{1}H NMR (600 MHz, $CDCl_3$) and (B) ^{13}C NMR (101MHz, CDCl3)



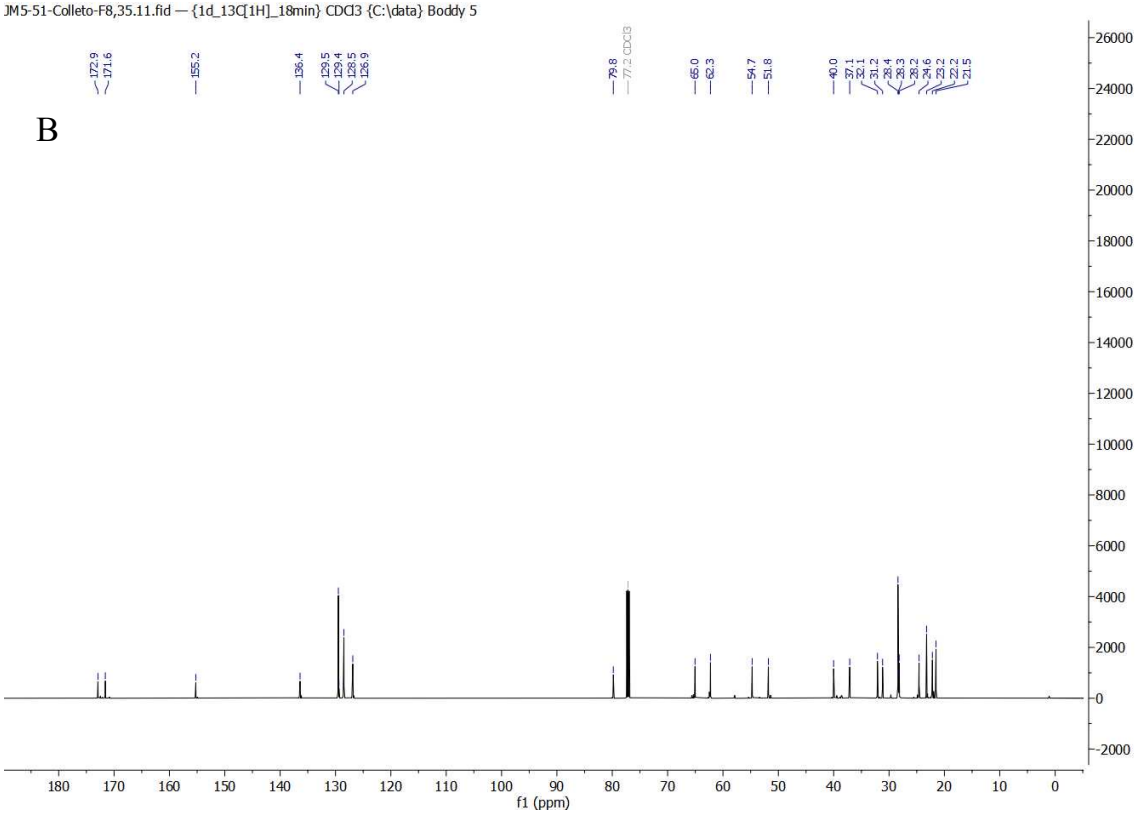


Spectra 3.25 of compound **3.6** (A) ^{1}H NMR (600 MHz, $CDCl_3$) and (B) ^{13}C NMR (101MHz, CDCl3)

A

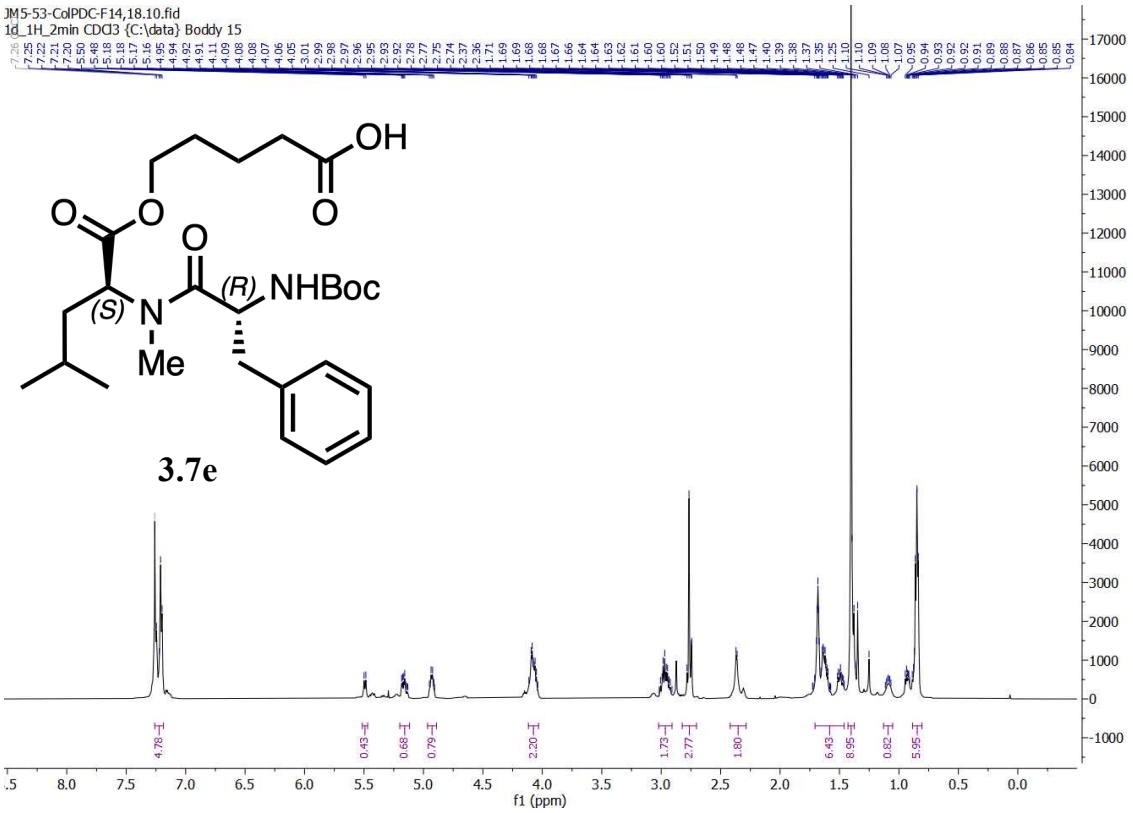


B

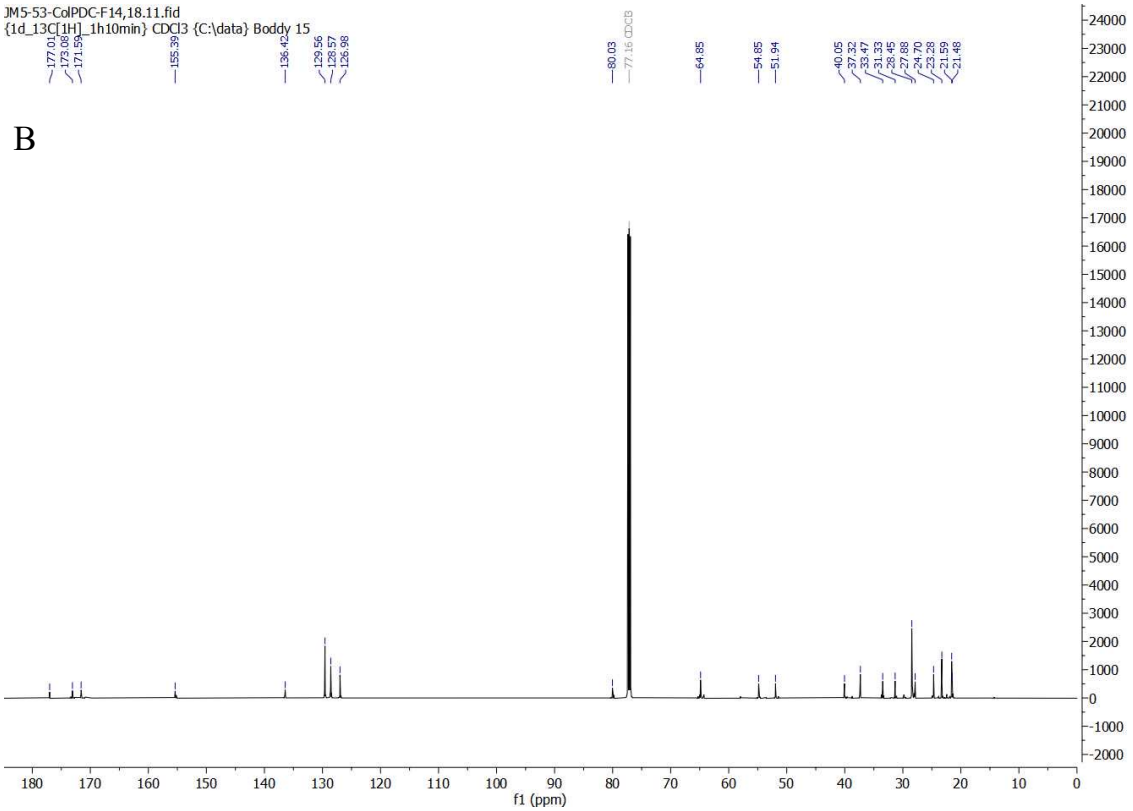


Spectra 3.26 of compound **3.7d** (A) ^{1}H NMR (600 MHz, $CDCl_3$) and (B) ^{13}C NMR (101MHz, CDCl3)

A

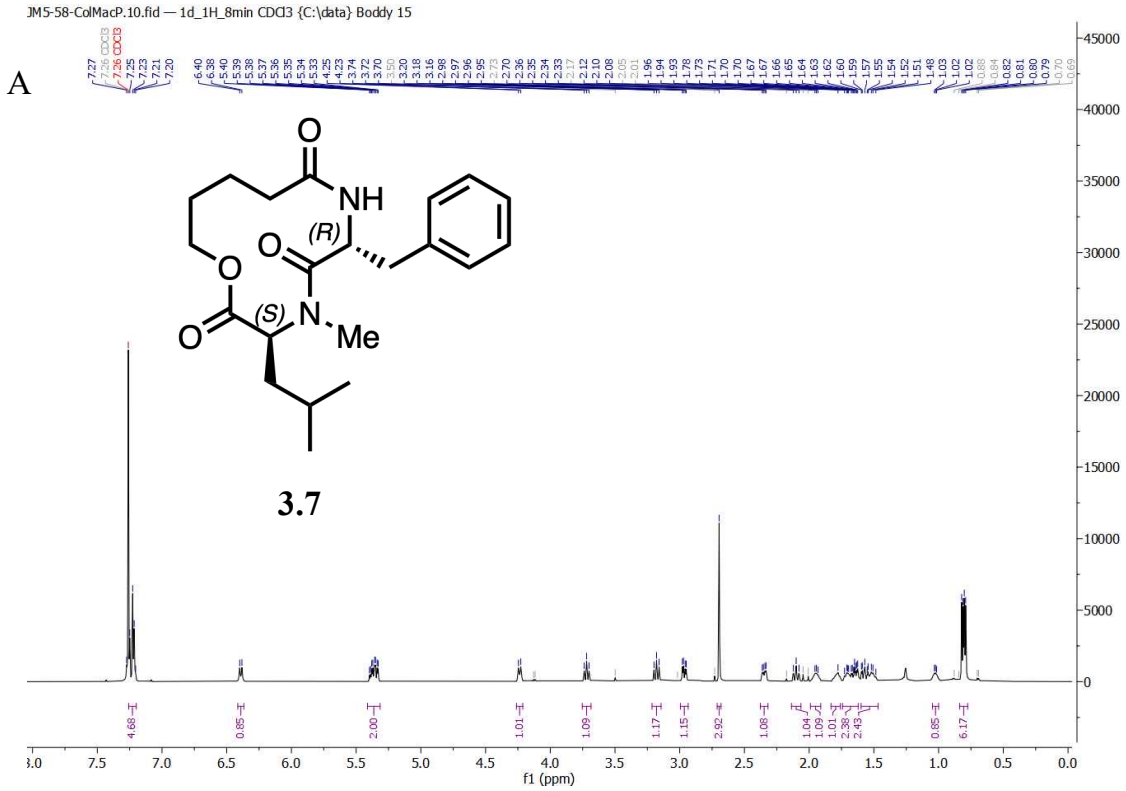


B

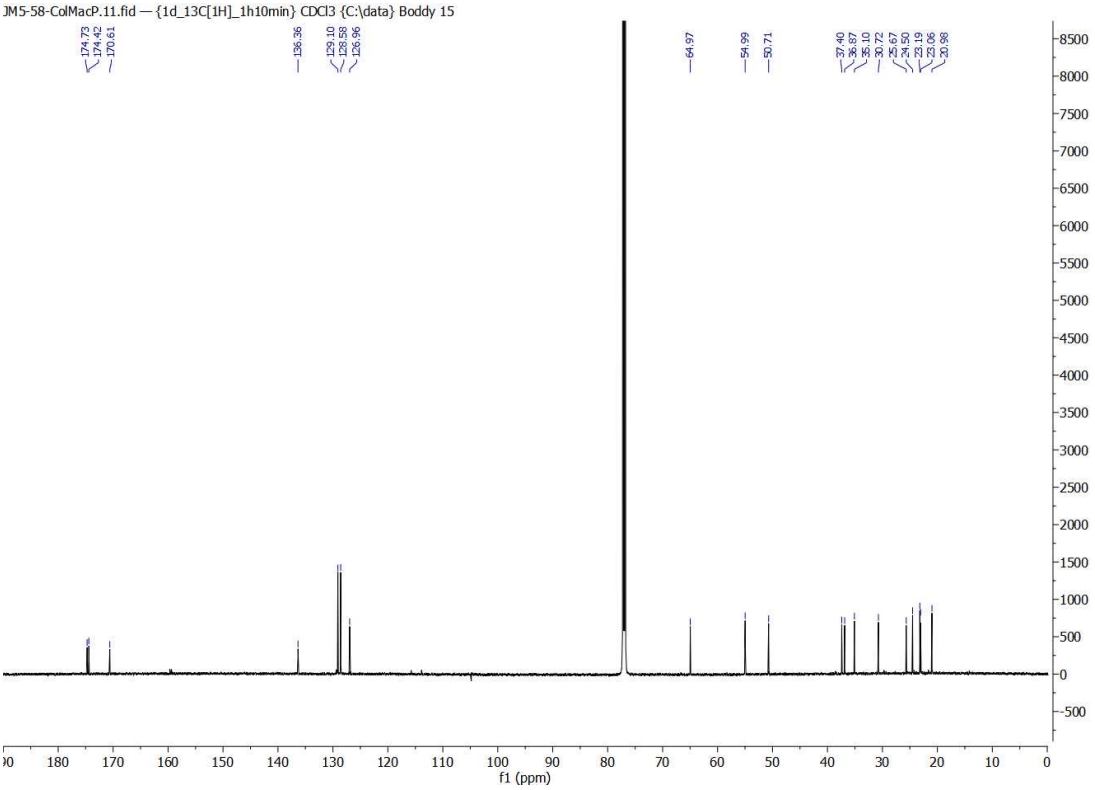


Spectra 3.27 of compound **3.7e** (A) ^{1}H NMR (600 MHz, $CDCl_3$) and (B) ^{13}C NMR (101MHz, CDCl3)

A

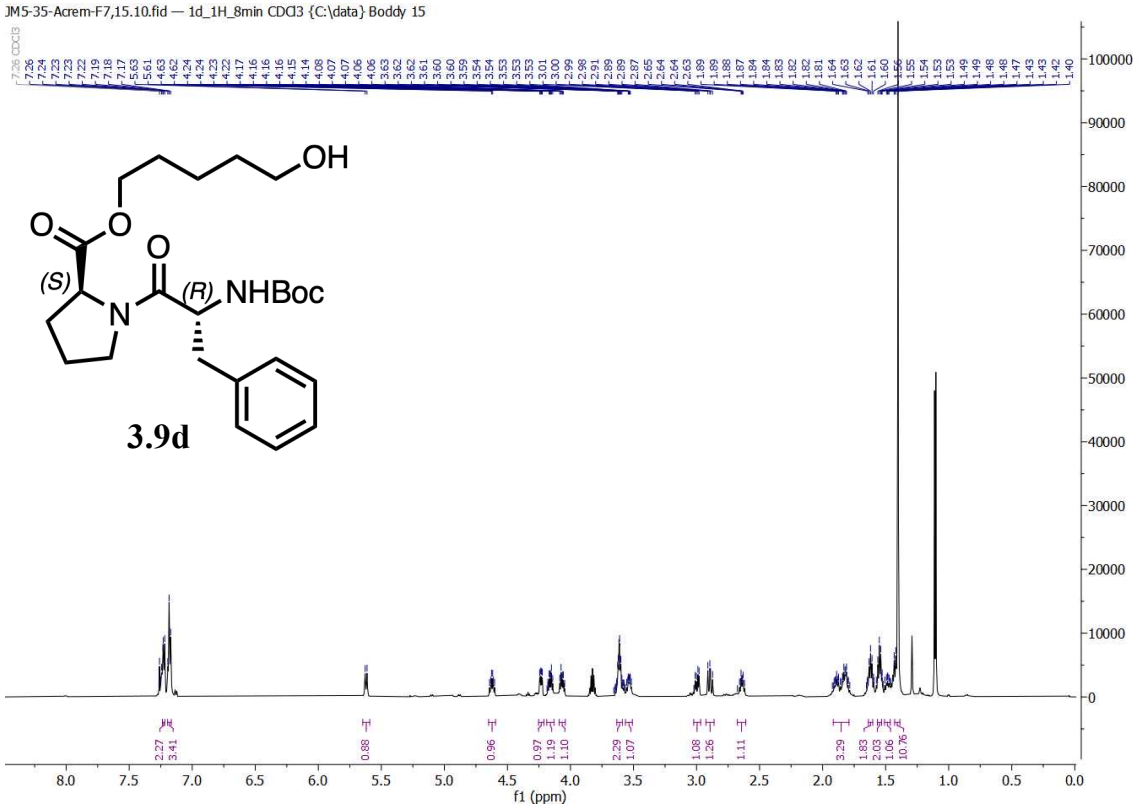


B

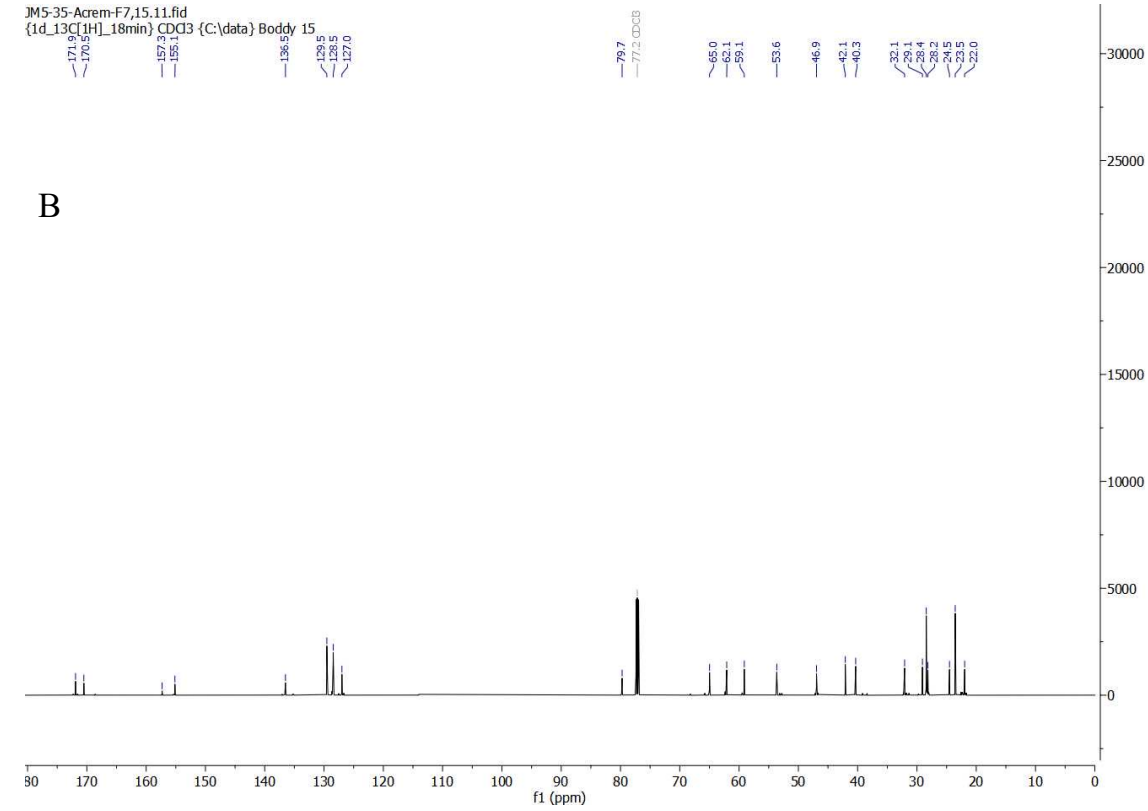


Spectra 3.28 of compound **3.7** (A) ^{1}H NMR (600 MHz, $CDCl_3$) and (B) ^{13}C NMR (101MHz, CDCl3)

A

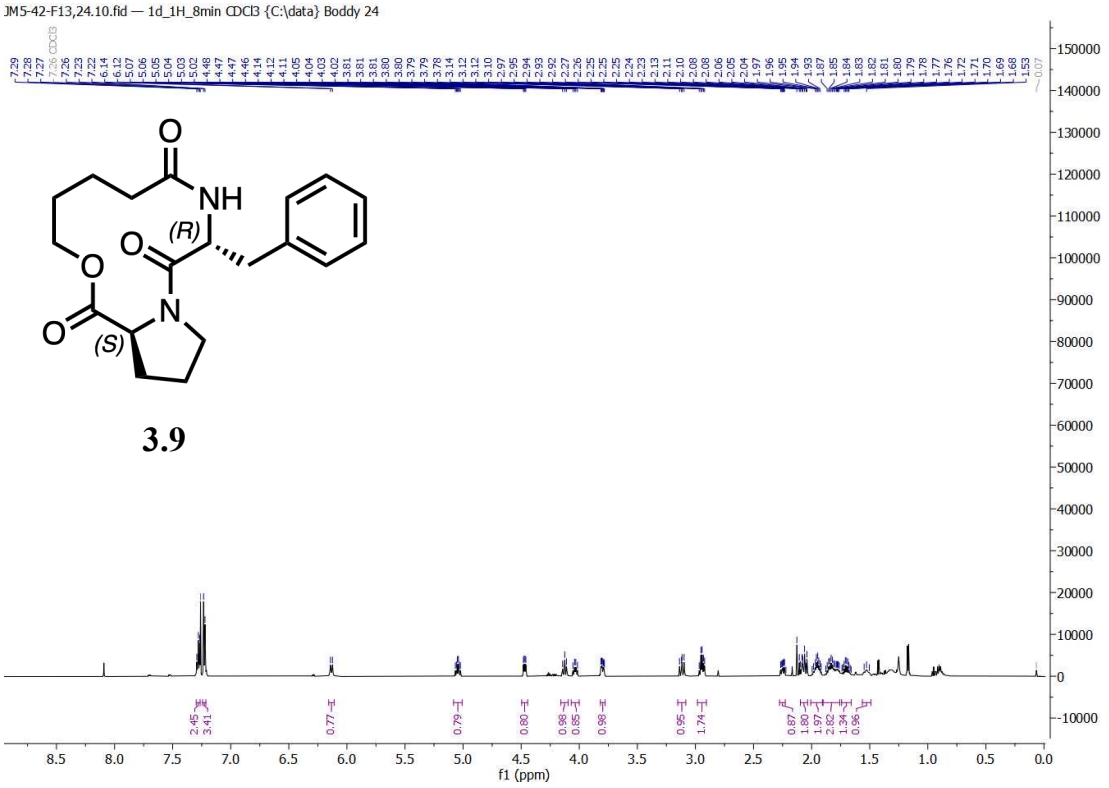


B



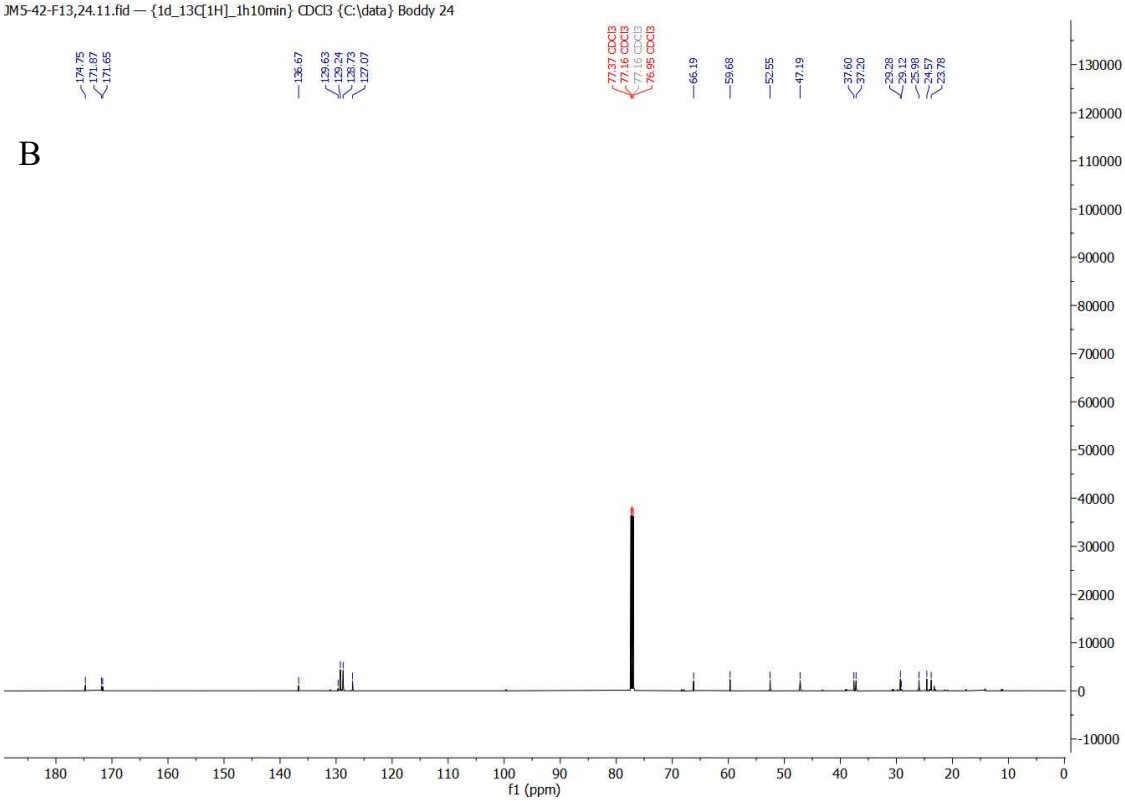
Spectra 3.29 of compound **3.9d** (A) ^{1}H NMR (600 MHz, $CDCl_3$) and (B) ^{13}C NMR (101MHz, CDCl3)

A



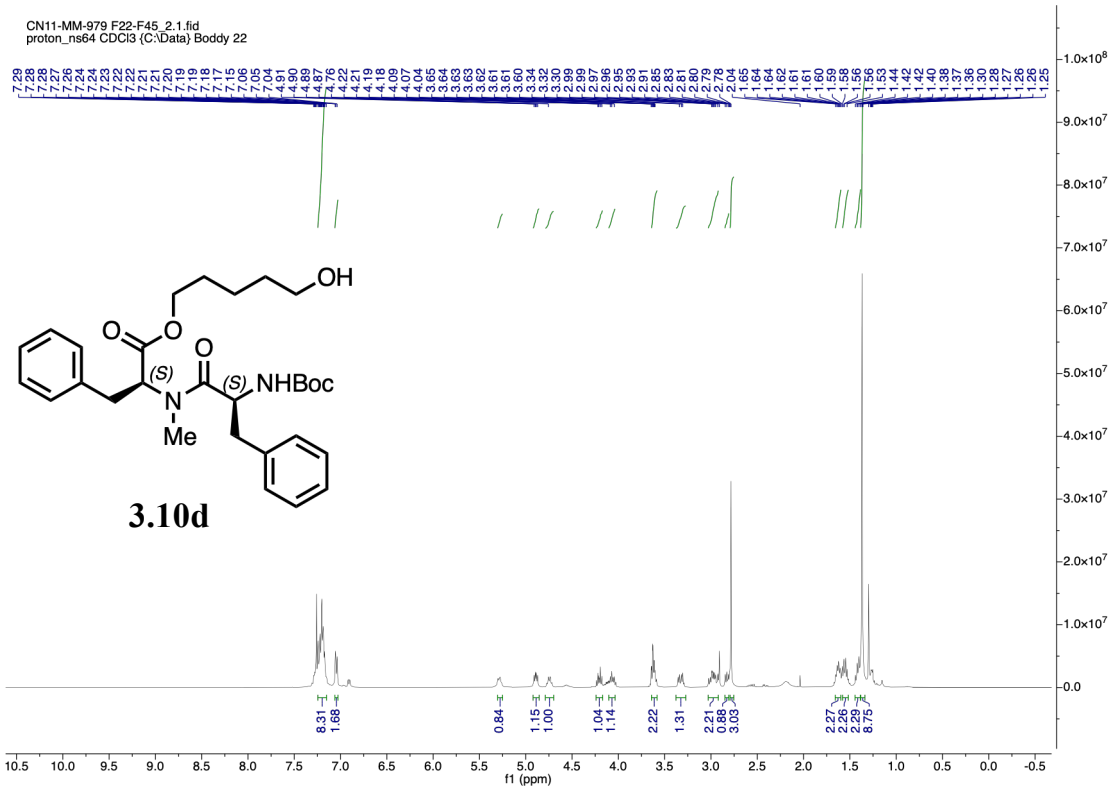
3.9

B

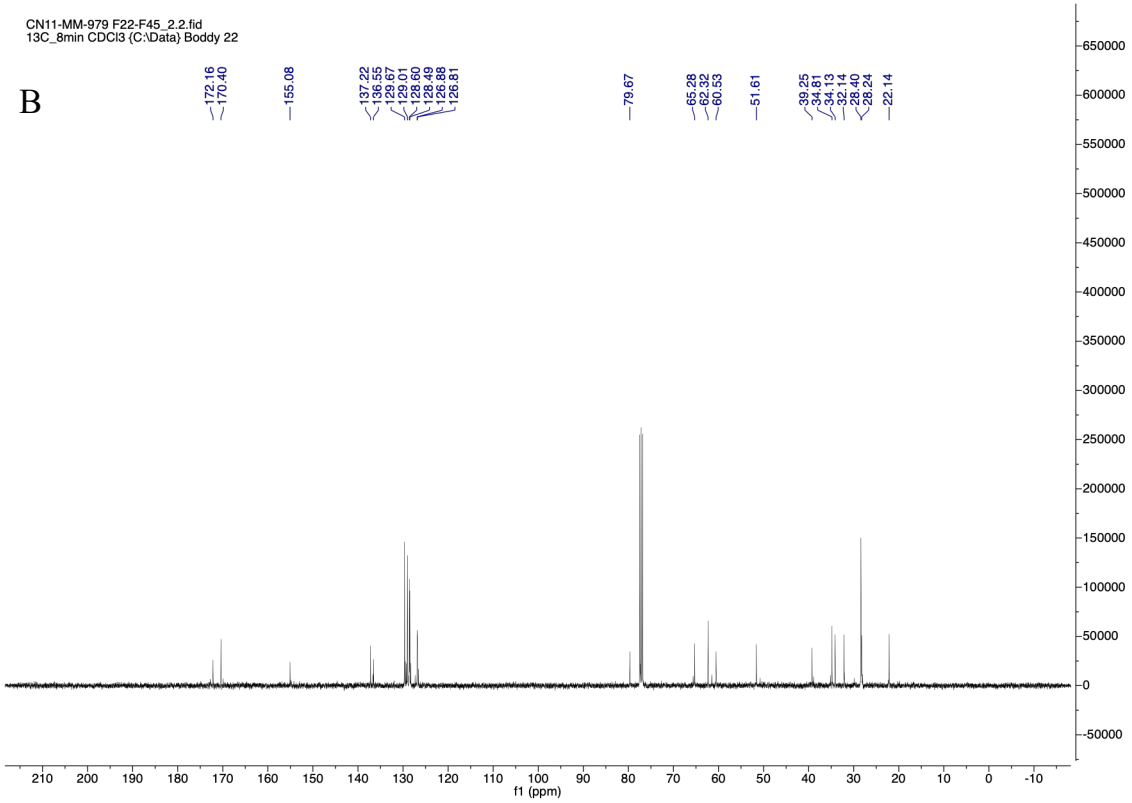


Spectra 3.30 of compound **3.9** (A) ^{1}H NMR (600 MHz, $CDCl_3$) and (B) ^{13}C NMR (101MHz, CDCl3)

A

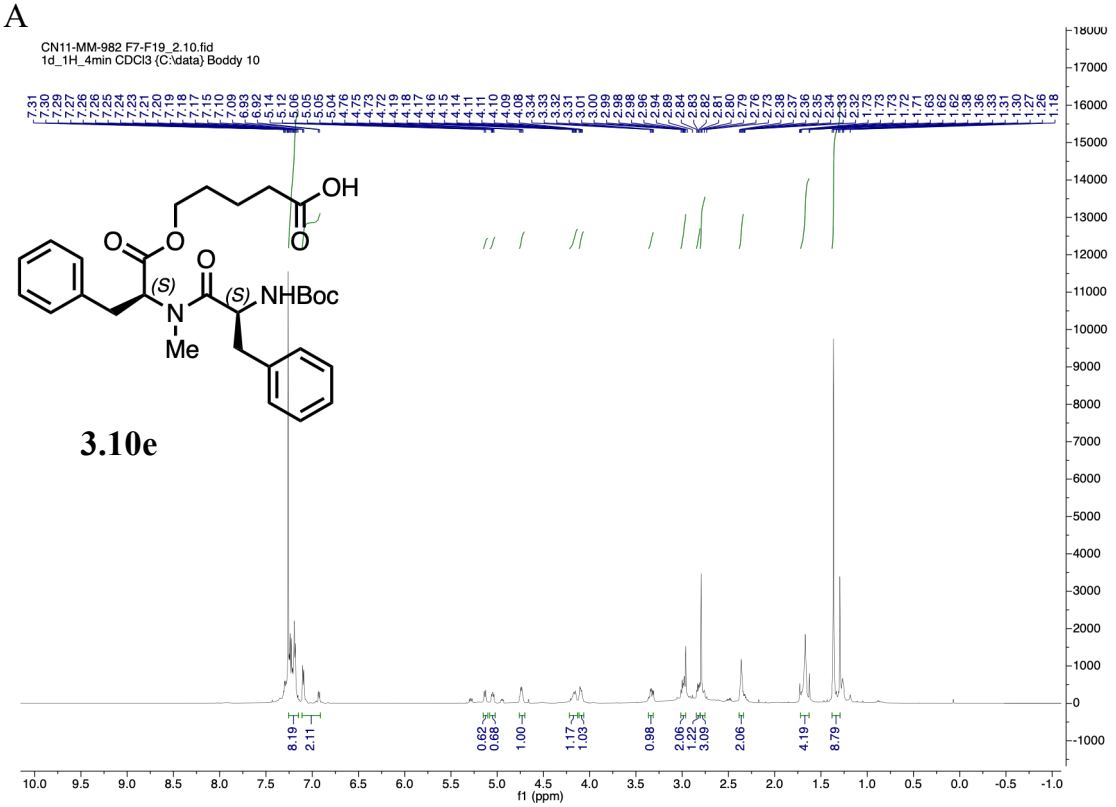


B

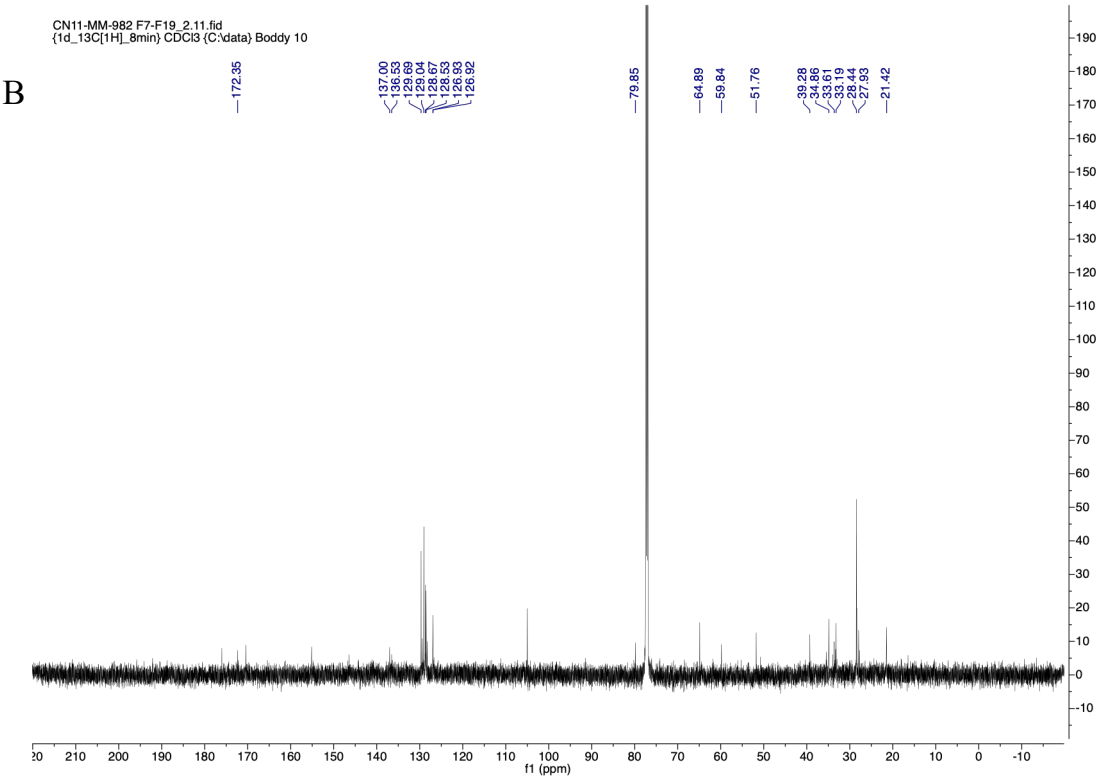


Spectra 3.31 of compound **3.10d** (A) ^{1}H NMR (600 MHz, $CDCl_3$) and (B) ^{13}C NMR (101MHz, CDCl3)

A

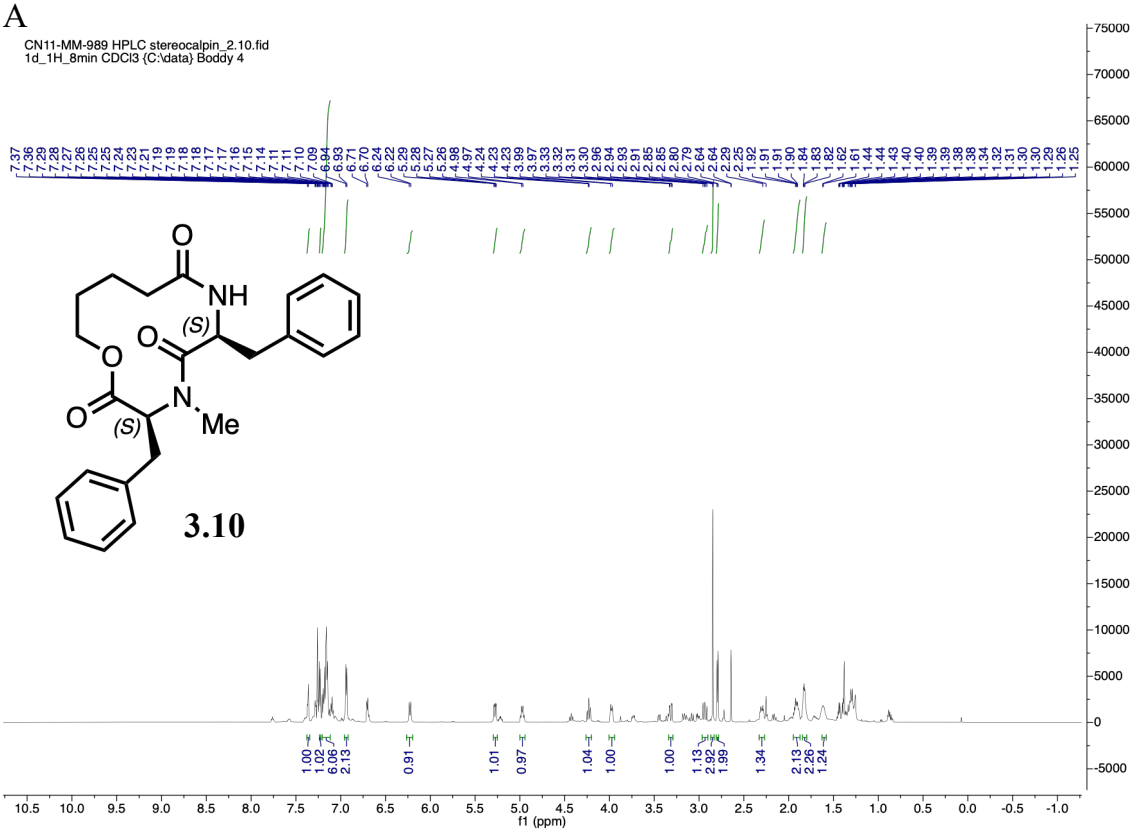


B

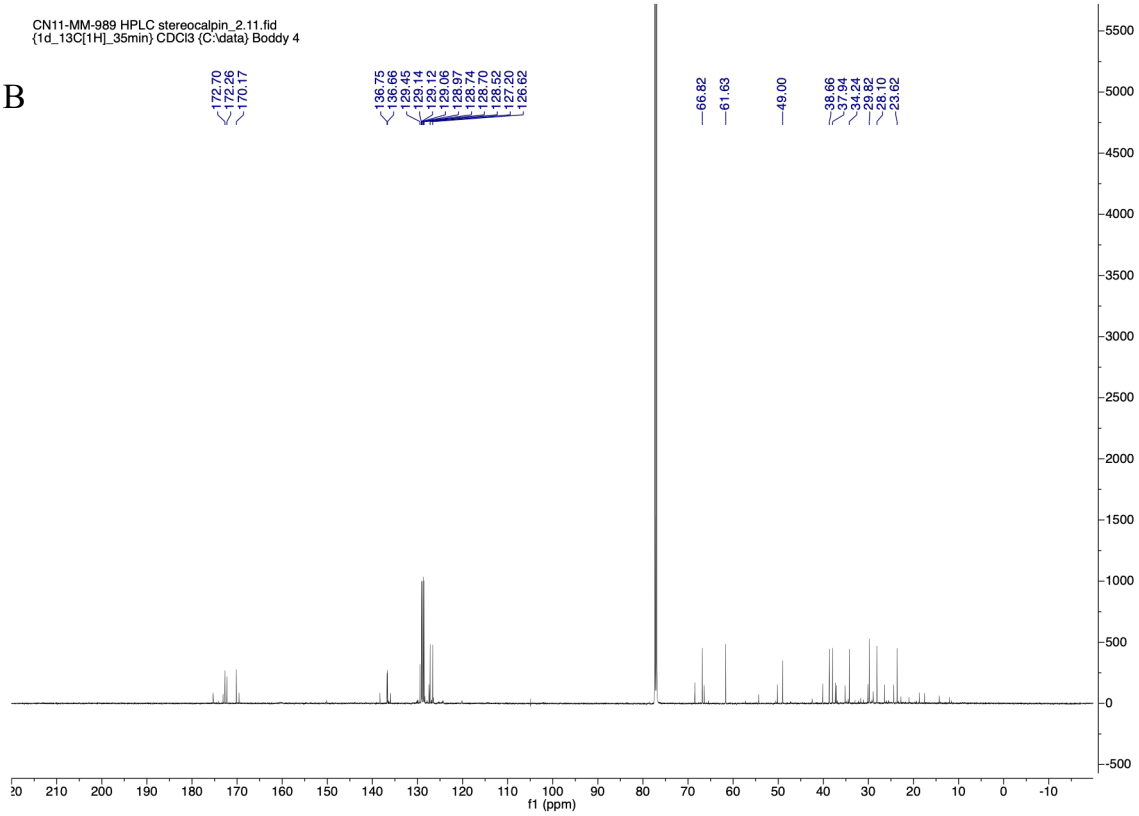


Spectra 3.32 of compound **3.10e** (A) ^{1}H NMR (600 MHz, $CDCl_3$) and (B) ^{13}C NMR (101MHz, CDCl3)

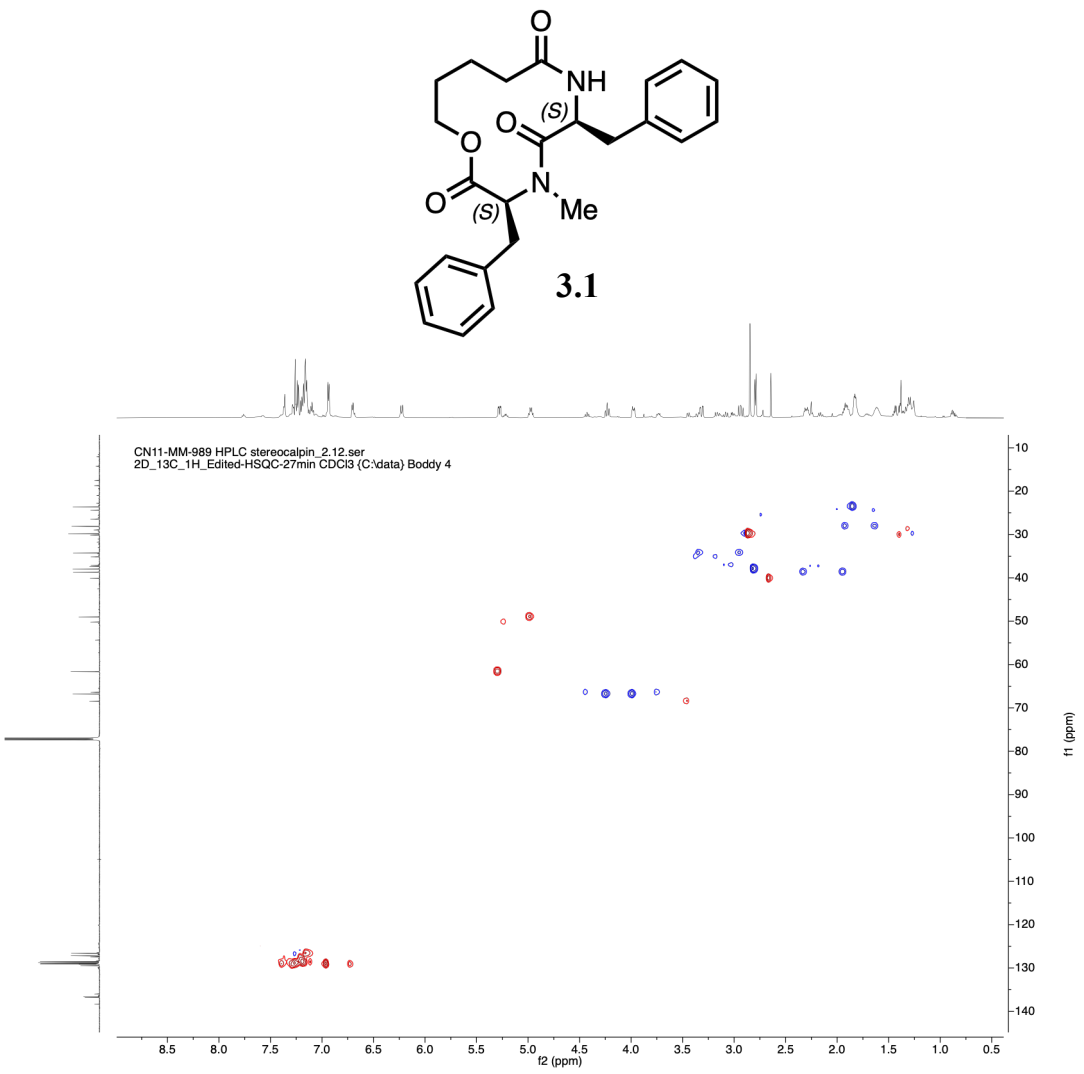
A



B

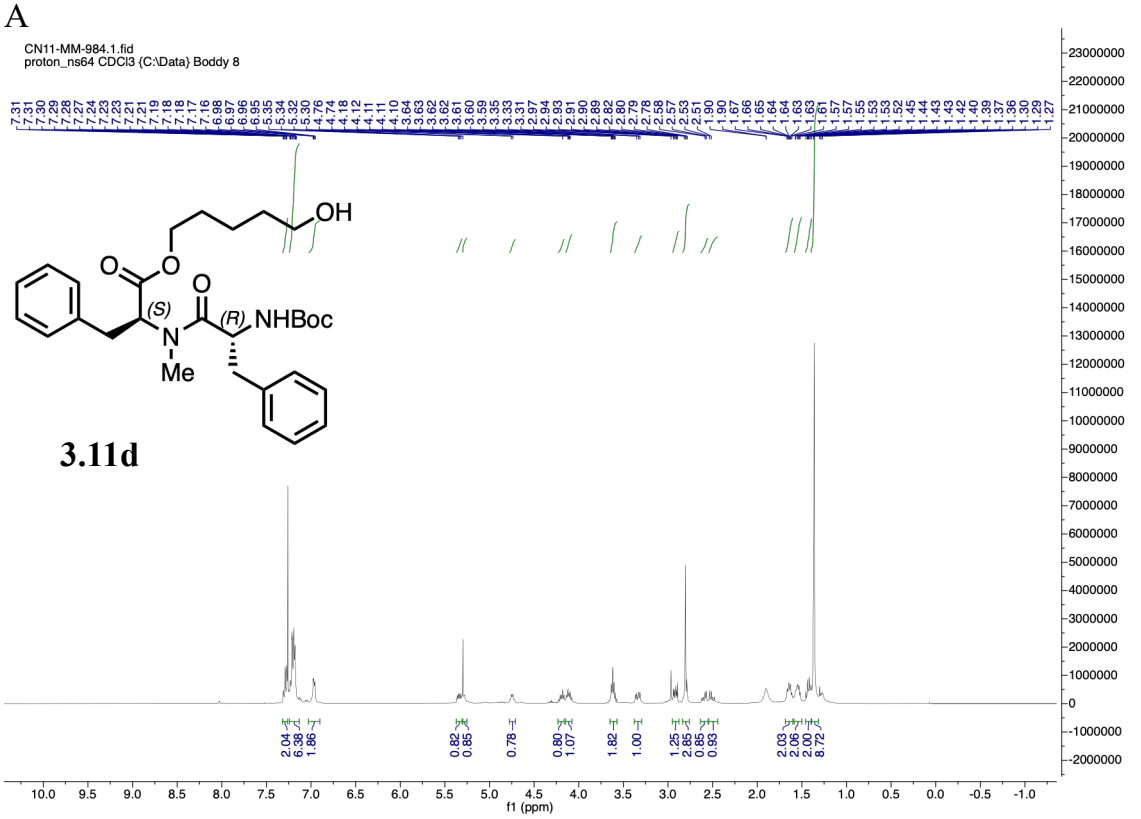


Spectra 3.33 of compound **3.10** (A) ^{1}H NMR (600 MHz, $CDCl_3$) and (B) ^{13}C NMR (101MHz, CDCl3)

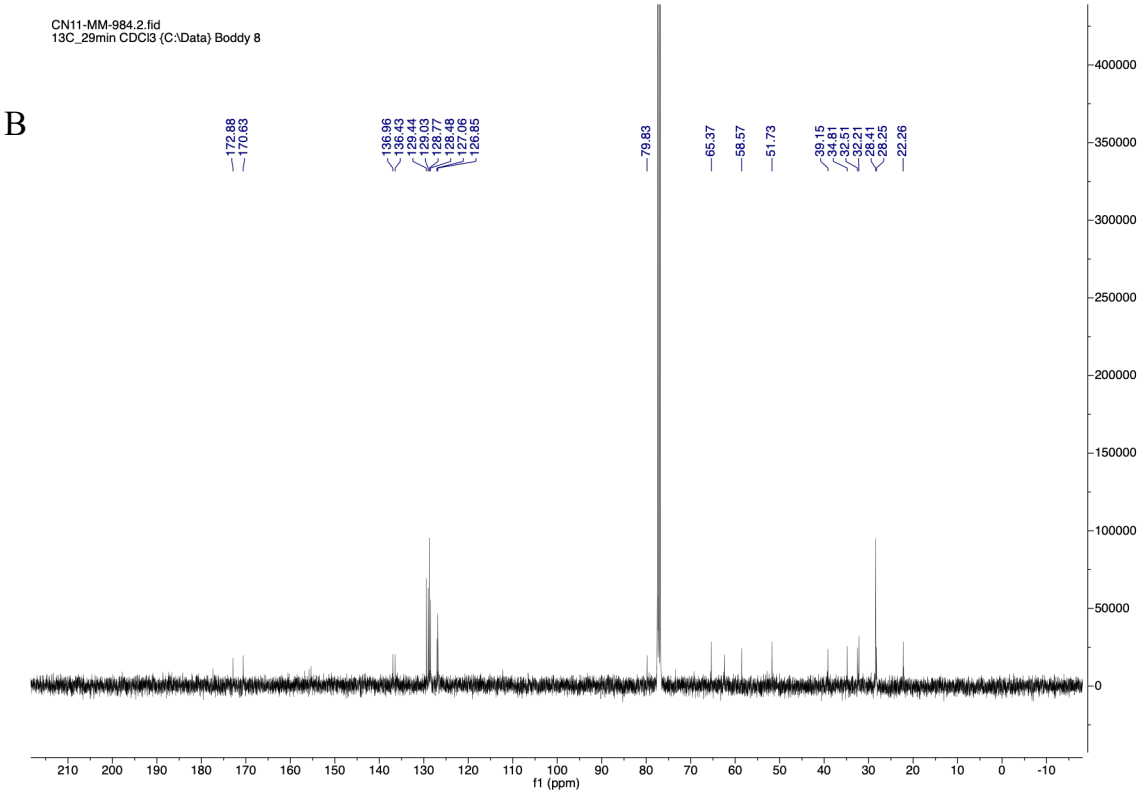


Spectra 3.34 of compound **3.10** HSQC ($CDCl_3$)

A

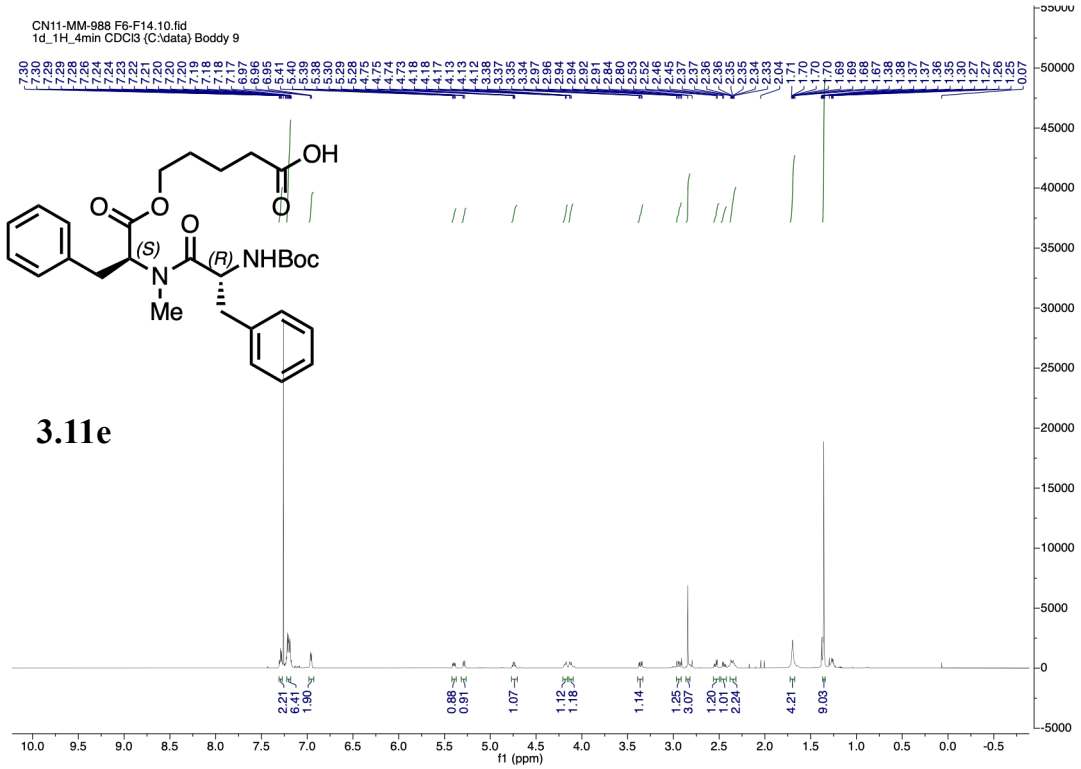


B

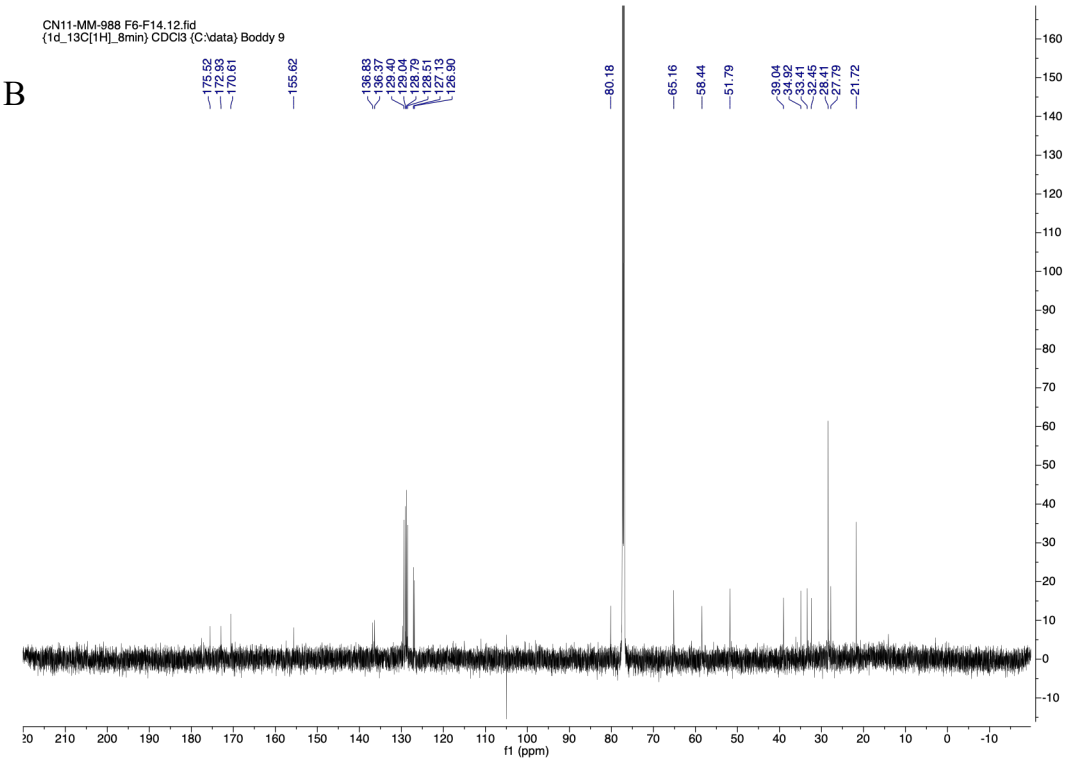


Spectra 3.35 of compound **3.11d** (A) ^{1}H NMR (600 MHz, $CDCl_3$) and (B) ^{13}C NMR (101MHz, CDCl3)

A

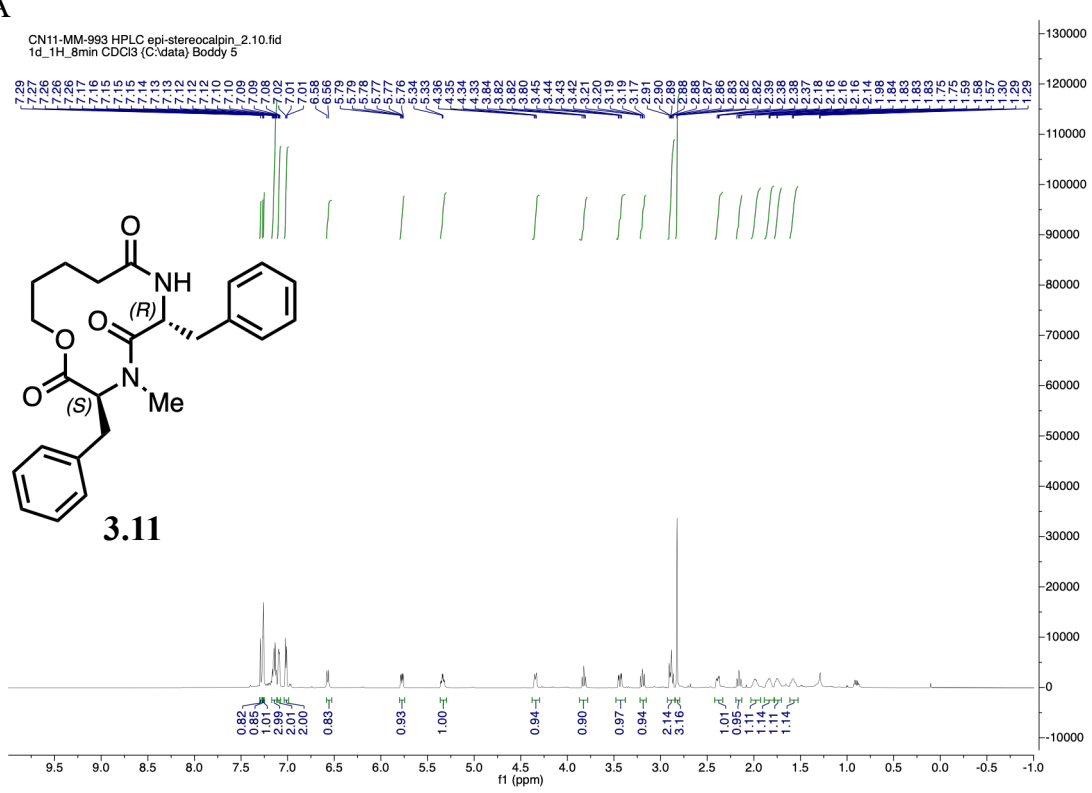


B

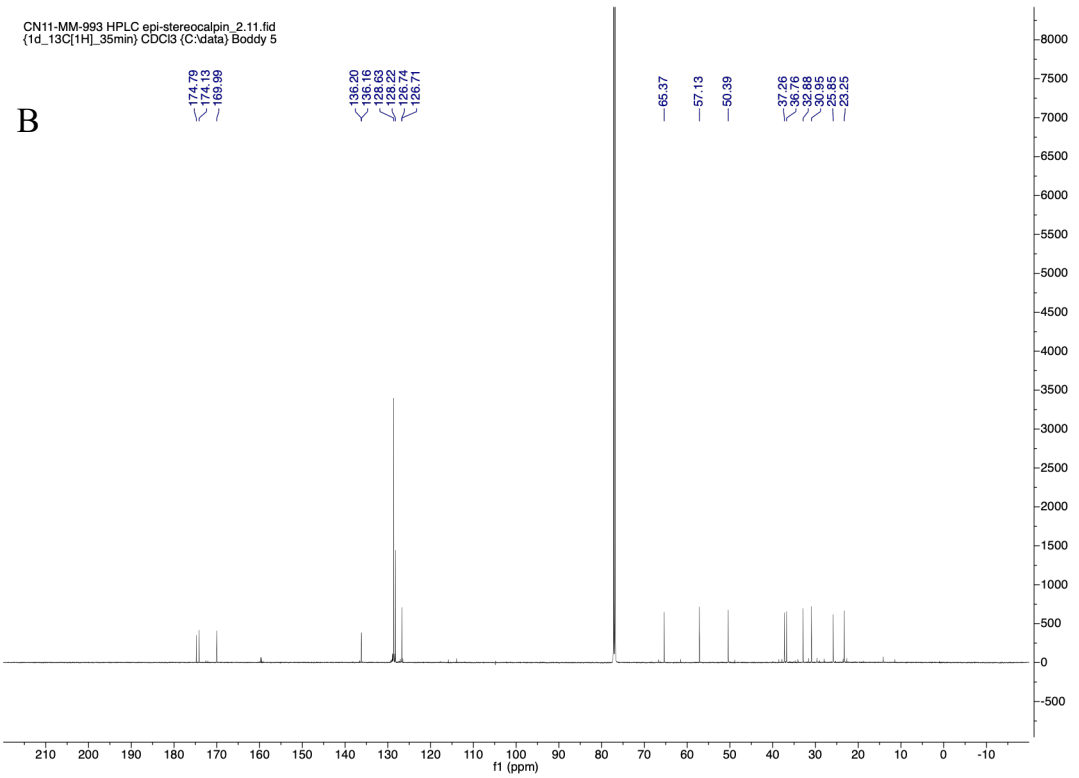


Spectra 3.36 of compound **3.11e** (A) ^{1}H NMR (600 MHz, $CDCl_3$) and (B) ^{13}C NMR (101MHz, CDCl3)

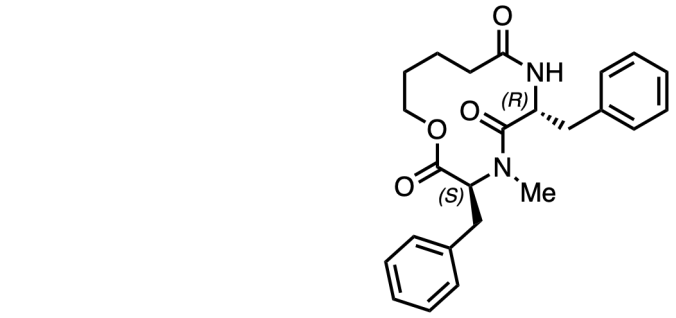
A



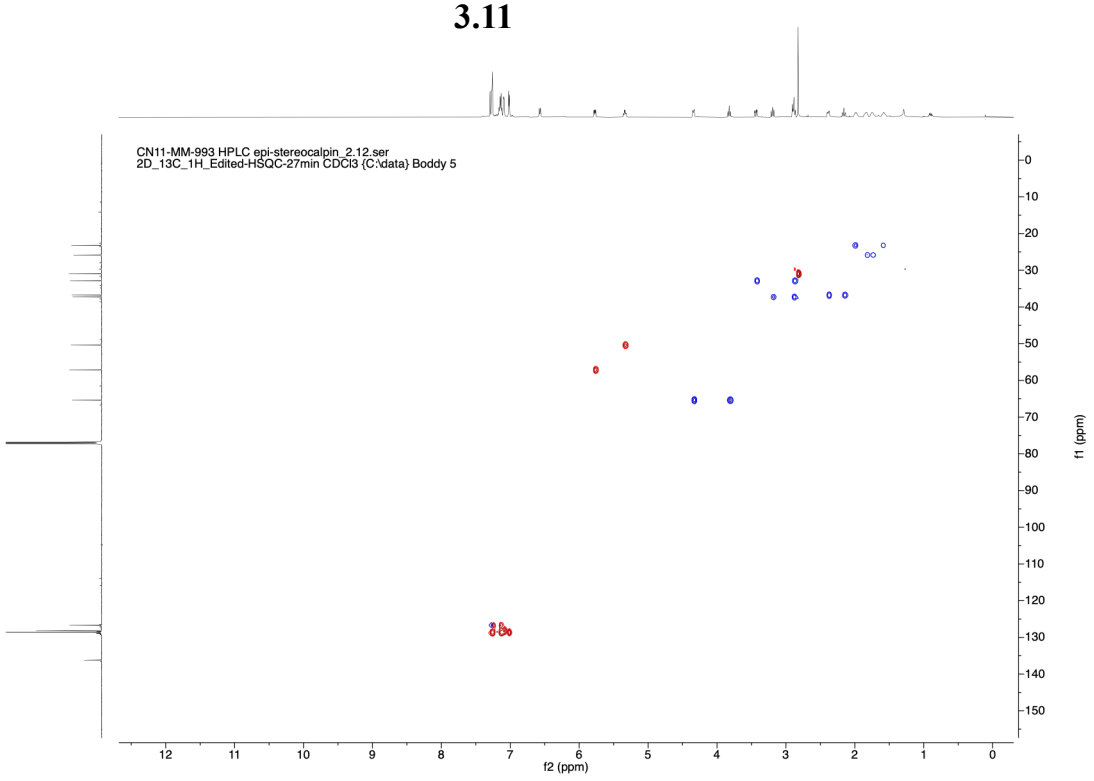
B



Spectra 3.37 of compound **3.11** (A) ^{1}H NMR (600 MHz, $CDCl_3$) and (B) ^{13}C NMR (101MHz, CDCl3)



3.11



Spectra 3.38 of compound **3.11** HSQC ($CDCl_3$)

CHAPTER IV.

Towards the Total Synthesis of Immunomodulide.

4.1 Introduction

The synthetic investigations described in Chapters II and III established the foundation required to undertake the total synthesis of Immunomodulide (**Figure 1.4**). Chapter II, which probes the synthesis of a simplified 12-membered core model system of immunomoduldie (**1.165**), accessed through two distinct macrolactamization disconnections, identified route C as the superior strategy. In route C, the macrocycle (**1.2-*anti***) is closed between the activated PKS fragment acid and the primary amine of the aromatic amino acid residue, preventing undesired epimerization at the activated acid upon ring-closure. Route C also established that Mitsunobu esterification was required to preserve the stereochemical integrity of the pipecolic acid residue during fragment coupling and highlighted the susceptibility of the reverse prenyl group on Trp indole nitrogen to migration under strongly acidic conditions.

Chapter III subsequently demonstrated that the indole ring itself is unstable to strongly oxidizing conditions, specifically PDC oxidation, unless protected as a carbamate, and validated TMSOTf and 2,6-lutidine as mild, carbamate-cleaving deprotection conditions capable of preserving the integrity of the reverse-prenylated indole nitrogen on Trp. Building on this foundation, the structure-activity relationship study described in Chapter III established the macrolactam backbone, and specifically its native D-Trp/L-Pip configuration, as the primary pharmacophoric determinant of immunomodulide's immunopotentiating activity. Additionally, probing preliminary activity across two synthesized analogue, demonstrated tolerance for

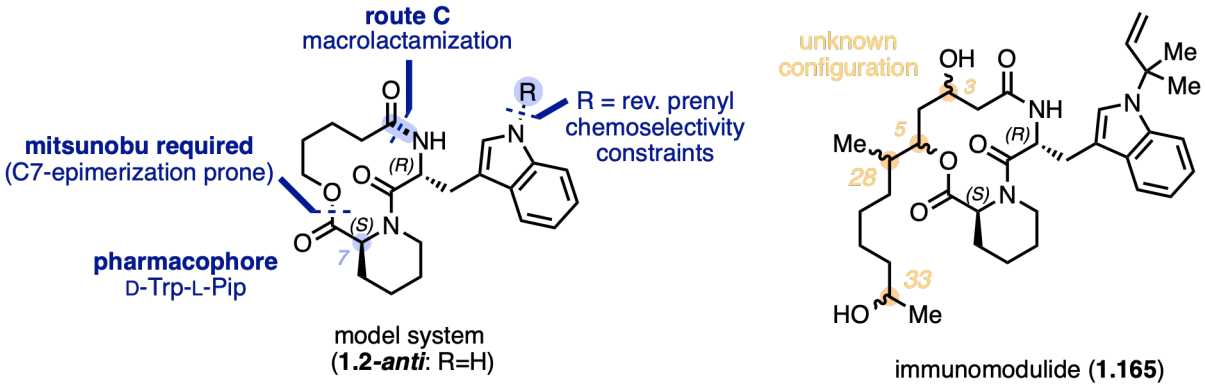


Figure 4.1. Summary of synthetic constraints established in Chapters II and III (left) and unresolved stereochemical challenges addressed in this chapter (right). Stereocenters of unknown configuration in the PKS fragment of immunomodulide (**1.165**) are highlighted in orange (C3, C5, C28, C33).

conservative substitutions at the aromatic side chain (D-Trp) and *N*-alkyl positions (L-Pip of the scaffold. Activity testing of the full analogue scope is currently ongoing.

Both studies carried out in these chapters were conducted using a simplified model system in which the PKS fragment was reduced to an achiral carbon chain, removing all stereochemical information present in the native fragment. This simplification was deliberately employed to isolate macrolactamization and pharmacophore elucidation from the unresolved stereochemistry of the native PKS fragment (see **Section 2.1.4** and **Section 3.1.4**).

As established in Chapter I (**Section 1.3.4**), the four stereocenters of the PKS fragment could not be assigned from the isolation data alone, and the limited quantity of isolated material (~2 mg) precluded X-ray crystallographic analysis, leaving structural validation by total synthesis as the only viable route to an unambiguous configurational assignment. The total synthesis of immunomodulide therefore requires resolution of the three challenges this substitution was designed to defer: (1) configurational assignment of the PKS fragment, (2) macrolactamization on the resulting stereochemically complex substrate, and (3) an unambiguous structural characterization of the fully elaborated natural product.

This chapter describes the structural assignment of the PKS fragment and the synthetic campaign undertaken toward the total synthesis of immunomodulide, applying the macrolactamization strategy and synthetic constraints established in Chapters II and III to the fully elaborated natural product target.

4.2 Defining the PKS Target (13C NMR stereochemical assignment)

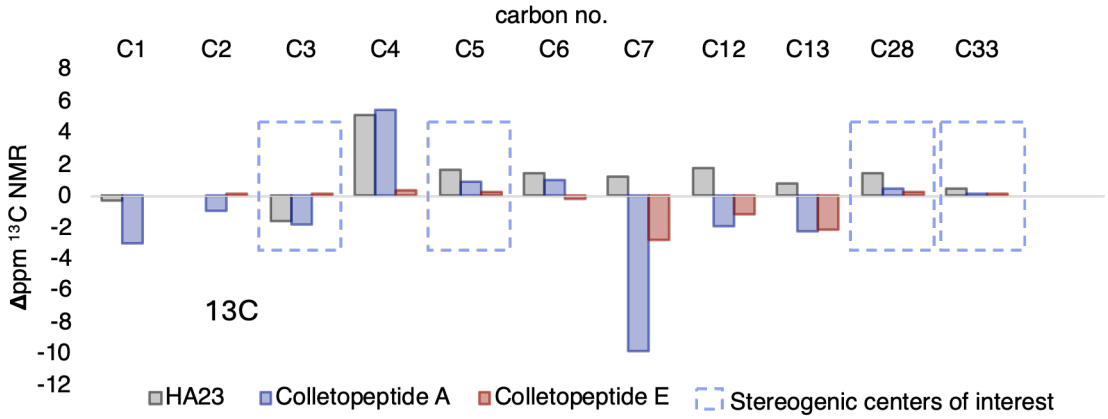
As established in Chapter I, the candidate biosynthetic gene cluster identified for immunomodulide provided confident assignment of the NRPS-derived D-Trp and L-Pip residues (**Section 1.3.1**), consistent with the epimerization domain, as well as the reverse-prenylated indole nitrogen, consistent with the dimethylallyltransferase encoded within the cluster. However, the absolute configuration of the four stereocenters within the PKS fragment of immunomodulide could not be resolved from the isolation data alone, leaving sixteen possible stereochemical permutations, which could not be addressed with NOE-based analysis. Resolving the configuration of the PKS fragment and defining a synthetic target, was essential in reducing the synthetic burden of a total synthesis campaign directed at characterizing immunomulide.

Two general strategies have been used within the fungal tridepsipeptide family to address comparable configurational ambiguity in the PKS fragment (**Section 1.2.6**). The first, an exhaustive synthetic approach exemplified by Kaneda's mirror-image strategy[1] for stereocalpin A[2], involves synthesis of the complete or reduced isomer set followed by direct spectroscopic comparison to the natural product, providing unambiguous assignment at considerable synthetic cost. In the context of immunomodulide, this approach would be viable, but synthetically labour intensive. The second, a biochemistry-guided approach developed by Takino et al. [3] in 2021 and applied to the acremolide A and B[4], HA23[5] and valactamide A[6], instead derived the stereochemical outcome from the established domain-level logic of fungal highly reducing PKS (hrPKS) enzymology. However, this approach has so far shown direct success only for acremolide A and HA23 which share an identical PKS-derived configuration, and does not serve to independently validate the model. Its earlier application to the valactamide A instead required several iterations against synthesized candidates before a confirmed structure was reached, indicating that the rule functions best as a heuristic starting hypothesis rather than a reliably predictive tool. Given these limitations, this approach was also not considered in the context of immunomodulide.

Beyond these two family-specific strategies, several general methods exist for configurational analysis of PKS-derived stereocenters. X-ray crystallography offers the most direct and unambiguous route to absolute configuration but requires a suitable crystalline derivative, which the limited quantity of isolated material did not permit (**Section 1.3.4**). Other strategies include J-based configuration analysis (JBCA)[7–9], chiral derivatization methods such as Mosher's method[10], and degradation-based methods (ozonolysis-[11] and hydrolysis-[12] based cleavages). However, JBCA requires well-resolved vicinal coupling constants and is poorly suited to flexible macrocyclic systems prone to conformational averaging. Conversely, Mosher-type derivatization and degradation-based methods would require substantially more material than was available for immunomodulide (**Section 1.3.4**) and would generally not be suitable (degradation-based methods) or only provide configurational information at hydroxyl-bearing centre, leaving the methyl-branched stereocenters unaddressed. Computational-based methods such as DP4[13,14] represent a viable alternative that would not have been constrained by the limited available material. However, this computational approach was not pursued in the present work.

Given the structural relatedness of immunomodulide to other characterized members of the 12-membered cyclic tridepsipeptide family, a separate approach was instead pursued. Total

synthesis campaigns within this compound family routinely confirm structural and stereochemical assignment by comparing the ^{1}H and ^{13}C NMR data of a synthesized candidate against those of the



Graph 4.1. Δppm of ^{13}C NMR shifts in d-methanol of immunomodulide (reference compound) and reported values for HA23, and Calletopeptide A, and E.

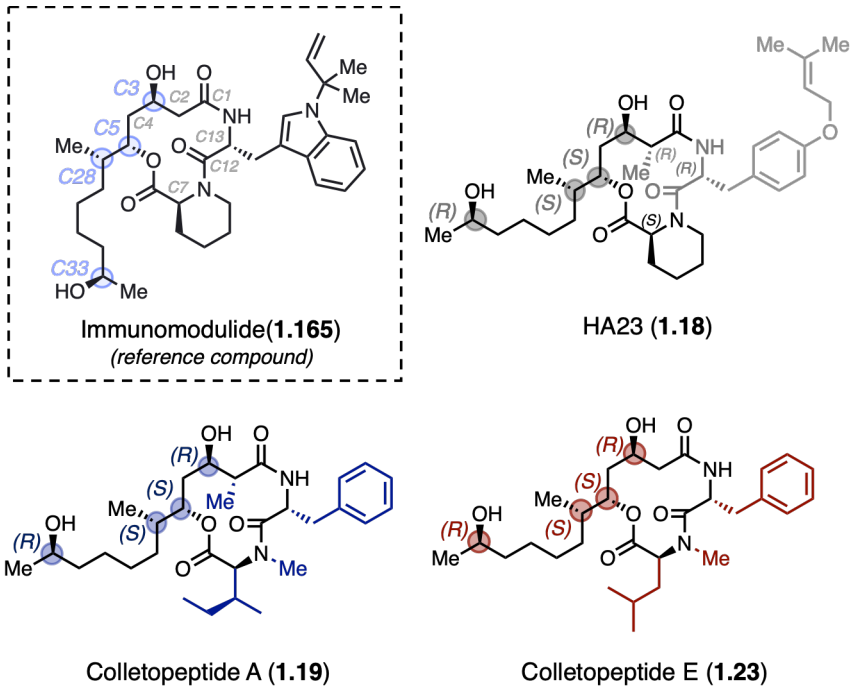
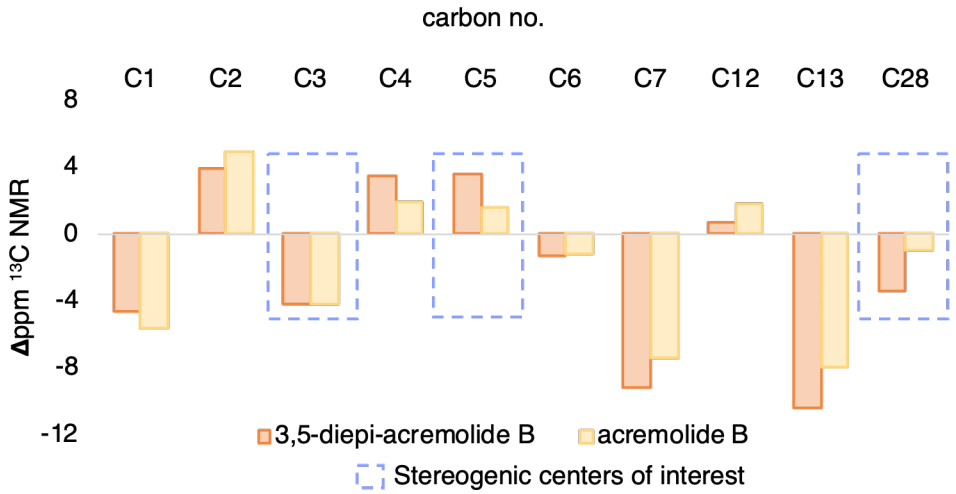


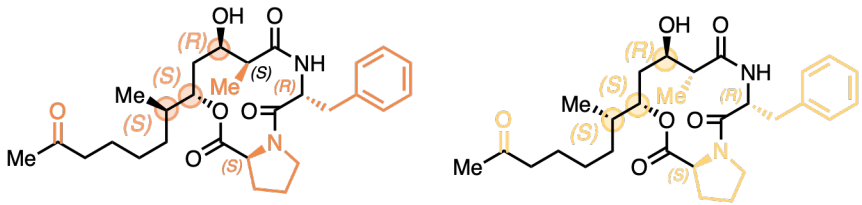
Figure 4.2. Δppm values of shared ^{13}C NMR signals between immunomodulide (**1.165**) and configurationally defined congeners HA23 (**1.18**), colletopeptide A (**1.19**), and colletopeptine E (**1.23**), recorded in d-MeOH. Stereocenters of interest (C3, C5, C28, C33) are indicated by dashed boxes. The minimal deviation observed for colletopeptide E across all positions, including the four stereocenters, identifies the 3R,5S,28S,33R configuration as the synthetic lead for immunomodulide.

isolated natural product[1,4,15]. This analysis flags any deviation as evidence of misassignment (**Section 1.2.5**)[16–20]. This same logic motivated the approach of comparing the ^{13}C NMR of immunomodulide against structurally related and configurationally defined tridepsipeptides.

Immunomodulide was thus compared against three structurally related, configurationally defined congeners bearing a shared PKS fragment: HA23[5,21], colletopeptide A[15,22], and colletopeptide E[23] (**Figure 4.2**). The change in chemical shift (Δppm) of each shared carbon (C1-C7, C12, C13, C28, and C33) was calculated relative to immunomodulide for each reference



Graph 4.2. Δppm of ^{13}C NMR shifts in d-DMSO of immunomodulide (reference compound), 3,6-diepi-acremolide B, acremolide B.



3,5-diepi-acremolide B (**1.62**)

acremolide B (**1.13**)

Figure 4.3. Δppm values of shared ^{13}C NMR signals between immunomodulide (**1.165**) and configurationally defined congeners 3,5-diepi-acremolide (**1.62**), and acremolide B (**1.13**), recorded in D-DMSO. Stereocenters of interest (C3, C5, C28, C33) are indicated by dashed boxes.

compound. Comparisons were carried out across all shared carbons and emphasis was placed on those within the macrolactone ring (C1-C7, C12-C13) and at the four unresolved PKS stereocenters (C3,C5, C28 and C33). Carbon shift values were expected to vary across the amino acid-derived carbons (C6-C7, C12-C13) given the differing residues present across the series

(immunomodulide: D-Trp/L-Pip; HA23: D-Tyr/L-Pip; colletopeptide A: D-Phe/L-Ile; colletopeptide E: D-Phe/L-Leu). This was confirmed by the significant deviations observed at C7, C12, and C13 (**Figure 4.2**), which ranged from +1.2 to -9.8 ppm, +1.8 to -1.9 ppm, and +0.8 to -2.2 ppm, respectively, across the three reference compounds, with colletopeptide A consistently showing the largest deviation at each of these positions. Beyond these amino acid carbons, HA23 and colletopeptide A also showed consistent deviations relative to immunomodulide across the

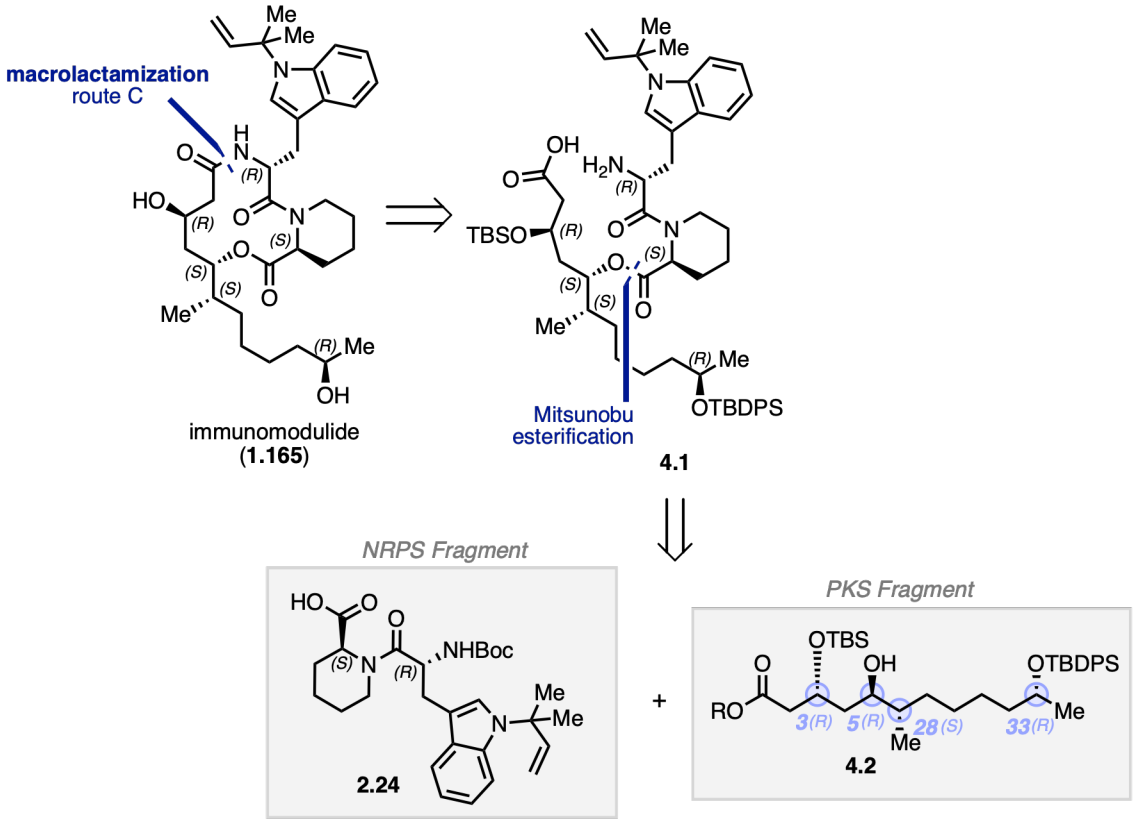


Figure 4.4. Retrosynthetic analysis of immunomodulide (**1.165**) via route C macrolactamization and Mitsunobu disconnection, revealing NRPS fragment **2.24** and PKS fragment **4.2**. PG = protecting group.

remaining carbons compared, including the four stereocenters of interest (C3, C5, C28, and C33), whereas colletopeptide E showed minimal deviation across this same set (**Figure 4.2**). This pattern is consistent with the C2 methyl substituent shared by HA23 and colletopeptide A which is absent in both immunomodulide and colletopeptide E. On this basis, the configuration of colletopeptide

E, (3R, 5S, 28S, 33R), was identified as the closest structural match to immunomodulide, narrowing the sixteen possible stereochemical permutations to a single synthetic lead.

To validate this approach, an analogous analysis was performed against 3,5-diepi-acremolide B (**1.62**) afforded by ElMarrouni[16] as well as acremolide B (**1.13**) synthesized and characterized by Xiao et al.[4] . Given the C5 (S) configured prediction on the basis of the colletopeptide E comparison (**Figure 4.2**), 3,5-diepi-acremolide B bearing the inverted (R) configuration at the C5 position and (S) configuration at C3, the analysis was expected demonstrate a true configurational mismatch that was predicted to be evident by drastic Δppm deviations across all carbons analyzed. Moreover, as C3 and C5 sit within the macrolactone and C5 represents the site of lactonization, configurational mismatches at these sites was expected to impose a more significant distortion on the already strained 12-membered ring than an equivalent mismatch at stereocenters along the hydrocarbon chain. This was confirmed (**Figure 4.3**), with deviations ranging from +3.9 to -10.5 ppm observed across the entire carbon set.

By contrast, acremolide B (**1.13**), which shares both the predicted C5 and C3 configurations with immunomodulide but is methylated at C2 and bears different amino acid residues, showed smaller overall deviations than the 3,5-diepi compound (**1.62**) across the stereocenters of interest, with Δppm values of -4.26, +1.55, and -0.97 ppm at C3, C5, and C28 respectively, compared to -4.16, +3.55, and -3.47 ppm for the 3,5-diepi compound. The notably smaller deviation at C28 in acremolide B is consistent with the 1,2-syn relationship between C5 and C28 being preserved when C5 adopts the correct configuration (S), whereas inversion at C5 in the diepi compound disrupts this relationship and propagates a larger chemical shift perturbation to C28. The residual deviations shared between both acremolide B and the diepi compound, particularly at C2, C3 and the amino acid-derived carbons C7 and C13, are attributable to the extra C2 methyl substitution and differing amino acid residues. A direct, single-variable comparison, isolating the effect of the C5 inversion alone without the confounding C2 methylation, would have offered a cleaner negative control for this second configurational analysis. However, no such related tridepsipeptide natural product bearing only the one configurational mismatch has been synthesized or isolated and reported in a directly comparable solvent system (CD_3OD or DMSO), precluding this more targeted comparison.

Together, these two analyses support both the assigned configuration of immunomodulide's PKS fragment and comparative ^{13}C NMR as a viable strategy for narrowing the stereochemical target prior to total synthesis.

4.3 A Retrosynthetic Analysis of Immunomodulide

With a configurational prediction of the PKS fragment complete (**Section 4.2**), a retrosynthetic analysis of immunomodulide was developed (**Figure 4.4**), building directly on the route C macrolactamization strategy established in Chapter II. Disconnection of the ring at the amide bond between the activated PKS fragment acid and the primary amine of the reverse-prenylated D-Trp residue reveals two key fragments **2.24** and **4.2**. The NRPS fragment (**2.24**), comprising the D-Trp(*N*-reverse-prenyl)-L-Pip dipeptide was already accessed in Chapter II (**Figure 2.8**), in three synthetic steps from Boc-D-Trp. As this fragment required no further optimization, the work described in this section largely centre on the design of a stereoselective route to the PKS fragment (**4.2**) to address the configuration of the stereocenters requiring validation through syntheses.

While the comparative ^{13}C NMR analysis described above was considered sufficient to confidently target the 3R, 5S, 28S, 33R final configuration, this assignment remained, a structural

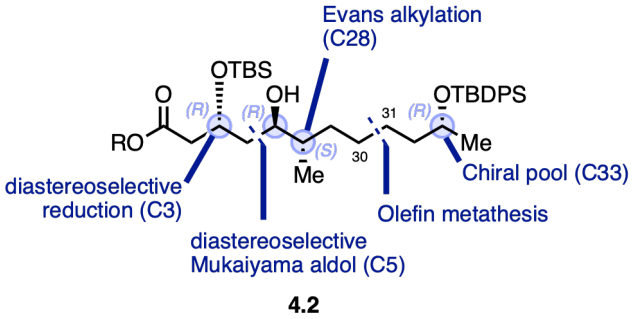


Figure 4.5. Summary of retrosynthetic analysis of the PKS fragment (**4.2**).

prediction rather than a definitively confirmed configuration. Given this, the retrosynthesis of the PKS fragment (**4.2**) was designed with tailorability as a guiding principle, such that each stereocenter could be selectively inverted and without requiring a complete redesign of the synthetic route. The configuration of each of the four PKS stereocenters was planned independently, allowing the stereochemical outcome at each position to be controlled by the choice of reagent, catalyst, or auxiliary employed at the corresponding bond-forming step, rather than being fixed by the synthetic route itself:

The C3 stereocenter was planned to be installed via diastereoselective ketone reduction, using either Evans-Saksena[24,25] or Narasaka-Prasad[26] conditions depending on the desired configuration relative to the adjacent C5 stereocenter, as these two methods are known to deliver opposite diastereomeric outcomes from a common β-hydroxy ketone substrate.

The C5 stereocenter, constituting the free hydroxyl that serves as the esterification handle in the Mitsunobu that joins the two fragments, was planned to be installed via a vinylogous Mukaiyama aldol reaction, with the diastereoselectivity of this step controlled through selection of the chiral Lewis acid catalyst employed. It is important to note that given that the Mitsunobu esterification proceeds with inversion of configuration at the alcohol-bearing carbon, (*R*)-configured alcohol at C5 was targeted as the inverse event upon Mitsunobu esterification would generate the desired ester with an (*S*) configured C5. This design also preserved tailorability at this position, as the (*R*)-configured C5 stereocenter could be accessed either by adjusting the chiral Lewis acid employed at the aldol stage, by using a stereo-retentive esterification strategy in place of Mitsunobu, or by performing a Mitsunobu-mediated double inversion.

The C28 stereocenter was planned to be installed via an Evans oxazolidinone auxiliary-controlled alkylation, with the auxiliary enantiomer selected to access the desired configuration.

The C33 stereocenter was introduced through a chiral pool approach, using commercially available methyl (*R*)-3-hydroxybutyrate as the starting material, which directly provides the desired (*R*)-configuration at C33 without requiring an asymmetric induction step.

Additionally, the C30 and C31 carbons were planned to be joined via a cross-metathesis reaction, enabling the left- and right-hand fragments of the PKS chain to be elaborated independently prior to coupling and hydrogenation to the desired saturated C30-C31 bond. With each stereocenter's installation strategy defined, the first-generation synthesis of the PKS fragment is described in Section 4.4.1.1.

4.4 Results and Discussion

4.4.1 Enantioselective Synthesis of the PKS Fragment

4.4.1.1 First-Generation Synthesis

Retrosynthetic analysis of the PKS fragment identified a common β-ketoester intermediate, **4.3**, accessible via two sequences (**Figure 4.6**). If **4.3** were accessed through disconnection A (**Figure 4.6**, left), the first step in the synthesis would begin with a Mukaiyama aldol reaction between fragments **4.6** and **4.7** to furnish olefin **4.4**, which would then require an olefin cross-metathesis with alkene **4.5** to complete the carbon chain. If **4.3** were instead accessed through

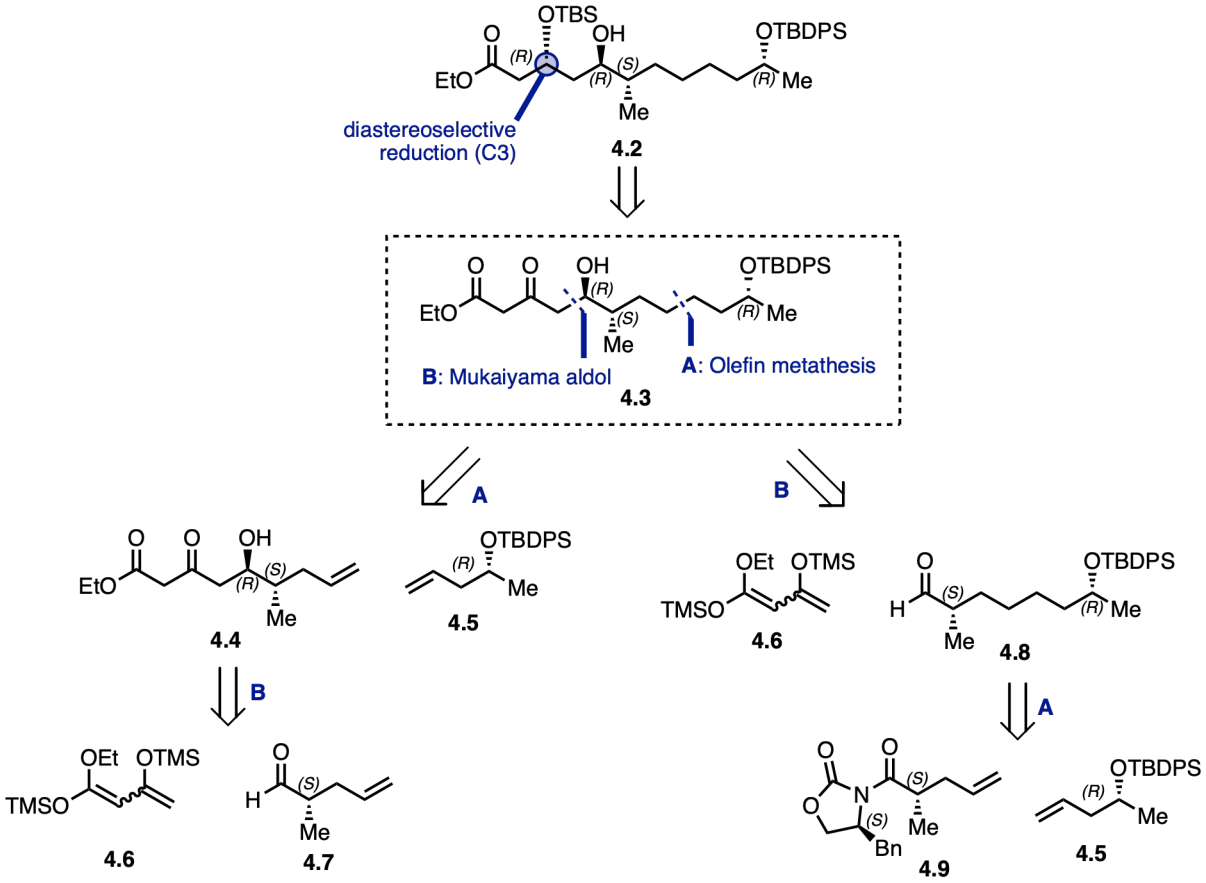


Figure 4.6. Retrosynthetic analysis of the PKS fragment (**4.2**). Two disconnection strategies (A: olefin metathesis; B: vinylogous Mukaiyama aldol) were considered for intermediate **4.3**, leading to divergent retrosynthetic pathways and common fragments **4.5** and **4.6.**

disconnection B (**Figure 4.6**, right), the synthesis would begin with an olefin cross-metathesis between alkene **4.9** and alkene **4.5** to furnish **4.8**, which would then require a Mukaiyama aldol with diene **4.6** to complete the chain.

The forward synthesis probing disconnection A was pursued first. This route began with construction of Chans' diene (**4.6**) which was achieved in two steps, starting from ethyl acetoacetate (**Figure 4.7**). Treatment of ethyl acetoacetate with NEt_3 and TMSCl in hexanes at room temperature afforded the *O*-silylated enol ether **4.10** via trapping of the enol tautomer. Treatment of this intermediate with LDA and TMSCl at -78°C to furnish Chans' diene **4.6** in 87%

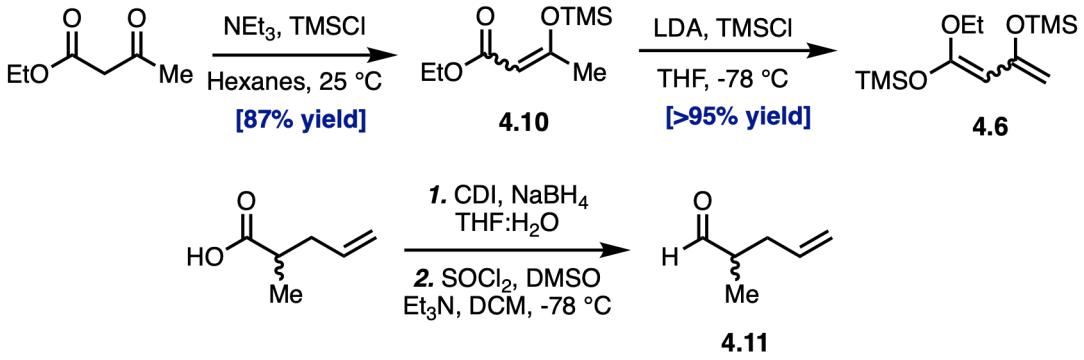


Figure 4.7. Synthesis of Chans' diene (**4.6**) from ethyl acetoacetate and attempted preparation of racemic aldehyde **4.11** via CDI-mediated reduction and Swern oxidation.

yield. Prior to investigating the asymmetric Mukaiyama aldol, the reaction was first planned to be evaluated using a racemic version of the aldehyde coupling partner. However, attempts to access the racemic aldehyde (**4.11**) via reduction of the corresponding commercially available racemic acid followed by Swern oxidation were unsuccessful, as the resulting aldehyde proved too volatile (bp 61 °C, 40 Torr) to isolate reliably. As the aldol reaction could not be evaluated without a robust sequence to access the aldehyde partner (**4.11**), it was concluded that an early-stage Mukaiyama aldol was synthetically impractical. As a robust route to **4.11** could not be established, an early-stage Mukaiyama aldol was deemed synthetically impractical, and the sequence was reordered according to disconnection B.

In this approach the cross-metathesis coupling was performed first, incorporating the alkene handle into a larger, less volatile fragment (**4.8**) prior to the Mukaiyama aldol step. To this end, alkene **4.9** and alkene **4.5** were prepared independently. Alkene **4.9**, bearing the C28 stereocenter, was accessed in two steps from pent-4-enoic acid. Acylation with (4S)-4-benzyl oxazolidinone under pivaloyl chloride/LiCl/Et_3N conditions afforded **4.12** in 58% yield, and subsequent α-methylation with CH_3I under NaHMDS enolization at -78°C delivered the α-methyl oxazolidinone **4.9** in 45% yield.

Alkene **4.5**, bearing the C33 stereocenter, was accessed in three steps from commercially available (*R*)-methyl 3-hydroxybutanoate. TBDPS protection of the free hydroxyl under standard imidazole/DMAP conditions afforded **4.13** in 96% yield. Then DIBAL reduction followed by

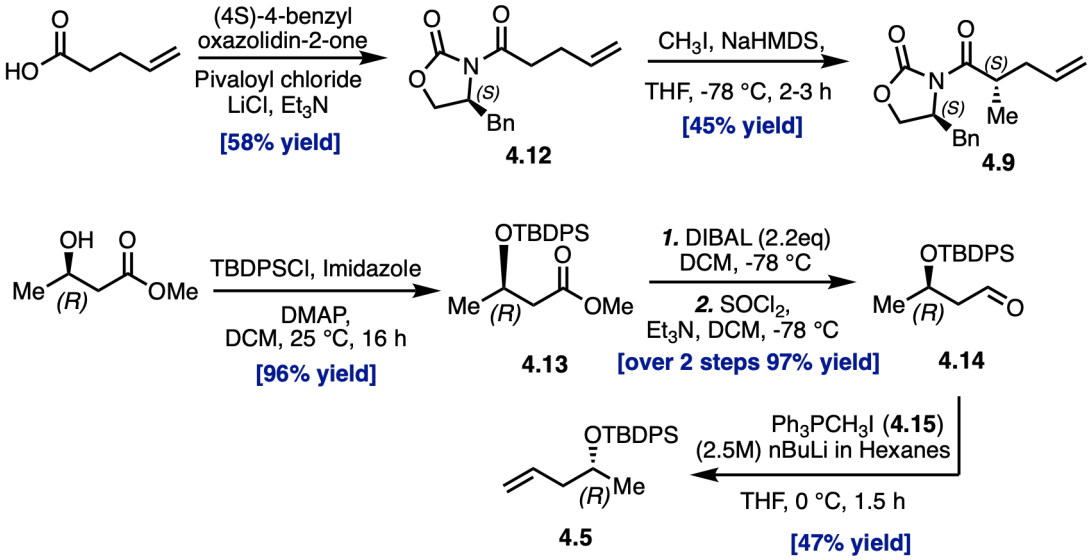
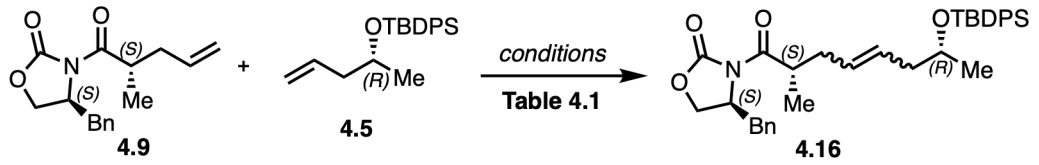


Figure 4.8. Synthesis of cross metathesis coupling partners **4.9** and **4.5**

Swern oxidation delivered aldehyde **4.14** in 97% yield over two steps. Wittig olefination conditions with Ph_3PCH_3I (**4.15**, prepared in one step from triphenylphosphine and methyl iodide[27]) were then employed to furnish the terminal alkene terminal alkene **4.5** in 47% yield.

A systematic screen of metathesis conditions was carried out to optimize this coupling (**Table 4.1**), varying catalyst identity (Grubbs I, Grubbs II, Hoveyda-Grubbs II), catalyst loading, and solvent. Given the type-I nature of both alkenes, given to their substitution patterns (mono substituted) and low steric bulk about the olefin, competitive homodimerization was anticipated. To bias the reaction toward the desired cross-metathesis product, non-equimolar alkene ratios were employed. This approach shifts the statistical distribution of metathesis events toward productive cross-coupling and is commonly employed when homodimerization pathways compete with the desired transformation[28]. Alkene **4.9** was selected as the limiting reagent throughout the entries screened, given the lower overall yield of its preparation relative to alkene **4.5**. However, entry 9 was performed to evaluate the effect of varying alkene stoichiometry on product formation and homodimerization.

Despite this optimization effort, yields remained consistently moderate across all conditions evaluated, and product formation was highly sensitive to reaction conditions. Increasing the reaction temperature by switching from DCM (40 °C) to DCE (84 °C) reduced the yield from 45.8% to 22.9% (entries 1 and 2), suggesting that elevated temperatures were detrimental, although solvent effects were not tested in isolation. Similarly, increasing catalyst loading proved



4.9 **4.5** **4.16**

Entry	**4.9** (equiv.)	**4.5** (equiv.)	Catalyst (equiv.)	Solvent	Temp (°C)	Time (h)	Yield % **4.9**-homodimer	Yield % **4.16**
1	1.0	10.0	G-I (0.1)	DCM	40	24	0	45.8
2	1.0	10.0	G-I (0.2)	DCE[d]	84	48	0	22.9
3	1.0	10.0	G-I (0.4)	DCM	40	24	0	14.5
4	1.0	4.0	G-I (0.4)	DCM	40	48	50.4	37.3
5	1.0	10.0[a]	G-II (0.2)	DCM	40	24	0	34.2
6	1.0	10.0	G-II (0.4)	DCM	40	24	0	18.8
7	1.0	10.0[a]	G-II (0.2)	DCM	40	20	0	83.8**
8	1.0	10.0	G-II (0.2)	DCM	40	48	0	44.2
9	10.0	1.0	G-II (0.1)	DCM	40	20	nd	44.9
10	1.0	10.0	HG-II (0.1)	DCM	40	20	0	40.0

Table 4.1. Optimization of the cross-metathesis reaction between **4.9** and **4.5**. Yields refer to NMR yields compared to limiting reagent. G-I = Grubbs 1st generation catalyst; G-II = Grubbs 2nd generation catalyst; HG-II = Hoveyda–Grubbs 2nd generation catalyst. Yield of cross-metathesis product. **not reproducible. n/d=not determined. [a]**4.5**-homodimer used

unproductive for both Grubbs I and Grubbs II catalysts, with yields decreasing from 45.8% to 14.5% (entries 1 and 3) and from 34.2% to 18.8% (entries 5 and 6), respectively. The importance of alkene stoichiometry was demonstrated in entry 4, where reducing the amount of alkene **4.5** from 10 to 4 equivalents resulted in significant formation of the **4.9**-homodimer (50.4%), confirming that self-metathesis represented a major competing pathway. Consequently, a large

excess of alkene **4.5** was maintained throughout subsequent studies to favour productive cross-metathesis.

Although a yield of 83.8% was obtained using Grubbs II catalyst and recycled homodimer-derived alkene **4.5** (entry 7), this result was not reproducible. Extending the reaction time from 20 h to 48 h under otherwise similar conditions reduced the yield to 44.2% (entry 8), indicating that prolonged reaction times were not beneficial. Finally, Hoveyda–Grubbs II afforded the desired product in 40.0% yield (entry 10), comparable to the yields obtained using both Grubbs I and Grubbs II catalysts under similar conditions (entry 1 and 8).

Overall, despite extensive optimization, the cross-metathesis remained insufficiently robust, with only moderate yields obtained under most conditions and a single high-yielding result that could not be reproduced. As this coupling occurred early in the synthesis, its moderate yield significantly compromised the overall efficiency of the route. Consequently, a second-generation approach to access the Mukaiyama aldol aldehyde precursor was pursued and is described in **Section 4.4.1.2**.

4.4.1.2 Second-Generation Synthesis

Given the limitations of the first-generation cross-metathesis route, an alternative strategy was developed to access the same aldehyde coupling partner required for the subsequent Mukaiyama aldol reaction. Rather than assembling the carbon framework through a low-yielding cross-

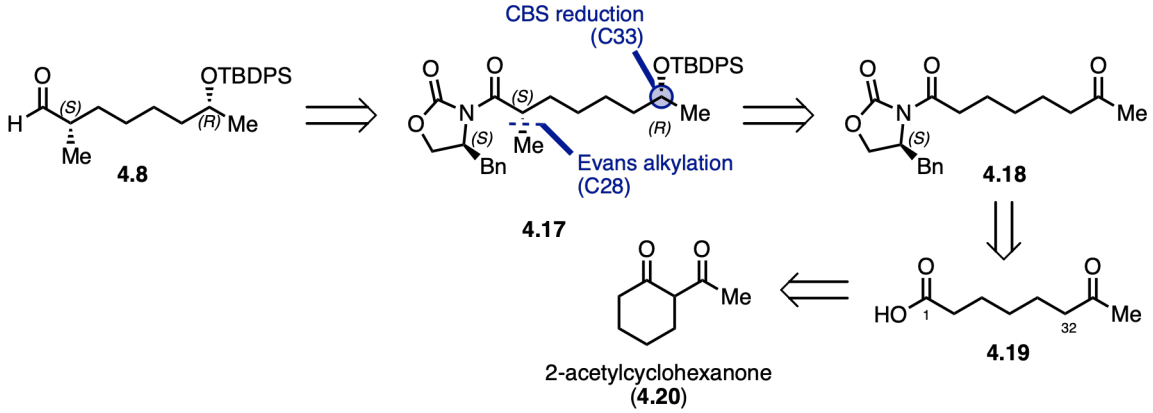


Figure 4.9. Retrosynthetic analysis of aldehyde **4.8** in the second-generation synthesis.

metathesis, the revised route exploited a retro-Claisen ring-opening of commercially available 2-acetylcyclohexanone to establish the full carbon skeleton in a single transformation.

Retrosynthetically, cleavage of the C1-C32 bond of the target aldehyde revealed a linear methyl ketone precursor accessible through retro-Claisen fragmentation of 2-acetylcyclohexanone (**Figure 4.9**). Importantly, this disconnection retained the modular stereochemical logic established in the first-generation route, whereby the C33 stereocenter could be installed through an enantioselective CBS reduction, while the C28 stereocenter was introduced through an Evans auxiliary-controlled alkylation, as in the first-generation route. Thus, the revised strategy preserved the ability to independently access alternative stereochemical permutations if required for future structure reassignment studies.

The synthesis commenced with retro-Claisen ring-opening of commercially available 2-acetylcyclohexanone (**4.20**) under basic conditions to furnish the corresponding keto acid **4.19** in 75% yield. Conversion of the acid to the corresponding Evans imide (**4.18**) proceeded in 60% yield, providing a substrate suitable for stereocontrolled installation of the C33 stereocenter. Treatment with (*S*)-Me-CBS catalyst and borane afforded the secondary alcohol **4.21** in 77% yield and 7.7 :1 d.r.

Mosher ester derivatization of the enantioenriched alcohol was attempted to confirm the configuration of C5 and d.r. However, the chemical shift differences between the two diastereomeric Mosher esters were insufficient for unambiguous configurational assignment. Given that the substituents α to the C5 Mosher ester didn't provide enough spatial information to

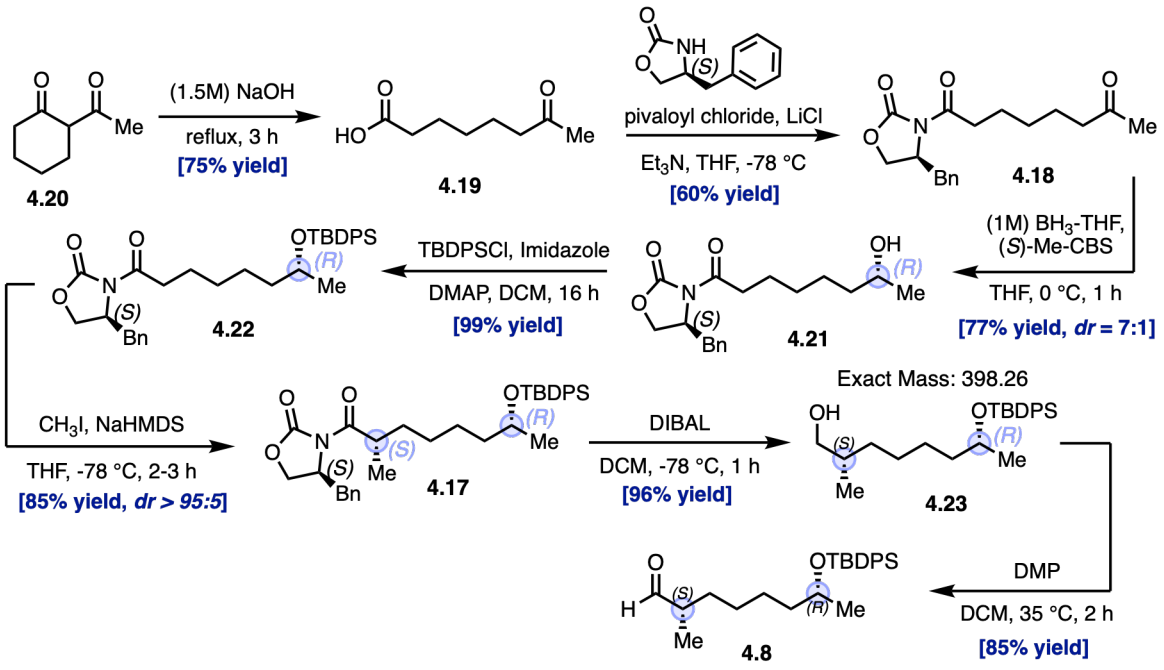


Figure 4.10. Forward synthesis of of aldehyde **4.8** (second-generation synthesis)

establish a reliable Δδ sign pattern across both faces, the (*R*) configuration was therefore assigned on the basis of the CBS facial selectivity model, and the d.r. of the reduction was confirmed by comparative ^{1}H NMR integration of the Mosher ester diastereomers relative to the racemic control (see **Section 4.8**).

Protection of the alcohol as the corresponding TBDPS ether (**4.22)** then proceeded in near quantitative yields (99%). Evans auxiliary-controlled methylation was employed to install the C28 stereocenter in 85% yield and excellent diastereoselectivity (>95:5 d.r., confirmed by NMR). Finally, **4.8** could be accessed in a one-step DIBAL reduction (65-72% yields), or in two steps employing 2.0eq of DIBAL to access the alcohol **4.X** (96% yields) followed by Dess–Martin oxidation (85% yields).

Overall, this route delivered the same aldehyde intermediate targeted in the first-generation synthesis while avoiding the problematic cross-metathesis step entirely. In addition to improving material throughput, the route originated from inexpensive commercially available starting materials, eliminated the need for a low-yielding fragment coupling reaction, and preserved stereochemical tailorability at both C28 and C33. Consequently, this retro-Claisen ring-opening sequence was adopted as the route of record for all subsequent synthetic studies.

4.4.1.3 Diastereoselectivity of the Vinylogous Mukaiyama Aldol

With a reliable route to the aldehyde coupling partner established, attention turned to installation of the C5 stereocenter through a diastereoselective vinylogous Mukaiyama aldol reaction. As outlined in the retrosynthetic analysis (**Section 4.3**), the (*R*)-configured alcohol at C5 was targeted at this stage, as the subsequent Mitsunobu esterification used to couple the PKS and NRPS fragments (**Figure 4.4**) was expected to proceed with inversion, ultimately furnishing the desired (*S*)-configured stereocenter in the predicted structure of immunomodulide.

The vinylogous Mukaiyama aldol reaction has emerged as a powerful method for the stereoselective construction of β-hydroxy carbonyl compounds, and numerous catalyst systems have been developed to control the stereochemical outcome of these transformations[29,30]. Broadly, these methods can be categorized according to the substrate class for which they were developed.

Aldehydes bearing a heteroatom β to the reacting carbonyl benefit from an additional facial bias element absent in purely α-substituted systems. This bias operates through either a closed, chelation-controlled transition state, in which the Lewis acid simultaneously coordinates the aldehyde carbonyl and the β-heteroatom to form a conformationally constrained cyclic intermediate (**TS-4.1**)[31,32]. Alternatively, selectivity can be achieved through an open-chain transition state (**TS-4.2**), in which facial selectivity arises from minimization of torsional strain and electrostatic repulsion between the β-heteroatom dipole and the carbonyl[33–35]. Both modes have been shown to deliver useful levels of diastereoselectivity for this substrate class[32,36]. In the

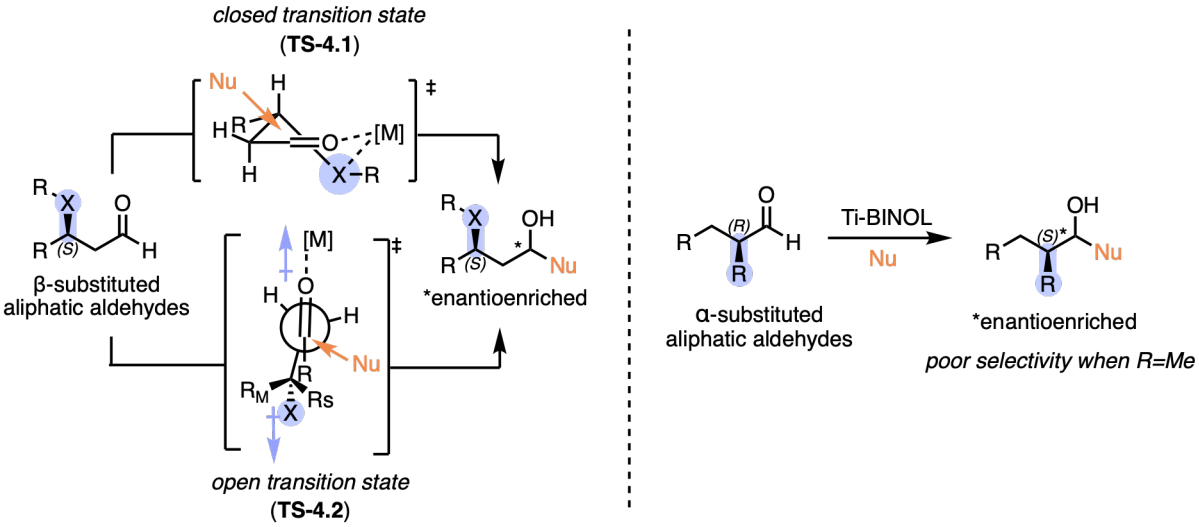


Figure 4.11. Strategies for diastereoselective nucleophilic addition to aliphatic aldehydes: β-heteroatom-substituted aliphatic aldehydes (left), Ti-BINOL-mediated addition to α-substituted aldehydes (right).

context of polyproprionate-derived natural products these modes of selectivity are common across total syntheses attempts given the classic 1,3-substitution pattern across these scaffolds[36–39]. Aldehydes bearing only α-substitution only, however, are limited to purely Felkin-controlled facial selectivity with no reinforcing contribution from a β-heteroatom. For this class of non-chelating aliphatic aldehydes, chiral titanium-BINOL complexes have instead been successfully applied, demonstrating excellent selectivity's for unhindered or aromatic a-substituted aldehyde substrates[40–43]. However, reports employing α-methyl substituted aldehydes specifically have consistently failed to produce useful diastereoselectivity, with moderate yields obtained at best[44]. This limitation was similarly encountered with the immunomodulide aldehyde, as described below (**Table 4.2**).

Given the documented failure of titanium-BINOL complexes on α-methyl substituted aliphatic aldehydes, catalyst-controlled approaches that do not rely on substrate chelation or a large steric gradient at the α-position were considered. Chiral oxazaborolidinium ion (COBI) catalysts represent one such class, operating through a well-defined chiral pocket rather than through substrate-directed coordination. These catalysts are derived from proline-based CBS oxazaborolidines, in which the pyrrolidine nitrogen and boron atom form the core of the bicyclic scaffold. First reported by Corey and co-workers[45] in Diels Alder chemistry, COBIs were

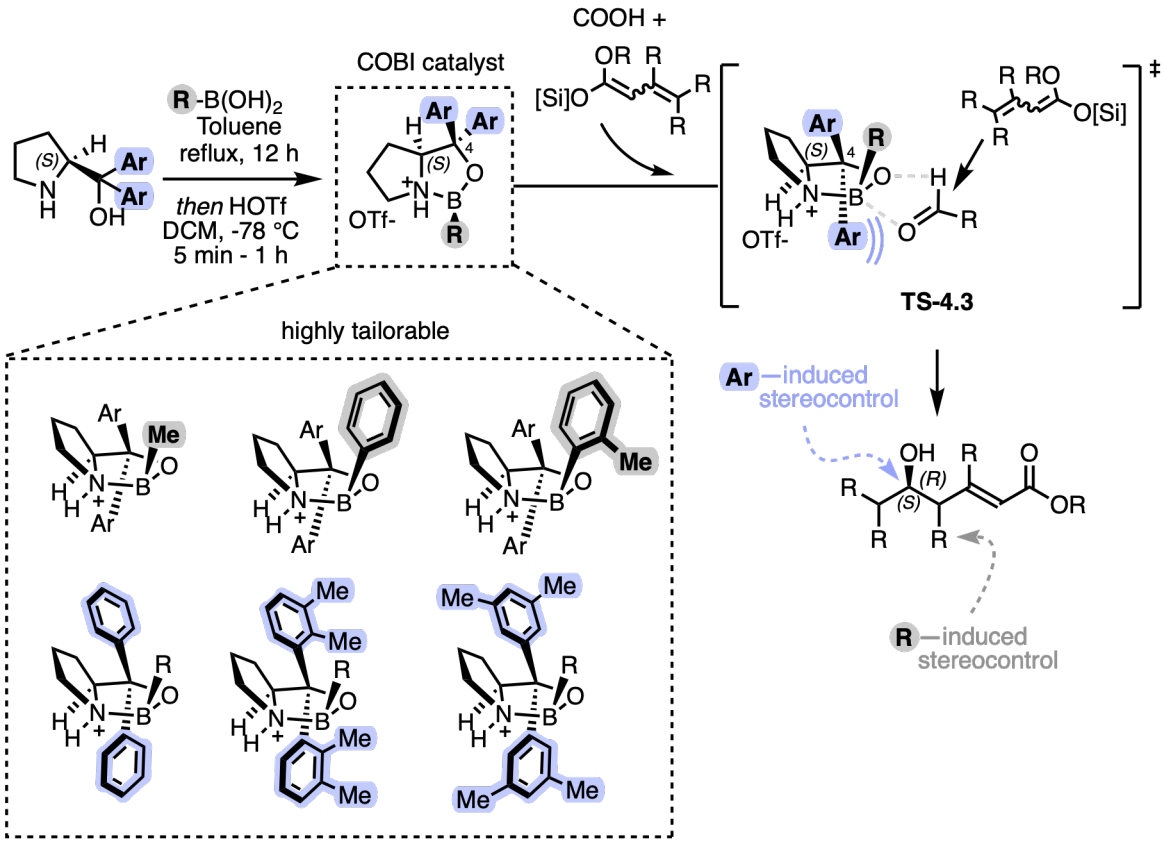


Figure 4.12. Generation of chiral oxazaborolidinium ion (COBI) catalyst from proline-derived amino alcohol and arylboronic acid, the and proposed transition state **TS-4.3** for the vinylogous Mukaiyama aldol reaction (ref 42). Aryl substituents at C4 (blue) control facial selectivity at the aldehyde (Ar-induced stereocontrol). Boron substituent R (grey) determines the binding orientation of the silyl nucleophile (R-induced stereocontrol). The modular scaffold accommodates structural variation at both positions.

subsequently applied to vinylogous Mukaiyama aldol by Boeckman and co-workers[46]. The study of COBIs and related oxazaborolidine-based chiral reagents have since been extended in its

application in bisvinylogous systems[47], Trp-based scaffolds[48], investigations of additives[48], and more broadly to natural product total synthesis[46,49–51].

These catalysts are generated in situ in two steps (**Figure 4.12**). Condensation of a proline-derived amino alcohol with a boronic acid in toluene at reflux affords the neutral CBS oxazaborolidine. Subsequent treatment with triflic acid at −78°C protonates the nitrogen to give the corresponding cationic oxazaborolidinium ion, substantially increasing the Lewis acidity of the boron centre. Upon coordination of the aldehyde to the Lewis acidic boron centre, the Re and Si faces of the carbonyl are rendered diastereotopic within the chiral environment of the catalyst. Facial selectivity arises from differential steric shielding by the C4 aryl substituent of the oxazaborolidine ring, directing nucleophilic attack to the less hindered face [46,52] (**Figure 4.12**). The modular nature of the CBS scaffold provides two independent handles on stereoselectivity according to Boeckman's model: variation of the C4 aryl groups (in blue, **Figure 4.12**) on the oxazaborolidine ring directs nucleophilic attack to one face of the coordinated aldehyde, while variation of the boron-bound substituent governs the orientation of the incoming silyl nucleophile, controlling diastereoselectivity at the terminal olefin carbon, when the it bears substituents (**Figure 4.12**)[46]. This two-parameter tunability makes these catalysts well suited to systematic optimization for a given substrate class, and makes COBIs a logical candidate for catalyst-controlled induction on a non-chelating α-substituted aliphatic aldehyde such as the immunomodulide aldehyde.

The C5 aldehyde **4.8** lacks the 1,3-heteroatom functionality required for productive Lewis acid chelation, placing it outside the scope of the β-substituted stereoinduction models discussed above. Stereochemical induction at this substrate therefore depends either on its intrinsic Felkin-Anh facial bias or on external catalyst control. As the target requires the 1,2-anti aldol product, Felkin-Anh control was predicted to deliver the undesired configuration. Lewis acid-mediated substrate-controlled conditions were nonetheless evaluated first to establish the intrinsic facial bias of **4.8**. Treatment with $BF_3{\cdot}OEt_2$ and $TiCl_4$ afforded high conversion but only modest diastereoselectivity, providing *syn:anti* ratios of 2:1 and 2.8:1 respectively (entries 1 and 2, **Table 4.2**). The weak intrinsic bias confirmed that **4.8** does not strongly favor either face under substrate control, encouraging investigations of external catalyst-controlled conditions.

$Ti(OiPr)_4$/(*R*)-BINOL conditions were evaluated as a catalyst-controlled alternative (entries 6–8). No product formation was detected under any of the Ti–BINOL conditions examined, regardless of the additive employed (none, LiCl, or 4Å molecular sieves). To determine

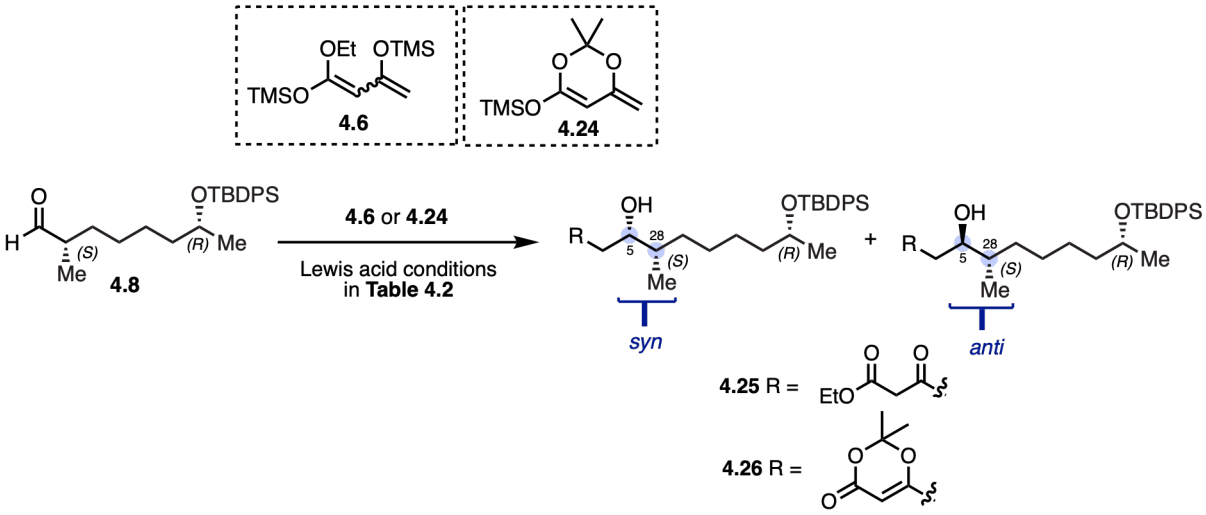
whether the absence of turnover reflected a catalyst incompatibility or an intrinsic limitation of titanium-based Lewis acids on this substrate, $Ti(OiPr)_4$ was evaluated in the absence of BINOL (entry 4). No conversion was observed, indicating that the OiPr ligands render the titanium centre insufficiently Lewis acidic to activate **4.8** toward nucleophilic addition. This is consistent with entry 3, in which $TiCl_2OiPr_2$ afforded less than 10% conversion, suggesting that partial chloride substitution partially restores Lewis acidity but remains inadequate. These results indicate that titanium-based stereocontrol on **4.8** is limited to substrate-controlled Felkin-Anh induction under $TiCl_4$ conditions, and that introduction of chelating or π-donor ligands required for asymmetric induction is incompatible with the Lewis acidity demands of this substrate.

Given the two-parameter tunability of COBI catalysts and their documented activity on non-chelating aldehydes, these were considered the most promising candidates for catalyst-controlled induction on **4.8**. High conversions were obtained under all COBI-derived conditions tested (entries 9-13), however, diastereoselectivity remained low across all variants. Both (*S*)-Me-CBS and (*S*)-Ph-CBS afforded the aldol product in approximately 2:1 d.r. (entries 4 and 5), comparable to the substrate-controlled results. Increasing steric bulk at the boron-bound substituent (Me, Ph, and o-tolyl) progressively attenuated conversion without any corresponding improvement in diastereoselectivity (entries 9,11, and 13), consistent with Boeckman's model. Addition of iPrOH as an additive with (*S*)-Ph-CBS completely suppressed product formation (entry 12), in contrast to reports suggesting that protic additives can improve selectivity via suppression of carbonyl activation by silicon[48,53,54]. Use of the enantiomeric (*R*)-Me-CBS catalyst produced only a marginal change in product distribution (1.6:1 d.r., entry 11), as expected given that inverting the configuration at boron does not alter the aryl environment responsible for aldehyde facial discrimination. The modest d.r. values across all COBI-derived conditions therefore reflect the limited intrinsic facial bias of **4.8** rather than a meaningful catalyst effect. Systematic variation of the C4 aryl substituents, which would require independent synthesis of the corresponding oxazaborolidines, was not pursued but remains a possible avenue for improving catalyst-controlled selectivity on this substrate class.

The modest stereocontrol observed across all aldehyde-activation strategies prompted consideration of an alternative approach in which chirality is introduced through the nucleophile rather than through activation of the electrophile. CuF_2/BINAP-based conditions, developed by Carreira and co-workers[55,56], operate through this complementary mechanism, in which fluoride-

mediated generation of a chiral copper dienolate transfers asymmetry directly at the γ-carbon of the vinylogous partner, bypassing the need for facial discrimination at the aldehyde entirely. Although CuF_2/BINAP demonstrated the highest selectivity on aromatic aldehyde substrates, yields of approximately 40% with high enantioselectivity were reported for aliphatic substrates[55], and this approach has since been applied successfully in four natural product total syntheses employing α-methyl-substituted aliphatic aldehydes[3,57–59]. These precedents warranted investigation of **4.8** under these conditions, using a TMS-dioxinone **4.24**
prepared in one step (see **Section 4.6**) as the vinylogous coupling partner in place of Chans' diene[55].

Unfortunately, no product formation was observed under these conditions in our hands. The absence of turnover is attributed to a practical limitation in the preparation of the nucleophile where removal of the salt byproducts generated during its synthesis could only be achieved by decanting, as attempted vacuum distillation consistently resulted in decomposition back to the dioxinone starting material. Residual LiCl in the reaction mixture is proposed to interfere with BINAP coordination to copper, via anion exchange to generate $CuCl_2$, which could disrupt formation of the active chiral copper complex and abolish asymmetric induction. Separately, Li^+ may coordinate the aldehyde carbonyl directly, rendering it less accessible to the chiral copper complex, further attenuating catalyst turnover. Given that cleaner nucleophile preparations have been reported to deliver high selectivity under CuF_2/BINAP conditions on closely related substrates[3,57–59], this approach remains a viable avenue for future investigation.



Entry	Diene	Lewis Acid (eq.)	Additive	Temp (°C)	Time (h)	Yield[a]	d.r. *(syn:anti)*
1[b]	**4.6**	BF_3OEt_2 (1.0)	--	-78	0.5	92%	2.2 : 1
2[b]	**4.6**	$TiCl_4$ (1.0)	--	-78	3	90%	2.8 : 1
3[b]	**4.6**	$TiCl_2O^iPr_2$ (1.0)	--	-78 to 25	16	< 10%	n/d
4[b]	**4.6**	$Ti(O^iPr)_4$ (1.0)	--	-78 to 25	72	0%	--
5[b]	**4.25**	BF_3OEt_2 (1.0)	--	-78	0.5	94%	2 : 1
6[c]	**4.6**	$Ti(O^iPr)_4$ (*R*)-BINOL (0.1)	--	-78 to 25	16	0%	--
7[c]	**4.6**	$Ti(O^iPr)_4$ (*R*)-BINOL (0.1)	LiCl (0.2)	-78 to 25	48	0%	--
8[c]	**4.6**	$Ti(O^iPr)_4$ (*R*)-BINOL (0.1)	4Å MS	-78 to 25	48	0%	--
9[d]	**4.6**	(*S*)-Me-CBS, HOTf (0.5)	--	-78	2.5	93%	2 : 1
10[d]	**4.6**	(*R*)-Me-CBS, HOTf (0.5)	--	-78	2.5	87%	1.6 : 1
11[d]	**4.6**	(*S*)-Ph-CBS, HOTf (0.5)	--	-78	2.5	54%	2 : 1
12[d]	**4.6**	(*S*)-Ph-CBS, HOTf (0.5)	iPrOH	-78	2.5	0%	--
13[d]	**4.6**	(*S*)-o-Tolyl-CBS, HOTf (0.5)	--	-78	2.5	40%	n/d
14[e]	**4.24**	CuF_2 (*R*)-BINAP (0.1)	--	-20	16	0%	--
15[e]	**4.24**	CuF_2 (*S*)-BINAP (0.1)	--	-20	16	0%	--

Table 4.2. Optimization of the vinylogous Mukaiyama aldol reaction between aldehyde **4.8** and Chans' diene **4.6** or TMS-dioxinone **4.24**. Diastereomeric ratios (syn:anti) refer to relative configuration at C5 and C28. [a]Yield determined by NMR. n/d = not determined. Carried out as per general procedure [b]A, [c]B, [d]C, [e]D (see **Section 4.6**)

The absence of meaningful stereocontrol across substrate-controlled, trityl cation, COBI-derived, and CuF_2/BINAP-based conditions, combined with the structural features of the aldehyde that place it outside the well-precedented substrate classes for each method, suggests that this substrate occupies a particularly difficult region of catalyst-controlled vinylogous Mukaiyama aldol chemistry. No conditions were identified that provided synthetically useful diastereoselectivity. The CuF_2/BINAP system could not be meaningfully assessed due to the nucleophile handling limitations described above, though it remains a credible avenue for future investigation alongside systematic variation of the C3 aryl substituents within the COBI framework. Rather than continuing optimization, the diastereomeric mixtures obtained from the aldol step were carried forward through the synthesis. Given the increasing structural complexity of subsequent intermediates, resolution via chromatography was anticipated to become more tractable at a later stage, as was seen purification of isomeric model substrates macrocycles investigated in Chapter II.

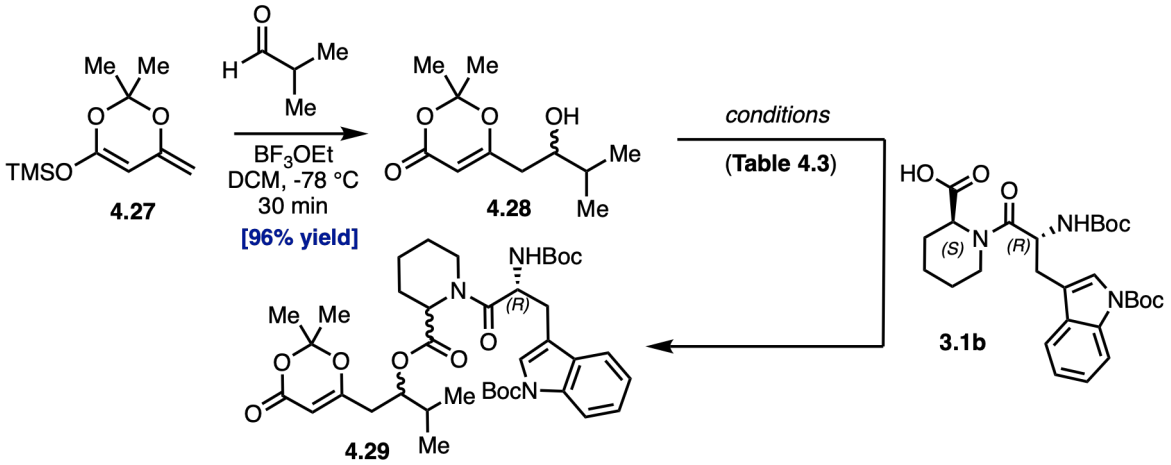
Importantly, these investigations led to the identification of the TMS-dioxinone **4.24** as the nucleophile of choice for all subsequent work. Unlike Chans' diene, the dioxinone functions as a protected β-ketoester equivalent, enabling direct elaboration toward the macrocyclization substrate without the functional group interconversions required in the original route. The low diastereoselectivity at C5 also rendered the planned diastereoselective reduction at C3 (**Figure 4.6**) impractical at this stage as both the Evans-Saksena and Narasaka-Prasad reduction protocols rely on the existing β-hydroxy group (C5) as a directing handle.

Carrying the aldol product forward as the dioxinone-derived β-ketoester instead allowed the diastereomeric mixture to be advanced directly into macrocyclization, where the increased structural complexity was expected to improve chromatographic resolution of the epimers. Reduction at C3 was therefore postponed until after macrocycle formation, where conformational constraints imposed by the ring were anticipated to provide additional facial bias not available in the acyclic intermediate. This strategy is explored further in **Section 4.4.2** and **4.4.3** where acylketene trapping is explored as an alternative method for ring-closure and sequence optimizations are investigated.

4.4.2 Evaluation of Acyl Ketene Ring-Closure in a Model System

With the dioxinone identified as the nucleophile of choice for the vinylogous Mukaiyama aldol reaction, attention turned to evaluating whether the dioxinone could serve a second strategic function: as a masked acyl ketene precursor for intramolecular ring closure. Thermal retro-hetero-Diels-Alder fragmentation of the dioxinone at elevated temperature generates a reactive acyl ketene intermediate, which can be intercepted by a suitable nucleophile. The indole NH of the tryptophan residue in the NRPS fragment was identified as a candidate intramolecular nucleophile for this purpose, offering a direct route to the macrolactam bond without requiring a separate macrolactonization or macrolactamization step.

To evaluate this strategy without expending the elaborated PKS aldehyde, a simplified model system was assembled in which isobutyraldehyde was used in the vinylogous Mukaiyama aldol reaction in place of the aldehyde synthesized in **Section 4.4.1**. This reaction proceeded smoothly generating **4.28** in 96% yields as a racemic mixture. This model preserves the functionality at the dioxinone terminus, and the C5 hydroxyl while conserving material. With the model PKS fragment in hand, coupling to the NRPS fragment (**3.1b, Figure 4.12**) was first attempted under planned



Mitsunobu conditions. Treatment with PPh_3 and DIAD in THF at room temperature failed to afford product (entry 1, **Table 4.3**), as did analogous conditions in toluene at elevated temperature (entry 2). Increasing the reagent stoichiometry with either DEAD or DIAD likewise returned no product or only trace conversion (entries 3 and 4). The failure of Mitsunobu conditions across all variants is attributed to the steric demands of the secondary alcohol in the dioxinone model fragment.

Figure 4.13. Assembly of model system **4.29** for evaluation of acyl ketene ring-closure.

Entry	Reagents (eq.)	Solvent	Temp (°C)	Yield
1	PPh3 (1.3), DIAD (1.3)	THF	0 to 25	0%
2	PPh3 (1.3), DIAD (1.3)	toluene	0 to 25	0%
3	PPh3 (4.0), DEAD (3.9)	THF	0 to 25	0%
4	PPh3 (4.0), DIAD (3.9)	toluene	0 to 25	<5%
5	EDC (1.2) DMAP (0.1)	DCM	25	60%

Table 4.3. Optimizations for esterification between dioxinone model **4.28** and simplified NRPS substrate **3.1b.**

Esterification using carbodiimide-mediated conditions (EDC, DMAP) at room temperature instead afforded the coupled product in 60% yield (entry 5, **Table 4.3**). These conditions were expected to epimerize the α-proton of the pipecolic acid residue, consistent with observations made during model system studies for route C (**Section 2.2.2**). At this stage, however, the racemic product was carried as the objective was to establish proof of concept for the acyl ketene ring-closure chemistry rather than to deliver a stereochemically defined intermediate. Optimization of the coupling step to suppress epimerization is addressed in **Section 4.4.3**.

The coupled ester was subjected to Boc deprotection with TFA in DCM at room temperature, liberating the free amine and providing the cyclization precursor (m/z 512, $[M+H]^+$). Heating in toluene at reflux for one hour triggered retro-hetero-Diels-Alder fragmentation of the dioxinone, generating the acyl ketene intermediate **4.30** in situ which was trapped intramolecularly by the indole NH of the tryptophan residue afforded the ring-closed product (**4.31**; *m/z* 476, $[M+Na]^+$, **Figure 4.14**). This confirmed that route C was still accessibly through acyl ketene trapping of the corresponding dioxinone rather than through tradition macrolactamization conditions explored in Chapter II. However, formation of the diketopiperazine (DKP) byproduct

(**4.32**; m/z 298, $[M+H]^+$) was observed as a major competing pathway (**Figure 4.14**). The DKP was isolated and fully characterized by NMR and HRMS (see experimental, **Section 4.6**), confirming its identity as the product of intramolecular condensation between the free amine and

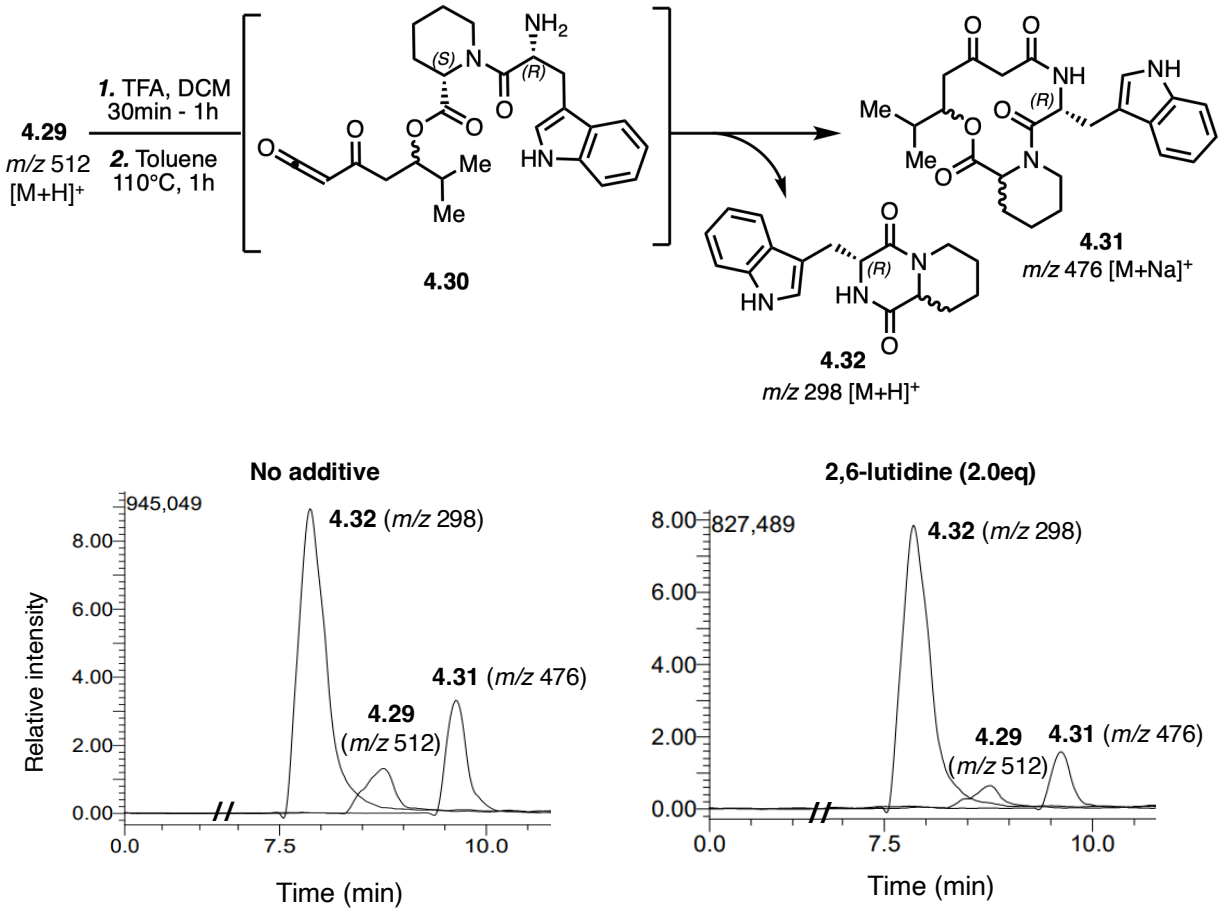


Figure 4.14. Testing acyl ketene trapping conditions in model **4.29** affords ring-closed macrolactam **4.31** and diketopiperazine **4.32** as a competing byproduct. Extracted ion chromatograms of LCMS trace at 1h in the absence (left) and presence (right) of 2,6-lutidine additive.

the adjacent pipecolic acid carbonyl. DKP formation via intramolecular condensation between the free amine and the adjacent pipecolic acid carbonyl is a known side reaction in this compound class, and has been documented in Zhao's attempt towards stereocalpin A[60]. The propensity for DKP formation is also well established to increase under thermal conditions and in the presence of base. Consistent with this, inclusion of 2,6-lutidine as an additive in a test reaction further promoted DKP formation at the expense of the desired ring-closed product, confirming that basic conditions are detrimental in this system (**Figure 4.14**).

These model system studies confirmed that acyl ketene trapping by the tryptophan indole NH is a viable macrolactamization strategy, while identifying two limitations requiring resolution before application to the full substrate. The thermal conditions required for acyl ketene generation are fundamentally incompatible with suppression of DKP formation, and epimerization at the pipecolyl stereocenter under EDC-mediated coupling conditions introduces a stereochemical liability at the outset. Efforts to address both limitations are ongoing and represent the most recent progress on this total synthesis, as described in **Section 4.4.3.**

4.4.3 Sequence Optimizations to Construct Immunomodulide

Before pursuing further optimization of the Route C ring-closure, the advanced PKS intermediate was briefly redirected toward the Route B ring-closure disconnection identified in

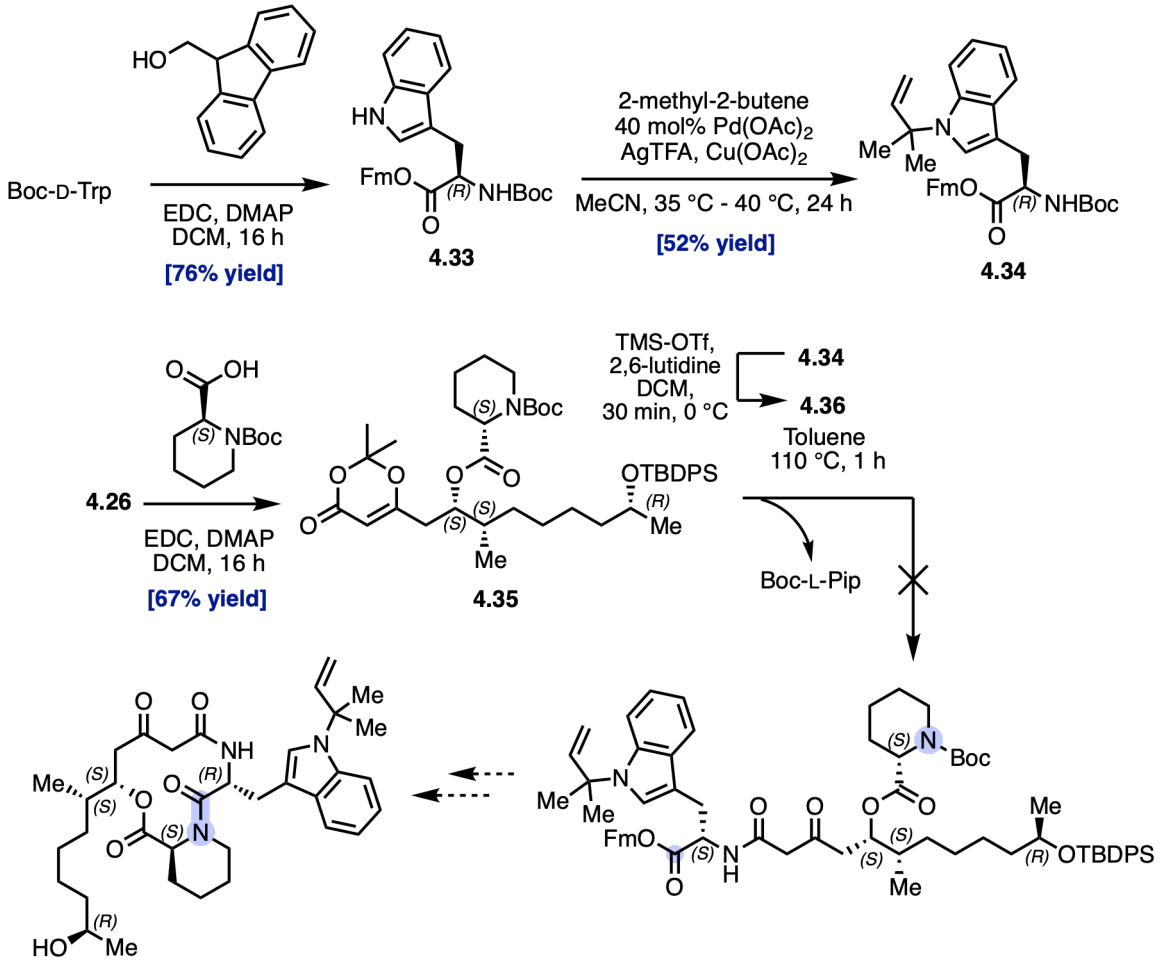


Figure 4.15 Attempted route B macrolactamization (blue) esterification-then-acyl ketene trapping of D-Trp coupling partner (**4.36**) results in decomposition of **4.35** in refluxing toluene conditions.

Chapter 2, in which the macrolactam bond is formed at the amide bond between the two amino acid residues rather than through acyl ketene trapping. This disconnection avoids the thermal conditions responsible for DKP formation in Route C entirely and represented a potentially rapid solution given that advanced material was already in hand.

To this end, the requisite D-Trp coupling partner (**4.34**) was prepared in two steps from Boc-D-Trp via EDC-mediated esterification with 9-fluorenylmethanol followed by reverse prenylation under palladium catalysis, affording **4.34** in 52% yield over two steps. Esterification of Boc-L-Pip with the C5 alcohol of PKS aldol product (**4.26**) using EDC and DMAP in DCM afforded the coupled intermediate **4.35** in 67% yield. Boc deprotection of **4.34** with TMSOTf and 2,6-lutidine in DCM at 0 °C was performed under mild conditions to avoid reverse prenyl migration, and the crude free amine **4.36** was carried directly into the next step without purification. Heating **4.35** in toluene at 110 °C for one hour to generate the acyl ketene intermediate in situ and effect trapping by the D-Trp fluorenyl ester resulted instead in decomposition of the PKS-Pip ester **4.35**. Instead, free pipecolic acid was detected in the reaction mixture, consistent with ester cleavage as a downstream consequence of dioxinone decomposition under the thermal conditions. To confirm this, **4.35** was heated in toluene at 110 °C, which produced the same

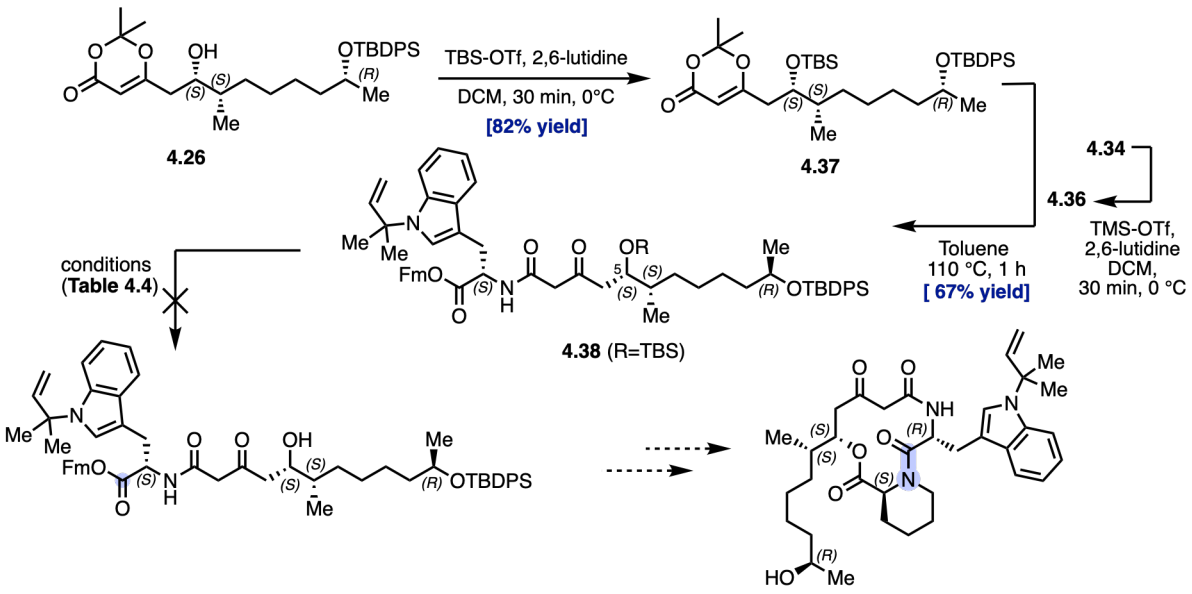


Figure 4.16. Attempted route B macrolactamization (in blue) via acyl ketene trapping by a D-Trp coupling partner (**4.36**)-then esterification and ring-closure reveals that deprotection of the C5 TBS ether is not possible under conditions examined (**Table 4.4**).

unidentified decomposition product, establishing that the PKS fragment itself is inherently unstable under these conditions independently of the coupling partner.

To circumvent the PKS fragment instability observed under the coupling-first sequence, the C5 alcohol of **4.26** was instead protected as a TBS ether using TBS-OTf and 2,6-lutidine in DCM at 0 °C, affording **4.37** in greater than 95% yield. Boc deprotection of the D-Trp coupling partner **4.34** was then performed under the same mild conditions (TMSOTf, 2,6-lutidine, DCM, 0 °C), and the crude free amine **4.36** was advanced directly into toluene reflux at 110 °C to effect

Condition	Observation
TBAF (3.0eq)	Ester hydrolysis
TBAF (3.0eq), AcOH (3.5eq), 72h	No change
4M HCl, MeOH	decomposition
1M HCl, MeOH	decomposition
PPTS, MeOH, 72h	No change
$BF_3 \cdot OEt_2$, DCM, -78°C	decomposition

Table 4.4. Conditions evaluated for deprotection of the C5 silyl ether of **4.38**. Reactions were monitored by LC-MS.

acyl ketene trapping, affording the Trp-coupled intermediate **4.38** in 67% yield. However, subsequent deprotection of the C5 silyl ether to unmask the TBS-protected alcohol could not be achieved under any conditions examined (**Table 4.4**), with neither the TBS nor TMS (not shown) protecting group removable without decomposition of the substrate. The origin of this failure was not established. Fluoride-mediated conditions (TBAF) could not be employed as they resulted in hydrolysis of the fluorenyl ester of the D-Trp residue. Buffered fluoride conditions (TBAF, AcOH) were therefore evaluated to suppress ester hydrolysis, but returned no deprotected product even after 72 hours. Strong acid conditions decomposed the reverse prenyl group on the tryptophan residue, and milder acidic conditions likewise failed to effect silyl ether removal. Silyl migration from the C5 oxygen to the enol of the adjacent β-ketoester, while not confirmed, may represent a contributing factor that renders the silyl group inaccessible to standard deprotection conditions. With no viable deprotection conditions identified that were compatible with the full functionality of the substrate, the Route B evaluation was abandoned and attention returned to Route C.

Attention returned to Route C, now with modifications informed by the limitations identified in the model system studies (**Section 4.4.2**). The epimerization observed under EDC-

mediated coupling conditions prompted evaluation of Yamaguchi esterification for coupling the intact NRPS fragment (**2.24**) to the PKS alcohol (**4.26**) (**Figure 4.17**), a method with precedent in

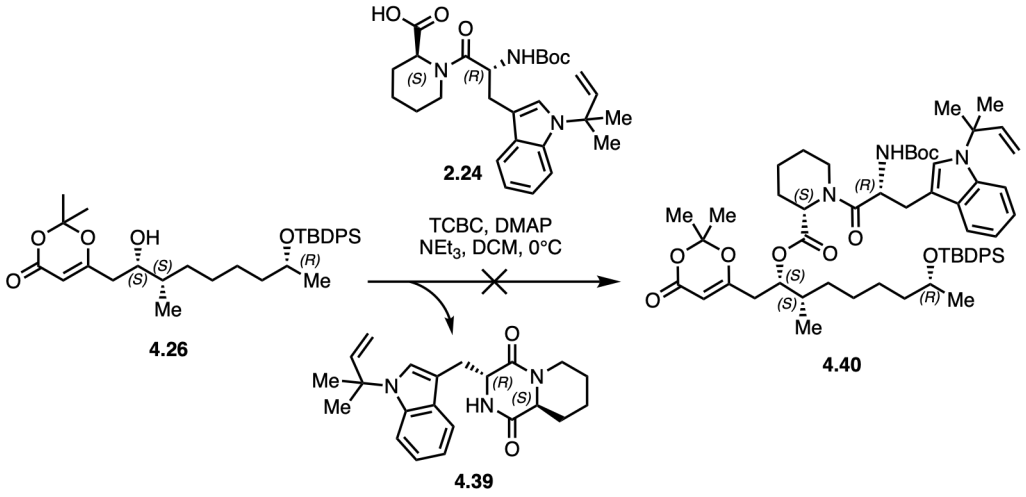


Figure 4.17. Yamaguchi esterification between PKS-dioxinone fragment **4.26** and NRPS fragment **2.24** affords DKP (**4.39**).

total synthesis attempts on related cyclic tridepsipeptide scaffolds[16]. However, the highly activated mixed anhydride intermediate promoted DKP formation even in the presence of the *N*-Boc protecting group on the pipecolic nitrogen, with the DKP (**3.29**) isolated and confirmed by NMR and HRMS. The susceptibility of the Boc-protected dipeptide to cyclization under these forcing activation conditions indicated that the Boc carbamate alone was insufficient to suppress DKP formation when the acylating species was sufficiently reactive. Di-Boc protection of the dipeptide nitrogen (Boc_2O, DMAP) was also attempted to further attenuate nucleophilicity but was unsuccessful under the conditions examined and may warrant revisiting under more forcing conditions.

These results established that coupling of the dipeptide fragment (**2.24**) to the PKS alcohol (**4.26**) was not viable regardless of the esterification method employed, and that stepwise installation of the amino acid residues was necessary. As such D-Trp(*N*-rev-prenyl) free acid **4.41** (**Figure 4.18**) was accessed instead, from its corresponding ester (**4.34**) via dimethylamine Fmoc removal at room temperature, affording **4.41** in 72% yield. Boc deprotection of the Pip-PKS fragment **4.35** with (4M) HCl in dioxane then liberated the free pipecolic amine, to which the D-Trp(*N*-rev-prenyl) acid **4.41** was appended under standard amidation conditions (HATU/DIPEA), affording the linear precursor **4.40** in 52% yield over two steps. With the linear precursor in hand, Boc deprotection was attempted using TMSOTf and 2,6-lutidine in DCM at 0 °C, and the resulting intermediate was advanced directly into the toluene reflux at 110 °C for acyl ketene ring-closure.

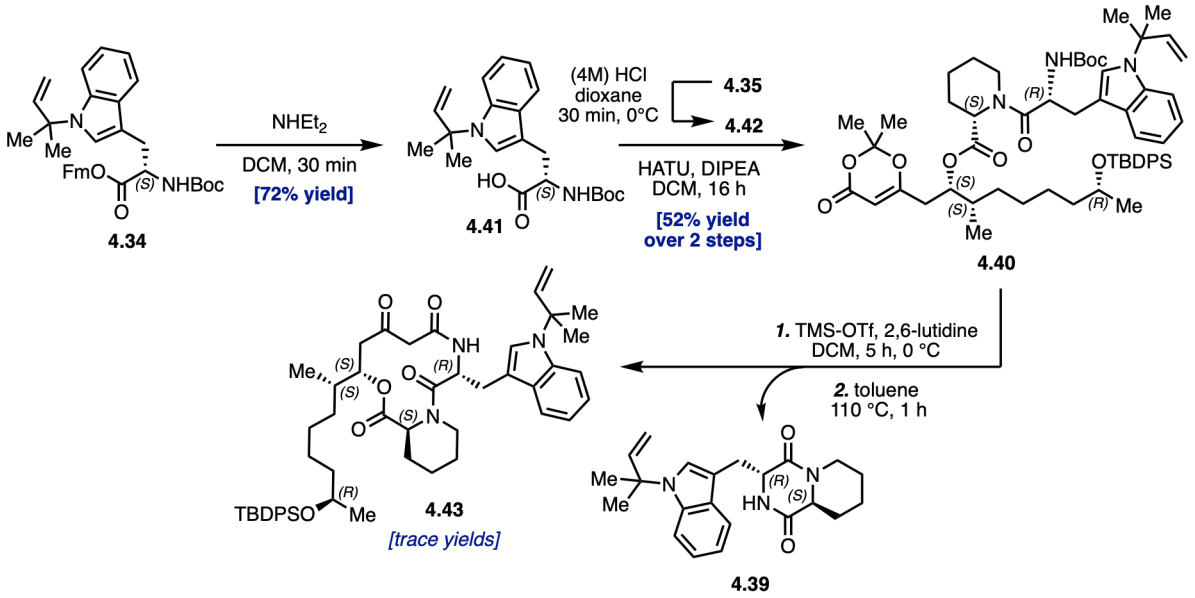


Figure 4.18 Synthesis of route C macrolactamization precursor **4.40** and acyl-ketene ring-closure attempt

Instead of effecting a clean Boc removal, TMSOTf is proposed to have activated the dioxinone toward ring-opening, effecting a rearrangement that resulted in ester cleavage and release of the NRPS fragment **2.24** as a free acid. This was consistent with TLC monitoring, showing disappearance of the starting material and the appearance of a new spot with an Rf consistent with the NRPS dipeptide acid. At that stage, the crude mixture was advanced directly into toluene reflux (step 2), where LC-MS analysis at 1 h showed evidence of the DKP (**4.49**) as the primary product (full spectroscopic characterization data pending), alongside unreacted

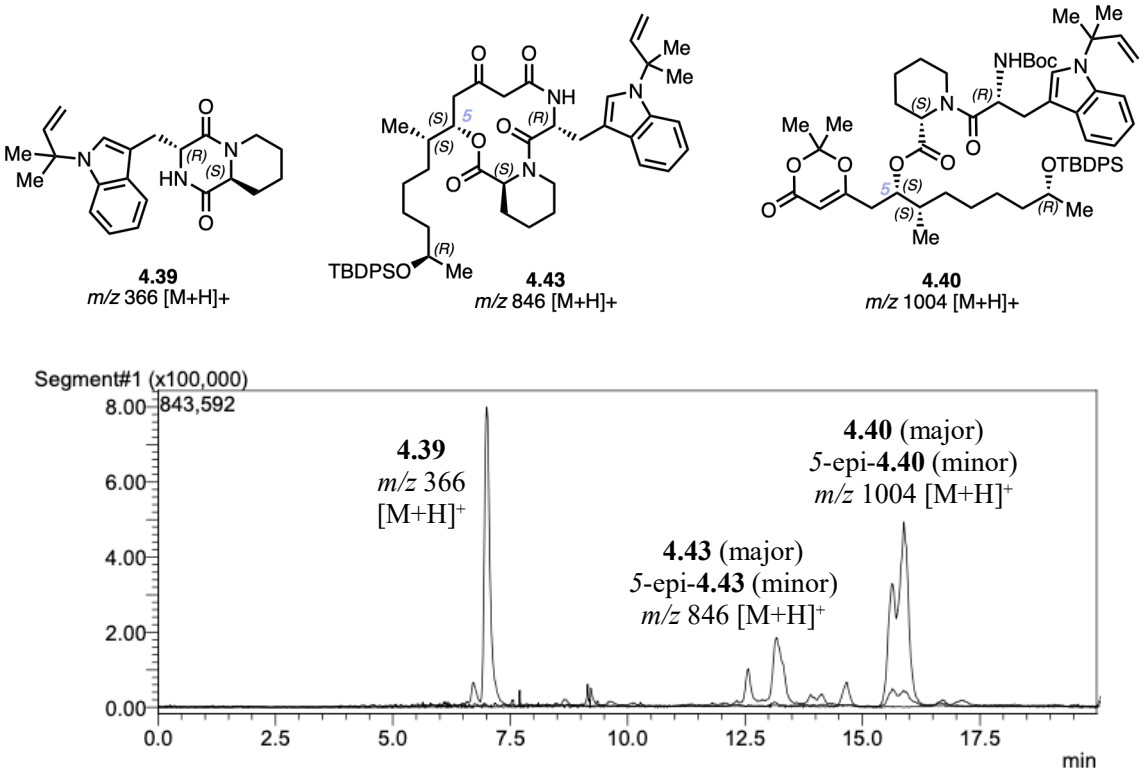


Figure 4.19. Reaction profile of acyl ketene ring-closing step. LC-MS extracted ion chromatogram (*m/z* 366, 846 and 1004) and structure of detected compounds shown: DKP **4.39** (*m/z* 366), unreacted starting material **4.40** (*m/z* 846) and product **4.43** (*m/z* 846).

starting material **4.40** and a low-intensity signal consistent with the expected mass of the macrolactam product **4.43** (**Figure 4.19**). At this stage, it remains to be determined whether DKP formation arises during ring-closure as a competing reaction (as anticipated by the model studies **Section 4.4.2**), or whether the DKP detected here formed from the dipeptide free acid intermediate generated during deprotection. What proportion of the observed DKP arises from each pathway is also to be determined. Importantly however, this observation confirmed that acyl ketene ring-

closure remained operative under these conditions, and that optimization of the upstream deprotection to improve the yield of cyclization-competent intermediate represents a critical priority.

Collectively, the studies described in this section identified three persistent bottlenecks in the assembly of the immunomodulide macrolactam. First, the ester linkage between the PKS fragment and the pipecolic residue demonstrated inherent instability under the thermal conditions required for bimolecular acyl ketene trapping, leading to dioxinone decomposition and subsequent ester cleavage observed (**Figure 4.15**). This instability was confirmed by heating the Pip-PKS fragment independently under the same conditions and precluded all synthetic sequences in which bimolecular acyl ketene trapping was attempted on the intact ester intermediate. Second, the C5 silyl ether introduced during the Route B sequence could not be removed under any conditions examined (**Figure 4.16**), as the substrate was incompatible with both fluoride- and acid-mediated deprotection, and Route B was not pursued further. Lastly, TMSOTf-mediated Boc deprotection of the linear precursor promoted PKS fragment decomposition, likely through unproductive activation of the dioxinone by the silyl Lewis acid (**Figure 4.18**). The first two constraints were addressed by redirecting the ring-closing strategy toward route C, which avoids both the bimolecular ester intermediate responsible for the first constraint and the C5 silyl ether responsible for the second. Current efforts are focused on identifying Boc deprotection conditions compatible with the dioxinone functionality, and on evaluating Lewis acid-mediated acyl ketene activation as a low-temperature alternative to the forcing thermal conditions that bias towards DKP formation. Work toward these objectives is ongoing.

4.5 Conclusions and Future Directions

The work described in this chapter addressed three challenges deferred from the model system studies of Chapters II and III: (1) configurational assignment of the PKS fragment, (2) stereoselective synthesis of that fragment, and (3) macrolactamization on the fully elaborated substrate.

Comparative ^{13}C NMR analysis against configurationally defined congeners of the 12-membered cyclic tridepsipeptide family narrowed the sixteen possible stereochemical permutations of the PKS fragment to a single synthetic lead, identifying the *3R,5S,28S,33R* configuration of colletopeptide E as the closest structural match to immunomodulide. This

assignment was supported by a negative control comparison against 2,5-diepi-acremolide B, which produced large Δppm deviations consistent with a confirmed configurational mismatch. A two-generation synthetic campaign was undertaken to access the PKS fragment. The first-generation route, relying on olefin cross-metathesis to assemble the carbon framework, was limited by moderate and irreproducible yields and was abandoned. The second-generation approach exploiting retro-Claisen ring-opening of 2-acetylcyclohexanone instead to access the backbone of the PKS fragment. This revised route delivered the aldehyde coupling partner **4.8** in fewer steps from inexpensive commercial starting materials, while preserving stereochemical tailorability at both C28 and C33.

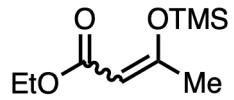
Diastereoselective installation of the C5 stereocenter via vinylogous Mukaiyama aldol reaction proved challenging. The immunomodulide aldehyde **4.8**, a non-chelating α-methyl substituted aliphatic aldehyde, sits outside the substrate classes for which chelation-controlled, titanium-BINOL-mediated have been demonstrated to deliver useful diastereoselectivity. No conditions evaluated afforded synthetically useful facial bias, and the CuF_2/BINAP system could not be meaningfully assessed due to nucleophile handling limitations arising from residual LiCl in the TMS-dioxinone preparation. A 2:1 diastereomeric mixture was carried forward, with chromatographic resolution deferred to a later stage. These investigations identified the TMS-dioxinone as the nucleophile of choice for all subsequent work, enabling direct access to macrocyclization intermediates and deferring the C3 reduction to the macrocyclic stage where conformational constraints may provide additional facial bias.

Model system studies established that acyl ketene trapping of the dioxinone by the tryptophan indole NH is a viable macrolactamization strategy, providing proof-of-concept for the Route C ring-closure via this alternatie strategy. However, the two limitations were identified were DKP formation under the thermal conditions required for acyl ketene generation, and epimerization at the pipecolyl α-carbon under EDC-mediated coupling conditions. Efforts to circumvent DKP formation through the Route B ring-closure disconnection were unsuccessful, as the PKS-Pip ester **4.35** intermediate demonstrated inherent instability under the thermal conditions required for bimolecular acyl ketene trapping, while C5 silyl ether deprotection of **4.38** in the alternative sequence could not be achieved under any conditions compatible with the full substrate functionality. Returning to Route C with stepwise NRPS fragment assembly using Boc-Pip suppressed epimerization, but a final TMSOTf-mediated Boc deprotection of the linear precursor

for cyclization promoted an uncharacterized rearrangement of the dioxinone accompanied by ester cleavage and DKP formation. Preliminary LC-MS evidence for the macrolactam product was nonetheless obtained, confirming that the acyl ketene ring-closure step itself remains operative.

Three priorities define the path forward from this chapter. First, the immediate synthetic bottlenecks identified in **Section 4.4.3**, namely the TMSOTf-mediated dioxinone rearrangement and DKP formation under thermal conditions, must be resolved before the acyl ketene ring-closure can be evaluated on the fully elaborated substrate. Second, once a clean route to the macrolactam is established, the C3 stereocenter can be addressed through diastereoselective reduction on the intact macrocycle, where conformational constraints not available in the acyclic intermediate may provide the facial bias that could not be achieved due to a poorly selective aldol. Third, and most critically, the synthesized macrolactam must be subjected to full spectroscopic characterization and compared against the isolated natural product to validate the *3R,5S,28S,33R* configurational assignment proposed in **Section 4.2.** Should a mismatch be identified, the tailorable retrosynthetic design described in **Section 4.3** permits selective inversion at any individual stereocenter without requiring a complete redesign of the synthetic route, providing a clear path to structural correction. Progress toward these objectives is ongoing.

4.6 Experimental Section

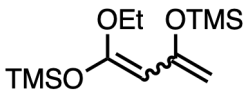


ethyl 3-((trimethylsilyl)oxy)but-2-enoate (4.10): as per literature reference[61]

Compound isolated as a 3:1 mixture of diastereomers. Major diastereomer is assigned:

^{1}H NMR (400 MHz, $CDCl_3$) δ 5.09 (s, 1H), 4.09 (q, 2H), 2.17 (s, 3H), 1.24 (t, *J* = 1.2 Hz, 3H), 0.25 (s, 9H).

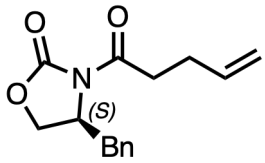
^{13}C NMR (101 MHz, $CDCl_3$) δ 169.6, 168.0, 99.7, 59.3, 20.7, 14.4, 0.2.



4-ethoxy-2,2,8,8-tetramethyl-6-methylene-3,7-dioxa-2,8-disilanon-4-ene (4.6): as per literature reference[61]

^{1}H NMR (400 MHz, $CDCl_3$) δ 4.47 (s, 1H), 4.13 (d, J = 1.4 Hz, 1H), 3.90 (d, J = 1.4 Hz, 1H), 3.76 (q, J = 7.0 Hz, 2H), 1.29 (t, J = 7.0 Hz, 3H), 0.25 (s, 6H), 0.20 (s, 6H).

^{13}C NMR (101 MHz, $CDCl_3$) δ 157.7, 153.6, 89.2, 77.9, 63.6, 14.4.



(S)-4-benzyl-3-(pent-4-enoyl)oxazolidin-2-one (4.12): as per literature reference[62]

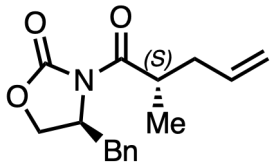
NEt3 (2.78 mL, 20mmol, 2.0eq) was added dropwise to a stirring solution of 4-pentenoic acid (1.0g, 10 mmol 1.0eq) in THF (dry) (0.25M) under inert atmosphere at -78°C. To this mixture, pivolyl chloride (1.48 mL, 12mmol, 1.2eq) was added dropwise and the resulting mixture was stirred for 20 minutes at -78°C after which it was allowed to warm to room temperature. The mixture was again cooled to -78°C and LiCl (1.2g, 30mmol, 3.0eq) was added followed by a solution of (4S)-4-benzyl oxazolidin-2-one (2.12g, 12mmol, 1.2eq) in THF (dry). Stirring was continued overnight as the reaction was left to warm to room temperature. The reaction was quenched with NH4Cl (sat.), the aqueous layers were extracted with EtOAc (x3). Organic layers

were combined and washed with brine, dried over MgSO4, filtered, and concentrated to afford the crude product. Purification was achieved via silica gel chromatography (10-20% EtOAc in Hexanes) to afford pure product **4.12** as a colourless oil (1.5g, 5.8mmol, 58% yield).

TLC (20% EtOAc/Hexanes): R_f= 0.4

^{1}H NMR (600 MHz, $CDCl_3$) δ 7.36 – 7.30 (m, 2H), 7.30 – 7.24 (m, 2H), 7.21 (dd, J = 7.0, 1.4 Hz, 2H), 5.94 – 5.84 (m, 1H), 5.11 (dt, J = 17.1, 1.6 Hz, 1H), 5.04 (dt, J = 10.2, 1.4 Hz, 1H), 4.68 (dddd, J = 10.8, 7.4, 3.2, 1.8 Hz, 1H), 4.24 – 4.14 (m, 2H), 3.30 (dd, J = 13.5, 3.4 Hz, 1H), 3.14 – 3.06 (m, 1H), 3.06 – 2.98 (m, 1H), 2.76 (ddd, J = 13.5, 9.7, 1.3 Hz, 1H), 2.50 – 2.43 (m, 2H).

^{13}C NMR (151 MHz, $CDCl_3$) δ 172.7, 153.6, 136.8, 135.4, 129.6, 129.1, 127.5, 115.9, 66.4, 55.4, 55.3, 38.1, 35.0, 28.3.



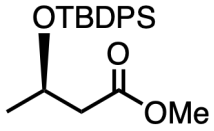
(S)-4-benzyl-3-((S)-2-methylpent-4-enoyl)oxazolidin-2-one (4.9): as per literature reference[62]

To a stirring solution of **4.12** (1.5g, 5.8mmol,1.0eq) in THF (dry) (0.4M) at -78°C under inert atmosphere, (1M) NaHDMS in THF (8.7mL, 8.7 mmol, 1.5eq) was added dropwise and the reaction was left to stir for 1 hour. Following this, drop-wise addition for Ch3I (1.44 mL, 23.2 mmol, 4.0eq) was executed at -78°C and stirring of the resulting mixture was continued for an additional 1-2 hours (until TLC shows reaction completion). Upon completion, the mixture was quenched with NH4Cl (sat.), the aqueous layers were extracted with ether (x2). Organic layers were combined and washed with brine, dried over MgSO4, filtered, and concentrated to afford the crude product. Purification of the alkene was achieved via silica column chromatography (20% EtOAc in Hexanes) to afford **4.9** as pale-yellow oil (712mg, 2.6mmol, 45% yield)

TLC (20% EtOAc/Hexanes): R_f= 0.5

^{1}H NMR (600 MHz, $CDCl_3$) δ 7.37 – 7.31 (m, 2H), 7.29 – 7.27 (m, 1H), 7.24 – 7.19 (m, 2H), 5.86 – 5.73 (m, 1H), 5.12 – 5.00 (m, 2H), 4.67 (dddd, J = 13.7, 7.3, 3.3, 0.8 Hz, 1H), 4.23 – 4.13 (m, 2H), 3.83 (h, J = 6.9 Hz, 1H), 3.33 – 3.24 (m, 1H), 2.77 (dd, J = 13.4, 9.6 Hz, 1H), 2.48 (dtt, J = 14.1, 7.0, 1.3 Hz, 1H), 2.20 (dtt, J = 13.9, 6.9, 1.2 Hz, 1H), 1.24 (dd, J = 6.9, 0.8 Hz, 3H).

^{13}C NMR (151 MHz, $CDCl_3$) δ 176.6, 153.2, 135.7, 135.4, 129.6, 129.1, 127.5, 117.2, 66.2, 55.5, 38.1, 37.7, 37.6, 17.2.



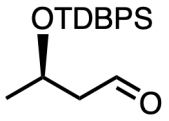
methyl (R)-3-((tert-butyldiphenylsilyl)oxy)butanoate (4.13)[63]**.**

To a stirring solution of Methyl (R)-3-hydroxybutyrate (2.0mL, 15.8, 1.0eq) in 40mL of dry DCM at -0°C under N_2 atmosphere, add imidazole (2.2g, 31.6mmol, 2.0 eq), TBDPSCl (5.2mL, 19.0, 1.2 eq) and DMAP (19.3mg, 0.158eq, 0.01eq). The reaction was left to stir vigorously overnight and warm to room temperature. Upon completion (determined by TLC), the reaction was diluted with H_2O and the aqueous layers were extracted with DCM (x2). The combined organic fractions were washed with brine, dried over Na2SO4, filtered and concentrated to afford **4.13** (6.0g, 16.82, 96% yield) as a colourless oil and was used in subsequent steps without the need for further purification.

TLC (10% EtOAc/Hexanes): R_f= 0.6

^{1}H NMR (400 MHz, $CDCl_3$) δ 7.69 (tt, J = 5.8, 1.6 Hz, 4H), 7.44 – 7.36 (m, 6H), 4.37 – 4.24 (m, 1H), 3.59 (s, 3H), 2.57 (dd, J = 14.6, 7.1 Hz, 1H), 2.45 – 2.34 (m, 1H), 1.12 (d, J = 6.1 Hz, 3H), 1.04 (s, 9H).

^{13}C NMR (101 MHz, $CDCl_3$) δ 171.9, 135.9, 135.8, 134.8, 134.3, 133.9, 129.7, 129.6, 127.7, 127.6, 127.5, 66.9, 51.4, 44.4, 26.9, 26.6, 23.6, 19.2.



(R)-3-((tert-butyldiphenylsilyl)oxy)butanal (4.14)[63]

An oven-dried flask was charged with **4.13** (6.89g, 19.3mmol, 1.0eq) in 96 mL of dry DCM under inert atmosphere. The stirring suspension was cooled to -78°C and (1M) DIBAL in THF (43mL, 43mmol, 2.2eq) was added dropwise. The reaction was left to warm to room temperature spontaneously overnight. Upon completion, the mixture was cooled to 0°C and stirred vigorously while EtOAc was added dropwise. After 15 minutes, a saturated solution of Rochelle's salt was

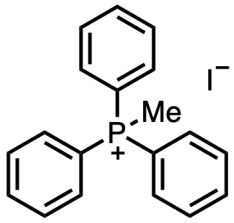
added and the mixture was left to stir for at least 30 minutes. The aqueous layer was extracted with EtOAc (x3), and organic layers were combined, washed with brine, dried over MgSO4 and filtered to afford the intermediate alcohol as a viscous oil. The product was sufficiently pure to use in the next step without further purification.

To a stirring solution of oxalyl chloride (3.31mL, 38.6mmol, 2.0eq) in 40mL of dry DCM at -78°C under inert atmosphere, was added DMSO (5.5mL , 77.2mmol, 4.0eq) dropwise. After 30 minutes of stirring, this mixture was transferred to a solution of the crude intermediate alcohol in 26mL of dry DCM dropwise and the resulting mixture was stirred for 1 hour. NEt3 (14.4mL, 96.5mmol, 5.0 eq) was then added dropwise, and the reaction was left to warm to room temperature over 30 minutes. Roughly 100mL of H_2O was then added and the aqueous layer was extracted with EtOAc. The organic layers were combined, washed with brine, dried over Na2SO4 and filtered to afford the aldehyde **4.14** (5.9g, 17.9mmol) in an 93% overall yield over two steps.

TLC (100% EtOAc/Hexanes): R_f= 0.5

^{1}H NMR (400 MHz, $CDCl_3$) δ 9.76 (dd, J = 2.9, 2.1 Hz, 1H), 7.70 – 7.66 (m, 4H), 7.45 – 7.35 (m, 6H), 4.35 (h, J = 6.1 Hz, 1H), 2.57 (q, J = 7.3 Hz, 2H), 2.54 – 2.41 (m, 2H), 1.18 (d, J = 6.2 Hz, 3H), 1.08 (s, 1H), 1.05 (d, J = 0.6 Hz, 6H).

^{13}C NMR (101 MHz, $CDCl_3$) δ 202.2, 135.9, 134.9, 134.1, 133.7, 130.0, 129.8, 129.7, 127.9, 127.8, 127.7, 77.4, 65.8, 52.9, 46.1, 27.0, 24.0, 19.3.

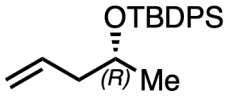


Methyltriphenylphosphonium iodide (4.15)

To a stirring mixture of triphenylphosphine (1.5g, 5.72mmol, X eq) in 14mL of benzene, methyl iodide (, 28.6mmol, 5.0eq) was added dropwise. The mixture was stirred for 24h under intert atmosphere. Upon completion, the mixture was filtered by vacuum filtration, and the precipitate was washed with hexanes before oven drying at 150°C. 2.2g (5.4mmol, 94% yield) of **4.15** was recovered as white powder and used in the next step without further purification.

^{1}H NMR (400 MHz, CDCl3) δ 7.85 – 7.64 (m, 15H), 3.20 (d, J = 13.2 Hz, 3H).

^{13}C NMR (101 MHz, $CDCl_3$) δ 135.3, 135.2, 133.4, 133.3, 130.6, 130.5, 119.4, 118.5, 12.0, 11.5.



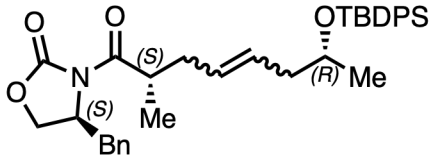
(R)-tert-butyl(pent-4-en-2-yloxy)diphenylsilane (4.5)[63]**.**

To a stirring solution of Ph3PCH3I (3.6g, 9.0mmol, 3.0eq) in 10mL of dry THF at 0°C, (2.5M) BuLi in hexanes (3mL, 7.5mmol, 2.5eq) was added dropwise and the resulting mixture was allowed to stir for 15-30 minutes until the formation of a deep orange solution. To this mixture a suspension of **4.14** (1.0g, 3.0mmol, 1.0 eq) in 90 mL of dry THF was added dropwise at 0°C. The resulting mixture was stirred for 1 hour, or until the starting material was completely consumed (determined by TLC). Upon completion, the mixture was quenched with NH4Cl (sat.), the aqueous layers were extracted with ether (x2). Organic layers were combined and washed with brine, dried over MgSO4, filtered, and concentrated to afford the crude product. Purification of the alkene was achieved via silica column chromatography at 100% Hexanes to afford 700mg (2.16mmol, 72% yield) of pure alkene **4.5** as a clear colourless oil.

TLC (10% EtOAc/Hexanes): R_f= 0.85

^{1}H NMR (400 MHz, $CDCl_3$) δ 7.71 (dddd, J = 7.9, 3.1, 1.6, 0.9 Hz, 4H), 7.40 (dddt, J = 14.4, 8.7, 7.7, 1.3 Hz, 6H), 5.85 – 5.71 (m, 1H), 5.02 – 4.94 (m, 2H), 3.92 (tdd, J = 6.3, 5.2, 0.9 Hz, 1H), 2.29 – 2.16 (m, 2H), 1.09 (dd, J = 5.4, 0.9 Hz, 11H).

^{13}C NMR (101 MHz, $CDCl_3$) δ 136.0, 136.0, 135.3, 134.9, 134.6, 129.6, 129.6, 127.6, 127.6, 116.9, 69.3, 44.1, 27.2, 23.0, 19.4.



(S)-4-benzyl-3-((2S,7R,E)-7-((tert-butyldiphenylsilyl)oxy)-2-methyloct-4-enoyl)oxazolidin-2-one (4.16).

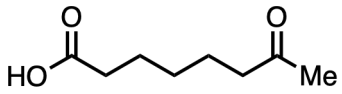
General procedure for Cross-Metathesis (Table 4.1) A representative procedure is described for entry 1. Alkenes **4.5** (700 mg, 2.16 mmol, 10.0 eq) and **4.9** (54.6 mg, 0.2 mmol, 1.0 eq) were

combined in 2mL of dry DCM. To this stirring mixture, 16.5 mg (0.02 mmol, 0.1 eq) of G-I catalyst was added and the reaction was left to stir at reflux (40 °C) under inert atmosphere for 24 h. The volatiles were removed under vacuum and the crude product was purified via silica column chromatography (gradient elution, 100% hexanes-10% EtOAc/hexanes) to afford pure **4.16** (52.1mg, 0.09mmol, 46% yield). Entries 2-10 were performed analogously, with variations in catalyst identity, catalyst loading, alkene stoichiometry, solvent, temperature, and reaction time as specified in **Table 4.1.**

TLC (10% EtOAc/Hexanes): R_f = 0.20

^{1}H NMR (400 MHz, $CDCl_3$) δ 7.68 (dt, J = 3.1, 1.7 Hz, 3H), 7.38 (dddd, J = 14.4, 8.8, 5.9, 2.6 Hz, 10H), 7.24 – 7.18 (m, 2H), 5.50 – 5.28 (m, 2H), 4.66 – 4.58 (m, 1H), 4.17 – 4.07 (m, 2H), 3.79 – 3.71 (m, 1H), 3.26 (dd, J = 13.2, 3.3 Hz, 1H), 2.76 (ddd, J = 13.3, 9.6, 2.0 Hz, 1H), 2.44 – 1.96 (m, 5H), 1.20 (dt, J = 6.8, 1.9 Hz, 3H), 1.05 (t, J = 2.8 Hz, 12H).

HRMS (ESI-TOF) *m/z* Calcd for $C_{35}H_{43}NO_4NaSi$ [M+Na]+ 592.2859, found 592.2830.



7-oxooctanoic acid (4.19)[64]

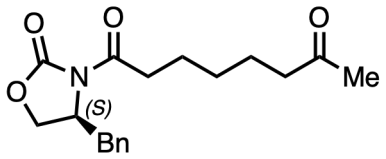
2-acetylcyclohexan-1-one (4g, 29.0mmol, 1.0eq) was refluxed overnight in 28mL of a 1.5M aqueous solution of NaOH. The solution was then cooled and washed with ethyl acetate before neutralizing with 1M HCl. The mixture was extracted with ethyl acetate after which the organic layer was collected, dried over MgSO4, filtered, and concentrated under reduced pressure to afford the product as a brown oil (3.4g, 75% yield).

TLC (50% EtOAc/Hexanes): R_f =0.41

^{1}H NMR (600 MHz, $CDCl_3$): δ 2.46 – 2.41 (m, 2H), 2.35 (tt, J = 7.6, 1.2 Hz, 2H), 2.15 – 2.11 (m, 3H), 1.67 – 1.62 (m, 2H), 1.61 – 1.56 (m, 2H), 1.34 (pd, J = 7.5, 1.6 Hz, 2H).

^{13}C NMR (151 MHz, $CDCl_3$): δ 209.17, 179.61, 43.52, 33.88, 30.04, 28.63, 24.53, 23.45.

HRMS (ESI-TOF) *m/z* Calcd for $C_8H_{14}O_3Na$, [M+Na]+ 181.084, found: 181.0833



(S)-1-(4-benzyl-2-oxooxazolidin-3-yl)octane-1,7-dione (4.18)

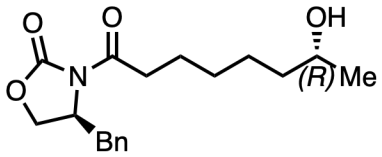
A flame-dried round bottom flask was charged with **4.19** (2.0g, 12.6mmol, 1.0eq) and 40mL of anhydrous THF under inert conditions. The suspension was cooled to -78°C, and trimethylamine (3.2mL, 25.0mmol, 2.0eq) added drop-wise, followed by pivolyl chloride (1.9mL, 15.2mmol, 1.2eq). The mixture was stirred for 1.5h, during which it was allowed to warm to room temperature. The mixture was cooled again to -78°C and lithium chloride (1.6g, 37.8mmol, 3.0eq) was added followed by a suspension of (*S*)-4-benzyl-oxazolidin-2-one (2.45g, 13.9mmol, 1.1eq) in 10mL of anhydrous THF. The mixture was stirred for 1h at -78°C, allowed to warm to room temperature overnight. The reaction was quenched with a saturated solution of NH_4Cl and diluted with ethyl acetate. The organic layer was extracted, washed with water and brine. The crude suspension was dried over $MgSO_4$, filtered and concentrated under reduced pressure. Purification via flash silica column chromatography with 30% ethyl acetate in hexanes, obtained the pure product as a colourless oil (2.4g, 60% yield).

TLC (50% EtOAc/Hexanes): R_f =0.61

^{1}H NMR (600 MHz, $CDCl_3$): δ 7.35 – 7.31 (m, 2H), 7.29 – 7.26 (m, 1H), 7.22 – 7.19 (m, 2H), 4.67 (ddt, *J* = 9.6, 7.6, 3.1 Hz, 1H), 4.23 – 4.13 (m, 2H), 3.29 (dd, *J* = 13.4, 3.4 Hz, 1H), 3.01 – 2.85 (m, 2H), 2.76 (dd, *J* = 13.4, 9.6 Hz, 1H), 2.45 (t, *J* = 7.4 Hz, 2H), 2.14 (s, 3H), 1.74 – 1.66 (m, 2H), 1.63 (p, *J* = 7.5 Hz, 2H), 1.39 (p, *J* = 7.7 Hz, 2H).

^{13}C NMR (151 MHz, $CDCl_3$): δ 209.05, 173.28, 153.59, 135.43, 129.55, 129.10, 127.49, 66.33, 55.29, 43.59, 38.07, 35.46, 30.05, 28.71, 24.10, 23.62.

HRMS (ESI-TOF) *m/z* Calcd for $C_{18}H_{24}O_4N$ [M+H]+ 318.1705, found: 318.1701



(S)-4-benzyl-3-((R)-7-hydroxyoctanoyl)oxazolidin-2-one (4.21)

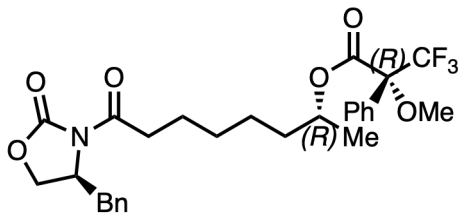
A flame-dried round bottom flask was charged (*S*)-(−)-2-Methyl-CBS-oxazaborolidine (1.78g, 6.4mmol, 1.3eq) and 12.4mL of anhydrous THF in inert conditions. To this suspension, a 1.0M solution of BH_3-THF (5.9mL, 5.9mmol, 1.2eq) was added dropwise and the mixture was left to stir for 15 to 30 min at room temperature. The mixture was cooled to -10°C in a salt-ice bath and a suspension of the **4.18** (1.57g, 4.95mmol, 1.0eq) in 3mL of anhydrous THF was added drop-wise. The reaction was left to warm to room temperature and the progress was monitored by TLC. Once complete (4h-16h), 1M HCl (7mL) and MeOH (7mL) was added and left to stir for an additional 30 min before the mixture was diluted with diethyl ether and extracted. The combined organic layers were dried over $MgSO_4$, filtered and concentrated under reduced pressure. Purification via flash silica column chromatography with a 30%–50% EtOAc in hexanes gradient, obtained the pure product as a colourless oil (1.24g, 77% yield, d.r.= 7.7:1).

TLC (50% EtOAc/Hexanes): R_f =0.37

^{1}H NMR (600 MHz, $CDCl_3$): δ 7.35 – 7.31 (m, 2H), 7.29 – 7.27 (m, 1H), 7.22 – 7.19 (m, 2H), 4.71 – 4.63 (m, 1H), 4.22 – 4.15 (m, 2H), 3.84 – 3.76 (m, 1H), 3.30 (dd, *J* = 13.4, 3.4 Hz, 1H), 3.01 – 2.87 (m, 2H), 2.77 (dd, *J* = 13.4, 9.6 Hz, 1H), 1.75 – 1.67 (m, 2H), 1.48 – 1.39 (m, 6H), 1.20 (dd, *J* = 6.2, 0.7 Hz, 3H).

^{13}C NMR (151 MHz, $CDCl_3$): δ 173.46, 153.61, 135.45, 129.57, 129.11, 127.50, 68.22, 66.32, 55.31, 39.26, 38.09, 35.59, 29.22, 25.64, 24.33, 23.70.

HRMS (ESI-TOF) *m/z* Calcd for $C_{18}H_{26}O_4N$ [M+H]+ 320.1862, found: 320.1855



(R)-8-((S)-4-benzyl-2-oxooxazolidin-3-yl)-8-oxooctan-2-yl (R)-3,3,3-trifluoro-2-methoxy-2-phenylpropanoate (4.21-(*R*)-MTPA**)**

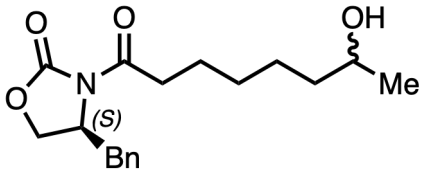
To a solution of alcohol **4.21** (35.7 mg, 0.112 mmol, 1.0 eq.) in 0.6mL of dry DCM were added (R)-Mosher's acid (36.68 mg, 0.157 mmol, 1.4 eq.), EDC (42.78 mg, 0.224 mmol, 2.0 eq.), and DMAP (0.68 mg, 0.0056 mmol, 0.05 eq.). The reaction was stirred at room temperature and monitored by TLC (30% EtOAc/hexanes) and LC-MS. Upon completion, the mixture was quenched with NaHCO3 and extracted with DCM (x3), the organic layers were comined and washed with brine, dried with Na2SO4 and concentrated. The crude residue was purified by flash silica gel column chromatography (10–30% EtOAc/hexanes) to afford 43.7mg of the Mosher ester **4.21**-(*R*)-MTPA (0.081 mmol, 73% yield) as clear pale yellow oil.

TLC (30% EtOAc/Hexanes): R_f = 0.50

^{1}H NMR (600 MHz, $CDCl_3$) δ 7.55 – 7.50 (m, 2H), 7.48 – 7.38 (m, 5H), 7.35 – 7.31 (m, 2H), 7.30 – 7.27 (m, 1H), 7.22 – 7.20 (m, 2H), 5.14 (dp, J = 7.5, 6.2 Hz, 1H), 4.69 – 4.65 (m, 1H), 4.23 – 4.14 (m, 2H), 3.58 – 3.54 (m, 3H), 3.30 (dd, J = 13.4, 3.4 Hz, 1H), 2.98 – 2.86 (m, 2H), 2.76 (dd, J = 13.4, 9.6 Hz, 1H), 1.69 (ddd, J = 8.7, 7.1, 3.3 Hz, 2H), 1.61 – 1.56 (m, 1H), 1.42 – 1.36 (m, 3H), 1.30 (dddd, J = 15.1, 6.7, 4.9, 1.9 Hz, 2H), 1.26 (d, J = 6.3 Hz, 3H).

^{13}C NMR (151 MHz, $CDCl_3$) δ 173.2, 166.2, 153.5, 135.3, 132.4, 129.5, 129.4, 129.1, 129.0, 128.7, 128.4, 128.3, 127.4, 127.3, 74.0, 66.2, 55.2, 38.0, 35.4, 35.4, 31.6, 28.8, 25.1, 24.1, 22.7, 19.5, 14.1.

HRMS (ESI-TOF) *m/z* Calcd for $C_{28}H_{32}NO_6F_3Na$ [M+Na]+ 588.2079, found 588.2059.



(4S)-4-benzyl-3-(7-hydroxyoctanoyl)oxazolidin-2-one (4.21-rac)

A round bottom flask was charged with **4.18** (35mg, 0.11, 0.1eq) and 0.27mL of dry THF. To this stirring suspension under inert conditions, BH3-THF was added dropwise at 0°C and the reaction was left to stir for 3h and warm to room temperature. Upon completion, the mixture was again cooled to 0°C and MeOH was added dropwise and left to stir for an additional 30 min before the mixture was diluted with diethyl ether and extracted. The combined organic layers were dried over

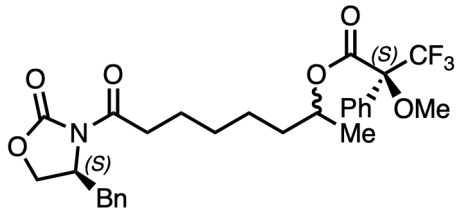
$MgSO_4$, filtered and concentrated under reduced pressure. Purification via flash silica column chromatography with a 30%–50% EtOAc in hexanes gradient, obtained the pure product **4.21-rac**, as a colourless oil (31mg, 0.1mmol, , 95% yield).

TLC (50% EtOAc/Hexanes): R_f =0.37

^{1}H NMR (400 MHz, $CDCl_3$) δ 7.36 – 7.28 (m, 3H), 7.22 – 7.18 (m, 2H), 4.67 (ddt, J = 9.7, 7.4, 3.2 Hz, 1H), 4.22 – 4.14 (m, 2H), 3.80 (td, J = 7.1, 4.5 Hz, 1H), 3.29 (dd, J = 13.4, 3.3 Hz, 1H), 3.02 – 2.83 (m, 2H), 2.76 (dd, J = 13.4, 9.6 Hz, 1H), 1.73 – 1.68 (m, 2H), 1.47 – 1.38 (m, 6H), 1.19 (d, J = 6.2 Hz, 3H).

^{13}C NMR (101 MHz, $CDCl_3$) δ 173.5, 153.6, 135.4, 129.5, 129.2, 129.1, 127.5, 68.2, 66.3, 55.3, 39.2, 38.0, 35.6, 29.2, 25.6, 24.3, 23.6.

HRMS (ESI-TOF) *m/z* Calcd for $C_{18}H_{26}O_4N$ [M+H]+ 320.1862, found: 320.1853



(R)-8-((S)-4-benzyl-2-oxooxazolidin-3-yl)-8-oxooctan-2-yl (S)-3,3,3-trifluoro-2-methoxy-2-phenylpropanoate (4.21-rac-MTPA)

Prepared as per **4.21-(*R*)-MTPA** using alcohol **4.21-rac** in the place of **4.21**. **4.21-rac** (20.5 mg, 0.064mmol, 1.0 eq.) yielded 23.4mg, **4.21-rac-MTPA** (0.043 mmol, 73% yield) as clear pale yellow oil.

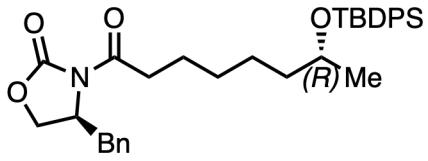
TLC (30% EtOAc/Hexanes): R_f = 0.49

^{1}H NMR (600 MHz, $CDCl_3$) δ 7.56 – 7.50 (m, 2H), 7.40 (dt, J = 5.3, 1.6 Hz, 3H), 7.33 (t, J = 7.3 Hz, 2H), 7.29 – 7.27 (m, 1H), 7.22 – 7.19 (m, 2H), 5.15 (ddd, J = 12.9, 7.1, 5.5 Hz, 1H), 4.66

(ddd, J = 12.9, 7.3, 3.3 Hz, 1H), 4.22 – 4.15 (m, 2H), 3.56 (dt, J = 12.0, 1.1 Hz, 3H), 3.30 (dd, J = 13.4, 3.4 Hz, 1H), 2.99 – 2.81 (m, 2H), 2.76 (dd, J = 13.4, 9.6 Hz, 1H), 1.70 (ddt, J = 16.5, 8.7, 4.1 Hz, 2H), 1.63 – 1.42 (m, 6H), 1.26 (s, 3H).

^{13}C NMR (151 MHz, $CDCl_3$) δ 173.3, 173.3, 166.3, 153.6, 135.4, 132.6, 129.7, 129.6, 129.1, 128.5, 128.5, 127.5, 127.4, 74.2, 66.4, 55.3, 38.1, 35.6, 35.5, 35.5, 31.7, 28.9, 25.3, 24.2, 22.8, 19.6, 14.3.

HRMS (ESI-TOF) *m/z* Calcd for $C_{28}H_{33}NO_6F_3$ [M+H]+ 536.2260, found 536.2246.



Preparation of (S)-4-benzyl-3-((R)–7—((tertbutyldiphenylsilyl)oxy)octanoyl) oxazolidin-2-one (4.22)

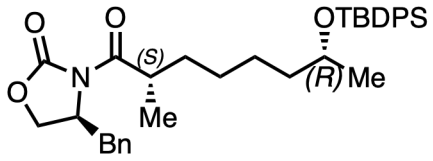
A round bottom flask was charged with alcohol **4.21** (1.24g, 3.88mmol, 1.0eq), imidazole (0.5g, 7.7mmol, 2.0eq), 4-dimethylaminopyridine (4.7mg, 0.04, 0.01eq) in 10mL of DCM. The stirring mixture was cooled to 0°C, after which tert-butyldiphenylchlorosilane (1.2mL, 4.7mmol, 1.2eq) was added drop-wise. The reaction was left to warm to room temperature overnight and progress was monitored by TLC. Once complete, H_2O was added, and the mixture was extracted trice with DCM. The combined organic fractions were dried over $MgSO_4$, filtered and concentrated under reduced pressure. Purification via flash silica column chromatography (100% hexanes—5% EtOAc in hexanes gradient) obtained the pure product as a colourless oil (2.1g, 99% yield).

TLC (15% EtOAc/Hexanes): R_f =0.32

^{1}H NMR (400 MHz, $CDCl_3$): δ 7.72 – 7.66 (m, 4H), 7.45 – 7.27 (m, 9H), 7.24 – 7.20 (m, 2H), 4.71 – 4.62 (m, 1H), 4.22 – 4.14 (m, 2H), 3.85 (h, *J* = 5.9 Hz, 1H), 3.30 (dd, *J* = 13.4, 3.3 Hz, 1H), 2.97 – 2.79 (m, 2H), 2.79 – 2.71 (m, 1H), 1.67 – 1.60 (m, 2H), 1.52 (ddd, *J* = 12.8, 6.4, 4.2 Hz, 1H), 1.41 (ddd, *J* = 13.2, 6.6, 1.8 Hz, 1H), 1.34 – 1.24 (m, 4H), 1.08 – 1.05 (m, 12H).

^{13}C NMR (101 MHz, $CDCl_3$): δ 173.48, 153.56, 136.02, 136.00, 135.45, 135.05, 134.69, 129.57, 129.55, 129.49, 129.08, 127.60, 127.51, 127.47, 69.61, 66.26, 55.27, 39.39, 38.06, 35.62, 29.28, 27.17, 25.17, 24.35, 23.38, 19.40.

HRMS (ESI-TOF) *m/z* Calcd for $C_{34}H_{44}O_4SiN$ [M+H]+ 558.3040, found: 558.3046



Preparation of (S)-4-benzyl-3-((2S,7R)-7-((tert-butyldiphenylsilyl)oxy)-2-methyloctanoyl)oxazolidin-2-one (4.17)

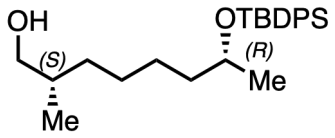
A suspension of **4.22** (92mg, 0.16mmol, 1.0eq) in 0.4mL anhydrous THF and inert conditions was cooled to -78°C. A 1M solution of NaHMDS in THF (0.25mL, 0.25mmol, 1.5eq) was added dropwise and left to stir at -78°C for 1h. To the stirring mixture, iodomethane (0.04mL, 0.66mmol, 4.0eq) was added and stirring was continued at -78°C for 2-3h, or until reaction was deemed completed by TLC. The reaction was quenched with a saturated solution of NH_4Cl and extracted thrice with ethyl acetate. The organic layers were combined and dried over $MgSO_4$, filtered and concentrated under reduced pressure. Purification via flash silica column chromatography with 10% ethyl acetate in hexanes, obtained the pure product as a colourless oil (80.1g, 85% yield, d.r.>95:5).

TLC (15% EtOAc/Hexanes): R_f =0.43

^{1}H NMR (600 MHz, $CDCl_3$): δ 7.60 – 7.57 (m, 4H), 7.32 – 7.17 (m, 9H), 7.14 – 7.11 (m, 2H), 4.57 (ddt, *J* = 10.0, 6.8, 3.4 Hz, 1H), 4.10 – 4.06 (m, 2H), 3.76 – 3.71 (m, 1H), 3.58 (h, *J* = 7.0 Hz, 1H), 3.18 (dd, *J* = 13.4, 3.3 Hz, 1H), 2.67 (dd, *J* = 13.4, 9.6 Hz, 1H), 1.59 (dq, *J* = 13.0, 7.4 Hz, 1H), 1.42 – 1.35 (m, 1H), 1.32 – 1.23 (m, 2H), 1.21 – 1.15 (m, 2H), 1.12 (d, *J* = 7.6 Hz, 2H), 1.11 – 1.09 (m, 3H), 0.96 (d, *J* = 0.9 Hz, 9H), 0.94 (d, *J* = 0.8 Hz, 3H).

^{13}C NMR (151 MHz, $CDCl_3$) δ 177.4, 153.2, 136.0, 136.0, 135.5, 135.1, 134.7, 129.6, 129.6, 129.5, 129.5, 129.1, 127.6, 127.5, 127.5, 69.7, 66.1, 55.5, 55.5, 39.4, 38.1, 37.8, 33.5, 27.5, 27.2, 25.5, 23.3, 19.4, 17.5.

HRMS (ESI-TOF) *m/z* Calcd for $C_{35}H_{46}O_4SiN$ [M+H]+572.3196, found: 572.3196



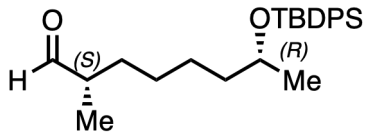
(2S,7R)-7-((tert-butyldiphenylsilyl)oxy)-2-methyloctanal (4.23)

A flame-dried round bottom flask was charged with (compound number, 1.0eq) in anhydrous DCM and inert conditions. The suspension was cooled to -78°C and DIBAL (2.0eq) was added slowly, drop-wise, over 10 min. The reaction was carefully monitored, maintain reaction conditions at -78°C and periodically checking reaction progress by TLC. Once reaction was deemed complete, acetone was added drop-wise to quench any excess DIBAL, and the mixture was allowed to carefully warm to room temperature. The crude mixture was concentrated under reduced pressure and purified via silica column chromatography (100% hexanes–15% ethyl acetate hexanes gradient).

TLC (15% EtOAc/Hexanes): R_f =0.35

^{1}H NMR (400 MHz, $CDCl_3$) δ 7.68 (ddt, J = 6.7, 3.8, 1.9 Hz, 4H), 7.50 – 7.30 (m, 6H), 3.82 (h, J = 6.0 Hz, 1H), 3.47 (dd, J = 10.5, 5.7 Hz, 1H), 3.38 (dd, J = 10.5, 6.6 Hz, 1H), 1.58 – 1.34 (m, 5H), 1.28 – 1.21 (m, 4H), 1.19 – 1.10 (m, 1H), 1.05 (d, J = 4.5 Hz, 12H), 0.88 (d, J = 6.7 Hz, 3H).

^{13}C NMR (101 MHz, $CDCl_3$) δ 136.0, 129.6, 129.5, 127.6, 127.5, 69.7, 68.5, 39.5, 35.8, 33.2, 27.2, 27.1, 25.6, 23.4, 19.4, 16.7.



(2S,7R)-7-((tert-butyldiphenylsilyl)oxy)-2-methyloctanal (4.8)

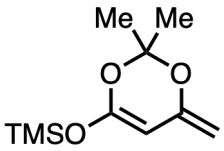
To a stirring solution of alcohol **4.23** (50 mg, 0.126 mmol, 1.0 equiv) in anhydrous DCM (1.26 mL) was added Dess–Martin periodinane (79.9 mg, 0.188 mmol, 1.5 equiv) under anhydrous conditions. The reaction was left for 2h to stir and heating (30-35°C) was used to speed up the oxidation reaction when sluggish. The reaction was quenched with a 10% aqueous solution of

sodium thiosulfate and extracted (x3) with DCM. The combined organic layers were dried over $MgSO_4$, filtered, and concentrated under reduced pressure. The crude residue was purified by silica column chromatography (100% hexanes-15% EtOAc /hexanes gradient) to afford aldehyde **4.8** (42.3 mg, 0.107 mmol, 85% yield) as a clear colourless oil. The aldehyde was stored at -20°C to minimize oxidative degradation.

TLC (20% EtOAc/Hexanes): R_f =0.65

^{1}H NMR (400 MHz, $CDCl_3$) δ 9.57 (d, J = 1.9 Hz, 1H), 7.71 – 7.63 (m, 4H), 7.45 – 7.33 (m, 6H), 3.83 (h, J = 6.0 Hz, 1H), 2.26 (qd, J = 6.8, 1.9 Hz, 1H), 1.69 – 1.56 (m, 3H), 1.52 – 1.43 (m, 1H), 1.43 – 1.28 (m, 1H), 1.29 – 1.12 (m, 3H), 1.08 – 1.02 (m, 15H).

^{13}C NMR (101 MHz, $CDCl_3$) δ 205.5, 136.0, 136.0, 135.0, 134.7, 129.6, 129.5, 127.6, 127.5, 77.4, 69.5, 46.4, 39.3, 30.6, 27.2, 27.1, 25.3, 23.4, 19.4, 13.4.

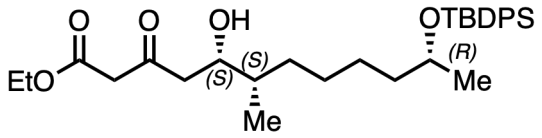


((2,2-dimethyl-4-methylene-4H-1,3-dioxin-6-yl)oxy)trimethylsilane (4.27)

A flame-dried flask was charged with DIPA (0.74 mL, 5.25 mmol, 1.5 eq) and 4mL of dry THF. The stirring suspension was cooled to -78°C, after which 2.1mL (5.25mmol, 1.5eq) of (2.5M) nBuLi in hexanes was added dropwise. The resulting solution was stirred for 30 min to generate LDA in situ. A solution of **4.8** (500mg, 3.5mmol, 1.0eq) in 3 mL of dry THF was then added dropwise at -78°C and left to stir for an 1 h. Following this, 0.75mL (5.95mmol, 1.7 eq) of freshly distilled TMSCl was added dropwise at -78°C, and the mixture was left to warm to room temperature over 1.5h. The reaction mixture was then filtered under inert atmosphere (Whatman 6900-2502 GD/X, 25 mm, 0.2 μm PVDF syringe filter) into a flame-dried flask, and the volatiles were removed under high vacuum. The crude product was analyzed by ^{1}H NMR to determine yield (86%) and carried forward to the next step without further purification.

^{1}H NMR (400 MHz, $CDCl_3$) δ 4.63 (s, 1H), 4.05 (s, 1H), 3.85 (s, 1H), 1.53 (s, 6H), 0.25 (s, 12H).

^{13}C NMR (101 MHz, $CDCl_3$) δ 153.4, 151.9, 102.6, 94.0, 85.0, 76.7, 24.6, 0.3.



ethyl (5S,6S,11R)-11-((tert-butyldiphenylsilyl)oxy)-5-hydroxy-6-methyl-3-oxododecanoate (4.25)

General Procedure A-Substrate-controlled Lewis acid conditions (entries 1-5, representative: entry 1, $BF_3 \cdot OEt_2$). A representative procedure is described for Entry 1. A solution of aldehyde **4.8** (60.9 mg, 0.15 mmol, 1.0 equiv) and diene **4.6** (84.9 mg, 0.31 mmol, 2.0 equiv) in dry DCM (0.4 mL) was cooled to -78 °C, and $BF_3 \cdot OEt_2$ (0.02 mL, 0.15 mmol, 1.0 equiv) was added dropwise. The reaction was monitored by TLC and deemed completed after 30 min. The reaction was quenched with NaHCO3 and the aqueous layer was extracted with DCM (3 ×). The combined organic layers were dried over Na_2SO_4, filtered, and concentrated under reduced pressure. The crude product was purified by flash column chromatography (10–15% EtOAc/hexanes) to afford **4.25** as an inseparable mixture of diastereomers (dr 2.2:1, syn:anti) in 92% yield. Entries 2–5 were performed analogously, with variations in Lewis acid, solvent, temperature, and reaction time as specified in **Table 4.2.**

General Procedure B- Ti-BINOL conditions (entries 6-8, (adapted from ref.[42]). A flame-dried flask was charged with (R)-BINOL (0.1 eq.) and dry DCM. Where indicated (Table 4.2) activated 4Å molecular sieves was added at this stage, and the mixture was stirred for 30 min prior to use. $Ti(OiPr)_4$ (0.1eq) was then added at room temperature and, where indicated (Table 4.2), dry LiCl (0.2 eq) was added at this stage. The mixture was then stirred for 30 min to generate the chiral titanium complex in situ. The solution was cooled to −78 °C, and a solution of aldehyde **4.8** (1.0 eq) in dry DCM was added dropwise, followed by dropwise addition of Chans' diene (**4.6**) (1.2 eq). The stirring mixture was left to warm to room temperature and stirred for 16-48 h. Reaction progress was monitored by TLC, which indicated no consumption of starting material under any of the conditions examined (entries 6-8). The reaction mixtures were quenched with saturated aqueous NH_4Cl, and unreacted aldehyde **4.8** was recovered following standard aqueous workup.

General Procedure C - COBI-catalyzed conditions (entries 9-13). Adapted from ref[50]

A flame-dried flask was charged with (S)-Me-CBS (0.5eq) and dry DCM. The resulting suspension was cooled to −78 °C, and TfOH (0.45 equiv) was added dropwise. After 1 h, a mixture of aldehyde **4.8** (1.0 equiv), Chans' diene **4.6** (1.25 equiv), and, where indicated in **Table 4.2**, isopropanol (1.1 eq), in dry DCM was added dropwise. The mixture was stirred at −78 °C for an additional 2.5 h, and the reaction was quenched with saturated aqueous $NaHCO_3$. The mixture was warmed to room temperature, and the layers were separated. The aqueous layer was extracted with DCM (x 3). The combined organic layers were dried over Na_2SO_4, filtered, and concentrated under reduced pressure. The crude residue was purified by flash column chromatography to afford **4.25** as an inseparable mixture of diastereomers. Entries 10-13 were performed analogously, using the indicated CBS catalyst (Me-CBS, Ph-CBS, or o-Tolyl-CBS), with variations in additive, time, and equivalents as specified in **Table 4.2**.

Characterization from General procedure A, entry 1:

TLC (15% EtOAc/Hexanes): R_f =0.24

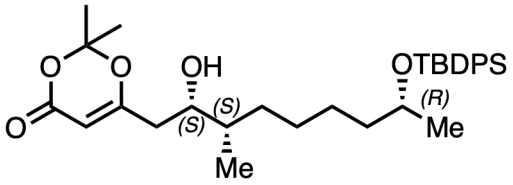
^{1}H NMR (600 MHz, $CDCl_3$) δ 7.70 – 7.66 (m, 4H), 7.44 – 7.39 (m, 2H), 7.39 – 7.34 (m, 4H), 4.21 (qd, J = 7.2, 0.9 Hz, 2H), 4.01 – 3.89 (m, 1H), 3.84 (q, J = 5.9 Hz, 1H), 3.49 (d, J = 2.2 Hz, 2H), 2.71 – 2.58 (m, 2H), 1.47 (tdd, J = 12.9, 8.5, 4.9 Hz, 2H), 1.41 – 1.34 (m, 2H), 1.31 – 1.21 (m, 7H), 1.18 – 1.13 (m, 1H), 1.05 (d, J = 1.2 Hz, 12H), 0.90 – 0.84 (m, 3H).

Diastereomer ratio (d.r.) = 2.2:1 (major:minor), determined by integration of the C5-H resonances (see spectral data). The major and minor diastereomers were assigned as the syn and anti aldol products, respectively, based on close agreement of the C5-H coupling pattern with literature values reported for an analogous system[58].

Major diastereomer: **^{1}H NMR (600 MHz, $CDCl_3$)** δ 3.98 (ddd, J = 9.2, 3.6, 3.6 Hz)

Minor diastereomer: **^{1}H NMR (600 MHz, $CDCl_3$)** 3.92 (ddd, J = 8.9, 5.6, 3.0 Hz),

^{13}C NMR (151 MHz, CDCl3) δ 204.2, 167.1, 136.0, 136.0, 135.1, 135.1, 134.8, 129.6, 129.5, 127.6, 127.5, 70.7, 69.7, 61.6, 50.1, 47.2, 39.5, 38.2, 38.1, 32.8, 27.4, 27.2, 25.6, 25.6, 23.4, 19.4, 14.3, 14.2.



6-((2S,3S,8R)-8-((tert-butyldiphenylsilyl)oxy)-2-hydroxy-3-methylnonyl)-2,2-dimethyl-4H-1,3-dioxin-4-one (4.26)

Synthetized as per General procedure A (vide supra), substituting TMS-dioxinone **4.24** for Chans' diene **4.6.** TMS-dioxinone **4.24** (64mg, 0.3mmol, 1.5 equiv)**,** aldehyde 4.8 (89 mg, 0.2 mmol, 1.0 eq), $BF_3 \cdot OEt_2$ (0.023mL, 0.2mmol, 1.0 eq, and dry DCM (2 mL) at -78°C. Purification by flash column chromatography (25% EtOAc/hexanes) afforded **4.26** as an inseparable mixture of diastereomers (d.r. 2:1, syn:anti) in 94% yield. spectroscopic data are reported for the mixture.

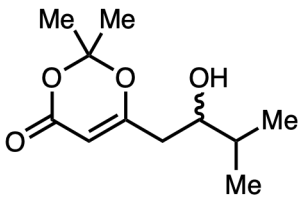
General Procedure D (see Table 4.2) - CuF_2/BINAP conditions (entries 14-15). Carried out as per ref[55]. No product formation was observed under either condition (entries 14 and 15, using (R)- and (S)-BINAP respectively), as determined by TLC and 1H NMR analysis of the crude reaction mixture, and starting materials were recovered following standard aqueous workup.

TLC (25% EtOAc/Hexanes): R_f =0.33

^{1}H NMR (400 MHz, $CDCl_3$) δ 7.68 (ddd, J = 7.9, 3.3, 1.5 Hz, 4H), 7.44 – 7.32 (m, 6H), 5.33 (t, J = 1.3 Hz, 1H), 3.88 – 3.68 (m, 2H), 2.38 – 2.19 (m, 2H), 1.70 (d, J = 1.9 Hz, 6H), 1.52 – 1.44 (m, 2H), 1.41 – 1.33 (m, 2H), 1.30 – 1.20 (m, 3H), 1.16 – 1.07 (m, 2H), 1.05 (d, J = 6.5 Hz, 12H), 0.88 (dd, J = 6.8, 3.3 Hz, 3H).

^{13}C NMR (101 MHz, $CDCl_3$) δ 169.9, 161.1, 136.0, 135.0, 134.8, 129.6, 129.5, 127.6, 127.5, 106.7, 95.1, 77.4, 73.0, 72.2, 69.6, 39.5, 39.1, 33.1, 32.0, 27.4, 27.2, 25.5, 24.9, 23.4, 19.4, 15.1, 13.8.

HRMS (ESI-TOF) *m/z* Calcd for $C_{32}H_{47}O_5Si$ [M+H+]+ 539.3193, found: 539.3196



6-(2-hydroxy-3-methylbutyl)-2,2-dimethyl-4H-1,3-dioxin-4-one (4.27)

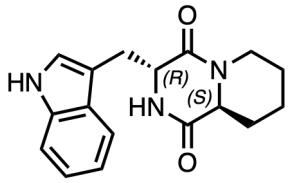
Synthetized as per General procedure A (vide supra), substituting TMS-dioxinone **4.24** for Chans' diene **4.6** and isobuteraldehyde for aldehyde **4.8.** TMS-dioxinone **4.24** (0.5mL, 1.87mmol, 1.5 equiv)**,** isobuteraldehude (0.113 mL, 1.24 mmol, 1.0 eq), $BF_3 \cdot OEt_2$ (0.15mL, 1.24 mmol, 1.0 eq, and dry DCM (20 mL) at -78 °C. Purification by flash column chromatography (25% EtOAc/hexanes) afforded 29.8mg **4.27** (0.14mmol, 96% yields) as a pale yellow oil.

TLC (15% EtOAc/Hexanes): R_f =0.20

^{1}H NMR (600 MHz, $CDCl_3$) δ 5.33 (s, 1H), 3.69 (ddd, J = 9.6, 5.2, 3.1 Hz, 1H), 2.41 (ddd, J = 14.6, 3.1, 0.8 Hz, 1H), 2.28 (dd, J = 14.6, 9.6 Hz, 1H), 1.75 – 1.70 (m, 8H), 1.70 (s, 8H), 0.95 (dd, J = 6.8, 1.6 Hz, 6H).

^{13}C NMR (151 MHz, $CDCl_3$) δ 169.9, 161.2, 106.7, 95.2, 73.6, 38.9, 33.9, 25.5, 24.9, 18.7, 17.3.

HRMS (ESI-TOF) *m/z* Calcd for $C_{11}H_{19}O_4$ [M+H+]+ 215.1283, Found 215.1277.



(3R,9aS)-3-((1H-indol-3-yl)methyl)hexahydro-4H-pyrido[1,2-a]pyrazine-1,4(6H)-dione (4.32)

4.32 was isolated as a byproduct during attempted acyl ketene ring-closure of (**Figure 4.14**) of **4.29.** A solution of **4.29** (5mg, 0.007mmol, 1.0 eq.) in dry toluene 1.4 mL was heated at 110 °C for 1 h under inert conditions. The reaction was cooled to room temperature and concentrated under reduced pressure. The crude residue was purified by flash column chromatography (10% methanol/DCM, 1% Et3N) to afford 1.4 mg of **4.32** (0.005mmol, 67% yield), alongside the desired macrolactam product **4.31**, which was detected by LC-MS but not isolated in sufficient quantity for full characterization.

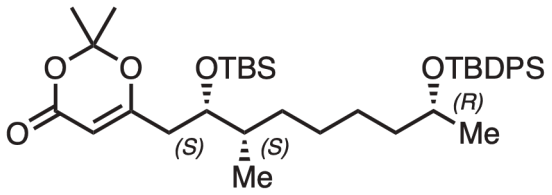
TLC (90% EtOAc/Hexanes): R_f =0.10

^{1}H NMR (400 MHz, $CDCl_3$) δ 8.67 (s, 1H), 7.59 – 7.53 (m, 1H), 7.38 (dt, J = 8.1, 1.0 Hz, 1H), 7.16 (ddd, J = 8.2, 6.9, 1.2 Hz, 1H), 7.08 (ddd, J = 8.0, 7.0, 1.1 Hz, 1H), 7.04 (d, J = 2.4 Hz, 1H), 6.42 (s, 1H), 4.55 (dp, J = 13.5, 2.0 Hz, 1H), 4.33 – 4.25 (m, 1H), 3.41 – 3.23 (m, 2H), 2.94 –

2.84 (m, 1H), 2.16 – 2.07 (m, 1H), 2.04 – 1.93 (m, 1H), 1.82 (t, J = 4.4 Hz, 1H), 1.63 – 1.53 (m, 1H), 1.39 – 1.34 (m, 1H), 1.30 – 1.20 (m, 3H).

^{13}C NMR (101 MHz, $CDCl_3$) δ 168.1, 165.0, 136.5, 127.0, 124.7, 122.4, 119.7, 119.1, 111.5, 108.9, 58.0, 55.2, 42.6, 31.4, 30.8, 24.4, 24.0.

HRMS (ESI-TOF) *m/z* Calcd for $C_{17}H_{20}N_3O_2$ [M+H+]+ 298.1554; Found 298.1554



6-((2S,3S,8R)-2-((tert-butyldimethylsilyl)oxy)-8-((tert-butyldiphenylsilyl)oxy)-3-methylnonyl)-2,2-dimethyl-4H-1,3-dioxin-4-one (4.37)

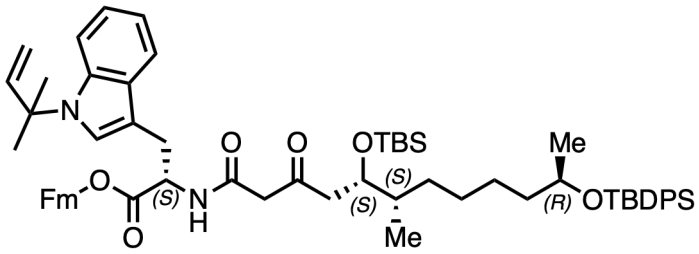
A flame-dried round-bottom flask was charged with **4.26** (38mg, 0.07 mmol, 1.0 eq.) and 0.7mL of dry DCM under inert atmosphere. The stirring suspension was cooled to 0C and 2,6-lutidine (0.016 mL, 0.14mmol, 2.0eq.) was added, after which TBSOTf (0.023mL, 0.1mmol, 1.5eq.) was added dropwise. The reaction was left to warm to room temperature and monitored for completion by TLC. After approximately 30 min, or upon completion, the mixture was quenched with NaHCO3 and extracted (x3) with DCM. The organic layers were combined, concentrated and the crude product was purified via silica column chromatography (10% EtOAc/hexanes) to afford 37.5mg (0.057, 82% yield) of pure **4.37** isolated as a clear colourless oil. The spectrum was reported as observed. The compound exists as a mixture of rotamers about the C5-silyl protected alcohol and diastereomers at C5, resulting in peak doubling/broadening for several resonances. Variable-temperature NMR was attempted to resolve rotamer-derived peak splitting (see Spectral Data, **Section 4.8**), but complete resolution of all signals could not be achieved due to the additional complexity introduced by the C5 diastereomeric mixture.

TLC (25% EtOAc/Hexanes): R_f =0.75

^{1}H NMR (600 MHz, $CDCl_3$) δ 7.68 (ddt, J = 7.5, 3.2, 1.5 Hz, 4H), 7.44 – 7.39 (m, 2H), 7.36 (td, J = 7.3, 1.6 Hz, 4H), 5.25 (s, 1H), 3.84 (ddd, J = 11.3, 7.7, 4.6 Hz, 2H), 2.29 (qdd, J = 13.9, 6.4, 2.7 Hz, 1H), 2.24 – 2.20 (m, 1H), 1.69 (s, 6H), 1.52 – 1.45 (m, 2H), 1.42 – 1.38 (m, 2H), 1.28 – 1.21 (m, 3H), 1.13 – 1.08 (m, 1H), 1.05 (s, 12H), 1.01 – 0.97 (m, 1H), 0.87 (s, 9H), 0.83 (d, J = 6.8 Hz, 3H), 0.02 (s, 6H).

^{13}C NMR (151 MHz, $CDCl_3$) δ 169.2, 168.8, 160.1, 134.9, 134.8, 133.9, 133.9, 133.6, 128.4, 128.4, 128.4, 128.4, 126.4, 126.4, 126.3, 105.3, 105.2, 94.2, 94.1, 71.8, 71.6, 71.6, 68.5, 68.5, 38.4, 38.4, 38.4, 38.3, 37.9, 37.7, 37.6, 37.4, 37.4, 36.4, 31.7, 31.0, 30.9, 28.7, 26.8, 26.7, 26.6, 26.6, 26.0, 24.9, 24.9, 24.8, 24.8, 24.8, 24.7, 24.5, 24.5, 24.4, 24.4, 23.4, 23.3, 23.3, 22.2, 22.2, 22.1, 18.2, 17.1, 17.0, 17.0, 13.3, 13.3, 12.9, 12.9, -4.0, -5.5, -5.5, -5.5, -5.6, -5.7.

HRMS (ESI-TOF) *m/z* Calcd for $C_{38}H_{61}O_5Si_2$ [M+H+]+ 653.4058; Found 653.4059.



((Nα-((5S,6S,11R)-5-((tert-butyldimethylsilyl)oxy)-11-((tert-butyldiphenylsilyl)oxy)-6-methyl-3-oxododecanoyl)-1-(2-methylbut-3-en-2-yl)-L-tryptophyl)oxy)fermium (4.38)

To a solution of **4.34** (37.7 mg, 0.068 mmol, 1.2 equiv) in 1mL of dry DCM at 0 °C was added 2,6-lutidine (0.039 mL, 0.34 mmol, 5.0 equiv) followed by dropwise addition of TMS-OTf (0.058 mL, 0.34 mmol, 5.0 equiv). The reaction was stirred at 0°C for 1-3 h and monitored by TLC. Upon completion, the reaction was quenched with saturated aqueous $NaHCO_3$ and concentrated under reduced pressure to dryness. The resulting crude residue (free amine **4.36**) was dissolved in minimal dry DCM and added dropwise to 2mL of dry toluene to dilute completely. **4.37** (37.3 mg, 0.057 mmol, 1.0 eq.) was added to the resulting suspension, and the mixture was heated to 110 °C for 1 h to effect acyl ketene ring-closure. The reaction was cooled to room temperature and concentrated under reduced pressure. The crude residue was purified via silica column chromatography 10-15% EtOAc/hexanes to afford 38.7mg of **4.38** (37mmol, 64% yield) as pale yellow viscous oil. The spectrum was reported as observed. The compound exists as a mixture of rotamers about the C5-silyl protected alcohol and diastereomers at C5, resulting in peak doubling/broadening for several resonances.

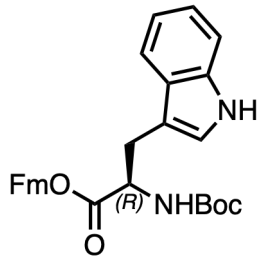
TLC (25% EtOAc/Hexanes): R_f =0.35

^{1}H NMR (600 MHz, $CDCl_3$) δ 7.73 (dt, J = 8.6, 4.7 Hz, 2H), 7.67 (dt, J = 6.4, 2.0 Hz, 4H), 7.54 (ddt, J = 10.1, 6.8, 3.2 Hz, 1H), 7.48 – 7.44 (m, 2H), 7.41 (dd, J = 9.4, 6.7 Hz, 4H), 7.36 (t, J = 7.4

Hz, 6H), 7.24 (s, 1H), 7.21 – 7.18 (m, 1H), 7.10 – 7.06 (m, 2H), 6.07 – 6.00 (m, 1H), 5.14 – 5.08 (m, 2H), 4.96 (qd, J = 6.0, 3.3 Hz, 1H), 4.39 – 4.31 (m, 1H), 4.24 – 4.17 (m, 1H), 4.08 (dp, J = 7.2, 3.8 Hz, 1H), 3.85 – 3.80 (m, 1H), 3.44 – 3.23 (m, 4H), 2.62 – 2.55 (m, 1H), 2.46 (ddd, J = 15.8, 11.5, 4.2 Hz, 1H), 1.66 (s, 6H), 1.48 – 1.45 (m, 2H), 1.37 (t, J = 5.2 Hz, 1H), 1.26 – 1.20 (m, 5H), 1.15 – 1.11 (m, 1H), 1.05 (s, 12H), 1.04 – 1.02 (m, 1H), 0.96 – 0.92 (m, 1H), 0.91 – 0.86 (m, 1H), 0.86 – 0.80 (m, 12H), 0.03 – -0.07 (m, 6H).

^{13}C NMR (151 MHz, $CDCl_3$) δ 171.7, 171.7, 165.4, 144.1, 143.6, 143.4, 141.2, 135.9, 135.9, 135.6, 135.6, 135.0, 134.6, 129.4, 129.4, 129.4, 127.8, 127.5, 127.5, 127.4, 127.4, 127.2, 127.1, 125.2, 125.1, 124.2, 124.1, 121.0, 121.0, 120.0, 119.0, 119.0, 118.7, 113.9, 113.4, 107.7, 72.1, 69.6, 69.5, 67.3, 59.0, 53.7, 53.3, 49.9, 49.8, 47.6, 46.5, 39.5, 39.5, 39.1, 39.0, 39.0, 33.0, 31.6, 31.6, 29.7, 27.9, 27.9, 27.8, 27.8, 27.6, 27.1, 25.8, 25.8, 25.7, 25.5, 25.5, 23.3, 23.2, 22.7, 19.3, 18.7, 18.0, 18.0, 17.4, 14.7, 14.1, 13.8, 1.0, -4.6, -4.6.

HRMS (ESI-TOF) *m/z* Calcd for $C_{64}H_{82}N_6O_2NaSi2$ [M+Na+]+ 1045.5935; Found: 1045.5933



(9H-fluoren-9-yl)methyl (tert-butoxycarbonyl)-D-tryptophanate (4.34)

A round-bottom flask was charged with Boc-D-Trp-OH (2.00 g, 6.57 mmol, 1.2 equiv), 9-fluorenemethanol (1.06 g, 5.48 mmol, 1.0 equiv), EDC (1.26 g, 6.57 mmol, 1.2 equiv), and DMAP (80.1 mg, 0.66 mmol, 0.1 equiv) in 65 mL of dry DCM. The reaction was stirred at room temperature for 16 h. The reaction was quenched with NaHCO3 and extracted with DCM (x3) and the organic layers were combined and dried under reduced pressure. The the crude residue was purified by flash column chromatography (20–30% EtOAc/hexanes) to afford **4.34** (2.74 g, 5.02 mmol, 76% yield).

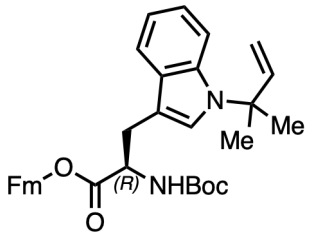
TLC (20% EtOAc/Hexanes) R_f =0.15

^{1}H NMR (400 MHz, $CDCl_3$) δ 8.00 (s, 1H), 7.77 – 7.72 (m, 2H), 7.56 (d, J = 7.9 Hz, 1H), 7.48 (dd, J = 7.5, 1.0 Hz, 1H), 7.43 (dd, J = 7.5, 1.0 Hz, 1H), 7.41 – 7.38 (m, 2H), 7.32 (d, J = 8.0 Hz, 1H), 7.29 – 7.26 (m, 2H), 7.19 (ddd, J = 8.2, 7.0, 1.3 Hz, 1H), 7.13 (td, J = 7.5, 1.1 Hz, 1H), 6.92

(d, J = 2.2 Hz, 1H), 5.10 (d, J = 8.3 Hz, 1H), 4.73 (q, J = 6.4 Hz, 1H), 4.34 (d, J = 7.2 Hz, 2H), 4.02 (t, J = 7.0 Hz, 1H), 3.26 (d, J = 5.8 Hz, 2H), 1.44 (s, 9H).

^{13}C NMR (101 MHz, $CDCl_3$) δ 172.5, 155.4, 143.7, 141.4, 136.2, 128.0, 127.3, 127.3, 125.2, 122.8, 122.4, 120.2, 120.1, 119.8, 118.9, 111.3, 110.5, 80.0, 67.3, 54.5, 46.8, 28.5, 28.3.

HRMS (ESI-TOF) *m/z* Calcd for $C_{30}H_{31}N_2O_4$ 483.2284, found: 483.2288



(9H-fluoren-9-yl)methyl Nα-(tert-butoxycarbonyl)-1-(2-methylbut-3-en-2-yl)-D-tryptophanate (4.36)

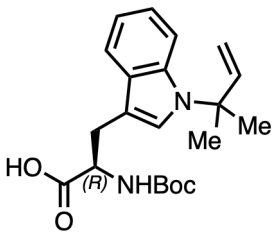
A flame-dried round-bottom flask was charged with **4.34** (500 mg, 0.91 mmol, 1.0 equiv), $Cu(OAc)_2$ (402 mg, 1.82 mmol, 2.0 equiv), and AgTFA (363.4 mg, 1.82 mmol, 2.0 equiv) in dry 9mL of dry MeCN. N2(g) was bubbled into the stirring mixture to ensure an inser atmosphere, after which 2-Methyl-2-butene (2.89 mL, 27.3 mmol, 30.0 equiv) followed by $Pd(OAc)_2$ (20 mg, 0.09 mmol, 0.1 equiv) and the reaction was heated to 35°C and left to stir for 1 h. $Pd(OAc)_2$ (20 mg, 0.09 mmol, 0.1 equiv) was added in three more successive portions at 1 h intervals (0.4 equiv total), after which the reaction was stirred at 35°C for an additional 16 h. The mixture was concentrated under reduced pressure and purified by flash column chromatography (30% EtOAc/hexanes) to afford 260mg of **4.36** (0.46mmol, 52% yields) as a yellow viscous oil.

TLC (30% EtOAc/Hexanes) R_f =0.72

^{1}H NMR (400 MHz, $CDCl_3$) δ 7.75 (dd, J = 7.6, 3.1 Hz, 2H), 7.58 – 7.52 (m, 1H), 7.50 (d, J = 7.5 Hz, 1H), 7.45 (dd, J = 8.4, 3.6 Hz, 2H), 7.39 (td, J = 7.5, 3.6 Hz, 2H), 7.27 (d, J = 3.0 Hz, 2H), 7.26 – 7.22 (m, 1H), 7.13 – 7.08 (m, 3H), 6.01 (dd, J = 17.4, 10.7 Hz, 1H), 5.16 – 5.04 (m, 3H), 4.80 – 4.73 (m, 1H), 4.35 – 4.24 (m, 2H), 3.97 (t, J = 7.3 Hz, 1H), 3.27 (d, J = 5.9 Hz, 2H), 1.62 (s, 6H), 1.45 (s, 9H).

^{13}C NMR (101 MHz, $CDCl_3$) δ 172.6, 155.4, 144.2, 143.7, 143.6, 141.4, 141.3, 135.7, 129.8, 128.0, 127.3, 127.3, 125.3, 123.9, 121.1, 120.2, 120.1, 119.1, 118.9, 114.0, 113.6, 108.3, 80.0, 67.5, 59.1, 54.7, 46.7, 28.5, 28.0, 27.9.

HRMS (ESI-TOF) *m/z* Calcd for $C_{35}H_{39}N_2O_4$ 551.2910, Found: 551.2922



Nα-(tert-butoxycarbonyl)-1-(2-methylbut-3-en-2-yl)-D-tryptophan (4.41)

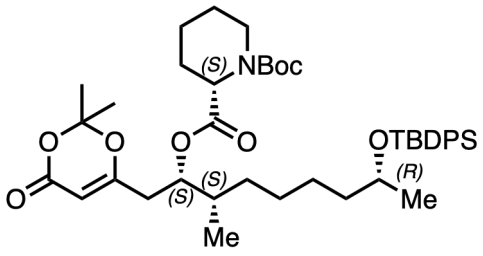
A round bottom flask was charged with **4.36** (60mg, 0.12mmol, 1.0eq.) and 3mL of DCM. To the stirring suspention, 1.5mL of diethylamine was added dropwise and the reaction progress was monitored by TLC. Once completion, the mixture was dried under reduced pressure and crude product was purified via silica gel chromatography (30% EtOAc/hexanes + 1% acetic acid) to afford 3.31mg of **4.41** (0.086 mmol, 72% yield) as a yellow solid.

TLC (30% EtOAc/Hexanes +1% acetic acid) $R_f = 0.12$

^{1}H NMR (600 MHz, $CDCl_3$) δ 7.58 (d, J = 7.7 Hz, 1H), 7.49 (d, J = 8.3 Hz, 1H), 7.16 (s, 1H), 7.11 (ddd, J = 8.5, 6.9, 1.5 Hz, 1H), 7.08 (td, J = 7.3, 1.1 Hz, 1H), 6.12 (dd, J = 17.5, 10.7 Hz, 1H), 5.23 – 5.10 (m, 2H), 5.01 (d, J = 8.0 Hz, 1H), 4.66 (d, J = 7.2 Hz, 1H), 3.36 (dd, J = 15.3, 5.7 Hz, 1H), 3.32 – 3.20 (m, 1H), 1.72 (s, 6H), 1.42 (s, 9H).

^{13}C NMR (151 MHz, $CDCl_3$) δ 176.5, 155.8, 144.2, 135.7, 129.7, 124.2, 121.1, 119.2, 118.9, 114.0, 113.7, 108.0, 80.4, 59.2, 54.4, 28.5, 28.0, 27.8.

HRMS (ESI-TOF) *m/z* Calcd for $C_{21}H_{28}N_2O_4Na$ [M+Na]+ 395.1947, found 395.1931.



1-(tert-butyl) 2-((2S,3S,8R)-8-((tert-butyldiphenylsilyl)oxy)-1-(2,2-dimethyl-4-oxo-4H-1,3-dioxin-6-yl)-3-methylnonan-2-yl) (S)-piperidine-1,2-dicarboxylate (4.35)

To a solution of **4.26** (80 mg, 0.148 mmol, 1.0 equiv) and Boc-L-Pip (47 mg, 0.205 mmol, 1.2 equiv) in 2mL of dry DCM were added EDC (41.3 mg, 0.216 mmol, 1.2 equiv) and DMAP (2.2

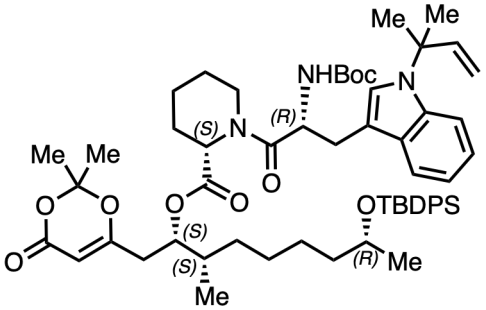
mg, 0.018 mmol, 0.1 equiv). The reaction was stirred at room temperature for 24h. The reaction was quenched with saturated aqueous NaHCO3 and the layers were separated. The aqueous layer was extracted with (x3)DCM, and the combined organic layers were washed with brine (x2), dried over Na2SO4, filtered, and concentrated under reduced pressure. The crude residue was purified by flash column chromatography (20% EtOAc/hexanes) to afford **4.35** (90.7 mg, 0.121 mmol, 67% yield).The spectrum was reported as observed. The compound exists as a mixture of rotamers about the ester, N-Boc and diastereomers at C5, resulting in peak broadening for several resonances.

TLC (25% EtOAc/Hexanes): $R_f = 0.40$

^{1}H NMR (400 MHz, $CDCl_3$) δ 7.67 (dq, J = 8.1, 2.0 Hz, 4H), 7.38 (dt, J = 14.2, 7.0 Hz, 6H), 5.26 (d, J = 3.0 Hz, 1H), 5.20 – 5.09 (m, 1H), 4.90 – 4.67 (m, 1H), 4.14 – 3.88 (m, 1H), 3.83 (p, J = 5.7 Hz, 1H), 3.01 – 2.75 (m, 1H), 2.50 (q, J = 6.7 Hz, 1H), 2.43 – 2.38 (m, 1H), 2.16 (d, J = 13.6 Hz, 1H), 1.67 (d, J = 7.7 Hz, 8H), 1.63 – 1.58 (m, 2H), 1.52 – 1.47 (m, 1H), 1.47 – 1.42 (m, 9H), 1.40 – 1.34 (m, 2H), 1.30 – 1.14 (m, 7H), 1.06 – 1.03 (m, 12H), 0.91 – 0.87 (m, 3H).

^{13}C NMR (151 MHz, $CDCl_3$) δ 171.5, 171.3, 168.3, 167.9, 167.9, 161.0, 160.9, 160.8, 155.8, 155.0, 136.0, 136.0, 135.0, 134.7, 129.6, 129.5, 127.6, 127.5, 107.0, 106.9, 106.9, 95.4, 95.2, 95.1, 80.3, 80.1, 80.0, 74.3, 73.8, 73.7, 69.6, 69.6, 54.9, 54.8, 53.8, 53.6, 42.1, 41.0, 39.5, 39.5, 39.4, 36.9, 36.7, 36.5, 35.1, 32.9, 31.1, 29.8, 28.5, 27.4, 27.3, 27.3, 27.3, 27.2, 27.2, 26.9, 25.6, 25.5, 25.4, 25.4, 24.9, 24.7, 23.3, 21.0, 19.4, 14.9, 14.3, 14.2.

HRMS (ESI-TOF) *m/z* Calcd for $C_{43}H_{63}NO_8SiNa$ [M+Na]+ 772.4221, Found 772.4243



(2S,3S,8R)-8-((tert-butyldiphenylsilyl)oxy)-1-(2,2-dimethyl-4-oxo-4H-1,3-dioxin-6-yl)-3-methylnonan-2-yl (S)-1-(Nα-(tert-butoxycarbonyl)-1-(2-methylbut-3-en-2-yl)-D-tryptophyl)piperidine-2-carboxylate (4.40)

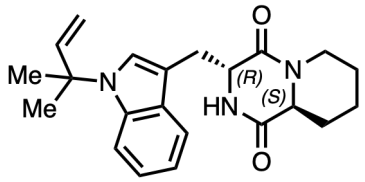
To a stirring solution of **4.34** (9.7mg, 0.013 mmol, 1.0 eq) in 0.1mL of 1,4-dioxane, 0.1mL of (2M) HCl in dioxane was added, and the reaction was left to stir until TLC showed complete Boc

deprotection. The volatiles were removed under reduced pressure and the crude product was re-dissolved in dry DCM. To this stirring suspension, **4.41** (5.8 mg, 0.015 mmol, 1.2 eq.), HATU (5.9 mg, 0.015 mmol, 1.2 equiv) and DIPEA (5.0 μL, 0.03 mmol, 2.0 equiv) were added. The reaction was left to stir for 16h at room temperature and quenched with NaHCO3. The mixture was extracted with DCM (x3), the organic layers were combined and concentrated. The crude residue was purified by silica gel column chromatography (gradient eluent: 10-25% EtOAc/hexanes) to afford 6.7mg of **4.40** (0.007mmol) 52% yield over two steps. Due to limited material, a ^{13}C NMR spectrum could not be obtained at the time. Compound identity was confirmed by HRMS and ^{1}H NMR analysis.

TLC (40% EtOAc/Hexanes) $R_f = 0.53$

^{1}H NMR (400 MHz, $CDCl_3$) δ 7.69 – 7.60 (m, 5H), 7.47 – 7.44 (m, 1H), 7.42 – 7.32 (m, 6H), 7.18 (d, J = 5.5 Hz, 1H), 7.08 (td, J = 6.9, 3.8 Hz, 2H), 6.27 (d, J = 1.4 Hz, 1H), 6.08 (ddd, J = 17.5, 10.7, 2.6 Hz, 1H), 5.60 – 5.47 (m, 1H), 5.30 – 5.14 (m, 4H), 5.09 (q, J = 4.1 Hz, 1H), 5.05 – 4.96 (m, 1H), 3.81 (h, J = 6.1 Hz, 1H), 3.43 (d, J = 13.2 Hz, 1H), 3.22 (dt, J = 13.2, 6.0 Hz, 1H), 3.08 (dd, J = 14.0, 9.6 Hz, 1H), 2.91 (t, J = 13.0 Hz, 1H), 2.52 – 2.30 (m, 2H), 1.96 (t, J = 9.3 Hz, 1H), 1.71 (d, J = 2.6 Hz, 6H), 1.66 – 1.61 (m, 6H), 1.57 (d, J = 7.9 Hz, 1H), 1.44 (s, 9H), 1.37 (d, J = 10.1 Hz, 2H), 1.29 (s, 1H), 1.23 – 1.15 (m, 4H), 1.04 (d, J = 3.3 Hz, 12H), 0.99 – 0.94 (m, 2H), 0.88 (q, J = 3.8 Hz, 2H), 0.85 – 0.81 (m, 3H), -0.09 (d, J = 14.8 Hz, 1H).

HRMS (ESI-TOF) *m/z* Calcd for $C_{59}H_{82}N_3O_9Si$ [M+H]+ 1004.5820, Found 1004.5838



(3R,9aS)-3-((1-(2-methylbut-3-en-2-yl)-1H-indol-3-yl)methyl)hexahydro-4H-pyrido[1,2-a]pyrazine-1,4(6H)-dione (4.39)

A flame-dried flask was charged with **4.40** (18mg, 0.018, 1.0eq) and 0.18 mL of dry DCM under inert conditions. To the stirring suspension 2,6-lutidine (0.011 mL, 0.099mmol, 5.5eq) was added and the mixture was cooled to 0°C. TMSOTF (0.016 mL, 0.09 mmol , 5.0 eq) was then added dropwise and the reaction was left to stir until **4.40** was no longer detected by TLC. The reaction was quenched with NaHCO3 and extracted with DCM (x3). The organic layers were

combined, washed with brine, dried with Na2SO4 and concentrated. The crude residue was taken up in a flame-dried vial under inert atmosphere, and 0.72 mL of dry toluene was added. The reaction was heated to reflux (110°C) and left to stir for 1 h. The crude residue was purified by flash column chromatography (80% EtOAC/hexane) to afford 5.5 mg of **4.32** (0.015, 83% yield), alongside the desired macrolactam product **4.43**, which was detected by LC-MS but not isolated in sufficient quantity for full characterization.

TLC (80% EtOAc/Hexanes): $R_f = 0.1$

HRMS (ESI-TOF) *m/z* Calcd for $C_{22}H_{32}N_3O_2$ [M+H]+ 366.2182, found 366.2153.

4.7 References

(1) Kaneda, M.; Inuki, S.; Ohno, H.; Oishi, S. *J. Org. Chem.* **2018**, *83* (6), 3047–3060.

(2) Seo, C.; Yim, J. H.; Lee, H. K.; Park, S. M.; Sohn, J. H.; Oh, H. *Tetrahedron Lett.* **2008**, *49* (1), 29–31.

(3) Takino, J.; Kotani, A.; Ozaki, T.; Peng, W.; Yu, J.; Guo, Y.; Mochizuki, S.; Akimitsu, K.; Hashimoto, M.; Ye, T.; Minami, A.; Oikawa, H. *Angew. Chem. - Int. Ed.* **2021**, *60* (43), 23403–23411.

(4) Xiao, Y.; Liu, J.; Jiang, Y.; Guo, Y.; Ye, T. *Molecules* **2024**, *29* (15), 3599.

(5) Feng, J.; Liu, J.; Ye, T. *Org. Lett.* **2025**, *27* (33), 9299–9303.

(6) Zhang, T.; Feng, J.; Oikawa, H.; Guo, Y.; Ye, T. *Precis. Chem.* **2024**, *2* (3), 120–126.

(7) Kim, M. C.; Machado, H.; Jang, K. H.; Trzoss, L.; Jensen, P. R.; Fenical, W. *J. Am. Chem. Soc.* **2018**, *140* (34), 10775–10784.

(8) Kim, D.-G.; Moon, K.; Kim, S.-H.; Park, S.-H.; Park, S.; Lee, S. K.; Oh, K.-B.; Shin, J.; Oh, D.-C. *J. Nat. Prod.* **2012**, *75* (5), 959–967.

(9) Moon, K.; Cui, J.; Kim, E.; Riandi, E. S.; Park, S. H.; Byun, W. S.; Kal, Y.; Park, J. Y.; Hwang, S.; Shin, D.; Sun, J.; Oh, K.-B.; Cha, S.; Shin, J.; Lee, S. K.; Yoon, Y. J.; Oh, D.-C. *Org. Lett.* **2020**, *22* (14), 5358–5362.

(10) Cui, J.; Hillman, P. F.; Kim, G. J.; Bui, T. T. M.; Moon, K.; Nam, S.-J.; Choi, H.; Oh, D.-C. *Nat. Prod. Rep.* **2025**, *42* (7), 1136–1174.

(11) Li, W.-S.; Luo, Z.; Zhu, Y.-L.; Yu, Y.; Wu, J.; Shen, L. *Mar. Drugs* **2020**, *18* (12), 590.

(12) Kwon, H. C.; Kauffman, C. A.; Jensen, P. R.; Fenical, W. *J. Am. Chem. Soc.* **2006**, *128* (5), 1622–1632.

(13) An, J. S.; Lee, J. Y.; Kim, E.; Ahn, H.; Jang, Y.-J.; Shin, B.; Hwang, S.; Shin, J.; Yoon, Y. J.; Lee, S. K.; Oh, D.-C. *J. Nat. Prod.* **2020**, *83* (9), 2776–2784.

(14) Hwang, S.; Heo, B. E.; Nguyen, T. Q.; Kim, Y. J.; Lee, S.-G.; Huynh, T.-H.; Kim, E.; Jo, S.-I.; Baek, M.-J.; Shin, E.-K.; Oh, J.; Park, C.; Yoon, Y. J.; Park, E.-J.; Kim, K. T.; Ryoo, S.; Lee, D.-G.; Wood, C.; Woo, M.; Kim, D.-D.; Paik, S.; Jo, E.-K.; Jang, J.; Oh, D.-C. *Angew. Chem. Int. Ed.* **2025**, *64* (1), e202412994.

(15) Chen, J.; Jiang, Y.; Yan, J.; Xu, C.; Ye, T. *Molecules* **2023**, *28* (20), 7194.

(16) Elmarrouni, A.; Fukuda, A.; Heras, M.; Arseniyadis, S.; Cossy, J. *J. Org. Chem.* **2010**, *75* (24), 8478–8486.

(17) Yadav, J. S.; Amrutapu, S. K.; Pabbaraja, S. *ChemistrySelect* **2017**, *2* (5), 1850–1853.
(18) Ghosh, A. K.; Xu, C. X. *Org. Lett.* **2009**, *11* (9), 1963–1966.
(19) Reddy, K. M.; Shashidhar, J.; Pottireddygari, G. R.; Ghosh, S. *Tetrahedron Lett.* **2011**, *52* (45), 5987–5991.
(20) Feng, J.; Liu, J.; Ye, T. *Org. Lett.* **2025**, *27* (33), 9299–9303.
(21) Feng, Y.; Blunt, J. W.; Cole, A. L. J.; Munro, M. H. G. *Org. Lett.* **2002**, *4* (12), 2095–2096.
(22) Feng, L.; Wang, J.; Liu, S.; Zhang, X.-J.; Bi, Q.-R.; Hu, Y.-Y.; Wang, Z.; Tan, N.-H. *J. Nat. Prod.* **2019**, *82*, 12.
(23) Lee, C.; Gong, J.; Kim, J.; Ko, H.; An, S.; Bang, S.; Deyrup, S. T.; Noh, M.; Shim, S. H. *J. Nat. Prod.* **2022**, *85* (3), 501–510.
(24) Saksena, A. K.; Mangiaracina, P. *Tetrahedron Lett.* **1983**, *24* (3), 273–276.
(25) Evans, D. A.; Chapman, K. T.; Carreira, E. M. *J. Am. Chem. Soc.* **1988**, *110* (11), 3560–3578.
(26) Narasaka, K.; Pai, H. C. *Chem. Lett.* **1980**, *9* (11), 1415–1418.
(27) Liu, W.; Li, L.; Chen, Z.; Li, C.-J. *Org. Biomol. Chem.* **2015**, *13* (22), 6170–6174.
(28) Chatterjee, A. K.; Choi, T.-L.; Sanders, D. P.; Grubbs, R. H. *J. Am. Chem. Soc.* **2003**, *125* (37), 11360–11370.
(29) Hosokawa, S. *Tetrahedron Lett.* **2018**, *59* (2), 77–88.
(30) Kalesse, M.; Cordes, M.; Symkenberg, G.; Lu, H.-H. *Nat. Prod. Rep.* **2014**, *31* (4), 563–594.
(31) Reetz, M. T.; Jung, A. *J. Am. Chem. Soc.* **1983**, *105* (14), 4833–4835.
(32) Evans, D. A.; Allison, B. D.; Yang, M. G.; Masse, C. E. *J. Am. Chem. Soc.* **2001**, *123* (44), 10840–10852.
(33) Chérest, M.; Felkin, H.; Prudent, N. *Tetrahedron Lett.* **1968**, *9* (18), 2199–2204.
(34) Leitereg, T. J.; Cram, D. J. *J. Am. Chem. Soc.* **1968**, *90* (15), 4019–4026.
(35) Reetz, M. T. *Angew. Chem. Int. Ed. Engl.* **1984**, *23* (8), 556–569.
(36) Evans, D. A.; Black, W. C. *J. Am. Chem. Soc.* **1992**, *114* (6), 2260–2262.
(37) Hume, P. A.; Furkert, Daniel. P.; Brimble, M. A. *J. Org. Chem.* **2014**, *79* (11), 5269–5281.
(38) Smith, T. E.; Kuo, W.-H.; Balskus, E. P.; Bock, V. D.; Roizen, J. L.; Theberge, A. B.; Carroll, K. A.; Kurihara, T.; Wessler, J. D. *J. Org. Chem.* **2008**, *73* (1), 142–150.

(39) Bhatt, U.; Christmann, M.; Quitschalle, M.; Claus, E.; Kalesse, M. *J. Org. Chem.* **2001**, *66* (5), 1885–1893.

(40) De Rosa, M.; Acocella, M. R.; Villano, R.; Soriente, A.; Scettri, A. *Tetrahedron Lett.* **2003**, *44* (32), 6087–6090.

(41) Soriente, A.; De Rosa, M.; Villano, R.; Scettri, A. *Tetrahedron Asymmetry* **2000**, *11* (11), 2255–2258.

(42) Soriente, A.; De Rosa, M.; Stanzione, M.; Villano, R.; Scettri, A. *Tetrahedron Asymmetry* **2001**, *12* (6), 959–963.

(43) Villano, R.; Acocella, M. R.; De Rosa, M.; Soriente, A.; Scettri, A. *Tetrahedron Asymmetry* **2004**, *15* (15), 2421–2424.

(44) Zimmer, R.; Peritz, A.; Czerwonka, R.; Schefzig, L.; Reißig, H.-U. *Eur. J. Org. Chem.* **2002**, *2002* (20), 3419–3428.

(45) Corey, E. J.; Sarshar, S.; Lee, D.-H. *J. Am. Chem. Soc.* **1994**, *116* (26), 12089–12090.

(46) Boeckman, Robert K.; Pero, J. E.; Boehmler, D. J. *J. Am. Chem. Soc.* **2006**, *128* (34), 11032–11033.

(47) Eggert, A.; Etling, C.; Millbrodt, L.; Schulz, G.; Kalesse, M. *Org. Lett.* **2021**, *23* (22), 8722–8726.

(48) Simsek, S.; Horzella, M.; Kalesse, M. *Org. Lett.* **2007**, *9* (26), 5637–5639.

(49) Senapati, B. K.; Gao, L.; Lee, S. I.; Hwang, G.-S.; Ryu, D. H. *Org. Lett.* **2010**, *12* (22), 5088–5091.

(50) Li, Q.; Seiple, I. B. *Tetrahedron* **2019**, *75* (24), 3309–3318.

(51) Li, Q.; Seiple, I. B. *J. Am. Chem. Soc.* **2017**, *139* (38), 13304–13307.

(52) Harada, T.; Yamamoto, Y.; Kusukawa, T. *Chem. Commun.* **2005**, No. 7, 859–861.

(53) Wang, X.; Adachi, S.; Iwai, H.; Takatsuki, H.; Fujita, K.; Kubo, M.; Oku, A.; Harada, T. *J. Org. Chem.* **2003**, *68* (26), 10046–10057.

(54) Hassfeld, J.; Christmann, M.; Kalesse, M. *Org. Lett.* **2001**, *3* (22), 3561–3564.

(55) Krüger, J.; Carreira, E. M. *J. Am. Chem. Soc.* **1998**, *120* (4), 837–838.

(56) Pagenkopf, B. L.; Krüger, J.; Stojanovic, A.; Carreira, E. M. *Angew. Chem. Int. Ed.* **1998**, *37* (22), 3124–3126.

(57) Tenenbaum, J. M.; Morris, W. J.; Custar, D. W.; Scheidt, K. A. *Angew. Chem. Int. Ed.* **2011**, *50* (26), 5892–5895.

(58) Snider, B. B.; Song, F. *Org. Lett.* **2001**, *3* (12), 1817–1820.

(59) Peng, W.; Han, F.; Liu, J.; Wang, C.; Minami, A.; Oikawa, H.; Guo, Y.; Ye, T. *Org. Lett.* **2025**, *27* (30), 8183–8188.

(60) Zhao, Z.; Wu, Y.; Li, Y. *Chin. J. Chem.* **2017**, *35* (7), 1185–1194.

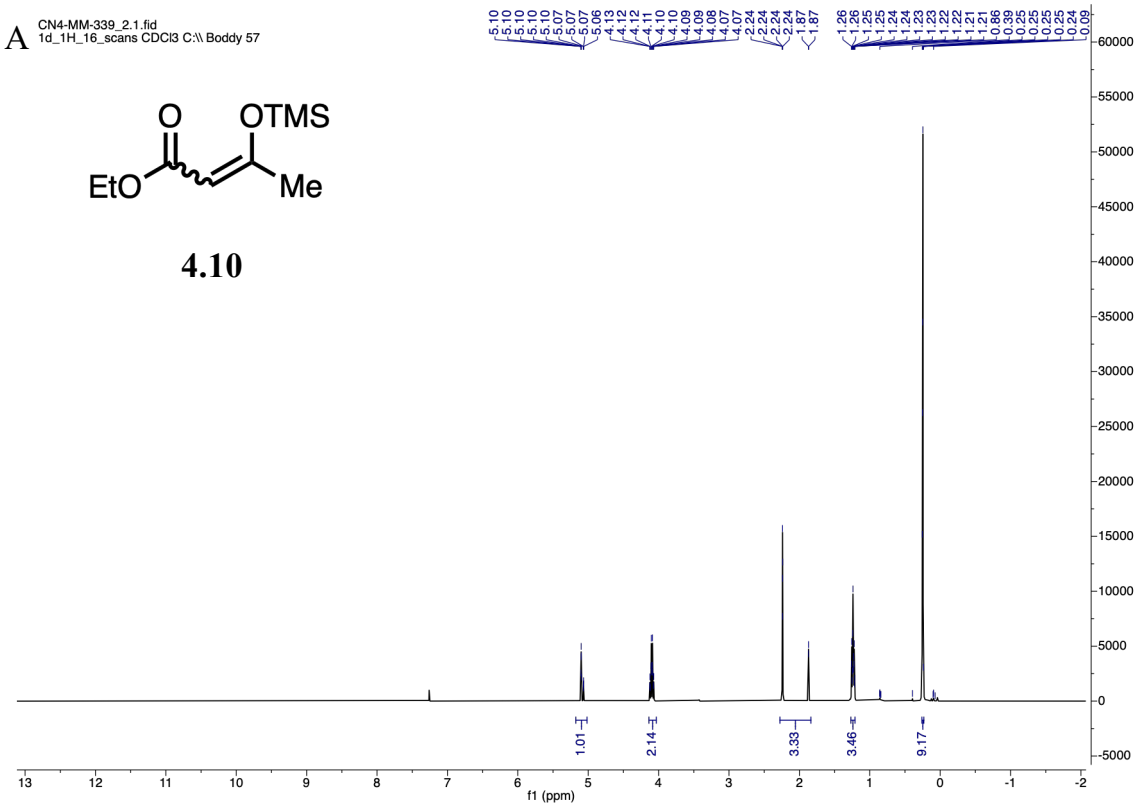
(61) Fujiwara, T.; Tsutsumi, T.; Nakata, K.; Nakatsuji, H.; Tanabe, Y. *Molecules* **2017**, *22* (1), 69.

(62) Kerhervé, J.; Botuha, C.; Dubois, J. *Org. Biomol. Chem.* **2009**, *7* (10), 2214–2222.

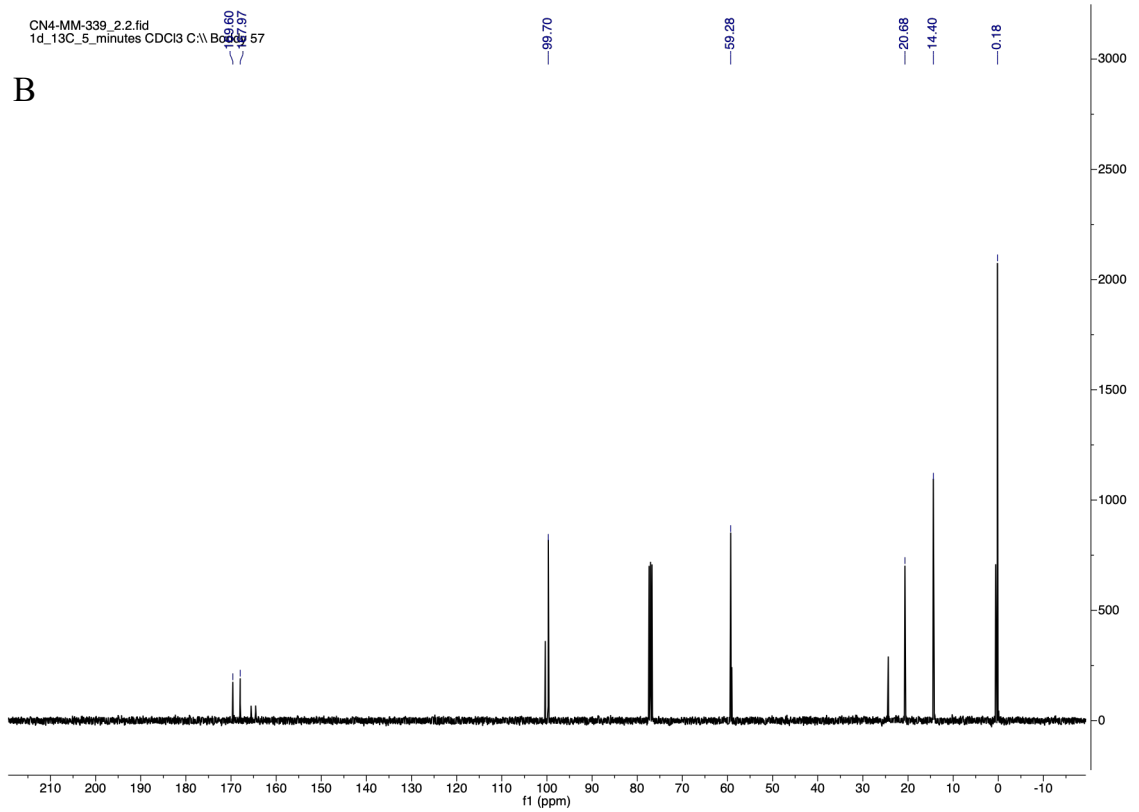
(63) Ren, H.; Wulff, W. D. *Org. Lett.* **2013**, *15* (2), 242–245.

(64) Birch, A. J.; Mani, N. S.; Rao, G. S. R. S. *J. Chem. Soc. Perkin 1* **1990**, No. 5, 1423–1427.

4.8 Appendix for Chapter IV
NMR Spectra:

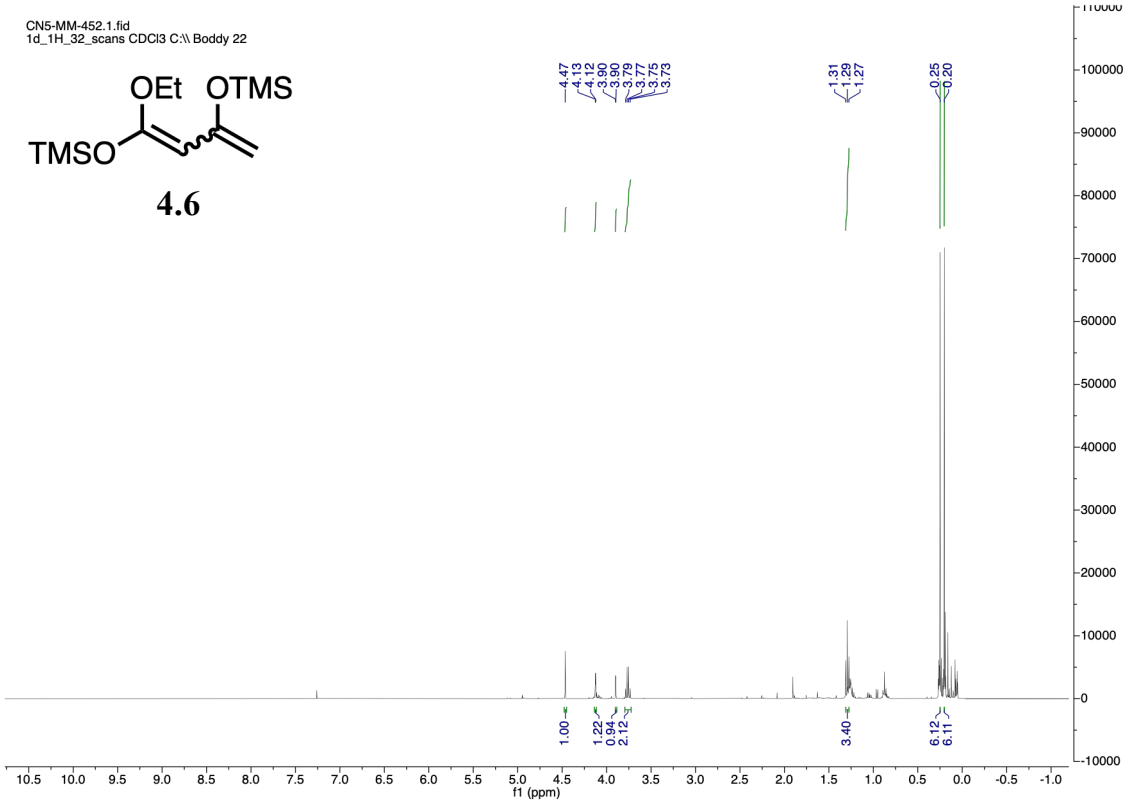


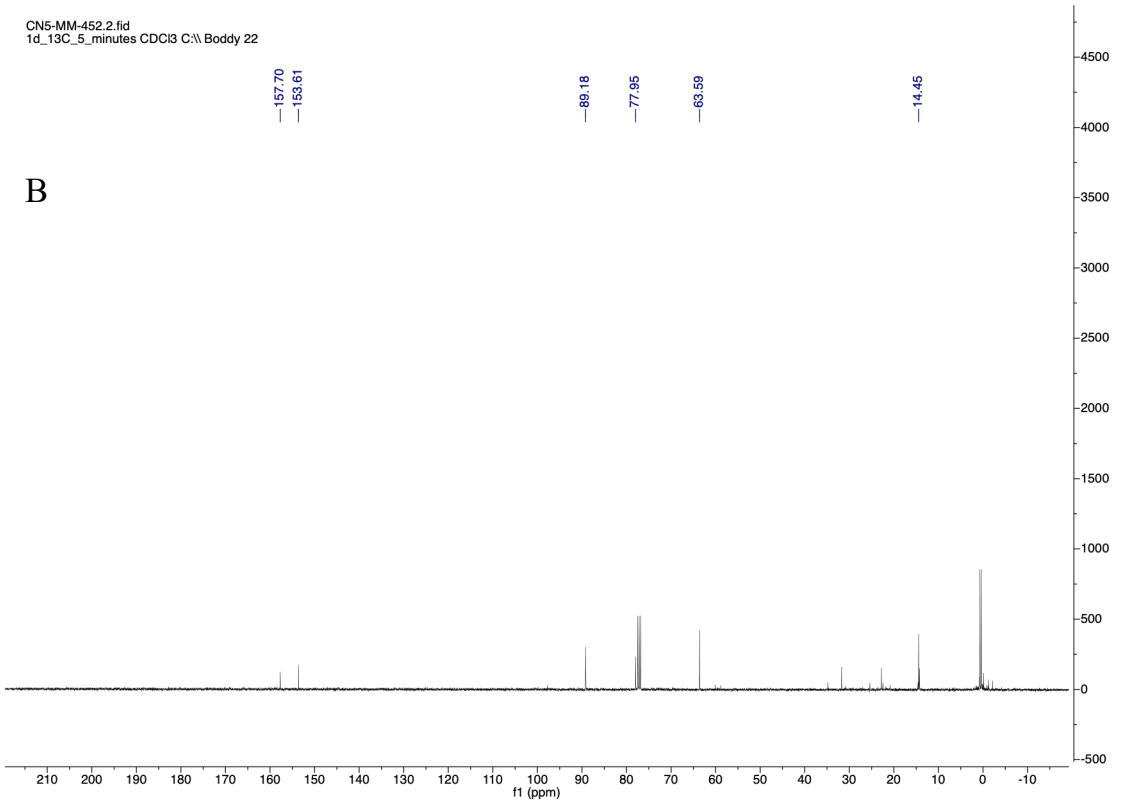
4.10



Spectra 4.1 of compound **4.10.** (A) ^{1}H NMR (400 MHz, $CDCl_3$) and (B) ^{13}C NMR (101 MHz, $CDCl_3$). Compound isolated as a 3:1 mixture of diastereomers. Major diastereomer is assigned in **Section 4.6**

A

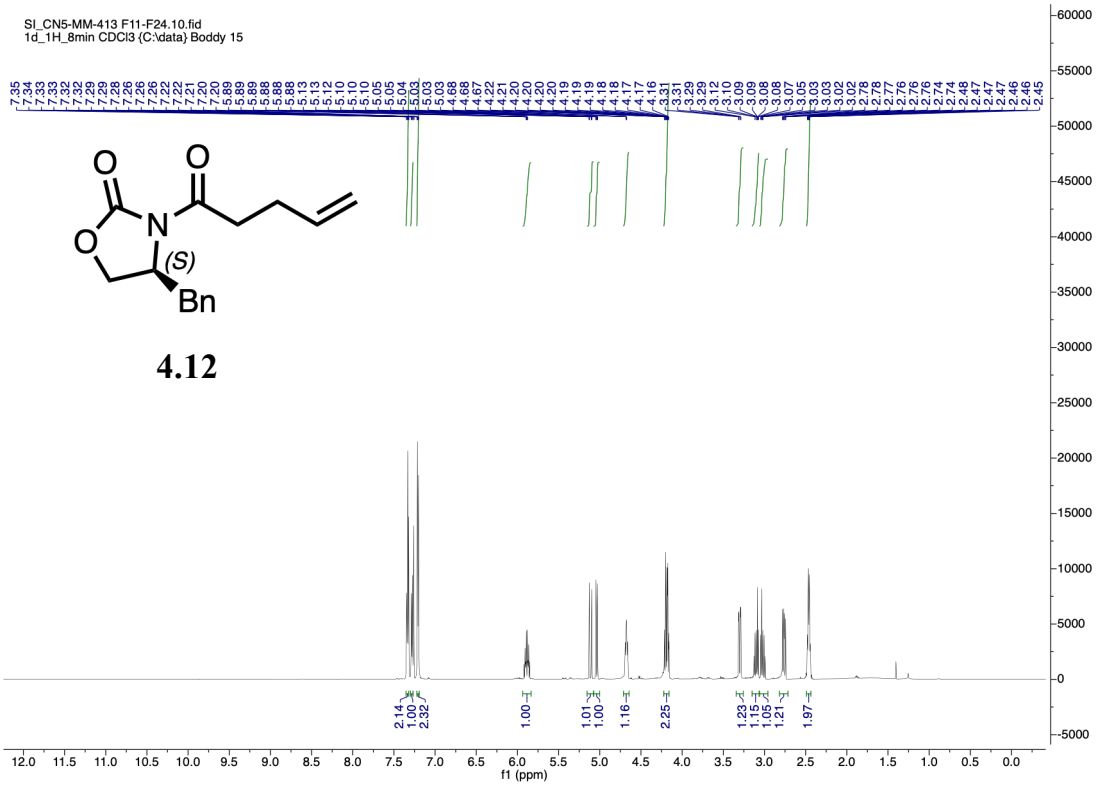




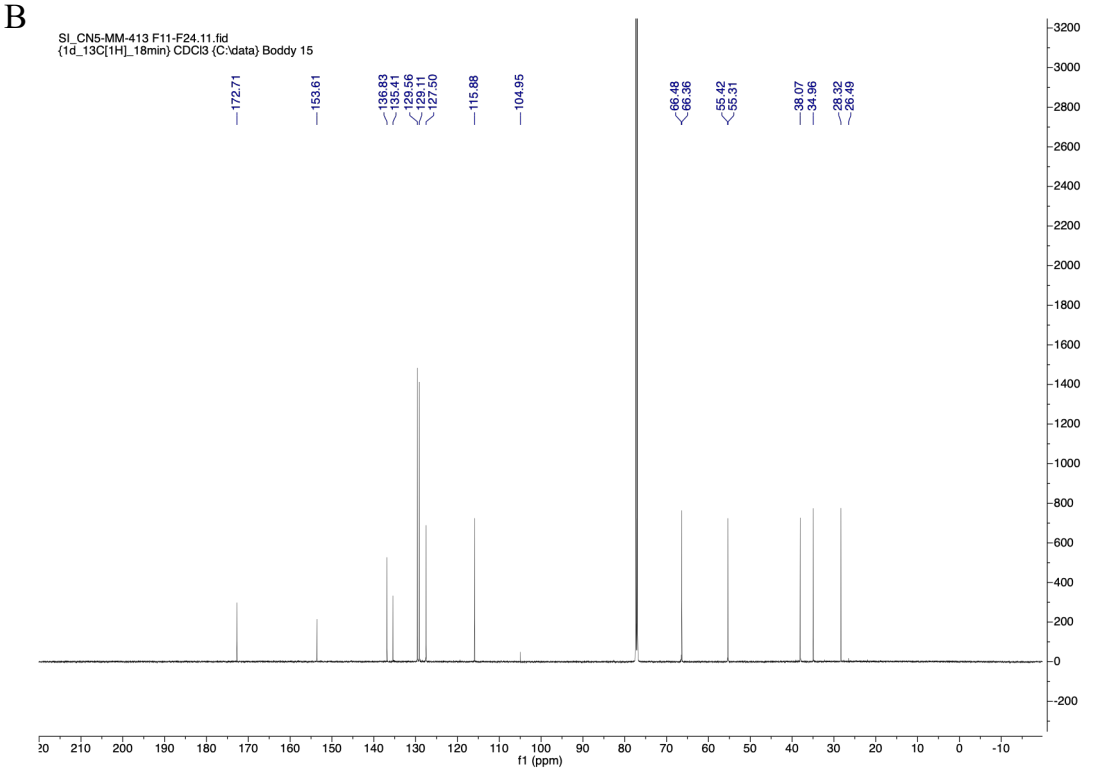
B

Spectra 4.2 of compound **4.6** (A) ^{1}H NMR (400 MHz, $CDCl_3$) and (B) ^{13}C NMR (101 MHz, $CDCl_3$)

A

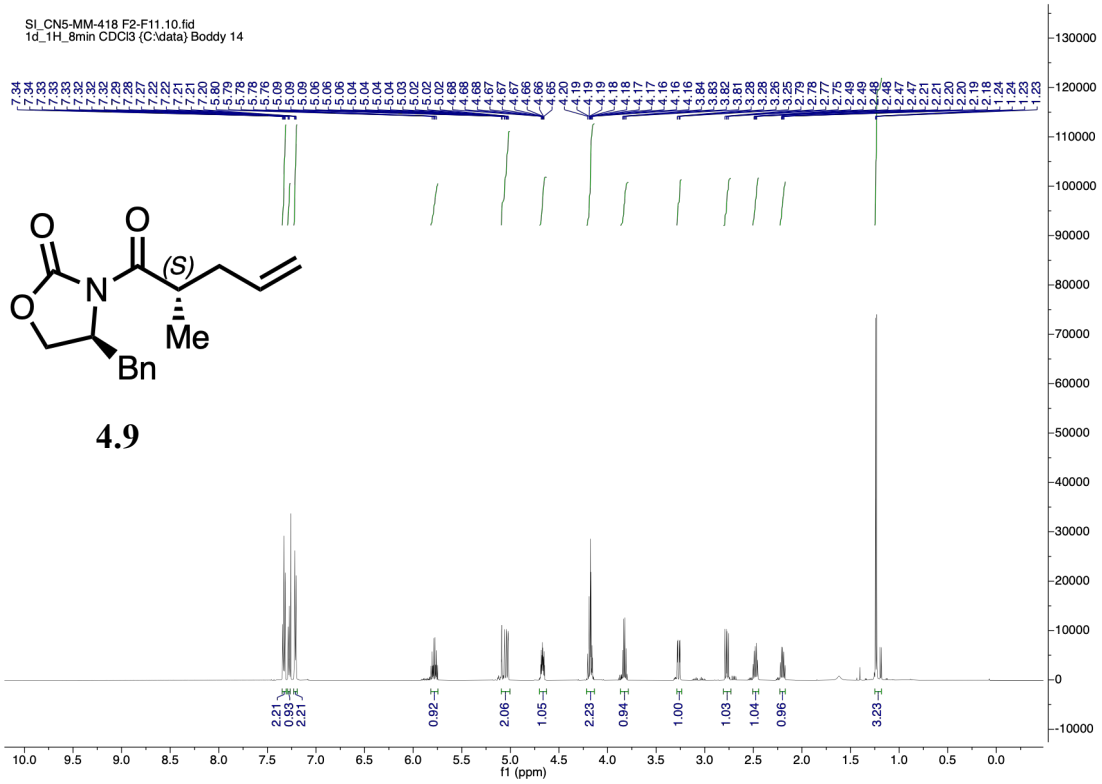


B



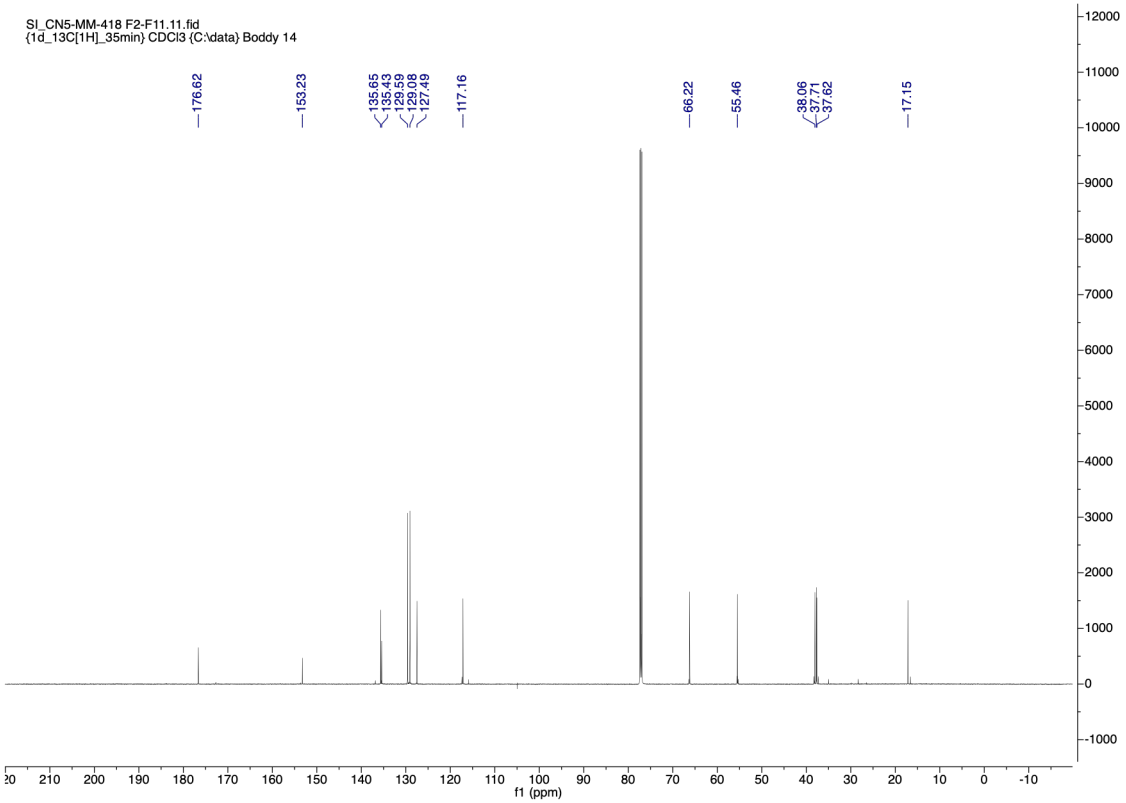
Spectra 4.3 of compound **4.12** (A) ^{1}H NMR (600 MHz, $CDCl_3$) and (B) ^{13}C NMR (101 MHz, $CDCl_3$)

A



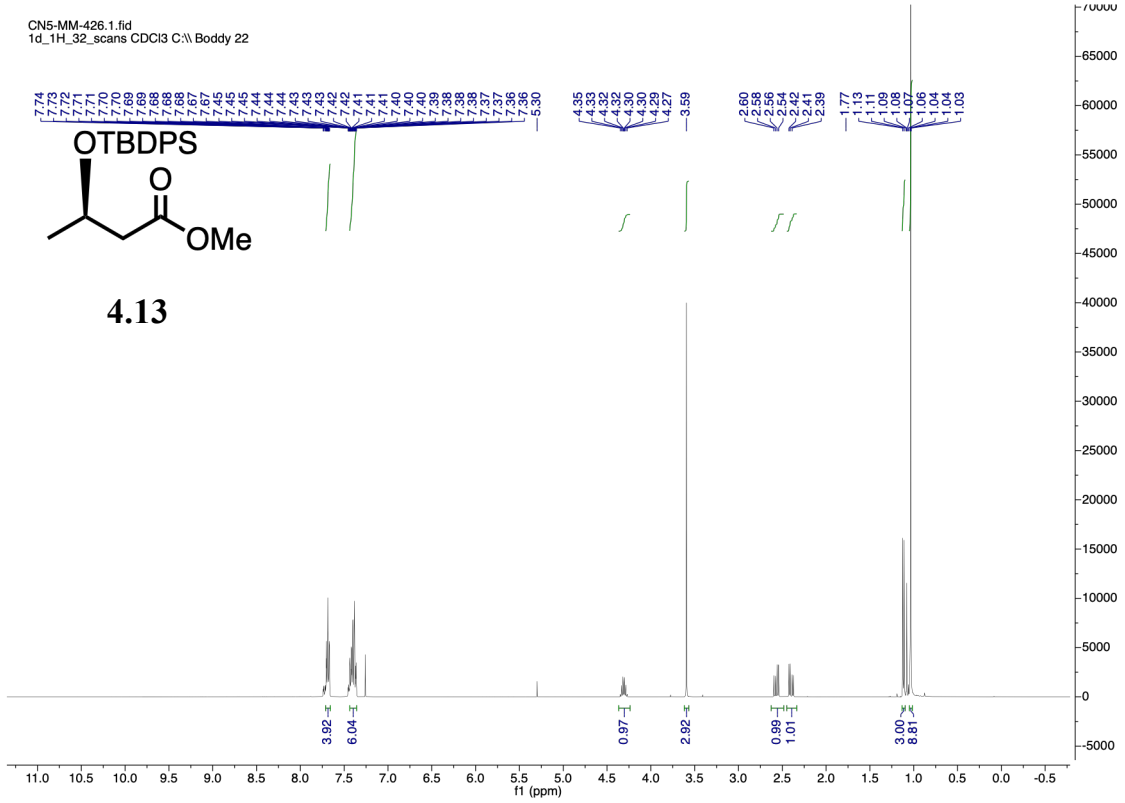
4.9

B

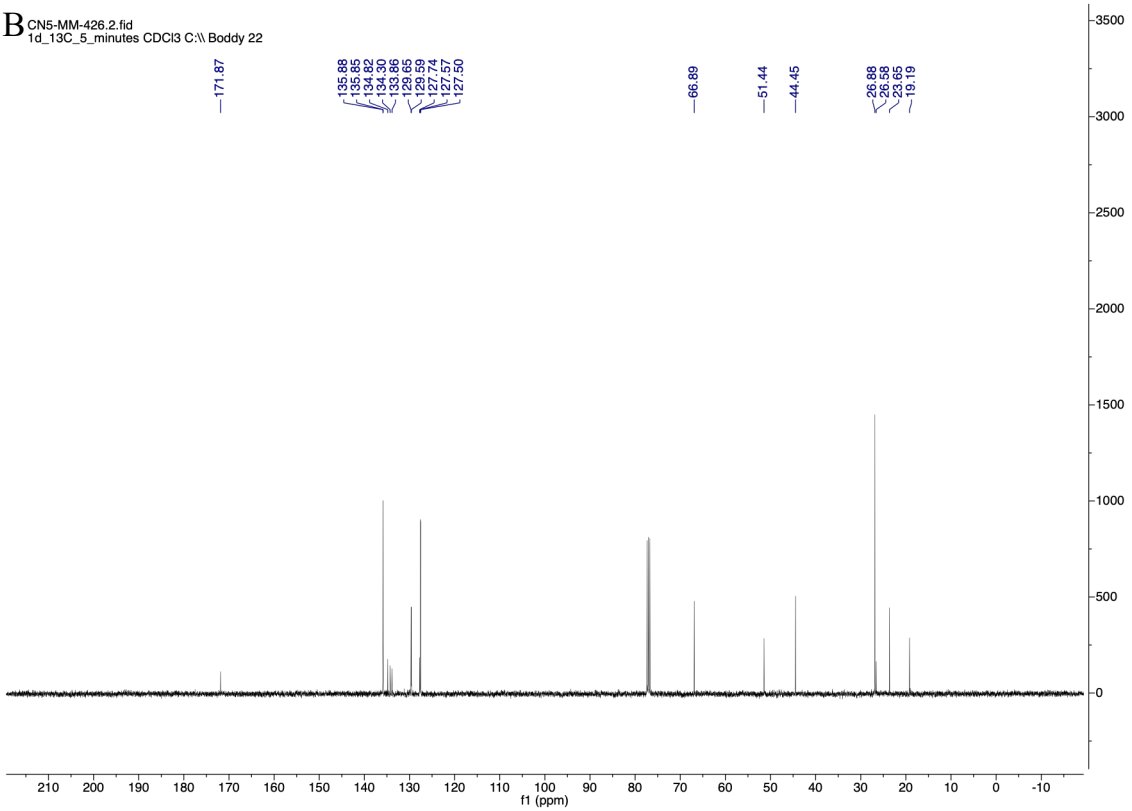


Spectra 4.4 of compound **4.9** (A) ^{1}H NMR (600 MHz, $CDCl_3$) and (B) ^{13}C NMR (101 MHz, $CDCl_3$)

A

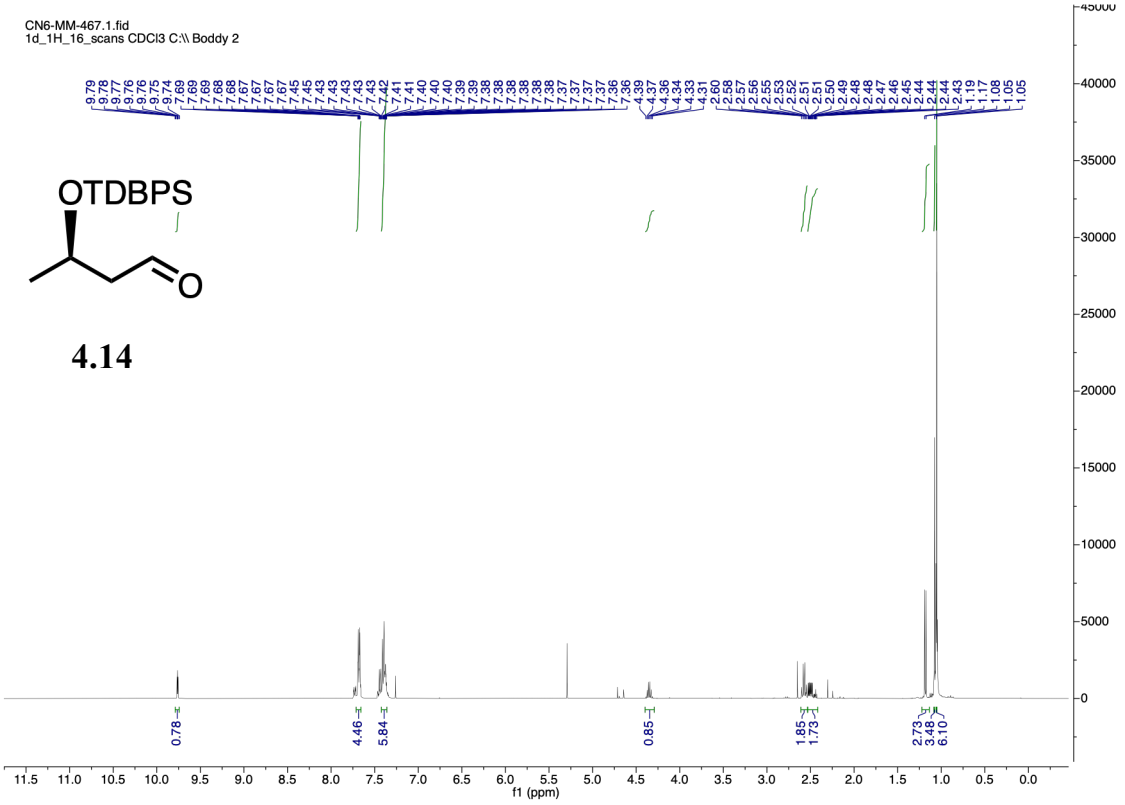


B



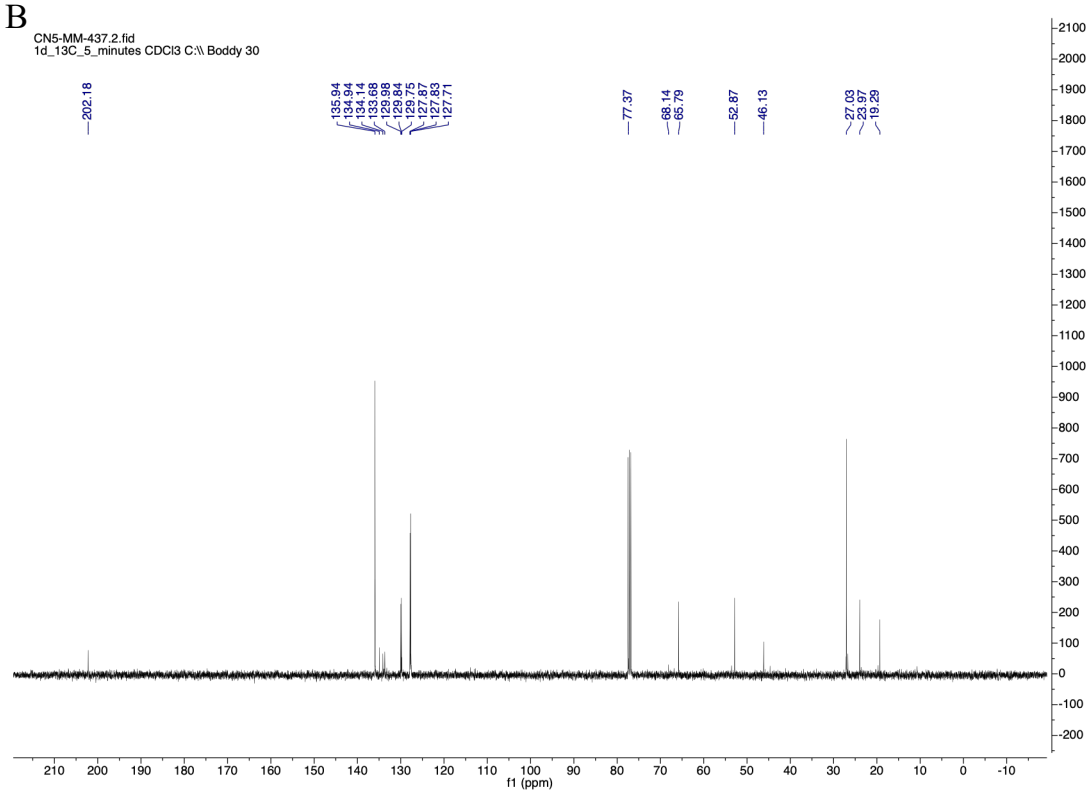
Spectra 4.5 of compound **4.13** (A) ^{1}H NMR (600 MHz, $CDCl_3$) and (B) ^{13}C NMR (101 MHz, $CDCl_3$)

A



4.14

B

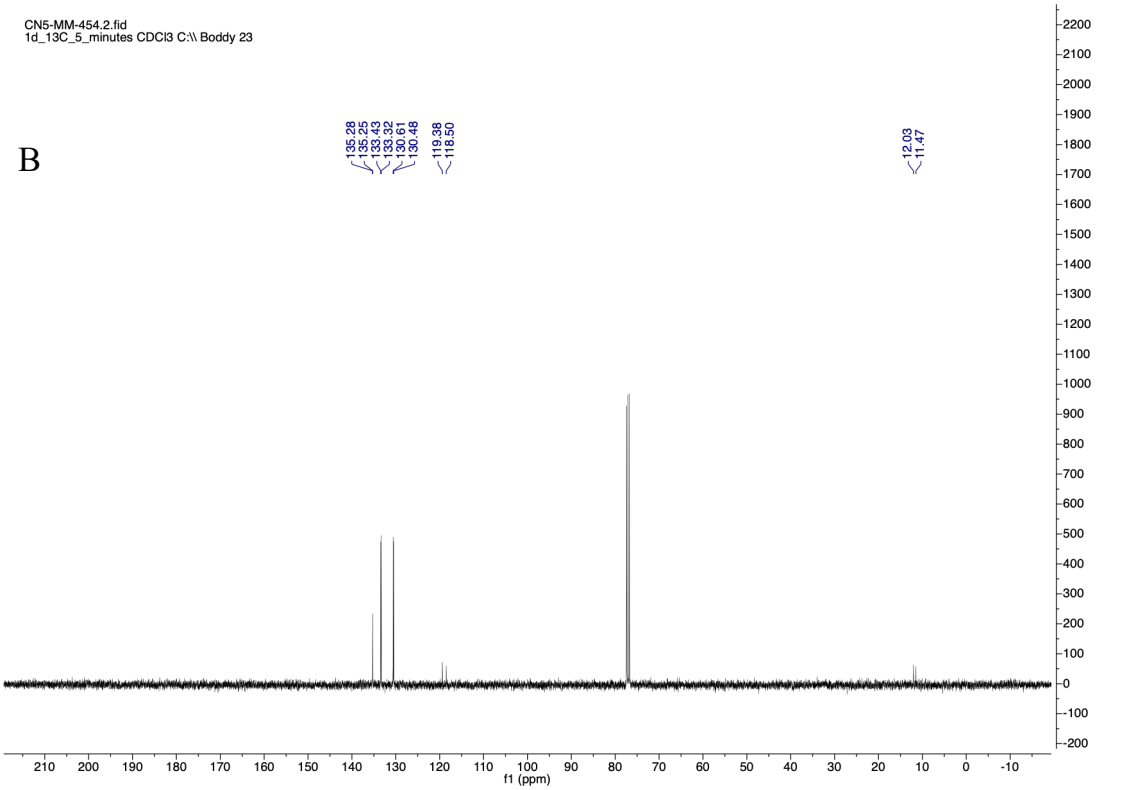


Spectra 4.6 of compound **4.14** (A) ^{1}H NMR (600 MHz, $CDCl_3$) and (B) ^{13}C NMR (101 MHz, $CDCl_3$)

A

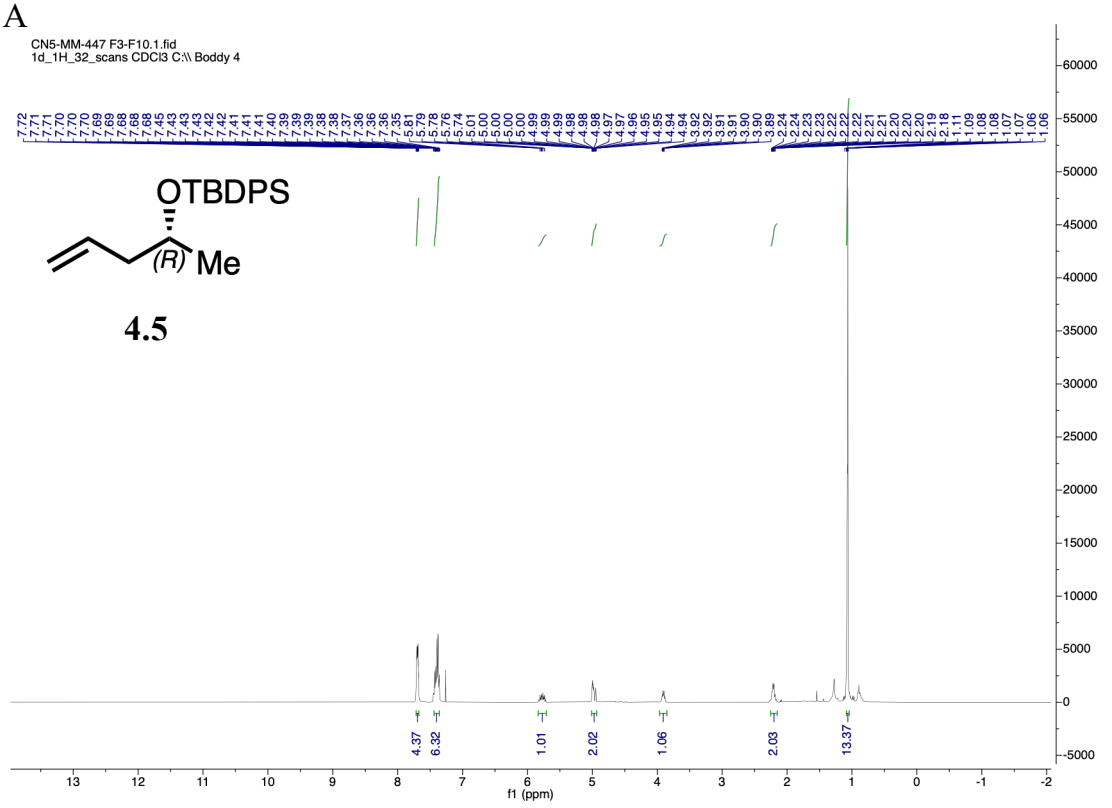


B

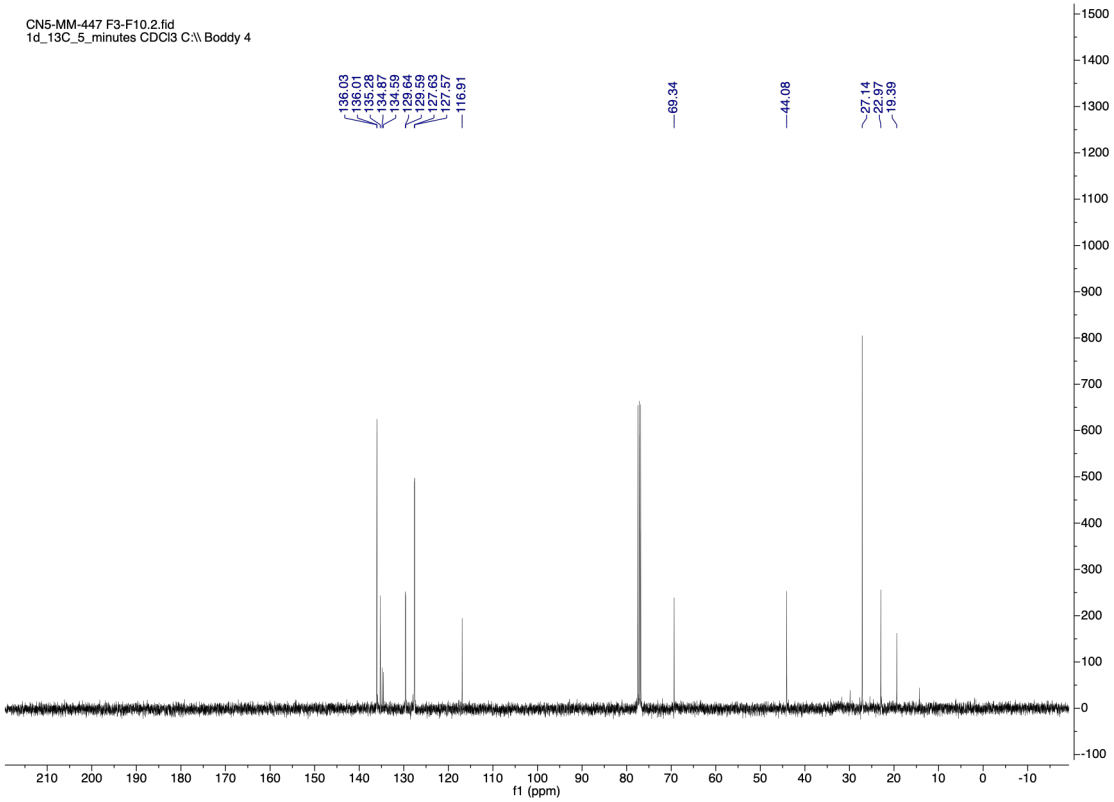


Spectra 4.7 of compound **4.15** (A) ^{1}H NMR (600 MHz, $CDCl_3$) and (B) ^{13}C NMR (101 MHz, $CDCl_3$)

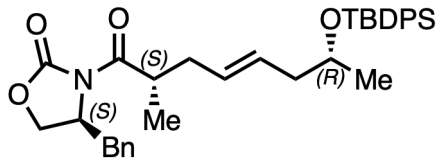
A



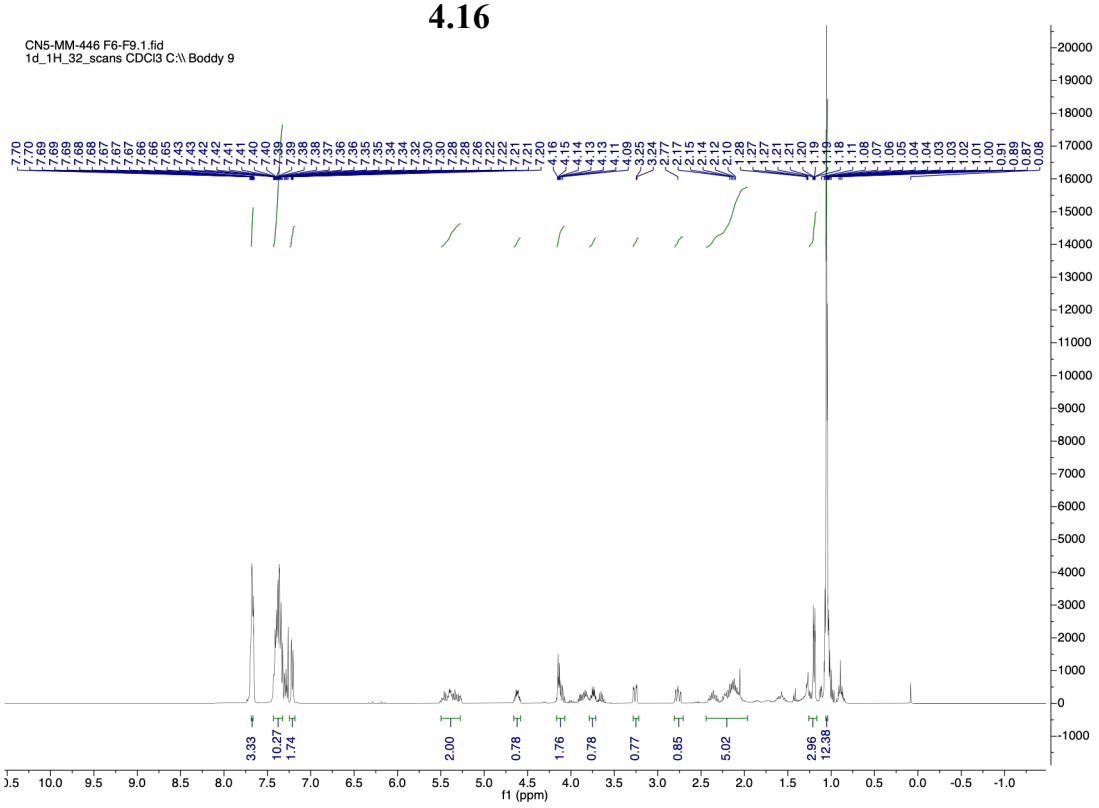
B



Spectra 4.8 of compound **4.5** (A) ^{1}H NMR (600 MHz, $CDCl_3$) and (B) ^{13}C NMR (101 MHz, $CDCl_3$)

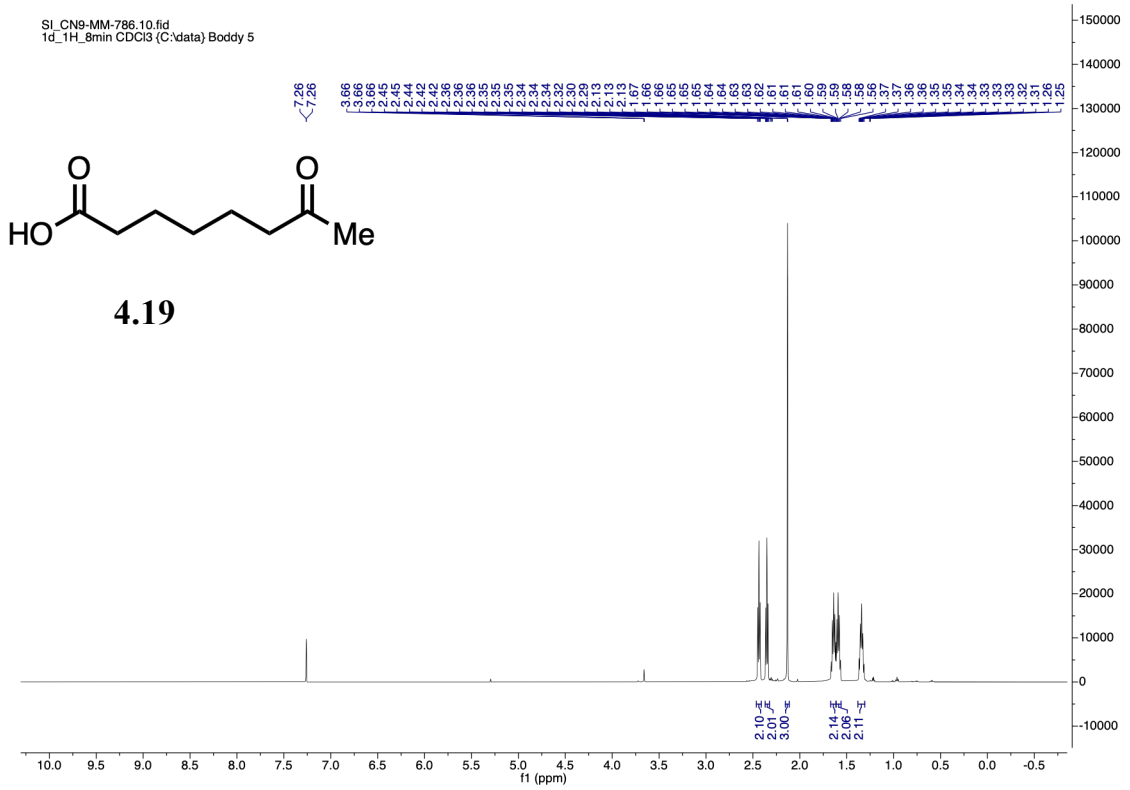


4.16



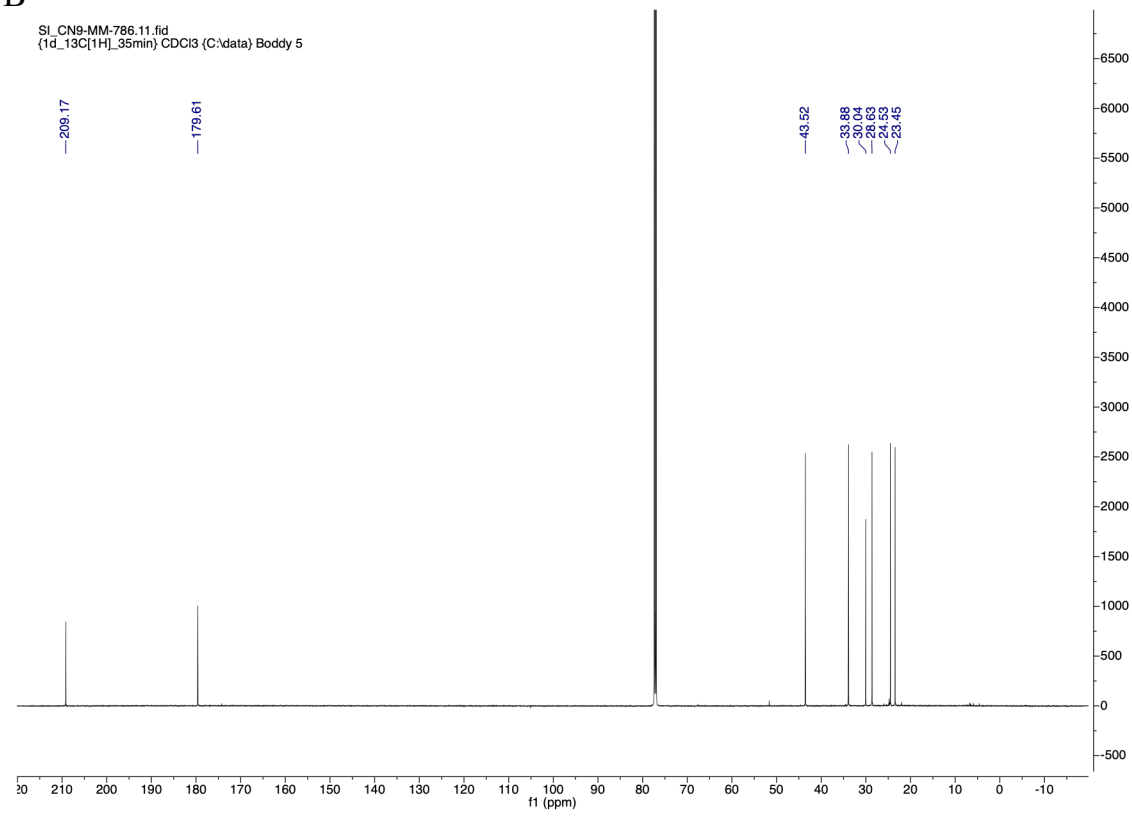
Spectra 4.9 of compound **4.16** ^{1}H NMR (600 MHz, $CDCl_3$)

A



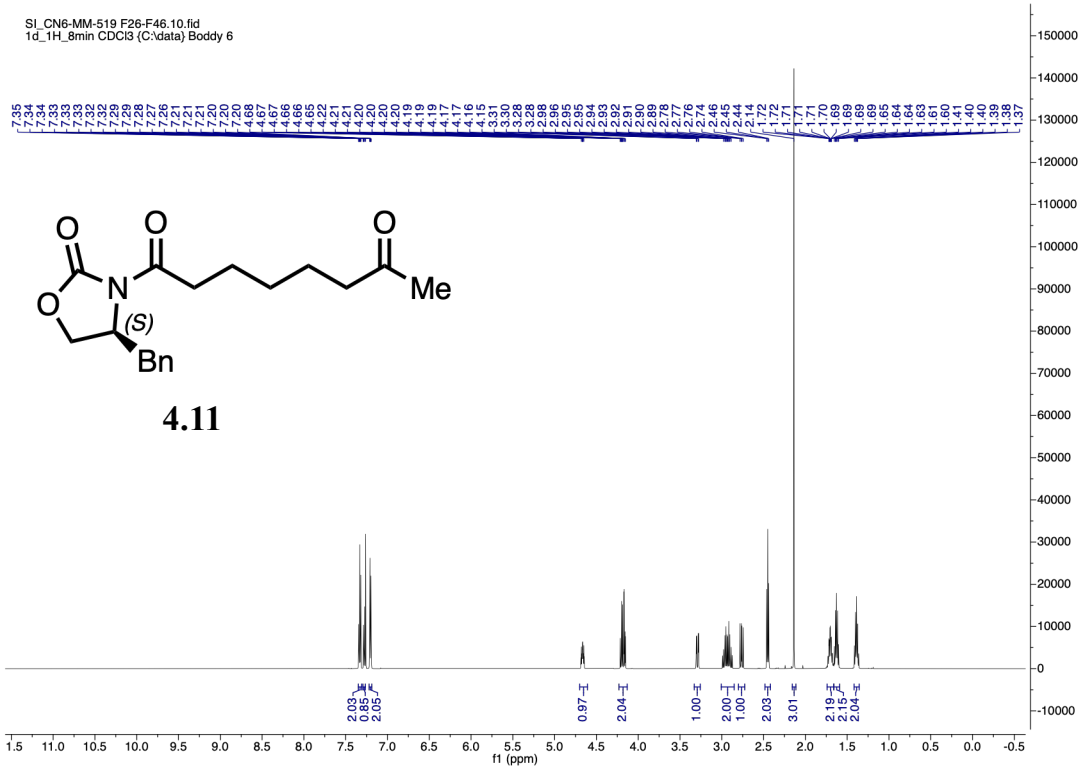
4.19

B



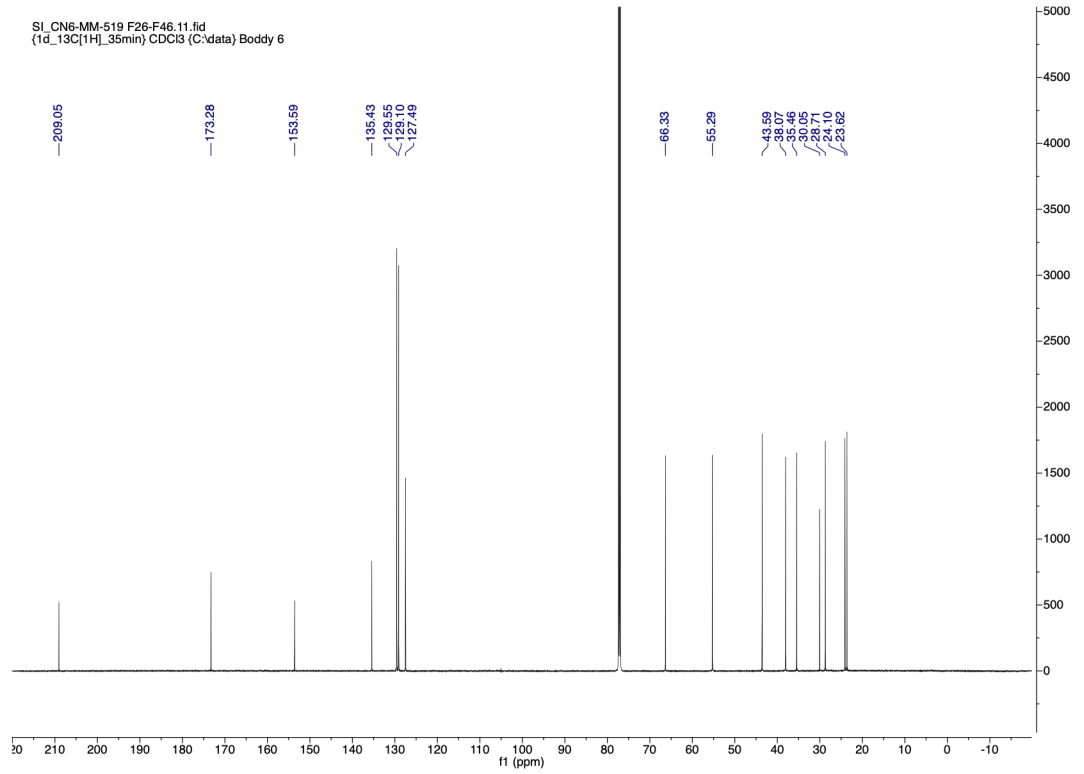
Spectra 4.10 of compound **4.19** (A) ^{1}H NMR (600 MHz, $CDCl_3$) and (B) ^{13}C NMR (101 MHz, $CDCl_3$)

A



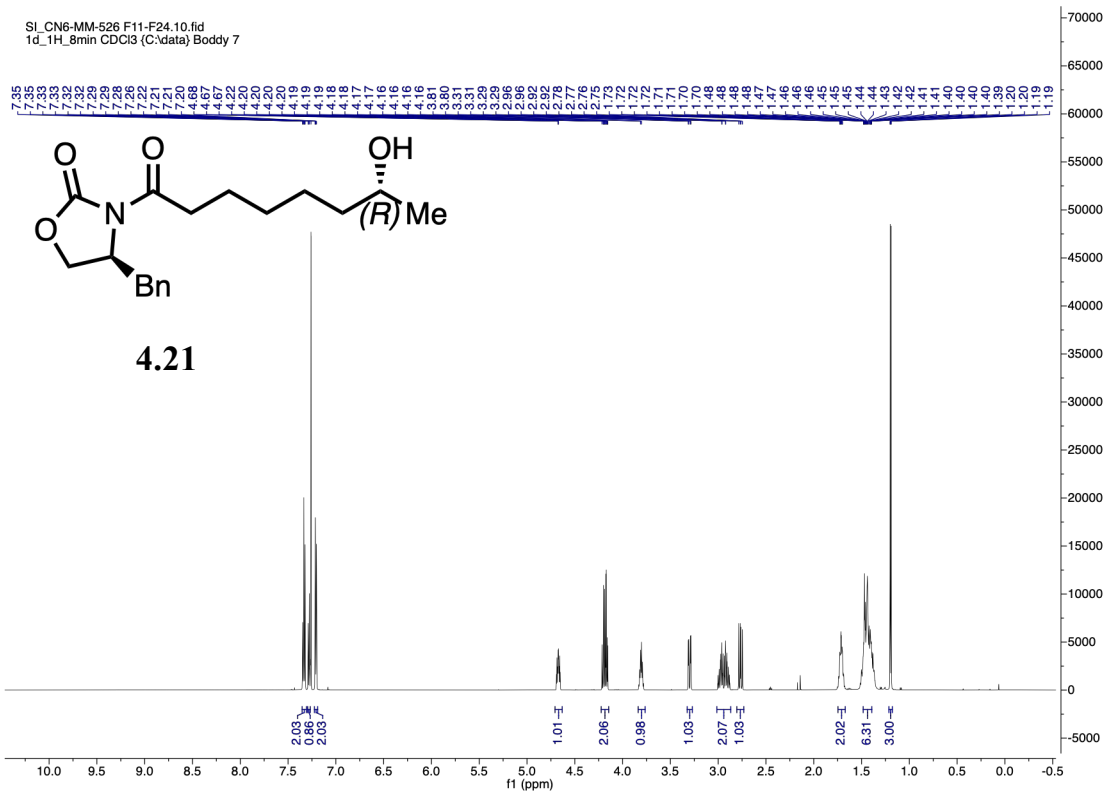
4.11

B

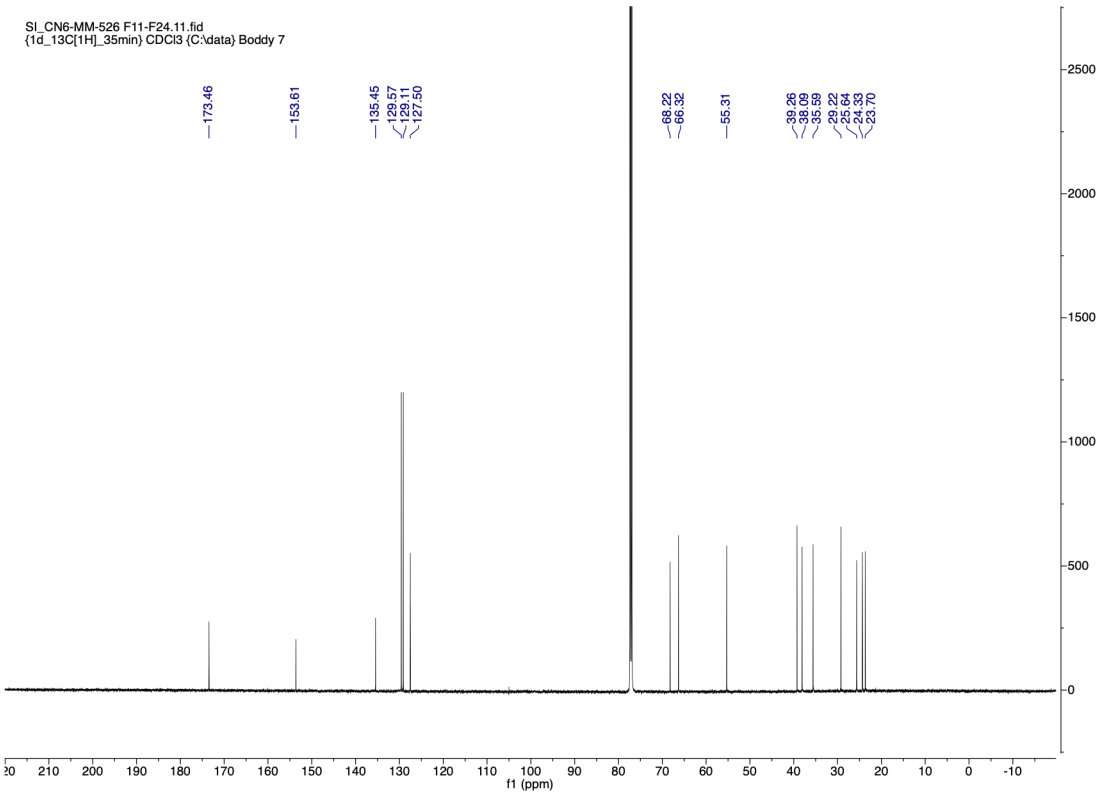


Spectra 4.11 of compound **4.18** (A) ^{1}H NMR (600 MHz, $CDCl_3$) and (B) ^{13}C NMR (101 MHz, $CDCl_3$)

A

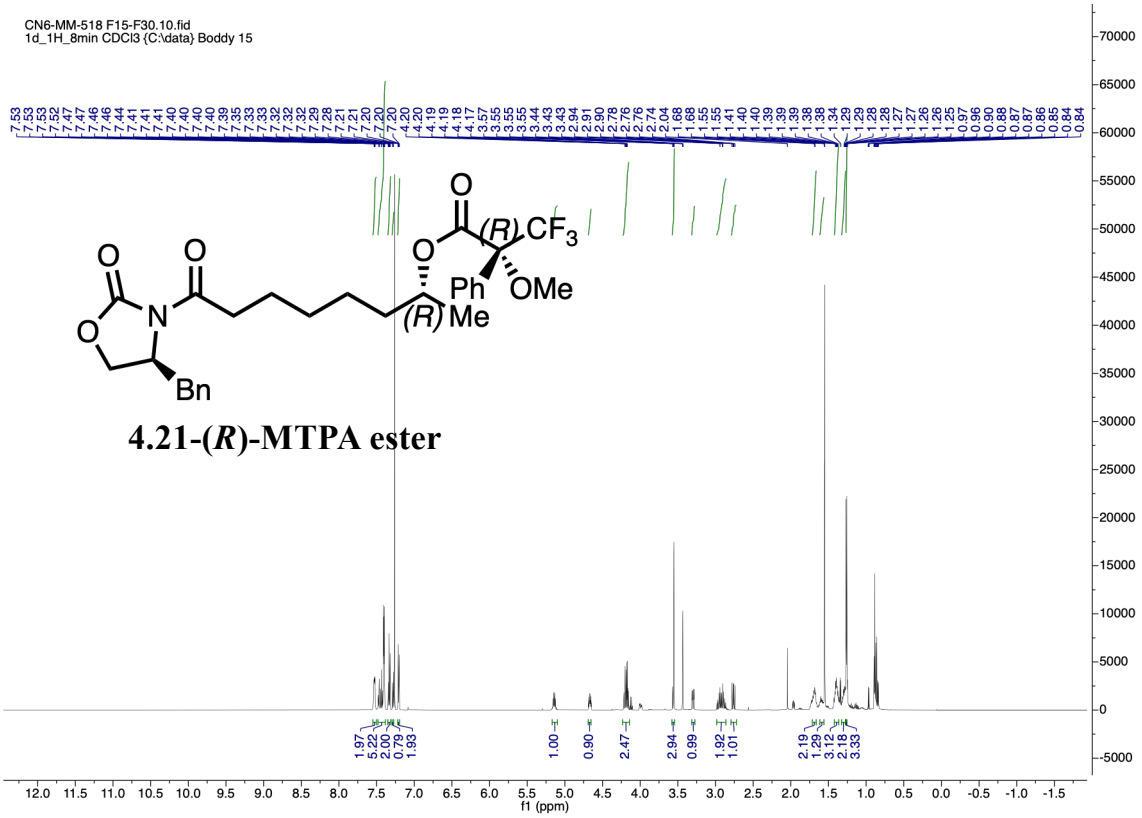


B

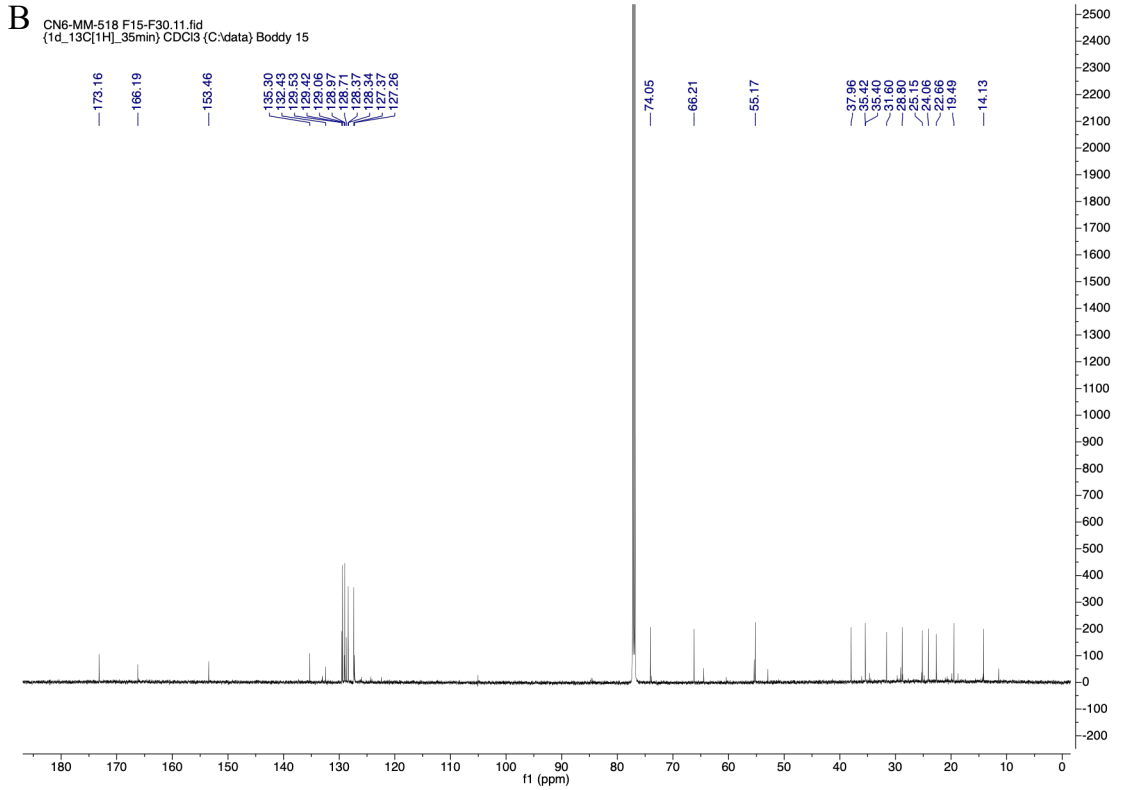


Spectra 4.12 of compound **4.21** (A) ^{1}H NMR (600 MHz, $CDCl_3$) and (B) ^{13}C NMR (101 MHz, $CDCl_3$)

A

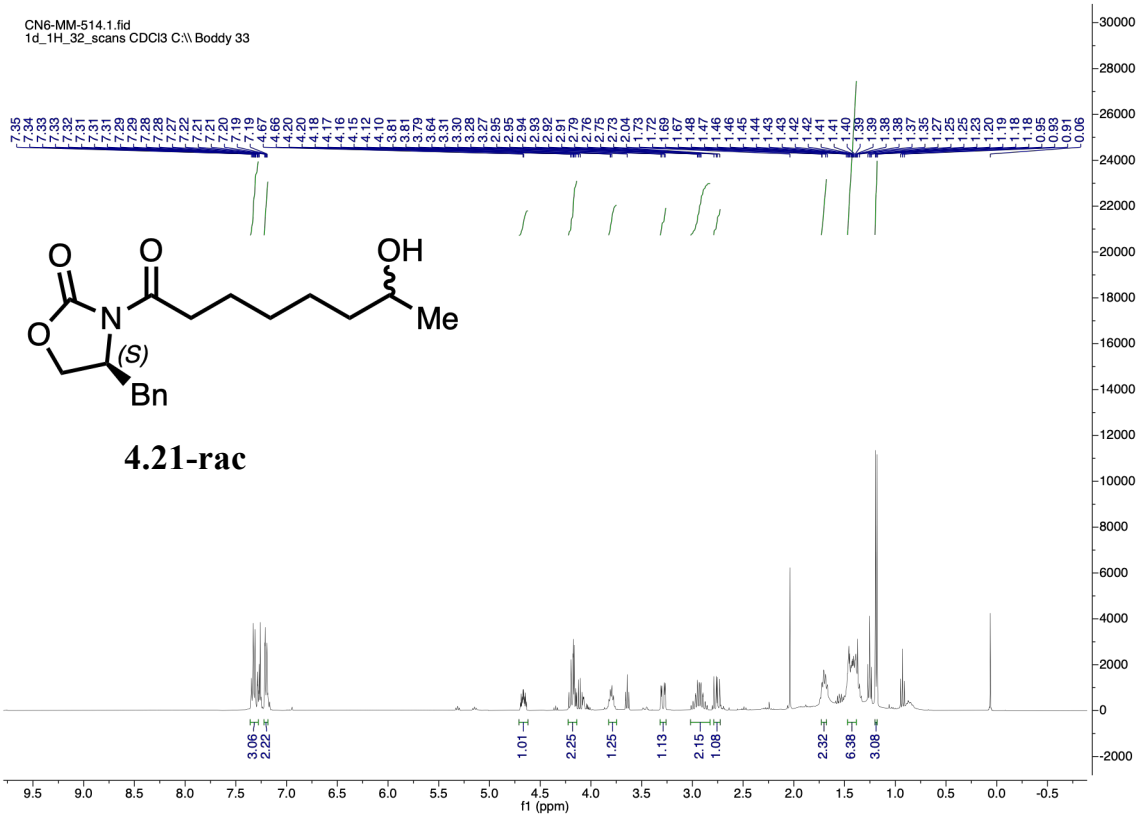


B

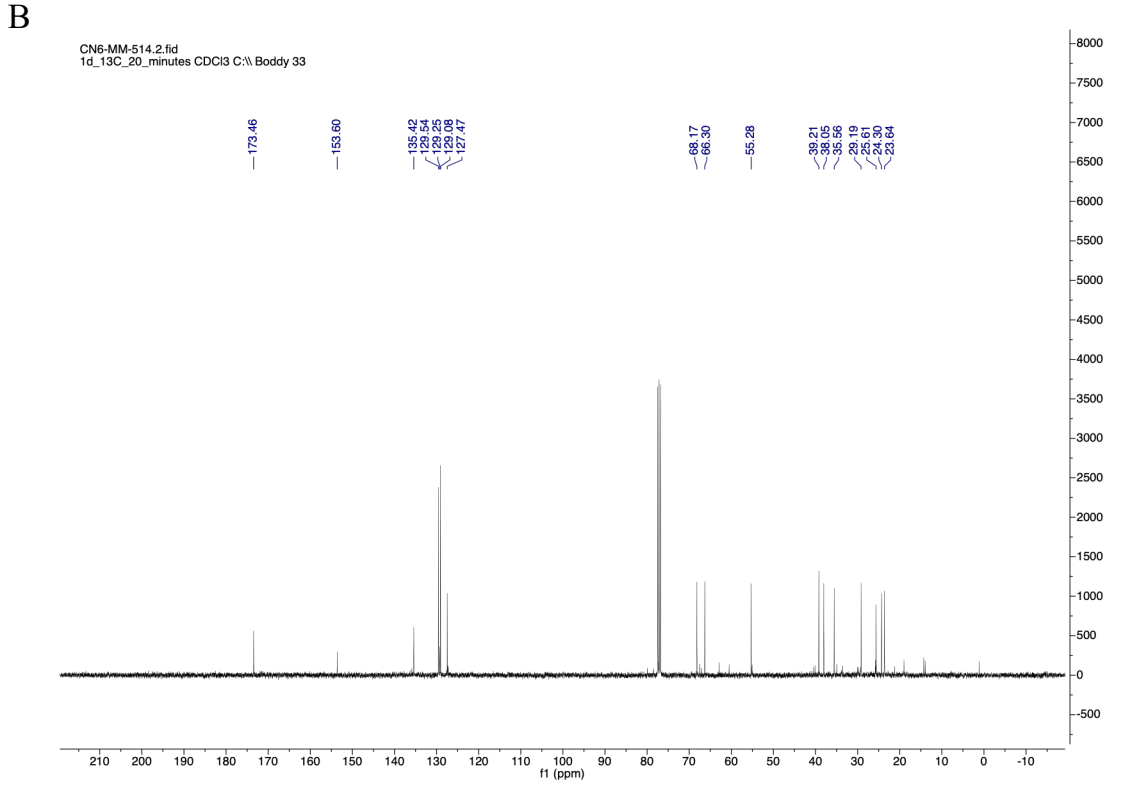


Spectra 4.13 of compound **4.21-(R)-MTPA ester** (A) ^{1}H NMR (600 MHz, $CDCl_3$) and (B) ^{13}C NMR (101 MHz, $CDCl_3$)

A

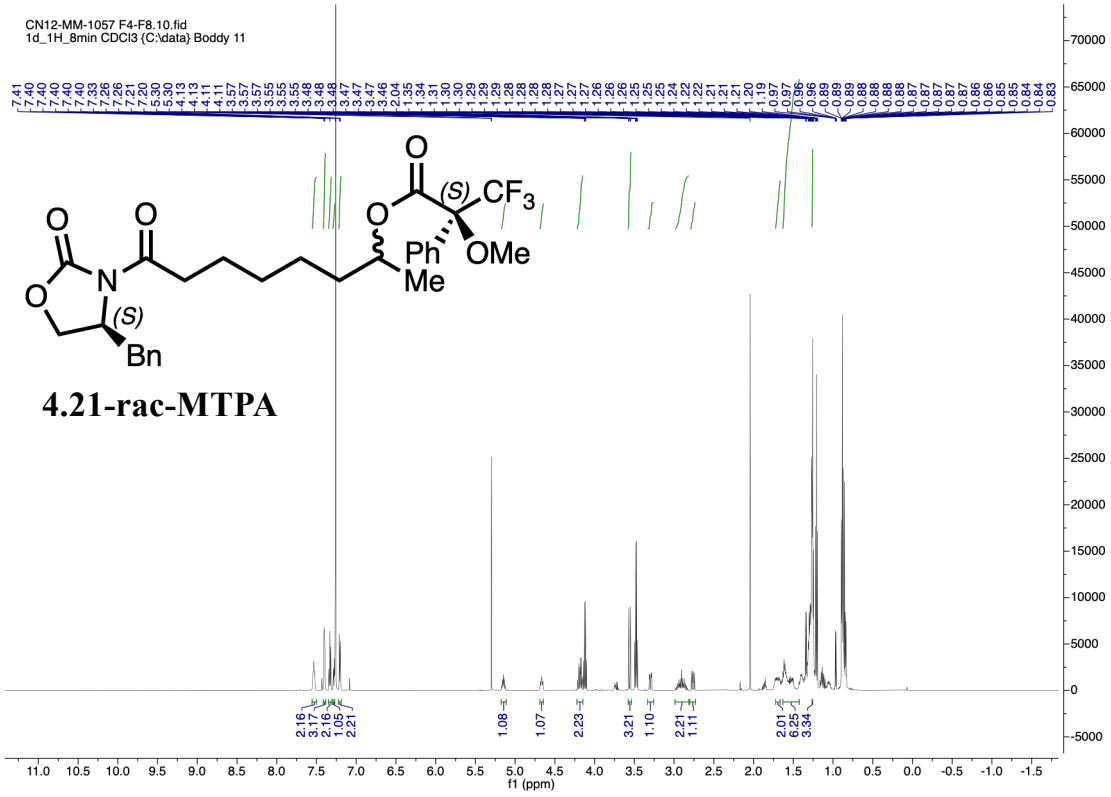


B

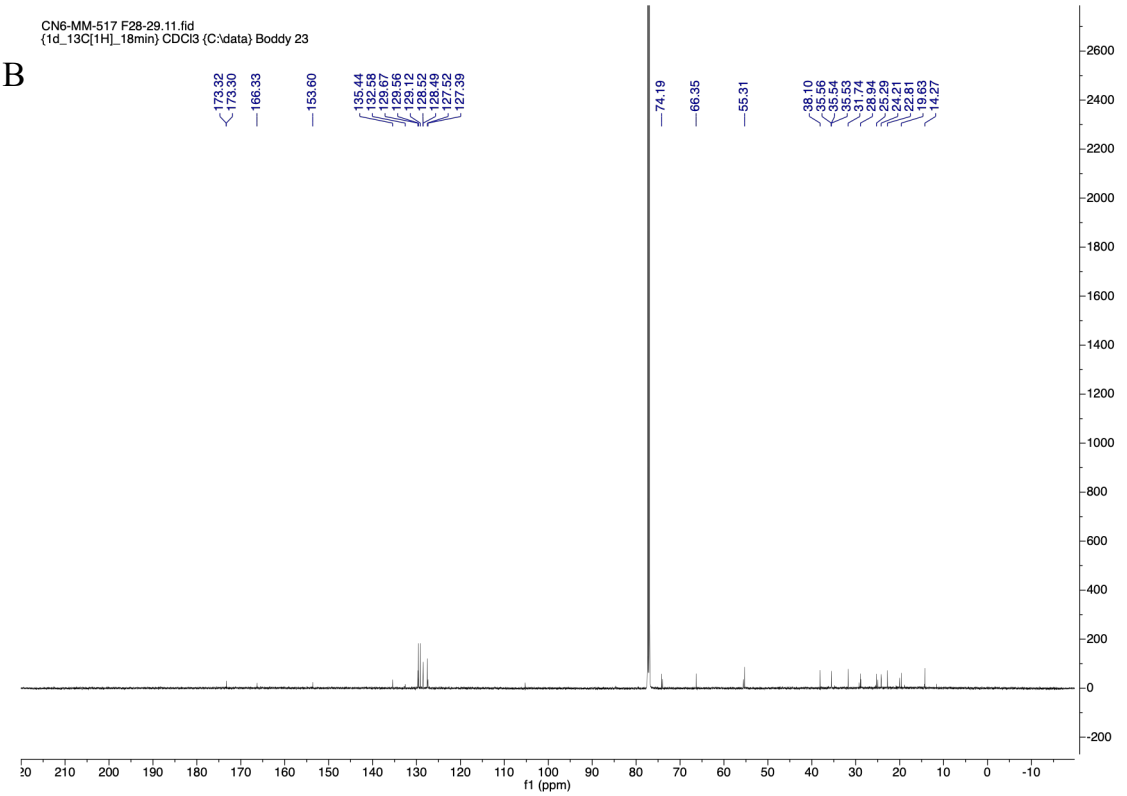


Spectra 4.14 of compound **4.21-rac** (A) ^{1}H NMR (400 MHz, $CDCl_3$) and (B) ^{13}C NMR (101 MHz, $CDCl_3$)

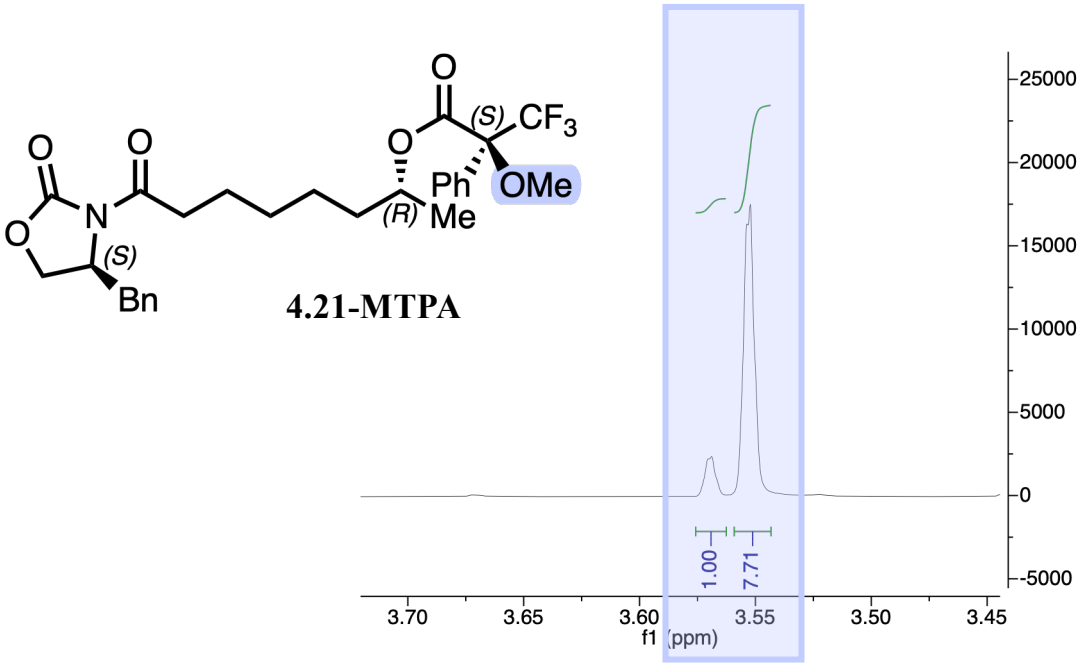
A



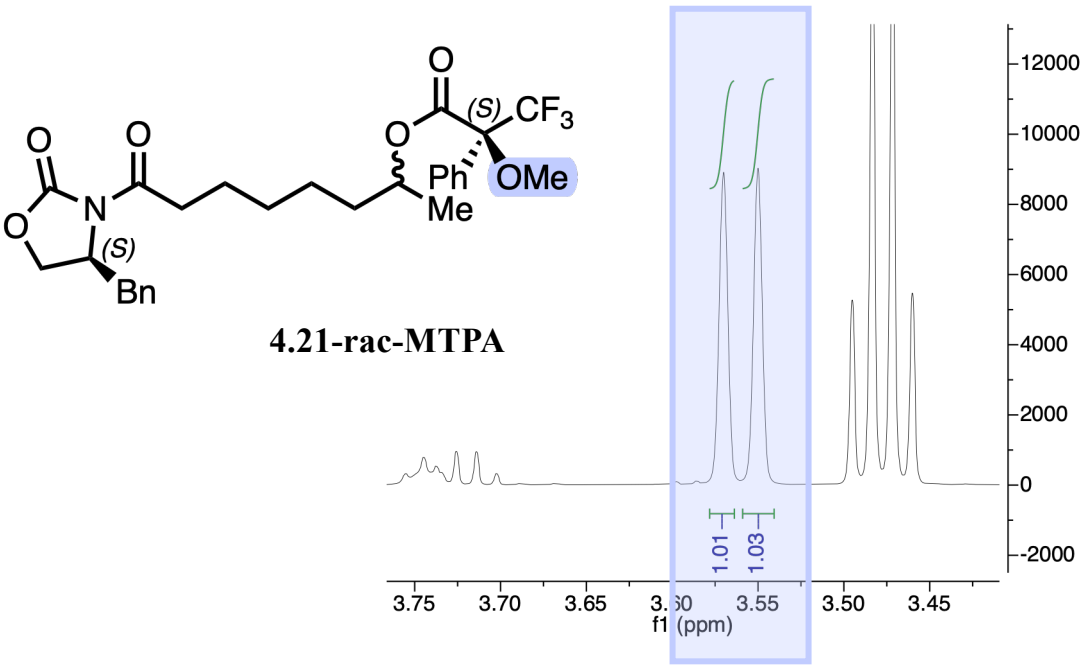
B



Spectra 4.15 of compound **4.21-rac-MTPA**(A) ^{1}H NMR (600 MHz, $CDCl_3$) and (B) ^{13}C NMR (101 MHz, $CDCl_3$)

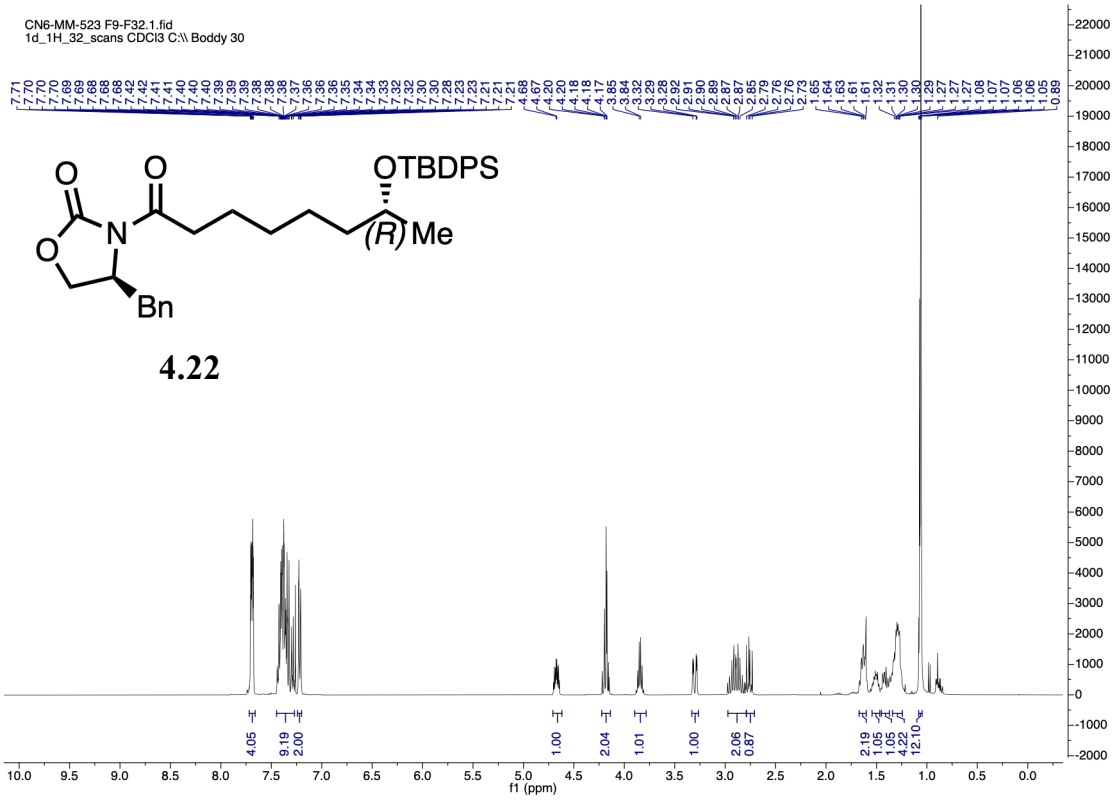


Spectra 4.16 of compound **4.21-MTPA** (A) ^{1}H NMR (600 MHz, $CDCl_3$) expanded in 3.45-3.70ppm region to show diastereomeric ration of C5 from integration of Mosher (-OMe) substitutent

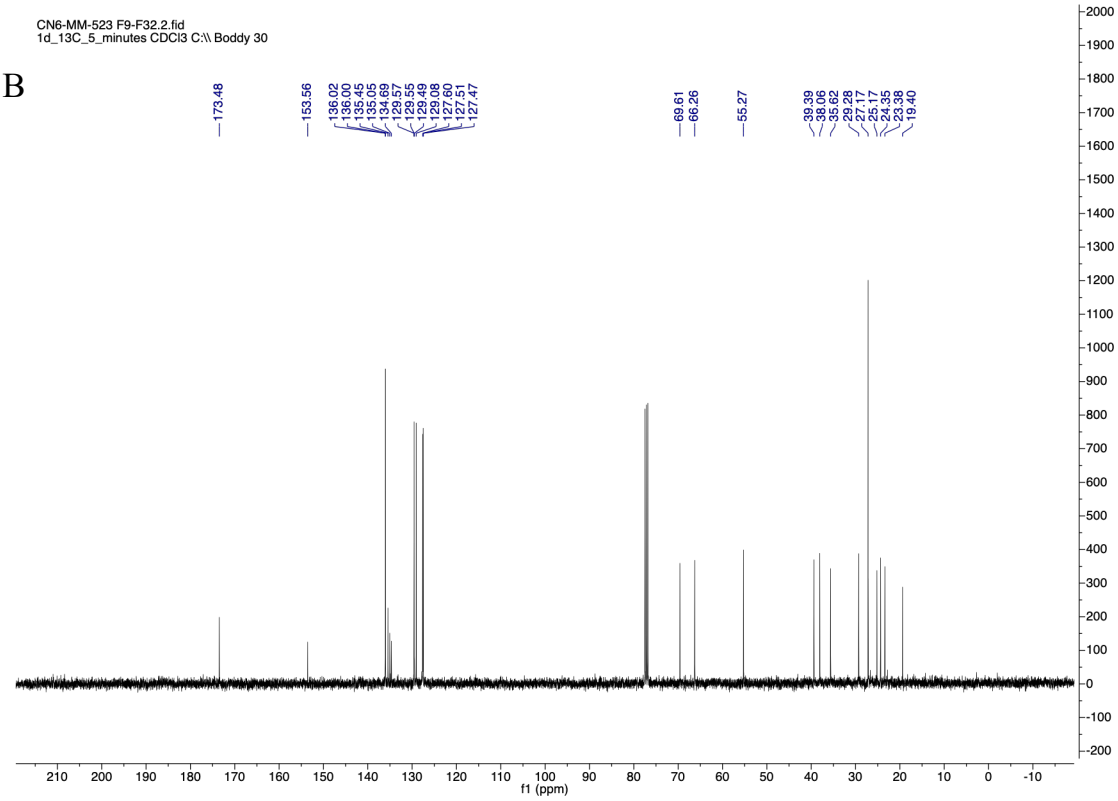


Spectra 4.17 of compound **4.21-rac-MTPA** (A) ^{1}H NMR (600 MHz, $CDCl_3$) expanded in 3.45-3.70ppm region to show diastereomeric ration of C5 from integration of Mosher (-OMe) substitutent

A

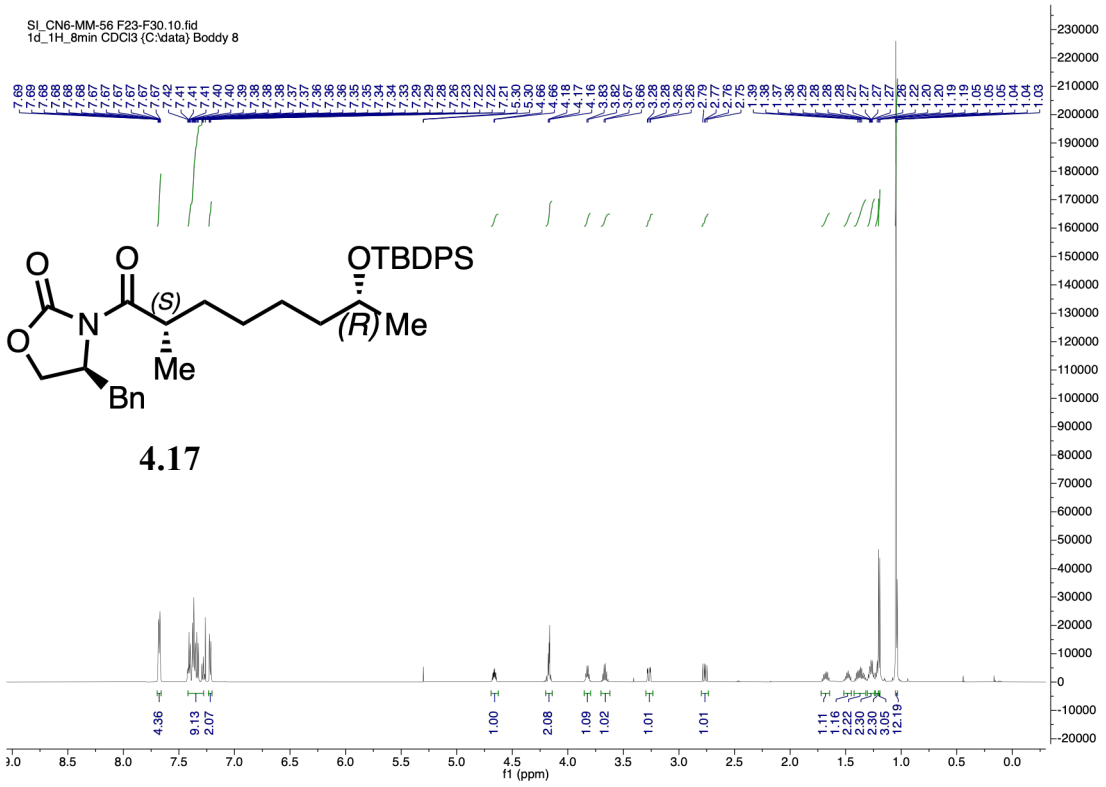


B

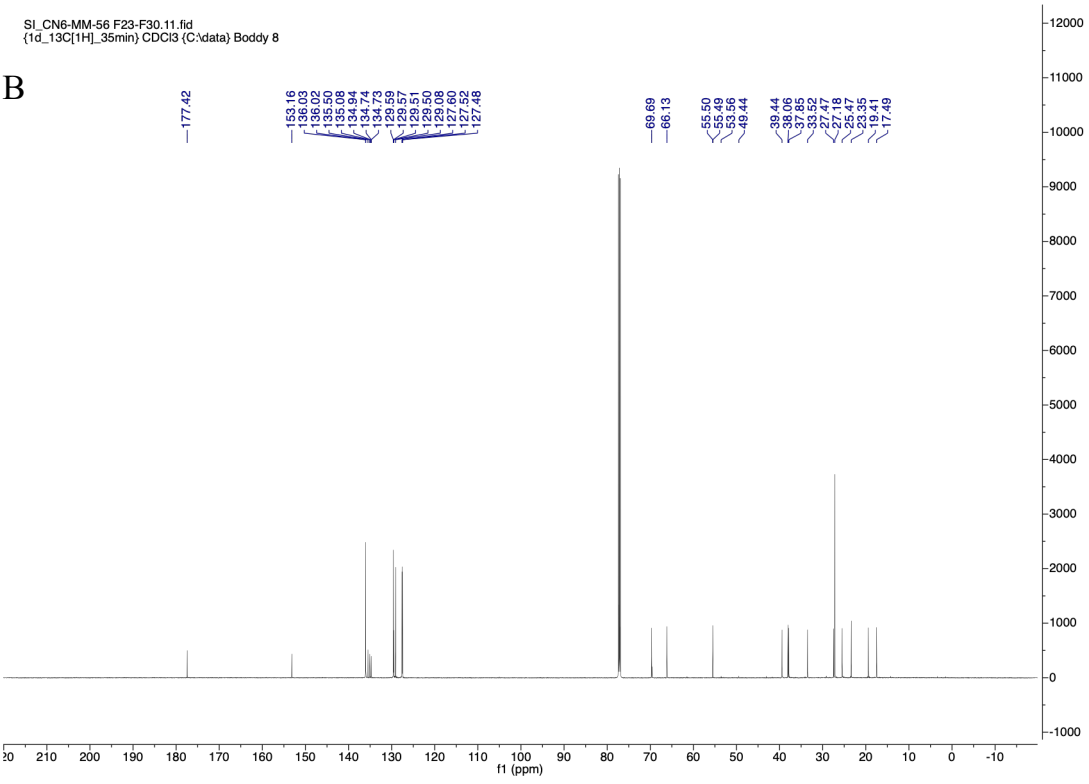


Spectra 4.18 of compound **4.22** (A) ^{1}H NMR (400 MHz, $CDCl_3$) and (B) ^{13}C NMR (101 MHz, $CDCl_3$)

A

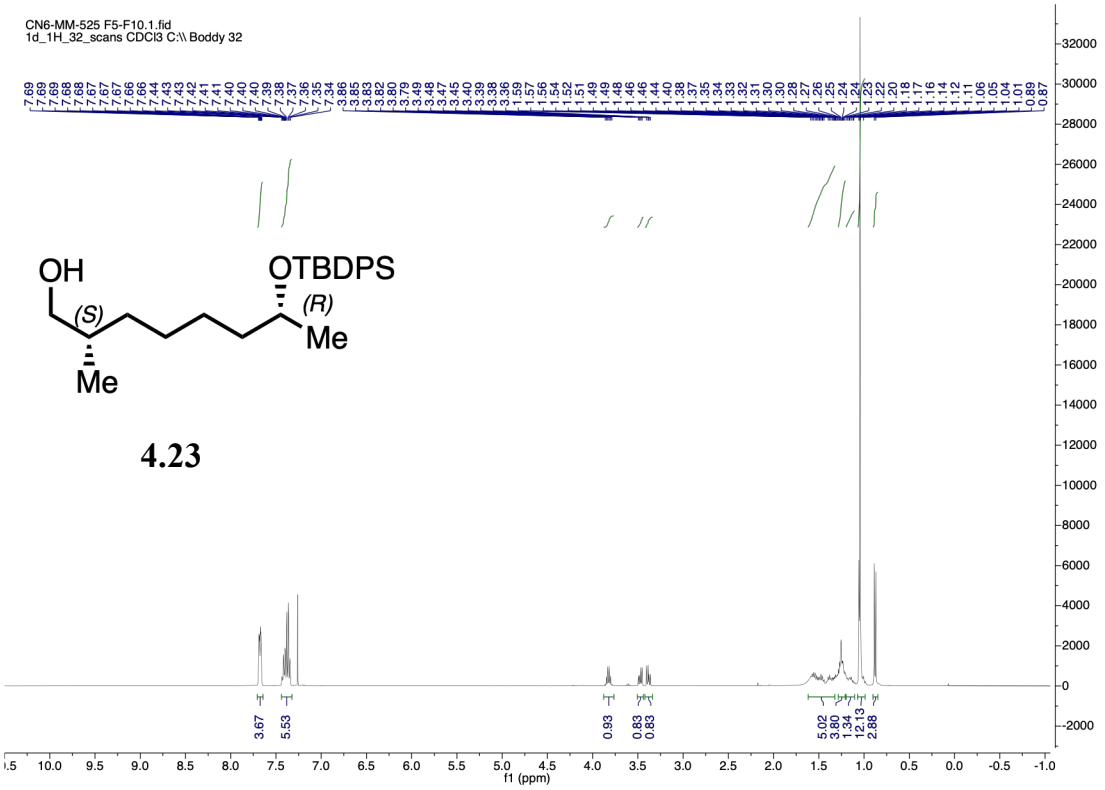


B

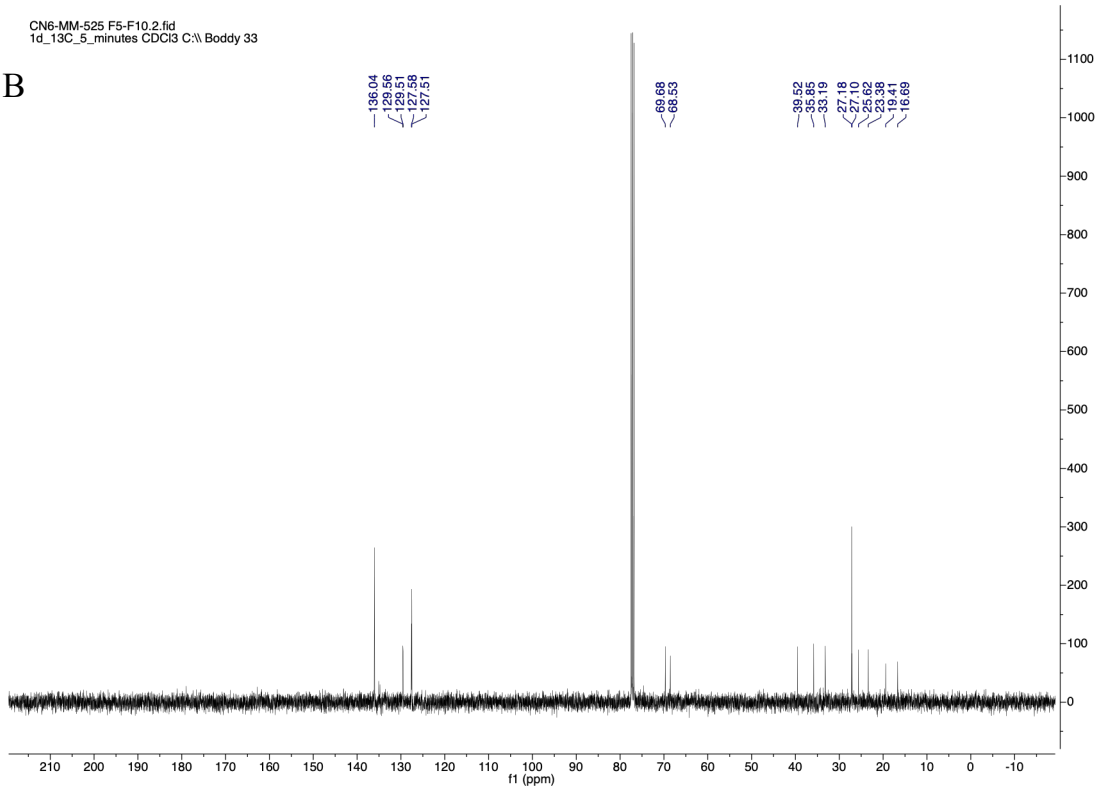


Spectra 4.19 of compound **4.17** (A) ^{1}H NMR (600 MHz, $CDCl_3$) and (B) ^{13}C NMR (101 MHz, $CDCl_3$)

A

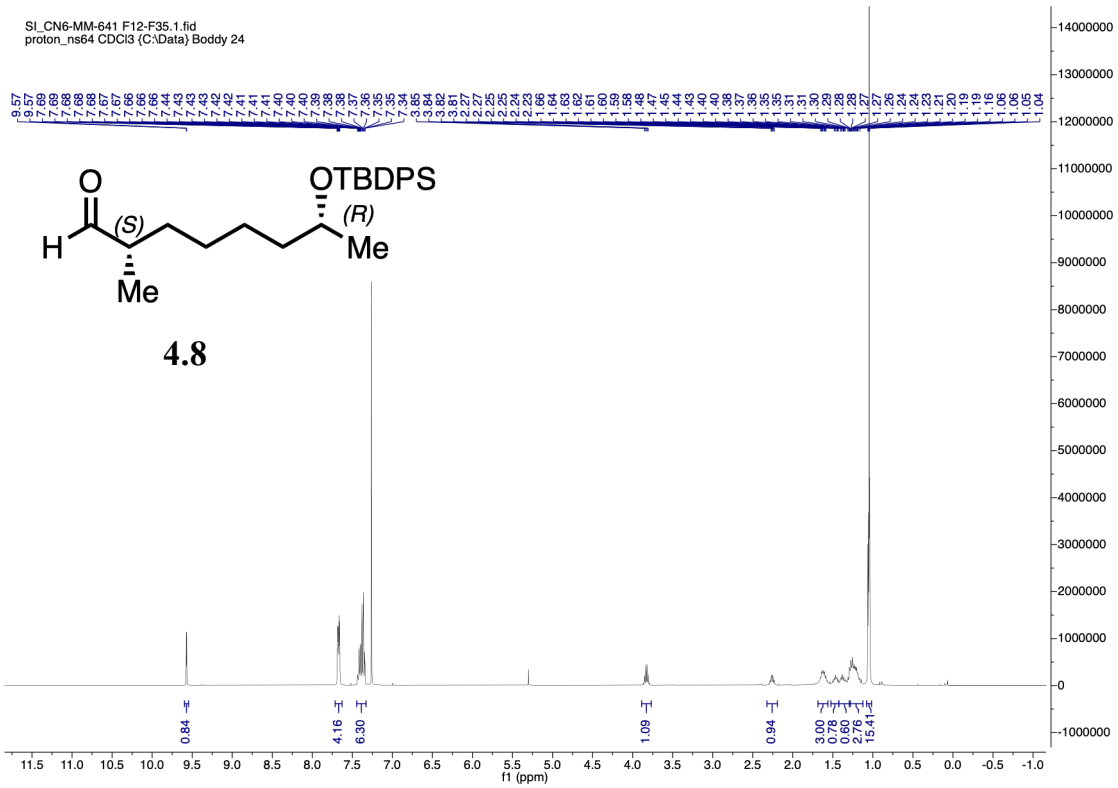


B

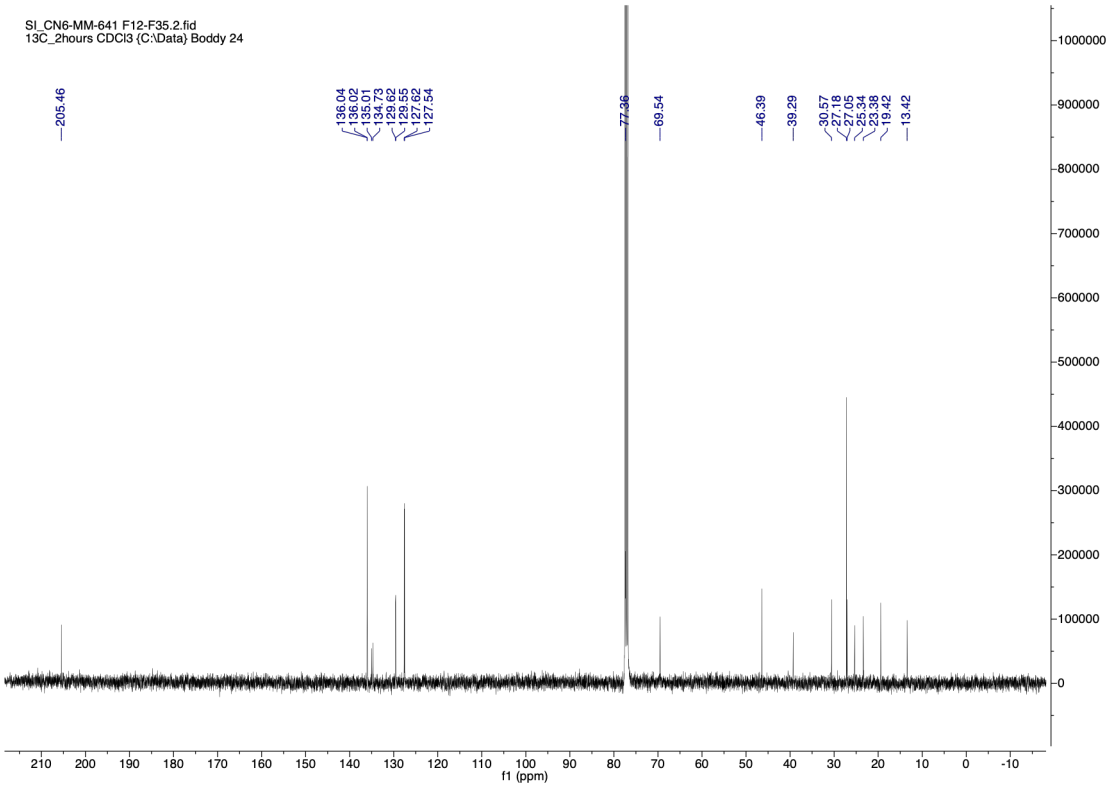


Spectra 4.20 of compound **4.23** (A) ^{1}H NMR (600 MHz, $CDCl_3$) and (B) ^{13}C NMR (101 MHz, $CDCl_3$)

A

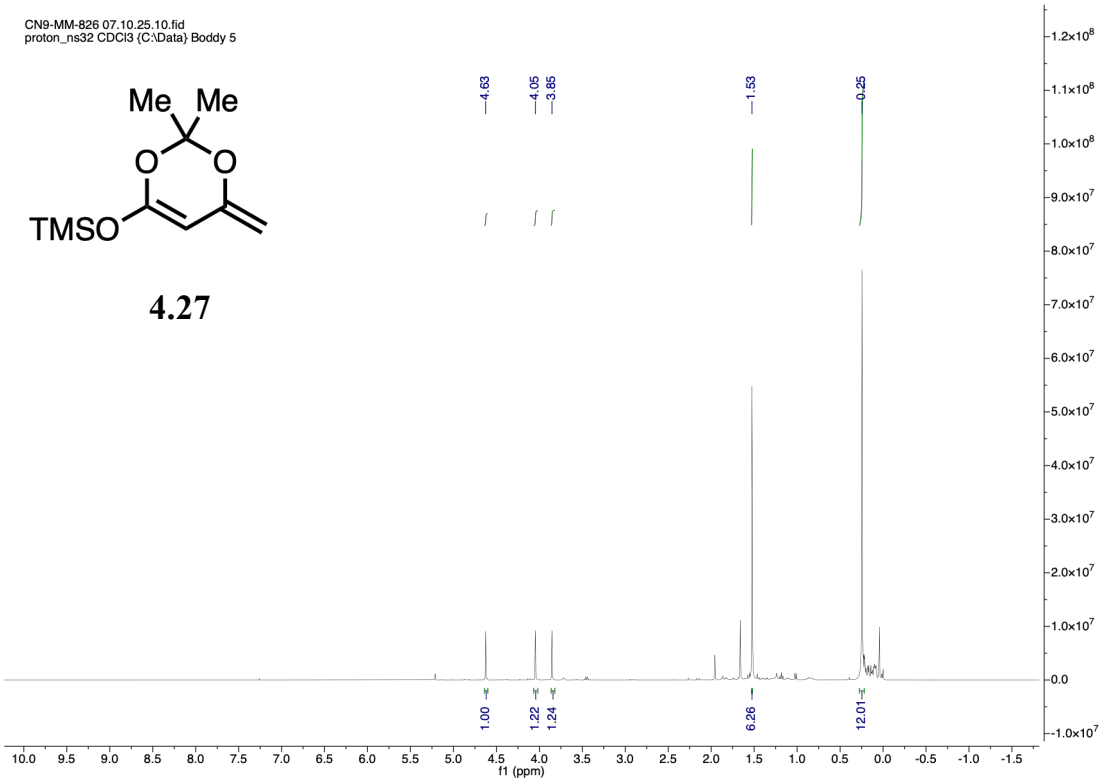


B

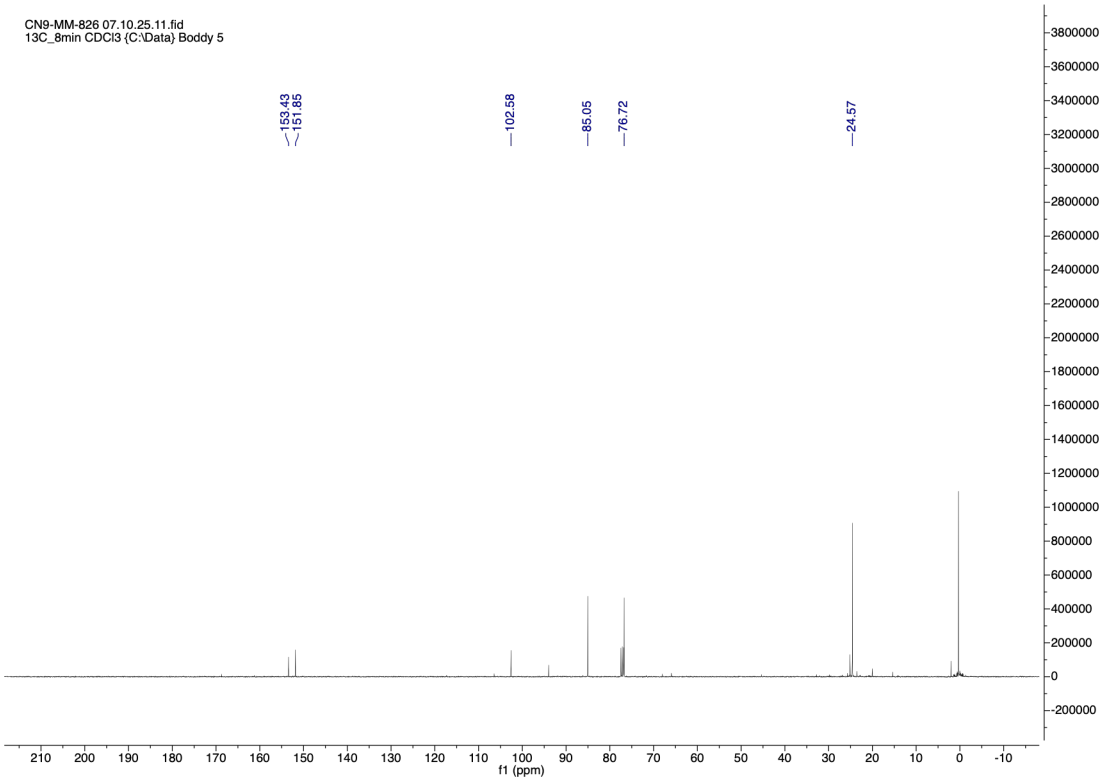


Spectra 4.21 of compound **4.8** (A) ^{1}H NMR (600 MHz, $CDCl_3$) and (B) ^{13}C NMR (101 MHz, $CDCl_3$)

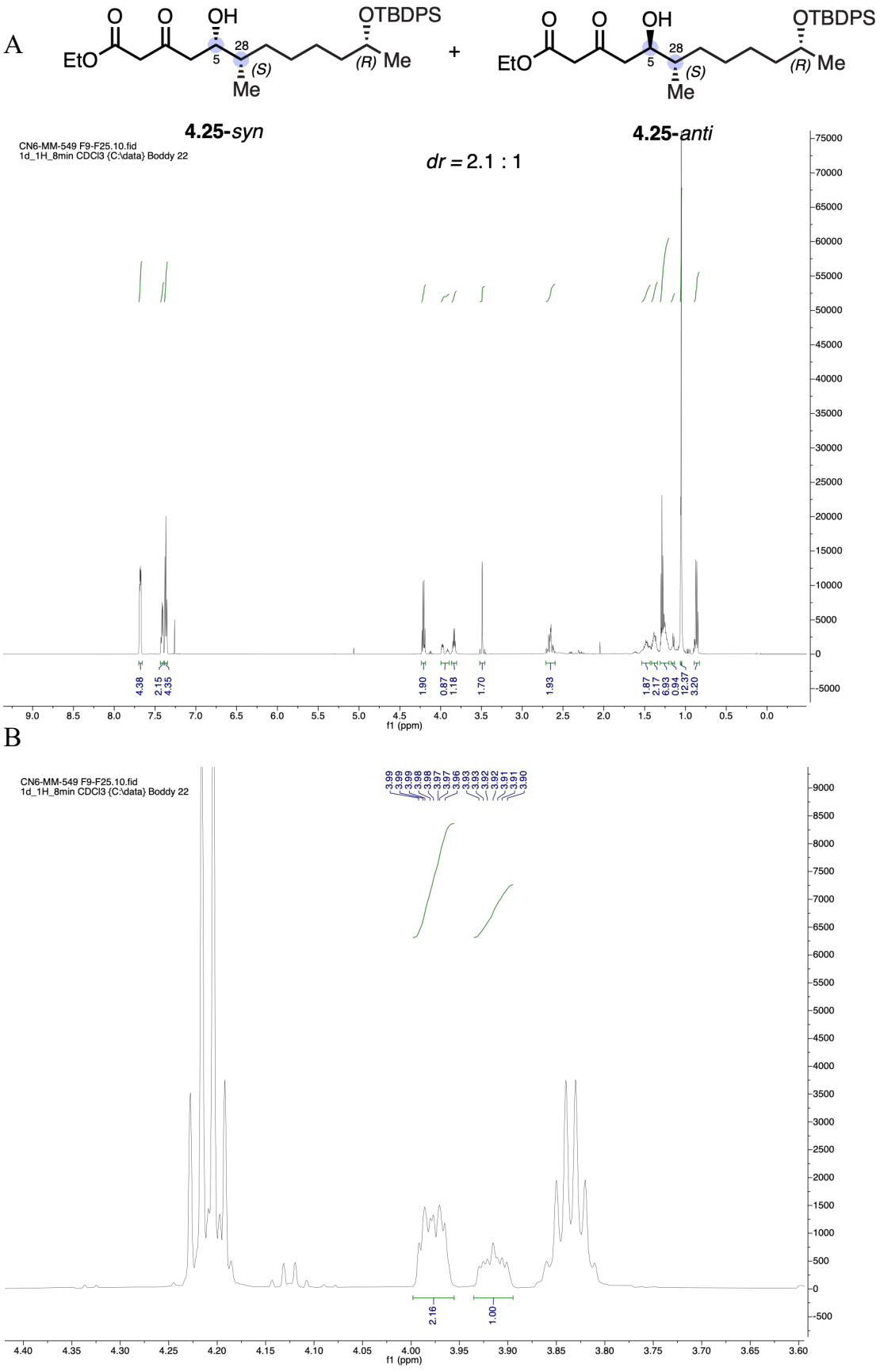
A



B

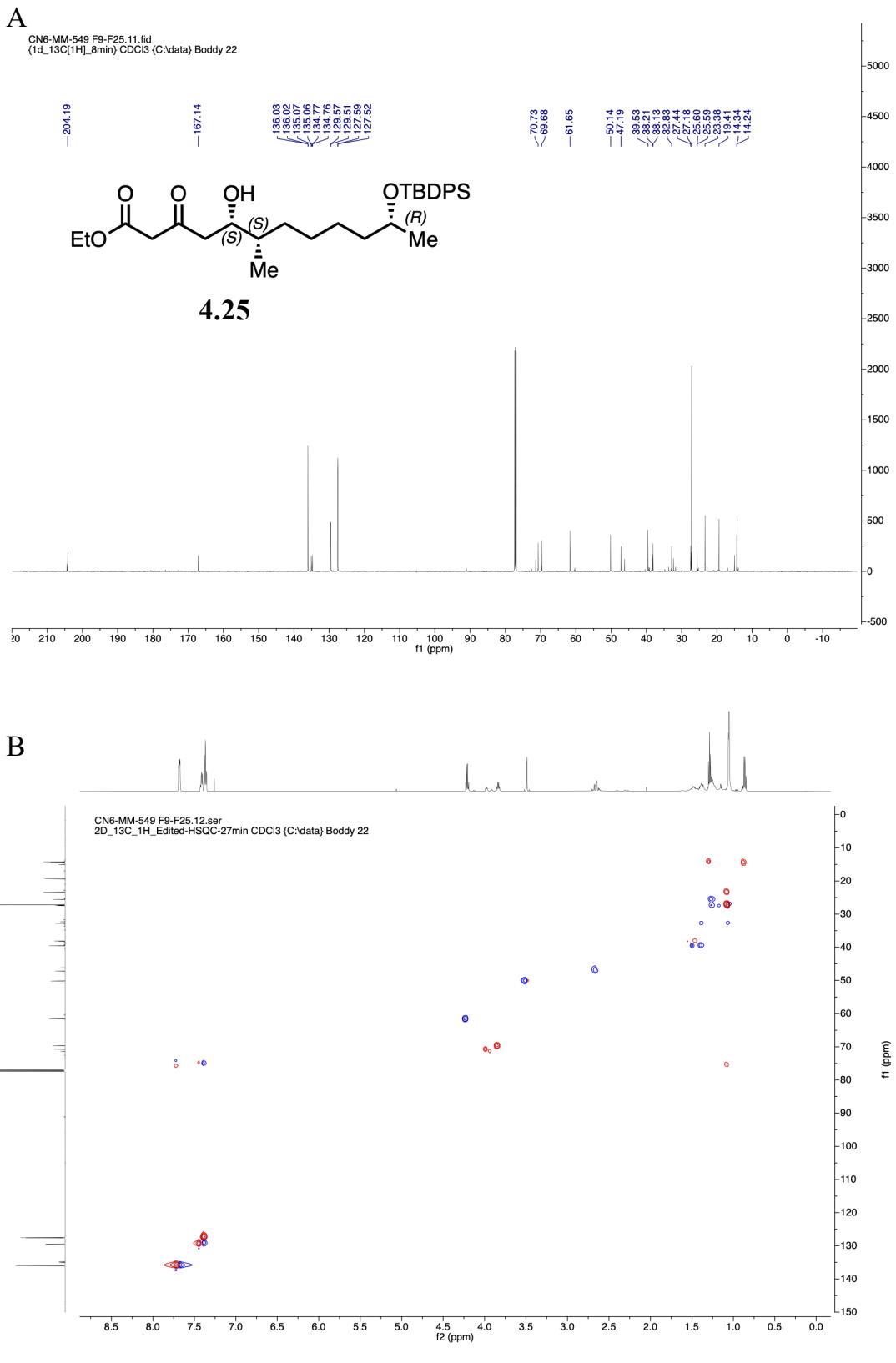


Spectra 4.22 of compound **4.27** (A) ^{1}H NMR (600 MHz, $CDCl_3$) and (B) ^{13}C NMR (101 MHz, $CDCl_3$)



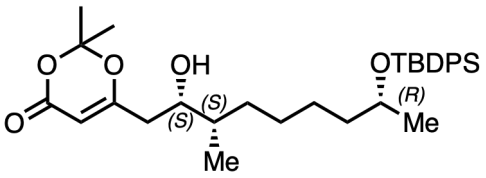
Spectra 4.23 of compound **4.25** mixture of diastereomers (A) ^{1}H NMR (600 MHz, $CDCl_3$) and (B) ^{1}H NMR (600 MHz, $CDCl_3$) of expanded C5 proton signal, integrated to determine diastereomeric ratio.

A

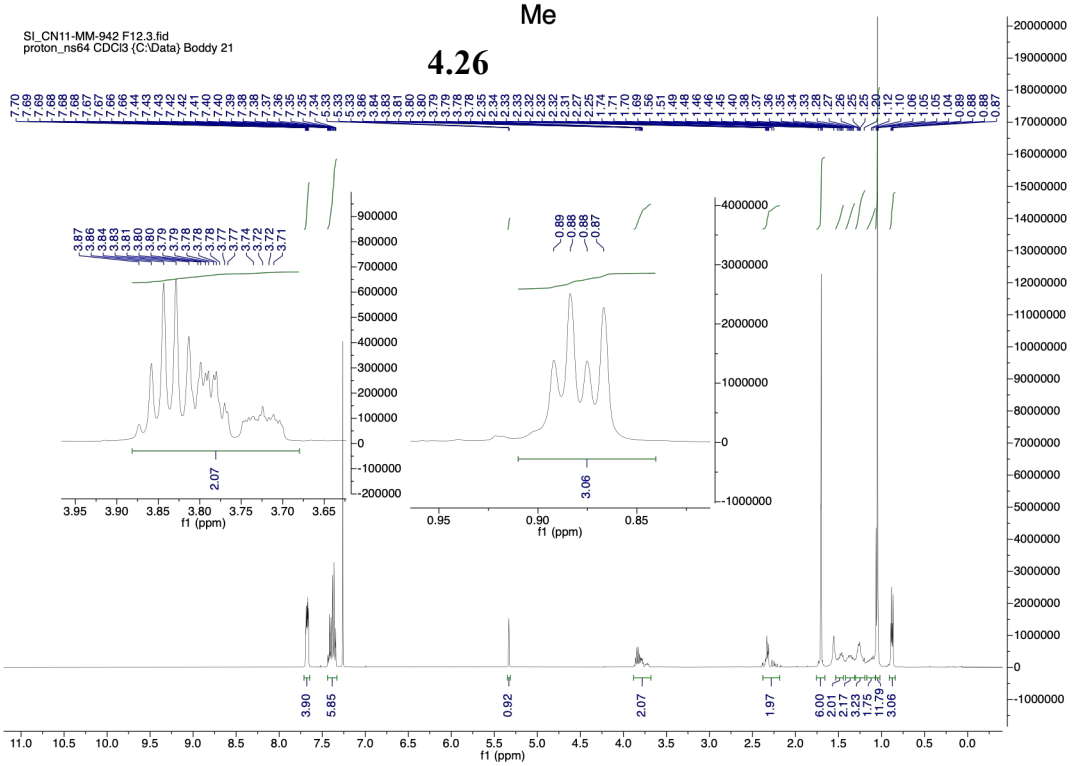


Spectra 4.24 of compound **4.25** as diastereomeric mixture (2.2:1, **4.25**-*syn* : **4.25**-*anti*) (A) ^{1}H NMR (600 MHz, $CDCl_3$) and (B) ^{13}C NMR (101 MHz, $CDCl_3$)

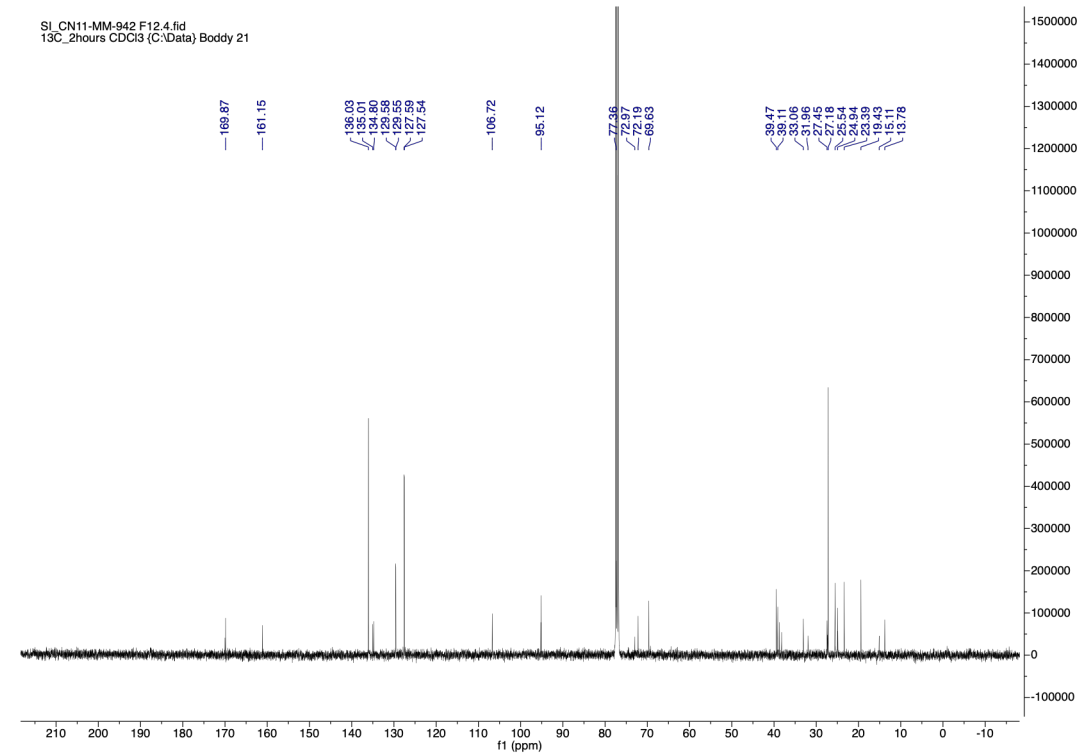
A



4.26



B

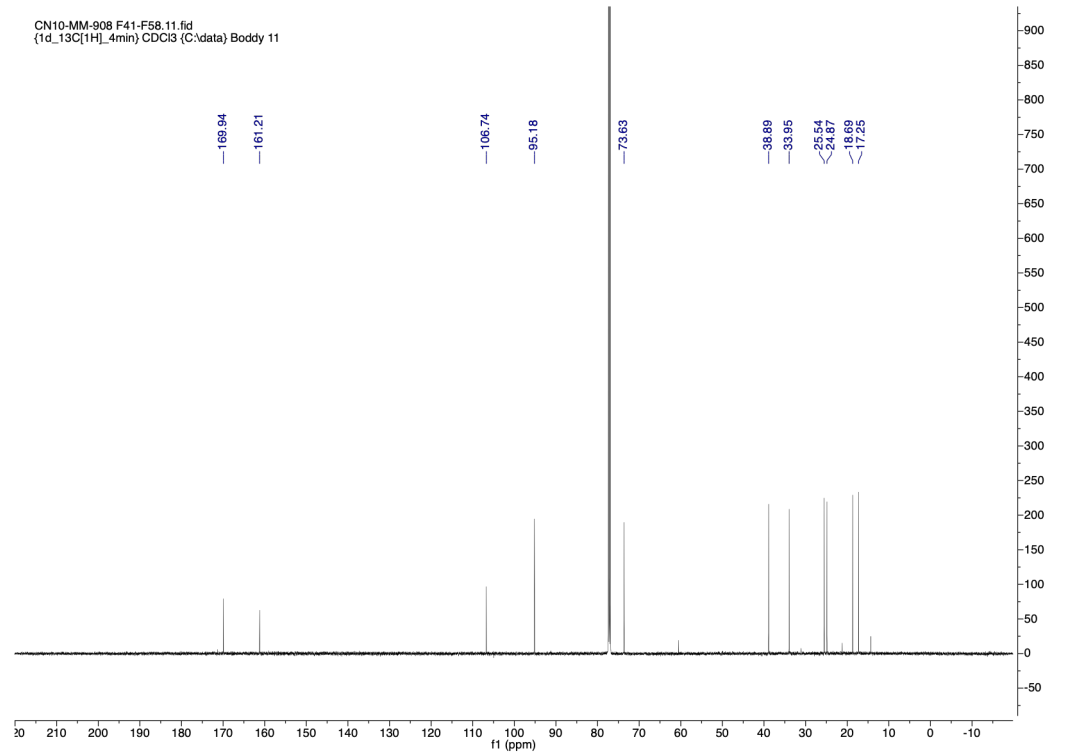


Spectra 4.25 of compound **4.26** as a 2:1 diasteromeric mixture (2:1, **4.26**-*syn* : **4.26**-*anti*) (A) ^{1}H NMR (600 MHz, $CDCl_3$) and (B) ^{13}C NMR (600 MHz, $CDCl_3$)

A

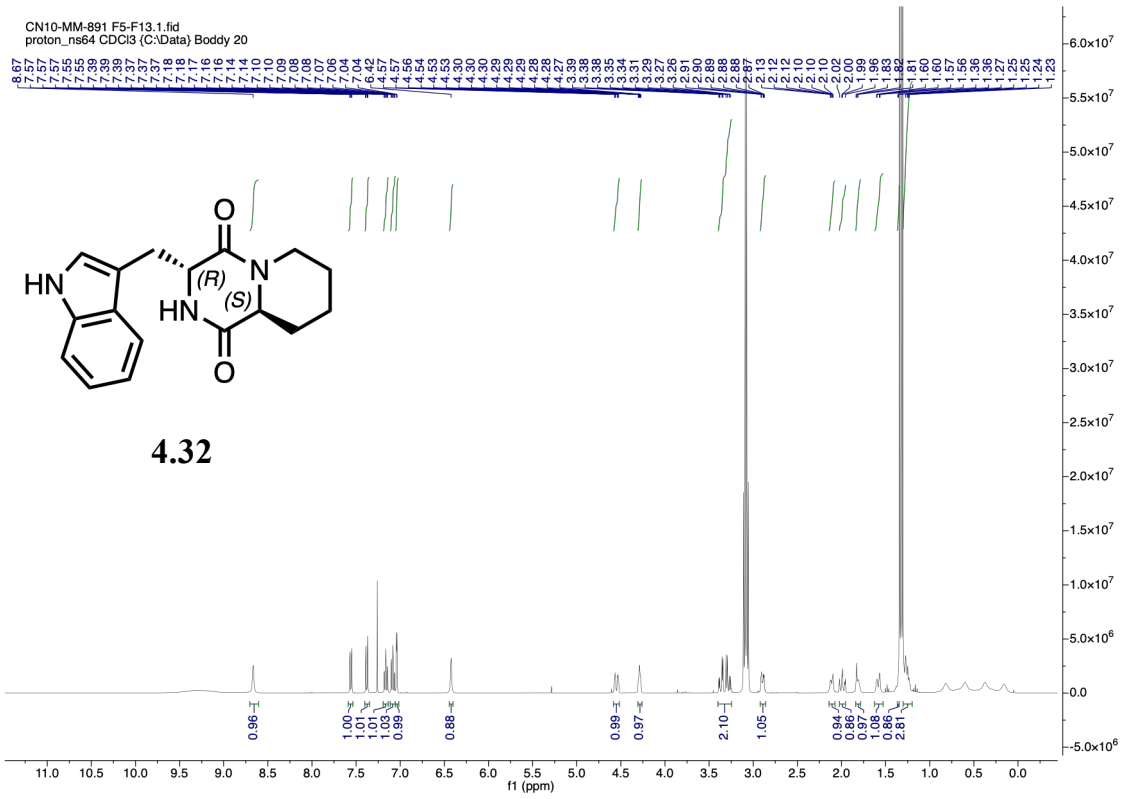


B

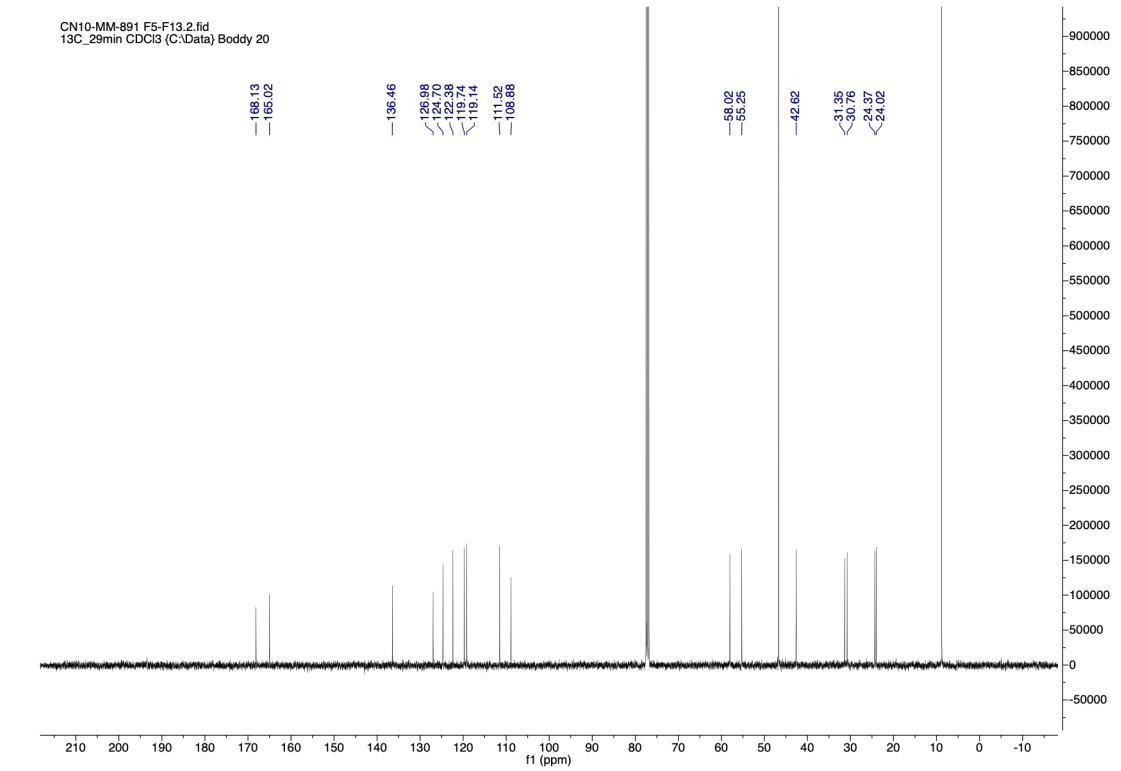


Spectra 4.26 of compound **4.27** (A) ^{1}H NMR (600 MHz, $CDCl_3$) and (B) ^{13}C NMR (600 MHz, $CDCl_3$)

A

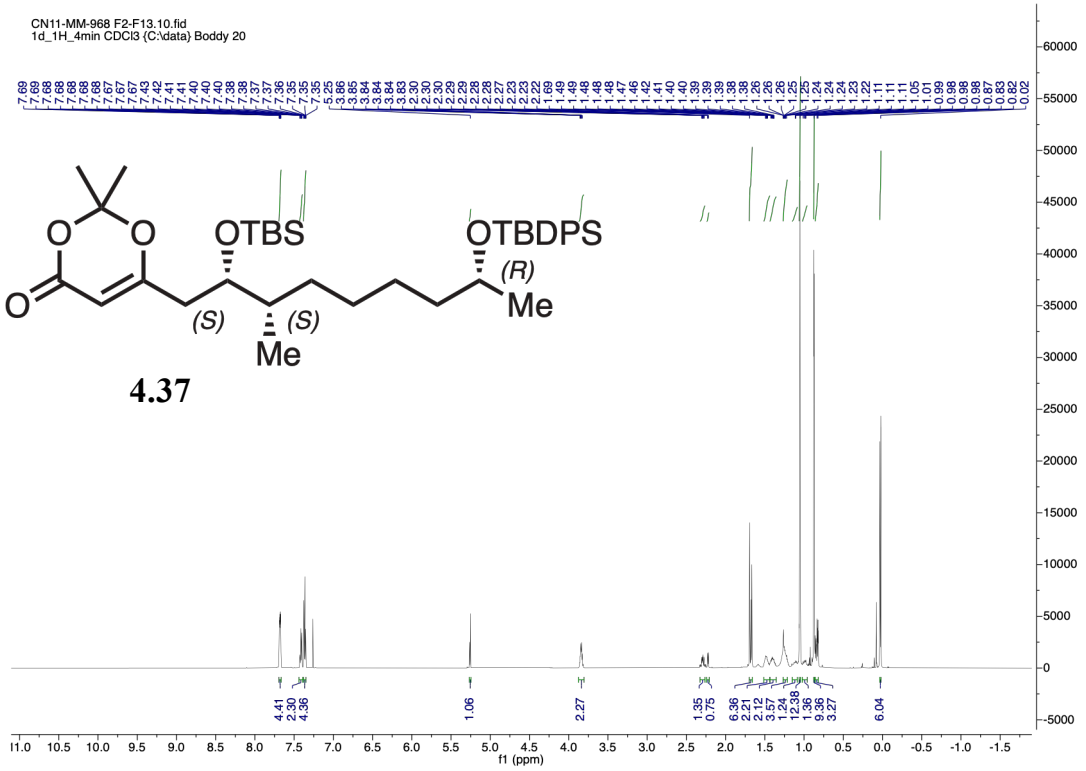


B

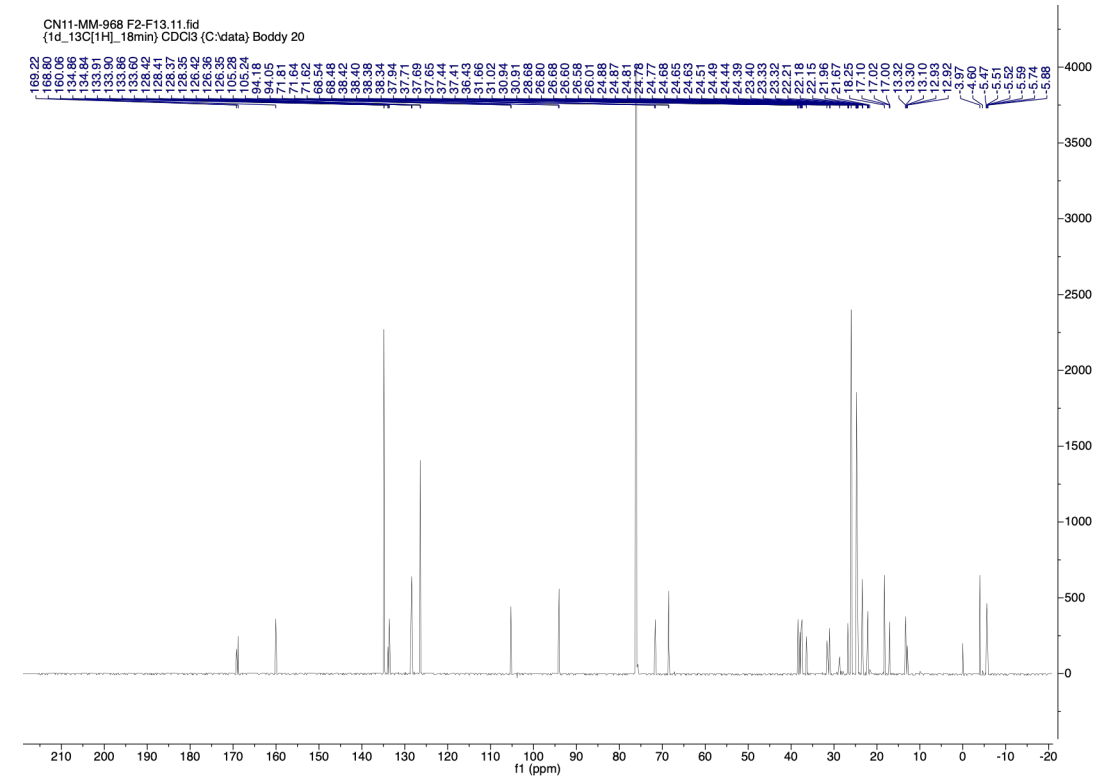


Spectra 4.27 of compound **4.32** (A) ^{1}H NMR (400 MHz, $CDCl_3$) and (B) ^{13}C NMR (101 MHz, $CDCl_3$). Unidentified peaks correspond to triethylamine impurity.

A

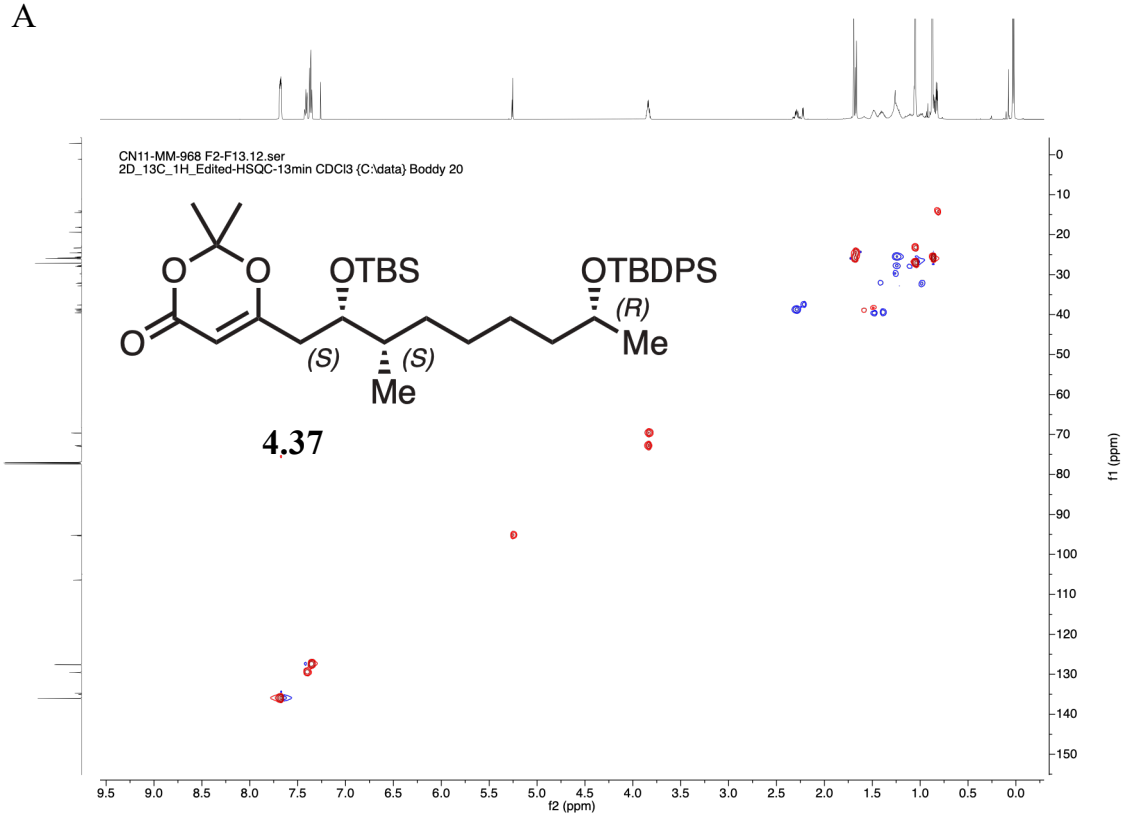


B

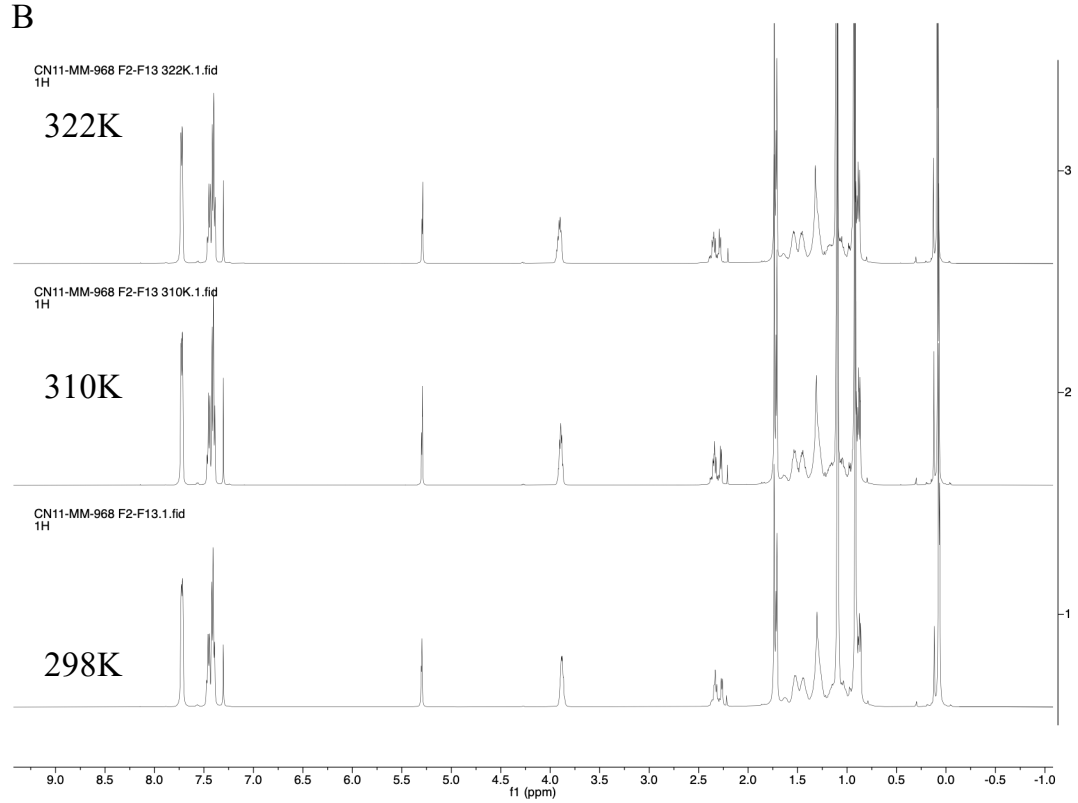


Spectra 4.28 of compound **4.37** (A) ^{1}H NMR (600 MHz, $CDCl_3$) and (B) ^{13}C NMR (101 MHz, $CDCl_3$)

A

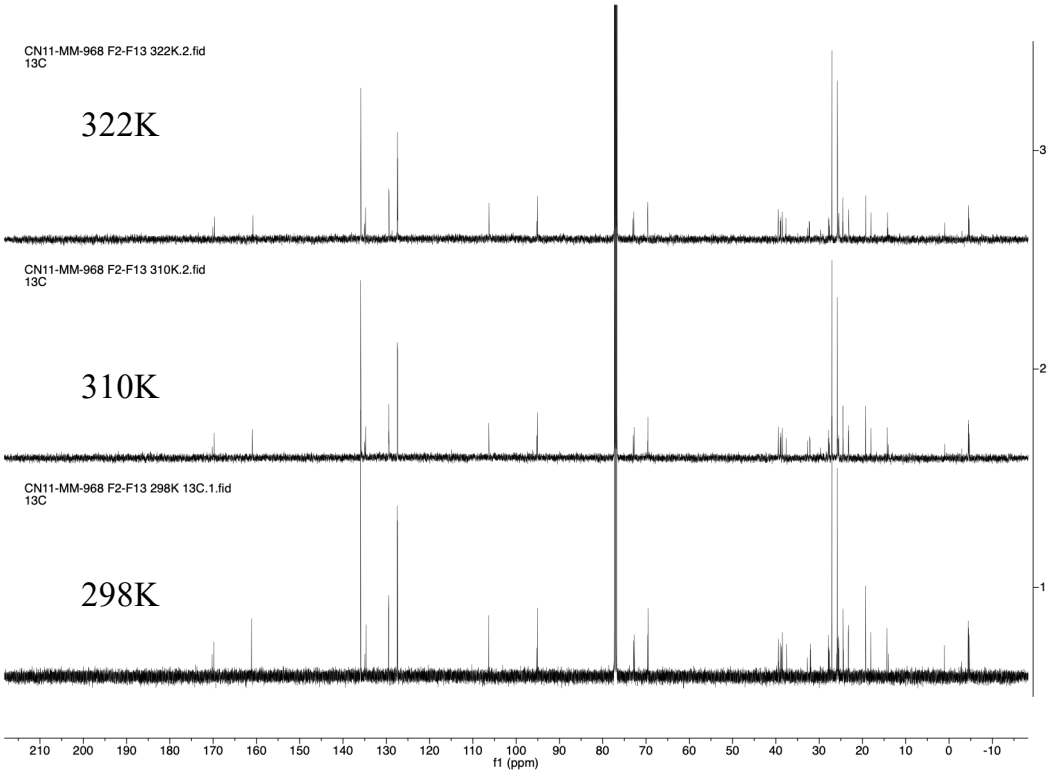


B

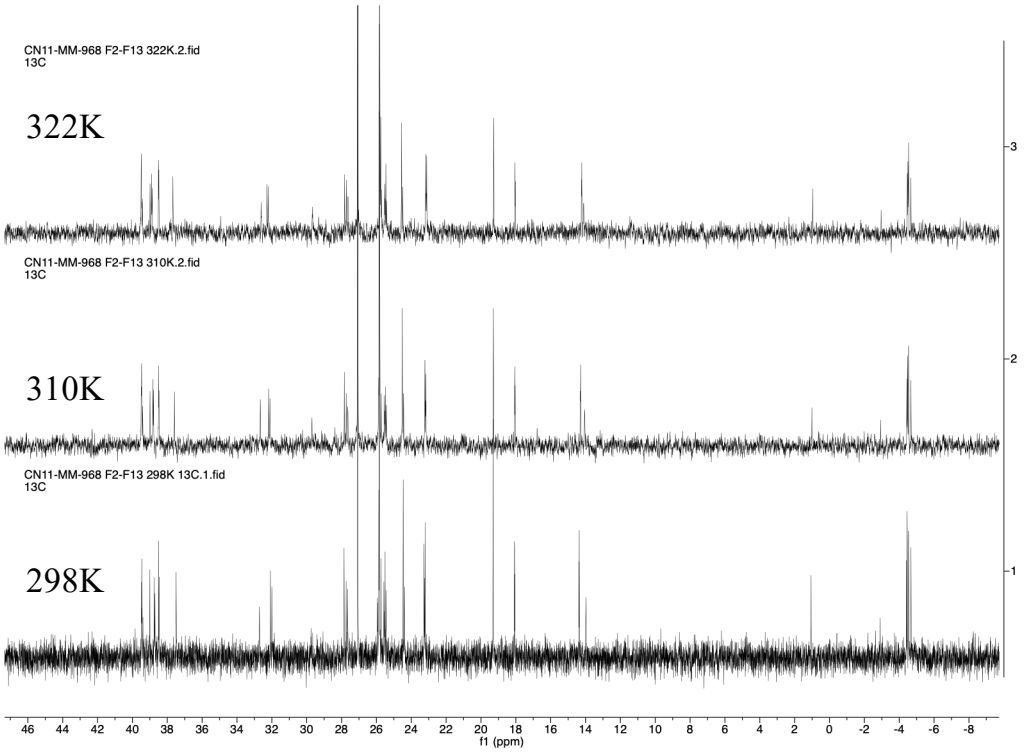


Spectra 4.29 of compound **4.37** (A) HSQC and (B) (A) VT NMR ^{1}H NMR (500 MHz, $CDCl_3$) recorded at 298K, 310K and 322K.

A

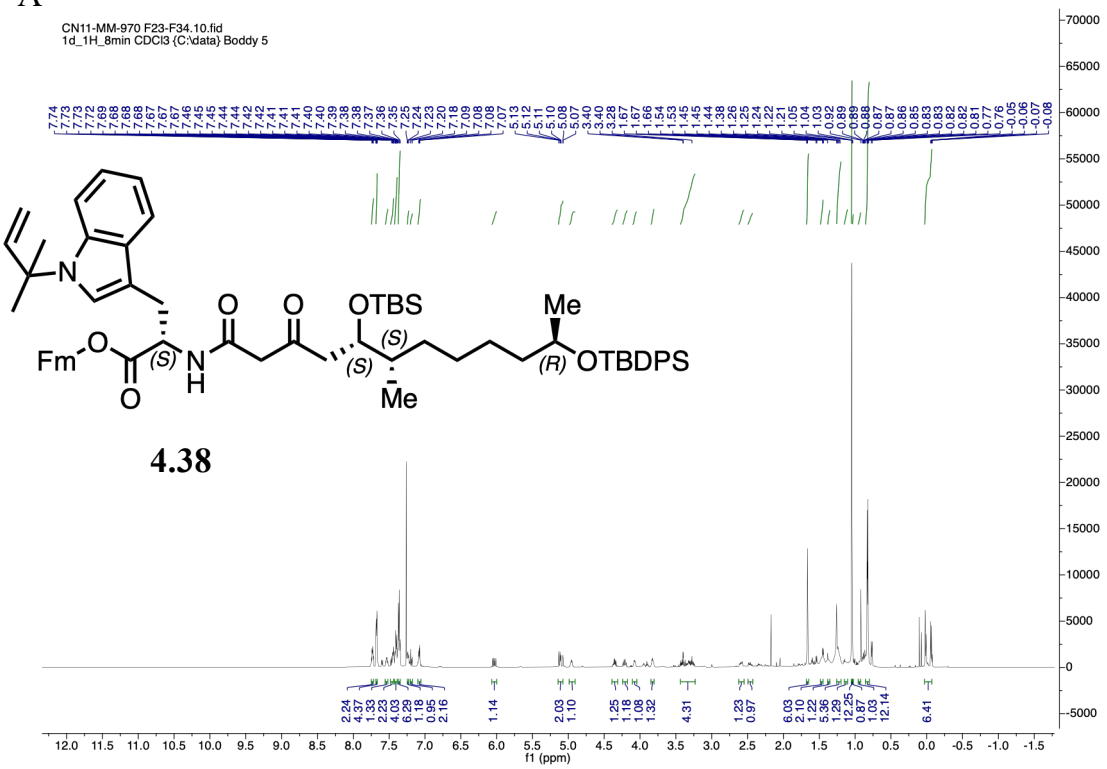


B



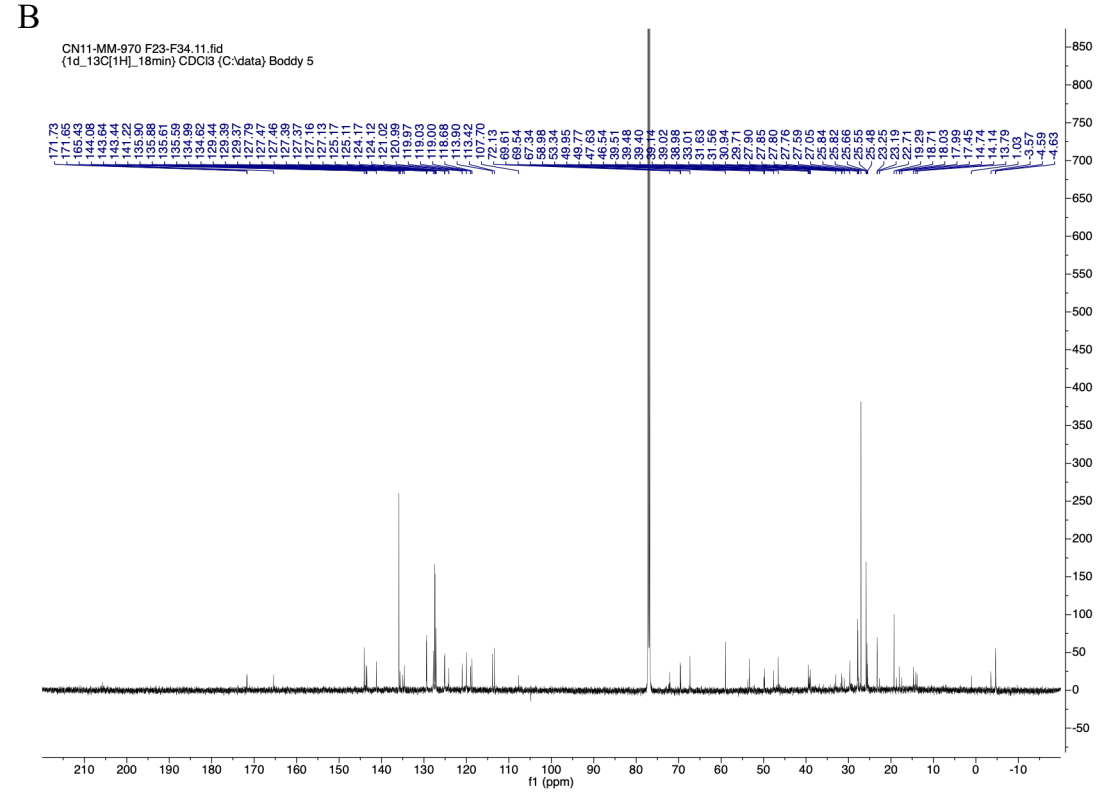
Spectra 4.30 of compound **4.37** (A) VT NMR ^{13}C NMR (101 MHz, $CDCl_3$) recorded at 298K, 310K and 322K. (B) Expanded VT ^{13}C NMR (101 MHz, $CDCl_3$) Spectra -8ppm to 46ppm

A



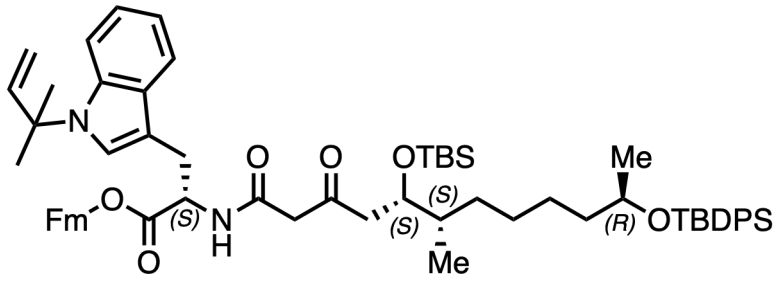
4.38

B

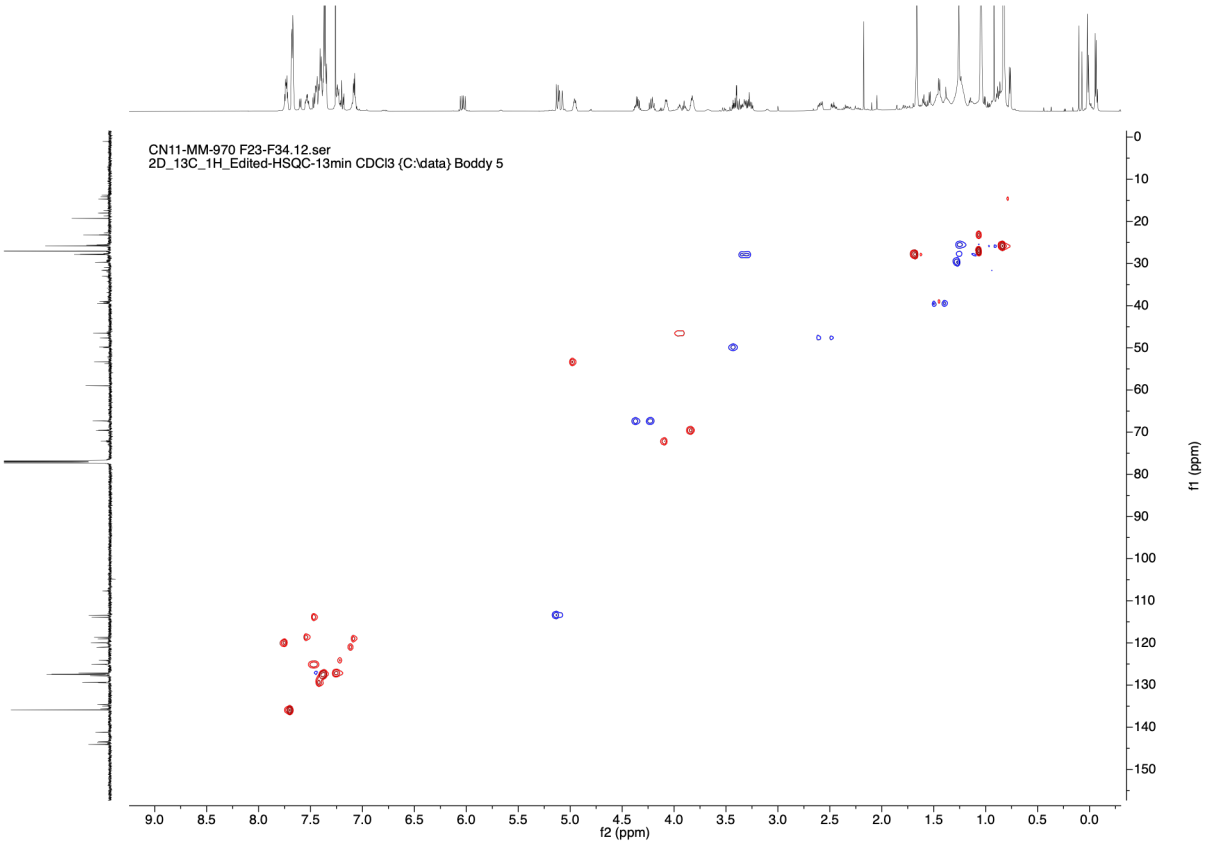


Spectra 4.31 of compound **4.38** (A) ^{1}H NMR (600 MHz, $CDCl_3$) and (B) ^{13}C NMR (101 MHz, $CDCl_3$)

A

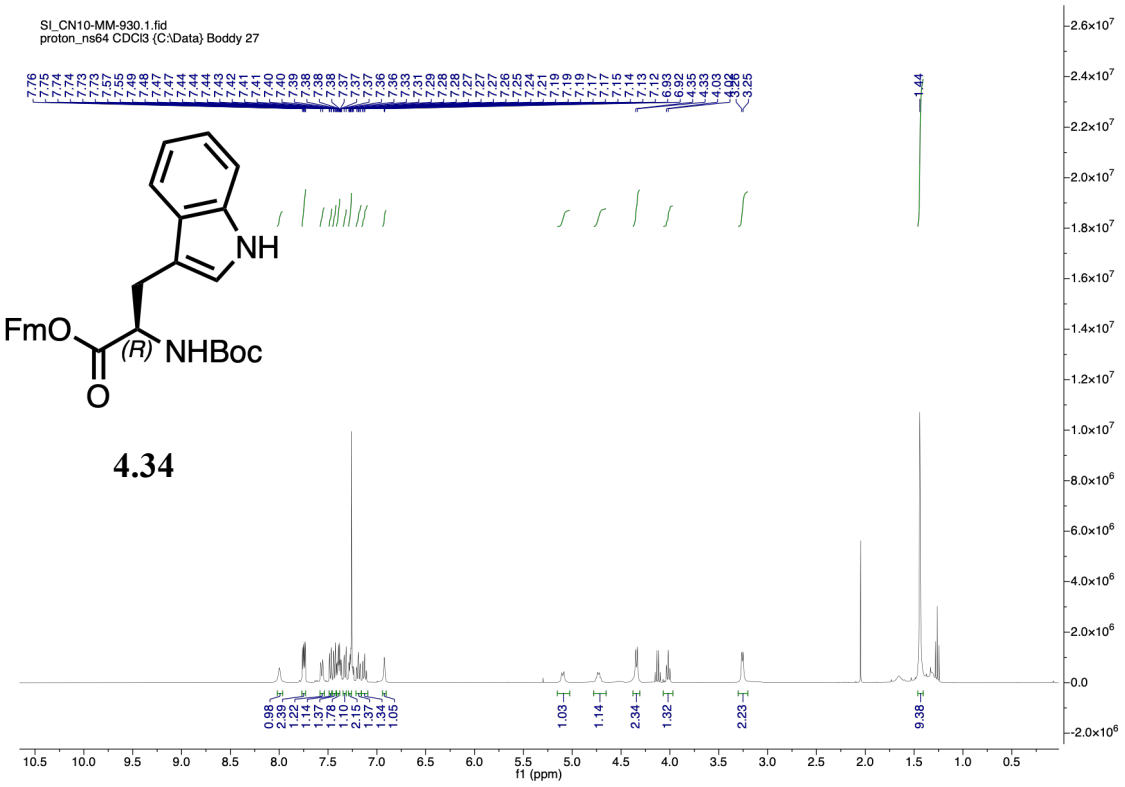


4.38

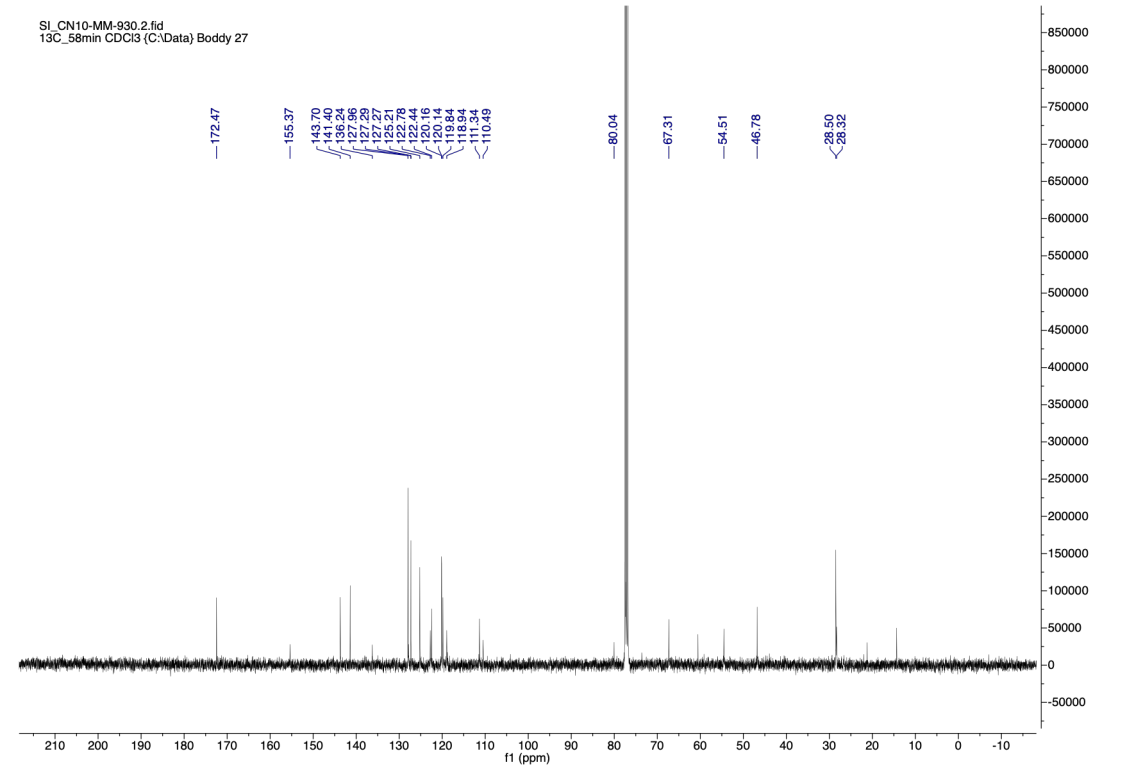


Spectra 4.32 HSQC of compound **4.38**

A

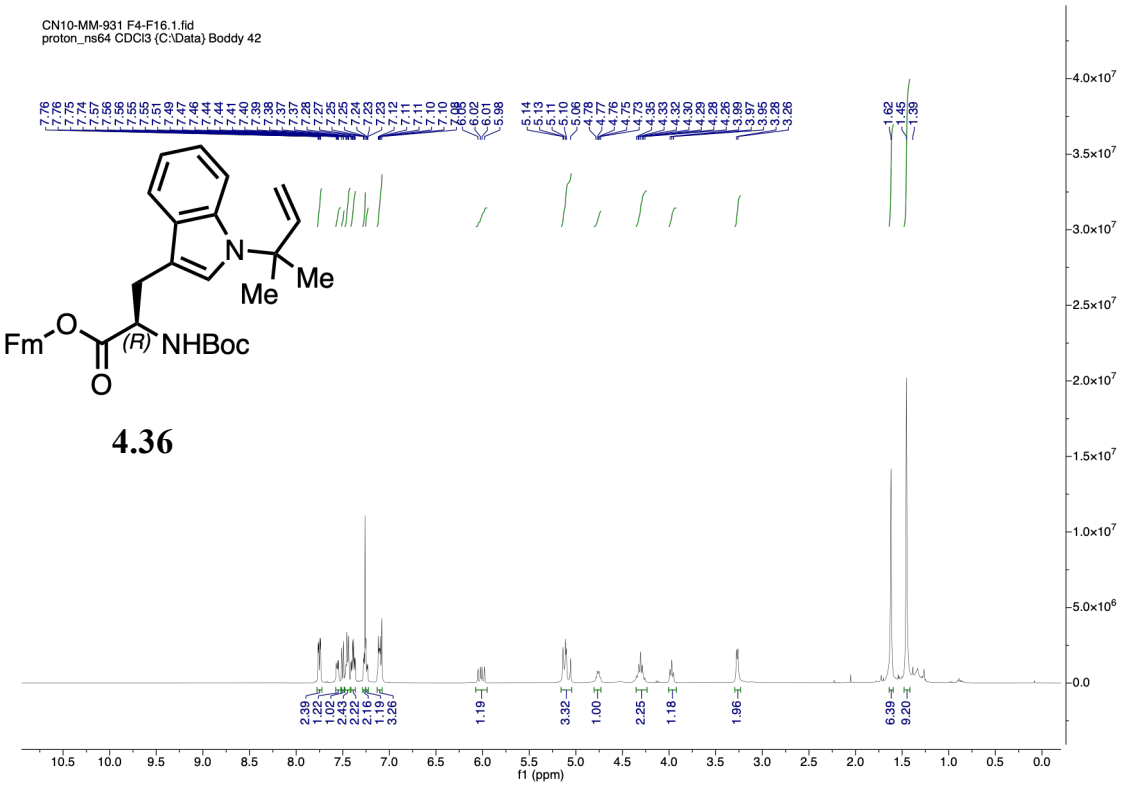


B



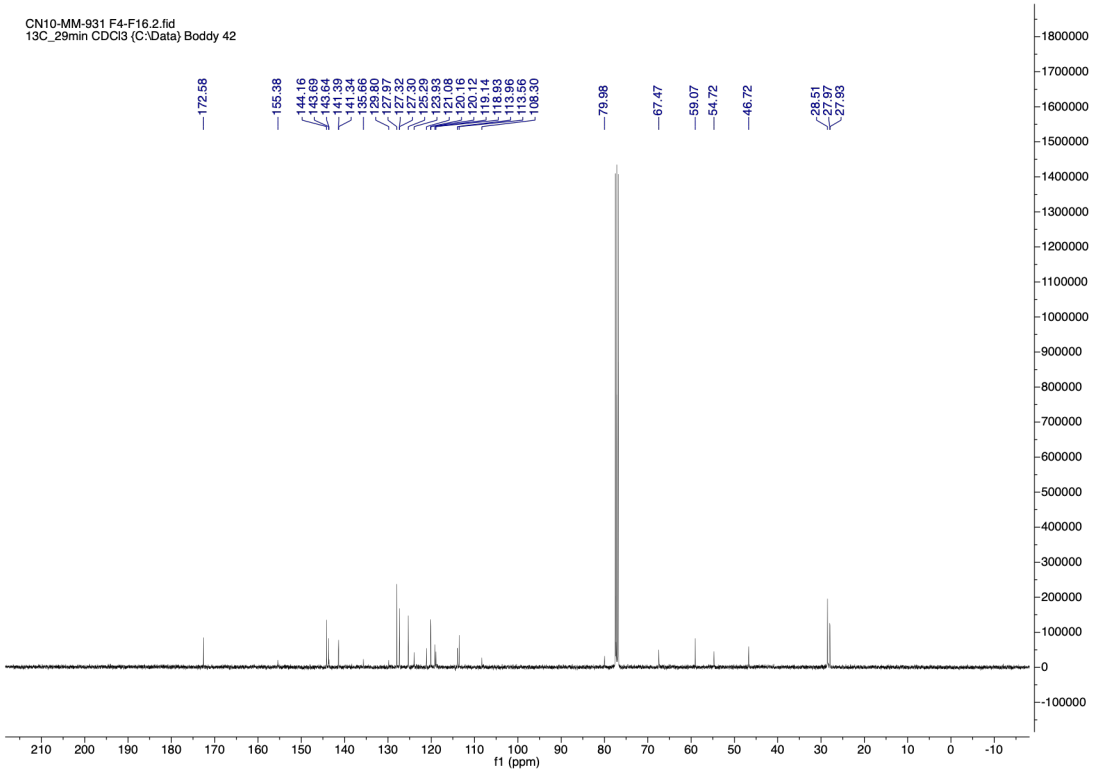
Spectra 4.33 of compound **4.34** (A) ^{1}H NMR (600 MHz, $CDCl_3$) and (B) ^{13}C NMR (101 MHz, $CDCl_3$)

A



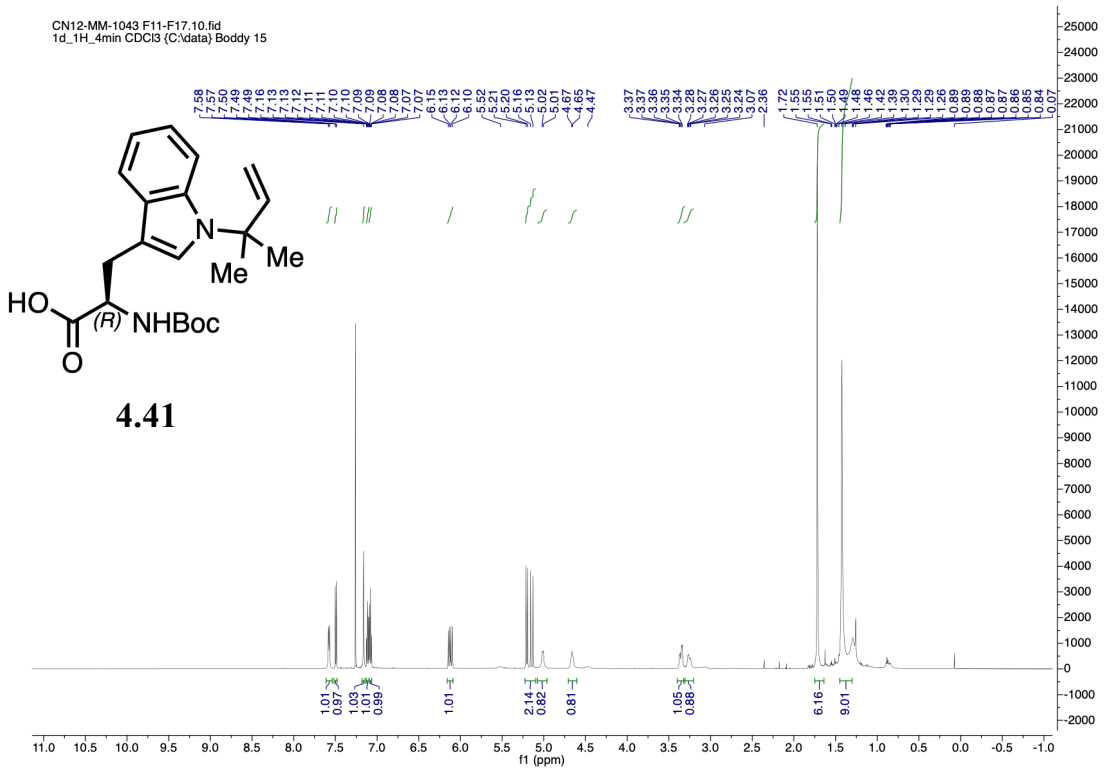
4.36

B



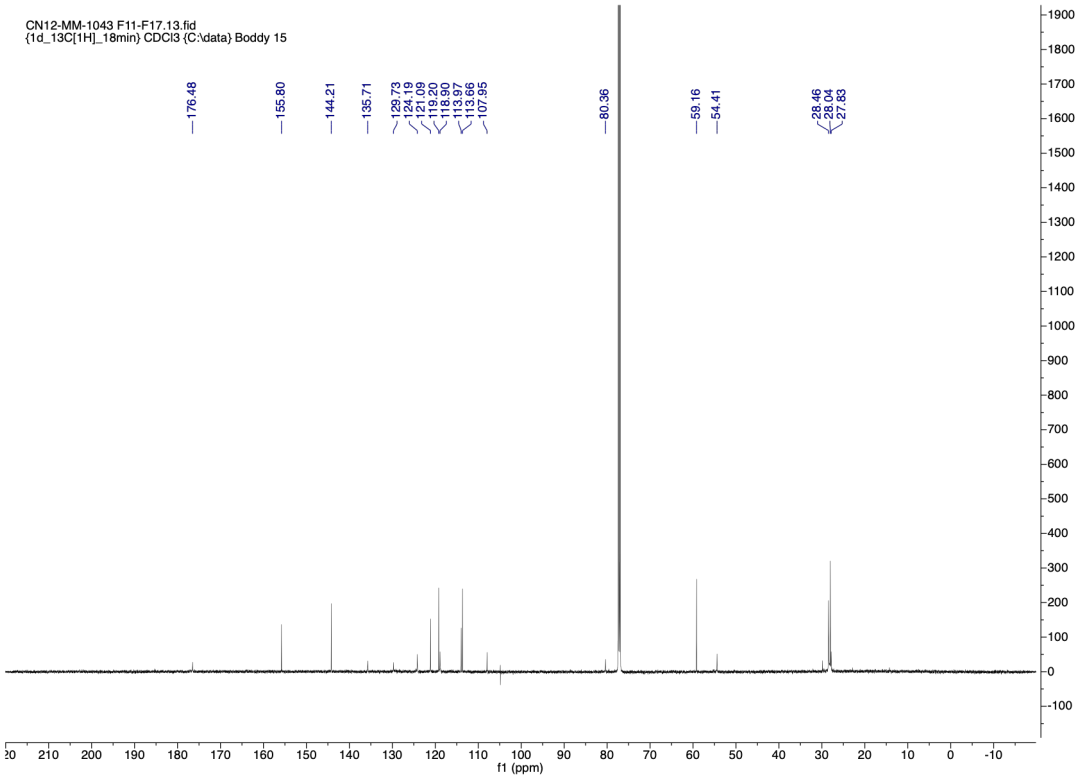
Spectra 4.34 of compound **4.36** (A) ^{1}H NMR (600 MHz, $CDCl_3$) and (B) ^{13}C NMR (101 MHz, $CDCl_3$)

A



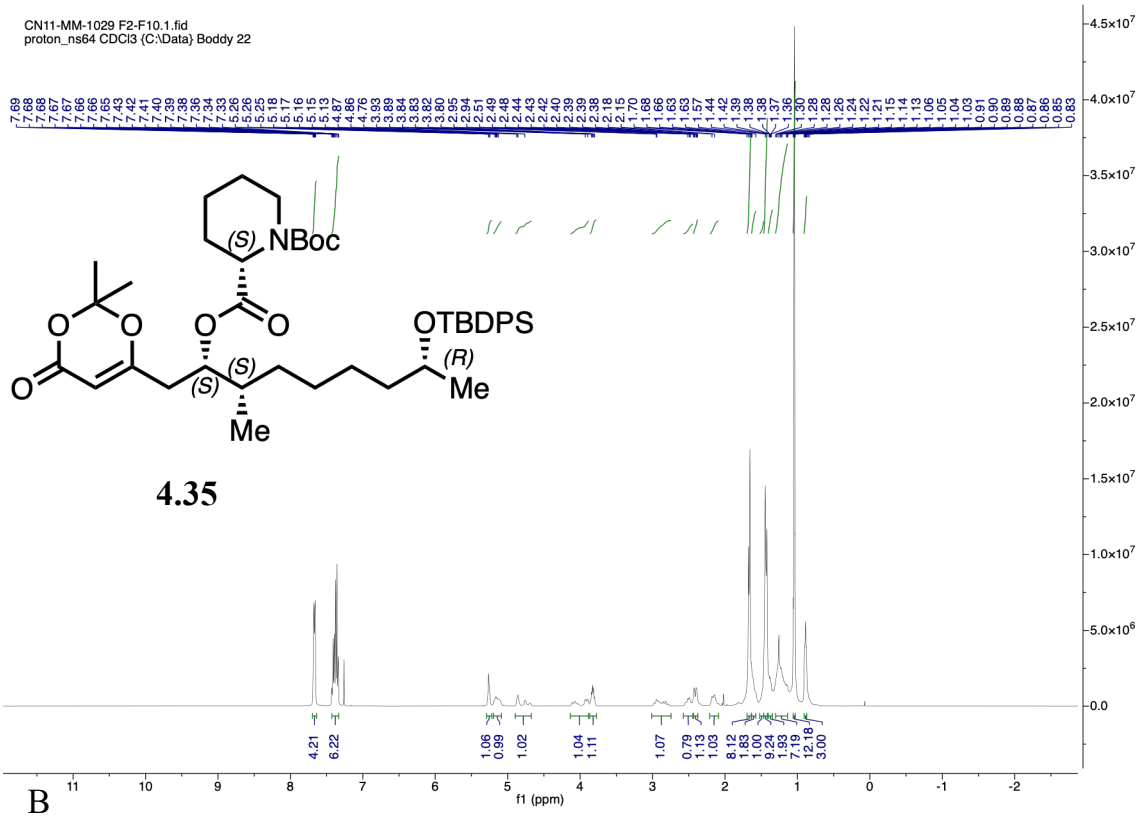
4.41

B



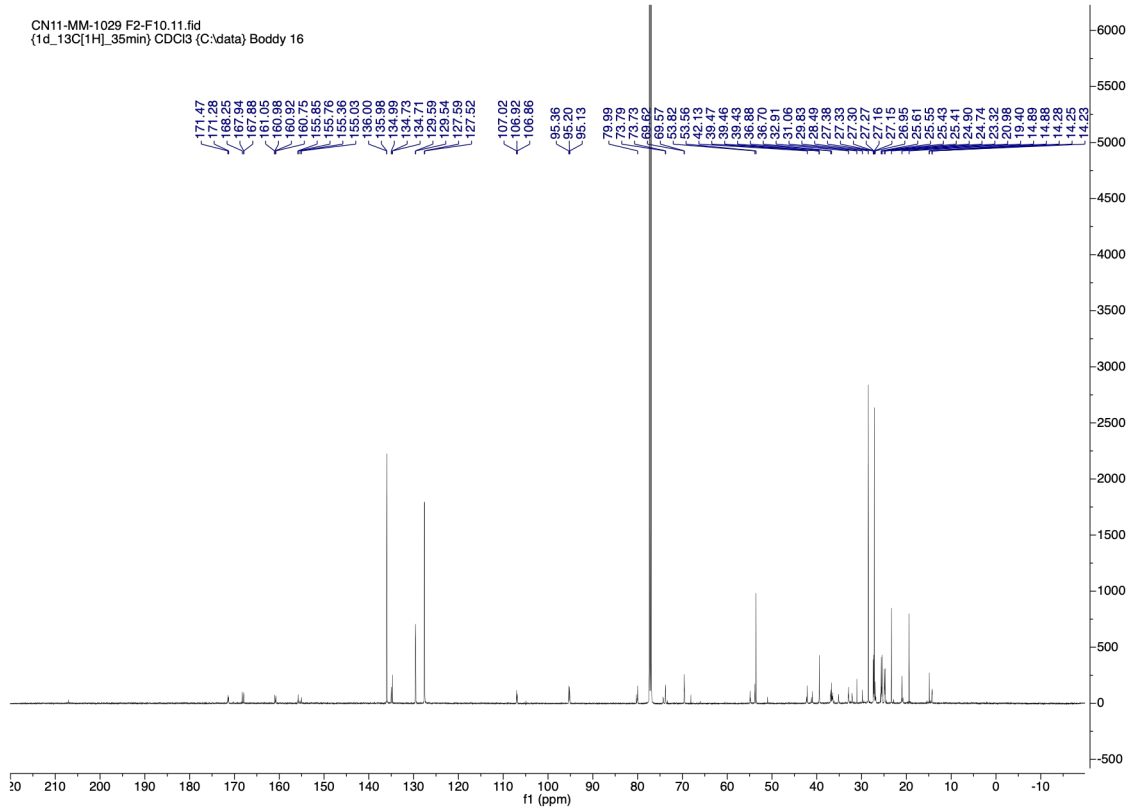
Spectra 4.35 of compound **4.41** (A) ^{1}H NMR (600 MHz, $CDCl_3$) and (B) ^{13}C NMR (101 MHz, $CDCl_3$)

A

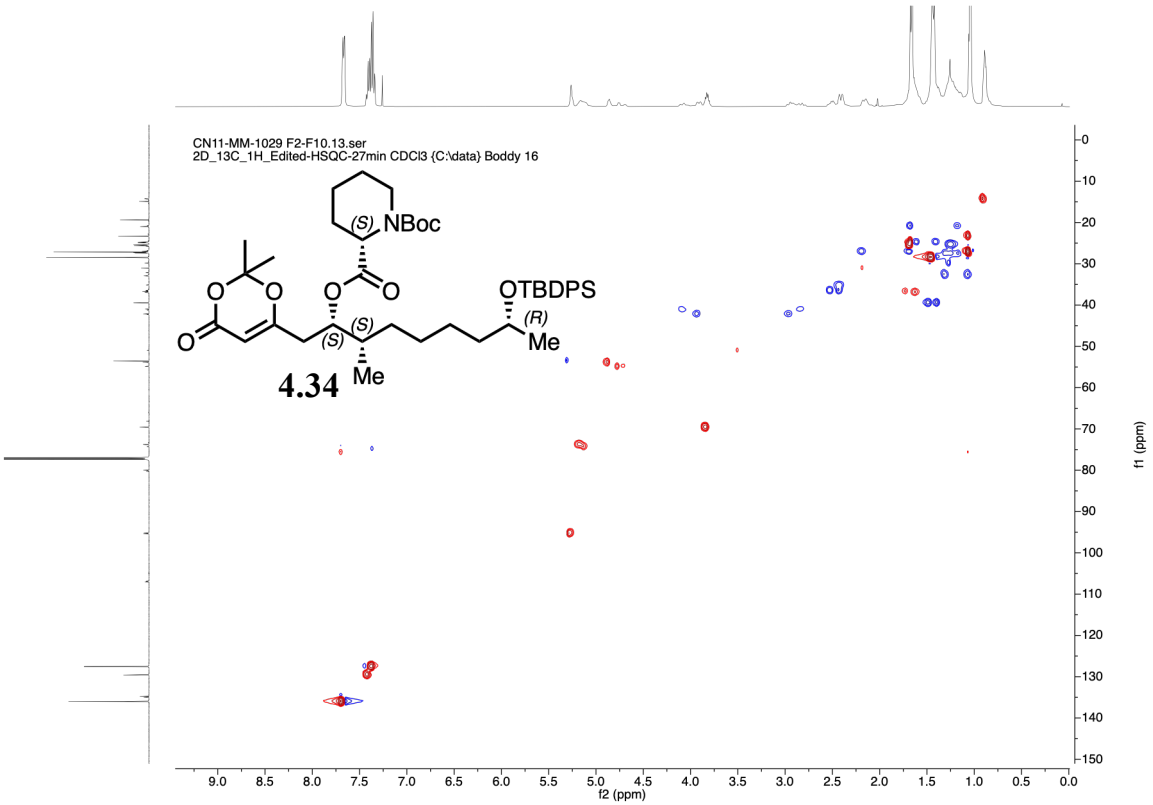


4.35

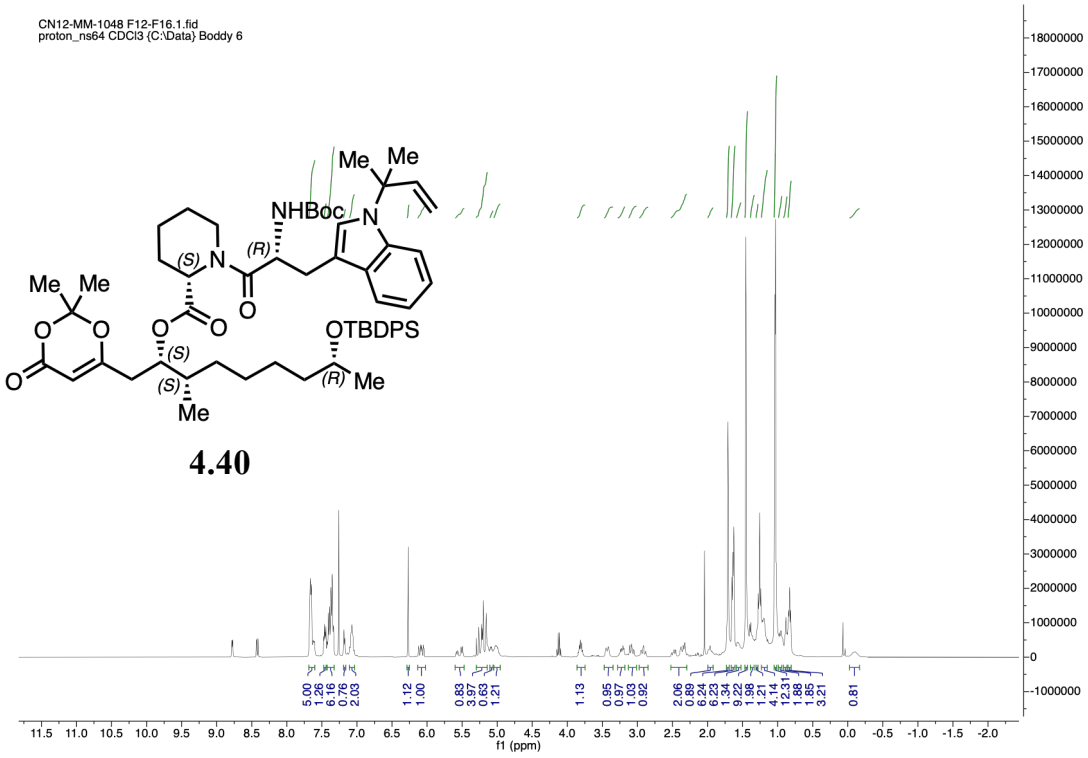
B



Spectra 4.36 of compound **4.35** (A) ^{1}H NMR (600 MHz, $CDCl_3$) and (B) ^{13}C NMR (600 MHz, $CDCl_3$)



Spectra 4.37 HSQC of compound **4.35**



Spectra 4.38 of compound **4.40** ^{1}H NMR (600 MHz, $CDCl_3$)

PART II.

The Total Synthesis of Fusahexin and its Biosynthetic Precursor, Prefusahexin

CHAPTER V.

The Total Synthesis of Fusahexin and Prefusahexin

5.1 Introduction to the Research Article Presented in this Chapter

Fusahexin (**5.1;** referred to as **1** in **Section 5.4**) is a macrocyclic hexapeptide natural product originally isolated from *Fusarium graminearum* by Westphal et al.[1] in 2021. Structurally, fusahexin is characterized by a heavily lipophilic peptidic backbone constituting alternating D- and L-configured amino acids (cyclo-(D-Ala-L-Leu -[D-allo-Thr-L-Pro]-D-Leu-L-Leu).

Intriguingly, **5.1** features a unique fused 6,5-bicyclic *N,O*-acetal moiety, arising from cross-

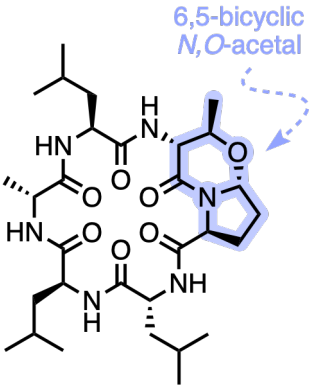


Figure 5.1. Structure of fusahexin featuring the unprescedented fused 5,6-bicyclic N,O-acetal

linking of the D-allo-Thr side chain alcohol to the δ-carbon of a neighbouring L-Pro residue, had not been observed in any other natural product prior to the isolation of fusahexin. Beyond its structural novelty, the acetal-based moiety found in fusahexin is closely related to dipeptide β-turn mimics developed for peptidomimetic applications[2–7,7–10], including antagonists of inhibitor of apoptosis proteins (IAPs)[2,11,12] and PD-1/PD-L1 pathway inhibitors[13], underscoring the broader relevance of this privileged scaffold in medicinal chemistry.

The discovery of **5.1** was enabled by overexpression of *NRPS4* in *F. graminearum*, which allowed Westphal et al. to unambiguously associate the gene with fusahexin production and establish *NRPS4* as the biosynthetic gene responsible for its assembly.Within the context of fungal virulence, Westphal et al. also found **5.1** to play an important functional role in *F. graminearum* physiology and pathogenicity. They noted that deletion of *NRPS4* (*ΔNRPS4*) resulted in loss of surface hydrophobicity, consistent with earlier observations in *F. graminearum* and related fungi, suggesting that fusahexin contributes directly or indirectly to the hydrophobic character of the fungal cell surface. Conversely, overexpression of *NRPS4* (OE::*NRPS4*) led to a water-repellent

phenotype slowed radial growth under osmotic stress conditions (1 M NaCl and 1 M sorbitol). Most notably, OE::*NRPS4* strains showed significantly impaired virulence on wheat relative to both wild-type and *ΔNRPS4* strains. Together, these phenotypic data implicate fusahexin as a natural product with a structural or regulatory role at the fungal cell surface, however, the exact mechanism by which it operates remain unknown.

Despite the structural characterization of fusahexin and its biosynthesis association with NRPS4, the biosynthetic mechanisms for the construction of the *N,O*-acetal remained an unresolved question prior to this work. Westphal's proposed NRPS product, cyclo-(D-Ala–L-Leu–D-allo-Thr–L-Pro–D-Leu–L-Leu) (dihydrofusahexin, **5.2**; **2** in **Section 5.4**), would require an oxidative transformation to generate the acetal of fusahexin; however, no candidate oxidase was identified within the fusahexin biosynthetic gene cluster, and the adenylation domain specificity for the installation of the fourth amino acid was inconclusive.

The work presented in this chapter addresses this gap through a synthesis-supported metabolomics strategy. A targeted gene deletion of *NRPS4* was generated in *F. graminearum* using CRISPR/Cas9 gene editing, and comparative UHPLC-HRMS metabolomics analysis of wild-type and *ΔNRPS4* strains ultimately led to the identification of a previously unknown cyclic hexapeptide, prefusahexin (**5.3**; **3** in **Section 5.4**), which incorporates L-ornithine in place of L-proline. The structure of prefusahexin was confirmed by total synthesis using Fmoc solid-phase peptide synthesis (SPPS) and HATU-mediated macrocyclization, and its role as a direct

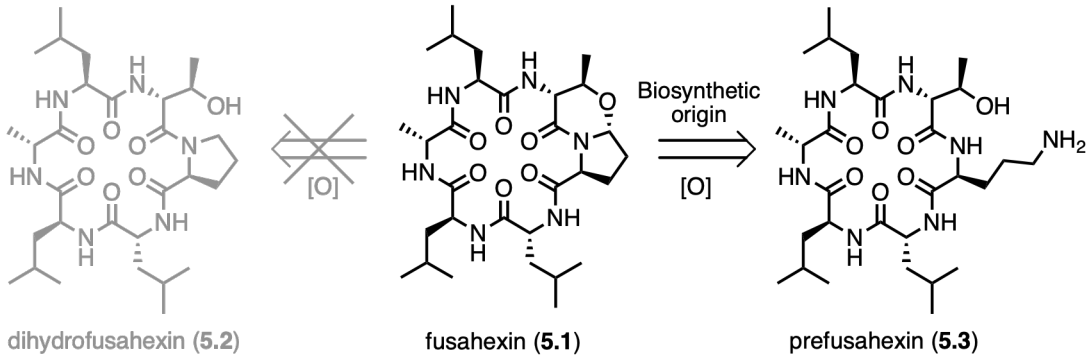


Figure 5.2. Revised biosynthesis of fusahexin (**5.1**). Prefusahexin (**5.3**), is identified as the direct biosynthetic precursor to **5.1** via an oxidative transformation [O] of the ornithine side chain. Dihydrofusahexin (**5.2**), is ruled out as a biosynthetic intermediate.

biosynthetic precursor to fusahexin was established. Furthermore, a biosynthesis-inspired total synthesis of fusahexin itself was achieved by incorporating a Weinreb amide surrogate for the

ornithine side chain, enabling selective DIBAL-H reduction to the aldehyde followed by acid-mediated cascade cyclization to the *N,O*-acetal. This work revises the proposed biosynthesis of fusahexin and establishes that the fusahexin biosynthetic gene cluster represents a split cluster[14,15], wherein the oxidative enzyme responsible for converting prefusahexin to fusahexin is encoded elsewhere in the genome.

5.2 Summary of Thesis Objectives (Part B)

Given the unresolved biosynthetic origin of the unique fused 6,5-bicyclic *N,O*-acetal of fusahexin (**5.1**), the work presented in Part II of this thesis was directed toward the identification of its direct biosynthetic precursor and the development of a biomimetic total synthesis providing experimental support for the proposed biosynthetic pathway. This objective was pursued in the form of three integrated objectives (summarized below) which constitute Chapter V of this thesis.

1. **Synthesis-Supported Identification and Structural Confirmation of the Direct Biosynthetic Precursor to Fusahexin (Section 5.4).** A CRISPR/Cas9-mediated deletion of *NRPS4* combined with comparative UHPLC-HRMS metabolomics profiling identified prefusahexin (**5.3**) as the direct biosynthetic precursor to **5.1**, ruling out the previously proposed dihydrofusahexin (**5.2**). The structure of **5.3** was confirmed by total synthesis and co-elution with the natural metabolite.

2. **Biosynthesis-Inspired Total Synthesis of Fusahexin (Section 5.4).** A total synthesis of **5.1** was achieved through incorporation of a Weinreb amide-functionalized glutamic acid surrogate during linear peptide assembly, enabling selective late-stage DIBAL-H reduction to the aldehyde followed by acid-promoted cascade cyclization to deliver **5.1** in high diastereomeric ratio, providing direct chemical support for the proposed biosynthetic oxidative cyclization mechanism.

3. **Biomimetic Oxidation of Prefusahexin as a Model for the Biosynthetic N,O-Acetal Formation (Section 5.5).** Building on the identification of **5.3** as the biosynthetic precursor to **5.1**, subsequent work investigated the chemical feasibility of the proposed oxidative transformation using a synthetic equivalent of the topaquinone (TPQ) cofactor found in copper

amine oxidases (CAOs). Treatment of **5.3** with a di-tert-butyl-ortho-benzoquinone surrogate reproduced the proposed oxidative backbone editing event, providing preliminary chemical evidence in support of CAO involvement in the biosynthesis of the **N,O**-acetal of fusahexin.

5.3 Author Contributions

The research presented in this chapter was conducted as a collaborative effort between the Boddy laboratory (Department of Chemistry and Biomolecular Sciences, University of Ottawa) and the Overy laboratory (Agriculture and Agri-Food Canada). The following is a summary of author contributions as described in the published manuscript:

C.N. (thesis author) designed and executed the total synthesis of prefusahexin (**5.3**), dihydrofusahexin (**5.2**), and fusahexin (**5.1**), including the preparation of all synthetic intermediates. C.N performed full spectroscopic characterization of all synthetic compounds by NMR and HRMS. **C.H.** performed the CRISPR/Cas9-mediated gene editing to generate knockout strain, conducted the spiking experiments, and contributed to the metabolomics experiments and data analysis along with **T.E.W**. **A.H**. and **A. S**. assisted with fungal culturing, extraction, and UHPLC-HRMS profiling experiments. **D. P. O.** co-supervised the biological and metabolomics components and contributed to the conception of the study, data interpretation, and manuscript preparation. **C. N. B.** conceived and supervised the project, directed the synthetic and metabolomics strategy, and contributed to the writing and revision of the manuscript.

5.4 Copyright

Section 5.5 is reproduced in accordance with the American Chemical Society's thesis reuse policy. Reprinted with permission from *Organic Letters,* **2026**, 28, 14, 4507-4511. Copyright 2026 American Chemical Society. The original publication can be accessed online at https://doi.org/10.1021/acs.orglett.6c00755

5.5 Synthesis-Supported Discovery of Prefusahexin, a Direct Fusahexin Biosynthetic Precursor

Claudia Natola[a], Carmen Hicks[b], Thomas E. Witte[b], Anne Hermans[b], Amanda Sproule[b], David P. Overy[b*], Christopher N. Boddy[a*]

[a]Department of Chemistry and Biomolecular Sciences, University of Ottawa, Ottawa, ON, Canada K1N 6N5

[b]Ottawa Research and Development Centre, Agriculture and Agri-Food Canada, Ottawa, ON, Canada.

5.5.1 Abstract

Cyclic hexapeptide fusahexin features a unique fused 6,5-bicyclic *N,O*-acetal, the biosynthetic origin of which is unresolved. Metabolomics analysis of a gene deletion in *Fusarium graminearum* revealed an Orn-containing intermediate, prefusahexin, as the product of nonribosomal peptide synthetase NRPS4. The chemical structure of prefusahexin was verified by total synthesis, and its predicted oxidized intermediate was synthesized and cyclized to fusahexin. These results establish prefusahexin as the key biosynthetic precursor to fusahexin.

5.5.2 Main Text

Fusahexin (**1** (**Figure 5.3**)) is a cyclic hexapeptide natural product containing alternating d- and l-configured amino acid residues[1] and is produced by the fungus *Fusarium graminearum*, along with other *Fusarium* spp.[16] In addition to its macrocyclic core, **1** is further cross-linked through the d-*allo*-Thr side chain alcohol to the δ-carbon of the neighboring residue, generating a fused 6,5-bicyclic *N,O*-acetal. This is a unique functional group that has not been observed in any other natural products, to the best of our knowledge. Intriguingly, related acetal-based dipeptide scaffolds were developed as β-turn mimics in the 1990s[3–10,17,18] and have been used in the

development of peptidomimetics as antagonists of inhibitor apoptosis proteins[2,11,12] and as PD-1/PD-L1 pathway inhibitors.[13]

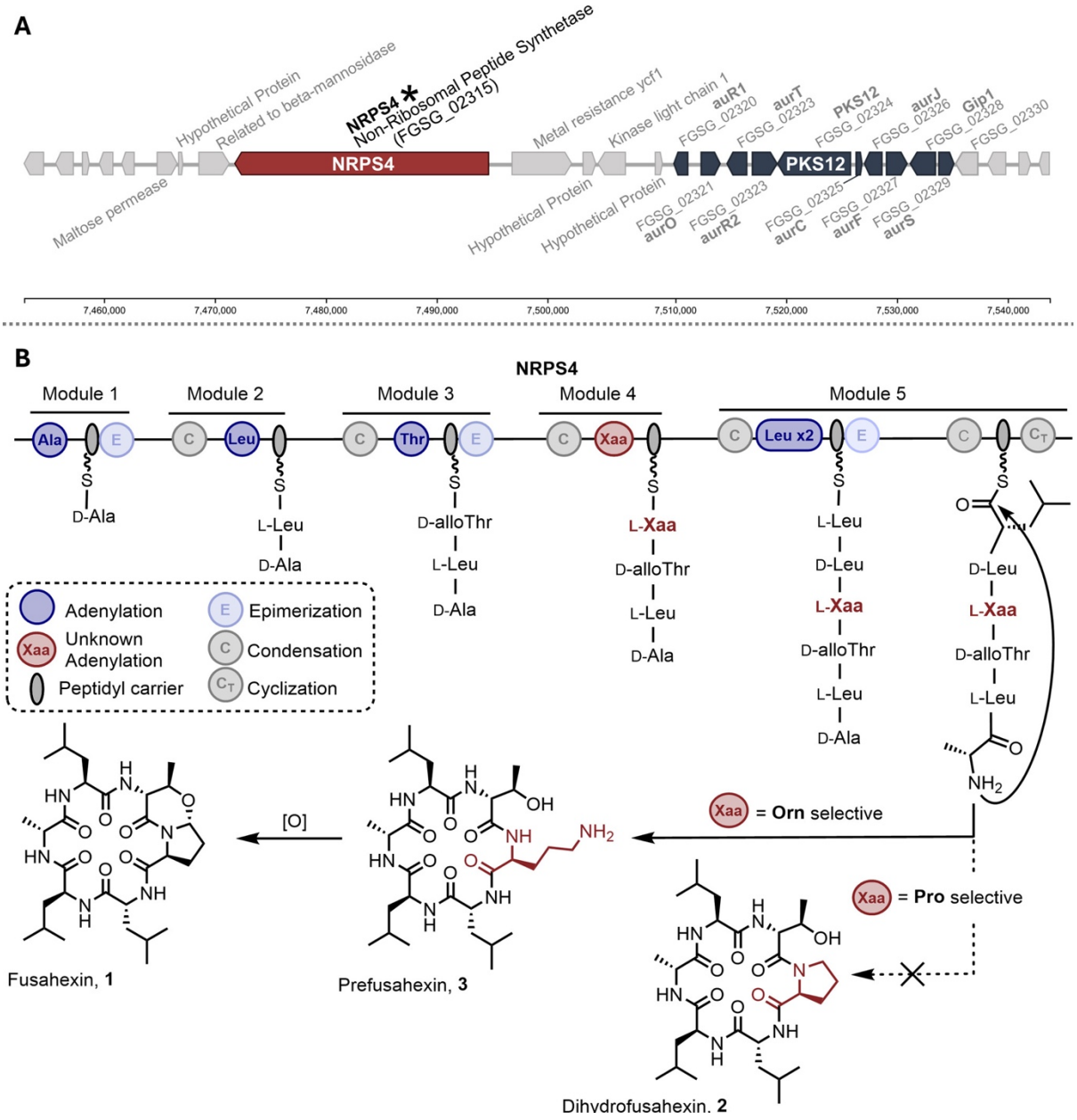


Figure 5.3 Revised biosynthesis of fusahexin showing intermediate prefusahexin leading to natural product fusahexin rather than the initially proposed dihydrofusahexin. (A) Biosynthetic gene cluster from *F. graminearum* chromosome 1 showing the NRPS gene cluster responsible for fusahexin biosynthesis. (B) Annotated protein encoded by NRPS4 from fusahexin biosynthesis that generates the newly identified intermediate prefusahexin via incorporation of L-Orn rather than L-Pro as initially proposed. Orn is oxidized by an, as of yet, unidentified enzyme to generate fusahexin.

Little is known about the biosynthesis of the *N,O*-acetal in fusahexin. Previous gene deletion experiments unambiguously associated fusahexin biosynthesis with nonribosomal peptide synthetase-encoding gene *NRPS4* (**Figure 5.3A**)[1]. Based on the architecture of the encoded NRPS, six amino acid residues are added one at a time to generate a linear hexapeptide, which is then cyclized. This rules out the incorporation of an *N,O*-acetal-containing building block. The proposed NRPS product is cyclo-(d-Ala-l-Leu-d-*allo*-Thr-l-Pro-d-Leu-l-Leu),[1] also here termed dihydrofusahexin (**2**), which must undergo oxidation to form **1** (**Figure 5.4B**). Examination of the

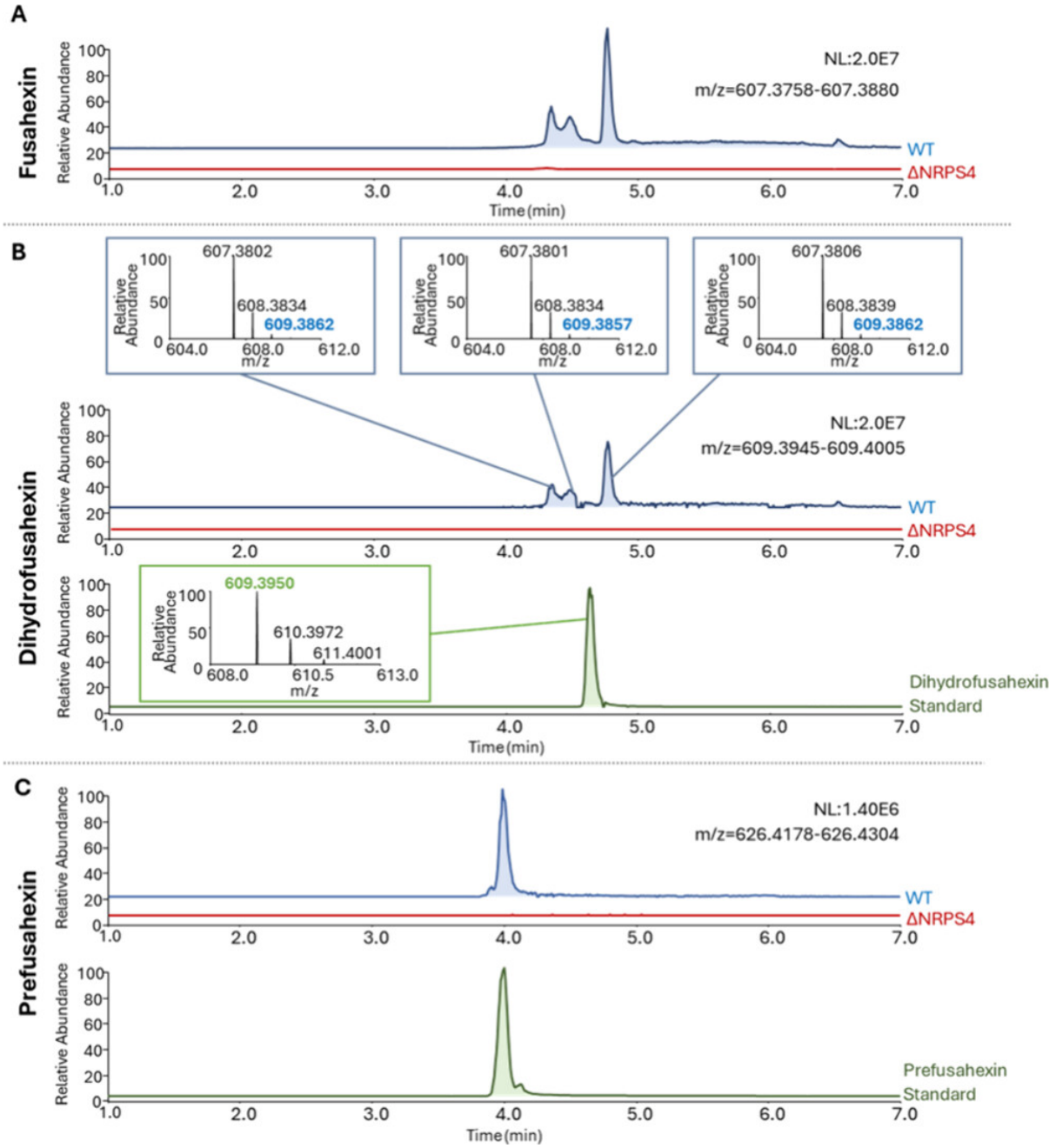


Figure 5.4. Extracted ion chromatograms (EICs) comparing targeted metabolite production between *F. graminearum* WT (blue trace) and Δ*NRPS4* (red trace) strains using a 5 ppm window around the theoretical $[M + H]^+$ *m*/*z* ion associated with fusahexin, dihydrofusahexin, and prefusahexin. (A) EIC confirming loss of fusahexin (and associated earlier eluting isomer and hydration products)[1] in Δ*NRPS4*. (B) EIC confirming the absence of dihydrofusahexin $[M + H]^+$ in both WT and Δ*NRPS4* strains as compared to the dihydrofusahexin standard. The detected peaks in the WT extract are associated with natural abundance isotopologue fusahexin ions containing two ^{13}C atoms (M + 2), which can be seen from the inset mass spectra. (C) EIC confirming the presence of prefusahexin in the WT and the absence in Δ*NRPS4* strains along with a comparison to the prefusahexin standard.

genomic neighborhood of the fusahexin biosynthetic gene cluster on chromosome 1 in representative *F. graminearum* strain DAOMC 233423 (**Figure 5.4A**) did not reveal any candidate oxidative enzymes,[19,20] such as a cytochrome P450, which would be able to oxidize the δ-carbon of the proline residue in **2** to generate **1**. Thus, the biosynthesis of this unique functional group in fusahexin remains a mystery.

We set out to experimentally identify the direct biosynthetic product from the fusahexin NRPS. In *F. graminearum*, the fusahexin biosynthetic gene cluster lies adjacent to the aurofusarin biosynthetic gene cluster[21] on chromosome 1 (accession number NC_026474.1 (**Figure 5.3A**)). A *NRPS4* gene deletion mutant (Δ*NRPS4*) was created by replacing *NRPS4* with a hygromycin resistance cassette using CRISPR/Cas9 gene editing of *F. graminearum* protoplasts (see Figure 5.S2). Metabolomics analysis of UPLC-HRMS culture extract profiles of the WT and Δ*NRPS4* strains confirmed the disruption of fusahexin biosynthesis (**Figure 5.4A**), consistent with previous studies.[1] In addition, the loss of production of a variety of mass features differing in retention time from fusahexin (and its documented earlier eluting isomer and hydration products[1]) was observed in the *ΔNRPS4* strain relative to the WT. Several of these NRPS4-dependent mass features were consistent with a biosynthetic intermediate derived from NRPS4 containing l-Orn in place of l-Pro, here termed prefusahexin **3** (**Figure 5.3B**).

Previous predictions of the biosynthesis of fusahexin[1] hypothesized the incorporation of l-Pro during the elongation of the peptide chain, resulting in the formation of dihydrofusahexin **2**. Bioinformatic analysis of the corresponding adenylation domain for its amino acid specificity was inconclusive, and given the low accuracy of fungal A domain specificity predictions[22,23] and the lack of experimental evidence for **2**, we hypothesized that **2** may not be a true intermediate in

fusahexin biosynthesis. To test this hypothesis, **2** was synthesized using standard Fmoc solid phase peptide synthesis (Fmoc-SPPS) and solution phase HATU-mediated macrocyclization (see Scheme 5.S1) for use as an authentic standard. No mass features with a retention time and pseudomolecular ions matching our synthetic standard were observed in our metabolomics data set (**Figure 5.4B**). While signals were observed for the $[M + H]^+$ *m*/*z* ion extraction of **2** (*m*/*z* 609.3945–609.4005) in the WT metabolomics data set (**Figure 5.4B**), these signals correspond to the natural abundance isotopologues of fusahexin and its associated isomeric *m*/*z* 607.3902 ions containing two ^{13}C atoms, as shown in the inset MS spectra of each of these mass features (**Figure 5.4B**). This assignment is further confirmed by comparing the retention times of these mass features in **Figure 5.4B** to the retention times of the fusahexins (**Figure 5.4A**). Together, these data suggest that **2** is not a biosynthetic intermediate of fusahexin.

To revise the fusahexin biosynthesis hypothesis, we evaluated the potential incorporation of nonproteinogenic amino acid L-Orn in place of L-Pro. Cyclization and offloading of the cyclic peptide intermediate would yield prefusahexin **3** (**Figure 5.3B**). We therefore synthesized an authentic prefusahexin standard (Scheme 5.S1) to evaluate our revised hypothesis. Exploration of

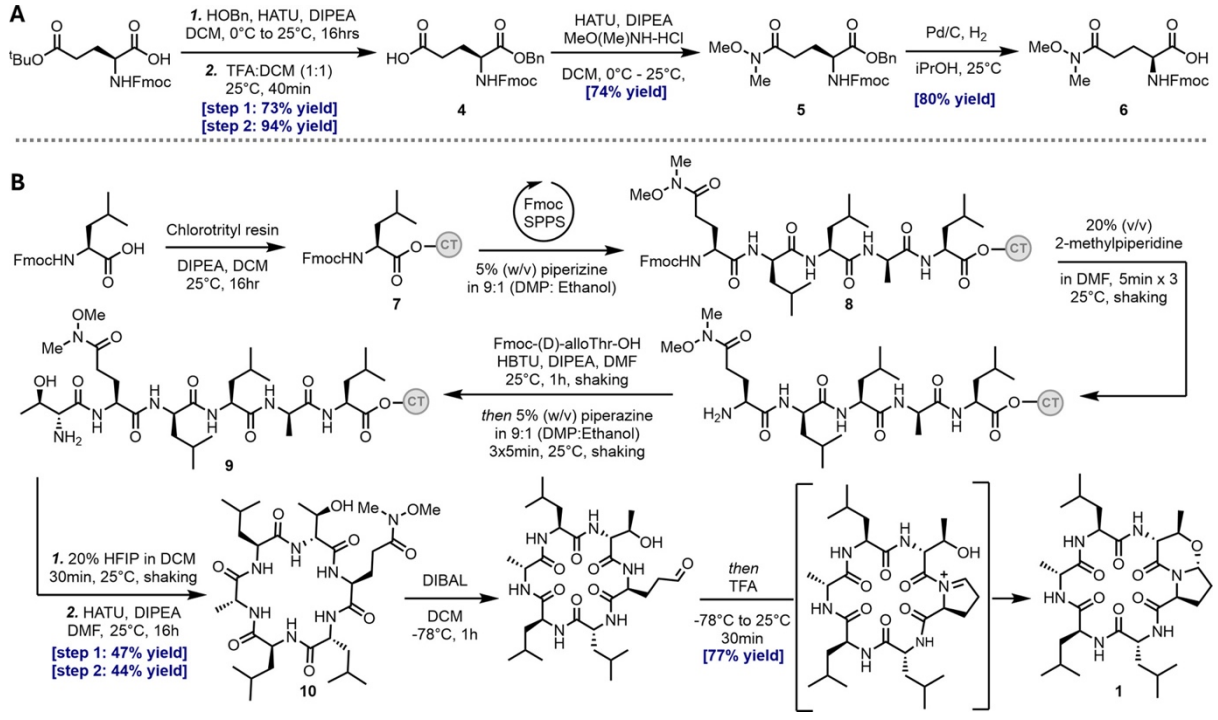


Figure 5.5 (A) Synthesis of l-Gln (Weinreb amide) noncanonical amino acid **6**. (B) Biosynthesis-inspired total synthesis of fusahexin **1**.

the metabolomics data set revealed the presence of a mass feature corresponding to the protonated pseudomolecular ion ($[M + H]^+$), which matched both the elution retention time and the observed and calculated $[M + H]^+$ *m*/*z* ion of prefusahexin in WT extracts and the absence of the expected $[M + H]^+$ ion in *ΔNRPS4* strain extracts (**Figure 5.4C**). Spiking experiments of the prefusahexin standard into WT extracts resulted in a corresponding increase in the expected $[M + H]^+$. These data confirm that prefusahexin is produced by *F. graminearum*, and its production is dependent on *NRPS4*. This is fully consistent with prefusahexin being a potential intermediate in fusahexin biosynthesis.

Although the enzyme that converts prefusahexin into fusahexin is unknown, we hypothesize that oxidation of the prefusahexin side chain primary amine by a nonclustered or cellular oxidase to the aldehyde should enable the generation of the *N,O*-acetal moiety seen in fusahexin. To test this transformation, we undertook the total synthesis of the proposed aldehyde intermediate to access fusahexin biomimetically (**Figure 5.5**). To enable synthetic access to the aldehyde in this polyfunctionalized macrocycle, we replaced L-Orn with the Weinreb amide[24] derivative of L-Gln, which we were confident could be selectively reduced to the aldehyde.[25]

Fmoc-protected L-Gln containing a side chain Weinreb amide, **6**, was synthesized in four steps in 41% yield from Fmoc-Glu(O*t*Bu)-OH (**Figure 5.5A**). Using automated Fmoc-SPPS, we synthesized the linear pentapeptide on the 2-ClTrtCl resin. Deprotection and coupling to Fmoc-D-*allo*-Thr were performed manually to limit undesirable pyroglutamate formation during microwave-assisted Fmoc deprotection.[26] Cleavage from the resin, followed by HATU-mediated ring closure, provided compound **10** in 44% yield. Reduction with DIBAL-H at −78 °C generated the aldehyde. Subsequent acidification with TFA triggered the cascade generating the *N,O*-acetal and smoothly producing fusahexin **1** in 77% yield (**Figure 5.5B**). Our synthetic fusahexin was indistinguishable from the natural product (Figure 5.S16), and NOE analysis confirmed the stereochemical configuration at the *N,O*-acetal (Figure 5.S17).

Bäuerlein and Geyer previously synthesized fusahexin.[27] Their synthesis generated an aldehyde dipeptide intermediate that underwent acid-catalyzed formation of the *N,O*-acetal, providing an important precedent for our synthesis. Their dipeptide intermediate was then elongated to a linear fusahexin precursor, which was macrocyclized via treatment with HATU to generate **1**. In contrast, our total synthesis mirrors the biosynthesis by assembling the *N,O*-acetal

on the macrocyclic hexapeptide as the last step, through the biosynthetically relevant aldehyde-containing macrocycle.

This study proposes a new biosynthetic intermediate for fusahexin **1**. We demonstrate that prefusahexin **3** rather than dihydrofusahexin **2** is formed by *F. graminearum* and that production of **3**, like that of **1**, is dependent on NRPS4. The successful conversion of our synthetic aldehyde derivative into fusahexin supports the hypothesis that the Orn side chain amine of prefusahexin **3** is enzymatically oxidized into the aldehyde, which then condenses to generate the unique fused 6,5-bicyclic *N,O*-acetal of fusahexin **1**.

Identification of the oxidative enzyme responsible for converting prefusahexin into fusahexin is still, however, unresolved. Analysis of the biosynthetic gene cluster does not reveal any gene encoding an enzyme that could reasonably catalyze this chemistry.[19,20] This suggests that it is a nonclustered oxidase.

It is notable that the aurofusarin biosynthetic gene cluster is immediately adjacent to the fusahexin biosynthetic gene cluster. Having two gene clusters that are in such proximity is highly unusual. We hypothesize that the insertion of the aurofusarin biosynthetic gene cluster into the 3′ end of the fusahexin biosynthetic gene cluster could have displaced the gene encoding this oxidase to a new location in the genome.[15,28] Regardless of the mechanism for loss of this gene, the fusahexin biosynthetic gene cluster represents an important example of a split biosynthetic gene cluster, and further examining how this occurred may shed light on the process by which natural product biosynthetic gene clusters diversify via transposition, recombination, gene conversion, inversion, and/or duplication.

5.5.3 Supplementary Information

Biological Materials and Methods

CRISPR-Cas9 mediated gene-editing:

All CRISPR Cas9 gene-editing procedures (PCR amplification of the HDR-HygB repair template; in vitro assembly of the Cas9-gRNA ribonucleoprotein complex; and *Fusarium graminearum* protoplast generation and transformation) were carried out in *F. graminearum* strain DAOMC 233423 using previously published procedures [29]. Gene-specific CRISPR-RNAs (crRNA) were designed for the *NRPS4* gene (FGSG_02315) with cleavage sites upstream of the translation start site and near the 3' end of target gene (**Table 5.S1**). Repair template amplification primers (**Table 5.S2**) were designed to contain 55-48 bp of homology adjacent to the gRNA-specified cleavage sites as well as 20 bp corresponding to up and downstream regions of hygromycin resistance sequences within the pRF-HU2 vector (regions pTrpC and hph depicted in **Figure 5.S1**). Additionally, putative transformants were isolated from a hygromycin-containing growth selection medium; target gene knockout confirmation was performed; and single-spored, axenic transformant strains obtained according to previously published procedures[29].

PCR and Southern Blot targeted gene knockout confirmation:

Selected knockout strains and WT control were cultured in S1M medium[29] lshaking at 28 °C and 170 rpm for 5 d and mycelium was then harvested via vacuum filtration and ground in liquid nitrogen using a mortar and pestle before gDNA isolation using a Illustra Nucleon Phytopure Genomic DNA Extraction Kit (GE Healthcare UK Limited, Buckinghamshire, UK) following manufacturer's protocol. PCR reactions were performed using amplification primers corresponding to the inserted hygromycin cassette as a positive control, and internal primers corresponding to the intended gene knockout (**Table 5.S3**). Final concentrations of 1x Titanium Taq buffer (with 3.5 mM $MgCl_2$), 0.1 mM dNTPs, 0.08 µM of both forward and reverse primers, 1x Titanium Taq polymerase (Clontech, Mountain View, California), were obtained with 2 µL of DNA template. Amplification was completed with initial denaturation at 95 °C, followed by 35 cycles consisting of denaturation at 95 °C for 15 s, elongation at 60 °C for 15 s and elongation at 72 °C for 30 s, with a final extension at 72 °C for 2 min. PCR products were visualized on a 1.5 % SYBR Safe agarose gel at 100 V for 30 min (**Fig 5.S2A & B**). All steps for DNA processing,

hybridization and Southern Blot analysis were carried out according to the published procedure[30]. The enzyme used for the DNA digest (KpnI) was selected in accordance with the target gene of interest in order to isolate the inserted hygromycin cassette within a 4-10kb fragment, allowing for the band to be visualized within the limits of the molecular ladder. Following the digestion, DNA was run on an agarose gel followed by DNA hybridization with a HygB specific probe (**Fig 5.S2C**).

Strains that demonstrated amplification of the hygromycin gene, as well as a lack of amplification of their respective gene of interest, were retained for further study and cryopreserved for long-term storage.

UHPLC-HRMS Metabolite Profiling and Metabolomics Analysis:

For metabolite profiling, both WT and *ΔNRPS4* strains were grown in 15 mL liquid slant cultures on MMK2 broth incubated at 28 °C, stationary at a 20° incline, in the dark, for 10 d (5 replicates per strain); two "negative" controls were prepared for each medium by inoculating with sterile water, followed by incubation to ensure the effects of media composition (mannitol (40 g), yeast extract (5 g), Murashige & Skoog salts (4.3 g) deionized water (1 L)) could be back-subtracted during metabolomics data processing[31] Mycelium and broth were then separated and extracted separately in 15 mL of ethyl acetate (in 125 mL Erlenmeyer flasks) shaking at 200 rpm at room temperature for 1 h. Solvent extracts were decanted, evaporated and then re-suspended in 1.5 mL MeOH and transferred into HPLC vials for UPLC-HRMS profiling.

Chemical profiling was completed using a Thermo Ultimate 3000 UPLC coupled to a Thermo LTQ Orbitrap XL HRMS and an UltiMate Corona VeoRS charged aerosol detector (Thermo Fisher Scientific Inc, Waltham, MS, USA). Chromatography was performed on a Phenomenex Kinetex 1.7 µm C_{18} column (50 × 2.1 mm, 100 Å) with a flow rate of 0.35 mL/min, using a mobile phase of H2O + 0.1 % formic acid (solvent A) and ACN + 0.1% formic acid (solvent B). The column was held at 5 % B for 0.5 min, ramped up to 95 % B over 4.5 min and held at 95 % B for 3.5 min. The mobile phase returned to 5% B over 1 min and was left to equilibrate for 3 min before the next injection. The HRMS was operated in positive electrospray ionization (ESI^+) mode with a 100–2000 *m/z* range and resolution of 30,000 using the following parameters: sheath gas flow 40, auxiliary gas flow 5, sweep gas flow 2, spray voltage 4.2 kV, capillary temperature 320 °C, capillary voltage 35 V, tube lens 100 V, AGC target 5E5 and maximum ion time 500 ms. All samples were injected in a randomized order and MeOH blanks were injected every six samples

in the sample sequence to assess for metabolite carry over and background subtraction during metabolomics data processing. Additionally, methanol solutions of synthesized metabolite standards for fusahexin, dihydrofusahexin, and prefusahexin were prepared to a concentration of 500 µg/mL, and, additionally, dihydrofusahexin and prefusahexin were independently spiked into aliquots of WT F. graminearum culture extract at ratios of 1:100 and 1:10 (v:v), for UPLC-HRMS profiling.

Metabolomics data pre-processing, data reduction, and statistical analysis were performed according to[31]. Pre-processing of the UPLC-HRMS raw data files was completed using MzMine 2.53[32] with previously reported data pre-processing parameters (Hicks et al., 2023). UPLC-HRMS profiles of both broth and mycelium extracts were processed together; all data were compiled into a representative matrix of metabolite mass features denoted with a retention time (RT) and mass to charge ratio (*m/z*). Exported pre-processed data matrices of mass feature peak height intensities were imported into R Studio for data processing, reduction and statistical analysis in the R environment[33]. To faciltate data comparison of the WT and *ΔNRPS4* strain culture extract profiles in the pre-processed data matrix, individual sample replicates were normalized to the total ion current by sample sums. Univariate analysis was completed using the 'MUMA' R package which utilizes both Welch's T tests and Wilcoxon-Mann Whitney U tests for normally and non-normally distribution mass features respectively based on Shapiro scores when determining p-values[34]. Visual inspection of the .RAW datafiles was performed to confirm metabolomics results using Thermo Xcalibur software with a ±5 ppm tolerance on the predicted exact mass.

Supplemental Tables

Table 5.S1. Primers used in the amplification of the hygromycin repair cassette. Sequences in yellow and green represent regions homologous to the pRF-HU2 vector downstream and upstream to the hygromycin resistance gene (hph) respectively. Sequences in black are homologous to the *F. graminearum* genome adjacent to intended Cas-9 cut sites.

Location	Primer Sequence 5'-3'
DOWN	AATAAAATGGTAAAATATCAGGAAAACATAACTAAAAACACGCCCGACAACTATTCCTTTGCCCTCGGAC
UP	GTCCGTTCGAACTGCGTTCCGCCGTTCTTTTTTGCAAAGTACAACATCGAATCGACAGAAGATGATATTGA

Table 5.S2. crRNA primer sequences used in the assembly of Cas-9 ribonucleoproteins.

Gene	crRNA Name	Sequence
FGSG_02315	02315gRNA-down1	ACUAAAAACACGCCCGACAAGUUUUAGAGCUAUGCU
	02315gRNA-up1	UUCGUCGUCGUGAUACAGUUGUUUUAGAGCUAUGCU

Table 5.S3. Internal primers used for the confirmation of the absence of *NRPS4* (FGSG_02315) and hygromycin (Hyg*) insertion cassette in the generated transformant strains.

Gene	Direction	Nt Count	Temp (°C)	Primer Sequence 5' - 3'	Amplicon Size (bp)
FGSG_02315	F1	20	57.5	TTCTCTCCGAAAACCTGCCG	545
	R1	20	57.1	GAGCTGGCTTTGGTTGAAGC	
Hyg*	F1	23	61.3	AGCTGCGCCGATGGTTTCTACAA	588
	R1	22	62.3	GCGCGTCTGCTGCTCCATACAA	

Supplemental Figures

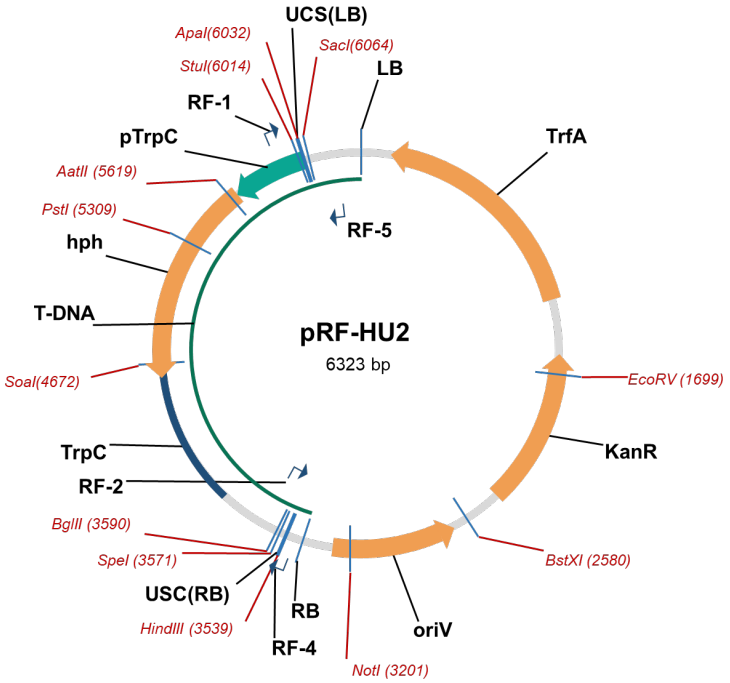


Figure 5.S1. pRF-HU2 vector map illustrating location of pTrpC and hph regions used in construction of Hygromycin repair templates.

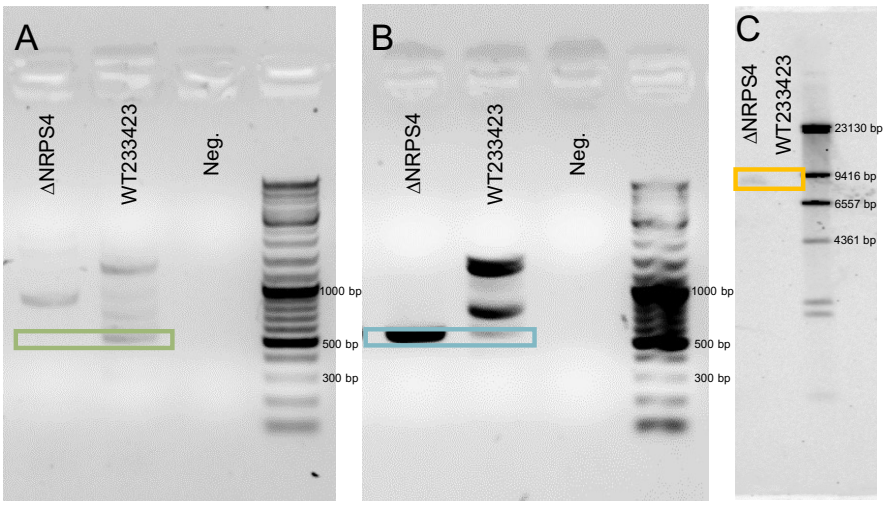


Figure 5.S2. Validation of knock out of *NRPS4* gene (FGSG_02315) and insertion of hygromycin resistance cassette in ΔNRPS4 strain. A) Gel electrophoresis of PCR amplification products using

primers internal to the *NRPS4* gene confirming gene presence in WT *F. graminearum* and absence of PCR product from ΔNRPS4 strain. B) Gel electrophoresis of PCR amplification products using primers internal to the hygromycin resistance gene confirming gene presence in ΔNRPS4 strain and absence of PCR product from WT *F. graminearum* strain. C) Southern blot analysis of ΔNRPS4 and WT *F. graminearum* strains with hybridization probe specific of the *hph* gene (expected fragment size of 8278 bp following DNA digest using Kpnl enzyme).

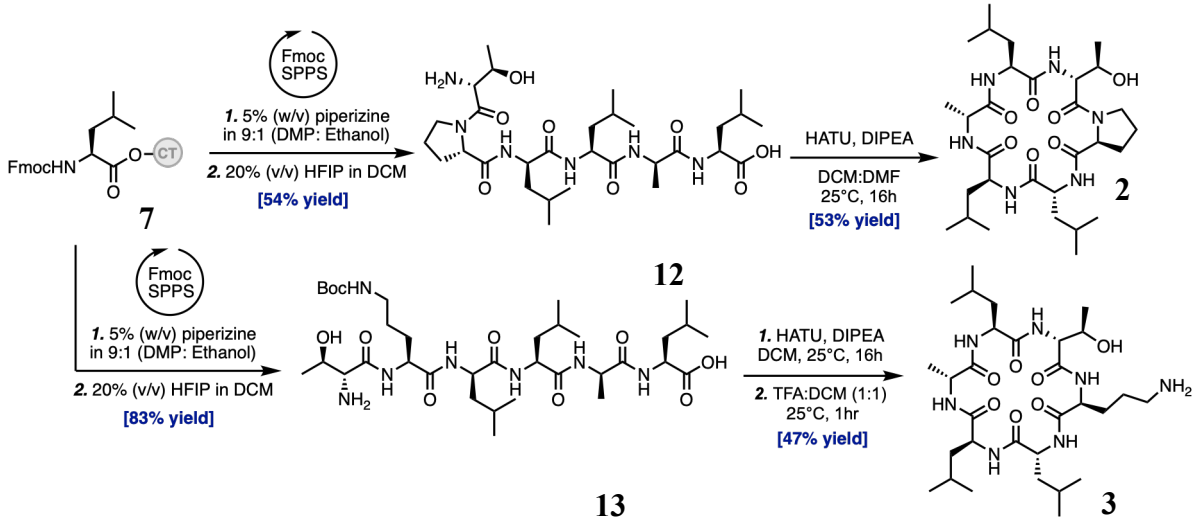
Chemical Material and Methods

General Experimental Procedures:

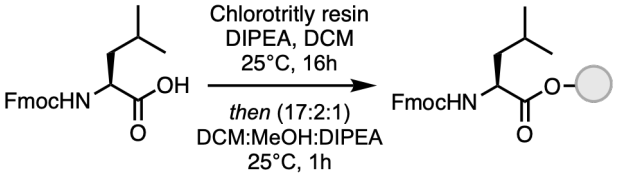
Solvents were purchased from Fisher Scientific. EDC-HCl, HATU and DIPEA were purchased from Oakwood Chemical (Estill, SC, USA), and all other chemicals were purchased from Sigma-Aldrich (Oakville, ON, Canada or Milwaukee,WI, USA). Reagents were all used without further purification unless otherwise specified. Reactions were carried out with dry solvents and under nitrogen atmosphere unless specified otherwise. Unless otherwise noted, solution-phase reactions were heated using conventional external heating (oil bath), and automated solid-phase peptide synthesis steps were conducted using microwave heating on a CEM Liberty Blue peptide synthesizer. Analytical thin layer chromatography (TLC) was carried out using commercially available 0.2mm aluminum-backed silica gel plates. Visualization was accomplished with UV light followed by dipping in CAM, Ninhydrin, Bromocresol green, Cerium sulfate, or $KMnO_4$ stain solution followed by heating when required. Reactions were monitored by LCMS using a Shimadzu LC20A HPLC coupled with a Shimadzu LCMS2020 single quad mass spectrometer with an ESI source, using a 5%-to-95% MeOH in Acetonitrile with 0.05% formic acid gradient over 15 min, unless otherwise specified. NMR spectroscopy was performed with either a Bruker Avance II operating at 400 MHz for ^{1}H and 100 MHz for ^{13}C spectra or a Bruker Avance III with a cryoprobe operating at 600 MHz for ^{1}H and 150 MHz for ^{13}C spectra. The chemical shifts are reported in parts per million (ppm) and were referenced to the residual solvent signal. High-resolution mass spectroscopy (HRMS) was conducted on a Micromass QTOF I (John L. Holmes Mass Spectroscopy Facility, Ottawa, ON, Canada). Structural assignments were made with additional information from gCOSY, gHSQC, and gHMBC experiments

Synthetic Procedures:

Supplemental Schemes

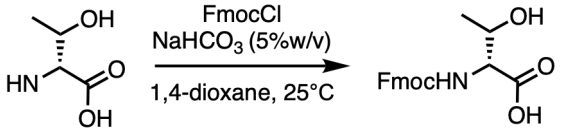


Scheme 5.S1. Synthesis of dihydrofusahexin (**2**), and prefusahexin (**3**).



Fmoc-L-leucine-O-Trt resin (7): 2-chlorotritryl chloride resin (1.0 g, 200-400 mesh, 0.4 mmol/g) in a fritted peptide vessel was added DCM (10 mL), allowing the resin to swell at room temperature for 30 min. Fmoc-L-Leu-OH (424 mg, 1.2 mmol, 1.2 eq) and DIPEA (0.85 mL, 4.8 mmol, 4.0 eq) were added to the solution, the vessel was agitated uncapped for 20 s and later capped and agitated overnight. The solution as flushed and washed with DCM (15 mL × 4). A capping solution of DCM:MeOH:DIPEA (17:2:1) was added to the vessel and agitated for 30 min. The solution was flushed, washed with DCM (15 mL × 4) and transferred to a round bottom flask to be dried under reduced pressure. The loading rate was determined with 2% DBU solution and spectrometric

analysis (Sigma-Aldrich, Fmoc Loading Test) to afford Fmoc-L-leucine-TrtCl resin with a loading rate of 0.8 mmol/g.

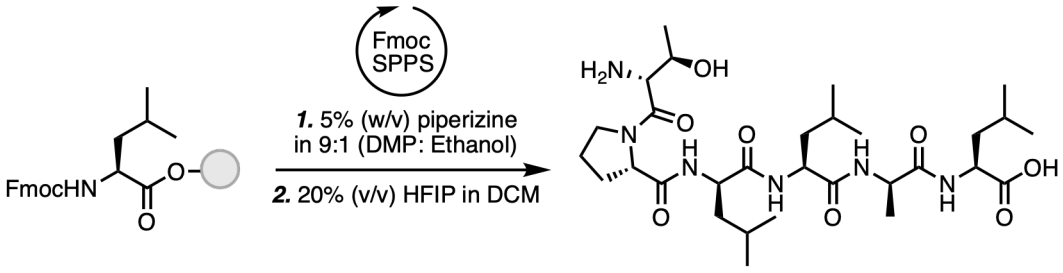


(((9H-fluoren-9-yl)methoxy)carbonyl)-D-*allo*-threonine (11): A flask was charged with commercially available D-*allo*-Thr-OH (1.0 g, 7.45 mmol, 1.0 eq) dissolved in 37 mL of a 5% (w/v) solution of $NaHCO_3$. To this stirring suspension, a solution of 9-Fluorenylmethoxycarbonyl chloride dissolved in 37 mL of 1,4-dioxane was added, and the mixture was left to stir at room temperature overnight. Upon completion, the aqueous layer was washed with 20 mL of diethyl ether and acidified to a pH of 2.0 with (1M) HCl. The aqueous layer was then extracted di ethyl ether (2 × 20mL), the organic layers were combined, washed with brine (1 × 20 mL), dried over $MgSO_4$, filtered, and concentrated under reduced pressure to afford Fmoc-D-*allo*-Thr-OH as a white powder (2.6 g, 7.3 mmol, 98% yield).

^{1}H NMR (600 MHz, MeOD) δ 7.80 (d, *J* = 7.6 Hz, 2H), 7.69 (dd, *J* = 7.4, 5.3 Hz, 2H), 7.41 – 7.37 (m, 2H), 7.31 (tt, *J* = 7.5, 1.1 Hz, 2H), 4.37 (qd, *J* = 10.6, 7.0 Hz, 2H), 4.27 – 4.21 (m, 2H), 4.09 (p, *J* = 6.3 Hz, 1H), 1.23 (d, *J* = 6.5 Hz, 3H).

^{13}C NMR (151 MHz, MeOD) δ 173.9, 158.7, 145.3, 145.2, 142.6, 128.8 (2C), 128.2, 126.3, 126.3, 120.9, 68.9, 68.1, 61.3, 48.4, 19.4.

HRMS (ESI-TOF) m/z: [M+Na]+ Calcd for $C_{19}H_{19}NO_5Na$ 364.1161; Found: 364.1183



D-*allo*-threonyl-L-prolyl-D-leucyl-L-leucyl-D-alanyl-L-leucine (12): Automated peptide synthesis was performed on a CEM liberty Blue peptide synthesizer at a 0.1 mmol scale. 0.125 g of Fmoc-L-leucine-2-TrtCl resin (resin loading rate of 0.8 mmol/g) was placed in the reaction vessel and the resin was allowed to swell in DMF for 5 min. Coupling cycles were programmed

at 50°C for 10 min with Fmoc-protected amino acids (0.2 M in DMF), HBTU (0.5 M in DMF) and DIPEA (2.0 M in DMF). Successive Fmoc deprotections were programmed at 50°C for 5 min using a solution of 20% piperazine (5% (w/v) in 9:1 NMP:EtOH). Upon completion of the automated SPPS cycle, the resin was transferred to a fritted vessel and flushed with DCM (10ml × 3). A microcleavage was performed to confirm the substrate by LCMS: approximately 5 mg of resin was aliquoted into a vial containing a solution of TFA:DCM (1:1) and stirred gently for 5 min. The mixture was filtered through a cotton pad and concentrated for LCMS analysis.

Resin cleavage: To the peptide-bound resin in the fritted vessel, 15 mL of 20% HFIP in DMF (v/v) was added. The vessel was capped and left to shake gently at room temperature. Upon completion, the resin was washed with 5 × 10mL DCM into a round bottle flask and concentrated under reduced pressure to obtain a 34.1 mg (54% yield, 0.054 mmol) of a crude white precipitate that was confirmed by LCMS and used in the next step without further purification (**Figure 5.S3**).
MS (ESI) m/z: [M + H]+ Calcd for C30H55N6O8 626.41; Found 626.60.

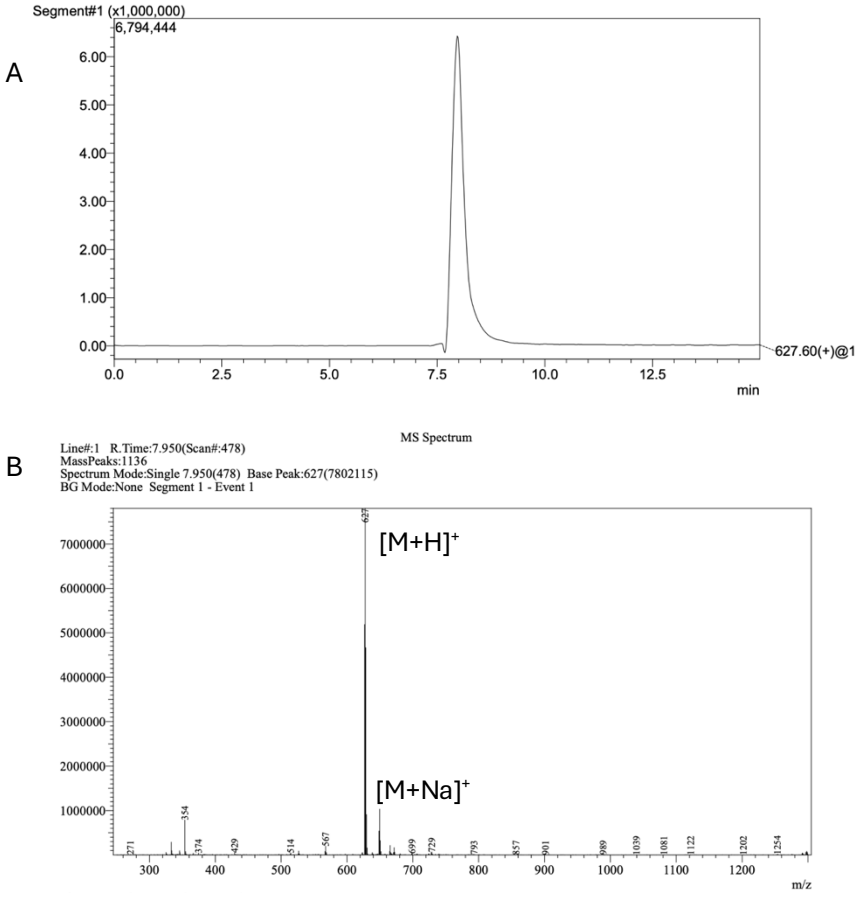
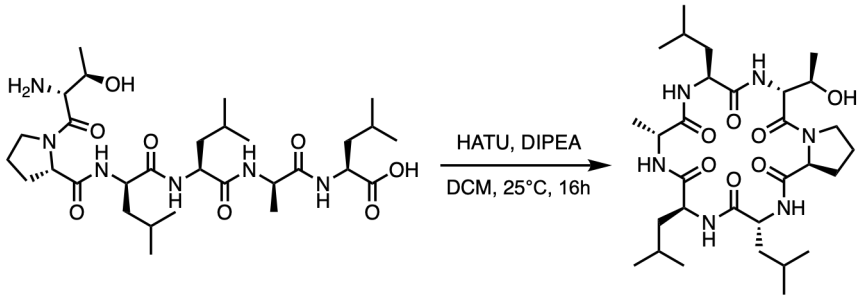


Figure 5.S3. (A) extraction ion chromatogram (EIC) and (B) mass spectrum (MS), indicating $[M+H]^+$ and $[M+Na]^+$ of intermediate **12.**

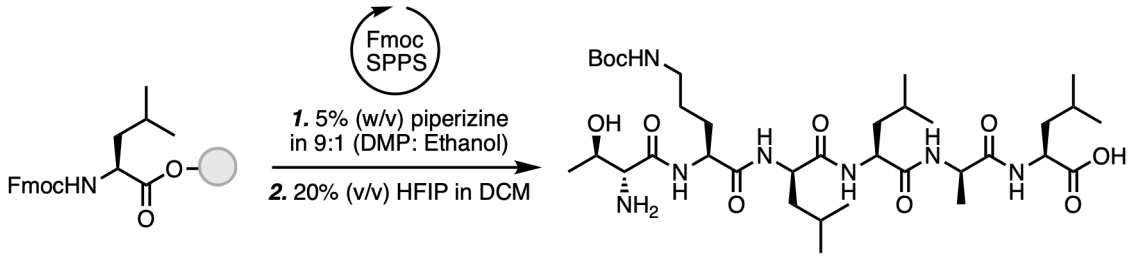


***cyclo*(L-leucyl-D-alanyl-L-leucyl-D-*allo*-threonyl-L-prolyl-D-leucine), Dihydrofusaxin (2):** Linear compound **6** (34.1 mg, 0.054 mmol,1.0 eq) was dissolved in DCM:DMF (5.4 mL) and HATU (62 mg, 0.163 mmol, 3.0 eq) and DIPEA (0.08 mL, 0.49 mmol, 9.0 eq) was added dropwise. The mixture was left to stir overnight at room temperature. Once complete, the mixture was concentrated via rotary evaporation while residual DMF was removed by drying over a stream of $N_{2\,(g)}$. The resulting concentrated mixture was purified by semipreparative reversed-phase HPLC to afford 17.4 mg (53% yield), dihydroxyfusahexin as a white powder.

^{1}H NMR (600 MHz, DMSO): δ 8.28 (d, *J* = 8.4 Hz, 1H), 8.18 (d, *J* = 7.9 Hz, 1H), 8.10 (d, *J* = 7.5 Hz, 1H), 8.00 (d, *J* = 7.8 Hz, 1H), 7.85 (d, *J* = 7.9 Hz, 1H), 5.34 – 5.30 (m, 1H), 4.99 (d, *J* = 5.5 Hz, 1H), 4.42 (dd, *J* = 8.1, 2.0 Hz, 1H), 4.37 (dd, *J* = 9.8, 7.7 Hz, 2H), 4.30 (q, *J* = 7.2 Hz, 2H), 4.15 (ddd, *J* = 9.7, 7.5, 5.4 Hz, 1H), 3.80 (dt, *J* = 8.8, 5.9 Hz, 1H), 3.72 (q, *J* = 8.7 Hz, 1H), 3.59 (d, *J* = 10.6 Hz, 1H), 2.11 (d, *J* = 11.9 Hz, 1H), 2.02 – 1.96 (m, 4H), 1.85 (d, *J* = 7.3 Hz, 2H), 1.70 (dq, *J* = 11.9, 8.5 Hz, 1H), 1.54 (dd, *J* = 14.1, 7.2 Hz, 2H), 1.47 (d, *J* = 7.6 Hz, 2H), 1.13 (d, *J* = 6.9 Hz, 3H), 1.06 (d, *J* = 6.1 Hz, 3H), 0.89 – 0.85 (m, 9H), 0.84 – 0.80 (m, 9H).

^{13}C NMR (151 MHz, DMSO) δ 171.6, 171.4, 170.9, 170.8, 170.7, 170.4, 67.2, 59.0, 56.5, 51.1, 50.8, 50.6, 47.4, 47.0, 41.5, 40.9, 40.3, 27.5, 24.3, 24.3, 24.3, 24.2, 23.1, 22.6, 22.6, 22.5, 22.3, 21.4, 20.5, 17.3.

HRMS (ESI-TOF) m/z: [M+Na]+ Calcd for $C_{30}H_{52}N_6O_7Na$ 631.3795; Found: 631.3798



D-*allo*-threonyl-L-ornicyl(Boc)-D-leucyl-L-leucyl-D-alanyl-L-leucine (13): Automated peptide synthesis was performed on a CEM Liberty Blue peptide synthesizer at a 0.1 mmol scale. 0.125 g of Fmoc-L-leucine-2-TrtCl resin (resin loading rate of 0.8 mmol/g) was placed in the reaction vessel and the resin was allowed to swell in DMF for 5 min. Coupling cycles were programmed at 50°C for 10 min with Fmoc-protected amino acids (0.2 M in DMF), HBTU (0.5 M in DMF) and DIPEA (2.0 M in DMF). Successive Fmoc deprotections were programmed at 50°C for 5 min using a solution of 20% piperazine (5% (w/v) in 9:1 NMP:EtOH). Upon completion of the automated SPPS cycle, the resin was transferred to a fritted vessel and flushed with DCM (10ml × 3). A microcleavage was performed to confirm the substrate by LCMS: approximately 5 mg of resin was aliquoted into a vial containing a solution of 20% HFIP in DCM and stirred gently for 30 min. The mixture was filtered through a cotton pad and concentrated for LCMS analysis.

Resin cleavage: To the peptide-bound resin in the fritted vessel, 15 mL of 20% HFIP in DMF (v/v) was added. The vessel was capped and left to shake gently at room temperature. Upon completion, the resin was washed with 5 ×10 mL DCM into a round bottle flask and concentrated under reduced pressure to obtain a 62 mg (83% yield, 0.083 mmol) of a crude white precipitate that was confirmed by LCMS (**Figure 5.S4**) and used in the next step without further purification.
MS (ESI) m/z: [M + H]+ Calcd for C35H66N7O10 744.49; Found 744.70

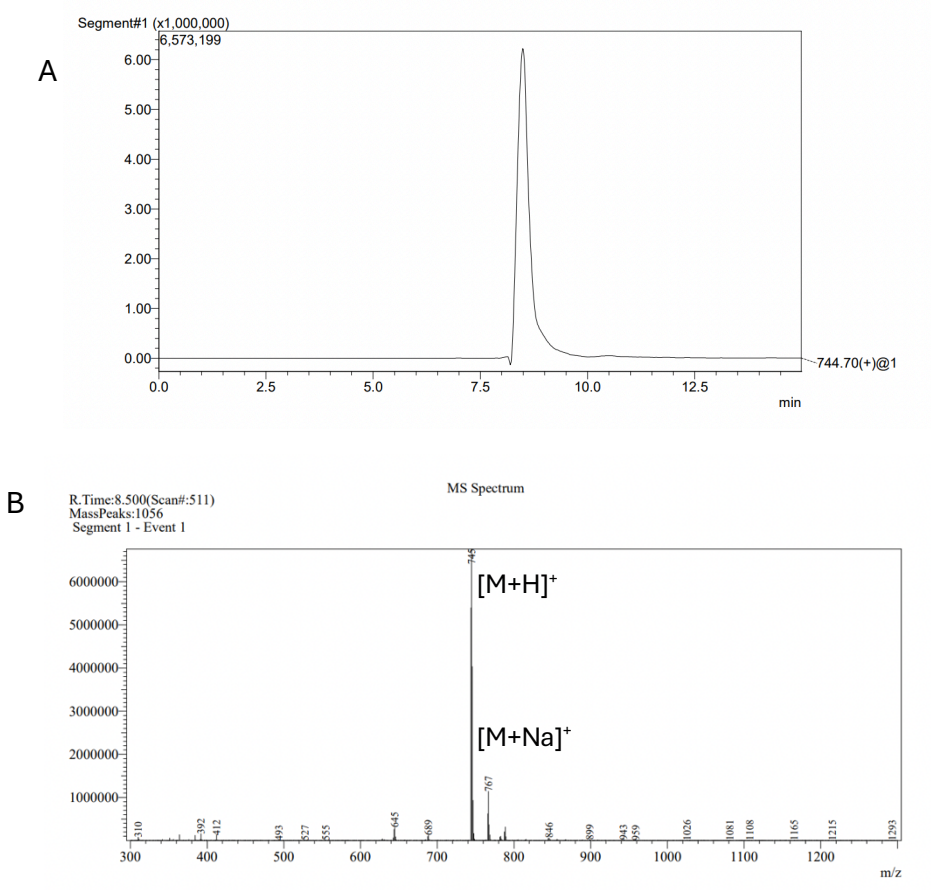
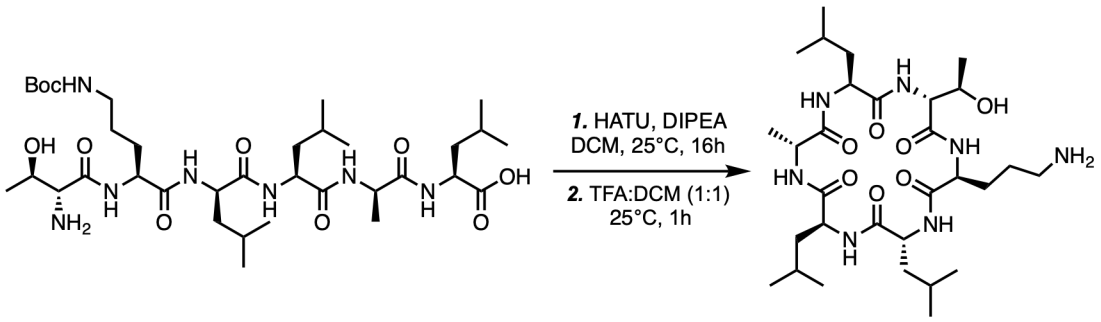


Figure 5.S4. (A) extraction ion chromatogram (EIC) and (B) mass spectrum (MS), indicating $M+H^+$ and $M+Na^+$ of intermediate **13.**



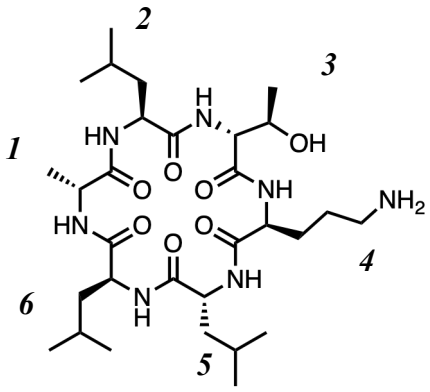
***cyclo*(L-leucyl-D-alanyl-L-leucyl-D-allothreonyl-L-ornicyl-D-leucine), Prefusahexin (3):** Linear D-allothreonyl-L-ornicyl(Boc)-D-leucyl-L-leucyl-D-alanyl-L-leucine. (62.0 mg, 0.083 mmol ,1.0 eq) was dissolved in DCM:DMF (8.3 mL) and HATU (95.0 mg, 0.23 mmol, 3.0 eq) and DIPEA (0.13 mL, 0.75 mmol, 9.0 eq) was added dropwise. The mixture was left to stir

overnight at room temperature. Once complete, the mixture was concentrated via rotary evaporation while residual DMF was removed by drying over a stream of $N_{2\,(g)}$. To the resulting concentrated mixture, 1% TFA in 1:4 ACN:H_2O was added, the suspension was sonicated for 10 min followed by centrifugation at 5000 RPM, 0°C for 40 min. The supernatant was discarded and the pellet was resuspended in the same 1% TFA in 1:4 ACN:H_2O by sonication. This process was repeated at least 3 times or until the supernatant appeared clear resulting in 40.5 mg (0.056 mmol, 67% yield) of macrocyclic product. The final product was obtained after deprotection, achieved via the suspension of the intermediate macrocycle in 0.2 mL DCM, followed dropwise addition of 0.2 mL TFA. The suspension of stirred at room temperature for 1h and concentrated under reduced pressure to reveal 25.1 mg (0.04 mmol, 47% yield) prefusahexin as a pale-yellow powder without the need for further purification.

^{1}H NMR (600 MHz, DMSO): δ 8.23 (d, *J* = 8.3 Hz, 1H), 8.12 (d, *J* = 8.5 Hz, 1H), 8.08 (d, *J* = 8.7 Hz, 1H), 8.05 (d, *J* = 7.9 Hz, 1H), 7.87 (d, *J* = 7.3 Hz, 1H), 7.75 (d, *J* = 8.3 Hz, 1H), 7.62 (s, 2H), 4.37 (dq, *J* = 15.2, 7.6 Hz, 2H), 4.27 (tdd, *J* = 14.0, 8.4, 5.9 Hz, 3H), 4.11 (t, *J* = 8.3 Hz, 1H), 3.83 (p, *J* = 6.5 Hz, 1H), 2.77 (t, *J* = 6.9 Hz, 2H), 1.65 – 1.61 (m, 1H), 1.55 – 1.45 (m, 14H), 1.13 (d, *J* = 6.8 Hz, 3H), 1.03 (d, *J* = 6.3 Hz, 3H), 0.87 (d, *J* = 2.3 Hz, 9H), 0.82 (d, *J* = 7.0 Hz, 9H).

^{13}C NMR (151 MHz, DMSO) δ171.4 (2C), 171.3, 170.9, 170.3, 169.9, 66.3, 58.1, 51.2, 50.8, 50.5, 50.2, 47.8, 41.0, 40.2, 40.1, 38.6, 29.0, 24.3, 24.3, 24.2, 23.3, 23.1, 22.8 (2C), 22.2, 22.1, 21.6, 20.2, 18.5

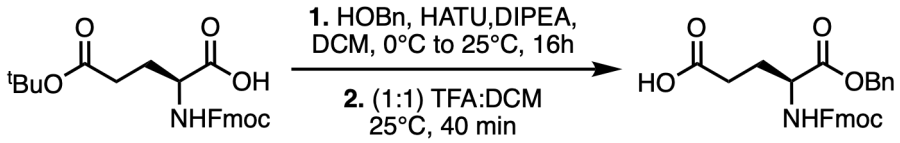
HRMS (ESI-TOF) m/z: [M+H]+ Calcd for $C_{30}H_{56}N_7O_7$ 626.4241; Found: 626.4240.



amino acid	position	δC	δH
1 (D-Ala)	-NH		7.87 (d, J = 7.3 Hz)
	α-CH	47.7	4.27 (tdd, J = 14.0, 8.4, 6.0 Hz)[a]
	β-CH3	18.5	1.13 (d, J = 6.9 Hz)
	C=O	171.4	
2 (L-Leu)	-NH		
	α-CH	50.7	4.27 (tdd, J = 14.0, 8.4, 6.0 Hz)[a]
	β-CH2	40.2	1.55 – 1.45 (m)[c]
	γ-CH	24.2-24.3[f]	1.55 – 1.45 (m)[c]
	d-CH	23.3, 22.7-21.6[g]	0.87 (d, *J* = 2.3 Hz)[d], 0.82 (d, *J* = 7.0 Hz)[e]
	C=O	171.3	
3 (D-alloThr)	-NH		8.08 (d, J = 8.7 Hz)
	α-CH	58.1	4.09 (t, J = 8.3 Hz)
	β-CH	66.3	3.83 (p, J = 6.5 Hz)
	γ-CH3	20.2	1.02 (d, J = 6.2 Hz)
	C=O	169.9	
4 (L-Orn)	-NH		7.75 (d, J = 8.2 Hz)
	α-CH	51.17	4.37 (dq, *J* = 15.2, 7.6 Hz)[b]
	β-CH2	23.0	1.55 – 1.45 (m)[c]
	y-CH2	29.0	1.65 – 1.61 (m), 1.55 – 1.45 (m)[c]
	d-CH2	38.6	2.77 (dd, J = 10.0, 4.2 Hz)f
	-NH2		7.62 (s)
	C=O	170.2	
5 (D-Leu)	-NH		8.12 (d, *J* = 8.5 Hz)
	α-CH	50.4	4.37 (dq, *J* = 15.2, 7.6 Hz)[b]
	β-CH2	41.0	1.55 – 1.45 (m)[c]
	γ-CH	24.2-24.3[f]	1.55 – 1.45 (m)[c]

			0.87 (d, *J* = 2.3 Hz)[d],
	d-CH	23.3, 22.7-21.6[g]	0.82 (d, *J* = 7.0 Hz)[e]
	C=O	171.4	
	-NH		8.23 (d, *J* = 8.3 Hz)
	α-CH	50.1	4.27 (tdd, J = 14.0, 8.4, 6.0 Hz)[a]
	β-CH2	40.1	1.55 – 1.45 (m)[c]
6 (L-Leu)	γ-CH	24.2-24.3[f]	1.55 – 1.45 (m)[c]
			0.87 (d, *J* = 2.3 Hz)[d],
	d-CH	23.3, 22.7-21.6[g]	0.82 (d, *J* = 7.0 Hz)[e]
	C=O	170.8	

Table 5.S4. Complete spectroscopic characterization of prefusahexin (**3**) displaying tabulated ^{1}H and ^{13}C chemical shifts in DMSO-d_6 (^{1}H 600 MHz, ^{13}C 151 MHz).
[a-g]Overlapping or partially overlapping signals .



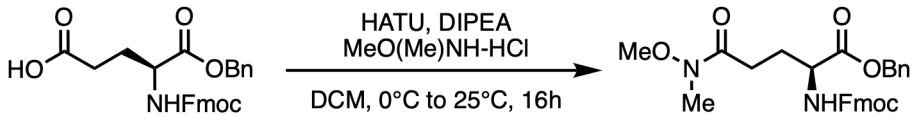
(*S*)-4-((((9H-fluoren-9-yl)methoxy)carbonyl)amino)-5-(benzyloxy)-5-oxopentanoic acid (4): A flame-dried flask equipped with a Teflon-coated magnetic stir bar and flushed with $N_{2(g)}$ was charged with Fmoc-Glu(OtBu)-OH (2.0 g, 4.7 mmol, 1.2 eq), HATU (1.7 g, 4.7 mmol, 1.2 eq) in 50 mL of DCM at 0°C. To this stirring solution, DIPEA (1.3 mL, 7.83 mmol, 2.0 eq) was added dropwise and stirring was continued for 15-20 min after which by Benzyl alcohol (0.41 mL, 3.91 mmol, 1.0 eq) was added. The reaction was left to warm to room temperature and stir overnight. Once complete, the stirring mixture was washed with (1M) HCl, saturated $NaHCO_3$, and brine, dried over $MgSO_4$, filtered, and concentrated under reduced pressure to afford the crude oil. Purification was achieved by silica gel flash chromatography (20% EtOAc in Hex) to yield 1.76 g (3.22 mmol, 73% yield) of pure product as a white powder. To a stirring suspension of the benzyl ester product (1.24 g, 2.4 mmol, 1.0 eq) in 12 mL DCM, equal volumes of TFA was added dropwise. The reaction was purged with $N_{2(g)}$ and left to stir for 40 min. Upon completion, the volatiles were removed under reduced pressure to afford 1.04 g (2.26 mmol, 94% yield) of sufficiently pure crude product **4**, isolated as a white powder which was used in the next step without further purification.

TLC (40%EtOAc in Hexane): Rf = 0.26

^{1}H NMR (600 MHz, $CDCl_3$) δ 7.76 (d, *J* = 7.6 Hz, 2H), 7.58 (d, *J* = 7.5 Hz, 2H), 7.40 – 7.37 (m, 2H), 7.36 – 7.29 (m, 7H), 5.47 (d, *J* = 8.2 Hz, 1H), 5.18 (s, 2H), 4.47 (td, *J* = 8.3, 5.1 Hz, 1H), 4.41 (q, *J* = 8.5 Hz, 2H), 4.20 (t, *J* = 7.1 Hz, 1H), 2.47 – 2.32 (m, 2H), 2.23 (dq, *J* = 13.8, 6.9 Hz, 1H), 2.02 – 1.93 (m, 1H).

^{13}C NMR (151 MHz, $CDCl_3$) δ 177.2, 171.7, 156.1, 143.7, 141.3, 141.3, 135.0, 128.7, 128.6, 128.4, 127.8, 127.1, 125.1, 125.1, 120.0, 120.0, 67.6, 67.2, 53.3, 47.2, 29.7, 27.5.

HRMS (ESI-TOF) m/z: [M+H]+ Calcd for $C_{27}H_{26}NO_6$ 460.1760; Found: 460.1790.



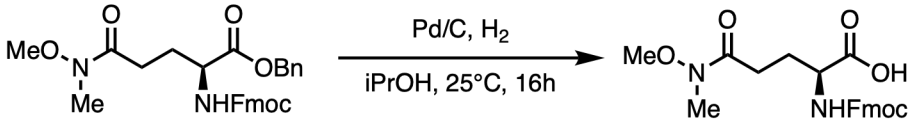
Benzyl N2-(((9H-fluoren-9-yl)methoxy)carbonyl)-N5-methoxy-N5-methyl-L-glutaminate (5): A flame-dried flask equipped with a Teflon-coated magnetic stir bar and flushed with $N_{2(g)}$ was charged with **4** (1.04 g, 2.26 mmol, 1.0 eq), HATU (1.28 g, 3.38 mmol, 1.5 eq) and 11.3 mL of DCM at 0°C. To this stirring solution, DIPEA (1.57 mL, 9.02 mmol, 4.0 eq) was added dropwise and stirring was continued for 15-20 min after which NH(Me)OM-HCl (329.0 mg, 3.38 mmol, 1.5 eq) was added. The reaction was left to warm to room temperature and stir overnight. Once complete, the stirring mixture was washed with (1M) HCl, saturated $NaHCO_3$, and brine, dried over $MgSO_4$, filtered, and concentrated under reduced pressure to afford the crude oil. Purification was achieved by silica gel flash chromatography (40% EtOAc in Hex) to yield 0.84 g (1.66 mol, 74% yield) of pure product **5** isolated as a white powder.

TLC (40%EtOAc in Hexane): Rf = 0.43

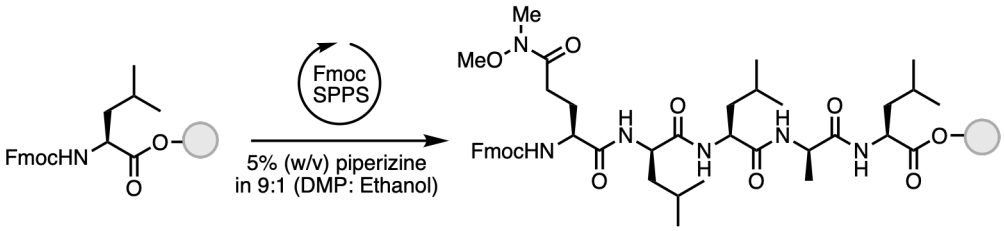
^{1}H NMR (600 MHz, CDCl3) δ 7.76 (d, J = 7.6 Hz, 2H), 7.60 (t, J = 8.3 Hz, 2H), 7.42 – 7.28 (m, 9H), 5.78 (d, J = 8.0 Hz, 1H), 5.25 – 5.12 (m, 2H), 4.45 (q, J = 7.4 Hz, 1H), 4.42 – 4.37 (m, 1H), 4.33 (t, J = 9.1 Hz, 1H), 4.22 (t, J = 7.3 Hz, 1H), 3.59 (s, 3H), 3.16 (s, 3H), 2.62 – 2.43 (m, 2H), 2.25 (dq, J = 13.4, 6.4 Hz, 1H), 2.09 (dq, J = 14.8, 7.7 Hz, 1H).

^{13}C NMR (151 MHz, CDCl3) δ 173.5, 172.1, 156.2, 144.1, 143.9, 141.4, 141.4, 135.5, 128.8, 128.6, 128.4, 127.8, 127.8, 127.2, 127.2, 125.4, 125.36, 120.1, 67.4, 67.3, 61.3, 54.1, 47.3, 32.4, 28.1, 26.8.

HRMS (ESI-TOF) m/z: [M+H]+ Calcd for $C_{29}H_{31}N_2O_6$ 503.2182; Found: 503.2202.



N2-(((9H-fluoren-9-yl)methoxy)carbonyl)-N5-methoxy-N5-methyl-L-glutamine (6): A flame-dried flask equipped with a Teflon-coated magnetic stir bar and flushed with $N_{2(g)}$ was charged with benzyl N2-(((9H-fluoren-9-yl)methoxy)carbonyl)-N5-methoxy-N5-methyl-L-glutaminate (0.84 g, 1.66 mmol, 1.0 eq), 8.3 mL of iPrOH and Pd/C (10% by weight) (17.6 mg, 0.17 mmol, 0.1 eq). A stream of $H_{2(g)}$ was bubbled in the stirring mixture for at least 10 min before the flask was sealed and left to stir in an $H_{2(g)}$ atmosphere overnight. Upon completion, the mixture was passed directly through a celite and washed with isopropanol. The combined filtrate was concentrated under reduced pressure to afford 0.547 mg (1.33 mmol, 80% yield) of crude product **6**, isolated as a white powder that was sufficiently pure to use in the next step without purification.
^{1}H NMR (400 MHz, $CDCl_3$) δ 7.76 (d, *J* = 7.6 Hz, 2H), 7.60 (t, *J* = 6.8 Hz, 2H), 7.40 (t, *J* = 7.5 Hz, 2H), 7.31 (t, *J* = 7.3 Hz, 2H), 6.06 (d, *J* = 6.6 Hz, 1H), 4.44 – 4.28 (m, 3H), 4.22 (t, *J* = 7.2 Hz, 1H), 3.70 (s, 3H), 3.23 (s, 3H), 2.95 (m, 1H), 2.66 (m, 1H), 2.27 (m, 1H), 2.06 (m, 1H).
^{13}C NMR (101 MHz, $CDCl_3$) δ 174.3, 174.1, 156.3, 143.9, 143.7, 141.3, 141.3, 127.8, 127.1, 125.2, 125.1, 120.00, 67.2, 61.4, 53.7, 47.1, 32.3, 28.5, 27.6.
HRMS (ESI-TOF) m/z: [M+H]+ Calcd for $C_{22}H_{25}N_2O_6$ 413.1713; Found 413.1725



***N*^{2}-(((9*H*-fluoren-9-yl)methoxy)carbonyl)-*N*^{5}-methoxy-*N*^{5}-methyl-L-glutaminyl-D-leucyl-L-leucyl-D-alanyl-L-leucine-TrtCl resin (8).** Automated peptide synthesis was performed on a CEM liberty Blue peptide synthesizer at a 0.1 mmol scale. 0.125 g of Fmoc-L-leucine-2-TrtCl resin (resin loading rate of 0.8 mmol/g) was placed in the reaction vessel and the resin was allowed to swell in DMF for 5 min. Coupling cycles were programmed at 50°C for 10 min with Fmoc-

protected amino acids (0.2 M in DMF), HBTU (0.5 M in DMF) and DIPEA (2.0 M in DMF). Successive Fmoc deprotections were programmed at 50°C for 5 min using a solution of 20% piperazine (5% (w/v) in 9:1 NMP:EtOH). Upon completion of the automated SPPS cycle, the resin was transferred to a fritted vessel and flushed with DCM (10mL × 3). A microcleavage was performed to confirm the substrate by LCMS: approximately 5.0 mg of resin was aliquoted into a vial containing a solution of 20% HFIP in DCM and stirred gently for 30 min. The mixture was filtered through a cotton pad and concentrated for LCMS analysis (**Figure 5.S5**) .

MS (ESI) m/z: [M + H]+ Calcd for $C_{43}H_{63}N_6O_{10}$ 823.46; Found 823.60.

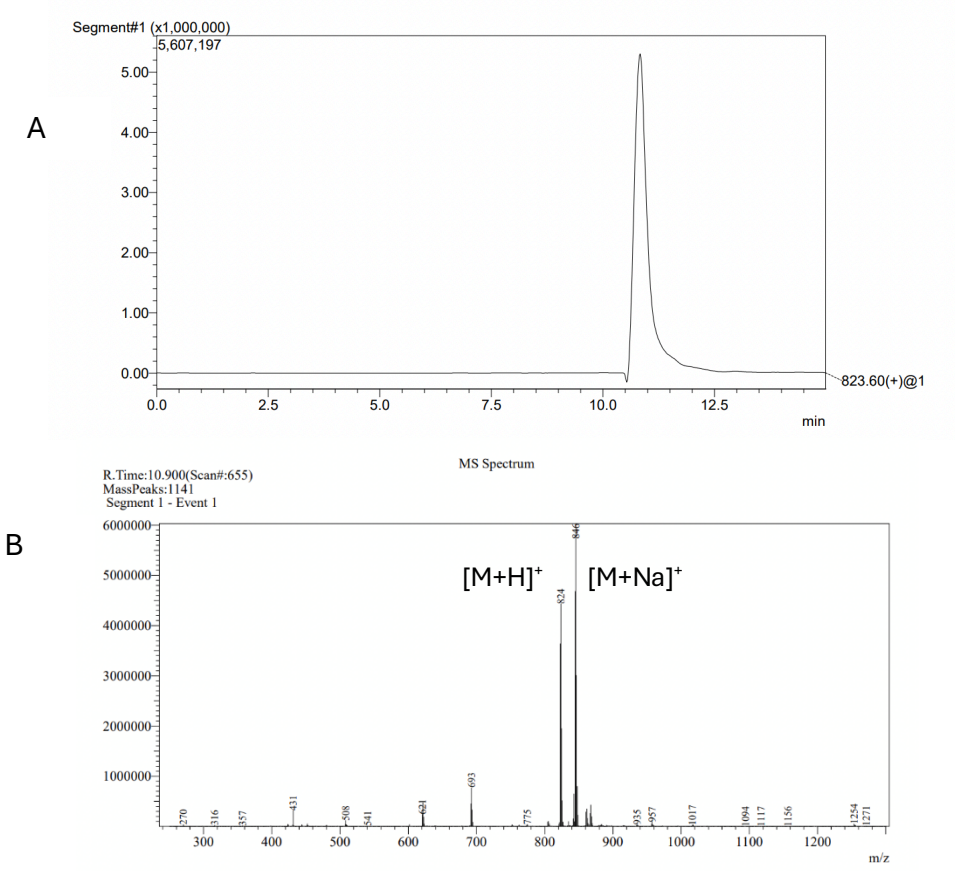
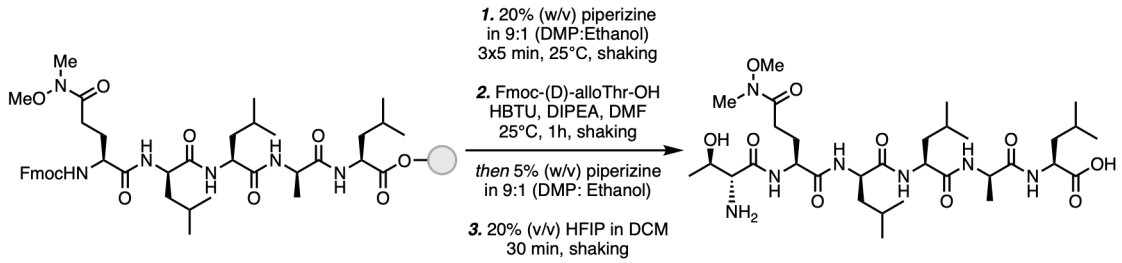


Figure 5.S5. (A) extraction ion chromatogram (EIC) and (B) mass spectrum (MS), indicating $[M+H]^+$ and $[M+Na]^+$ of intermediate **8** following a microcleavage, generating the free acid**.**



N^2-((((9*H*-fluoren-9-yl)methoxy)carbonyl)-D-*allo*-threonyl)-N^5-methoxy-N^5-methyl-L-glutaminyl-D-leucyl-L-leucyl-D-alanyl-L-leucine (9): Manual solid phase peptide synthesis was performed for the installation of the last amino acid on resin. To the fritted vessel charged with N^2-(((9H-fluoren-9-yl)methoxy)carbonyl)-N^5-methoxy-N^5-methyl-L-glutaminyl-D-leucyl-L-leucyl-D-alanyl-L-leucine-TrtCl resin, 5.0 mL of 20% 2-methylpiperidine in DMF (v/v) was added and left to shake gently for 5 min. This was repeated two more times before the resin was washed with 5 ×10 mL DCM. Following this, the fritted vessel was charged with N5-methoxy-N5-methyl-L-glutaminyl-D-leucyl-L-leucyl-D-alanyl-L-leucine-TrtCl resin, 6.0 mL of DMF, followed by 0.2 g (0.6 mmol, 6.0 eq) of (((9H-fluoren-9-yl)methoxy)carbonyl)-D-*allo*-threonine, 0.23 g (0.6 mmol, 6.0 eq) of HBTU and 0.35 mL (2.0 mmol, 20.0 eq)of DIPEA. The mixture was left to shake for 30 min at room temperature after which the fritted vessel was flushed with DCM (10 mL × 3). A microcleavage was performed to confirm the substrate by LCMS: approximately 5.0 mg of resin was aliquoted into a vial containing a solution of TFA:DCM and stirred gently 5 min. The mixture was filtered through a cotton pad and concentrated for LCMS analysis directly in the next step without further purification. To the peptide-bound resin in the fritted vessel charged with N^2-((((9*H*-fluoren-9-yl)methoxy)carbonyl)-D-allothreonyl)-N^5-methoxy-N^5-methyl-L-glutaminyl-D-leucyl-L-leucyl-D-alanyl-*L*-leucine-TrtCl resin, 5.0 mL of a deprotection cocktail (of 5% (w/v) piperazine in 9:1 (DMP:Ethanol)) was added and left to shake gently for 5 min. The solvent was expelled through the frit, and the procedure was repeated two more times for a total of three rounds od deprotection. Once complete, the resin was washed with 5 × 5 mL DCM. A 15 mL of the resin cleavage cocktail was prepared (20% HFIP in DCM) and applied to the resin in the fritted vessel. The vessel was left to shake gently at room temperature for 30 min. The contents of the vessel were drained directly into a round bottom flask and the resin was washed with 5 × 5 mL DCM directly into the flask. The crude linear peptide was concentrated under reduced pressure to afford

33.0 mg (0.047 mmol, 47% yield) of **9** as a white powder that was used directly in the next step without further purification after LCMS (**Figure 5.S6**).

MS (ESI) m/z: [M + H]+ Calcd for $C_{32}H_{60}N_7O_{10}$ 702.44; Found 702.30.

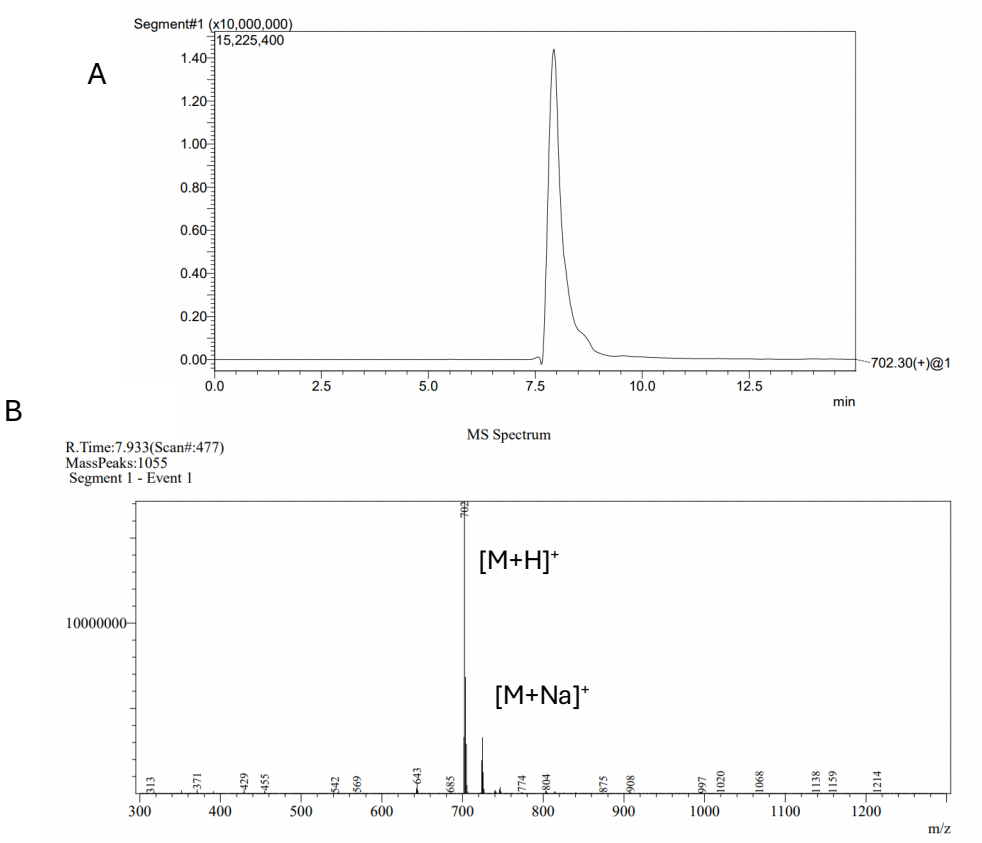
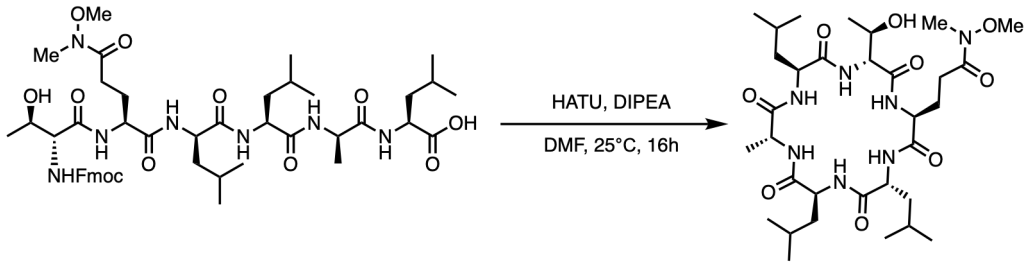


Figure 5.S6. (A) extraction ion chromatogram (EIC) and (B) mass spectrum (MS), indicating $[M+H]^+$ and $[M+Na]^+$ of intermediate **9.**



Cyclo(N^2-(D-*allo*-threonyl)-N^5-methoxy-N^5-methyl-L-glutaminyl-D-leucyl-L-leucyl-D-alanyl-L-leucine) (10): Linear N^2-(D-*allo*-threonyl)-N^5-methoxy-N^5-methyl-L-glutaminyl-D-leucyl-L-

leucyl-D-alanyl-L-leucine (120.0 mg, 0.171 mmol, 1.0 eq) was dissolved in DCM (6.8 mL) and HATU (194.0 mg, 0.51 mmol, 3.0 eq) and DIPEA (0.27 mL, 1.54 mmol, 9.0 eq) was added dropwise over 5 min. The mixture was left to stir overnight at room temperature. Once complete, the mixture was concentrated and 1%TFA in 1:4 ACN:H_2O was added. The suspension was sonicated for 10 min followed by centrifugation at 5000 RPM, 0° C for 40 min. The supernatant was discarded and the pellet was resuspended in the same 1% TFA in 1:4 ACN:H_2O by sonication. This process was repeated at least 3 times or until the supernatant appeared clear resulting in 51.0 mg (44% yield) of macrocyclic product. LCMS analysis confirmed isolation of desired product (**Figure 5.S7**). The product was used crude, without the need for further purification.

MS (ESI) m/z: [M + Na]+ Calcd for C32H57N7O9Na 706.41; Found 706.60.

HRMS (ESI-TOF) m/z: [M+H]+ Calcd for $C_{32}H_{58}N_7O_9$ 684.4296; Found: 684.4274.

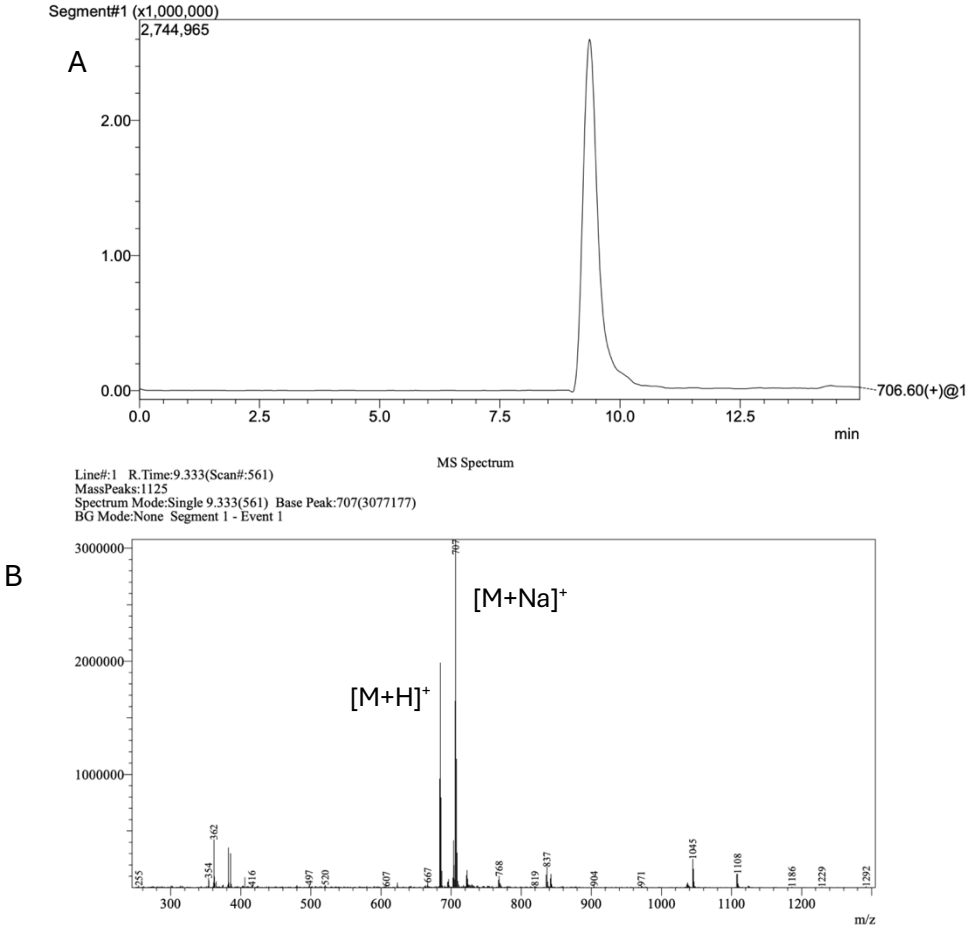
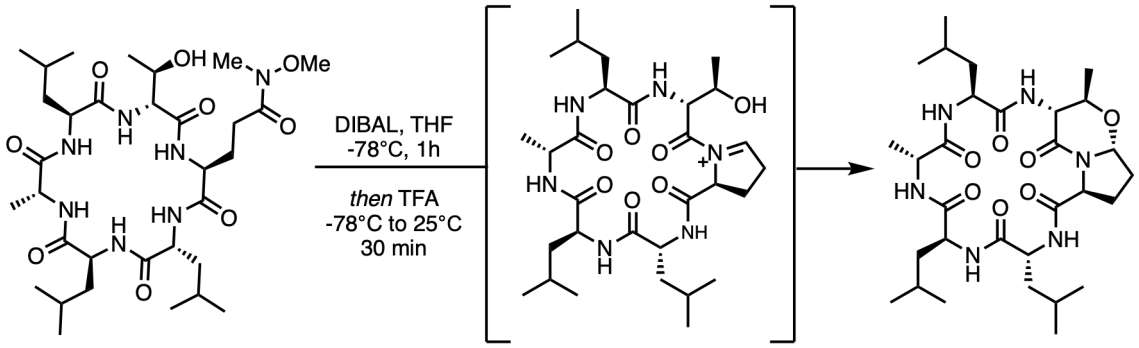


Figure 5.S7. (A) extraction ion chromatogram (EIC) and (B) mass spectrum (MS), indicating $[M+H]^+$ and $[M+Na]^+$ of intermediate **10.**



Fusahexin (1): A flame-dried round bottom flask equipped with a Teflon coated magnetic stir bar was charged with 3-((2*S*,5*R*,8*S*,11*R*,14*S*,17*R*)-17-((*R*)-1-hydroxyethyl)-5,8,14-triisobutyl-11-methyl-3,6,9,12,15,18-hexaoxo-1,4,7,10,13,16-hexaazacyclooctadecan-2-yl)-*N*-methoxy-*N*-methylpropanamide (1.4 mg, 0.002 mmol, 1.0 eq), and (0.04 mL) of dry THF. The suspension was cooled to -78°C and a solution of DIBAL (1M in Hex) (0.01 mL,0.006 mmol, 6.0 eq) was added dropwise. The reaction was left to stir for 1h at -78°C after which TFA was added dropwise. Following the addition, the reaction was removed from the cold bath and left to warm to room temperature over 30 min. Once complete, the volatiles were removed via rotary evaporation and the crude mixture was purified by semipreparative reverse-phase HPLC to afford the cyclic compound, fusahexin (1.2 mg, 77% yield). Spectroscopic data are in agreement with those previously reported[1,27]. Spectral overlay provided in **Fig 5.S16**).

^{1}H NMR (600 MHz, DMSO) δ 8.51 (d, J = 8.0 Hz, 1H), 8.00 (d, J = 8.5 Hz, 1H), 7.74 (d, J = 7.8 Hz, 1H), 7.71 (d, J = 8.6 Hz, 1H), 7.64 (d, J = 8.8 Hz, 1H), 5.51 (t, J = 6.0 Hz, 1H), 4.41 – 4.21 (m, 6H), 3.84 (p, J = 6.5 Hz, 1H), 2.34 (dd, J = 13.2, 6.7 Hz, 1H), 2.07 – 1.95 (m, 2H), 1.92 – 1.85 (m, 1H), 1.71 (dt, J = 12.5, 5.9 Hz, 1H), 1.58 – 1.45 (m, 6H), 1.37 (dt, J = 14.0, 7.0 Hz, 1H), 1.31 – 1.27 (m, 1H), 1.24 – 1.23 (m, 3H), 1.15 (d, J = 6.9 Hz, 3H), 0.88 (t, J = 5.7 Hz, 6H), 0.84 – 0.79 (m, 12H).

HRMS (ESI-TOF) m/z: [M+Na]+ Calcd for $C_{30}H_{50}N_6O_7Na$ 629.3639; Found 629.3647

Table 5.S5. Comparison of selected diagnostic ^{1}H NMR data for fusahexin (1). Selected diagnostic ^{1}H NMR signals are compared for isolated fusahexin[8], literature-reported synthetic fusahexin[7] and fusahexin synthesized in this work. Overlapping signals and exchangeable amide protons are excluded from the comparison. $\Delta\delta = \delta$(this work) − δ(isolated[8]).

Amino acid, position	δH (mult, J in Hz)			Δδ (ppm)
	Isolated*	Literature-reported synthetic**	This work	
Ala(1), β-CH_3	1.16 (d, 6.9)	1.15	1.15 (d, 6.9)	−0.01
Thr(3), β-H	3.85 (dq, 6.3, 8.6)	3.84	3.84 (p, 6.5)†	−0.01
Thr(3), γ-CH_3	1.25 (d, 6.3)	1.24	1.24–1.23 (m)†	−0.01 to −0.02
Pro(4), δ-CH	5.51	5.52	5.51 (t, 6.0)†	0.00

* Literature values of isolated fusahexin correspond to the assigned ^{1}H NMR data reported for fusahexin by Westpal et al. (600MHz, 308K, DMSO-d_6)[8]

** Literature synthetic values correspond to the assigned ^{1}H NMR data reported for synthetic fusahexin in by Bäuerlein et al. (600MHz, 310K, DMSO-d_6)[7]

† Apparent multiplicities in crowded regions may vary due to signal overlap; chemical shift is the primary basis for comparison.

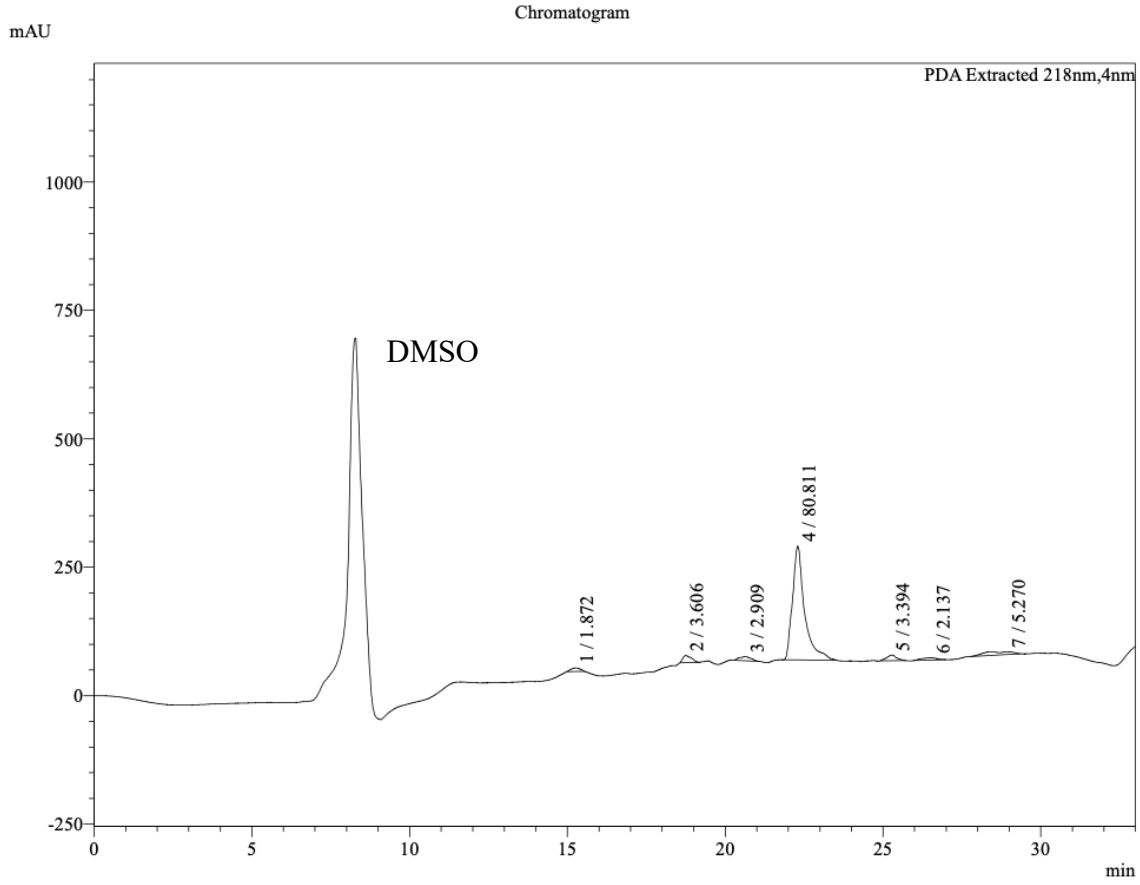


Figure 5.S8. *rp* HPLC chromatogram of fusahexin (**1**) (peak 4) ran at a flowrate of 10mL/min from 5%-95% (ACN in H2O) over 33 min, detected at 218 nm. Peak number / Area % over detected peaks.

For NMR spectra see **Section 5.8** (Appendix to Chapter V)

5.6 Future Directions and Preliminary Results

5.6.1 Identifying oxidative enzyme responsible for converting prefusahexin to fusahexin

The work presented in this chapter establishes prefusahexin (**5.3**) as the direct biosynthetic precursor to fusahexin (**5.1**) and implicates an oxidative transformation of the ornithine side chain primary amine as the key step generating the unique fused 6,5-bicyclic *N,O*-acetal.

However, the identity of the enzyme responsible for this oxidation remains unresolved. As discussed in the manuscript, analysis of the fusahexin biosynthetic gene cluster in *F. graminearum* did not reveal any candidate oxidase, suggesting that the responsible enzyme is non-clustered and that the fusahexin biosynthetic gene cluster represents a split cluster[14,15]. One hypothesis is that the insertion of the aurofusarin biosynthetic gene cluster at the 3′ end of *NRPS4* may have displaced the gene encoding this oxidase to a new genomic locus in *F. graminearum.*

A promising candidate class for this non-clustered oxidase that could convert prefusahexin

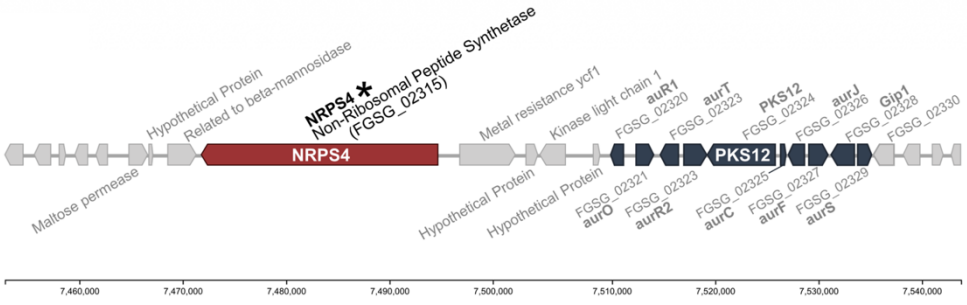


Figure 5.3 Biosynthetic gene cluster of fusahexin (**5.1**) in *F. graminearum*, showing the ajdacent aurofusarin (PKS12) biosynthetic gene cluster at the 3′ end of NRPS4. Adapted from Section 5.5. ref 14.

to fusahexin are the copper amino oxidases (CAOs). CAOs catalyze the oxidative deamination of primary amines to aldehydes using a topaquinone (TPQ) cofactors and molecular oxygen, generating hydrogen peroxide and ammonia as byproducts. The oxidation of the ornithine δ-amine of prefusahexin (**5.3**) to the corresponding δ-aldehyde by a CAO would be mechanistically consistent with the proposed biosynthetic logic, as the resulting aldehyde intermediate would spontaneously undergo intramolecular cyclization with the adjacent D-allo-Thr side chain alcohol to the *N,O*-acetal, as was demonstrated in our total synthesis of fusahexin[35] (**Section 5.5**).

Current work in the Boddy laboratory is investigating CAO involvement in the biosynthesis of **5.1** across fusahexin-producing *Fusarium* strains has led to the identification of

CAO-encoding gene adjacent to the candidate NRPS4 gene cluster in *Fusarium avenaceum* (unpublished). This finding provides preliminary bioinformatic evidence consistent with CAO involvement in the oxidative transformation of **5.3** to **5.1**. Notably, a putative CAO-encoding gene in *F. graminearum* has been localized to a separate chromosome entirely, further supporting fusahexin's split cluster architecture and genomic displacement of this key biosynthetic element.

5.6.2 Biomimetic Oxidation of Prefusahexin Using a Synthetic TPQ Equivalent

To probe the chemical feasibility of the CAO-mediated oxidation hypothesis, a biomimetic reaction was developed using a synthetic equivalent of the TPQ cofactor. Ortho-quinones are well-established synthetic surrogates for TPQ in biomimetic oxidation chemistry[36–44], and 3,5-di-tert-butyl-o-benzoquinone (**5.4**) was selected as a practical equivalent based on previously reported successes and availability[44,45].

Treatment of prefusahexin (**5.3**) with the ortho-quinone surrogate (**5.4**) in aqueous acetonitrile under aerobic conditions, followed by acidification with TFA, was found to produce fusahexin (**5.1**), as confirmed by LCMS analysis monitoring the extracted ion chromatograms for the $[M+H]^+$ ion at m/z 607.3 and the $[M+Na]^+$ ion at m/z 626.3 (**Figure 5.4**).

These results provide direct chemical evidence that oxidation of the ornithine side chain

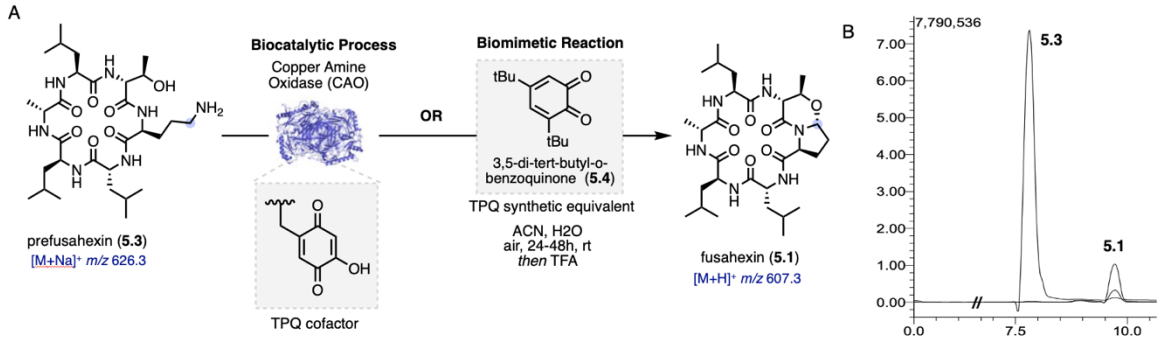


Figure 5.4. A. Biomimetic oxidation of prefusahexin (**5.3**) to fusahexin (**5.1**) using 3,5-di-tert-butyl-o-benzoquinone (**5.4**) as a synthetic equivalent of the topaquinone (TPQ) cofactor of copper amine oxidases (CAOs). B. LCMS extracted ion chromatograms (XICs) of the biomimetic oxidation at 48h monitoring the $[M+Na]^+$ ion at *m/z* 626.3 and the $[M+H]^+$ ion at *m/z* 607.3 confirm formation of **5.1** as the major product, with residual **5.3** observed.

primary amine, followed by spontaneous acid-promoted condensation, is a viable route from prefusahexin to fusahexin. This biomimetic transformation reproduces the proposed biosynthetic

oxidative backbone editing event in a single synthetic operation, and supports the hypothesis that a CAO-type enzyme performs this chemistry in vivo.

Experimental Note. Prefusahexin (0.9 mg, 0.0013 mmol, 1.0 eq.) was dissolved in 0.02mL aqueous acetonitrile (1:4 ACN:H_2O) in an HPLC vial and treated with 3,5-di-tert-butyl-o-benzoquinone (1.6 mg, 5.6 eq.) under aerobic conditions at room temperature for 24–48 h. The reaction mixture was acidified with one drop of TFA and analyzed directly by LCMS. Product identity was confirmed by retention time matching with synthetic fusahexin.

5.5.3 Outlook

Together, these preliminary results suggest that the biosynthesis of the unique 6,5-bicyclic *N,O*-acetal of fusahexin proceeds through CAO-mediated oxidative deamination of the prefusahexin ornithine side chain, followed by spontaneous intramolecular *N,O*-acetal formation. Outstanding questions include whether the stereochemical outcome at the *N,O*-acetal is enzyme-controlled or arises from the thermodynamic preference of the macrocyclic scaffold. In addressing this outstanding question, future work will be directed at heterologous expression of the native CAO, and enzymatic assays with synthetic prefusahexin as the substrate to enable the use of CAO as a biocatalyst. This direction could ultimately support the use of CAO as a biocatalytic tool for the rapid and stereoselective construction of the privileged 6,5-bicyclic N,O-acetal scaffold, expanding access to this structural motif for future peptidomimetic and chemotherapeutic applications.

5.7 Conclusions

The work presented in this chapter addressed a major question in the biosynthesis of fusahexin (**5.1**): the identity of the direct NRPS4 product and the origin of its unique fused 6,5-bicyclic *N,O*-acetal. Through an interdisciplinary approach involving investigative metabolomics, CRISPR/Cas9 gene editing, UHPLC-HRMS profiling and synthesis, prefusahexin (**5.3**) was identified and validated as the direct biosynthetic precursor to fusahexin. The structure of **5.3** was unambiguously confirmed by an automated SPPS-enabled total synthesis and co-elution with the natural metabolite, and the previously proposed intermediate dihydrofusahexin (**5.2**) was ruled out as a biosynthetic intermediate.

A biosynthesis-inspired total synthesis of fusahexin (**5.1**) enabled by late-stage backbone editing was also achieved through the incorporation of a Weinreb amide-functionalized glutamic acid surrogate. A reduction triggered cascade enabled by DIBAL-H delivered the aldehyde intermediate that cyclized under acidic conditions to the to the desired *N,O*-acetal. This synthesis mirrors the proposed biosynthetic pathway and provides direct chemical evidence that oxidation of the ornithine side chain of **5.3** is sufficient to trigger spontaneous cyclization to the *N,O*-acetal, generating **5.1** diastereoselectively.

Finally, fusahexin was found to has a split biosynthetic gene cluster arrangement in *F. graminearum* wherein the oxidative enzyme responsible for the key late-stage transformation of **5.3** to **5.1** is encoded outside the cluster. Recent bioinformatic evidence from *Fusarium avenaceum*, where a CAO-encoding gene was identified adjacent to the NRPS4 cluster, combined with the localization of a candidate CAO-encoding gene to a separate chromosome in *F. graminearum*, is consistent with genomic displacement of this biosynthetic element and implicates copper amine oxidases as the likely responsible enzyme class. The successful biomimetic oxidation of **5.3** using a synthetic TPQ equivalent to deliver **5.1** provides further chemical support for this hypothesis.

With synthetic access to **5.1** and **5.3** now established, this platform opens the door to future biological investigations of fusahexin's role in fungal virulence and cell surface hydrophobicity. More broadly, the biocatalytic potential of the implicated CAO enzyme may offer a stereoselective route to the 6,5-bicyclic *N,O*-acetal scaffold and related acetal-containing motifs of synthetic and medicinal interest.

5.8 References

(1) Westphal, K. R.; Bachleitner, S.; Severinsen, M. M.; Brundtø, M. L.; Hansen, F. T.; Sørensen, T.; Wollenberg, R. D.; Lysøe, E.; Studt, L.; Sørensen, J. L.; Sondergaard, T. E.; Wimmer, R. *J. Nat. Prod.* **2021**, *84* (8), 2070–2080.

(2) Vamos, M.; Welsh, K.; Finlay, D.; Lee, P. S.; Mace, P. D.; Snipas, S. J.; Gonzalez, M. L.; Ganji, S. R.; Ardecky, R. J.; Riedl, S. J.; Salvesen, G. S.; Vuori, K.; Reed, J. C.; Cosford, N. D. P. *ACS Chem. Biol.* **2013**, *8* (4), 725–732.

(3) Bäuerlein, C.; Geyer, A. *J. Org. Chem.* **2025**, *90* (31), 11142–11150.

(4) Sun, H.; Moeller, K. D. *Org. Lett.* **2002**, *4* (9), 1547–1550.

(5) Sun, H.; Martin, C.; Kesselring, D.; Keller, R.; Moeller, K. D. *J. Am. Chem. Soc.* **2006**, *128* (42), 13761–13771.

(6) Zhang, X.; Jiang, W.; Schmitt, A. C. *Tet. Lett.* **2001**, *42* (30), 4943–4945.

(7) Chalmers, D. K.; Marshall, G. R. *J. Am. Chem. Soc.* **1995**, *117* (22), 5927–5937.

(8) Claridge, T. D. W.; Hulme, C.; Kelly, R. J.; Lee, V.; Nash, I. A.; Schofield, C. J. *Bioorg. & Med. Chem. Lett.* **1996**, *6* (4), 485–490.

(9) Baldwin, J. E.; Hulme, C.; Schofield, C. J.; Edwards, A. J. *J. Chem. Soc., Chem. Commun.* **1993**, No. 11, 935–936.

(10) Nagai, U.; Sato, K. *Tet. Lett.* **1985**, *26* (5), 647–650.

(11) COSFORD, N. D. P.; VAMOS, M. D. Inhibitor of Apoptosis Protein (Iap) Antagonists. WO2014085489A1, June 5, 2014.

(12) PACHE, L.; CHANDA, S. K.; VAMOS, M. D.; Cosford, N. D. P.; Teriete, P.; MARLETT, J.; Diaz, A.; Young, J. A. T. Use of Inhibitor of Apoptosis Protein (IAP) Antagonists in HIV Therapy. US10300074B2, May 28, 2019.

(13) Jiang, S. ; Zhou, G. ; Hao, H. ; Miao, Q. ; Wu, X. ; Zhang, K. ; Qiu, Y. Macrocyclic Compound for Inhibiting PD-1/PD-L1 and Application Thereof. CN112010940B, 2019.

(14) Gómez-Olarte, S.; Bolaños, N. I.; Echeverry, M.; Rodríguez, A. N.; Cuéllar, A.; Puerta, C. J.; Mariño, A.; González, J. M. *Front. Immunol.* **2019**, *10*, 1671.

(15) Sauters, T. J. C.; Rokas, A. *Curr. Biol.* **2025**, *35* (11), R527–R544.

(16) Witte, T. E.; Hermans, A.; Sproule, A.; Hicks, C.; Talhouni, T.; Schneiderman, D.; Harris, L. J.; Eranthodi, A.; Foroud, N. A.; Chatterton, S.; Overy, D. P. *J. Fungi* **2024**, *10* (12), 821.

(17) Slomczynska, U.; Chalmers, D. K.; Cornille, F.; Smythe, M. L.; Beusen, D. D.; Moeller, K. D.; Marshall, G. R. *J. Org. Chem.* **1996**, *61* (4), 1198–1204.

(18) Chiou, W.-H.; Mizutani, N.; Ojima, I. *J. Org. Chem.* **2007**, *72* (6), 1871–1882.

(19) Ozaki, T. *Biosci. Biotechnol. Biochem.* **2023**, *87* (8), 809–818.

(20) Walsh, C. T. *Nat. Prod. Rep.* **2023**, *40* (2), 326–386.

(21) Frandsen, R. J. N.; Nielsen, N. J.; Maolanon, N.; Sørensen, J. C.; Olsson, S.; Nielsen, J.; Giese, H. *Mol. Microbiol.* **2006**, *61* (4), 1069–1080.

(22) Noriler, S.; Navarro-Muñoz, J. C.; Glienke, C.; Collemare, J. *Genomics* **2022**, *114* (6), 110525.

(23) Zhang, Z.; Zhou, Y.; Xie, S.; Liu, R.-Z.; Huang, Z.; Saravana Kumar, P.; Feng, G.; Yuan, F.; Zhang, L. *J. Am. Chem. Soc.* **2025**, *147* (36), 32662–32670.

(24) Balasubramaniam, S.; Aidhen, I. S. *Synthesis* **2008**, *2008* (23), 3707–3738.

(25) Douat, C.; Heitz, A.; Paris, M.; Martinez, J.; Fehrentz, J.-A. *J. of Pept. Sci.* **2002**, *8* (11), 601–614.

(26) Monti, A.; Caporale, A.; Ruvo, M.; Doti, N. *J. of Pept. Sci.* **2026**, *32* (1), e70064.

(27) Bäuerlein, C.; Geyer, A. *J. Org. Chem.* **2025**, *90* (31), 11142–11150.

(28) Olarte, R. A.; Menke, J.; Zhang, Y.; Sullivan, S.; Slot, J. C.; Huang, Y.; Badalamenti, J. P.; Quandt, A. C.; Spatafora, J. W.; Bushley, K. E. *BMC Genomics* **2019**, *20* (1), 120.

(29) Hicks, C.; Witte, T. E.; Sproule, A.; Hermans, A.; Shields, S. W.; Colquhoun, R.; Blackman, C.; Boddy, C. N.; Subramaniam, R.; Overy, D. P. *Journal of Fungi* **2023**, *9* (7), 695.

(30) Gebbie, L. *Methods in Molecular Biology* **2014**, *1099*, 159–177.

(31) Witte, T. E.; Overy, D. P. *Methods Mol. Biol.* **2022**, *2456*, 349–365.

(32) Pluskal, T.; Castillo, S.; Villar-Briones, A.; Orešič, M. *BMC Bioinformatics* **2010**, 11 1, 395.

(33) R Core Team. *R: A Language and Environment for Statistical Computing*; R Foundation for Statistical Computing: Vienna, 2022.

(34) Gaude, E.; Chignola, F.; Spiliotopoulos, D.; Spitaleri, A.; Ghitti, M.; Garcia-Manteiga, J. M.; Mari, S.; Musco, G. *Curr. Metabolomics* **2013**, *1* (2), 180–189.

(35) Natola, C.; Hicks, C.; Witte, T. E.; Hermans, A.; Sproule, A.; Overy, D. P.; Boddy, C. N. *Org. Lett.* **2026**, *28* (14), 4507–4511.

(36) Esguerra, K. V. N.; Xu, W.; Lumb, J.-P. *Chem.* **2017**, *2* (4), 533–549.

(37) Largeron, M.; Fleury, M.-B. *Science* **2013**, *339* (6115), 43–44.

(38) Yuan, H.; Yoo, W.-J.; Miyamura, H.; Kobayashi, S. *J. Am. Chem. Soc.* **2012**, *134* (34), 13970–13973.

(39) Wendlandt, A. E.; Stahl, S. S. *Org. Lett.* **2012**, *14* (11), 2850–2853.

(41) Wang, L.; Yang, H.; Cui, J.; Chen, X.; Yu, B.; Zhang, X. *Chem.* **2026**, *12* (2), 102744.

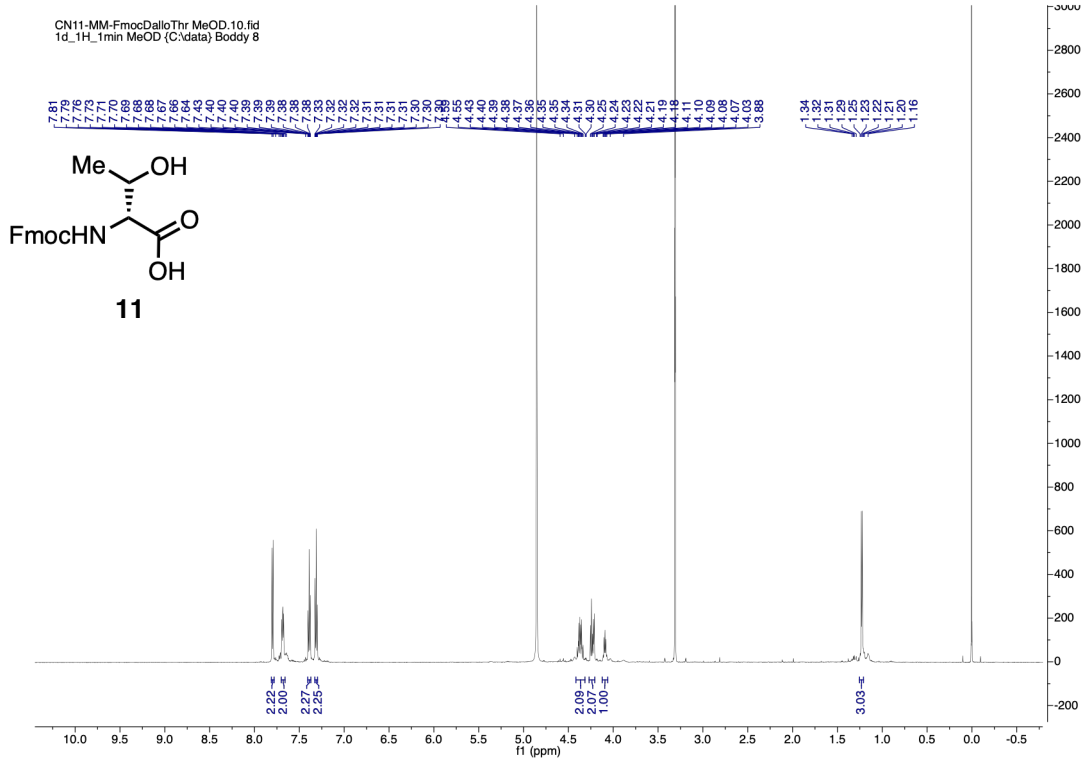
(42) Ohshiro, Y.; Itoh, S.; Kurokawa, K.; Kato, J.; Hirao, T.; Agawa, T. *Tet. Lett.* **1983**, *24* (33), 3465–3468.

(43) Prosser, L. C.; Talbott, J. M.; Garrity, R. P.; Raj, M. *Org. Lett.* **2023**, *25* (33), 6206–6210.

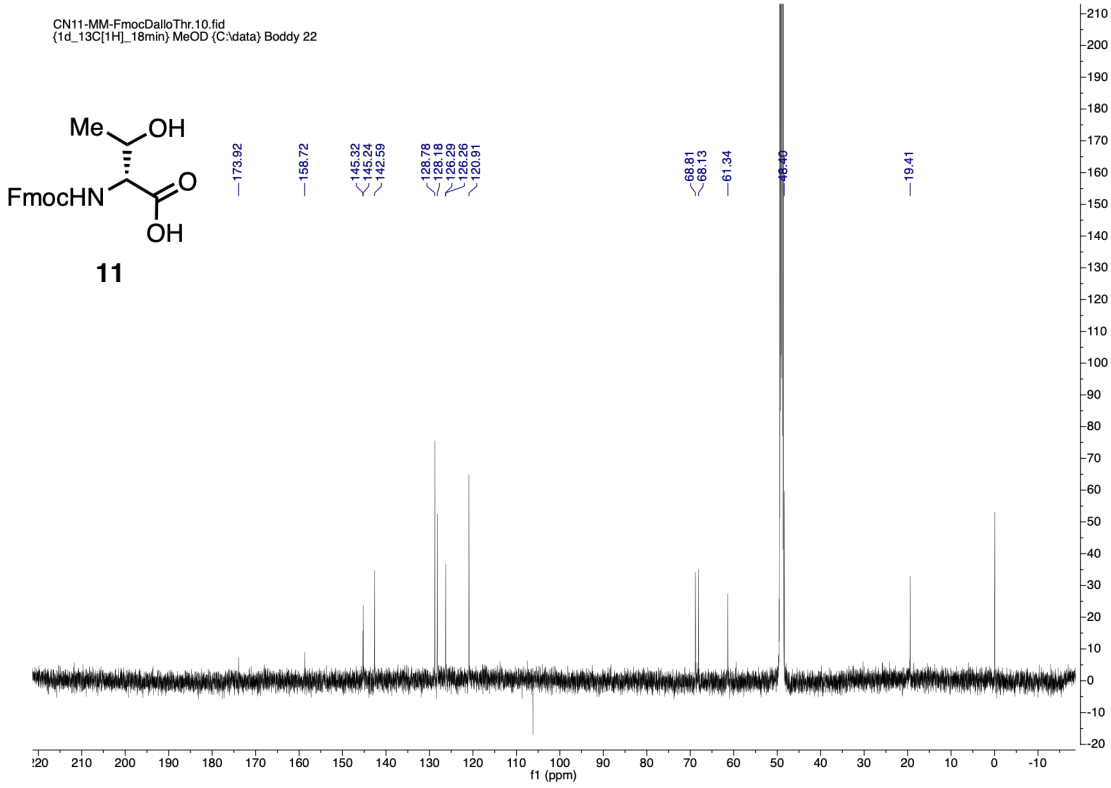
(44) Vasu, D.; Arriba, A. L. F. de; A. Leitch, J.; Gombert, A. de; J. Dixon, D. *Chem. Sci.* **2019**, *10* (11), 3401–3407.

(45) Rong, H.-J.; Cheng, Y.-F.; Liu, F.-F.; Ren, S.-J.; Qu, J. *J. Org. Chem.* **2017**, *82* (1), 532–540.

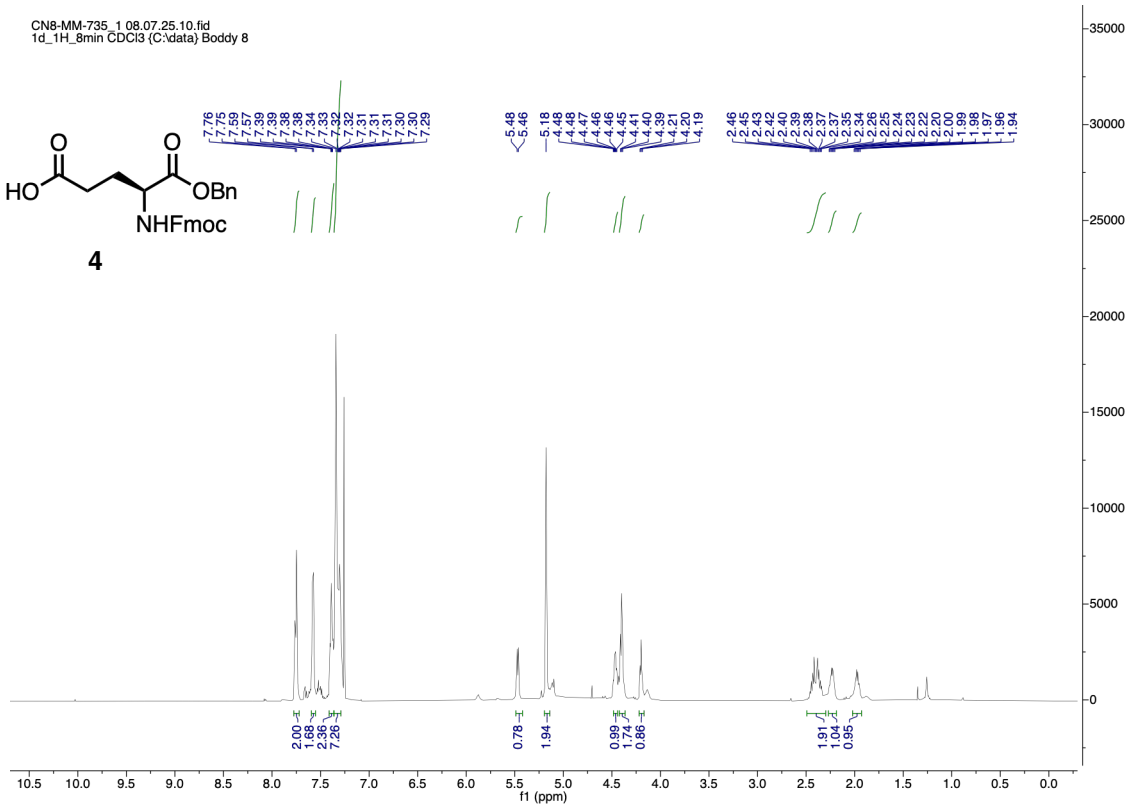
5.9 Appendix to Chapter V
NMR Spectra:



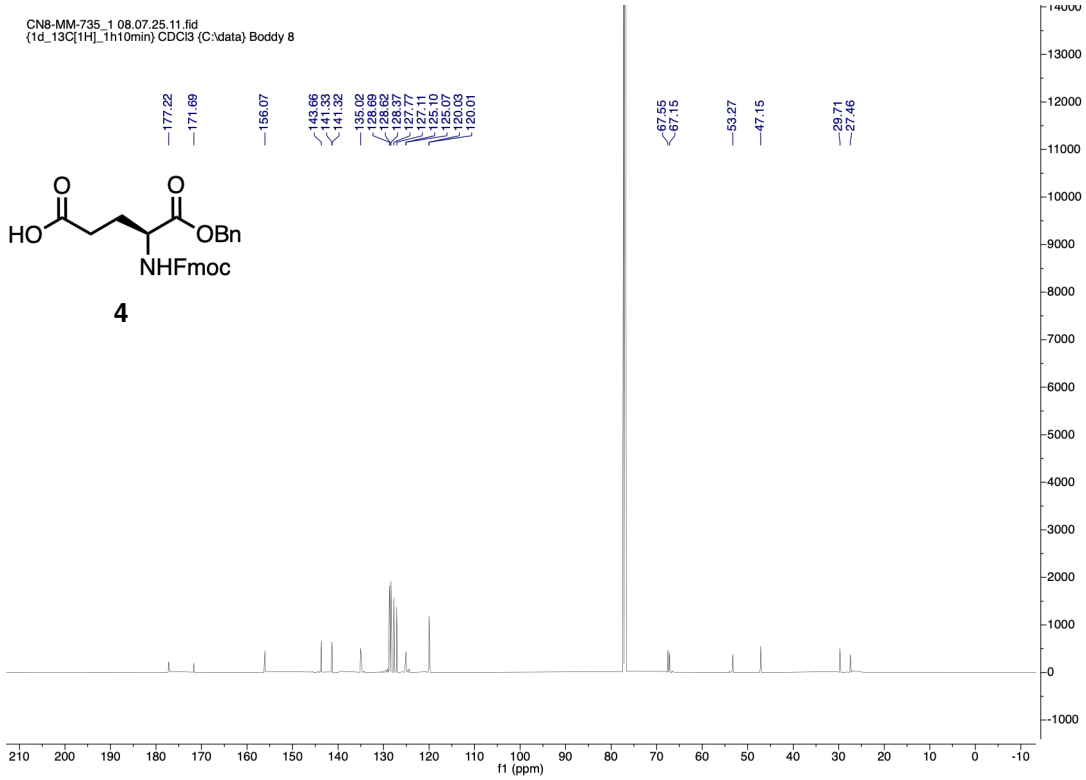
Spectra 5.1 ^{1}H NMR (600 MHz, MeOD with TMS) of (((9H-fluoren-9-yl)methoxy)carbonyl)-D-*allo*-threonine (**11**)



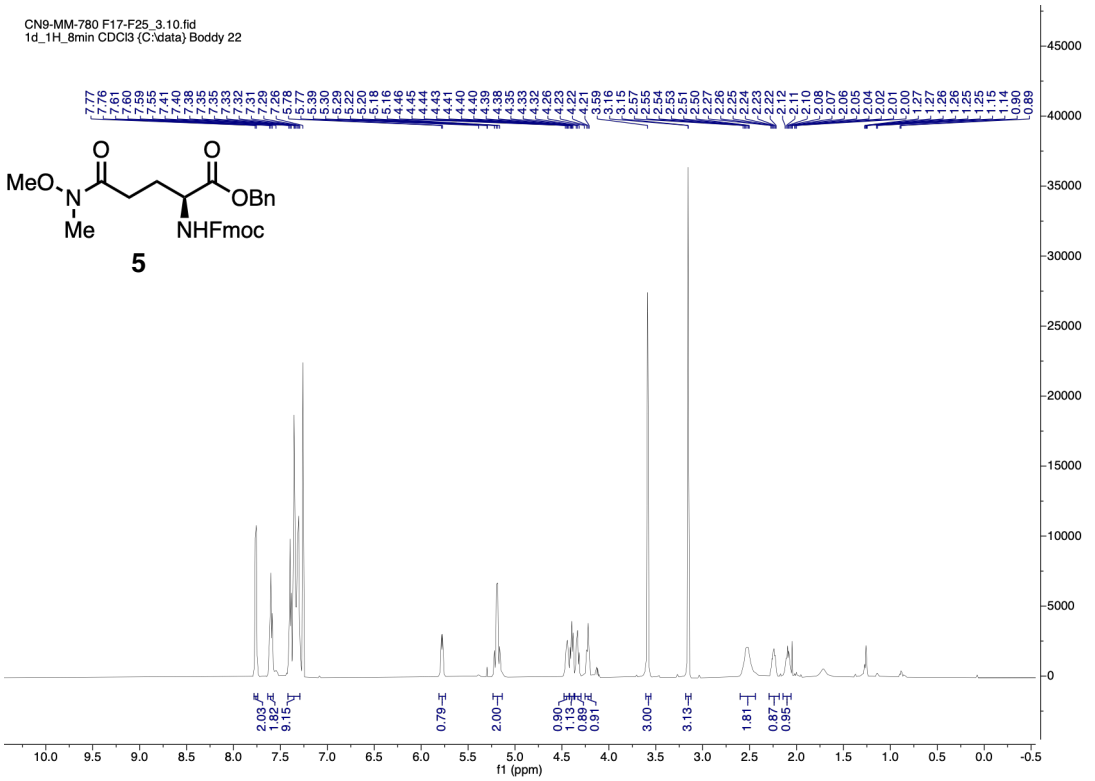
Spectra 5.2 ^{13}C NMR (151 MHz, MeOD with TMS) of (((9H-fluoren-9-yl)methoxy)carbonyl)-D-*allo*-threonine (**11**)



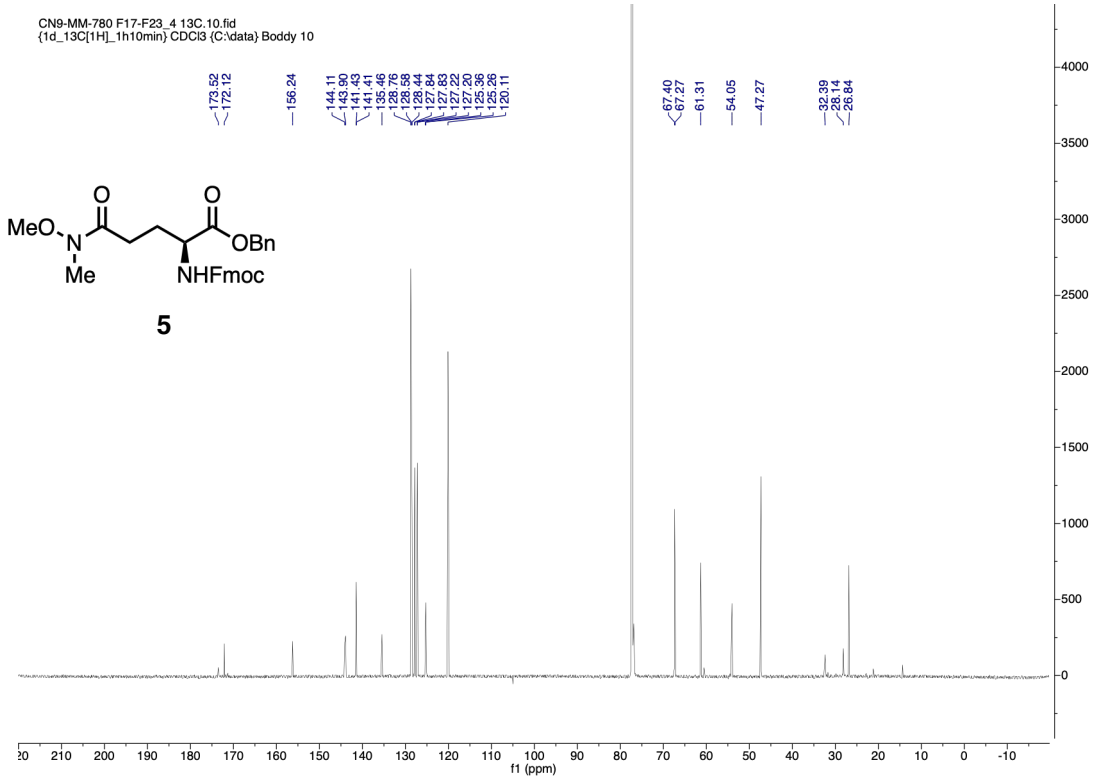
Spectra 5.3 ^{1}H NMR (600 MHz, CDCl3) of (S)-4-((((9H-fluoren-9-yl)methoxy)carbonyl)amino)-5-(benzyloxy)-5-oxopentanoic acid (**4**)



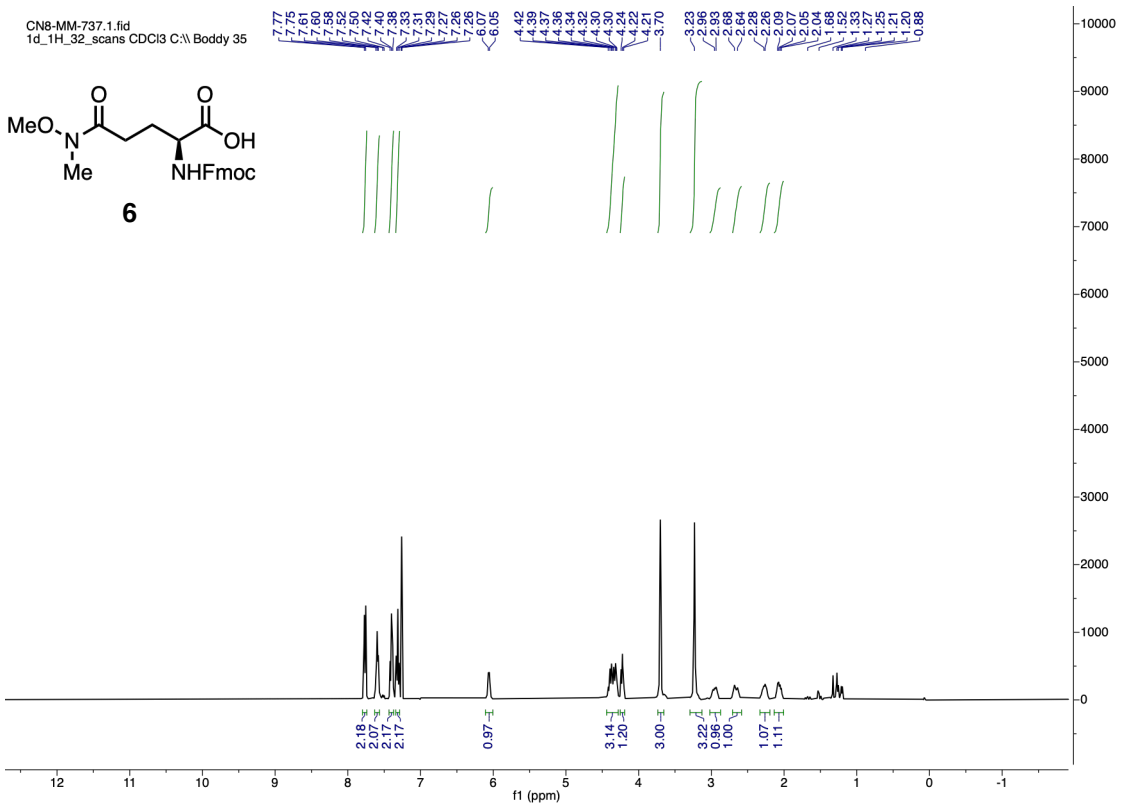
Spectra 5.4 ^{13}C NMR (151 MHz, $CDCl_3$) of (S)-4-((((9H-fluoren-9-yl)methoxy)carbonyl)amino)-5-(benzyloxy)-5-oxopentanoic acid (**4**)



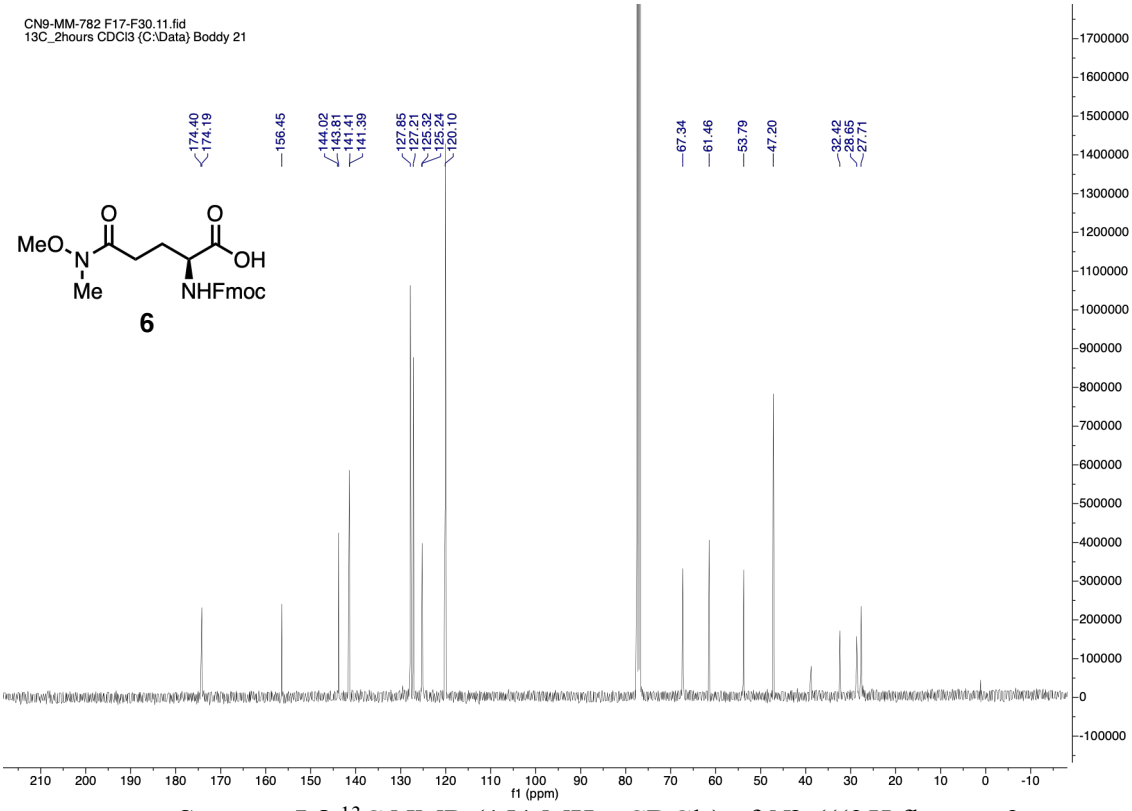
Spectra 5.5[1]H NMR (600 MHz, CDCl3) of benzyl N2-(((9H-fluoren-9-yl)methoxy)carbonyl)-N5-methoxy-N5-methyl-L-glutaminate (**5**)



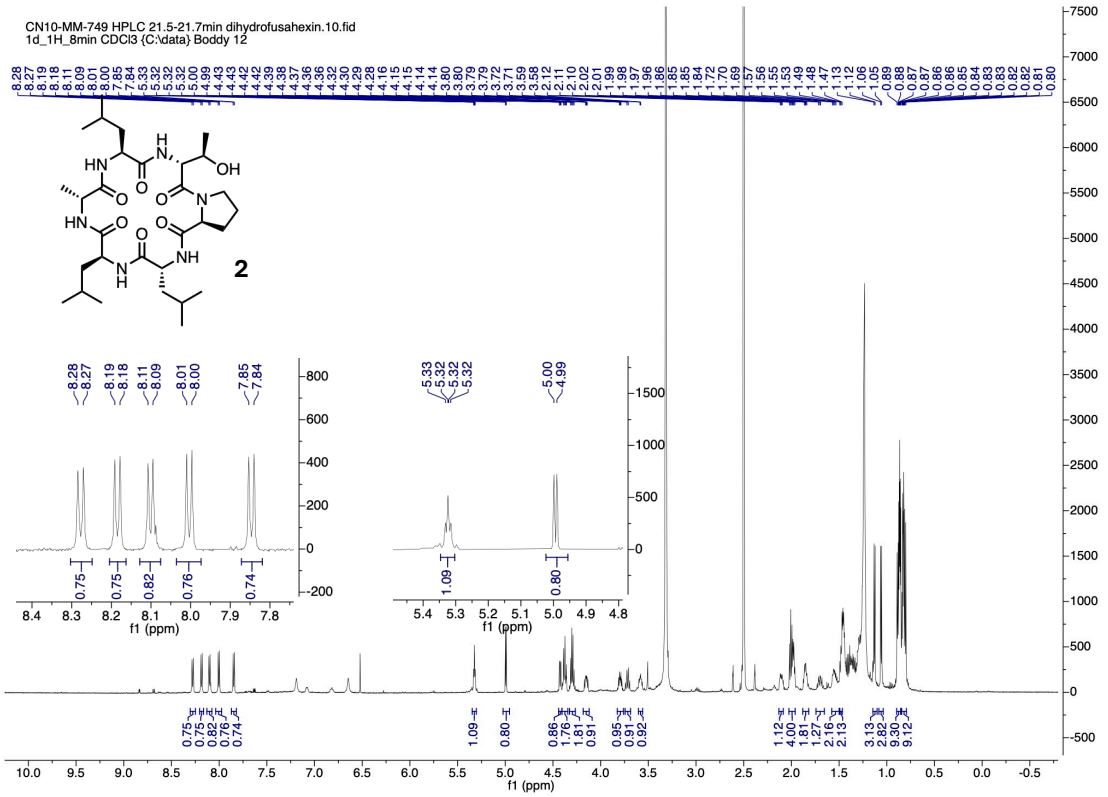
Spectra 5.6 [13]C NMR (151 MHz, $CDCl_3$) of benzyl N2-(((9H-fluoren-9-yl)methoxy)carbonyl)-N5-methoxy-N5-methyl-L-glutaminate (**5**)



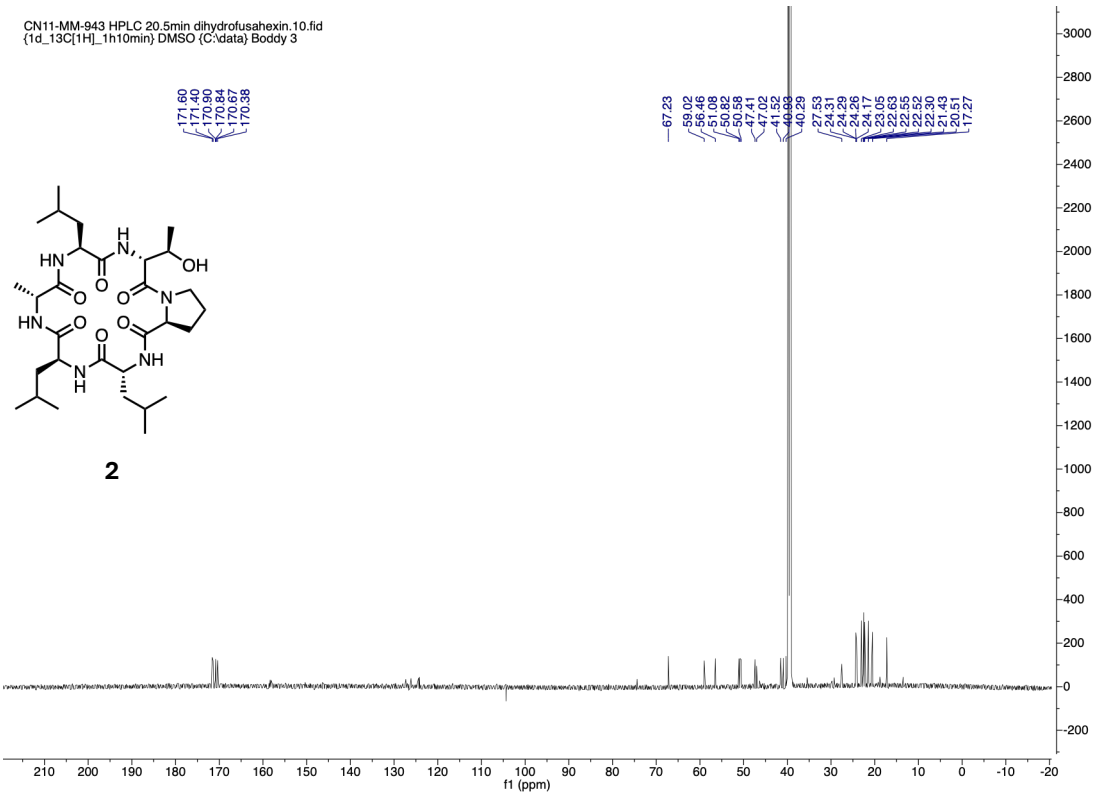
Spectra 5.7 ^{1}H NMR (600 MHz, CDCl3) of *N*2-(((9*H*-fluoren-9-yl)methoxy)carbonyl)-*N*5-methoxy-*N*5-methyl-*L*-glutamine (**6**)



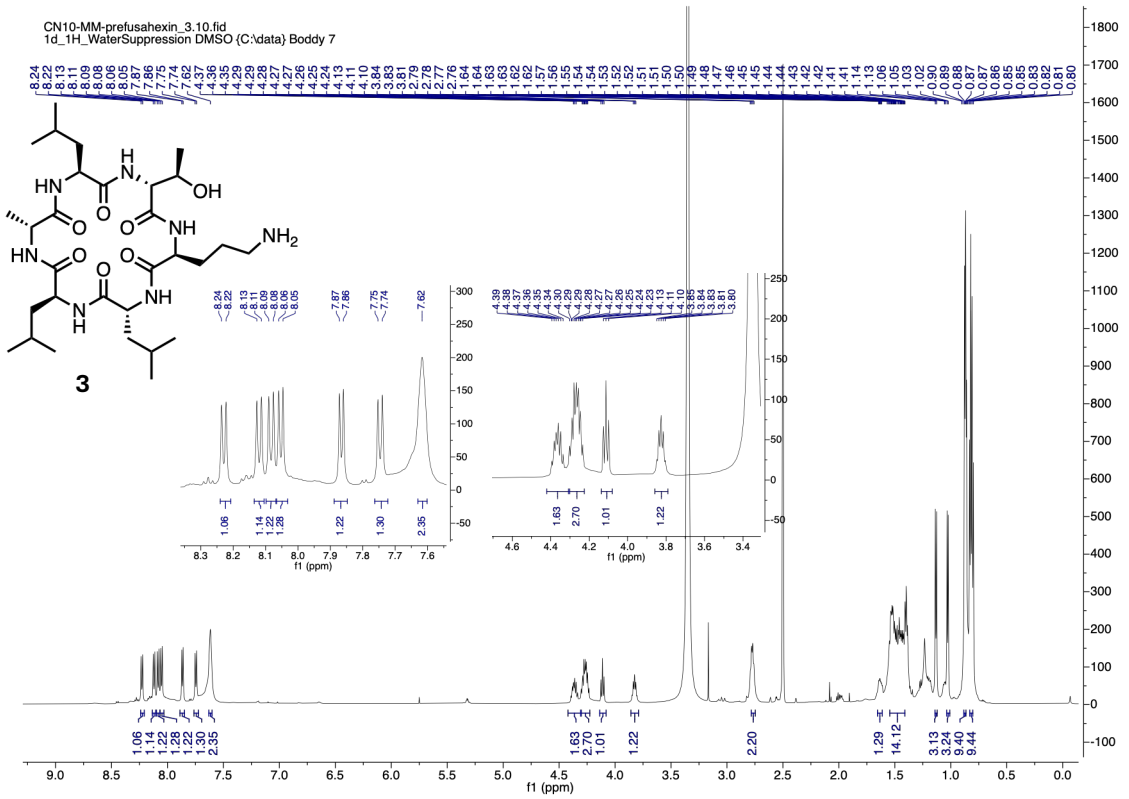
Spectra 5.8 ^{13}C NMR (151 MHz, $CDCl_3$) of *N*2-(((9*H*-fluoren-9-yl)methoxy)carbonyl)-*N*5-methoxy-*N*5-methyl-*L*-glutamine (**6**)



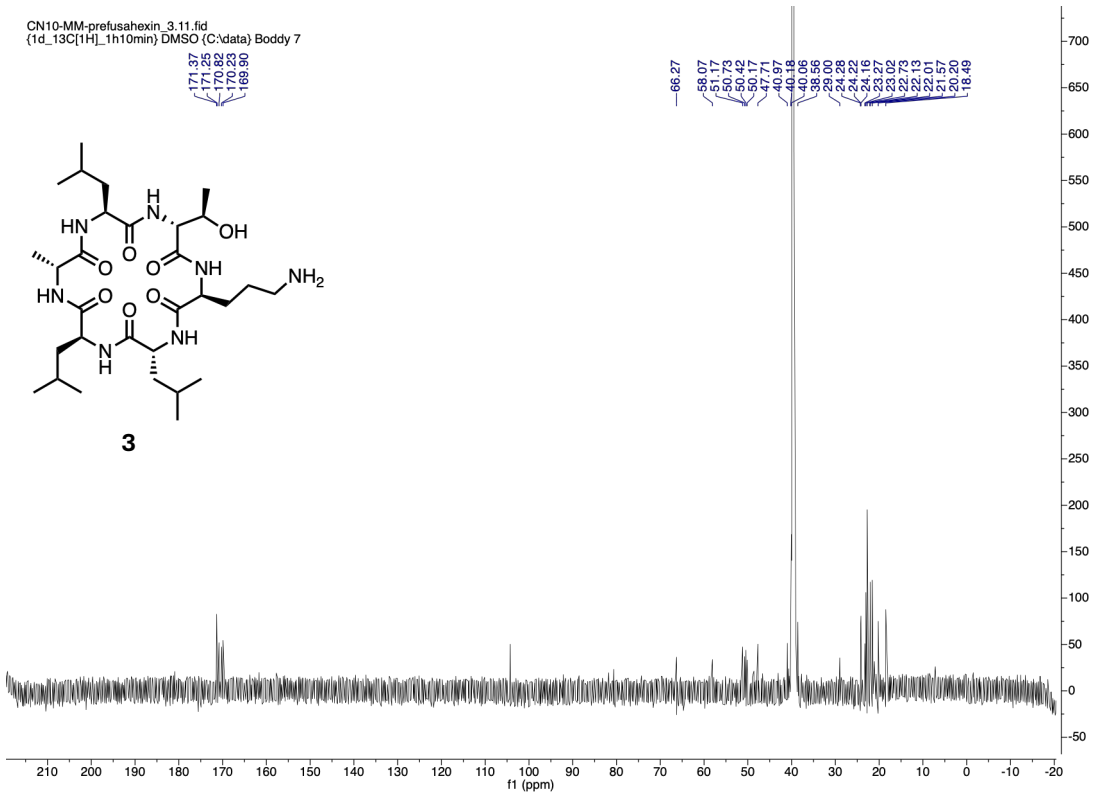
Spectra 5.9 ^{1}H NMR (600 MHz, DMSO-d_6) of Dihydrofusahexin (**2**) with expanded views of the amide region and the δH Pro



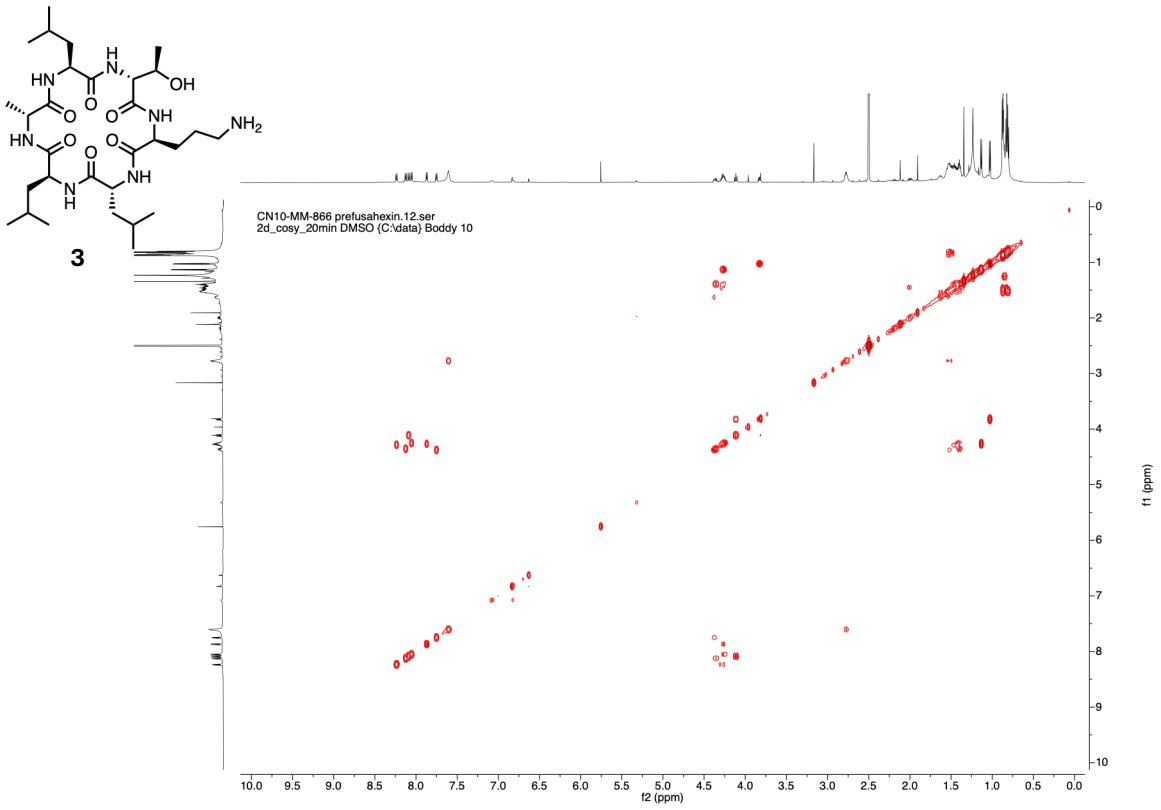
Spectra 5.10 ^{13}C NMR (151 MHz, DMSO-d_6) of Dihydrofusahexin (**2**)



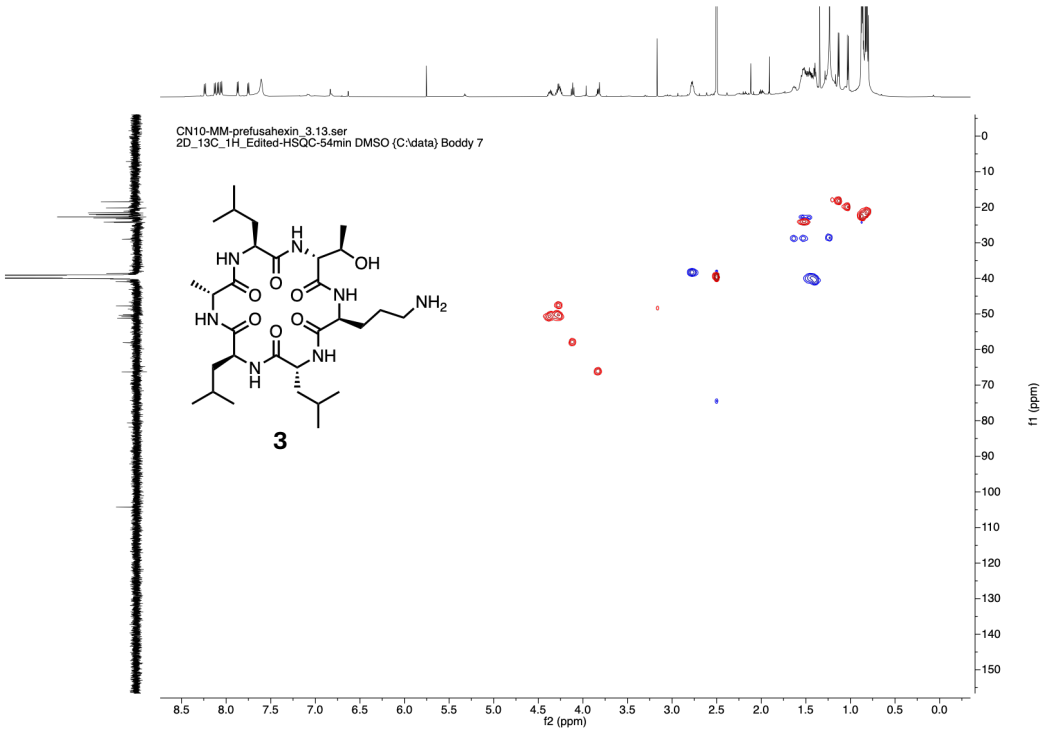
Spectra 5.11 ^{1}H NMR (600 MHz, DMSO-d_6) of Prefusahexin (**3**) recorded with water suppression. Expanded views of the amide and α-H regions.



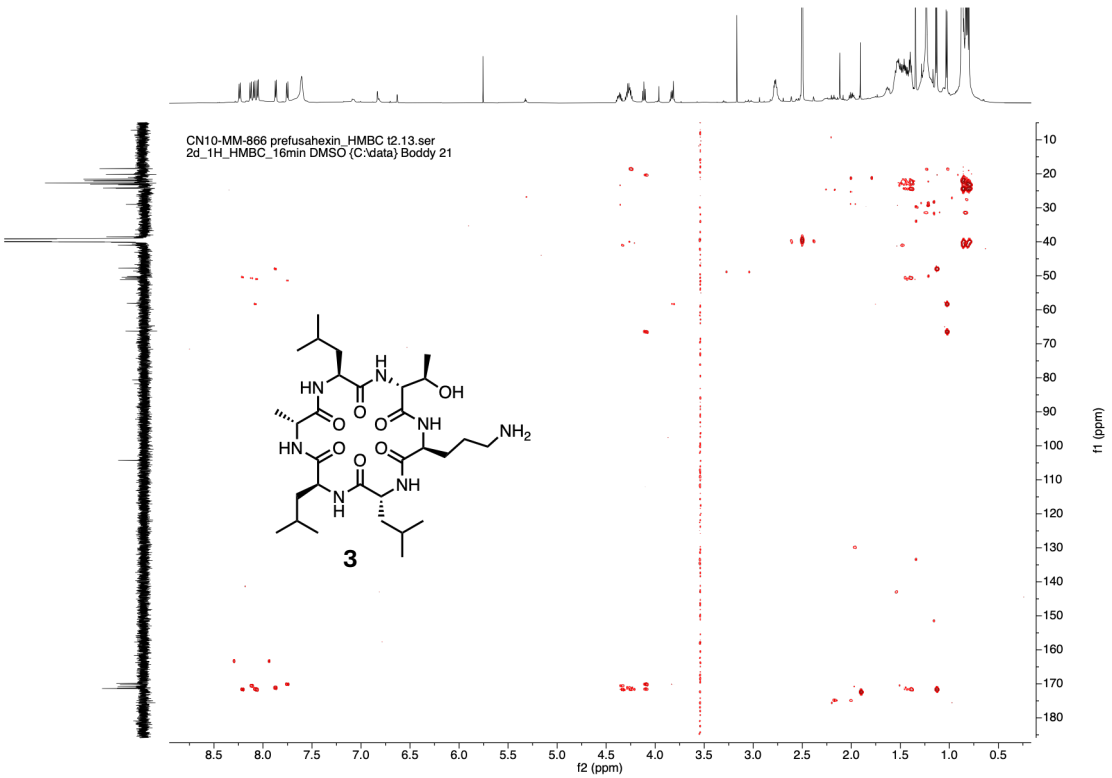
Spectra 5.12 ^{13}C NMR (151 MHz, DMSO-d_6) of Prefusahexin (**3**)



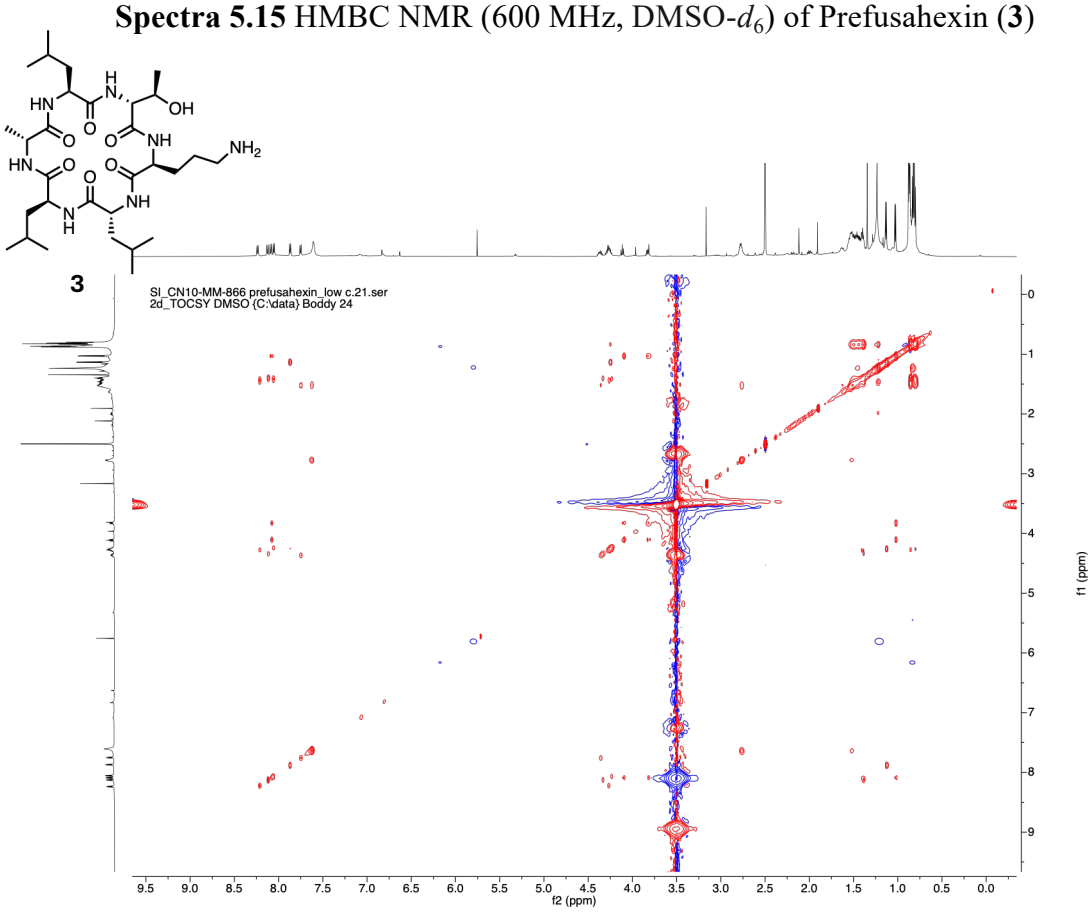
Spectra 5.13 COSY NMR (600 MHz, DMSO-d_6) of Prefusahexin (**3**)



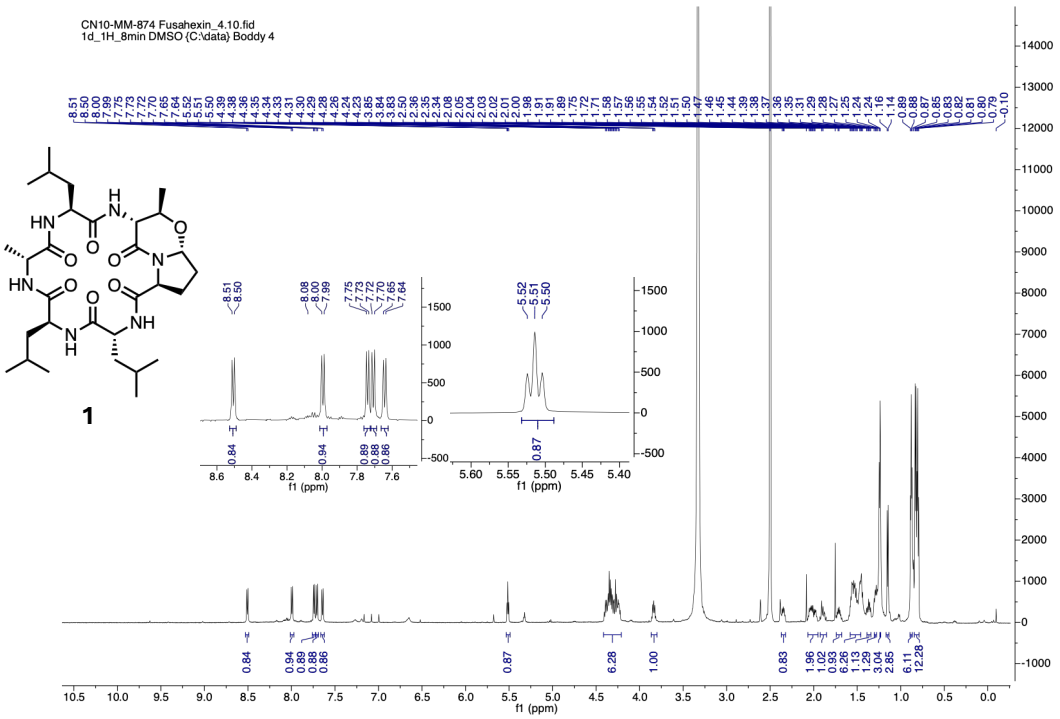
Spectra 5.14 HSQC NMR (151 MHz, DMSO-d_6) of Prefusahexin (**3**)



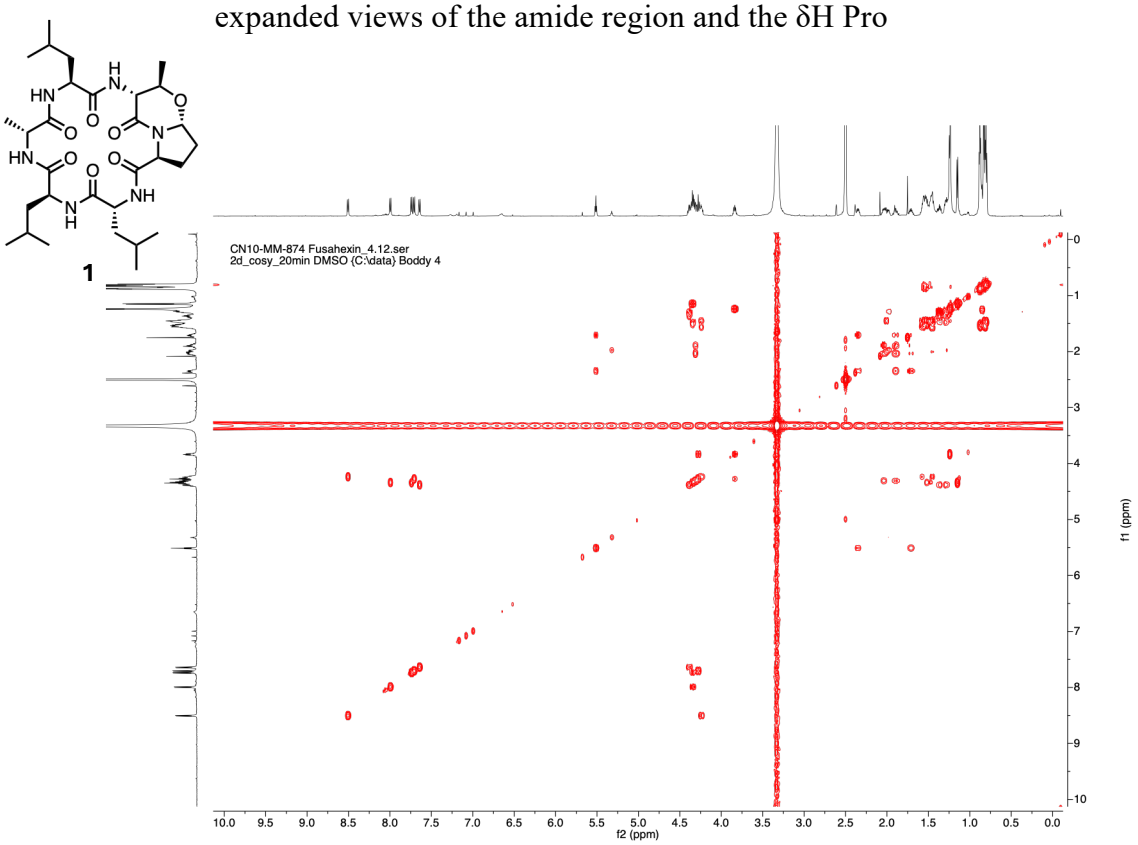
Spectra 5.15 HMBC NMR (600 MHz, DMSO-d_6) of Prefusahexin (**3**)



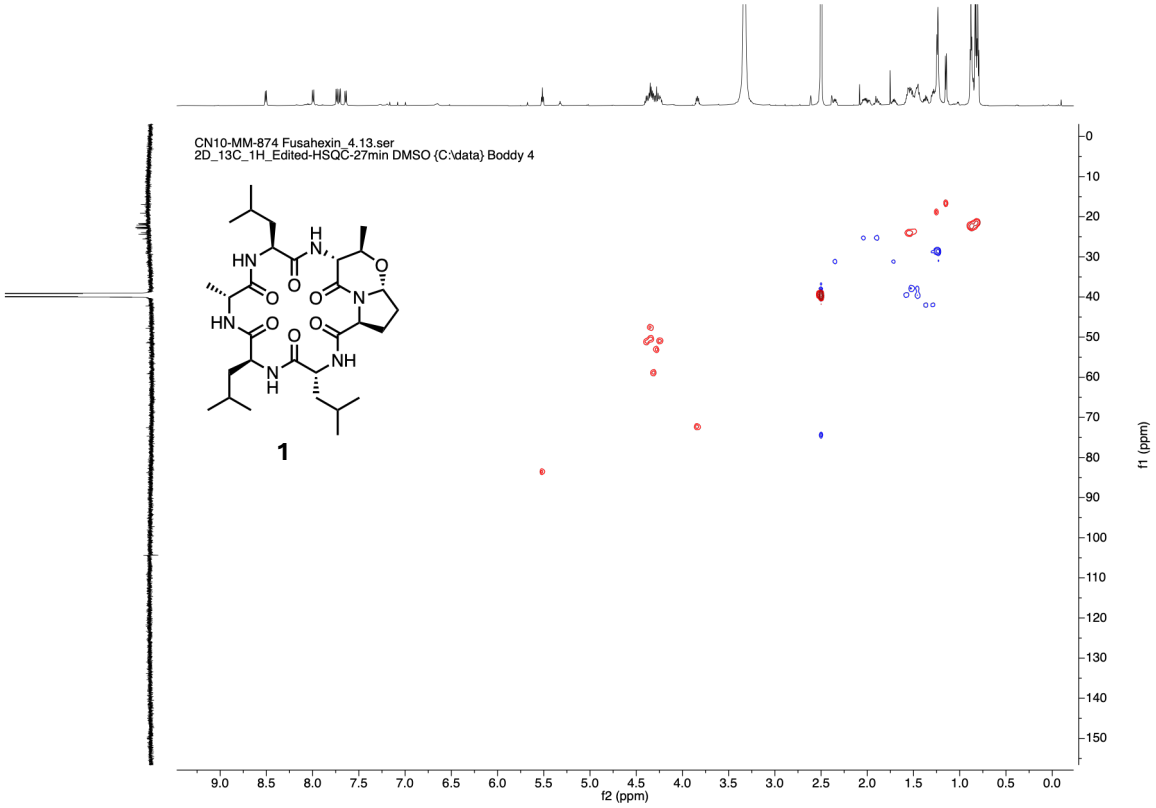
Spectra 5.16 TOCSY NMR (600 MHz, DMSO-d_6) of Prefusahexin (**3**)



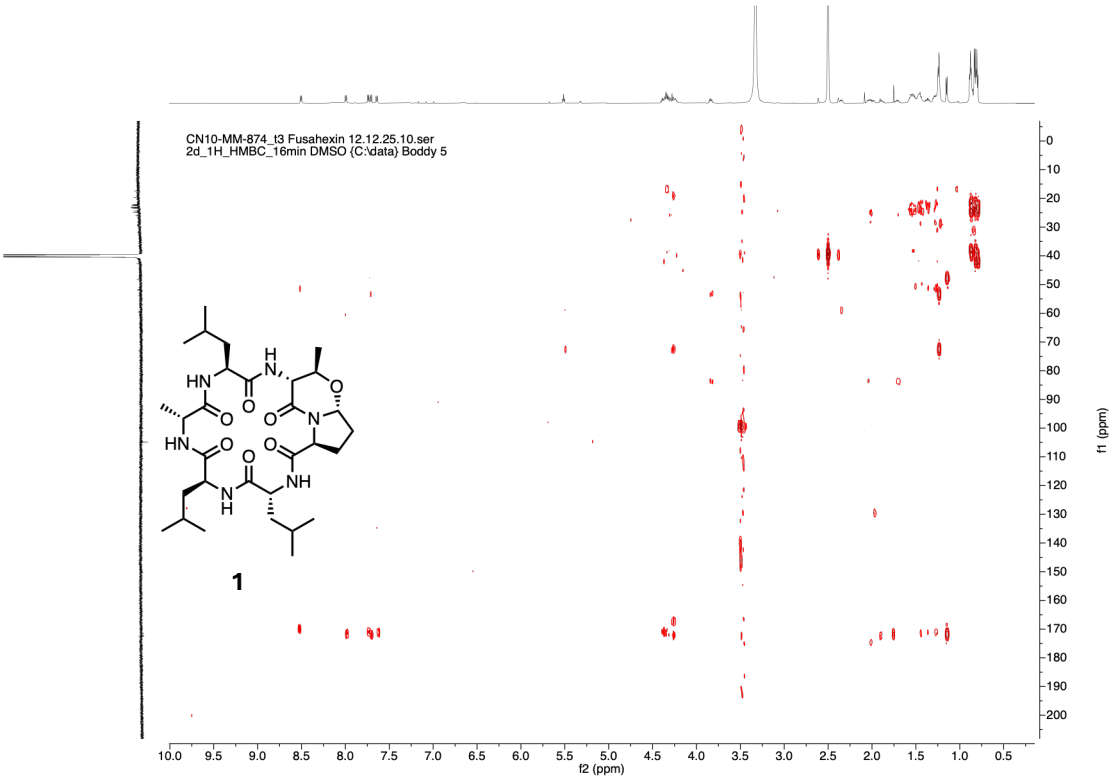
Spectra 5.17 ^{1}H NMR (600 MHz, DMSO-d_6) of Fusahexin (**1**) with expanded views of the amide region and the δH Pro



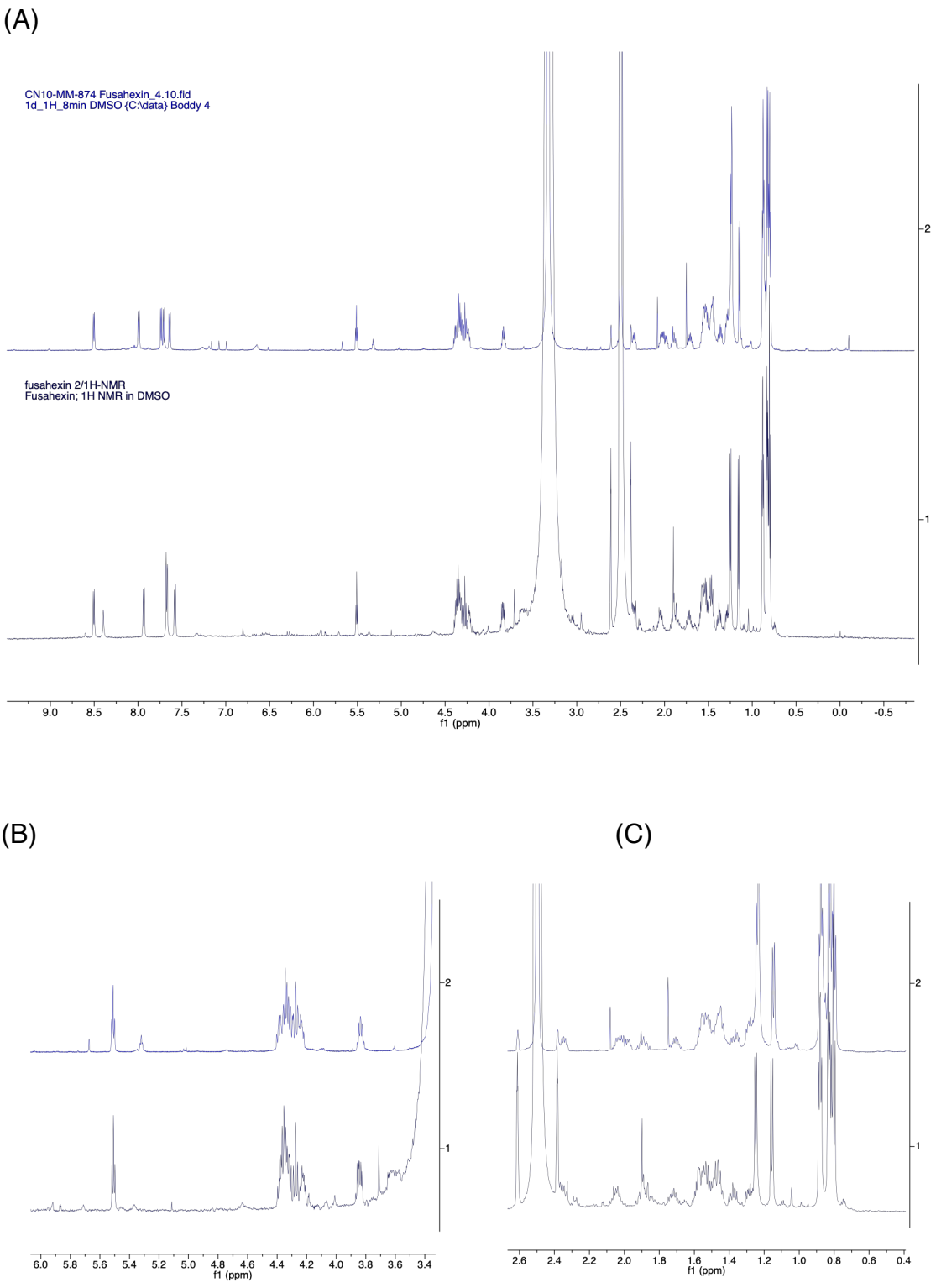
Spectra 5.18 COSY NMR (600 MHz, DMSO-d_6) of Fusahexin (**1**)



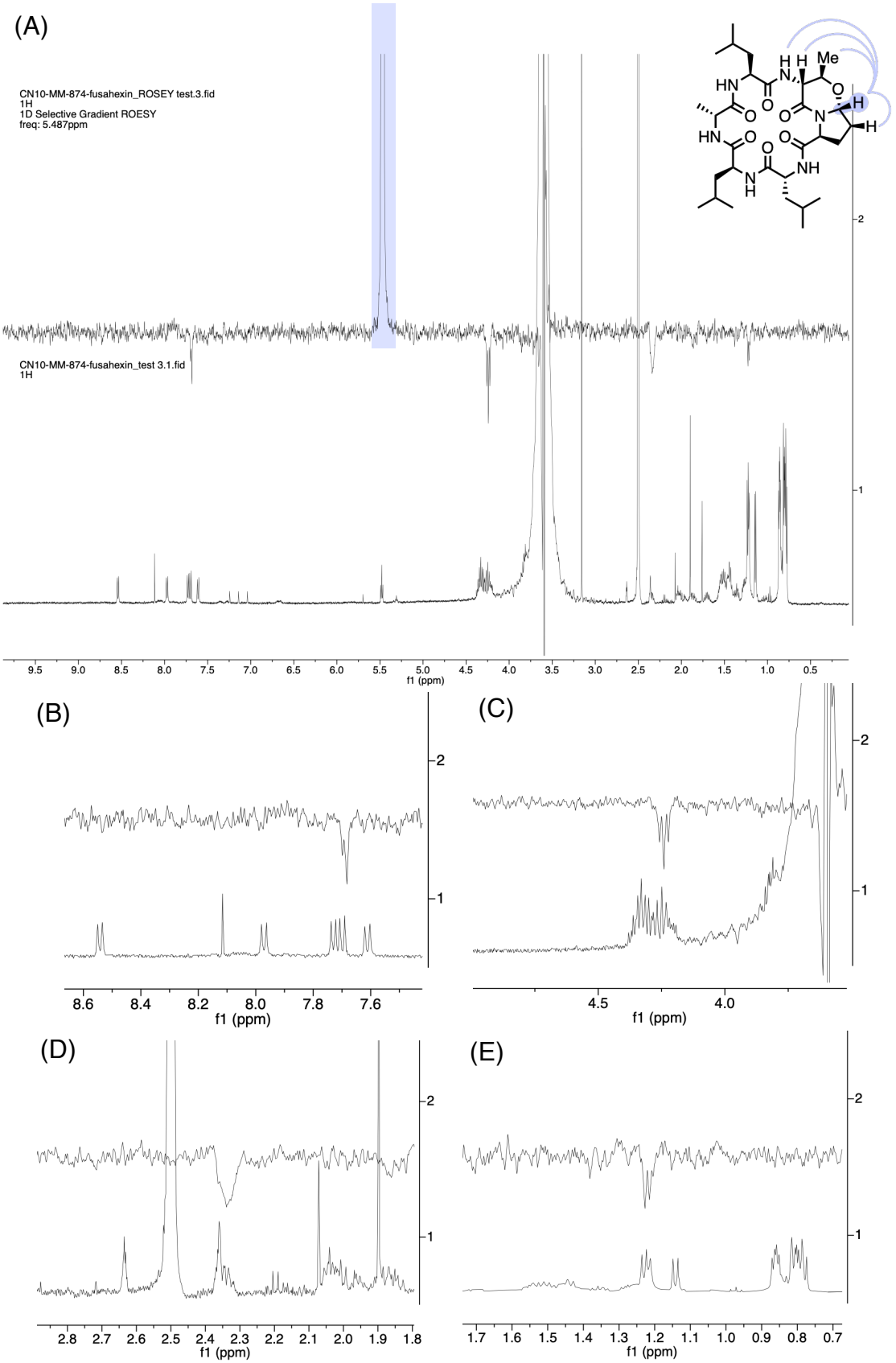
Spectra 5.19 HSQC (151 MHz, DMSO-d_6) of Fusahexin (**1**)



Spectra 5.20 HMBC (151 MHz, DMSO-d_6) of Fusahexin (**1**)



Spectra 5.21 (A) Overlay ^{1}H NMR spectra of synthetic Fusahexin, **1**, (blue; top) with the literature-reported spectrum[6] (navy; bottom) of the natural isolate from *Fusarium graminearum*. Expanded regions between (B) δ 3.5–6.0ppm and (C) δ 0.5–3.0ppm are shown to highlight diagnostic resonances.



Spectra 5.22 (A) Overlay of 1D selective gradient ROSEY irradiated at δ 5.547 ppm (highlight) (top spectrum) with ^{1}H NMR spectra of fusahexin (**1**) (bottom spectrum). Expanded regions between (B) δ 7.6–8.4 ppm, (C) δ 3.0–5.0ppm, (D) δ 1.8–2.8 ppm, and (E) δ 0.7–1.7 ppm are shown to highlight diagnostic resonances.

5.10 Appendix to Chapter V
Copyright license

AMERICAN CHEMICAL SOCIETY LICENSE TERMS AND CONDITIONS

Jul 02, 2026

This Agreement between Claudia Natola ("You") and American Chemical Society ("American Chemical Society") consists of your license details and the terms and conditions provided by American Chemical Society and Copyright Clearance Center.

License Number	6280840030100
License date	Jun 02, 2026
Licensed Content Publisher	American Chemical Society
Licensed Content Publication	Organic Letters
Licensed Content Title	Synthesis-Supported Discovery of Prefusahexin, a Direct Fusahexin Biosynthetic Precursor
Licensed Content Author	Claudia Natola, Carmen Hicks, Thomas E. Witte, et al
Licensed Content Date	Apr 1, 2026
Licensed Content Volume	28
Licensed Content Issue	14
Volume number	28
Issue number	14
Type of Use	Thesis/Dissertation
Requestor type	Author (original work)
Format	Electronic
Portion	Full article
Title of new work	Synthetic Studies Toward Fusarium-Derived Natural Products: Total Syntheses of Immunomodulide, Fusahexin, and Prefusahexin
Institution name	University of Ottawa
Expected presentation date	Aug 2026
The Requesting Person / Organization to Appear on the License	Claudia Natola
Requestor Location	[redacted]
Payment Type	Invoice
Email Address	
Billing Address	[redacted]
Total	**0.00 USD**
Terms and Conditions	

American Chemical Society's Policy on Thesis and Dissertations

If your university requires you to obtain permission, you must use the RightsLink permission system.
See RightsLink instructions at https://pubs.acs.org/page/copyright/permissions.html.

This is regarding request for permission to include **your** paper(s) or portions of text from **your** paper(s) in your thesis. Permission is now automatically granted; please pay special attention to the **implications** paragraph below. The Copyright Subcommittee of the Joint Board/Council Committees on Publications approved the following:

Copyright permission for published and submitted material from thesis and dissertations
ACS extends blanket permission to students to include in their thesis and dissertations their own articles, or portions thereof, that have been published in ACS journals or submitted to ACS journals for publication, provided that the ACS copyright credit line is noted on the appropriate page(s).

Publishing implications of electronic publication of thesis and dissertation material
Students and their mentors should be aware that posting of thesis and dissertation material on the Web prior to submission of material from that thesis or dissertation to an ACS journal may affect publication in that journal. Whether Web posting is considered prior publication may be evaluated on a case-by-case basis by the journal's editor. If an ACS journal editor considers Web posting to be "prior publication", the paper will not be accepted for publication in that journal. If you intend to submit your unpublished paper to ACS for publication, check with the appropriate editor prior to posting your manuscript electronically.

Reuse/Republication of the Entire Work in Thesis or Collections: Authors may reuse all or part of the Submitted, Accepted or Published Work in a thesis or dissertation that the author writes and is required to submit to satisfy the criteria of degree-granting institutions. Such reuse is permitted subject to the ACS' "Ethical Guidelines to Publication of Chemical Research" (https://pubs.acs.org/page/policy/ethics/index.html#b); the author should secure written confirmation (via letter or email) from the respective ACS journal editor(s) to avoid potential conflicts with journal prior publication*/embargo policies. Appropriate citation of the Published Work must be made. If the thesis or dissertation to be published is in electronic format, a direct link to the Published Work must also be included using the ACS Articles on Request author-directed link - see https://pubs.acs.org/page/policy/articlesonrequest/index.html
* Prior publication policies of ACS journals are posted on the ACS website at https://pubs.acs.org/page/policy/prior/index.html
If your paper has not yet been published by ACS, please print the following credit line on the first page of your article: "Reproduced (or 'Reproduced in part') with permission from [JOURNAL NAME], in press (or 'submitted for publication'). Unpublished work copyright [CURRENT YEAR] American Chemical Society." Include appropriate information.
If your paper has already been published by ACS and you want to include the text or portions of the text in your thesis/dissertation, please print the ACS copyright credit line on the first page of your article: "Reproduced (or 'Reproduced in part') with permission from [FULL REFERENCE CITATION.] Copyright [YEAR] American Chemical Society." Include appropriate information.
Submission to a Dissertation Distributor: If you plan to submit your thesis to UMI or to another dissertation distributor, you should not include the unpublished ACS paper in your thesis if the thesis will be disseminated electronically, until ACS has published your paper. After publication of the paper by ACS, you may release the entire thesis (**not the individual ACS article by itself**) for electronic dissemination through the distributor; ACS's copyright credit line should be printed on the first page of the ACS paper.
v1.4

Questions? E-mail us at customercare@copyright.com.

CHAPTER VI.

Conclusions and Future Directions

6.1 Overview

Fungal natural products represent a structurally diverse and biologically rich source of molecular scaffolds, the full characterization of which demands the integration of chemical synthesis, biosynthetic investigation, and biological evaluation. The work described in this thesis applies this integrated approach to two macrocyclic fungal natural products, organized around two distinct research programs. The first, spanning Chapters I-IV, concerns the total synthesis and biological investigation of immunomodulide, a PKS-NRPS hybrid-derived 12-membered cyclic tridepsipeptide with plant immunopotentiating activity. The second, described in Chapter V, addresses the biosynthetic characterization and total synthesis of fusahexin[1], a macrocyclic hexapeptide assembled by a nonribosomal peptide synthetase from *Fusarium graminearum*.

Chapter I reviewed the emerging family of fungal-derived 12-membered cyclic tridepsipeptides, establishing the structural, biosynthetic, and synthetic landscape within which immunomodulide is situated and identifying the recurring synthetic challenges that informed the campaign described in subsequent chapters. Chapter II described the total synthesis of a simplified macrolactam model system of immunomodulide, evaluating two macrolactamization disconnections and identifying route C as the superior strategy while establishing key synthetic constraints applicable to the fully elaborated target. Chapter III extended the model system studies into a preliminary structure-activity relationship campaign, identifying the native D-Trp/L-Pip macrolactam configuration as the primary pharmacophoric determinant of immunomodulide's plant immunopotentiating activity and demonstrating tolerance for conservative structural substitutions at the aromatic and *N*-alkyl positions. Chapter IV described the configurational assignment of the PKS fragment by comparative ^{13}C NMR analysis, the two-generation enantioselective synthesis of the PKS aldehyde coupling partner, and the ongoing synthetic campaign toward the total synthesis of Immunomodulide. This work has advanced to the macrolactamization precursor and preliminary LC-MS evidence for the macrolactam product has been obtained. Chapter V addressed the biosynthetic and structural characterization of fusahexin, identifying prefusahexin as its direct biosynthetic precursor, achieving the total syntheses of both natural products, and implicating copper amine oxidases as the enzymatic class responsible for the key late-stage oxidative cyclization.

6.2 The 12-Membered Cyclic Tridepsipeptide Family

The comparative analysis presented in Chapter I revealed a structurally conserved subfamily of fungal PKS-NRPS natural products that has attracted sustained synthetic interest while remaining incompletely characterized both biologically and biosynthetically. The consistent failure of macrolactonization-based ring-closure across all reported synthetic campaigns[2,3], in contrast to the selective success of macrolactamization strategies[3–9], establishes a practical design principle that should guide future synthetic planning for any member of this class. Equally important is the recurring documentation of diketopiperazine[10] formation and amino acid epimerization[3–5] as competing pathways in macrolactamization, which reflect fundamental chemical constraints of the *N*-alkylated macrolactam scaffold that remain unresolved.

A significant gap that remains across this family is the absence of biochemically characterized biosynthetic gene clusters for most members. To date, only the xylacremolide-producing BGC has been functionally characterized[11], and the biosynthetic origins of the acremolides[12], colletopeptides[13], colletotrichamides[14], HA23[15], and stereocalpins[16,16], remain inferred by analogy. Targeted genome mining and heterologous expression campaigns directed at the producing organisms of these metabolites would substantially advance the understanding of hrPKS programming logic within this subfamily and could enable the discovery of related cryptic metabolites. The biochemistry-based stereochemical prediction model developed by Takino et al[17]. has shown promise in reducing the synthetic burden of configurational assignment for acremolides and HA23, but its limitations in the valactamide[18] series and the absence of independent biosynthetic validation for most family members suggest that it should remain a hypothesis-generating tool rather than a definitive assignment method. As such, total synthesis remains the most reliable route to unambiguous configurational assignment for members of this class.

6.3 Toward the Total Synthesis of Immunomodulide

The synthetic campaign described in Chapters II through IV represents the first total synthesis effort directed at immunomodulide and the first systematic investigation of its PKS fragment configuration.

Investigations on ring-closing approaches, clarify the design constraint for route B-type disconnections in this scaffold, and support the limitations in this approach as observed across literature reported attempts that target this ring closing strategy[3–5]. The systematic evaluation

carried out in Chapter II, spanning multiple activation methods and both diastereomeric linear precursors defines the source of epimerization to be mode of activation and suggests that attempts that pursue route B disconnections should be optimized on this front to limit stereochemical scrambling. Furthermore, these results validate route C as the superior disconnection for this scaffold, assuming DKP formation can be managed through orthogonal protecting groups, reduced temperature, and non-basic conditions.

The comparative ^{13}C NMR analysis established a viable strategy for narrowing the stereochemical target space prior to synthesis, reducing sixteen possible permutations to a single synthetic lead through comparison against configurationally defined congeners. The identification of colletopeptide E[19] as the closest structural match, and the confirmation of the 1,2-syn relationship between C5 and C28 through the acremolide B[7,12] comparison, provide convergent lines of evidence for the 3R,5S,28S,33R configurational assignment that will be tested upon completion of the synthesis. Overall this strategy offers a complementary, empirical alternative to this biosynthetic prediction model developed by Takino et al.[17]. By comparing spectroscopic data against configurationally defined congeners, this approach narrows the stereochemical target space prior to synthesis without reliance entirely on biosynthetic assumptions. Its extension to other family members with unresolved PKS-derived stereocenters would provide an independently validated cross-check for the Takino model where applicable and serve as the primary assignment strategy where it is not.

Preliminary LC-MS evidence for the macrolactam product confirms that acyl ketene ring-closure via route C is operative, and that the synthesis is stalled at the deprotection step rather than at macrolactamization. The most immediate synthetic priorities are identifying Boc deprotection conditions compatible with the dioxinone functionality and evaluating Lewis acid-mediated acyl ketene activation (Chapter IV) as a lower-temperature alternative to thermal retro-hetero-Diels-Alder fragmentation, and work toward both objectives is ongoing in the Boddy laboratory.

Once the macrolactam is obtained in sufficient quantity for full characterization, comparison against the isolated natural product will provide the definitive test of the 3R,5S,28S,33R configurational assignment. The tailorable retrosynthetic design, in which each stereocenter was planned for independent installation, permits selective inversion at any individual position without requiring route redesign, providing a clear path to structural correction if needed. Reduction at C3, deferred from the acyclic stage due to the insufficient facial bias at the adjacent

C5 center, may be addressable on the intact macrocycle where conformational constraints can be exploited. The overall synthetic platform developed here, including the retro-Claisen route to the PKS aldehyde and the stepwise NRPS assembly strategy using Boc-Pip, provides a reliable and modular framework for accessing immunomodulide and its future analogs.

More broadly, the combination of pathway analysis establishing the PKS-NRPS hybrid architecture, together with the comparative ^{13}C NMR strategy resolving the PKS-derived stereocenters, and the tailorable synthetic design permitting targeted correction, offers a general strategy for accelerating configurational assignment across the hrPKS-NRPS tridepsipeptide family, allowing a proposed stereochemistry to be tested and, if necessary, corrected through targeted inversion rather than route redesign.

6.4 Immunomodulide as a Plant Immune Potentiator

Pathogen resistance continues to erode the effectiveness of existing crop protection strategies[20]. By identifying immunomodulide as a potentiator of the plant immune system and defining where the scaffold can be modified without loss of activity, this work lays the groundwork for a viable alternative to conventional agrochemicals facing rising resistance.

The SAR campaign described in Chapter III establishes the first pharmacophore model for any member of the 12-membered cyclic tridepsipeptide class in the context of plant innate immunity. The finding that the D-Trp/L-Pip configuration is a strict requirement for ROS burst potentiation, while conservative substitutions at both the aromatic side chain and the *N*-alkyl position are tolerated, defines the conformational and configurational requirements of the scaffold in a way that directly informs future analog design. The tolerance for D-Phe and L-Pro substitution suggests that the aromatic side chain and the *N*-alkyl group contribute to activity through shape complementarity rather than through specific polar contacts with a biological target.

DC3000 colonization assays confirmed that the ROS burst potentiation observed for immunomodulide and the model system translates into a meaningful reduction in bacterial colonization, which is the critical agrochemical relevance criterion. Finalization of the full analog library is ongoing among colleagues in the Boddy laboratory, and biological evaluation of this library by our collaborators is pending its completion. If confirmed across the analog series, these results would establish immunomodulide as a promising lead scaffold for the development of novel

plant immune potentiators, motivating further analog synthesis and optimization toward field application.

The broader question of whether immunopotentiating activity is a general feature of the 12-membered cyclic tridepsipeptide scaffold, or specific to the immunomodulide pharmacophore, has not yet been addressed. Testing of the tridepsipeptide family analog set, including the colletopeptide-, acremolide-, stereocalpin- and HA23-inspired analogs synthesized in Chapter III, in the ROS burst and DC3000 assays is ongoing, will answer this question, and could identify additional active scaffolds within a structurally diverse but synthetically accessible chemical space.

A key future direction is determining the mechanism by which immunomodulide potentiates PAMP-triggered immunity, which remains unknown and represents one of the most scientifically significant open questions arising from this work. A clickable analog installed at a position confirmed tolerant of modification, such as the aromatic side chain or the terminal hydroxyl of the PKS chain, would enable activity-based protein profiling or fluorescent target identification experiments in plant cell systems.

6.5 Biosynthesis and Synthesis of Fusahexin

The work described in Chapter V resolved a central mechanistic question in fusahexin biosynthesis and delivered the first total syntheses of both fusahexin and its direct precursor prefusahexin[21]. Notably, the biomimetic reduction-cyclization cascade central to this synthesis, in which reductive unmasking of the ornithine-derived aldehyde triggers, diastereoselective cyclization to the bicyclic *N,O*-acetal, proceeded in 77% yield, and 10:1 dr. This result demonstrated that this key step mirrors the proposed biosynthetic transformation both mechanistically and in practical efficiency. As with the immunomodulide campaign, this work shows the strength of pairing pathway analysis with chemical synthesis for characterizing structurally novel fungal metabolites and resolving their biosynthesis. The synthetic platform established in Chapter V, providing access to both prefusahexin and fusahexin, underpins the mechanistic and biological investigations described below.

The identification of the split biosynthetic gene cluster arrangement in *F. graminearum,* with the oxidative enzyme encoded on a separate chromosome, represents an unusual genomic organization that challenges the conventional BGC-centric framework for fungal secondary

metabolite discovery. The identification of a CAO-encoding gene adjacent to the NRPS4 cluster in *F. avenaceum*, combined with the successful biomimetic oxidation of prefusahexin using a synthetic TPQ equivalent, provides strong chemical support for CAO-mediated oxidative cyclization as the final biosynthetic transformation. Heterologous expression of this candidate CAO enzyme is currently underway, with the goal of testing this proposed mechanism by applying the expressed enzyme to prefusahexin as a biocatalyst.

Beyond its mechanistic significance, the finding that a simple oxidation event is sufficient to trigger spontaneous diastereoselective cyclization to the bicyclic *N,O*-acetal provides a biomimetic design principle applicable to the synthesis of related fused acetal-containing scaffolds. As discussed in Chapter V, this motif, though unprecedented among natural products prior to fusahexin, is structurally related to dipeptide β-turn mimics developed for peptidomimetic applications[22–27,27–30], including IAP antagonists[22,31,32] and PD-1/PD-L1 pathway inhibitors[33]. This biomimetic oxidation strategy is not confined to fusahexin, and the same quinone-mediated approach is currently being applied within the group to construct a related scaffold in a separate total synthesis target, extending this design principle beyond the fusahexin scaffold.

Lastly, the biological role of fusahexin in *Fusarium* pathogenicity and cell surface hydrophobicity, proposed based on structural analogy with fusarinine and related siderophore-like metabolites[1], has not yet been directly tested. With synthetic access to fusahexin and prefusahexin now established, future biological investigations can address whether fusahexin contributes to virulence in *F. graminearum* infection of wheat. This question is of direct relevance to the management of Fusarium head blight disease, which persists as one of the most economically damaging cereal diseases worldwide[34].

6.6 Conclusion

The work described in this thesis advances the synthesis, structural characterization, and biological understanding of two structurally distinct *Fusarium*-derived natural products, while contributing broadly to the synthetic methodology available for accessing macrocyclic scaffolds. The immunomodulide campaign establishes the first pharmacophore model for plant immunopotentiating activity within the 12-membered cyclic tridepsipeptide class and brings the total synthesis to the stage of preliminary macrolactam formation, with a clear path to completion through ongoing optimization of the deprotection and ring-closure sequence. The fusahexin

campaign delivers the first total syntheses of both fusahexin and prefusahexin and identifies the enzymatic logic underlying the key biosynthetic transformation, opening the door to further mechanistic and biological investigations. Together, these studies demonstrate the value of pairing total synthesis with biosynthetic and biological analysis for characterizing structurally novel fungal natural products. In doing so, they position both programs to move beyond structural and mechanistic characterization toward applications with direct agricultural and biocatalytic relevance. Immunomodulide stands as a candidate scaffold for crop protection strategies less vulnerable to pathogen resistance, while the fusahexin studies open the door to investigating its role in fungal virulence and to expanding our biocatalytic toolbox for constructing medicinally relevant *N,O*-acetal-containing scaffolds.

6.7 References

(1) Westphal, K. R.; Bachleitner, S.; Severinsen, M. M.; Brundtø, M. L.; Hansen, F. T.; Sørensen, T.; Wollenberg, R. D.; Lysøe, E.; Studt, L.; Sørensen, J. L.; Sondergaard, T. E.; Wimmer, R. *J. Nat. Prod.* **2021**, *84* (8), 2070–2080.

(2) Yadav, J. S.; Amrutapu, S. K.; Pabbaraja, S. *ChemistrySelect* **2017**, *2* (5), 1850–1853.

(3) Reddy, K. M.; Shashidhar, J.; Pottireddygari, G. R.; Ghosh, S. *Tetrahedron Lett.* **2011**, *52* (45), 5987–5991.

(4) Feng, J.; Liu, J.; Ye, T. *Org. Lett.* **2025**, *27* (33), 9299–9303.

(5) Ghosh, A. K.; Xu, C. X. *Org. Lett.* **2009**, *11* (9), 1963–1966.

(6) Elmarrouni, A.; Fukuda, A.; Heras, M.; Arseniyadis, S.; Cossy, J. *J. Org. Chem.* **2010**, *75* (24), 8478–8486.

(7) Xiao, Y.; Liu, J.; Jiang, Y.; Guo, Y.; Ye, T. *Molecules* **2024**, *29* (15), 3599.

(8) Chen, J.; Jiang, Y.; Yan, J.; Xu, C.; Ye, T. *Molecules* **2023**, *28* (20), 7194.

(9) Kaneda, M.; Inuki, S.; Ohno, H.; Oishi, S. *J. Org. Chem.* **2018**, *83* (6), 3047–3060.

(10) Zhao, M. X.; Zeng, E. Z.; Li, Y.; Wang, C. J. *J. Mater. Chem. B* **2014**, *2* (42), 7351–7359.

(11) Schalk, F.; Fricke, J.; Um, S.; Conlon, B. H.; Maus, H.; Jäger, N.; Heinzel, T.; Schirmeister, T.; Poulsen, M.; Beemelmanns, C. *RSC Adv.* **2021**, *11* (31), 18748–18756.

(12) Ratnayake, R.; Fremlin, L. J.; Lacey, E.; Gill, J. H.; Capon, R. J. *J. Nat. Prod.* **2008**, *71* (3), 403–408.

(13) Feng, L.; Wang, J.; Liu, S.; Zhang, X.-J.; Bi, Q.-R.; Hu, Y.-Y.; Wang, Z.; Tan, N.-H. *J. Nat. Prod.* **2019**, *82*, 12.

(14) Bang, S.; Lee, C.; Kim, S.; Song, J. H.; Kang, K. S.; Deyrup, S. T.; Nam, S. J.; Xia, X.; Shim, S. H. *J. Org. Chem.* **2019**, *84* (17), 10999–11006.

(15) Feng, Y.; Blunt, J. W.; Cole, A. L. J.; Munro, M. H. G. *Org. Lett.* **2002**, *4* (12), 2095–2096.

(16) Seo, C.; Yim, J. H.; Lee, H. K.; Park, S. M.; Sohn, J. H.; Oh, H. *Tetrahedron Lett.* **2008**, *49* (1), 29–31.

(17) Takino, J.; Kotani, A.; Ozaki, T.; Peng, W.; Yu, J.; Guo, Y.; Mochizuki, S.; Akimitsu, K.; Hashimoto, M.; Ye, T.; Minami, A.; Oikawa, H. *Angew. Chem. - Int. Ed.* **2021**, *60* (43), 23403–23411.

(18) Zhang, T.; Feng, J.; Oikawa, H.; Guo, Y.; Ye, T. *Precis. Chem.* **2024**, *2* (3), 120–126.

(19) Lee, C.; Gong, J.; Kim, J.; Ko, H.; An, S.; Bang, S.; Deyrup, S. T.; Noh, M.; Shim, S. H. *J. Nat. Prod.* **2022**, *85* (3), 501–510.

(20) Jinna, Z.; Khan, T.; Kanwal, N.; Zhenji, W. *Cell. Mol. Biol.* **2025**, *71* (5), 43–48.

(21) Natola, C.; Hicks, C.; Witte, T. E.; Hermans, A.; Sproule, A.; Overy, D. P.; Boddy, C. N. *Org. Lett.* **2026**, *28* (14), 4507–4511.

(22) Vamos, M.; Welsh, K.; Finlay, D.; Lee, P. S.; Mace, P. D.; Snipas, S. J.; Gonzalez, M. L.; Ganji, S. R.; Ardecky, R. J.; Riedl, S. J.; Salvesen, G. S.; Vuori, K.; Reed, J. C.; Cosford, N. D. P. *ACS Chem. Biol.* **2013**, *8* (4), 725–732.

(23) Bäuerlein, C.; Geyer, A. *J. Org. Chem.* **2025**, *90* (31), 11142–11150.

(24) Sun, H.; Moeller, K. D. *Org. Lett.* **2002**, *4* (9), 1547–1550.

(25) Sun, H.; Martin, C.; Kesselring, D.; Keller, R.; Moeller, K. D. *J. Am. Chem. Soc.* **2006**, *128* (42), 13761–13771.

(26) Zhang, X.; Jiang, W.; Schmitt, A. C. *Tetrahedron Lett.* **2001**, *42* (30), 4943–4945.

(27) Chalmers, D. K.; Marshall, G. R. *J. Am. Chem. Soc.* **1995**, *117* (22), 5927–5937.

(28) Claridge, T. D. W.; Hulme, C.; Kelly, R. J.; Lee, V.; Nash, I. A.; Schofield, C. J. *Bioorg. Med. Chem. Lett.* **1996**, *6* (4), 485–490.

(29) Baldwin, J. E.; Hulme, C.; Schofield, C. J.; Edwards, A. J. *J. Chem. Soc. Chem. Commun.* **1993**, No. 11, 935–936.

(30) Nagai, U.; Sato, K. *Tetrahedron Lett.* **1985**, *26* (5), 647–650.

(31) COSFORD, N. D. P.; VAMOS, M. D. Inhibitor of Apoptosis Protein (Iap) Antagonists. WO2014085489A1, June 5, 2014.

(32) PACHE, L.; CHANDA, S. K.; VAMOS, M. D.; Cosford, N. D. P.; Teriete, P.; MARLETT, J.; Diaz, A.; Young, J. A. T. Use of Inhibitor of Apoptosis Protein (IAP) Antagonists in HIV Therapy. US10300074B2, May 28, 2019.

(33) Jiang, S. ; Zhou, G. ; Hao, H. ; Miao, Q. ; Wu, X. ; Zhang, K. ; Qiu, Y. Macrocyclic Compound for Inhibiting PD-1/PD-L1 and Application Thereof. CN112010940B, 2019.

(34) Chin, T.; Pleskach, K.; Tittlemier, S. A.; Henriquez, M. A.; Bamforth, J.; Withana Gamage, N.; Ashfaq, T.; Lee, S. J.; Kurera, M. S.; Patel, B.; Walkowiak, S. *Can. J. Plant Pathol.* **2023**, *45* (3), 277–289.